AD-A174 931   ENVIRONMENTAL AND WATER QUALITY OPERATIONAL STUDIES:    1/5
              MIXING IN RIVERS(U) CORNELL UNIV ITHACA NY DEPT OF
              CIVIL ENGINEERING  E R HOLLEY ET AL  SEP 86
UNCLASSIFIED  WES/TR/E-86-11 DACW39-83-M-0737           F/G 8/8        NL
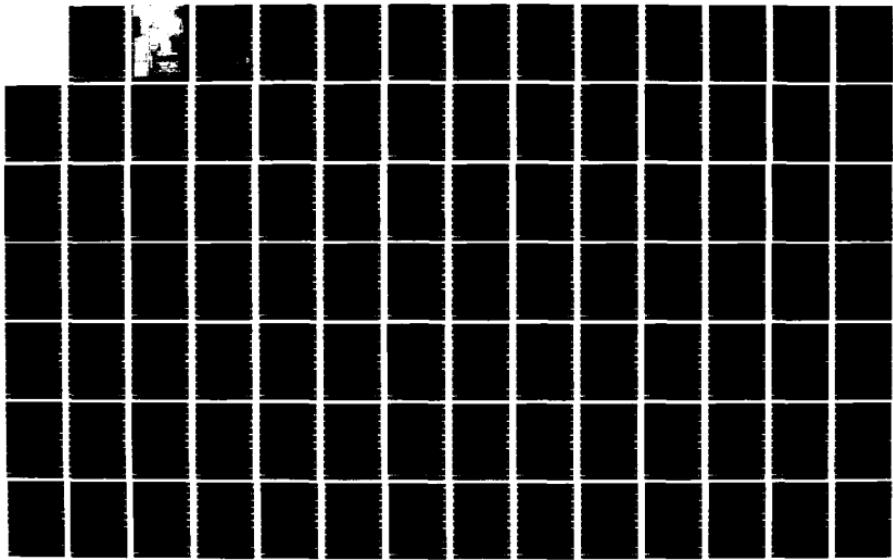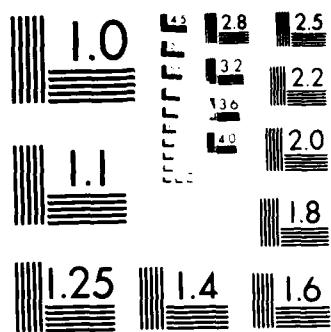
MICROCOPY RESOLUTION TEST CHART

NATIONAL BUREAU OF STANDARDS 1963 A

US Army Corps
of Engineers

AD-A174 931

ENVIRONMENTAL AND WATER QUALITY
OPERATIONAL STUDIES

TECHNICAL REPORT E-86-11

# MIXING IN RIVERS

by

Edward R. Holley

8902 Rockcrest Drive
Austin, Texas 78759

Gerhard H. Jirka

Department of Civil Engineering
Cornell University
Ithaca, New York 14850

September 1986

Final Report

Approved For Public Release; Distribution Unlimited

86 12 09

ADA 174931

(12)

# REPORT DOCUMENTATION PAGE

Form Approved
OMB No 0704 0188
Exp Date Jun 30 1986

| 1a REPORT SECURITY CLASSIFICATION<br>Unclassified | 1b RESTRICTIVE MARKINGS |
|---|---|

| 2a SECURITY CLASSIFICATION AUTHORITY | 3 DISTRIBUTION/AVAILABILITY OF REPORT |
|---|---|
| 2b DECLASSIFICATION/DOWNGRADING SCHEDULE | Approved for public release; distribution unlimited |

| 4 PERFORMING ORGANIZATION REPORT NUMBER(S) | 5 MONITORING ORGANIZATION REPORT NUMBER(S)<br>Technical Report E-86-11 |
|---|---|

| 6a NAME OF PERFORMING ORGANIZATION | 6b OFFICE SYMBOL (If applicable) | 7a NAME OF MONITORING ORGANIZATION<br>USAEWES<br>Environmental Laboratory |
|---|---|---|

| 6c ADDRESS (City, State, and ZIP Code)<br>8902 Rockcrest Drive, Austin, TX 78759;<br>Ithaca, NY 14850 | 7b ADDRESS (City, State, and ZIP Code)<br>PO Box 631<br>Vicksburg, MS 39180-0631 |
|---|---|

| 8a NAME OF FUNDING/SPONSORING ORGANIZATION<br>US Army Corps of Engineers | 8b OFFICE SYMBOL (If applicable) | 9 PROCUREMENT INSTRUMENT IDENTIFICATION NUMBER |
|---|---|---|

8c ADDRESS (City, State, and ZIP Code)

Washington, DC 20314-1000

10. SOURCE OF FUNDING NUMBERS

| PROGRAM ELEMENT NO | PROJECT NO | TASK NO | WORK UNIT ACCESSION NO |
|---|---|---|---|
| | | | EWQOS IC.3 |

11. TITLE (Include Security Classification)

Mixing in Rivers

12. PERSONAL AUTHOR(S)
Holley, Edward R., and Jirka, Gerhard H.

| 13a TYPE OF REPORT<br>Final report | 13b TIME COVERED<br>FROM _____ TO _____ | 14 DATE OF REPORT (Year, Month, Day)<br>September 1986 | 15 PAGE COUNT<br>423 |
|---|---|---|---|

16. SUPPLEMENTARY NOTATION
Available from National Technical Information Service, 5285 Port Royal Road, Springfield, VA 22161.

| 17 COSATI CODES | | | 18 SUBJECT TERMS (Continue on reverse if necessary and identify by block number) |
|---|---|---|---|
| FIELD | GROUP | SUB-GROUP | Hydraulic transport processes     Riverine mixing |
| | | | Jets     Rivers |
| | | | Plumes     Solute transport |

19. ABSTRACT (Continue on reverse if necessary and identify by block number)

This manual provides a discussion of the fundamental transport processes and the governing equations for mixing of solutes in rivers. Both the initial mixing associated with the momentum and buoyancy of the effluent discharge and the ambient transport following the initial mixing are considered in detail. Experimental considerations are discussed, and applications of the transport equations for both initial and ambient mixing problems are presented.

DTIC
ELECTE
DEC 1 0 1986
S D
E

| 20 DISTRIBUTION/AVAILABILITY OF ABSTRACT<br>☒ UNCLASSIFIED/UNLIMITED ☐ SAME AS RPT ☐ DTIC USERS | 21 ABSTRACT SECURITY CLASSIFICATION<br>Unclassified |
|---|---|
| 22a NAME OF RESPONSIBLE INDIVIDUAL | 22b TELEPHONE (Include Area Code)    22c OFFICE SYMBOL |

DD FORM 1473, 84 MAR     83 APR edition may be used until exhausted
All other editions are obsolete

PREFACE

39-83-M-0737

This report was prepared under Contract No. DACW83-M-0737 during
the period November 1982 to November 1984 as part of the Environmental
and Water Quality Operational Studies (EWQOS), Work Unit IC.3 entitled
"Improve and Verify Riverine Water Quality and Ecological Predictive
Techniques." The EWQOS Program is sponsored by the Office, Chief of
Engineers (OCE), US Army, and is assigned to the US Army Engineer Water-
ways Experiment Station (WES) under the purview of the Environmental
Laboratory (EL). The OCE Technical Monitors for EWQOS were Dr. John
Bushman, Mr. Earl Eiker, and Mr. James L. Gottesman.

Chapters 1, 4, 5, 6, 7, and part of 8 were prepared by
Dr. Edward R. Holley, Austin, Tex. Chapters 2, 3, and the remainder of
8 were prepared by Dr. Gerhard H. Jirka, Ithaca, N. Y. Mr. Aaron Stein
of the Water Quality Modeling Group (WQMG), Ecosystem Research and
Simulation Division (ERSD), EL, WES, monitored the effort under the
direct supervision of Mr. Mark Dortch, Chief, WQMG. The review and
preparation of this report were directed by Ms. Sandra Bird, WQMG; the
authors express their appreciation for her thorough review. She
detected may of the errors in the draft of this report. General
supervision was provided by Mr. Donald L. Robey, Chief, ERSD, and
Dr. John Harrison, Chief, EL. Dr. J. L. Mahloch was Program Manager
of EWQOS.

Copyrighted figures were used courtesy of the American Society
of Civil Engineers and the American Geophysical Union.

COL Allen F. Grum, USA, was the previous Director of WES.
COL Dwayne G. Lee, CE, is the present Commander and Director.
Dr. Robert W. Whalin is Technical Director.

This report should be cited as follows:

Holley, E. R., and Jirka, G. H. 1986. "Mixing in Rivers,"
Technical Report E-86-11, US Army Engineer Waterways Experiment
Station, Vicksburg, Miss.

1

CONTENTS

CONVERSION FACTORS, NON-SI to SI (METRIC)
UNITS OF MEASUREMENT

Non-SI units of measurement used in this report can be converted to SI (metric) units as follows:

| Multiply | By | To Obtain |
| --- | --- | --- |
| cubic feet per second | 0.02831685 | cubic metres per minute |
| Fahrenheit degrees | 5/9 | Celsius degrees* |
| feet | 0.3048 | metres |
| feet per second | 0.3048 | metres per second |
| gallons (US liquid) | 3.785412 | cubic decimetres |
| miles (US statute) | 1.609347 | kilometres |
| pounds (mass) | 0.4535924 | kilograms |
| square feet per second | 0.09290304 | square metres per second |

---

* To obtain Celsius (C) temperature readings from Fahrenheit (F) readings, use the following formula: $C = (5/9) (F - 32)$. To obtain Kelvin (K) readings, use $K = (5/9)(F - 32) + 273.15$.

MIXING IN RIVERS

CHAPTER 1.  INTRODUCTION

US Army Corps of Engineer (CE) activities, such as reservoirs or
dredged material disposal sites, can potentially affect water quality in
rivers.  Channelization projects and impoundments may alter the hy-
draulic transport properties of a river.

Many factors influence water quality in rivers, including the
amount and type of pollutant input, biological and chemical processes,
geometric and hydraulic characteristics of the river, methods and loca-
tion for discharges, physical and chemical properties of the pollutant,
and hydraulic transport processes.  This report deals only with the dis-
charge and transport of solutes, i.e. substances that are dissolved in
the water.  No direct consideration is given to many other important
aspects of water quality in rivers, including pollutant-sediment inter-
actions, insoluble pollutants, and specifics of biological and chemical
processes.

There are also many types of rivers; in fact, there are so many
types that it is difficult to find meaningful names for the various
categories.  This problem is compounded by the fact that the categoriza-
tions which have been developed are for purposes other than identifying
the various characteristics which influence the hydraulic transport
processes.  Some of the widely used descriptions of rivers are braided
streams, pool-and-riffle streams, and run-of-the-river reservoirs.  It
is even difficult to state a clear definition of the distinction between
rivers and reservoirs; for this report, the distinction is based on riv-
ers having an absence of significant natural stratification and of sig-
nificant, long-term wind effects.  In this report, additional stream
categories are free-flowing streams and streams with irregular cross
sections.  A free-flowing stream is defined as one with an unobstructed
cross section which varies in size and shape in some systematic fashion
along the stream length and with an identifiable thalweg.  Irregular
cross sections are ones in which the variations in the bottom profile

5

are randomly distributed and have heights which are on the same order of magnitude as the flow depths.

Calculation of transport in rivers can require different methods depending on the type of river, distance from input site, and type of injection. This report provides criteria for selection of computational techniques. Analytical solutions and "desk-top" type calculations are given where possible and appropriate. No specific numerical solution techniques are discussed, but guidelines for choosing the necessary complexity of a numerical model are implicit through much of the discussion.

This report is organized in three major sections. The first section (Chapters 2 and 3) presents a discussion of initial mixing associated with the momentum and buoyancy of the effluent discharge; the second section (Chapters 4 - 7) discusses ambient transport after the end of whatever initial mixing may be present; the third section (Chapter 8) gives some example applications for both initial mixing and ambient transport. In the first two sections, the discussion begins with various considerations related to the theory of the problem at hand and to the important physical mechanisms. Particularly in the second section (Chapters 4 - 6), there is a detailed treatment of the basics of ambient transport, beginning with the fundamental equations and going through various calculated concentration distributions. In the first two sections, emphasis is placed on the theoretical, fundamental, and physical concepts because of the firm belief of the authors that an understanding of these concepts is essential for the appropriate interpretation of experimental results and the appropriate use of these results for predictive purposes. Thus, it must be emphasized that the reader cannot skip or skim over the portions on basic concepts and then be able to make intelligent and proper use of the principles illustrated in the latter portions devoted to applied aspects.

# CHAPTER 2. FUNDAMENTAL ASPECTS OF JETS AND PLUMES

## 2.1 INTRODUCTION

### 2.1.1 Definition and Importance

Any natural river or man-made watercourse has its associated mean advective field and turbulent characteristics. The understanding of these transport processes and their mathematical formulation is a key ingredient for a successful prediction of any pollutant introduced into such a watercourse.

The actual method of introduction or discharge of the pollutant also can influence the subsequent transport pattern. This is to be expected, as in practice a pollutant discharge is a finite amount of inflow (in case of a continuous discharge) or a finite amount of mass (in case of an "instantaneous" or slug discharge) that is released into the river. Thus, the release initially will more or less disturb the ambient (or natural) transport pattern and will generate its own mean advective and turbulence fields. This active, discharge-induced transport process is generally called the initial mixing phase.

The mixing in this initial phase is governed by the dynamic characteristics and by the geometry of the discharge relative to the ambient conditions. The discharge dynamics are controlled mainly by the momentum and the buoyancy of the inflow. For example, high-velocity (i.e. high-momentum) injections are associated with rapid mixing close to the discharge. On the other hand, highly buoyant inflows, due to the density differences relative to the ambient water, can be associated with strongly divergent mixing patterns; they may increase mixing if coupled with vertically rising or falling trajectories, or they may inhibit mixing if the trajectory is blocked, forming, for instance, a warm water layer at the river surface.

The discharge geometry may range from surface channels that enter a river laterally, to submerged single pipes located on the river bottom, to multiport diffusers in which a feeder pipe spans the river width

7

(or a portion thereof) and has a multitude of smaller nozzles or parts.

The initial mixing phase has paramount engineering importance for managing the actual environmental impact of a discharge. It is in this phase that the engineer can actually control the amount of mixing and, if desired, can achieve a very high degree of dilution that may rapidly reduce pollutant concentrations to acceptable levels. In contrast, the intensity of ambient transport and mixing processes is frequently much lower and cannot be further affected by engineering design.

The information on initial mixing is organized as follows. The fundamental aspects of jet diffusion under the influence of initial momentum and buoyancy, respectively, are presented in Chapter 2. This discussion includes the underlying physical phenomena and their mathematical treatment, with particular emphasis on the simple, yet powerful, integral analysis technique. Some idealized conditions, namely a stagnant and infinitely large receiving water, are assumed in the initial stages of that discussion. Yet it will be evident later that the integral analysis can be readily extended to more realistic conditions as they prevail in riverine discharges. Chapter 3 then deals with the application of that technique to the three major classes of riverine discharges: Submerged single-port discharges (Section 3.1), submerged multiport discharges (Section 3.2), and surface discharges (Section 3.3). In each of these cases, the significant features of the underlying predictive model are explained and major results, which are useful for design or analysis purposes, are presented.

Throughout Chapters 2 and 3, maximum emphasis is placed on the initial mixing phases produced by continuous, steady-state discharges into rivers. The initial mixing produced by instantaneous releases (e.g. accidental dumps or field experimental tracer slug releases) is of lesser importance in routine environmental assessment and is analyzed briefly in Section 3.5. Examples are presented in Chapter 8.

## 2.1.2 Physical Processes

Consider a large ambient body of water that is stagnant and of
uniform density. If an aqueous discharge is introduced locally into
this water body by means of a port or nozzle, the velocity discontinu-
ity between the discharged fluid and the ambient fluid causes an
intense shearing action. In the general case of engineering applica-
tions where the discharge Reynolds number is large enough, i.e. where

$$Re = \frac{U_o D}{\nu} \gtrsim 2000$$

in which $U_o$ = discharge velocity, $D$ = discharge diameter, and $\nu$ =
kinematic viscosity, the flow breaks rapidly down into a turbulent mo-
tion. The width of the zone of high turbulent intensity increases in
the direction of the flow by incorporating ("entraining") more of the
outside, nonturbulent fluid into this zone. In this manner, any in-
ternal concentrations (e.g. of fluid momentum or of pollutants) become
diluted by the entrainment of ambient water. Inversely, one can speak
of the fact that both fluid momentum and pollutants (solutes) become
gradually diffused into the ambient field.

The initial velocity discontinuity may arise in different fash-
ions. In a "pure jet" (also called "momentum jet" or "nonbuoyant jet"),
the initial momentum flux in the form of a high-velocity injection
causes the turbulent diffusion. In a "pure plume," the initial buoy-
ancy flux leads to local vertical accelerations which then lead to tur-
bulent diffusion. In the general case of a "buoyant jet" (also called
a "forced plume"), a combination of initial momentum flux and buoyancy
flux is responsible.

From a mathematical viewpoint, it is possible in all of these
cases to employ simplified equations of the fluid motion. These equa-
tions take account of the narrow, elongated shape of the turbulent zone
and, hence, are of boundary-layer type. The equations may be further
simplified by integrating across the local jet cross section, thereby

9

yielding a one-dimensional equation set. This is the approach of "jet integral analysis" and will be demonstrated in the following paragraphs.

## 2.2 SIMPLE ROUND JETS

### 2.2.1 Physical Description

The actual instantaneous physical appearance of a simple round jet, i.e. one which is discharged with no buoyancy into a large, stagnant receiving water body of uniform density, is sketched in Figure 1a. Following the release from the nozzle, the jet flow becomes unstable at its boundary and breaks down into the turbulent motion. Typically, the size of the turbulent eddies increases with increasing distance along the trajectory. Thus, the jet goes from an initial fine-scale turbulent structure to an increasingly coarser one.

From an engineering viewpoint the actual instantaneous velocity and concentration distributions are often of secondary importance. The primary interest lies mostly in the mean (time-averaged over the time scale of the turbulent fluctuations) behavior as indicated in Figure 1b. The jet then exhibits a straight trajectory (in the absence of buoyancy), and all jet properties are distributed in a bell-shaped profile around that trajectory. In fact, one may define a "nominal width," $b$, at which a jet property (e.g. the velocity) attains a certain percentage of its maximum centerline value. One major characteristic of jets is their slender appearance, i.e. the local width $b$ is much less than the local distance along the trajectory ($b/s \ll 1$). By continuity this implies further that the forward velocities $u$ in the jet are considerably larger than the transverse velocities $v$ in the radial direction $r$ ($v/u \ll 1$). Even further, the pressure within the jet is approximately equal to the outside (hydrostatic) pressure in the ambient fluid as the transverse accelerations are negligible.

### 2.2.2 Governing Equations and Boundary Conditions

With these statements--all corresponding to the "boundary layer nature" of the flow--the time-averaged equations for the turbulent jet motion are

Continuity:
$$\frac{\partial u}{\partial s} + \frac{1}{r} \frac{\partial rv}{\partial r} = 0 \qquad (2.2.1)$$

Forward momentum:
$$u \frac{\partial u}{\partial s} + v \frac{\partial u}{\partial r} = -\frac{1}{r} \frac{\partial}{\partial r} (r \overline{u'v'}) \qquad (2.2.2)$$

Scalar conservation:
$$u \frac{\partial c}{\partial s} + v \frac{\partial c}{\partial r} = -\frac{1}{r} \frac{\partial}{\partial r} (r \overline{c'v'}) \qquad (2.2.3)$$
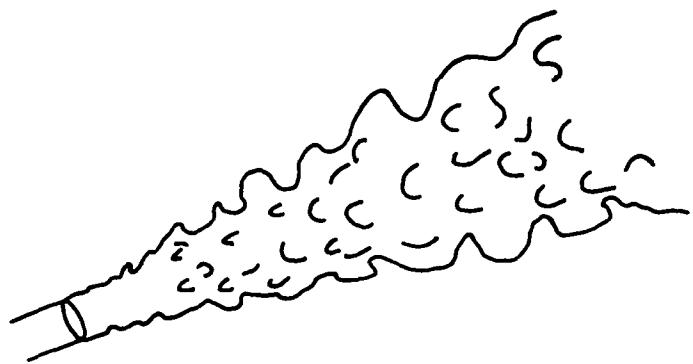


a.   Instantaneous appearance
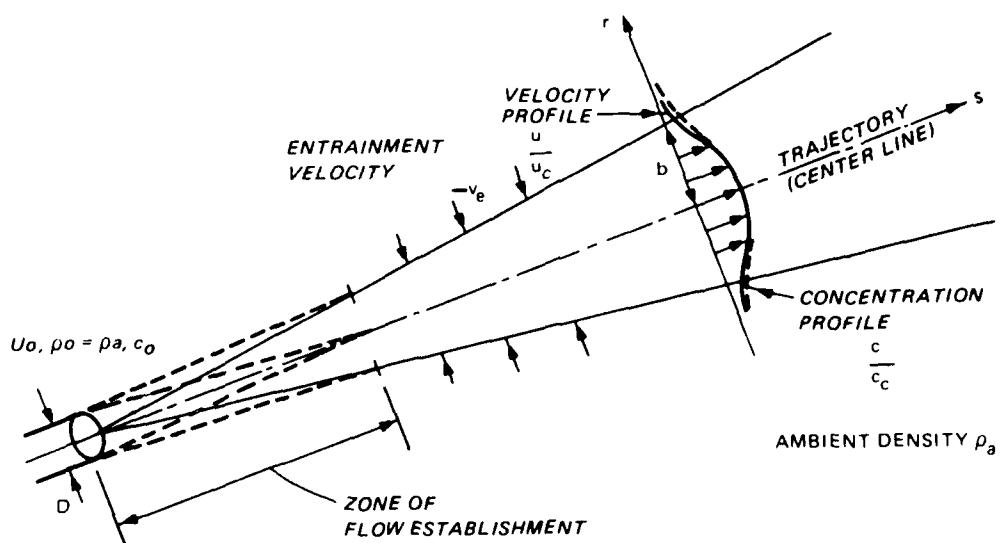


b.   Time-averaged conditions

Figure 1.   Simple round jet in uniform stagnant ambient
water body

11

The transverse momentum equation is negligible. In these equations the mean velocities $u$ and $v$ correspond to the local axisymmetric coordinates $s$ and $r$, respectively; $c$ is the mean pollutant concentration. The correlation terms $\overline{u'v'}$ and $\overline{c\,v'}$ represent the net lateral turbulent diffusion of momentum and pollutant mass due to the fluctuating jet properties (Reynolds terms) in which the primed quantities $u'$, $v'$, and $c'$ denote the temporal deviations from the temporal mean quantities $u$, $v$, and $c$. All turbulent diffusion terms in the s-direction have been neglected relative to the lateral terms, as have been molecular diffusion terms. Assuming uniform conditions at the beginning of the jet, the initial conditions for this equation system are

$$u = U_o , \quad c = c_o \quad \text{at} \quad s = 0 , \quad r \leq D/2 \qquad (2.2.4)$$

and the boundary conditions are

$$\left.\begin{array}{l} u \to 0 , \quad \dfrac{\partial v}{\partial r} \to 0 , \quad c \to 0 \\[2mm] \overline{u'v'} \to 0 , \quad \overline{c'v'} \to 0 \end{array}\right\} \text{at} \quad r \to \infty \qquad (2.2.5)$$

with symmetry about the centerline ($r = 0$).

There are different techniques--similarity solutions, eddy viscosity approaches, integral analysis, and direct numerical integration--for the solution of this equation set, all of which require one or more empirical (experimentally determined) coefficients for final closure of the equation system. A simple, sufficiently accurate and highly versatile approach is jet integral analysis.

The integral analysis proceeds by a priori selecting similarity functions to represent the relative transverse distribution of jet properties, such as velocities and concentrations. Thus, one does not, in fact, solve for these distributions (as a complete solution would require), but initially assumes profiles that approximate the actual observed bell-shaped profiles, for example,

12

$$\frac{u}{u_c} = f\left(\frac{r}{b}\right), \quad \frac{c}{c_c} = F\left(\frac{r}{b}\right) \tag{2.2.6}$$

in which $u_c$ and $c_c$ are the local centerline values and $b$ the local width. A frequently used profile assumption is a Gaussian (normal) distribution

$$\frac{u}{u_c} = f\left(\frac{r}{b}\right) = \exp\left(-\frac{r^2}{b^2}\right)$$

$$\frac{c}{c_c} = F\left(\frac{r}{b}\right) = \exp\left(-\frac{r^2}{\lambda^2 b^2}\right) \tag{2.2.7}$$

Thus, in Eq. 2.2.7 the nominal width (b) of the velocity profile has been defined as the position where the local velocity is $1/e = 37$ percent of the centerline velocity. The dispersion factor $\lambda$ in the concentration profile is introduced to account for the fact that the profiles of scalar quantities (e.g. concentration, temperature, etc.) are found experimentally to be somewhat wider ($\lambda > 1$) than the velocity profile. Other profile assumptions for $f$ and $F$ may be found in the literature, e.g. cosine functions, polynomials, or even rectangular ("top-hat") distributions. Two points must be noted in this respect: (a) the final functional relationships are unaffected by the choice of the profiles; (b) the empirical constants (e.g. entrainment coefficients or spreading constants), however, depend on the profile specification, and care must be exercised when quoting such values.

Also, when making such profile specifications, one must obviously exclude the initial zone of flow establishment (Figure 1) that exists just after the discharge and in which an adjustment between the efflux profile (approximately uniform) and the final established profile takes place. However, no major error is introduced in practical applications since the length of flow establishment is short ($\sim 6D$). Alternatively, an adjustment via a virtual origin can be made (Figure 1) or an analysis of the zone of flow establishment can be performed.

13

Having made these profile specifications (Eq. 2.2.6), the local bulk flux quantities can be defined by integration across the jet cross section.

Volume flux: $\qquad Q = 2\pi \int_0^\infty u r \, dr$

Momentum flux (kinematic): $\qquad M = 2\pi \int_0^\infty u^2 r \, dr \qquad$ (2.2.8)

Scalar (pollutant) mass flux: $Q_c = 2\pi \int_0^\infty u c r \, dr$

Using Eq. 2.2.6 these can be expressed as:

$$Q = 2\pi I_1 u_c b^2$$

$$M = 2\pi I_2 u_c^2 b^2 \qquad\qquad (2.2.9)$$

$$Q_c = 2\pi I_3 u_c c_c b^2$$

in which the "integral constants" are:

$$I_1 = \int_0^\infty f(\eta) \eta \, d\eta \;, \quad I_2 = \int_0^\infty f^2(\eta) \eta \, d\eta \;, \quad I_3 = \int_0^\infty f(\eta) F(\eta) \eta \, d\eta \quad (2.2.10)$$

and $\eta = r/b$ . Using the Gaussian functions (Eq. 2.2.7), these become

$$I_1 = \frac{1}{2} \;, \qquad I_2 = \frac{1}{4} \;, \qquad I_3 = \frac{1}{2} \frac{\lambda^2}{1 + \lambda^2} \qquad (2.2.11)$$

In just the same manner, it is possible to integrate, $2\pi \int_0^\infty [ \quad ] r \, dr$ , the three governing equations (Eqs. 2.2.1 to 2.2.3). Using the boundary conditions (Eq. 2.2.5) and the bulk quantities (Eq. 2.2.8), one obtains:

14

Volume flux conservation: $\dfrac{dQ}{ds} + 2\pi(rv)\big|_{r\to\infty} = 0$       (2.2.12)

Momentum flux conservation: $\dfrac{dM}{ds} = 0$       (2.2.13)

Scalar flux conservation: $\dfrac{dQ_c}{ds} = 0$       (2.2.14)

The term $2\pi(rv)\big|_{r\to\infty}$ in Eq. 2.2.12, where $\infty$ means "sufficiently out-side the jet" as in boundary layer terminology, is a non-zero quantity; this term from Eq. 2.2.12 represents the net flow toward the jet that is induced in the outside fluid by the "turbulent pumping action" within the jet. Using the jet width $b$ as the characteristic length, this term is usually expressed as

$$2\pi(rv)\big|_{r\to\infty} = -2\pi b v_e \qquad (2.2.15)$$

in which $v_e$ is called the "entrainment velocity." With this conven-tion Eq. 2.2.12 becomes

$$\frac{dQ}{ds} = 2\pi b v_e \qquad (2.2.16)$$

expressing the increasing volume flux along the trajectory.

2.2.3 Closure of the Equation Set

Note that it was not necessary to specify the turbulent correla-tion terms $\overline{u'v'}$ and $\overline{v'c'}$ in the governing equations (Eqs. 2.2.2 and 2.2.3). The transverse integration with the similarity functions and the boundary conditions (Eq. 2.2.5) eliminated the correlation terms. However, the usual closure problem, i.e. some way of relating the turbulence effects to the mean flow quantities, is not avoided alto-gether, since the integral equations contain the unknown parameters $v_e$ and $\lambda$ . The two dynamically important equations at this point are Eqs. 2.2.13 and 2.2.16. Their solution would describe the dependence

15

of $s$ of the two variables $u_c(s)$ and $b(s)$. The system is not closed, however, as the entrainment velocity $v_e(s)$ is not specified at this stage. Some additional physical arguments on jet behavior must be given to proceed any further. Either of two closure statements can be given.

a. **Closure statement I.** It is readily observed experimentally (as sketched in Figure 1b) and can also be deducted by physical reasoning (using dimensional similarity arguments first given by Prandtl, see Schlichting 1968), that the jet width grows linearly with distance, i.e. $b \sim s$. Using this statement, one can completely bypass Eq. 2.2.16 and simply use the following equation set

$$\frac{db}{ds} = k_j$$

$$\frac{d}{ds}\left(2\pi I_2 u_c^2 b^2\right) = 0$$

(2.2.17)

in which $k_j$ = jet spreading coefficient . The parameter $\lambda$ (or $\lambda b$) can be obtained by comparison of the rates of spreading of scalar (e.g. concentration) and velocity distributions.

b. **Closure statement II.** Alternatively, using the same physical reasoning, Morton, Taylor, and Turner (1956) first demonstrated that the entrainment velocity must be proportional to the centerline velocity $v_e \sim u_c$. This leads to the equation set

$$\frac{d}{ds}\left(2\pi I_1 u_c b^2\right) = 2\pi \alpha_j u_c b$$

$$\frac{d}{ds}\left(2\pi I_2 u_c^2 b^2\right) = 0$$

(2.2.18)

in which $\alpha_j$ = jet entrainment coefficient defined by the expression $v_e = \alpha_j u_c$ .

The advantage of the spreading approach is that $k_j$ is a readily determined constant from experimental data. The advantage of

16

the entrainment approach, however, is that it can be more easily extended to describe more complicated buoyant jet motions (other than simple jets or plumes). For the two approaches to be consistent, a comparison of the two equation sets shows

$$\alpha_j = I_1 k_j \qquad (2.2.19)$$

Thus, once $k_j$ is determined from experimental data, the corresponding $\alpha_j$ is readily computed. It is stressed again that the numerical values of both coefficients depend on the similarity function selected.

## 2.2.4 Solutions

The final solutions of the now-closed equation system are summarized in Table 1, which lists the functional dependence of both bulk variables and local variables on the distance s . In deriving these solutions it is convenient to consider the following bulk flux initial conditions

$$\left. \begin{array}{l} M_o = U_o^2 a_o \\[1em] Q_o = U_o a_o \\[1em] Q_{co} = U_o c_o a_o \end{array} \right\} \qquad \text{at} \quad s = 0 \qquad (2.2.20)$$

where the discharge area $a_o = \frac{\pi}{4} D^2$ , is used instead of the diameter, as was done in specifying the original initial conditions in Eq. 2.2.4. Furthermore, the solutions listed in Table 1 apply only sufficiently far away from the source (where the effects of the zone of flow establishment are no longer important), or about $s \geq 6D$ . The related dilution parameters, either in bulk (flux) form or as the minimum centerline value, are also given.

Finally, the empirical constants that must be evaluated from experimental data are summarized in Table 2, which is restricted to the Gaussian profiles specified in Eq. 2.2.9. The values given are

17

<div align="center">

Table 1

Solutions for the Axisymmetric Jet and Plume*

</div>

| | Round Jet | Round Plume |
|---|---|---|
| **Initial Discharge Parameters:** | | |
| $a_o = \frac{\pi}{4} D^2$ | $M_o = U_o^2 a_o$ | $M_o$** |
| | $Q_o = U_o a_o$ | $Q_o$ |
| | $Q_{co} = U_o c_o a_o$ | $Q_{co}$ |
| | | $J_o = U_o g_o' a_o$ |

**Bulk Variables:**

Momentum flux

| $M = 2\pi I_2 u_c^2 b^2$ | $M = M_o$ | $M = \frac{1}{2} (\pi I_2)^{1/3} \left( \frac{I_4}{I_1 I_3} J_o \frac{\alpha_p}{5} \right)^{2/3} (3s)^{4/3}$ |
|---|---|---|

Discharge

| $Q = 2\pi I_1 u_c b^2$ | $Q = \left( \frac{2\pi M_o}{I_2} \right)^{1/2} \alpha_j s$ | $Q = \left( \frac{I_4 \pi^2}{I_1 I_2 I_3} J_o \right)^{1/3} \left( \frac{\alpha_p}{5} \right)^{4/3} (3s)^{5/3}$ |
|---|---|---|

Scalar flux

| $Q_c = 2\pi I_3 u_c c_c b^2$ | $Q_c = Q_{co}$ | $Q_c = Q_{co}$ |
|---|---|---|

Buoyancy flux

| $J = 2\pi I_3 u_c g_c' b^2$ | -- | $J = J_o$ |
|---|---|---|

**Local Variables:**

| Width | $b = k_j s = \frac{\alpha_j}{I_1} s$ | $b = k_p s = \frac{3}{5} \frac{\alpha_p}{I_1} s$ |
|---|---|---|
| Centerline velocity | $u_c = \left( \frac{M_o}{2\pi I_2} \right)^{1/2} \frac{I_1}{\alpha_j s}$ | $u_c = \frac{1}{2} \left( \frac{I_4}{3\pi I_2 I_3} J_o \right)^{1/3} \left( \frac{5}{\alpha_p} I_1 \right)^{2/3} s^{-1/3}$ |
| Centerline concentration (buoyancy) | $c_c = \frac{Q_{co}}{I_3} \left( \frac{I_2}{2\pi M_o} \right)^{1/2} \frac{I_1}{\alpha_j s}$ | $g_c' = c_c \frac{J_o}{Q_{co}}$ $= \left( \frac{I_2}{I_4} \right)^{1/3} \left( \frac{I_1}{I_3} \frac{J_o}{\pi} \right)^{2/3} \left( \frac{5}{\alpha_p} \right)^{4/3} (3s)^{-5/3}$ |

**Dilutions:**

Bulk dilution:

| $S = \frac{Q}{Q_o}$ | $S = \frac{1}{Q_o} \left( \frac{2\pi M_o}{I_2} \right)^{1/2} \alpha_j s$ | $S = \frac{1}{Q} \left( \frac{I_4 \pi^2}{I_1 I_2 I_3} J_o \right)^{1/3} \left( \frac{\alpha_p}{5} \right)^{4/3} (3s)^{5/3}$ |
|---|---|---|

Centerline (minimum) dilution:

| $S_c = \frac{c_o}{c_c} = \frac{g_o'}{g_c'}$ | $S_c = \frac{I_3}{I_1} S$ | $S_c = \frac{I_3}{I_1} S$ |
|---|---|---|

---

\* Solutions are accurate outside the region of flow establishment $s \geq 6D$ .

** $M_o$ is constrained to

$$M_o = \left( \frac{5}{4} \frac{I_2^{3/2} I_4}{I_3} \frac{1}{\sqrt{2\pi} \alpha_p} J_o Q_o^2 \right)^{2/5}$$

in order to have simple plume conditions.

Table 2

Empirical Constants for the Axisymmetric Jet and Plume

with Gaussian Profile Specification (Eq. 2.2.7)*

| | Round Jet** | Round Plume |
|---|---|---|
| Spreading coefficient | $k_j = 0.110$ | $k_p = 0.100$ |
| Ratio $\alpha/k$ | $\dfrac{\alpha_j}{k_j} = \dfrac{1}{2}$ | $\dfrac{\alpha_p}{k_p} = \dfrac{5}{6}$ |
| Entrainment coefficient | $\alpha_j = 0.055$ | $\alpha_p = 0.083$ |
| Scalar dispersion coefficient | $\lambda_j = 1.20$ | $\lambda_p = 1.20$ |
| Equilibrium Froude number[†] | $F_{\ell j} = \infty$ | $F_{\ell p} = 4.66$ |

---

\* The above constants are based on the data surveys of Jirka,
Abraham, and Harleman (1975); Chen and Rodi (1980); and List (1982).

\*\* Round jet integral coefficients for Gaussian profiles are:

$$I_1 = \frac{1}{2} \ , \quad I_2 = \frac{1}{4} \ , \quad I_3 = \frac{1}{2} \frac{\lambda^2}{1+\lambda^2} \ , \quad I_4 = \frac{\lambda^2}{2} \ .$$

[†] $\quad F_\ell = \dfrac{u_c}{\left(g_c' b\right)^{1/2}}$ .

representative averages of the earlier data summaries of Jirka,
Abraham, and Harleman (1975); Chen and Rodi (1980); and List (1982).

## 2.3  SIMPLE ROUND PLUMES

### 2.3.1  Physical Description

An instantaneous view of a plume motion is shown in Figure 2a.
Here the motion is generated by releasing, at a ccnstant rate, water
that is lighter (density $\rho_o$ ) than the ambient water (density $\rho_a$ ),
i.e. $\rho_o < \rho_a$ .  The resulting motion is then driven by buoyant forces
and occurs along a vertical trajectory.  A local fluid element within
the plume with density $\rho$  will experience a buoyant acceleration  $g'$
relative to the outside fluid

$$g' = \frac{\rho_a - \rho}{\rho_a} g \qquad\qquad (2.3.1)$$

that is directed opposite to the direction of the total gravitational
acceleration g (for a plume with positive buoyancy, as being considered
here).  The motion of a turbulent plume, in comparison to the simple
jet (Figure 2a), often shows coarse large-scale meandering features, a
difference due to the buoyant accelerations.

The time-averaged conditions are indicated in Figure 2b and
again display bell-shaped distributions.  The plume exhibits a similar
narrow boundary-layer nature as the simple jet, so that the same
assumptions hold.

### 2.3.2  Governing Equations and Boundary Conditions

Compared to the simple jet equations (Eqs. 2.2.1-2.2.3), two
changes are expected:  a buoyant acceleration term in the momentum

20
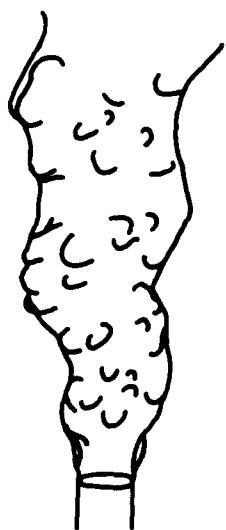
a.   Instantaneous appearance
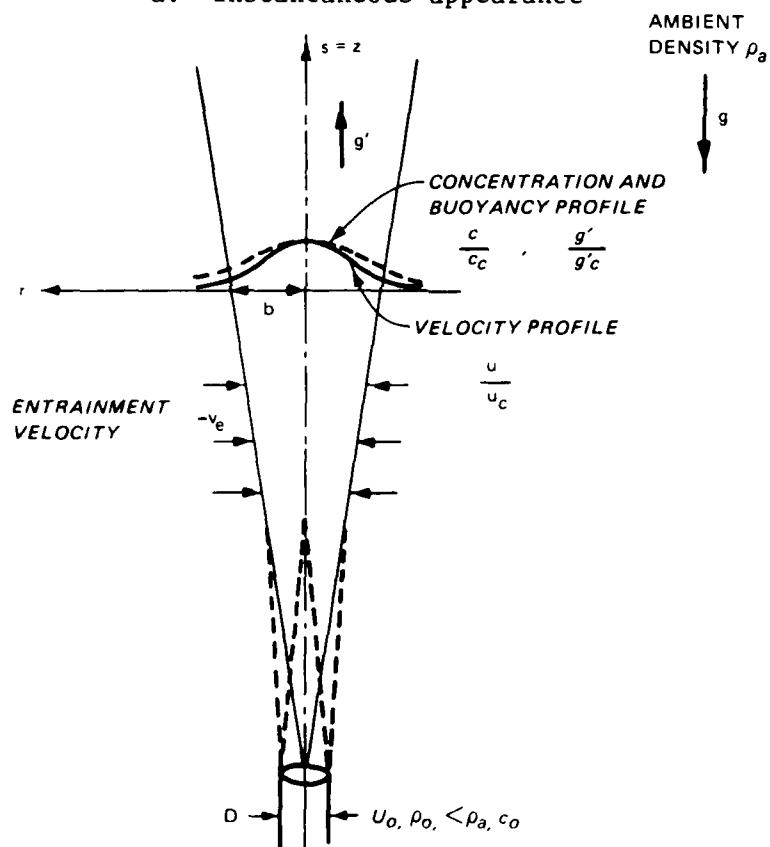
b.   Time-averaged conditions

Figure 2.   Simple round plume in uniform stagnant ambient water body

21

equation and an additional buoyancy conservation equation. Thus, the following equations apply:

Vertical momentum: $\quad u \dfrac{\partial u}{\partial s} + v \dfrac{\partial u}{\partial r} = -\dfrac{1}{r} \dfrac{\partial}{\partial r} (r \overline{u'v'}) + g'$ (2.3.2)

Buoyancy conservation: $u \dfrac{\partial g'}{\partial s} + v \dfrac{\partial g'}{\partial r} = -\dfrac{1}{r} \dfrac{\partial}{\partial r} (r \overline{(g')'v'})$ (2.3.3)

in addition to Eqs. 2.2.1 and 2.2.3. The quantity $(g')'$ denotes the turbulent fluctuation of buoyancy from its mean value, and the correlation $\overline{(g')'v'}$ is the transverse turbulent diffusive flux of buoyancy. In writing Eq. 2.3.2, the Boussinesq approximation has been made by assuming that the density is constant in all terms except the gravity term $g'$. This is acceptable in practical problems since the density deviations from the ambient density are usually small (e.g., < 3 percent in case of fresh water plumes in the ocean or estuaries).

The initial conditions on the system of plume equations (Eqs. 2.2.1, 2.2.3, 2.3.2, and 2.3.3) are

$$\left.\begin{aligned} g' &= g_o' \\[1em] u &= U_o = F_{\ell p} \frac{I_2^{5/4}}{8^{1/4} I_1 I_3^{1/2}} \left(g_o' D\right)^{1/2} \\[1em] c &= c_o \end{aligned}\right\} \text{at} \quad s = 0 , \quad r \le \frac{D}{2} \qquad (2.3.4)$$

and lateral boundary conditions are

$$g' \to 0 , \quad \overline{(g')'v'} \to 0 \qquad \text{at} \quad r \to \infty \qquad\qquad (2.3.5)$$

in addition to Eq. 2.2.5. The particular constraint on $U_o$, in which $F_{\ell p}$ is a plume Froude number which is defined in Table 2, is explained below.

An integral analysis of the plume can proceed in the same spirit as for the jet case. Since the local buoyancy is a scalar quantity, it

22

will be distributed similarly to the concentration profile (Eq. 2.2.6) so that

$$\frac{g'}{g'_c} = \frac{c}{c_c} = F\left(\frac{r}{b}\right) \tag{2.3.6}$$

in which $g'_c$ is the maximum (centerline) value. An additional bulk flow quantity is

$$\text{Buoyancy flux:} \quad J = 2\pi \int_0^\infty ug'r\,dr = 2\pi I_3 u_c g'_c b^2 \tag{2.3.7}$$

in addition to those defined in Eqs. 2.2.8 and 2.2.9. Cross-sectional integration of Eqs. 2.3.2 and 2.3.3 yields

$$\text{Momentum flux conservation:} \quad \frac{dM}{ds} = 2\pi I_4 g'_c b^2 \tag{2.3.8}$$

$$\text{Buoyancy flux conservation:} \quad \frac{dJ}{ds} = 0 \tag{2.3.9}$$

which apply together with Eqs. 2.2.16 and 2.2.17. The new term on the right-hand side of Eq. 2.3.8 represents the bulk acceleration effect of plume buoyancy in which the integration constant is

$$I_4 = \int_0^\infty F(\eta)\eta\,d\eta \tag{2.3.10}$$

which becomes for a Gaussian profile

$$I_4 = \frac{\lambda^2}{2} \tag{2.3.11}$$

23

### 2.3.3 Closure of the Equation Set

It is important to realize that the only dynamically important parameter within the pure plume is its buoyancy flux. The local momentum flux, in turn, is controlled by the buoyancy flux and increases with position s . Thus, the plume can be seen as a perfect equilibrium motion in which the buoyancy forces control the inertial (momentum) forces. A ratio of gravity and inertial forces can be expressed in the usual manner by a local densimetric Froude number:

$$F_\ell^2 = \frac{u_c^2}{g_c' b} = \sqrt{2\pi} \; \frac{I_1^2 I_3}{I_2^{5/2}} \frac{M^{5/2}}{JQ^2} \tag{2.3.12}$$

In an equilibrium motion, the force ratio and hence the Froude number must be constant along the plume path so that

$$F_\ell = \text{const.} = F_{\ell p} \tag{2.3.13}$$

Differentiating Eq. 2.3.12 with respect to S and setting $dF_\ell^2/ds = 0$ yield the equilibrium condition

$$\frac{5}{2} \frac{1}{M} \frac{dM}{ds} - \frac{2}{Q} \frac{dQ}{ds} - \frac{1}{J} \frac{dJ}{ds} = 0 \tag{2.3.14}$$

that governs the plume equation system (Eqs. 2.2.16, 2.3.8, and 2.3.9). Since the simple plume is a self-similar motion just as the simple jet (although with different dynamics since one is driven by buoyancy flux and the other by momentum flux), the same general closure principles can be used.

#### Closure statement I

Plume spreading: $\dfrac{db}{ds} = k_p$ \hfill (2.3.15)

24

<u>Closure statement II</u>

$$\text{Plume entrainment:} \quad \frac{dQ}{ds} = 2\pi\alpha_p u_c b \qquad (2.3.16)$$

The numerical values for the plume spreading coefficient $k_p$ and plume entrainment coefficient $\alpha_p$ will, in general, be different from the jet case due to their differences in turbulent structure.

The consistency condition between Eqs. 2.3.15 and 2.3.16, namely

$$\alpha_p = \frac{5}{3} I_1 k_p \qquad (2.3.17)$$

is obtained from substitution into the governing equations, and the value of the plume Froude number is

$$F_{\ell p} = \left( \frac{5}{4} \frac{I_1 I_4}{I_2} \frac{1}{\alpha_p} \right)^{1/2} \qquad (2.3.18)$$

### 2.3.4 <u>Solutions</u>

The solutions for the axisymmetric plume are included in Table 2 for comparison to the jet. These solutions were obtained using the following initial conditions for the bulk variables:

$$\left.\begin{aligned}
J_o &= U_o g_o' a_o \\[4pt]
Q_o &= U_o a_o \\[4pt]
M_o &= \left( \frac{5}{4} \frac{I_2^{3/2} I_4}{I_3} \frac{1}{\sqrt{2\pi}\,\alpha_p} J_o Q_o^2 \right)^{2/5} \\[4pt]
Q_{co} &= U_o c_o a_o
\end{aligned}\right\} \quad \text{at} \quad s = 0 \qquad (2.3.19)$$

The condition on the momentum flux is necessary to ensure that the initial efflux meets the plume equilibrium condition (Eq. 2.3.18). This

25

requirement is also reflected in the earlier statement on initial conditions (Eq. 2.3.4). If the actual momentum flux differs materially from that specified in Eq. 2.3.19, the motion will not be that of a pure plume (at least in the initial stages), since $F_\ell \neq F_{\ell p}$. In particular, if the actual momentum flux is larger than $M_o$, the case of the general buoyant jet results (section 2.6). Cases in which the actual initial momentum flux is less than $M_o$ (starved or retarded plumes) are probably not of much practical relevance for riverine discharges but may occur in other situations such as effluxes from natural-draft cooling towers.

Empirical constants for the round plume are juxtaposed to the jet values in Table 2.

Finally, it should be noted that all the comments and equations in this paragraph apply also in the same manner to a negatively buoyant plume, for which the discharge density $\rho_o$ is larger than the ambient density $\rho_a$. In that case, the definition diagram in Figure 2b must be reversed with $z$ pointing downward and $g'$ would still represent a local buoyant acceleration in the direction $z$.

## 2.4  PLANE JETS AND PLUMES

The other fundamental geometry, in addition to the axisymmetric round case, is the two-dimensional plane jet or plume. No specific illustrations or definition diagrams are given here, as the instantaneous appearances and time-averaged conditions closely resemble those depicted in Figure 1 (jet) or Figure 2 (plume), respectively. The only difference lies in the fact that the two-dimensional motion originates from a slot (extending two-dimensionally into and out from the paper) whose total width is denoted by $B$ (instead of the port diameter $D$), and the transverse coordinate is denoted by the normal distance $n$ (instead of the radial distance $r$). The same boundary layer type approximations that have been introduced earlier lead to the following equation sets and solutions. Since the developments parallel those in the previous sections, the equations in this section are presented without much discussion.

26

### 2.4.1 Plane Jets

Governing equations:

Continuity:

$$\frac{\partial u}{\partial s} + \frac{\partial v}{\partial n} = 0 \tag{2.4.1}$$

Forward momentum:

$$u\,\frac{\partial u}{\partial s} + v\,\frac{\partial u}{\partial n} = -\,\frac{\partial}{\partial n}\,\overline{u'v'} \tag{2.4.2}$$

Scalar conservation:

$$u\,\frac{\partial c}{\partial s} + v\,\frac{\partial c}{\partial n} = -\,\frac{\partial}{\partial n}\,\overline{c'v'} \tag{2.4.3}$$

Initial conditions:

$$u = U_o \;,\; c = c_o \qquad \text{at}\quad s = 0 \;,\; -\frac{B}{2} \le n \le \frac{B}{2} \tag{2.4.4}$$

Boundary conditions:

$$\left.\begin{array}{l} u \to 0 \;,\; \dfrac{\partial v}{\partial n} \to 0 \;,\; c \to 0 \\[2mm] \overline{u'v'} \to 0 \;,\; \overline{c'v'} \to 0 \end{array}\right\} \quad \text{at}\quad n \to \pm\infty \tag{2.4.5}$$

with symmetry conditions at the centerline $n = 0$ .

General profile definitions:

$$\frac{u}{u_c} = f\left(\frac{n}{b}\right) \;,\; \frac{c}{c_c} = F\left(\frac{n}{b}\right) \tag{2.4.6}$$

Gaussian profiles (specific case):

$$\frac{u}{u_c} = \exp\left(-\,\frac{n^2}{b^2}\right) \;,\; \frac{c}{c_c} = \exp\left(-\,\frac{n^2}{\lambda^2 b^2}\right) \tag{2.4.7}$$

Bulk flux quantities (per unit length in the direction of the slot):

Volume flux:

$$q = \int_{-\infty}^{\infty} u\,dn = i_1 u_c b \tag{2.4.8}$$

27

Momentum flux:
$$m = \int_{-\infty}^{\infty} u^2 dn = i_2 u_c^2 b \qquad (2.4.9)$$

Scalar mass flux:
$$q_c = \int_{-\infty}^{\infty} ucdn = i_3 u_c c_c b \qquad (2.4.10)$$

with the integral constants

$$i_1 = \int_{-\infty}^{\infty} f(\eta) d\eta ,$$

$$i_2 = \int_{-\infty}^{\infty} f^2(\eta) d\eta , \qquad (2.4.11)$$

$$i_3 = \int_{-\infty}^{\infty} f(\eta) F(\eta) d\eta$$

and $\eta = n/b$ .

For the Gaussian profiles

$$i_1 = \sqrt{\pi} , \quad i_2 = \sqrt{\pi/2} , \quad i_3 = \lambda \sqrt{\pi/(1+\lambda^2)} \qquad (2.4.12)$$

The integrated conservation equations are:

Volume flux conservation:
$$\frac{dq}{ds} + 2v\Big|_{n \to \pm\infty} = 0 \qquad (2.4.13)$$

Momentum flux conservation:
$$\frac{dm}{ds} = 0 \qquad (2.4.14)$$

Scalar flux conservation:
$$\frac{dq_c}{ds} = 0 \qquad (2.4.15)$$

The term $v\big|_{n \to \pm\infty} = \pm v_e$ is again denoted as the entrainment velocity of the ambient flow introduced as the jet periphery.

From similarity arguments, two closure statements are possible:

28

Jet spreading: $\quad \dfrac{db}{ds} = k_j$ $\hfill$ (2.4.16)

instead of the volume flux conservation, Eq. 2.4.13.

Closure statement II

Jet entrainment: $\quad \dfrac{dq}{ds} = 2\alpha_j u_c$ $\hfill$ (2.4.17)

in which $k_j$ and $\alpha_j$ are the jet spreading and jet entrainment
coefficients for the two-dimensional jet with the consistency condition

$$\alpha_j = \frac{i_1}{4} k_j \hfill (2.4.18)$$

Because of the geometry difference, their numerical values (as obtained
from experimental data) bear no relation to those for the round jet.

Final solutions are summarized in Table 3 based upon the bulk
initial conditions

$$\left. \begin{aligned} m_o &= U_o^2 B \\ q_o &= U_o B \\ q_{co} &= U_o c_o B \end{aligned} \right\} \quad \text{at } s = 0 \hfill (2.4.19)$$

and are restricted to the established flow region $s \gtrsim 5B$ . The empi-
rical coefficients are given in Table 4.

## 2.4.2 Plane Plumes

Governing equations (together with Eqs. 2.4.1 and 2.4.3):

Forward momentum: $\quad u \dfrac{\partial u}{\partial s} + v \dfrac{\partial u}{\partial n} = -\dfrac{\partial}{\partial n} \overline{u'v'} + g'$ $\hfill$ (2.4.20)

Buoyancy conservation: $\quad u \dfrac{\partial g'}{\partial s} + v \dfrac{\partial g'}{\partial n} = -\dfrac{\partial}{\partial n} \overline{(g')'v'}$ $\hfill$ (2.4.21)

Table 3

Solutions for the Two-Dimensional Jet and Plume*

| | Plane Jet | Plane Plume |
|---|---|---|
| <u>Discharge Parameters:</u> | $m_o = U_o^2 B$ | $m_o$ ** |
| | $q_o = U_o B$ | $q_o$ |
| | $q_{co} = U_o c_o B$ | $q_{co}$ |
| | | $j_o = U_o g_o' B$ |

<u>Bulk Variables:</u>

Momentum flux

$$m = i_2 u_c^2 b \qquad m = m_o \qquad m = \left(\frac{2i_2 i_4^2}{i_1 i_3^2}\right)^{1/3} \alpha_p^{1/3} j_o^{2/3} s$$

Discharge

$$q = i_1 u_c b \qquad q = \left(4\alpha_j \frac{i_1}{i_2} m_o s\right)^{1/2} \qquad q = \left(\frac{4 i_1 i_4}{i_2 i_3}\right)^{1/3} \alpha_p^{2/3} j_o^{1/3} s$$

Scalar flux

$$q_c = i_3 u_c c_c b \qquad q_c = q_{co} \qquad q_c = q_{co}$$

Buoyancy flux

$$j = i_3 u_c g_c' b \qquad -- \qquad j = j_o$$

<u>Local Variables:</u>

Width

$$b = k_j s = \frac{4}{i_1} \alpha_j s \qquad b = k_p s = \frac{2}{i_1} \alpha_p s$$

Centerline velocity

$$u_c = \left(\frac{1}{4\alpha_j} \frac{i_1}{i_2} \frac{m_o}{s}\right)^{1/2} \qquad u_c = \left(\frac{i_1 i_4}{2 i_2 i_3}\right)^{1/3} \left(\frac{j_o}{\alpha_p}\right)^{1/3} = const.$$

Centerline concentration (buoyancy)

$$c_c = \frac{q_{co}}{i_3} \left(\frac{i_1 i_2}{4\alpha_j m_o s}\right)^{1/2} \qquad g_c' = c_c \frac{j_o}{q_{co}}$$

$$= \left(\frac{i_1^2 i_2}{4 i_3^2 i_4}\right)^{1/3} \left(\frac{j_o}{\alpha_p}\right)^{2/3} \frac{1}{s}$$

<u>Dilutions:</u>

Bulk dilution

$$S = \frac{q}{q_o} \qquad S = \frac{1}{q_o} \left(4\alpha_j \frac{i_1}{i_2} m_o s\right)^{1/2} \qquad S = \frac{1}{q_o} \left(\frac{4 i_1 i_4}{i_2 i_3}\right)^{1/3} \alpha_p^{2/3} j_o^{1/3} s$$

Centerline (minimum) dilution

$$S_c = \frac{c_o}{c_c} = \frac{g_o'}{g_c'} \qquad S_c = \frac{i_3}{i_1} S \qquad S_c = \frac{i_3}{i_1} S$$

---

\* Solutions are accurate outside the region of flow establishment, $s \geq 5B$ .

\** $m_o$ is constrained to

$$m_o = \left(\frac{i_2^2 i_4}{2 i_1^2 i_3^2 p}\right)^{1/3} q_o j_o^{1/3}$$

in order to have pure plume conditions.

Table 4

Empirical Constants for the Two-Dimensional Plane Jet and
Plume with Gaussian Profile Specification (Eq. 2.4.7)*

| | Plane Jet** | Plane Plume |
|---|---|---|
| Spreading coefficient | $k_j = 0.135$ | $k_p = 0.147$ |
| Ratio $\alpha/k$ | $\dfrac{\alpha_j}{k_j} = \dfrac{\sqrt{\pi}}{4}$ | $\dfrac{\alpha_p}{k_p} = \dfrac{\sqrt{\pi}}{2}$ |
| Entrainment coefficient | $\alpha_j = 0.060$ | $\alpha_p = 0.130$ |
| Scalar dispersion coefficient | $\lambda_j = 1.35$ | $\lambda_p = 1.30$ |
| Equilibrium Froude number[†] | $F_{\ell j} = \infty$ | $F_{\ell p} = 3.54$ |

* The above constants are based on the data surveys of Jirka,
Abraham, and Harleman (1975); Chen and Rodi (1980); and List (1982).
** Plane jet integral coefficients for Gaussian profiles are:

$$i_1 = \sqrt{\pi} \ , \quad i_2 = \sqrt{\pi/2} \ , \quad i_3 = \lambda \sqrt{\pi/(1+\lambda^2)} \ , \quad i_4 = \lambda\sqrt{\pi}$$

† $\quad F_\ell = \dfrac{u_c}{\left(g_c' b\right)^{1/2}}$ .

Initial conditions:

$$g' = g'_o \ , \quad u = U_o = F_{\ell p}\left(\frac{i_2^3}{i_1^3 i_3}\right)^{1/2} \left(g'_o B\right)^{1/2} \ , \quad c = c_o$$

$$(2.4.22)$$

$$\text{at} \quad s = 0 \ , \ -\frac{B}{2} \leq n \leq \frac{B}{2}$$

Boundary conditions (together with Eq. 2.4.5):

$$g' \to 0 \ , \quad \overline{(g')'v'} \to 0 \qquad \text{at} \quad n \to \pm \infty \qquad (2.4.23)$$

Bulk flow quantities (together with Eqs. 2.4.8 - 2.4.10):

$$\text{Buoyancy flux:} \quad j = \int_{-\infty}^{\infty} u g' dn = i_3 u_c g'_c b \qquad (2.4.24)$$

with the assumption that $g'$ is distributed similarly to $c$

$$\frac{g'}{g'_c} = \frac{c}{c_c} = F\left(\frac{n}{b}\right) \qquad (2.4.25)$$

Integral equations (together with Eqs. 2.4.13 and 2.4.15):

$$\text{Momentum flux conservation:} \quad \frac{dm}{ds} = i_4 g'_c b \qquad (2.4.26)$$

$$\text{Buoyancy flux conservation:} \quad \frac{dj}{ds} = 0 \qquad (2.4.27)$$

with $i_4 = \int_{-\infty}^{\infty} F(n) dn$ or for the Gaussian profile $i_4 = \lambda\sqrt{\pi}$ .

<u>Closure statement I</u>:

$$\text{Plume spreading:} \quad \frac{db}{ds} = k_p \qquad (2.4.28)$$

<u>Closure statement II</u>:

$$\text{Plume entrainment:} \quad \frac{dq}{ds} = 2\alpha_p u_c \qquad (2.4.29)$$

in which $k_p$ and $\alpha_p$ are plume spreading and plume entrainment coefficients, respectively, with the consistency condition

$$\alpha_p = \frac{i_1}{2} k_p \qquad (2.4.30)$$

and the value of plane plume Froude number is

$$F_{\ell p} = \left( \frac{i_1 i_4}{2 i_2} \frac{1}{\alpha_p} \right)^{1/2} \qquad (2.4.31)$$

The initial conditions

$$
\left.
\begin{aligned}
j_o &= U_o g_o' B \\[2mm]
q_o &= U_o B \\[2mm]
m_o &= \left( \frac{i_2^2 i_4}{2 i_1^2 i} \frac{1}{\alpha_p} \right)^{1/3} q_o j_o^{1/3} \\[2mm]
q_{co} &= U_o c_o B
\end{aligned}
\right\} \qquad \text{at} \quad s = 0 \qquad (2.4.32)
$$

yield the final plume solutions given in Table 3 in which the buoyancy flux $j_o$ is the only dynamically significant variable. The empirical constants for the plane plume are listed in Table 4.

33

## 2.5 EXTENSIONS OF THE INTEGRAL ANALYSIS

The results that have been derived in the preceding sections are all rigorous and exact based on the existence of a similarity function and based on the assumed closure scheme. Thus, the previous results are limited to these simple conditions for which the assumption of self-similarity holds, namely sources of momentum flux or of buoyancy flux, respectively, issuing into unlimited, stagnant, and homogeneous receiving water. Actual environmental conditions in rivers, channels, lakes, reservoirs, or estuaries are always more complex, involving combined momentum/buoyancy sources, crossflow, ambient stratification, finite boundaries, etc. Due to the number of parameters involved, these motions cannot be expected to be self-similar. Nevertheless, as is shown in sections 2.6-2.9, the integral analysis technique is extremely flexible and powerful and can be extended to include many of these practical complexities. A host of such extensions, loosely called "jet models," exists in the literature. It must be realized that any of these models contain some ad hoc assumptions and approximations. As a minimum requirement, any such model should be demonstrated to reduce reasonably well to the exact limiting conditions of the jet and plume. It is for that reason that the detailed solutions for these cases, together with the approximate physical constants, have been listed in Tables 1-4.

## 2.6 BUOYANT JETS: COMBINED MOMENTUM/BUOYANCY SOURCES

The general buoyant jet in a uniform, stagnant, and infinite receiving water, discharged at an angle $\theta_o$ with the horizontal, will have a curved trajectory as shown in Figure 3. Using the same definitions of the bulk variables that have been given in the preceding sections (and in Tables 1 and 3), it is straightforward to write the governing integral equations without going through a formal integration process.*

---

* Actually, the assumption of a small trajectory curvature is inherent in the following, and acceptable in most practical cases. See Schatzmann (1978) for a more detailed development.
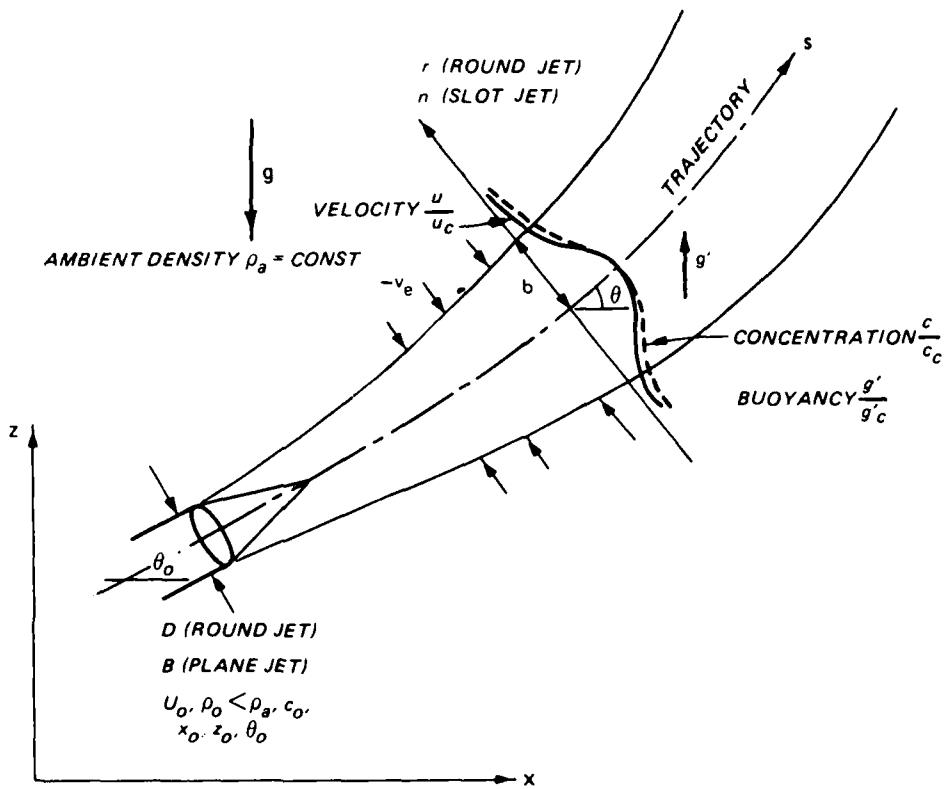
Figure 3. Round buoyant jet in uniform stagnant infinite
receiving water

### 2.6.1 Round Buoyant Jets

Volume flux conservation:    $\dfrac{dQ}{ds} = 2\pi\alpha u_c b$    (2.6.1)

Alternatively, one can use another closure assumption:

Jet spreading:    $\dfrac{db}{ds} = k$    (2.6.2)

Note that both $\alpha$ and $k$ are written in general form, without any subscript.

35

Axial momentum flux conservation:

$$\frac{dM}{ds} = 2\pi I_4 g_c' b^2 \sin \theta \qquad (2.6.3)$$

i.e., only the $\sin \theta$ component of buoyancy produces acceleration in the axial direction.

Horizontal momentum flux conservation:

$$\frac{d}{ds} (M \cos \theta) = 0 \qquad (2.6.4)$$

i.e., no acceleration in the horizontal direction.

Scalar flux conservation: $\qquad \frac{dQ_c}{ds} = 0 \qquad\qquad (2.6.5)$

Buoyancy flux conservation: $\quad \frac{dJ}{ds} = 0 \qquad\qquad (2.6.6)$

In addition, it is necessary to relate the local coordinate system $(s, \theta)$ to the fixed global one $(x, z)$

$$\frac{dx}{ds} = \cos \theta \qquad (2.6.7)$$

$$\frac{dz}{ds} = \sin \theta \qquad (2.6.8)$$

This system of seven ordinary differential equations is fully specified by seven initial conditions at $s = 0$. These are the initial bulk fluxes $M_o$, $J_o$, $Q_o$ and $Q_{co}$ (alternatively, given by $U_o$, $g_o' = g(\rho_a - \rho_o)/\rho_a$, $c_o$, and $D$) and the geometry $x_o$, $z_o$, and $\theta_o$. In fact, as discussed earlier, initial conditions should really be specified at the end of the zone of flow establishment (several

36

diameters away from the actual discharge). Often, however, this difference is negligible. If necessary, more detailed (though approximate) treatments of this zone may be consulted (Hirst 1972 or Jirka and Fong 1981).

At this point, before the equation system can be solved, the first closure dilemma in buoyant jet analysis arises: Which of the two equations, Eq. 2.6.1 or 2.6.2, should be used and how should the coefficients $\alpha$ or $k$ be chosen? This is a critical question as a buoyant jet initially has a more jet-like (momentum-dominated) behavior, but in the final stage approaches a plume-like (buoyancy-dominated) behavior. However, as can be seen from Table 2, the coefficients for these two limiting stages do not agree. The following possibilities exist then:

a. Use Eq. 2.6.2 and assume $k = \text{const.} = k_p$ (since the final stage always behaves like a simple plume). This is the basis of the model of Abraham (1963) and, clearly, a good proposition since the variability in $k$ is minor (10 percent, Table 2). The main disadvantage of the jet spreading approach, however, is that it cannot be easily extended to other cases, such as crossflows, etc.

b. Use Eq. 2.6.1 and assume $\alpha = \text{const.} = \alpha_p$. This was assumed originally by Fan (1967) and is incorporated into the predictive nomograms of Fan and Brooks (1967) and Shirazi and Davis (1972). In view of the strong variability of $\alpha$ (Table 2), it is probably the most imprecise method of buoyant jet analysis, though the errors may be tolerable in practice.

c. Use Eq. 2.6.1, but specify a variable entrainment coefficient that depends on the local jet properties, as described by the local Froude number, Eq. 2.3.12, and the local angle $\theta$. One such possibility that is directly derived from the above equation set with the assumption $db/ds = \text{const.} = k_p$ is

$$\alpha = I_1 k_p + \frac{I_1 I_4}{2 I_2} \frac{\sin \theta}{F_\ell^2} \tag{2.6.9}$$

37

Another approach (Fox 1970, Hirst 1972) uses the mean energy equation for the buoyant jet to give

$$\alpha = \alpha_j + \lambda_p^2 \left( \frac{2\lambda_p^2 - 1}{1 + \lambda_p^2} \right) \frac{\sin \theta}{F_\ell^2} \qquad (2.6.10)$$

Other transitions, sometimes based only on fitting transitions between the two limiting stages, can be found in the literature (e.g. Schatzmann 1978, List 1982). The difference between these model predictions is often minor. Actual predictions are presented in Section 3.1.2.

## 2.6.2  Plane (Slot) Buoyant Jets

The development is entirely parallel to the round case with the following governing equations:

$$\frac{dq}{ds} = 2\alpha u_c b \qquad (2.6.11)$$

$$\frac{db}{ds} = k \qquad (2.6.12)$$

$$\frac{dm}{ds} = I_4 g_c' b \sin \theta \qquad (2.6.13)$$

$$\frac{d}{ds} (m \cos \theta) = 0 \qquad (2.6.14)$$

$$\frac{dq_c}{ds} = 0 \qquad (2.6.15)$$

$$\frac{dj}{ds} = 0 \qquad (2.6.16)$$

$$\frac{dx}{ds} = \cos \theta \qquad (2.6.17)$$

$$\frac{dz}{ds} = \sin \theta \qquad (2.6.18)$$

38

Initial conditions are given by the flux variables per unit width $m_o$ , $j_o$ , $q_o$ , and $q_{co}$ (or $U_o$ , $g_o'$ , $c_o$ , and B) and by the geometry $x_o$ , $z_o$ and $\theta_o$ .

Also, the closure problem is similar to the round jet case, as can be seen from Table 4. Again the constant spreading assumption (Abraham 1963) is preferable over the constant entrainment coefficient assumption (Fan 1967). Variable entrainment models can be specified as

$$\alpha = \frac{i_1}{4} k_p + \frac{i_1 i_4}{2 i_2} \frac{\sin\theta}{F_\ell^2} \tag{2.6.19}$$

from the above equation set, or as

$$\alpha = \alpha_j + \lambda\sqrt{\pi}\left(\sqrt{2} - \sqrt{\frac{3}{1 + \lambda^2}}\right)\frac{\sin\theta}{F_\ell^2} \tag{2.6.20}$$

(Jirka, Abraham, and Harleman 1975) using the jet energy equation.

## 2.7  EFFECT OF AMBIENT DENSITY STRATIFICATION

If the receiving water is stratified with a stable density gradient ($d\rho_a/dz < 0$ , i.e. the ambient density $\rho_a(z)$ decreases upward), then the buoyancy flux is not conserved along the jet trajectory but is constantly decreasing. Eventually the buoyant jet will reach, and may even overshoot, its terminal level $z_t$ at which the local internal jet density is equal to the ambient density $\rho_a(z_t)$ . The jet will then become trapped at this level and spread horizontally in the form of a gravitational current. The jet mechanics prior to the terminal level are readily described with the integral technique if two extensions are made. First, the buoyancy profiles are now defined with respect to the local reference buoyancy

39

$$g' = \frac{\rho_a(z) - \rho}{\rho_a(z)} g \qquad (2.7.1)$$

instead of Eq. 2.3.1, leading to modification of Eqs. 2.3.6 and 2.4.25, respectively. Second, from mass balance requirements, the buoyancy flux is decreasing at the same rate at which it is diluted with ambient water of lesser density. This leads to

$$\frac{dJ}{ds} = Q \frac{d\rho_a}{ds} \qquad (2.7.2)$$

for the round jet, instead of Eq. 2.6.6, and to

$$\frac{dj}{ds} = q \frac{d\rho_a}{ds} \qquad (2.7.3)$$

for the plane jet, instead of Eq. 2.6.16. Inherent in these expressions is the assumption that the average density of the entrained water is equal to the density at the level of trajectory (centerline). This excludes cases of very rapid local changes, such as steep pycnoclines in lakes, reservoirs, or estuaries.

## 2.8 EFFECTS OF AMBIENT CROSSFLOW

When a round buoyant jet is discharged into an ambient crossflow of velocity $u_a$ , then it will be deflected in the direction of the crossflow. This deflection is brought about by two force mechanisms, a pressure drag force $F_D$ and a force $F_e$ due to the entrainment of crossflow momentum. Referring to Figure 4, this situation is readily described in the integral analysis framework provided that several adjustments are made. First, neglecting the horseshoe or "kidney" shape (Fischer et al. 1979) which actually exists and assuming that the jet may be approximated by a circular cross section, the velocity profile in the jet cross section is made up of the ambient velocity

40
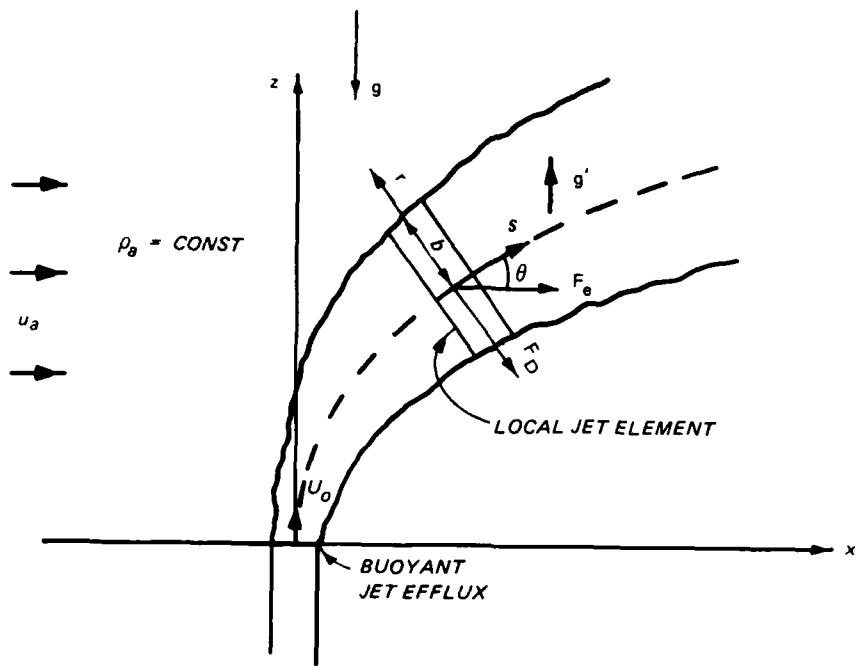
Figure 4. Round buoyant jet in ambient crossflow (side-
view for $\theta_o$ = 90 deg)

component in the direction of the trajectory $u_a \cos \theta$ and the bell-
shaped jet portion

$$u = u_c f\left(\frac{r}{b}\right) + u_a \cos \theta \qquad (2.8.1)$$

This, then, affects the definition of all jet bulk flux variables, $M$ ,
$J$ , $Q$ and $Q_c$ . The definition of the kinematic drag force normal to
the jet axis and per unit length of the jet axis is

$$F_D = \frac{1}{2} C_D u_a^2 \sin^2 \theta \quad (2b) \qquad (2.8.2)$$

in which $C_D$ is a drag coefficient (of order of unity), the width of

41

the "jet body" is simply taken as 2b , and the entrainment force (entrainment of momentum) is

$$F_e = u_a \frac{dQ}{ds} \qquad (2.8.3)$$

The governing momentum equations, Eqs. 2.6.3 and 2.6.4, are amplified to

$$\frac{dM}{ds} = 2\pi I_4 g_c' b^2 \sin\theta + F_e \cos\theta \qquad (2.8.4)$$

$$\frac{d}{ds}(M \cos\theta) = F_e + F_D \sin\theta \qquad (2.8.5)$$

Also, it is observed in bent-over jets that the entrainment mechanism is considerably more vigorous and the entrainment velocity not simply proportional to $u_c$ as in the previous case. Several analyses have suggested that jet entrainment in crossflows has a second contribution once the jet is strongly bent over but still slowly rising. This second contribution is similar to that of a horizontal line element of fluid that is rising due to an initial vertical impulse of momentum or due to initial buoyancy in a stagnant ambient fluid. The rising line element experiences turbulent growth and entrainment that is proportional to the velocity of rise. Since the strongly bent-over jet is similar to this line element, this second entrainment mechanism can be added to the original entrainment mechanism associated with the excess of forward jet velocity relative to the surrounding fluid. The result is

$$\frac{dQ}{ds} = 2\pi\alpha u_c b + 2\pi\alpha_2 u_a \sin\theta \cos\theta \, b \qquad (2.8.6)$$

where $\alpha$ is of the same form as for a buoyant jet (e.g. Eq. 2.6.9 or 2.6.10) and $\alpha_2$ is of the order of 0.5. Entrainment models of this type have been used by Abraham (1970) and Jirka and Fong (1981).

42

No integral analysis is possible for the crossflow deflection of plane buoyant jets. The deflecting mechanism is highly complicated in this case, with eddying and reentrainment in the wake zone behind the jet.

Finally, the effect of ambient turbulence becomes invariably important at larger distances from the origin when the jet turbulent intensity decreases to the same order as the ambient intensity. In a way, this provides a transition to the passive diffusion in the far-field, as discussed in Chapters 4-7.

## 2.9 EFFECTS OF FINITE BOUNDARIES

The jet analyses that have been discussed so far apply only to the case in which the jet dimension is small with respect to the dimensions of the receiving water. In this case, the pressure field can be assumed as unperturbed (hydrostatic) throughout. The effects of finite boundaries encompass the following four distinct problem areas.

### 2.9.1 Jets Discharging Parallel to Boundaries

The dynamic pressure deviation near the jet due to the jet entrainment velocity is of the order of $\Delta p \sim v_e^2$. This is, in general, a negligible quantity since $v_e = \alpha u_c$. However, if a boundary (either a solid boundary or a free surface) is located in the vicinity of the entraining jet boundary, then the velocity of the approaching entrainment flow will become larger than $v_e$ due to the geometric restrictions. Hence, larger pressure deviations will occur unevenly at the jet boundary, exerting a force on the jet. Consequently, the jet may attach to the boundary due to the low pressure zone (a form of the Coanda effect).

### 2.9.2 Interference of Round Jets

This is a problem somewhat analogous to the previous case and occurs in multiport diffuser discharges. The individual round jets merge into a two-dimensional plume. This is discussed in Section 3.2.

43

### 2.9.3 Jet Impingement on Boundaries

In this case the jet flow approaches normal to, or nearly normal to, a solid boundary or a free surface. Upon impingement the jet will spread in both directions. The thickness of the resulting spreading layer determines the length of the actual jet zone and the amount of dilution that can be achieved up to the impingement level (Sections 3.1 and 3.2).

### 2.9.4 Buoyant Jets at the Free Surface

In this case the vertical buoyant force, in combination with the free surface which inhibits any upward motion, influences the jet flow in two ways. An overall effect is that the lateral jet spreading is in excess of the usual jet-like spreading. Also, the local turbulent entrainment at the jet bottom interface is inhibited. This is the topic of Section 3.3.

## 2.10 NONDIMENSIONAL PARAMETERS AND BUOYANT JET SCALES

As in all physical or engineering problems, the dynamics of initial jet mixing are governed by certain parameters that describe a given situation. Such parameters can be derived using the requirements of dimensional consistency. In the following, two representations of parameters or scales are introduced. Each of these representations has its own particular advantage for characterizing jet/plume behavior and for displaying results. The two types of representations are intimately related, however, as will be demonstrated.

### 2.10.1 Nondimensional Parameters Based on Detailed Efflux Conditions

Using the actual dimensions and discharge conditions, the set of parameters in Table 5 describes a buoyant jet mixing problem. In case of stratification, $g_o'$ and $\Delta\rho_o$ refer to conditions at the level of the discharge, and a linear density gradient is assumed in the definition of $T$ .

44

Table 5

Nondimensional Parameters for Buoyant Jet Problems

| Type of Buoyant Jet | Round | Plane (Slot) |
|---|---|---|
| Discharge densimetric Froude number | $F_o = \dfrac{U_o}{\sqrt{g_o' D}}$ | $F_s = \dfrac{U_o}{\sqrt{g_o' B}}$ |
| Initial angle | $\theta_o$ | $\theta_o$ |
| Stratification parameter | $T = -\dfrac{\Delta\rho_o}{D d\rho_a/dz}$ | $T = -\dfrac{\Delta\rho_o}{B d\rho_a/dz}$ |
| Crossflow parameter | $R = u_a/U_o$ | $R = u_a/U_o$ |

The meaning of the densimetric Froude number is of particular interest. Its magnitude characterizes the initial ratio of inertial to buoyant forces within the discharge and determines whether the discharge behaves more nearly like a jet (large $F_o$ or $F_s$) in its initial phases or more nearly like a plume (small $F_o$ or $F_s$) from the very beginning.

### 2.10.2 Scales Based on Bulk Efflux Quantities

a. Momentum length scales. It has been noted earlier that the two fundamental bulk (integral) quantities that affect buoyant jet behavior in quiescent homogeneous ambient water are the initial momentum flux and the initial buoyancy flux. Considering then the dimensions of these quantities (first two rows of Table 6), it is possible by dimensional reasoning to define length scales as given in the third row of Table 6.

The resulting length scales are appropriately called "momentum length scales" since they are a measure for the distance from the orifice for which the momentum effects are important. For the initial trajectory of a buoyant jet over a length less than the momentum length

45

scale, the discharge should behave like a jet, while for the final
trajectory it will behave like a plume. Thus, from a practical point
of view, the length-scale computation gives direct insight into the
expected size and extent of a buoyant jet problem. The momentum length
scale is also the obvious length variable for the scaling of buoyant
jet properties and allows a simplified representation of results from
any buoyant jet computation or exponent. By substitution, it may be
verified that the momentum length scales are linked to the initial
orifice scale (D or B) via the densimetric Froude numbers, as shown in
the last row of Table 6.

Table 6

Length Scales for Buoyant Jet Problems

| | Round Buoyant Jet | Slot Buoyant Jet |
|---|---|---|
| Momentum flux [dimensions] | $M_o$ $\left[L^4/T^2\right]$ | $m_o$ $\left[L^3/T^2\right]$ |
| Buoyancy flux [dimensions] | $J_o$ $\left[L^4/T^3\right]$ | $j_o$ $\left[L^3/T^3\right]$ |
| Momentum length scales | $\ell_M = \dfrac{M_o^{3/4}}{J_o^{1/2}}$ | $\ell_m = \dfrac{m_o}{j_o^{2/3}}$ |
| Relationship to Froude number | $\ell_M = \left(\dfrac{\pi}{4}\right)^{1/4} DF_o$ | $\ell_m = BF_s^{4/3}$ |

_b_. __Crossflow length scales__. In the presence of a crossflow
with velocity $u_a$ [L/T] , the buoyant jet behavior can be represented
by additional length scales. To form these, one must consider the
effects of momentum flux and of buoyancy flux separately. For a momen-
tum source only (round jet) one obtains:

$$\text{Jet-crossflow length scale:} \quad \ell_{Mu} = \frac{M_o^{1/2}}{u_a} = \left(\frac{\pi}{4}\right)^{1/2} D \frac{1}{R} \quad (2.10.1)$$

46

This would be a measure of the distance over which a jet could penetrate into a crossflow before it becomes strongly deflected. For a buoyancy source only (round plume):

$$\text{Plume-crossflow length scale:} \quad \ell_{Ju} = \frac{J_o}{u_a^3} = \frac{\pi}{4} D \frac{1}{R^3 F_o^2} \qquad (2.10.2)$$

with a similar physical meaning.

In the general case of a round buoyant jet, both scales are present in addition to $\ell_m$ (defined in Table 6). It is then the relative magnitude of these three scales that determines the composite geometry (trajectory) and mixing (dilution) of the resulting motion (Wright 1977).

<u>c</u>. <u>Stratification length scales</u>. Additional scales can be obtained through consideration of the ambient density gradient, $-\frac{1}{\rho_a} \frac{d\rho_a}{da} [L^{-1}]$. These scales are not further pursued here due to their limited significance in riverine mixing problems. (For further information, see Wright 1977 or Fischer et al. 1979.)

2.10.3 <u>Comments</u>

In the following sections, both length scales and nondimensional parameters are used to characterize the dynamics of initial mixing processes. It is important to understand the complementary role of these representations. In simple problems with few physical variables, the use of the dynamic length scales is especially powerful and attractive. (See, for example, Section 3.1, Figures 6 and 7.) When more variables enter the problem, however, it then becomes necessary to include the ratios of individual length scales with each other and with the source dimensions (D or B). Such ratios are then, in fact, equal to or proportional to the nondimensional parameters. For example, the ratio $\ell_m/D$ corresponds to a Froude number (Table 6) which, for small values ($F_o \lesssim 5$), has a distinctly separate influence on round buoyant jet behavior (Figure 7).

47

A study of the following sections and of the examples in Chapter 8 should show that the key for a successful analysis of an initial mixing problem is to separate the important quantities from the unimportant ones. Often, dominant ones depend on the region of interest, and some iterations and inspections may be necessary in the process of finding them. The different techniques of dimensional analysis discussed above are useful aids in that process.

CHAPTER 3.   INITIAL MIXING ANALYSIS FOR VARIOUS
TYPES OF DISCHARGES

The three most important geometries for continuous discharges in
riverine applications (as well as in run-of-the-river reservoirs, estu-
aries, and coastal waterways) are the single-port submerged discharge,
the multiport submerged diffuser, and the surface discharge from free
surface flow in a canal.  Important physical characteristics and pre-
dictive methods for these three cases are summarized in Sections 3.1-
3.3 of this chapter.  Section 3.4 summarizes discharge-induced strati-
fication effects in rivers; these effects can arise when the discharge
flow rate is a substantial fraction of the river flow and when buoyancy
is present.  The most important applications in this respect are cool-
ing water flows from thermal power stations.  Finally, in Section 3.5,
a brief review is given of the initial mixing effects for instantaneous
discharges since they may be of interest in connection with accidental
spills or in tracer tests.

3.1  SUBMERGED SINGLE PORT DISCHARGES

3.1.1  Introduction

This section is organized as follows:  First, basic solutions
for buoyant jets in stagnant infinite receiving water are presented.
The stagnant water case is usually a lower bound on the initial mixing
capacity of any outfall and, in fact, is a good approximation to mixing
in low-velocity conditions such as run-of-the-river reservoirs.  Sec-
ond, solutions for buoyant jets in crossflows with unlimited depth are
given.  In the third portion, the effects of boundaries and of shallow
water depth are considered.  Solutions for ambient stratification ef-
fects are not given here since those are of limited practical impor-
tance in riverine mixing.  For details on this aspect, the reader is
referred to Jirka, Abraham, and Harleman (1975); Wright (1977); and
Fischer et al. (1979).

The basic geometry is that of a single round outfall pipe of
diameter  D  discharging the effluent.  It should be noted that the

results are directly transferable to other pipe geometries of arbitrary cross-sectional area $a_o$. An equivalent round pipe diameter can always be calculated by $D = (4a_o/\pi)^{1/2}$ and beyond a sufficiently large distance the jet behavior is identical. Assuming a rectangular opening $a_o = \ell_1 \ell_2$ with length $\ell_1$ and width $\ell_2$ (where $\ell_1 > \ell_2$), an estimate of that distance is

$$s = \frac{1}{k} \sqrt{a_o} \sqrt{\frac{\ell_1}{\ell_2}} \qquad\qquad (3.1.1)$$

in which $k$ is the spreading coefficient (Table 2).

In the following, emphasis is put on simple, commonly occurring jet situations (mostly vertical and horizontal discharge angles). For more complex situations, these simple cases may serve as a first approximation or more detailed models must be used (e.g. Hirst 1972, Shirazi and Davis 1972, Schatzmann 1978, Jirka and Fong 1981).

### 3.1.2 Solutions for Stagnant Water

a. Vertical round buoyant jet. This jet will have a straight vertical trajectory. The solution for the bulk dilution can be obtained directly from the buoyant jet equation system, Eqs. 2.6.1-2.6.8, with $\theta = \theta_o = 90$ deg and closure assumption Eq. 2.6.2,

$$S = \frac{Q}{Q_o} = \left(\frac{2\pi I_1^2}{I_2}\right)^{1/2} \left[M_o^{3/2} + \frac{3}{4}\left(\frac{2\pi I_2 I_4^2}{I_3^2}\right)^{1/2} J_o kz^2\right]^{1/3} \frac{kz}{Q_o} \qquad (3.1.2)$$

as given by Abraham (1963). Using the appropriate Gaussian profile coefficients (Table 2), the corresponding centerline dilution in normalized form is

$$\frac{S_c}{F_o} = 0.178 \left[\left(\frac{z}{DF_o}\right)^3 + 0.203 \left(\frac{z}{DF_o}\right)^5\right]^{1/3} \qquad (3.1.3)$$

50

and is plotted as the solid line in Figure 5. The solution consists of a transition from a pure jet regime (first part of Eq. 3.1.3) to a pure plume regime (second part).

b. Horizontal round buoyant jet. The trajectories of round buoyant jets with different Froude numbers $F_o$ are displayed in Figure 6, using experimental data and different model predictions. This figure shows the usual degree of agreement, typical for buoyant jet problems. The governing dynamics are immediately apparent from Figure 6. Buoyant jets with large momentum flux for a given buoyancy flux (high $F_o$) penetrate much further along the horizontal axis, while buoyancy dominated jets (low $F_o$) are quickly deflected in the vertical direction.

The benefit of the length scale representation (Table 6) can be seen from Figure 7; all the data for high $F_o$ ($\geq$ 5) collapse into a single curve due to the limited number of governing physical variables (only $M_o$ and $J_o$). For small $F_o$, a minor, yet persistent, deviation exists. This is due to the fact that the source diameter D (or alternatively, the initial discharge $Q_o$) is an additional nonnegligible physical variable in this Froude number range. The curve in Figure 7 (and also in Figure 5) is based on Abraham's (1963) model that has been found to be in good agreement with data (Roberts 1977). Values of the jet width are also marked. The centerline dilution for horizontal jets is shown in Figure 5 in comparison to the vertical case. From a practical viewpoint, Figure 5 demonstrates that for low submergences ($z/DF_o \leq$ 10) higher mixing can be attained with a horizontal jet. For larger submergences, however, the jet approaches the pure vertical plume behavior so that the initial momentum and the angle of discharge behavior are not important.

c. Vertical round negatively-buoyant jet. If a dense effluent is issued vertically upward or a light effluent vertically downward, then the action of buoyancy is against the direction of the initial flow. Thus, the buoyant jet will penetrate to a maximum level $z_m$ from the outlet before falling back, somewhat similar to the action of a vertical water fountain in air. Two measures of the jet action in

51
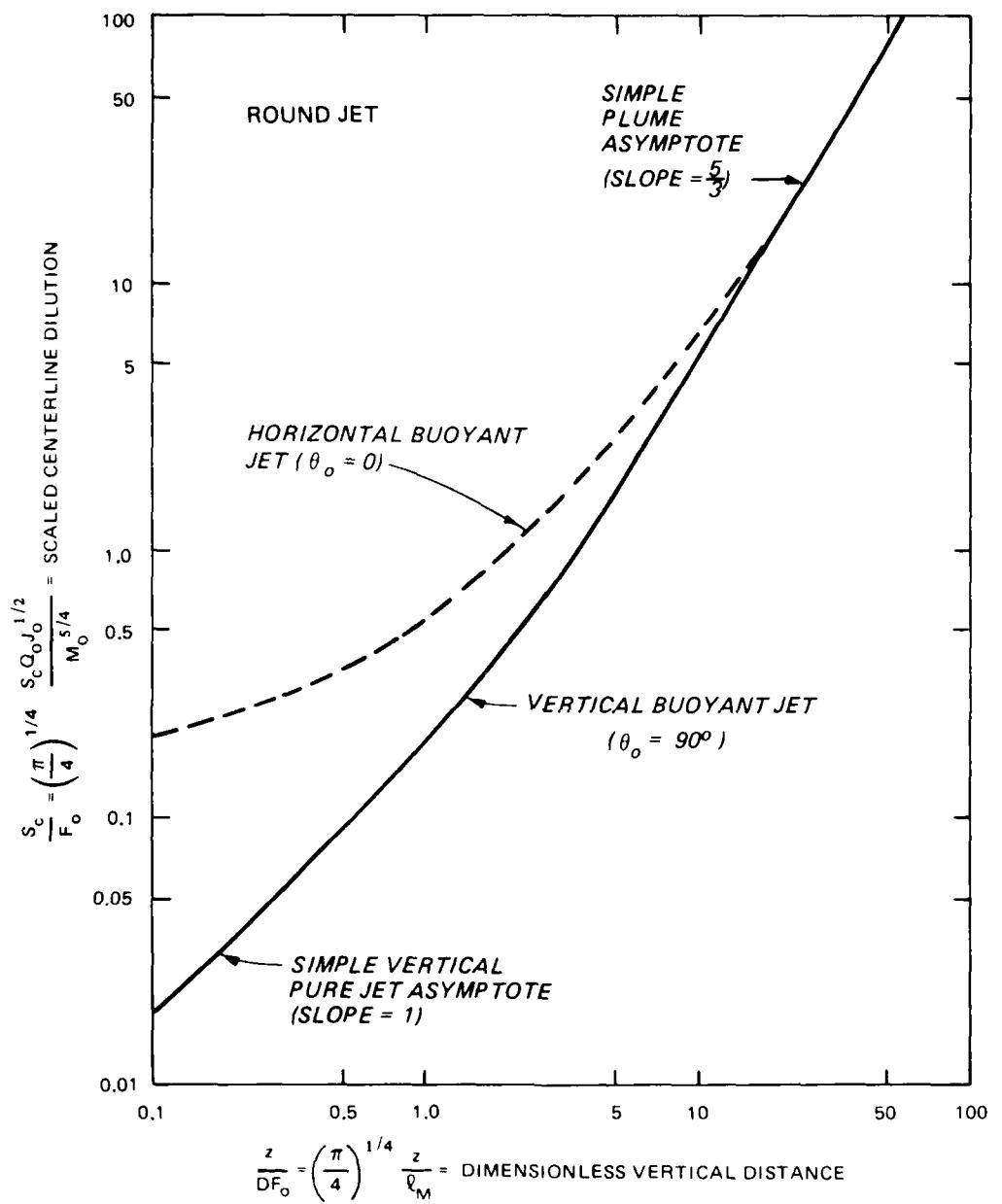
Figure 5. Centerline dilution for vertical and horizontal round buoyant jets in deep, stagnant, unstratified water

52
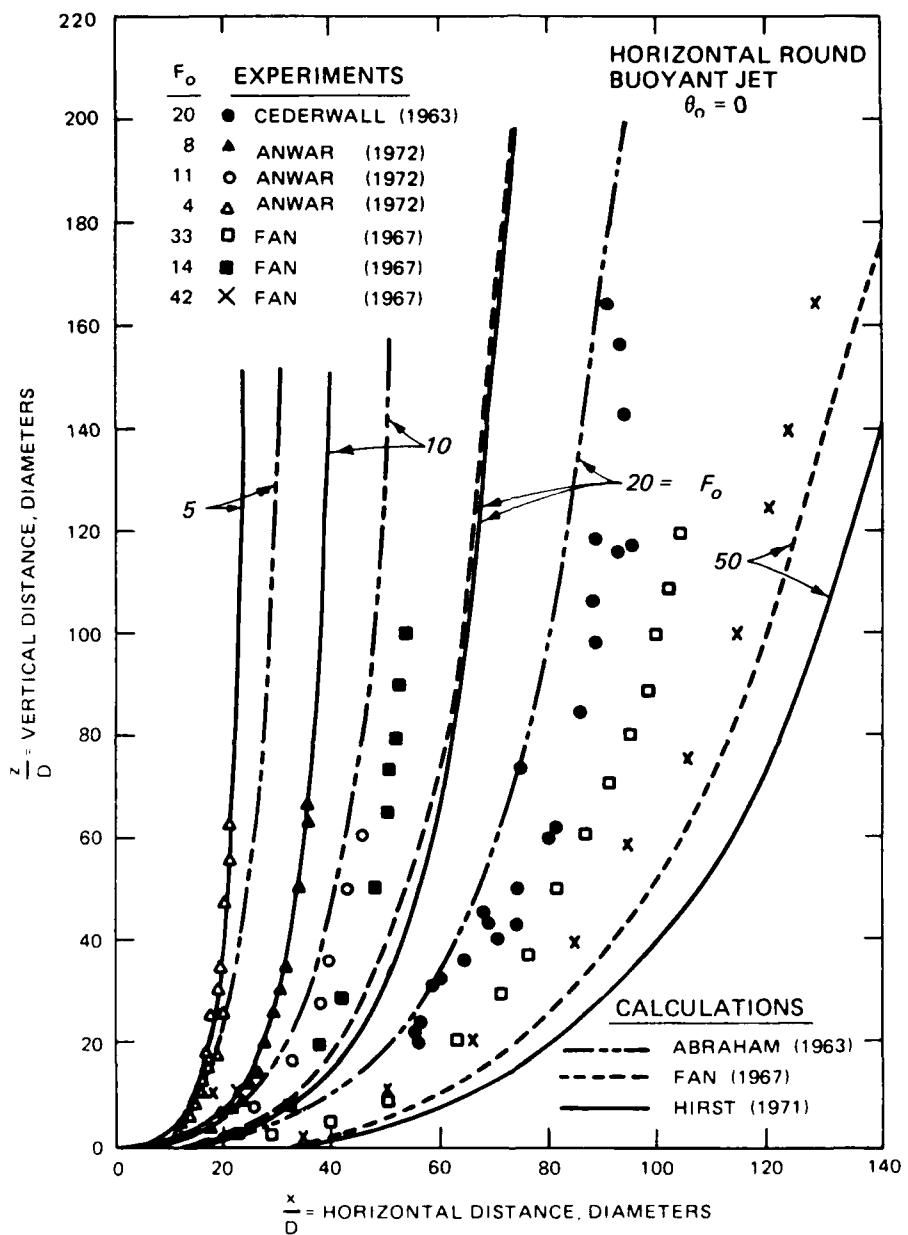
Figure 6.  Experimental and calculated trajectories for round
horizontal buoyant jets
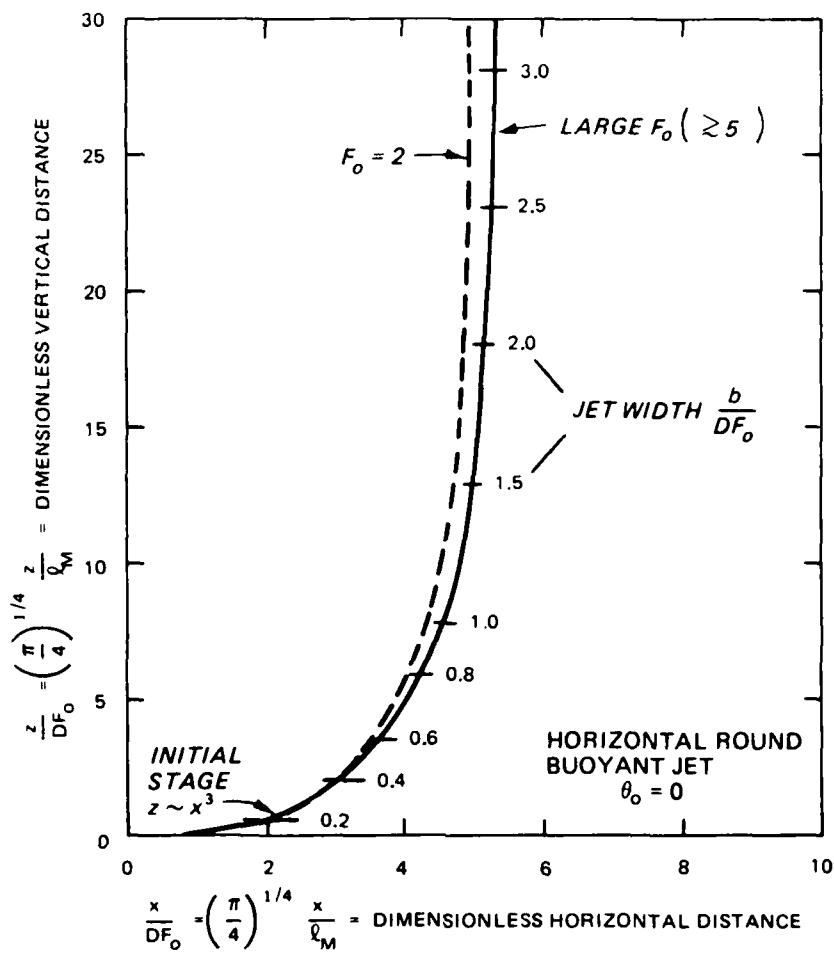
Figure 7. Nondimensional trajectory for round horizontal buoyant jets

this case are the vertical penetration level $z_m$ ,

$$\frac{z_m}{DF_o} = \left(\frac{\pi}{4}\right)^{1/4} \frac{z_m}{\ell_m} = C \tag{3.1.4}$$

where the constant $C$ is approximately 1.9 and the dilution $S_m$ at that level,

$$\frac{S_m}{F_o} = 0.23 \tag{3.1.5}$$

54

Both estimates are based on Abraham's work (1967). Note that in these cases the absolute value of $g_o'$ is used in the definition of $F_o$ (Table 5) since $g_o'$ is a negative quantity.

### 3.1.3 Solutions for Flowing Ambient

a. Vertical round buoyant jet (crossflow). The buoyant jet intrudes vertically into the crossflow but becomes gradually deflected into the direction of the crossflow. The vertical intrusion comes about by the action of the initial momentum and/or of the initial buoyancy. Using the scales of influence defined earlier, it is therefore illustrative to describe the trajectory and mixing relationships for two regimes:

(1) Jet with negligible buoyancy in crossflow, $\ell_M/\ell_{Mu} \gg 1$. Here, the momentum length scale $\ell_M$, which represents the relative influence of momentum compared to buoyancy, is so large that the jet becomes well deflected before buoyancy plays any role. Trajectories (normalized by $\ell_{Mu}$) and center-line dilutions are plotted in Figure 8 based on several data sources compiled by Wright (1977). The jet conditions are described by different power laws (slopes in double logarithmic plots) for the initial phase (small influence of buoyancy) and the final phase (greater influence of buoyancy) (Fischer et al. 1979). The breakpoint between these phases is described by $x \approx \ell_{Mu}$ as expected.

(2) Plume with negligible initial momentum in crossflow, $\ell_M/\ell_{Ju} \ll 1$. In this case the momentum length is so short that the deflection mechanism is immediately controlled by the interaction of buoyancy and crossflow. Trajectories and dilutions are summarized in Figure 9.

(3) General case. Of course, in the general case of a buoyant jet (significant momentum and buoyancy) in a crossflow, the overall jet trajectory will be described by several of the phases included in Figures 8 and 9. In that case, it is necessary to carefully delineate the different regimes by calculating the appropriate length scales and then

55
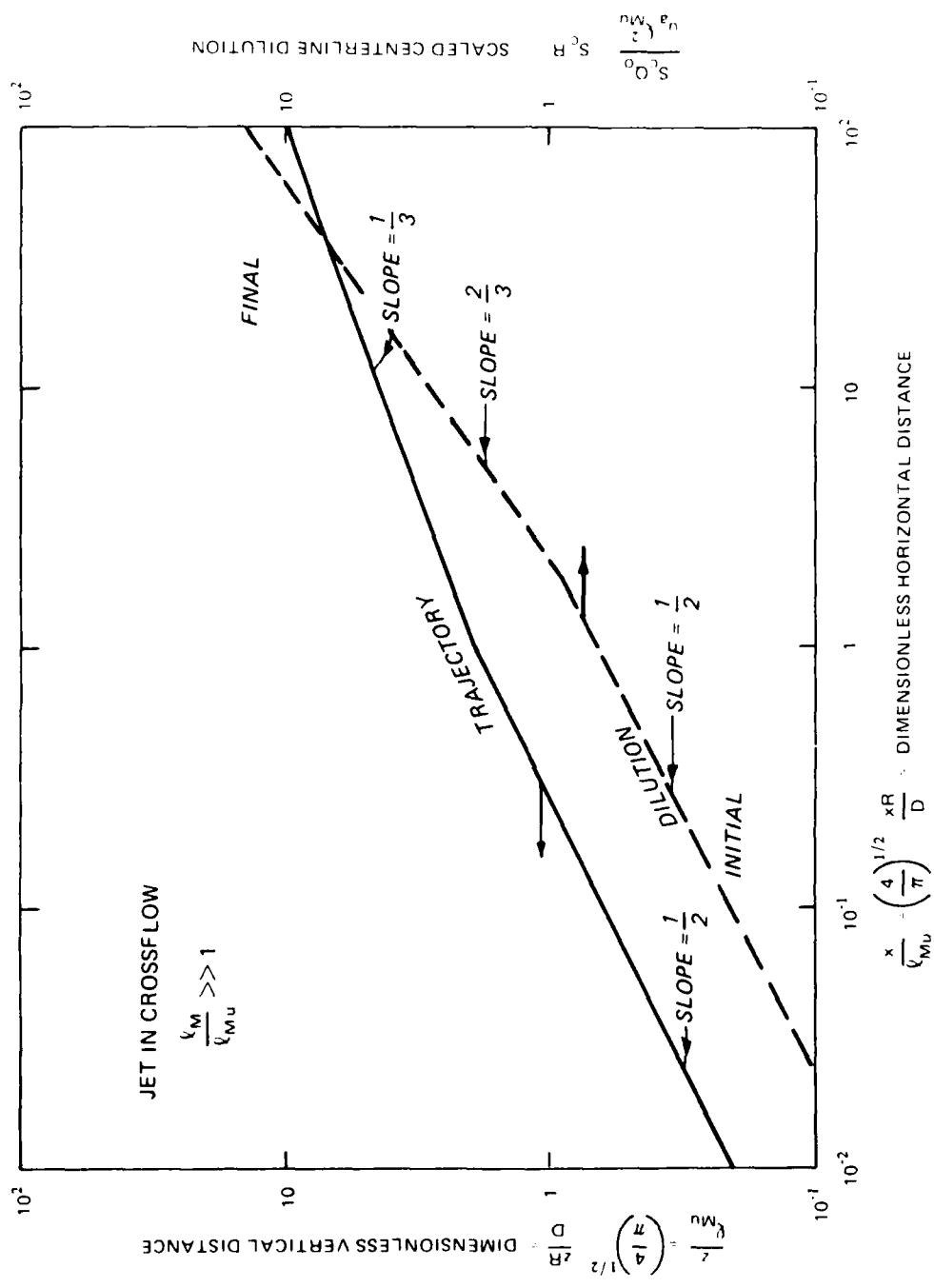
Figure 8. Trajectory and centerline dilution for round jets in a crossflow (after Wright 1977)

PLUME IN CROSSFLOW

$\dfrac{\ell_M}{\ell_{Ju}} \ll 1$

FINAL

SLOPE $= \dfrac{2}{3}$

SLOPE $= \dfrac{3}{4}$

TRAJECTORY

INITIAL

y-axis (left): $\dfrac{z}{\ell_{Ju}} = \dfrac{4}{\pi}\,\dfrac{z}{D}\;R^3 F_o^2$   DIMENSIONLESS VERTICAL DISTANCE

y-axis (right): $\dfrac{S_c Q_o}{u_a \ell_{Ju}^2} = \dfrac{4}{\pi}\,S_c R^5 F_o^4$   SCALED CENTERLINE DILUTION

x-axis: $\dfrac{x}{\ell_{Ju}} = \dfrac{4}{\pi}\,\dfrac{x}{D}\;R^3 F_o^2$   DIMENSIONLESS HORIZONTAL DISTANCE
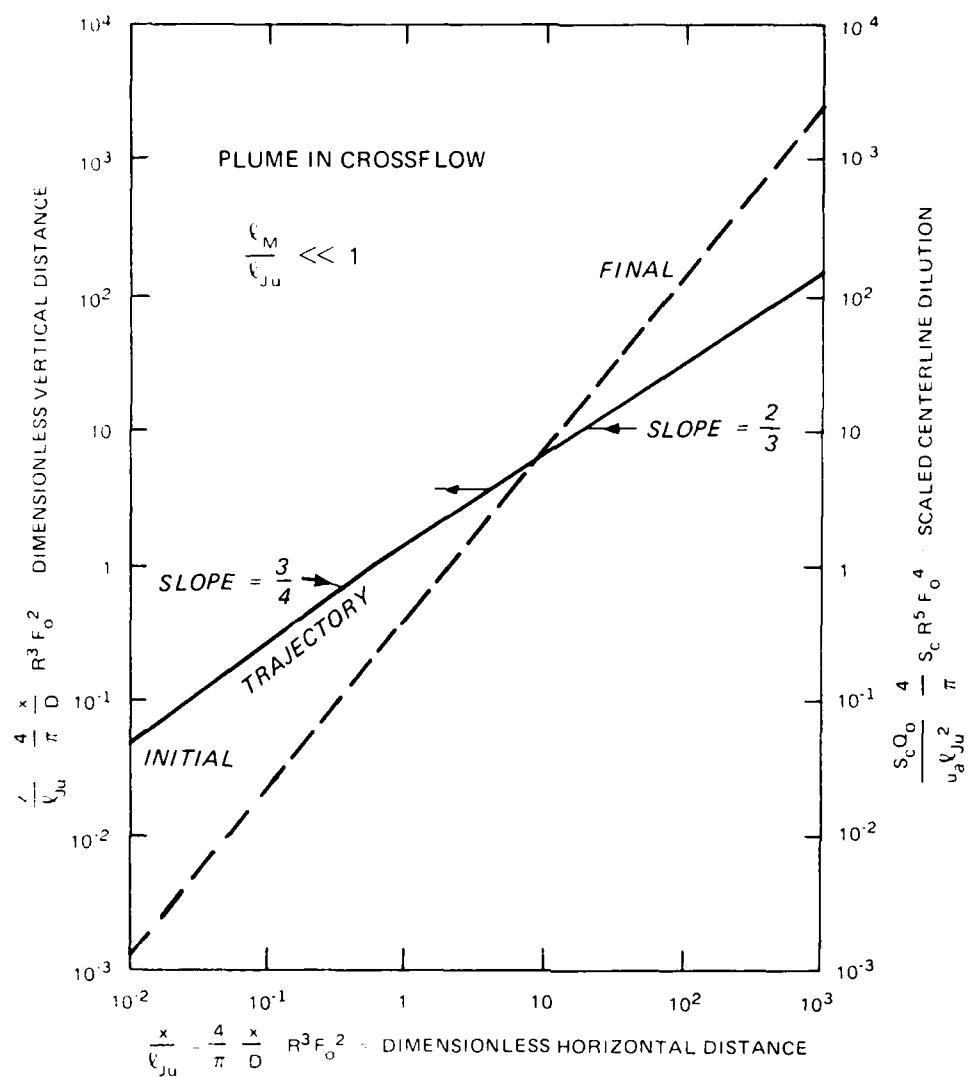
Figure 9.  Trajectory and centerline dilution for round plumes
in a crossflow

selecting the appropriate relationships.  This process is illustrated
in example 1 of Chapter 8.  (See also Fischer et al. 1979.)

   b.  Horizontal round buoyant jet (co-flow).

   (1)  Jet with negligible buoyancy in co-flow.  In the case of a
co-flowing jet that issues parallel to the direction of the ambient
flow, the jet travels along with the ambient flow and the excess veloc-
ities become dissipated by turbulent diffusion while the total excess
momentum flux  $\Delta M_o$  is preserved.  For this reason it is preferable to

57

scale all jet relationships with a modified jet-crossflow length scale (compare to Eq. 3.1.2)

$$\ell^*_{Mu} = \frac{\Delta M_o^{1/2}}{u_a} = \left(\frac{\pi}{4}\right)^{1/2} D \frac{(1 - R)^{1/2}}{R} \tag{3.1.6}$$

where $\Delta M_o = (U_o - u_a) U_o D^2 \pi/4$. With this scaling, the jet properties, such as width and dilution, can be plotted uniquely as shown in Figure 10. The jet trajectory is straight in the direction of the flow.

(2) Jet with negligible initial momentum in co-flow. It is to be expected that in the final stage the jet behavior will be identical to that for the final stage of the pure plume in crossflow (Figure 9)
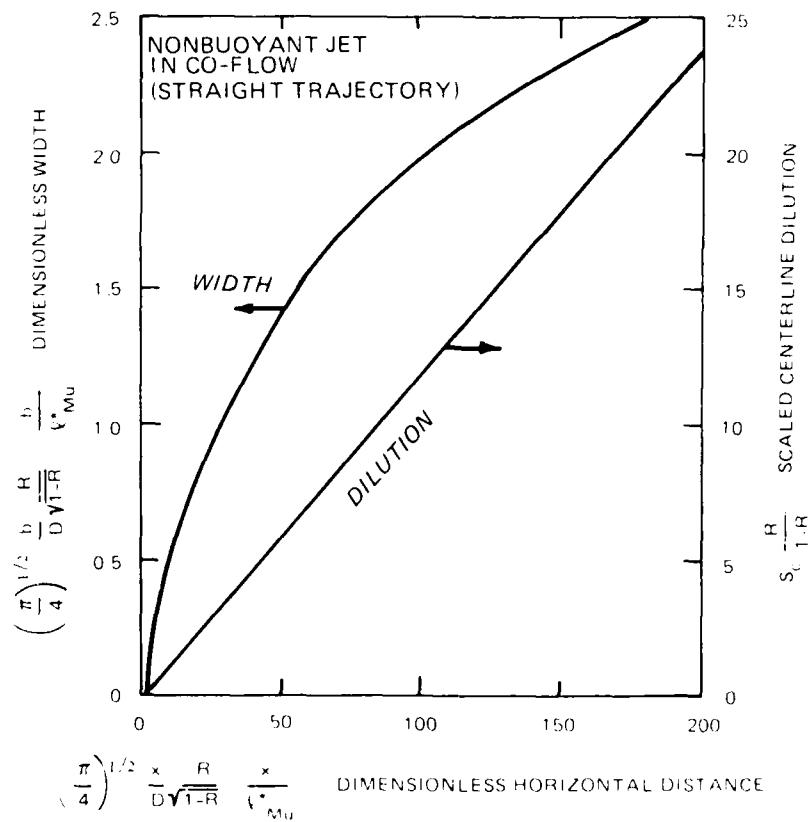


Figure 10. Dilution and jet width for nonbuoyant
co-flowing jets (after Rodi 1975)

58

since the momentum generated by the buoyancy is dominant in both cases. Thus, the appropriate scale for the final stage is $\ell_{Ju}$. However, in the initial stage ($x < \ell_{Ju}$), the jet will be behaving similar to the initial trajectory of the buoyant jet in stagnant flow ($z \sim x^3$, Abraham 1963, and Figure 7 for $x \lesssim 3\ell_M$), but with horizontal advection by the ambient flow, leading to a quadritic ($z \sim z^2$) trajectory. The length of the initial region is further influenced by the modified scale $\ell_{Mu}^*$, or in parametric fashion by $\ell_{Ju}/\ell_{Mu}^*$. The complete dilution and trajectory relationships are displayed in Figure 11 and are based on data from McQuivey, Keefer, and Shirazi (1971) neglecting, however, the effect of ambient turbulence that is considered in a passive diffusion process.

### 3.1.4 Interaction with Surface

In the two preceding sections, the ambient water depth was assumed to be unlimited. However, the actual water depth $H$ can have a profound effect on jet dynamics and mixing. Figure 12 illustrates the two major possibilities that can occur when a buoyant jet exists in stagnant water with a finite depth (or more generally, in water with a small crossflow as indicated by $\ell_{Mu}/H \gg 1$).

In the following, a criterion for discharge stability (absence of recirculation) is provided. In applications, this criterion must first be consulted to decide whether the rising portion of a single-port discharge behaves as a simple buoyant jet or as an unstable recirculating one. Next, dilution predictions for the unstable jet are given. Finally, the impingement process for stable jets is discussed.

a. *Criterion for discharge stability (deep-water conditions)*. In the stable discharge configuration (also called deep-water condition) the buoyant jet simply rises to the free surface (Zone 1 in Figure 12a) and then impinges (Zone 2). The flow after impingement may increase suddenly in thickness (internal hydraulic jump, Zone 3) until a stratified counterflow regime (Zone 4) is encountered.

Analysis of the four hydrodynamic zones indicated in Figure 12a indicates a limiting dynamic condition at which the situation becomes unstable as $H/DF_o$ decreases. This condition for a vertical discharge

59
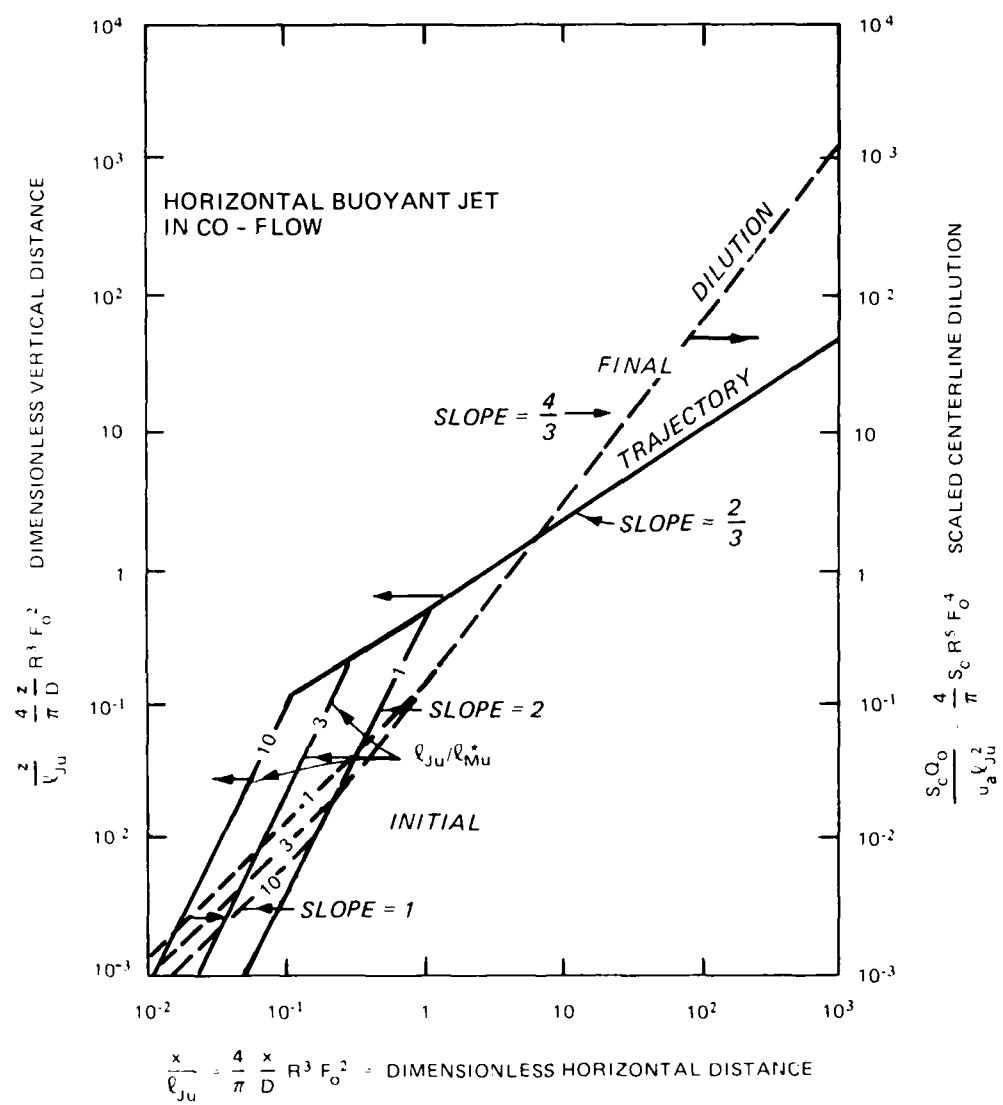
Figure 11. Trajectory and dilution for buoyant jets in co-flow
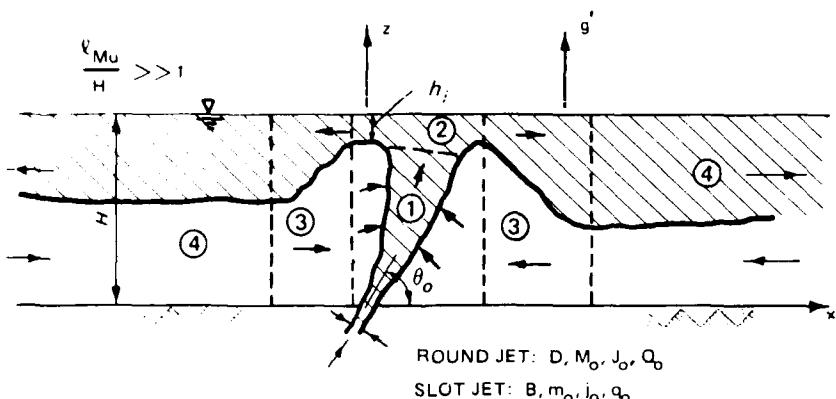
① SUBMERGED BUOYANT JET REGION
② SURFACE IMPINGEMENT REGION
③ INTERNAL HYDRAULIC JUMP REGION
④ STRATIFIED COUNTERFLOW REGION

a.   Stable discharge configuration
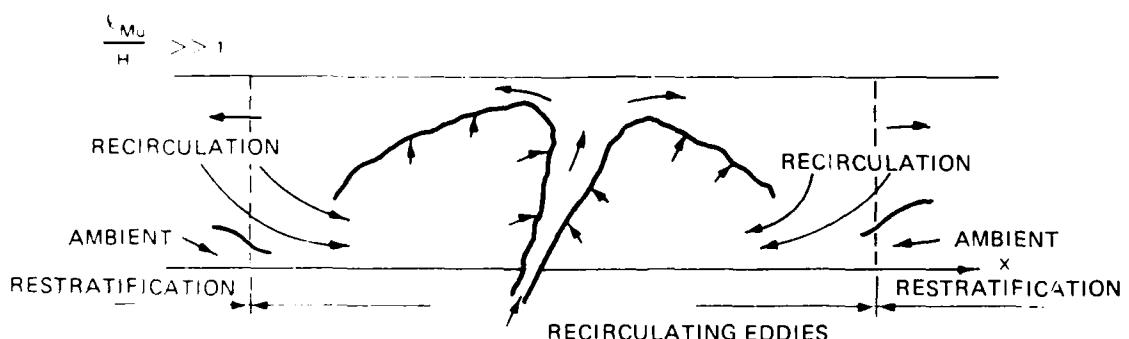


b.   Unstable discharge configuration

Figure 12.   Two major discharge configurations for buoyant jets in
finite water depth and small crossflow

is indicated as the stability criterion (Lee and Jirka 1981, Jirka
1982a) in the parameter domain of $F_o$ and $H/D$ in Figure 13.   For
$H/D \gtrsim 10$ , the criterion is simply a straight line given by

$$\frac{H}{DF_o} = 0.22 \tag{3.1.7}$$

or

$$\frac{\ell_M}{H} = 4.3 \tag{3.1.8}$$

61

Figure 13 was developed for a vertical jet ($\theta_o$ = 90 deg); how-
ever, data analysis (Jirka 1982a) indicates that at least the stability
criterion is approximately applicable to nonvertical ($\theta_o$ < 90 deg) con-
ditions as well.
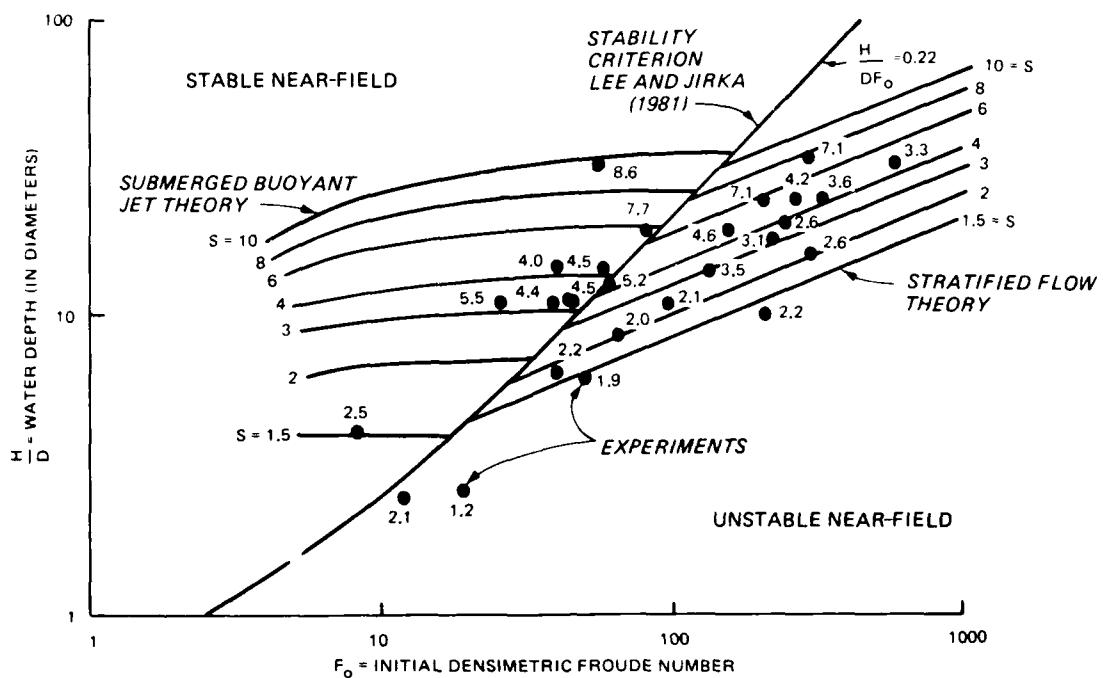


Figure 13.  Stability criterion and bulk dilution for vertical round
buoyant jets in finite water depth

b.  Bulk dilution for unstable discharge (shallow-water) condi-
tions.  The unstable discharge configuration (or shallow-water condi-
tion) is radically different.  Here, the jet does not have enough
buoyant stability after the impingement process to have a gradual
transition to the stratified counterflow nor to allow the ambient
inflow required to supply the entrainment for Zone 1.  Rather, unstable
recirculating eddies develop around the jet leading to repeated reen-
trainment of discharged water.

Experimental data for the bulk dilution  S  that occurs at the
edge of the recirculating ("boil") region (Figure 12b) of an unstable
jet are shown in Figure 13, together with theoretical predictions.
This dilution factor  S  is a measure of the mixing that the discharge
has experienced once it leaves the recirculating zone and flows into

the stratified far-field zone (indicated by the dashed line section in Figure 12b). For unstable conditions, the dilution equation is

$$\frac{S}{F_o} = 0.9 \left(\frac{H}{DF_o}\right)^{5/3} \tag{3.1.9}$$

or,

$$S \frac{Q_o J_o^{1/2}}{M_o^{5/4}} = 1.3 \left(\frac{H}{\ell_M}\right)^{5/3} \tag{3.1.10}$$

Comparison of Eqs. 3.1.9 and 3.1.10 with the simple plume solution (Eq. 3.1.3) indicates the same functional relationships but with a considerably higher coefficient in the unstable case due to the additional entrainment that occurs in the recirculating process.

    <u>c</u>.  <u>Surface impingement for stable discharge conditions</u>.

    (1)  <u>Stagnant or weak crossflow</u> ($\ell_{Mu}/H \gg 1$). It is necessary to know the thickness $h_i$ of the surface impingement layer (Fig. 12a) because active jet entrainment takes place only up to the level $z_i = H - h_i$. Lee and Jirka's (1981) analysis for vertical jets gives $h_i \approx 0.2H$ if $H/D \geq 4$, while for small $H/D < 4$, $h_i$ is better presented as $h_i \approx 0.4 \, D$ (i.e. scaled by the diameter). For nonvertical jets, Abraham (1963) gives a more general result, namely, $h_i \approx 0.10 \, L_p$ where $L_p$ is the length of the curved jet path. The bulk dilution in the surface boil region above an impinging jet is therefore calculated as the mean dilution $S$ of the buoyant jet at the level $z_i$ above the discharge port. The values thus calculated are actually drawn as iso-lines in the stable domain portion of Figure 13.

    (2)  <u>Crossflow</u> ($\ell_{Mu}/H \approx 1$). When a bent-over buoyant jet in a crossflow approaches the free surface, there exists the possibility of jet bifurcation, i.e., the jet can actually split into two branches that travel downstream while separating further. This mechanism is related to the internal double vortex structure that exists in bent-over jets but has been neglected so far in the discussion as it is of limited

63

importance for trajectory or dilution prediction in deep water. Discussions and models of the bifurcation mechanism have been given, for example, by Jirka and Fong (1981), who also gave further references. The conditions under which bifurcation occurs have not been well defined. However, as a general guideline, it is expected that the impingement process dominates for $\ell_{Mu}/H \gg 1$ , while for $\ell_{Mu}/H \ll 1$ , the crossflow deflection may be so strong that any bifurcation may not be evident. Perhaps $\ell_{Mu}/H \approx 1$ (possibly 1/3 to 3) is most conducive to significant bifurcation. However, it must be emphasized that these values are primarily conjecture at this time. When bifurcation does occur, the simplest approximation, following Abdelwahed and Chu (1978), is that the angle of each spreading branch relative to the crossflow direction is equal to the trajectory angle at the point of surface impingement (= $\tan^{-1} dz/dx$) and that the dilution in the two branches after bifurcation is equal to that of the simple momentum jet (using the dilution diagram of Figure 8).

### 3.2 SUBMERGED MULTIPORT DISCHARGES (DIFFUSERS)

The submerged multiport diffuser is probably the most effective mixing device for natural water bodies. It causes a rapid dilution of the effluent. This is achieved by discharging the effluent through a series of individual small ports or nozzles that are spaced along a main feeder pipe. Thus, the effluent is distributed over a large distance. A multiport diffuser is made up of many round jets. However, in usual designs, these jets rapidly merge, thereby forming a two-dimensional plane jet. Thus, all the fundamental results derived in Section 2.4 are of interest here. The aspects of this initial jet-merging are discussed in the following section. Next, the discharge stability of multiport discharges in finite water depths is examined. Then results for deep-water diffusers are presented, followed by those for shallow-water diffusers. The latter category is of special importance for cooling water discharges from thermoelectric power plants.

## 3.2.1  Jet Interference (Equivalent Slot Jet)

Two types of jet interference are illustrated in Figure 14. In a unidirectional diffuser (when all nozzles point in one direction), the round jets merge laterally into a plane buoyant jet (Figure 14a). Using the spreading coefficients  k  listed in Table 2 and considering that the actual jet or plume width is larger by about a factor of 2
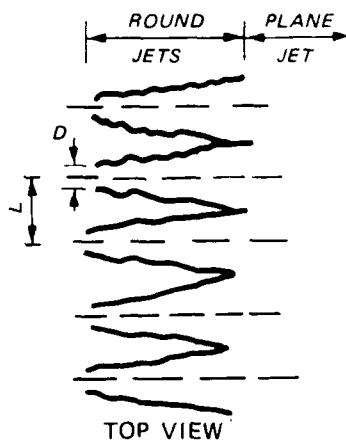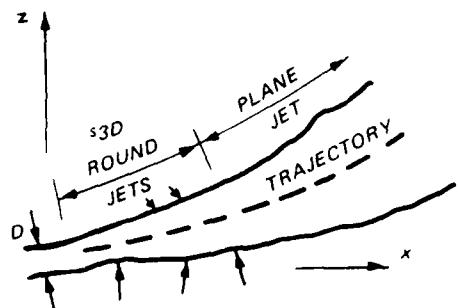
SIDE VIEW                              TOP VIEW

a.  Jets merging in unidirectional diffuser

SIDE VIEW                    TOP VIEW A - A
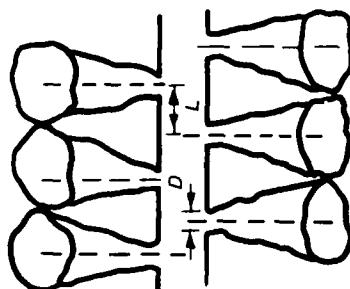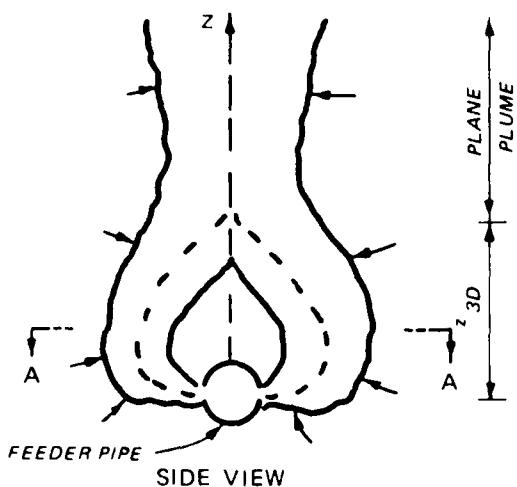
b.  Jets merging in alternating diffuser

Figure 14.  Interference of multiport diffuser discharges forming two-dimensional (slot) jets or plumes

(since the  k  coefficients describe the  1/e  width), the distance
$s_{3D}$  to the beginning of the merging region is

$$\frac{s_{3D}}{L} \approx 2 \qquad\qquad (3.2.1)$$

in which L is the nozzle spacing. A more complicated merging process
takes place for alternating diffusers (alternate nozzles pointing in
opposite directions) as shown in Figure 14b. Here the buoyant jets
from both sides are bent toward each other (due to the low-pressure
region formed by the jet entrainment) and ultimately form a vertically
rising plane plume. An expression for the vertical merging distance
$z_{3D}$  is (Jirka and Harleman, 1973)

$$\frac{z_{3D}}{LF_o} \approx 1 \qquad\qquad (3.2.2)$$

In either case, the dynamics of the plane buoyant jet beyond the
distance of merging,  $s > s_{3D}$ , can be described by the two-dimensional
relationships given in Section 2.4. The only requirement is that the
correct total flux quantities are prescribed. If $M_o$ , $J_o$ , $Q_o$ , and
$Q_{co}$ are the fluxes through each nozzle, then the correct two-
dimensional flux quantities that must be specified at the origin
(s = 0) are

$$m = \frac{M_o}{L} \ , \quad j_o = \frac{J_o}{L} \ , \quad q_o = \frac{Q_o}{L} \ , \quad q_{co} = \frac{Q_{co}}{L} \qquad\qquad (3.2.3)$$

where  L  is the nozzle spacing. Alternatively, the correct width  B
and Froude number of an "equivalent slot jet" are

$$B = \frac{D^2\pi}{4L} \ , \quad F_s = F_o\left(\frac{4L}{D\pi}\right)^{1/2} \qquad\qquad (3.2.4)$$

66

For practical designs, the fictitious width  B  is a small dimension
(of the order of centimeters).  The equivalent slot diffuser is a con-
venient and accurate representation of multiport diffuser dynamics as
demonstrated by Cederwall (1971) and Jirka and Harleman (1973).  The
use of an equivalent slot implies that the initial three-dimensional
effects are of no importance for larger distances ($s > s_{3D}$) and that
the direct two-dimensional results are sufficiently precise and, of
course, much simpler.  If more detail is desired in the region before
merging ($s < s_{3D}$), then appropriate calculations for the individual
round jets must be made as discussed in the previous sections, and then
matched to the two-dimensional results at  $s = s_{3D}$ .

## 3.2.2  Criterion for Discharge Stability for Multiport Diffusers

a.  Stagnant water.  Reference is again made to Figure 12, which
also applies for two-dimensional conditions.  The stability criterion
is plotted in Figure 15 for the slot jet parameter domain of  $F_s$  and
$H/B$  and shows a significant dependence on the discharge angle  $\theta_o$ .
Note that the alternating diffuser (Figure 14b) is represented by
$\theta_o = 90$ deg , i.e. a vertical buoyant jet.  For the region  $H/B \geq 200$ ,
the criterion is given by

$$\frac{H}{BF_s^{4/3}} = 1.84 \left(1 + \cos^2 \theta_o\right)^2 \qquad (3.2.5)$$

or

$$\frac{\ell_m}{H} = \frac{m_o}{j_o^{2/3} H} = \frac{0.54}{\left(1 + \cos^2 \theta_o\right)^2} \qquad (3.2.6)$$

This criterion (Jirka 1982b) divides the stable discharge domain (deep-
water conditions) in which buoyant jet theories (Section 3.2.3) are
directly applicable from the unstable domain (shallow-water condition)
in which flow recirculation and breakdown occur so that alternative
predictive theories (Section 3.2.4) must be used.

67
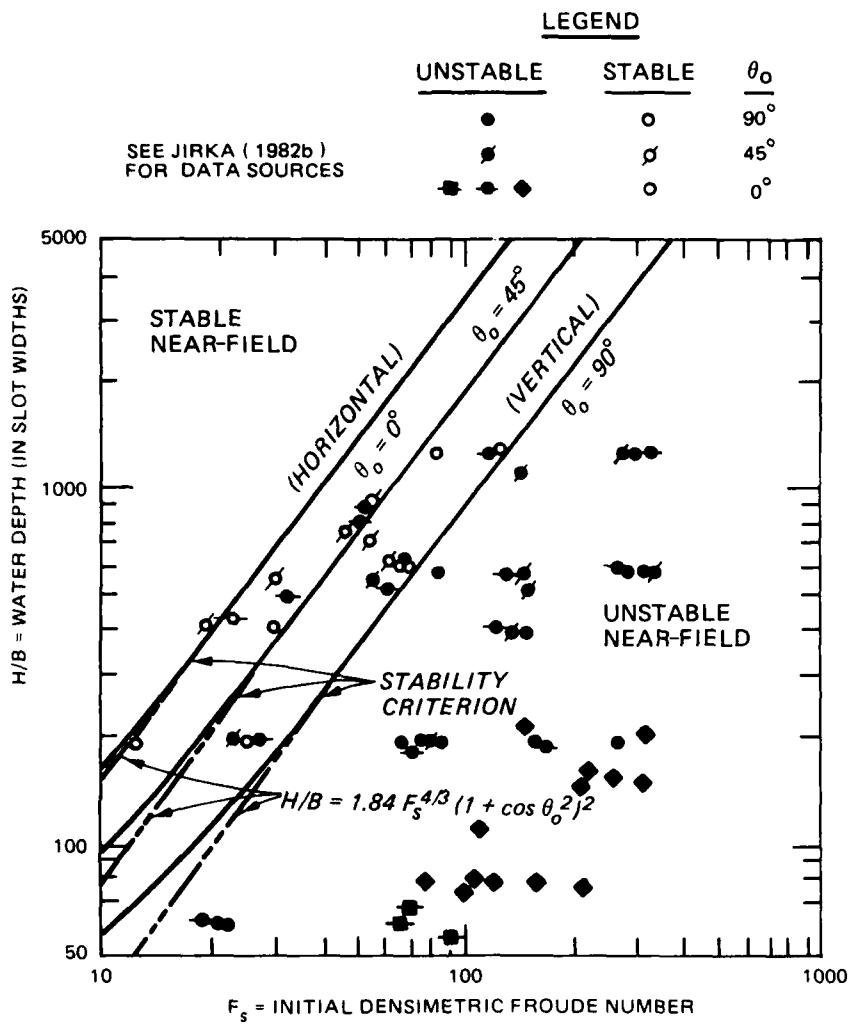
Figure 15. Stability diagram for multiport diffusers
and slot jets (after Jirka 1982)

b. **Flowing ambient.** If a diffuser pipe is perpendicular to an
ambient flow, then the total ambient momentum $m_a = u_a^2 H$ will be a
further destabilizing mechanism on the diffuser flow field. Jirka
(1982b) has shown that the stagnant water criterion (Eq. 3.2.5 or
3.2.6) can be expanded in this case to

$$\frac{m_o(1 + \cos \theta_o) + m_a}{j_o^{2/3} H} = 0.54 \qquad (3.2.7)$$

68

Thus, when the combined normalized momentum flux on the left-hand side of the above equation exceeds 0.54, the flow will break down into a fully mixed region. In case of strong crossflow, the entire water depth downstream from the diffuser line will then be occupied by the mixed effluent. However, this does not preclude the possibility of eventual restratification due to particular boundary conditions in the far-field. Such possibilities are discussed in Section 3.4.

### 3.2.3 Deep Water Diffusers

#### a. Stagnant water.

(1) Vertical slot jet. The governing plane buoyant jet equation system (Eqs. 2.6.11-2.6.18) can be integrated with $\theta = \theta_o = 90$ deg , $s = z$ , and the constant spreading assumption (Eq. 2.6.12) to give a bulk dilution

$$S = \frac{q}{q_o} = \frac{i_1}{i_2^{1/2}} \left( m_o^{3/2} + \frac{i_2^{1/2} i_4}{i_3} j_o k^{1/2} z^{3/2} \right)^{1/3} \frac{k^{1/2} z^{1/2}}{q_o} \qquad (3.2.8)$$

(Abraham 1963, Jirka and Harleman 1979). With all coefficients specified (from Table 4) the normalized centerline dilution is

$$\frac{S_c}{F_s^{2/3}} = 0.481 \left[ \left( \frac{z}{BF_s^{4/3}} \right)^{3/2} + 0.837 \left( \frac{z}{BF_s^{4/3}} \right)^3 \right]^{1/3} \qquad (3.2.9)$$

The solution is plotted in Figure 16 and shows the characteristic transition between the initial jet regime and the final plume regime. (Compare also to Figure 5 for the round jet.) Figure 16 is applicable only in the region where the individual jets have merged (Eqs. 3.2.1 and 3.2.2).

(2) Horizontal slot jet. The nondimensional trajectory and jet widths are shown in Figure 17 based on Abraham's (1963) model. The centerline dilution predictions are given in Figure 16 for comparison with the vertical jet, again showing a higher dilution for the

69
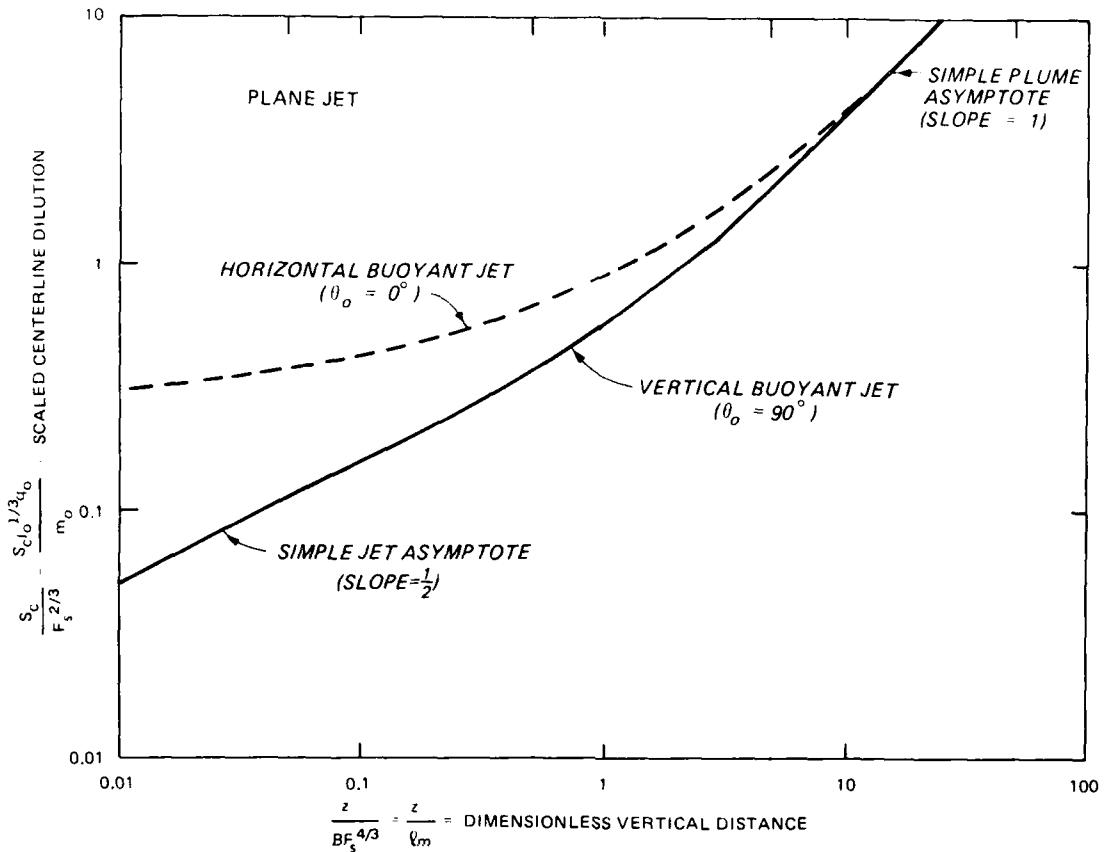
Figure 16. Centerline dilution for vertical and horizontal slot buoy-
ant jets (multiport diffusers) in deep, stagnant, unstratified water

horizontal jet up to $z/\ell_m \approx 10$ when the asymptotic plume regime is
attained.

(3) <u>Negatively buoyant vertical slot jet</u>. This situation is
frequently encountered with the disposal of heavy fluids (e.g. concen-
trated industrial or cooling water blowdown). The maximum vertical
penetration level is of the order of

$$\frac{z_m}{BF_s^{4/3}} = \frac{z_m}{\ell_m} \approx 1.0 \tag{3.2.10}$$

and the associated dilution at that level is

70

$$\frac{S_m}{F_s^{2/3}} \approx 0.4 \qquad\qquad (3.2.11)$$

with $|g_o'|$ used in the Froude number definition.
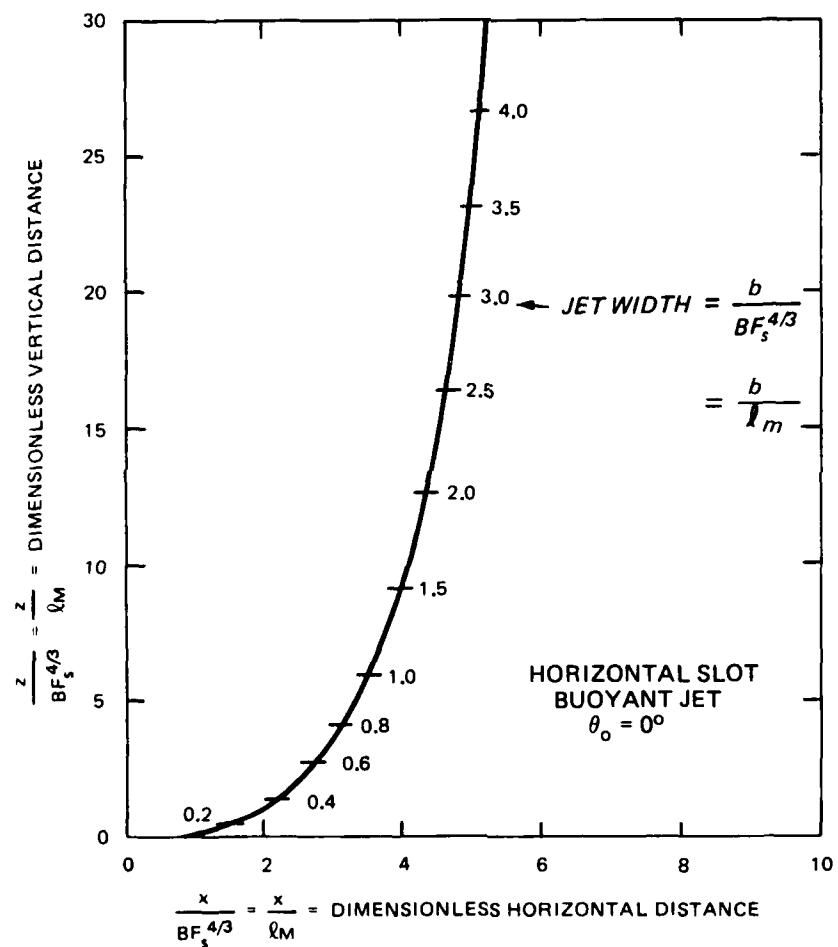


Figure 17. Nondimensional trajectory for horizontal
slot buoyant jets (multiport diffusers) in deep,
stagnant, unstratified water

<u>b</u>. <u>Surface impingement</u>. For positively buoyant discharges, the
thickness of the surface impingement layer that defines the upper end
of active jet entrainment is approximately

$$\frac{h_i}{H} = 0.16 \qquad (3.2.12)$$

based on Jirka and Harleman's (1973) theory and experiments.

<u>c</u>. <u>Weak Ambient Crossflow</u>. The strong destabilizing effect of
ambient crossflow has been discussed in connection with Eq. 3.2.7.
However, when the ambient crossflow is too weak to cause complete ver-
tical mixing, it may have an inhibiting effect on dilution as the
entrainment on the downstream (lee) side of the diffuser plume becomes
blocked. Studies by Roberts (1977) indicate for weak crossflow that a
dilution at the water surface $S_s$ is

$$\frac{S_s}{F_s^{2/3}} = 0.27 \, \frac{H}{BF_s^{4/3}} = 0.27 \, \frac{H}{\ell_m} \qquad (3.2.13)$$

Comparison to the plume solution (second expression in bracket of
Eq. 3.2.9, which yields $S_c/F_s^{2/3} = 0.45 \, z/\ell_m$ ) shows that this dilution
is considerably less than would occur under stagnant conditions even if
account is taken of the impingement layer.

3.2.4 <u>Shallow-Water Diffusers</u>

<u>a</u>. <u>Coflowing unidirectional diffuser</u>. This is a beneficial
diffuser arrangement for effluent disposal in riverine situations.
Referring to Figure 18, the diffuser discharges in the direction of the
river flow. The discharge is strongly unstable due to the combined
action of diffuser and ambient momentum. The result is a vertically
fully mixed plume (Figure 18). The mixing mechanism in this case con-
sists of back entrainment as ambient river water is accelerated from
upstream and carried over the diffuser and of more gradual side
entrainment.

72

PLAN VIEW

RIVERBANK

SLIPSTREAM

SIDE ENTRAINMENT

BACK

ENTRAINMENT

$L_d$

$C_c L_d$

RIVER BANK OR

SYMMETRY LINE

$Q_d$

SIDE VIEW

$u_a$

VERTICALLY MIXED PLUME

5 TO 10 H
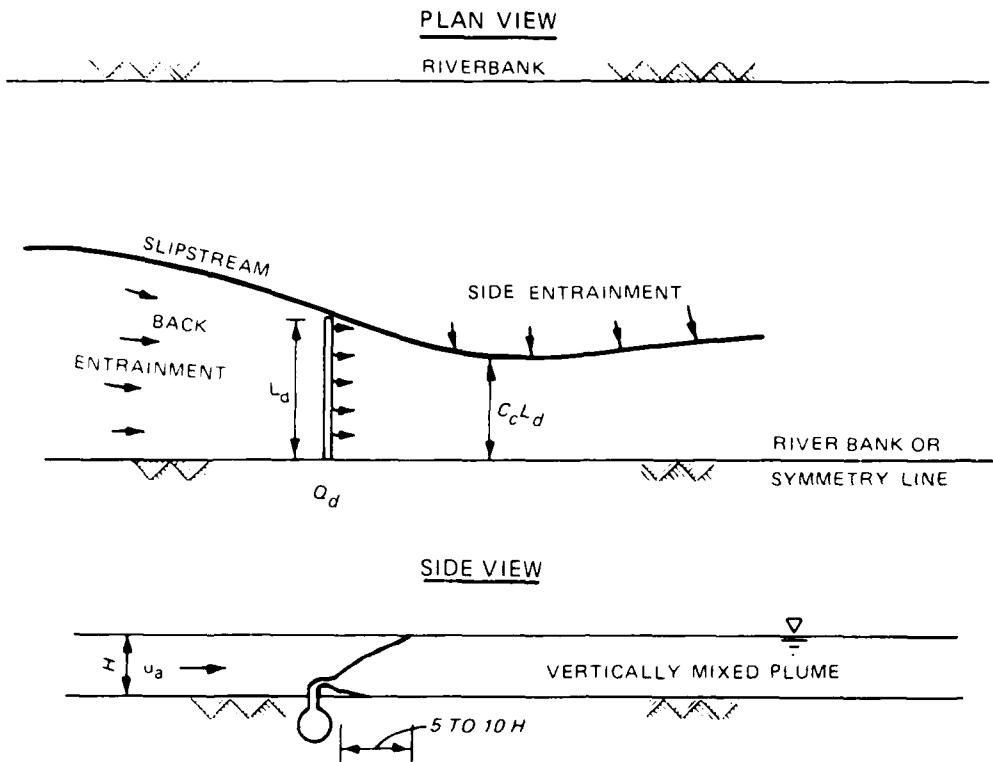
Figure 18.  Co-flowing unidirectional diffuser in a river

From the viewpoint of rapid mixing, the back entrainment contribution is more important in the diffuser dynamics.  An analysis by Adams (1982) (also Jirka 1982b) gives the bulk dilution downstream from the diffuser due to back entrainment (i.e. neglecting side entrainment):

$$S = \frac{1}{2} V + \frac{1}{2} \left( V^2 + \frac{2 m_o H}{q_o^2} \right)^{1/2} \qquad (3.2.14)$$

in which $V = u_a H/q_o$ is the volume flux ratio between ambient and discharge flow.  For the stagnant case ($V = 0$), this result reduces to

73

$$S = \frac{\left(m_o H/2\right)^{1/2}}{q_o} \qquad\qquad (3.2.15)$$

i.e., it is only the diffuser momentum flux per unit width $m_o$ that is responsible for mixing. Once the diffuser operates in the shallow-water domain (which is ascertained by consulting the stability criterion, Section 3.2.2), the buoyancy flux is dynamically unimportant for mixing and hence does not appear in Eq. 3.2.14 or 3.2.15. The above results are based on an assumption of a constant river depth $H$ and constant discharge characteristics $m_o$ and $q_o$ . If the depth varies along the diffuser length and if it is desired to achieve a constant dilution $S$ along the diffuser, then Eq. 3.2.15 indicates that $m_o$ and $q_o$ should be varied along the length in such a manner as to keep the quantity $q_o^2/m_o$ (which is equal to $B$ ) a constant fraction of $H$ . For a "weak" diffuser whose momentum is negligible compared to the ambient momentum, the dilution is given by $S \approx V$ , i.e. mixing is simply achieved as ambient flow sweeps over the diffuser line.

A further feature of the unidirectional diffuser dynamics is the contraction that takes place downstream. The plume width is restricted to $C_c L_d$ , which is less than the actual diffuser length $L_d$ . For shallow water, the contraction coefficient is given by

$$C_c = \frac{1}{2} + \frac{1}{2}\left(1 + \frac{2m_o}{m_a}\right)^{-1/2} \qquad\qquad (3.2.16)$$

in which $m_a = u_a^2 H$ is the ambient kinematic momentum flux. Again, in the limiting case of a stagnant ambient, the most severe contraction ($C_c = 1/2$) is obtained.

Of course, the bulk dilution equation (Eq. 3.2.14) is valid only if the actual river flow ($Q_R = u_a HW$ in which $W$ = river width) is larger than the required entrainment flow $(S-1)Q_d$ , in which $Q_d$ is

the total diffuser flow ($Q_d = q_o L_d$). In that case, the remaining
river flow $[Q_R - (S-1) Q_d]$ passes through the river cross section that
is not occupied by the diffuser. However, if the river flow is small
$[Q_R < (S - 1)Q_d]$, then recirculation must take place, i.e., mixed water
from the downstream region will return to the back-entrainment region.
The new average dilution is then controlled by the river so that
$S_R = Q_R/Q_d + 1$ . This river-controlled condition always applies if the
diffuser extends fully across the river.

A complete analysis of the full diffuser plume, including the
shape of the slipstream and the gradual side entrainment, has been
given by Lee and Jirka (1980).

b. Other diffuser types. There are several other diffuser
types, namely the unidirectional crossflowing diffuser, the staged
diffuser, and the alternating diffuser. All of these operate in the
unstable shallow-water regime, the latter also relying on buoyancy flux
as a dynamic variable that contributes to mixing. These types have
emerged predominantly in the direct heat disposal of once-through cool-
ing water from thermoelectric power plants, especially in coastal
regions. Those types are of limited importance in river applications.
For a complete discussion, the reader is referred to Jirka (1982b).

3.3 SURFACE DISCHARGES

The oldest and least costly approach to effluent disposal into
rivers, lakes, and reservoirs is the use of a surface canal that enters
at the shoreline. Three possibilities exist regarding the buoyancy of
the effluent:

a. If the effluent is nonbuoyant ($g_o' = 0$) and if the water
depth is great enough not to provide any inhibition to the inflow re-
quired for entrainment, the jet will behave exactly like the nonbuoyant
jets considered in Section 3.1 except that the water surface will act
as a symmetry plane. If the water is stagnant, then the jet trajectory
will be straight; if there is crossflow, the jet will be deflected ac-
cording to the trajectory laws displayed in Figure 8.

75

b. If the effluent is heavier than the receiving water, it will sink away from the water surface, thereby forming a submerged buoyant jet. Again, this is exactly the situation considered in Section 3.1.3. If the ambient is stagnant, the predictive diagrams of Figures 5 and 7 (with $\theta_o = 0$ deg and z pointing vertically downward) are applicable. Often, however, the vertical fall will soon be limited by shallow ambient depth. A complicated three-dimensional trajectory arises for crossflows since the jet issues laterally into the flow but is then deflected sideways. Detailed models (such as Hirst 1972) must be consulted in those cases.

c. If the effluent is lighter than the ambient water, there is a buoyant surface jet. The rest of this section is devoted to this type of jet.

### 3.3.1 Buoyant Surface Jet in Deep Stagnant Water

a. Basic features. Figure 19 is a definition diagram for a buoyant surface jet. The jet issues from a canal of depth $h_o$ and width $2b_o$. Very close to the discharge point, the jet behaves essentially as a nonbuoyant jet with linear spreading. However, at larger distances buoyancy exerts an increasing effect on two levels of jet behavior. On a small scale, it dampens the turbulent vertical entrainment at the jet bottom and, on a larger scale, it causes continuous lateral spreading of the jet. Thus, the buoyant jet becomes gradually thinner while spreading strongly laterally. During this process the local densimetric Froude number ($F_L = u_c/(g_c'h)^{1/2}$) is constantly decreasing from its initial large value. This Froude number ultimately reaches a value of unity at a distance called the transition distance ($x_t$). At this distance the lateral spreading motion becomes of the same order as the forward motion. Thus, the jet has completely collapsed into a far-field "pool" of buoyant fluid. This far-field motion has completely different dynamics, is inherently unsteady in large receiving water bodies, and may begin with an abrupt transition internal hydraulic jump from the buoyant-jet near-field to the far-field (Figure 19). These aspects are discussed by Jirka, Adams, and

76
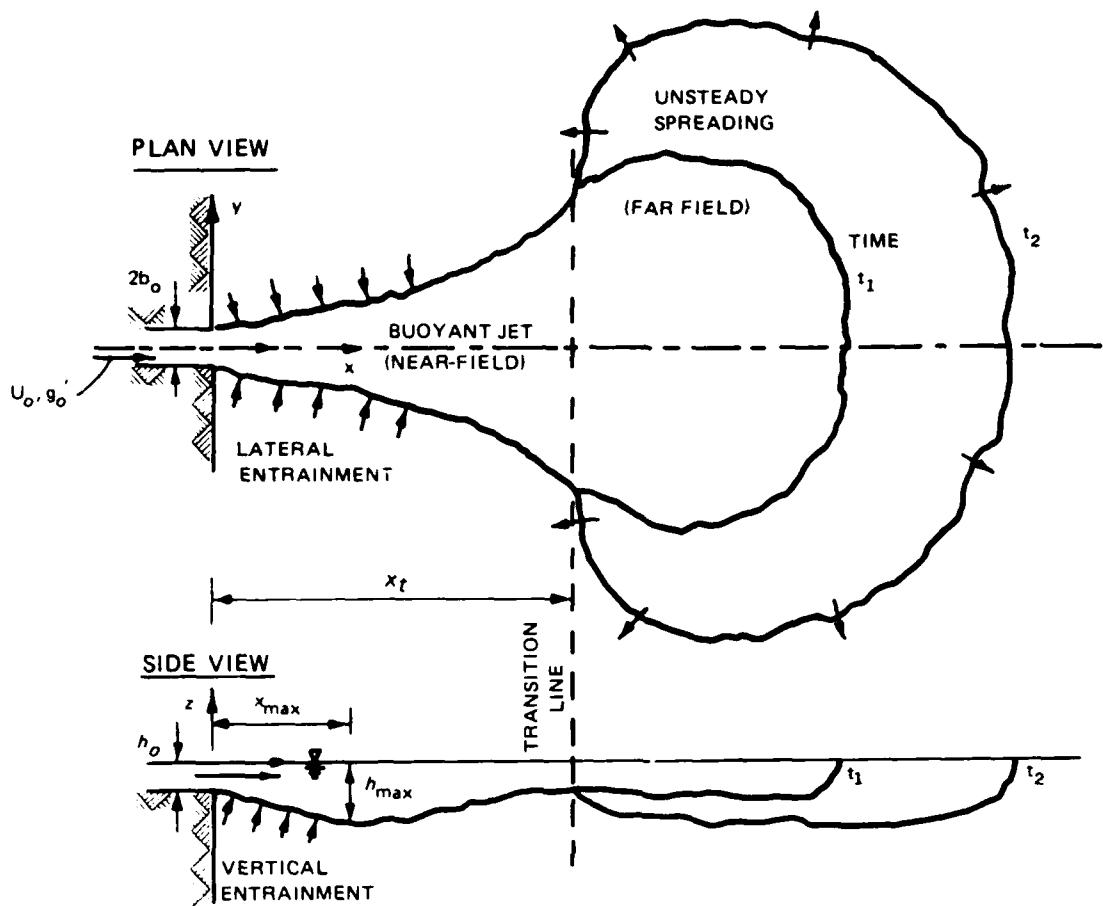
Figure 19. Definition diagram for buoyant surface discharge in deep, stagnant receiving water

Stolzenbach (1981). Only the near-field region ($x < x_t$) is a true jet regime.

 b. **Nondimensional parameters and scales.** Since the exact geometry of the buoyant surface jet channel is frequently quite important (in contrast to the submerged applications), a somewhat different parameterization is introduced here. The rectangular channel (Figure 19) has a length scale

$$L_o = \sqrt{h_o b_o} \tag{3.3.1}$$

77

i.e., the square root of half the channel cross section, and an aspect ratio

$$A = \frac{h_o}{b_o} \qquad (3.3.2)$$

A surface jet Froude number is then

$$F_o' = \frac{U_o}{\sqrt{g_o' L_o}} \qquad (3.3.3)$$

These discharge channel parameters are related to the momentum length scale ($\ell_M$, in which the total fluxes appear, Table 6) by

$$\ell_M = 2^{1/4} L_o F_o' \qquad (3.3.4)$$

As usual, the momentum length scale ($\ell_M$) is a measure of the relative influence of momentum flux and buoyancy flux on jet behavior.

     c. <u>Nondimensional solutions</u>. The nondimensional geometry and the centerline dilution are plotted in Figure 20. The half-width and half-depth lines relate to the positions where the scalar concentration and buoyancy are one-half the centerline values (corresponding to 83 percent of the usual Gaussian width definitions). The full width and depth lines are somewhat wider and describe the edge of the jet where the scalar quantities are essentially zero (or negligible). It is evident from Figure 20 that the buoyant surface jet flattens out considerably as the axial distance increases.

     Some important parameters for the surface jet are the maximum depth

$$\frac{h_{max}}{L_o F_o'} = 0.42 \qquad \text{or} \qquad \frac{h_{max}}{\ell_M} = 0.35 \qquad (3.3.5)$$

78

occurring at a distance

$$\frac{x_{max}}{L_o F'_o} = 5.5 \qquad \text{or} \qquad \frac{x_{max}}{\ell_M} = 4.6 \qquad (3.3.6)$$

and the transition distance

$$\frac{x_t}{L_o F'_o} \approx 15 \qquad \text{or} \qquad \frac{x_t}{\ell_M} \approx 13 \qquad (3.3.7)$$

Initially the dilution increases linearly with distance (as for a non-buoyant jet $F'_o \to \infty$ , Table 1) but it gradually destabilizes and reaches a plateau value (indicative of the damping of vertical entrainment) at the transition. This plateau value is called the stable centerline dilution

$$\frac{S_{cs}}{F'_o} \approx 1.0 \qquad (3.3.8)$$

Thus, the buoyant surface jet has a definite limit on its mixing capacity (unlike the submerged buoyant jet in deep receiving water).

Finally, it should be emphasized that the basic solutions in Figure 20 have been plotted for the asymptotic range $F'_o >> 1$ . The effect of finite Froude numbers (as usual, an indication of additional dynamic effects of a large source size) can be considered in two steps. First, as long as $F'_o$ is reasonably large, $F'_o \gtrsim 3$ in practice, the asymptotic solution is valid in the later phases of jet spreading (large distance $x$ ), but a finite source effect is present in the outlet vicinity. This is indicated qualitatively by the dot-dashed lines in Figure 20; the length of the affected zone is inversely related to $F'_o$ . Second, for even smaller Froude numbers, $1 \lesssim F'_o \lesssim 3$ , the dynamic effect of the finite source is felt throughout the jet evolution up to its final transition. All buoyant surface jet properties, including

79
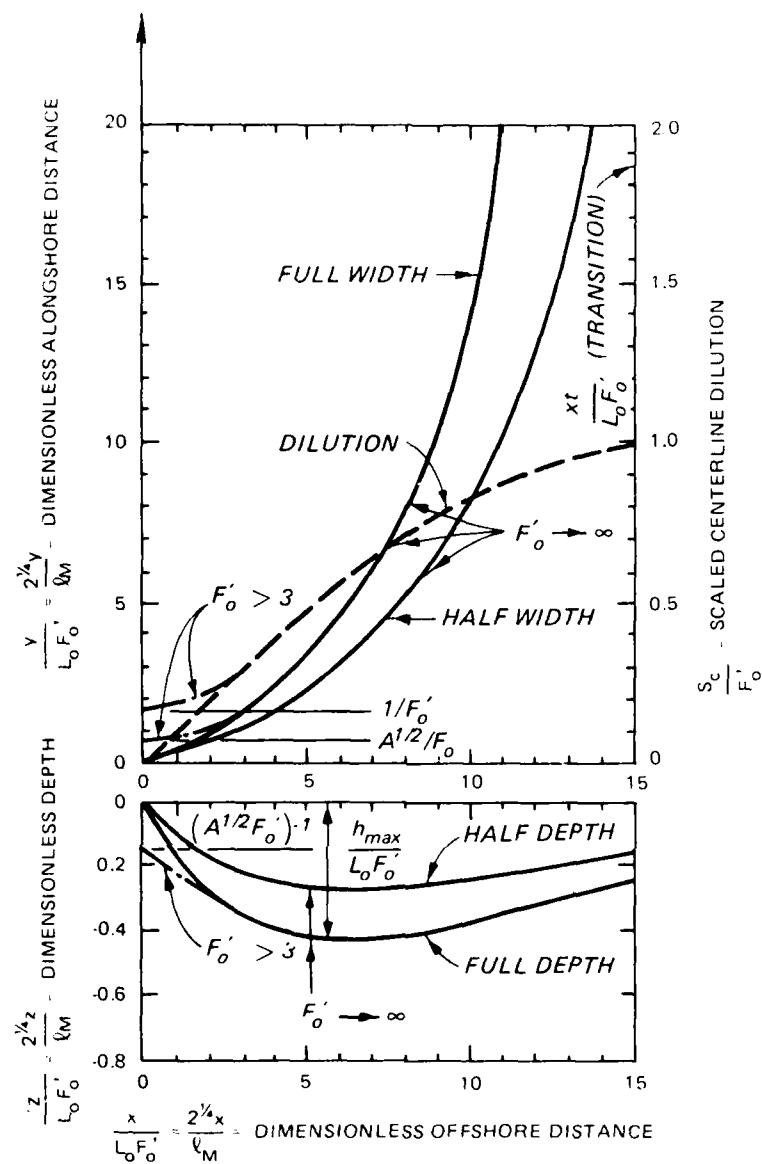
Figure 20. Nondimensional geometry and center-
line dilution for buoyant surface jets in deep,
stagnant receiving water (after Jirka et al.
1981)

geometry and dilution, are then dependent on $F_o'$ and on $A$ and cannot
any longer be scaled uniquely as was done in Figure 20. As an example,
the normalized stable centerline dilution (Eq. 3.3.8) becomes

$$\frac{S_{cs}}{F'_o} \approx \left[ 1 + \frac{1}{\left(F'_o\right)^2} \right] \qquad (3.3.9)$$

as a more general expression that is approximately valid down to $F'_o \approx 1$ for a wide range of aspect ratios, $0.1 < A < 2$ (Jirka, Adams, and Stolzenbach 1981). In general, the complete situation of low Froude number surface jets ($F'_o < 3$) with arbitrary aspect ratios may be examined with appropriate mathematical models (e.g., Stolzenbach and Harleman 1971; Shirazi and Davis 1974), but with the additional caution that the fluid mechanical aspects in this range of strong buoyancy effects are, in fact, poorly understood and, hence, inadequately modeled.

### 3.3.2 Effects of Shallow Receiving Water

If the depth of the receiving water is small enough to interfere significantly with the inflow required for entrainment or if the depth is less than the maximum jet penetration depth ($h_{max}$), the jet mixing capacity is adversely affected. Examination of data (Jirka, Adams, and Stolzenbach 1981) has shown that the effect of limited depth is felt if

$$\frac{h_{max}}{H} > 0.75 \qquad (3.3.10)$$

which provides a definition of shallow-water conditions. Note that with Eq. 3.3.5 this condition can be expressed alternatively as

$$\frac{H}{L_o F'_o} < 0.56 \qquad \text{or} \qquad \frac{H}{\ell_M} < 0.47 \qquad (3.3.11)$$

In the absence of a crossflow, the most noticeable consequence of shallow-water conditions is a reduction of the centerline dilution by a factor of approximately

$$r_s = \left(\frac{0.75}{h_{max}/H}\right)^{0.75} \quad \text{for} \quad \frac{h_{max}}{H} > 0.75 \qquad (3.3.12)$$

Thus, if the centerline dilution under shallow-water conditions is required, one can simply multiply the deep-water dilution $S_c$ plotted in Figure 20 or its stable value $S_{cs}$ (Eq. 3.3.8) by the reduction factor $r_s$.

### 3.3.3 Buoyant Surface Jet in Ambient Crossflow

a. Basic Features. The behavior of surface jets in crossflows is again strongly dependent upon the depth of the receiving water. If deep-water conditions prevail, the crossflow causes a bent-over trajectory by virtue of the usual deflecting mechanisms, the drag force, and the force that arises from the entrainment of ambient momentum. Typically, buoyant surface jets in crossflows do not have a transition with a stable limiting dilution.

In shallow receiving water, where the buoyant jet occupies a portion or all of the available depth, the crossflow has even stronger effects. The ambient flow is blocked by the jet, leading to much stronger deflection and to limitation of the entrainment on the downstream side. Eventually, the jet becomes partially attached to the shoreline, and recirculation results with a buildup of effluent concentrations and reduced dilutions. This difference between free and shoreline-attached jets is shown in Figure 21.

A criterion for shoreline attachment has been presented in Jirka, Adams, and Stolzenbach (1981):

$$R \left(\frac{h_{max}}{H}\right)^{3/2} > 0.05 \qquad (3.3.13)$$

where $h_{max}$ is given by Eq. 3.3.5. Thus, cases with strong crossflow (large $R = u_a/U_o$) and shallow water (large $h_{max}/H$) are highly prone to attach to the shoreline.
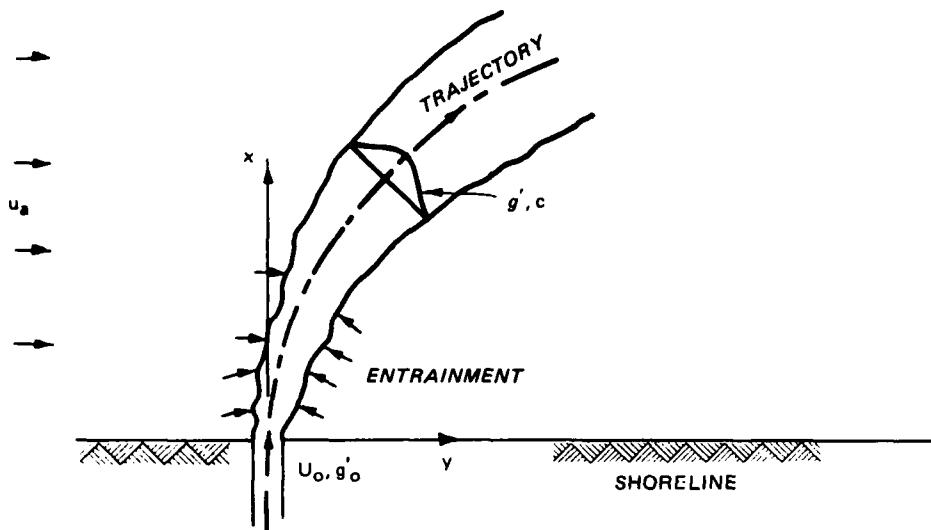
a. Nonattached (free) jet
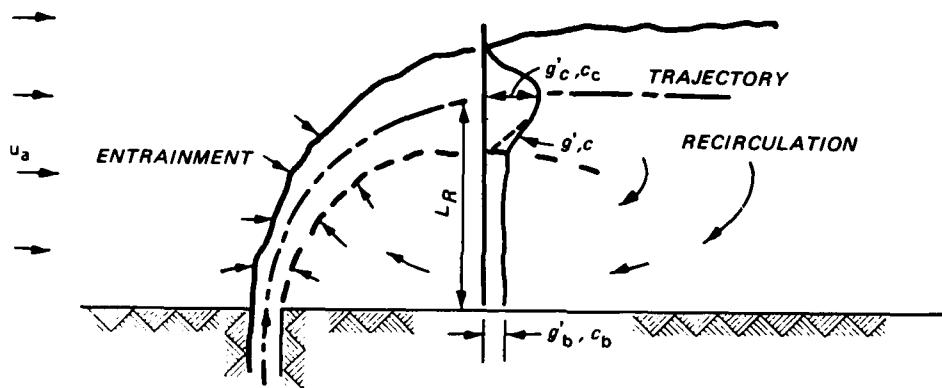


b. Shoreline-attached jet

Figure 21. Two modes of behavior of buoyant surface jets in
ambient crossflows

b. Nonattached (free) jets. The trajectories of buoyant sur-
face jets become highly complicated as they are affected by a multitude
of parameters ($F_o'$, R, $h_{max}/H$) or, alternatively, a multitude of length
scales. Jirka, Adams, and Stolzenbach (1981) argued that the trajec-
tory laws should, in first order, be similar to those for a pure momen-
tum jet in a crossflow (Figure 8) since it is the initial momentum that
pushes the jet offshore. There is some support for this argument if
buoyant jet data are plotted according to these laws, as is done in

83

Figure 22. (Note the change in the notation for the axes; see also
Figure 21.) However, there is also a clear dependence upon the param-
eter $F_o'R$ which is equal to the length scale ratio $2^{1/4}\ell_M/\ell_{Mu}$ , where
$\ell_{Mu}$ is defined as $\sqrt{2}\,L_o/R$ for the surface jet case. Jets with
strong buoyancy (small $F_o'R$ ) are seen to penetrate further into the
crossflow. This effect is presumably due to the decrease of both drag
and entrainment forces as the buoyant jet flattens out rapidly.
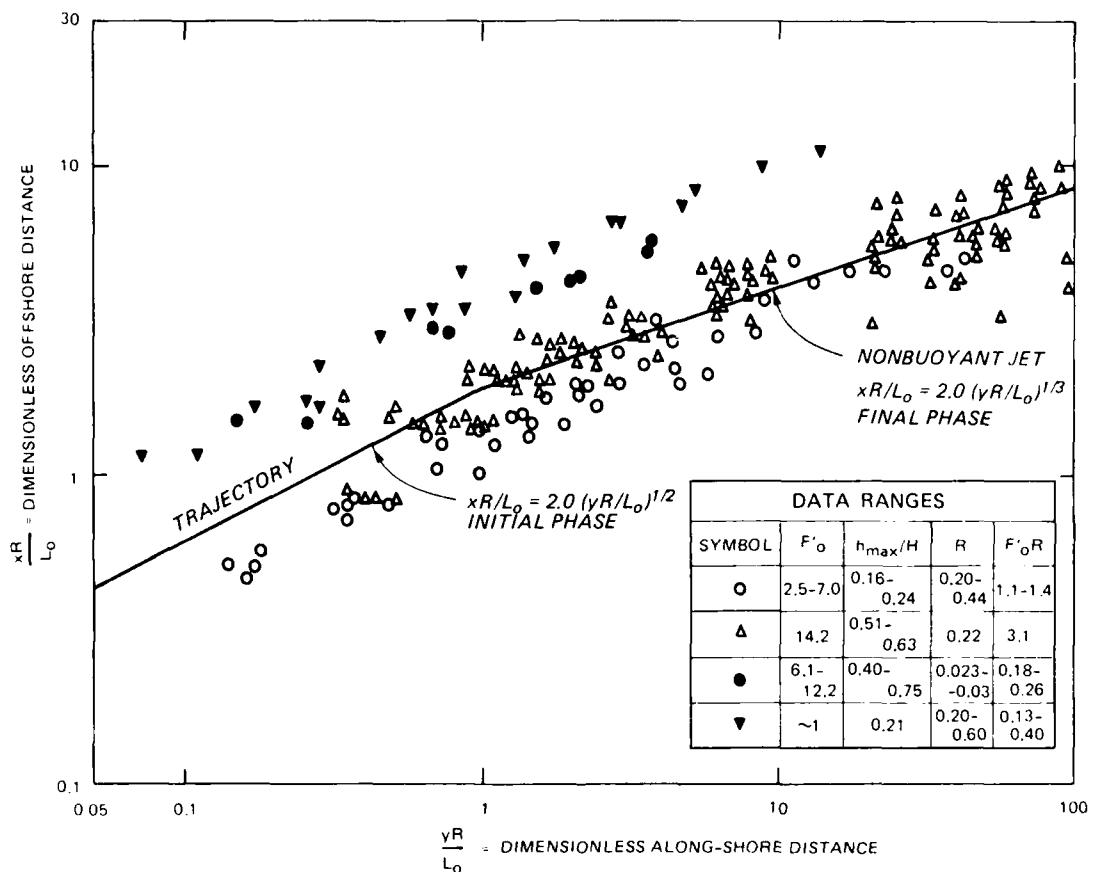


Figure 22. Nondimensional trajectories of buoyant surface jets in
crossflows

The situation is less clear as regards the mixing characteris-
tics (centerline dilutions) for buoyant jets in crossflow. It appears
that a single unique dilution plot can no longer be valid because of
the several parameter combinations. It is at this point that actual
surface buoyant jet models or resulting design nomograms have to be

84

consulted (e.g., Stolzenbach and Harleman 1971, Shirazi and Davis 1974).

c. Shoreline-attached jets. Near-field mixing is even more complex for shoreline-attached jets. Detailed studies (Adams, Stolzenbach, and Harleman 1975) indicate that the near-field mixing is considerably lower than for free jets. Depending upon the degree of blocking, the degree of reentrainment of already mixed effluent water may be up to 100 percent so that the surface jet entrains ambient undiluted water from only one side. Thus, for conservative purposes, the dilution of attached jets can be estimated as 50 percent of that of nonattached jets. Also, the width $L_R$ of the recirculating zone (Figure 21b) may be approximated from the jet-crossflow length scale

$$L_R \approx \ell_{Mu} \qquad\qquad (3.3.14)$$

with the definition of $\ell_{Mu}$ discussed in the preceding paragraph.

## 3.4  DISCHARGE-INDUCED STRATIFIED FLOW

### 3.4.1  Introduction

The near-field mixing induced by the three basic continuous discharge geometries (the submerged single-port discharge, the submerged multiport diffuser, and the surface discharge) is analyzed in the preceding sections. These analyses show that the near-field mixing is strong if there are large initial momentum fluxes (i.e. large densimetric Froude numbers). On the other hand, due to the stabilizing effect of the buoyancy flux or due to a limited receiving water geometry, there is always a definite limit on the achievable mixing.

If the amount of near-field mixing is denoted by an overall dilution ratio S , as estimated by the preceding analyses for each specific situation, the water that leaves the initial mixing zone may have a residual density difference $\Delta\rho$ :

$$\Delta\rho = \rho_a - \rho = \frac{\Delta\rho_o}{S} \qquad (3.4.1)$$

where $\Delta\rho_o$ is the initial discharge density difference. The density difference at the end of the initial mixing zone has an associated buoyant acceleration

$$g' = \frac{\Delta\rho}{\rho_a} g \qquad (3.4.2)$$

Thus, there is the possibility that, outside of the near-field mixing zone, this acceleration will produce additional motion (or stratified flow) relative to the undisturbed ambient flow. Obviously, the character of the motion induced by $g'$ depends heavily on the ambient geometry and flow field. In the following, only a few special (yet common) situations are discussed. There are numerous other situations that may arise and may require special analysis and consultation of the relevant literature. It must be stressed that the stratified flow does not contribute any significant amount of additional effective mixing, but rather causes a redistribution of the effluent in the receiving water.

The importance of the motion induced by $g'$ is in direct relation to the amount of the discharge flow. The motion is most important for large effluents, such as cooling water from thermal power plants, for which the stratified flow may effect a redistribution of the mixed effluent over large distances.

### 3.4.2 Arrested Wedges

Figure 23 presents a schematic illustration of one situation in which stratified flow is induced by the interaction of the ambient flow and the mixed discharge. The near-field is indicated by the cross-hatched region whose dimensions may be estimated from the relationships given in the earlier sections. As indicated in the plan view in the figure, the near-field may extend across the whole river width or may

86

SURFACE WEDGE
$L_i$

AMBIENT
$q_a$

$\Delta\rho$

$\tau_i$

$q$

$\Delta\rho$

$H(x)$

AMBIENT

POSSIBLE
INCREASING
DEPTH $H(x)$

BOTTOM WEDGE

ELEVATION VIEW

NEAR-FIELD
MIXING ZONE
(SUBMERGED OR
SURFACE DISCHARGE)

$q_a$

SURFACE
WEDGE
FRONT

BOTTOM
WEDGE
FRONT

x

(ENTIRE RIVER WIDTH
OR LATERAL SECTION)

PLAN VIEW
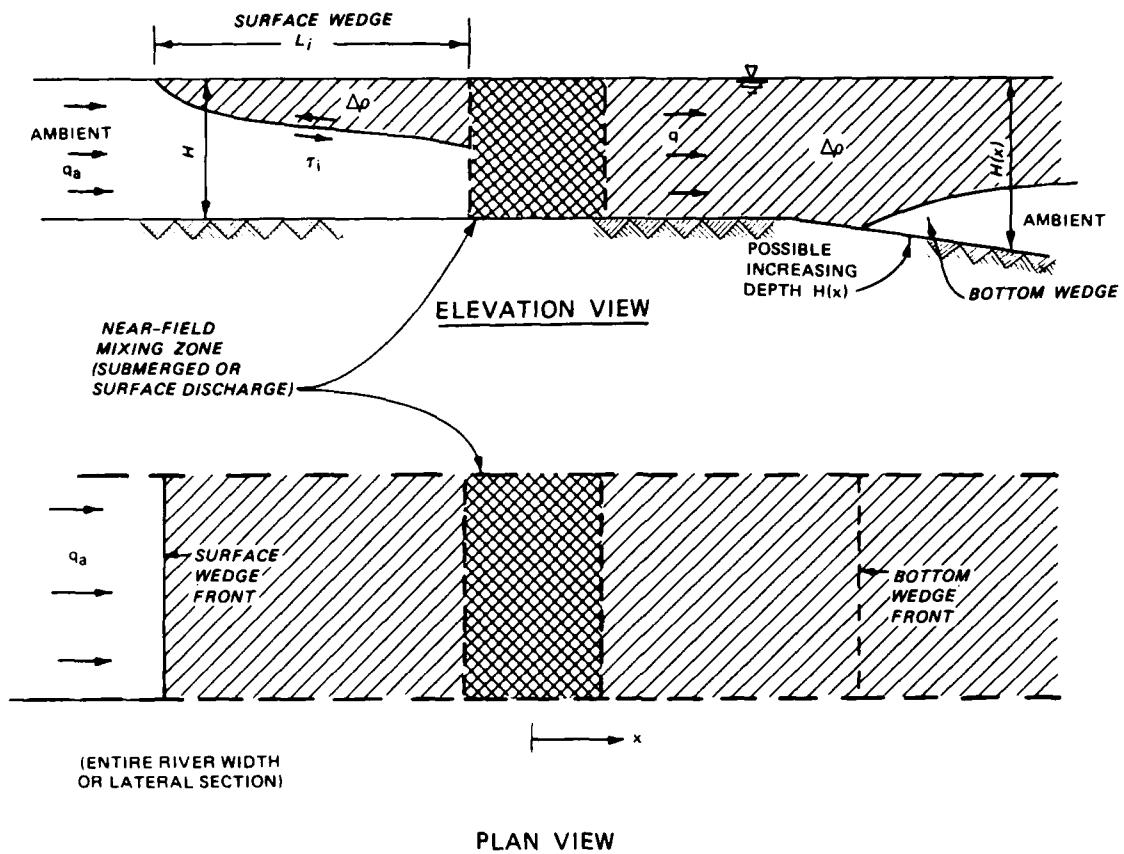
Figure 23.  Schematic diagram for wedge intrusions formed by a buoyant
discharge in riverine situations

occupy only a certain portion (e.g. given by the diffuser length in
Figure 18).

Two examples of stratified flow are shown in Figure 23 namely, a
surface wedge (or underflow) and a bottom wedge (or overflow), in an
ambient flow which is characterized by a discharge per unit width of
$q_a$  (= $u_a H$).  The surface wedge results from the buoyant acceleration
g' causing an intrusion of part of the mixed discharge upstream
against the ambient flow.  The upstream motion is opposed by pressure
forces from the ambient flow passing under the wedge and by frictional
forces, represented by an interfacial shear stress (Figure 23)

87

$$\tau_i = \rho_a \frac{f_i}{8} (\Delta u)^2 \qquad (3.4.3)$$

where $\Delta u$ is the local velocity difference across the interface be-
tween the two layers and $f_i$ is a Darcy-Weisbach interfacial friction
factor. For steady-state conditions, there is internal circulation but
no net flow in the arrested wedge.

In an analogous fashion, a bottom wedge may form downstream as
the mixed discharge rises and the more dense ambient fluid intrudes
under the wedge. Even though the initial mixing region may be calcu-
lated to extend only partially across the river, the buoyant accelera-
tions would generally be expected to spread the mixed discharge across
the full width of the river surface if they are sufficient to cause
wedges to develop. Also, the bottom wedge can form in rivers only if
the initial mixing region does not extend across the full width of the
river; otherwise, there would be no source of ambient water to intrude
under the mixed discharge.

There are numerous possible variations to the situation depicted
in Figure 23. For example, both wedges may be absent (expelled), or
the downstream wedge may intrude all the way to the near-field mixing
zone (thereby supplying downstream water for the near-field mixing), or
the downstream zone may be made up of co-flowing upper (mixed) and lower
(ambient) layers. The prediction of any particular situation depends
on the ambient geometry and requires the techniques of two-layer stra-
tified flow theory (e.g. Harleman 1961; Jirka, Abraham, and Harleman
1975). Only a few fundamental results of that theory are given below.

a. Criterion for stratified-flow intrusions. A wedge driven by
the buoyancy $g'$ can intrude against the ambient flow only if the
densimetric Froude number is less than some critical value (C), i.e. if

$$\frac{u_a}{\sqrt{|g'|H}} = \frac{q_a}{\sqrt{|g'|H^3}} < C \qquad (3.4.4)$$

88

The absolute value of $g'$ is used since Eq. 3.4.4 applies both to the surface wedge ($g' > 0$) and to the bottom wedge ($g' < 0$). Theoretical analysis gives $C = 1$. However, in practice $C$ is on the order of 0.6 to 0.7.

Referring to the downstream section of Figure 23, Eq. 3.4.4 may be used in inverted form to estimate the local depth $H(x)$ which marks the intrusion point, i.e.,

$$H(x) = \left( \frac{|g'| C^2}{q^2} \right)^{1/3} \qquad (3.4.5)$$

where $q$ designates the mixed downstream flow rate.

b. __Estimates of intrusion lengths.__ If Eq. 3.4.4 is satisfied so that an intrusion takes place, the steady-state wedge shape and length $L_i$ are governed by a balance of buoyant, inertial, pressure, and frictional forces. Normalized solutions for intrusion lengths in a channel with a horizontal bottom (constant $H$ and negligible bottom slope) are plotted in Figure 24a for surface wedges and Figure 24b for bottom wedges. The surface wedge length depends both on the interfacial friction factor ($f_i$) and the channel bottom friction factor ($f_o$). For field conditions, $f_i$ is typically in the range of 0.005 to 0.01 and the ratio $f_i/f_o$ in the range 0.5 to 1.0. For the bottom wedge, the solution depends only on $f_i$ if there is no net flow in the wedge. In both cases, a smaller Froude number (a smaller ambient flow rate or increased buoyancy) gives a longer wedge length.

It is also of interest to note that wedges can originate at critical flow sections where strong changes in the flow geometry take place. This may be the edge of a near-field mixing section (Figure 23) or the exit section into a large reservoir or water body, as sketched in Figure 24. Two-layer stratified flows are dynamically similar to (one-layer) open-channel flow, and the role and existence of critical flow sections are also analogous. (For more details, see Jirka, Abraham, and Harleman 1975.)
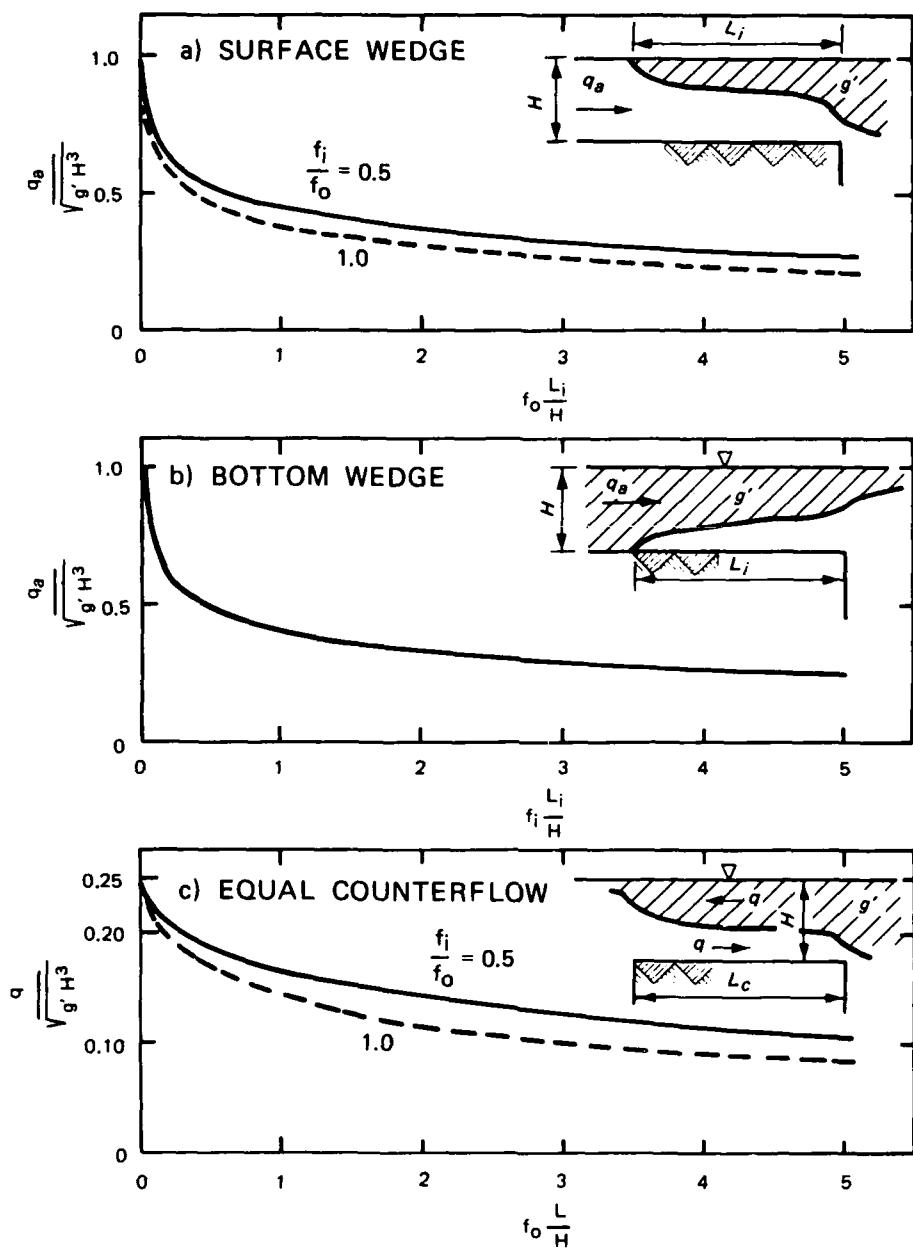
Figure 24.   Nondimensional solutions for stratified flow
intrusions and counterflows

## 3.4.3  Stratified Counterflow

Occasionally, a buoyant effluent may be discharged into an arti-
ficial lagoon or natural cove with the purpose of premixing it with the
ambient water before discharging it into a river or reservoir

90

(Figure 25). If the cove is connected to the main water body by a channel or constricted flow region, the amount of premixing that can be achieved may be limited by the stratified flow condition in the channel. At steady state, if the dilution is reasonably large so that the ambient inflow is much larger than the initial discharge flow rate $Q_o$ , equal amounts of ambient inflow and mixed outflow must pass through the channel. The dynamics of this stratified counterflow are again governed by a balance of buoyant, inertial, pressure, and frictional forces, and the flow will be bounded by critical sections at both ends of the channel.



PLAN VIEW

ELEVATION VIEW
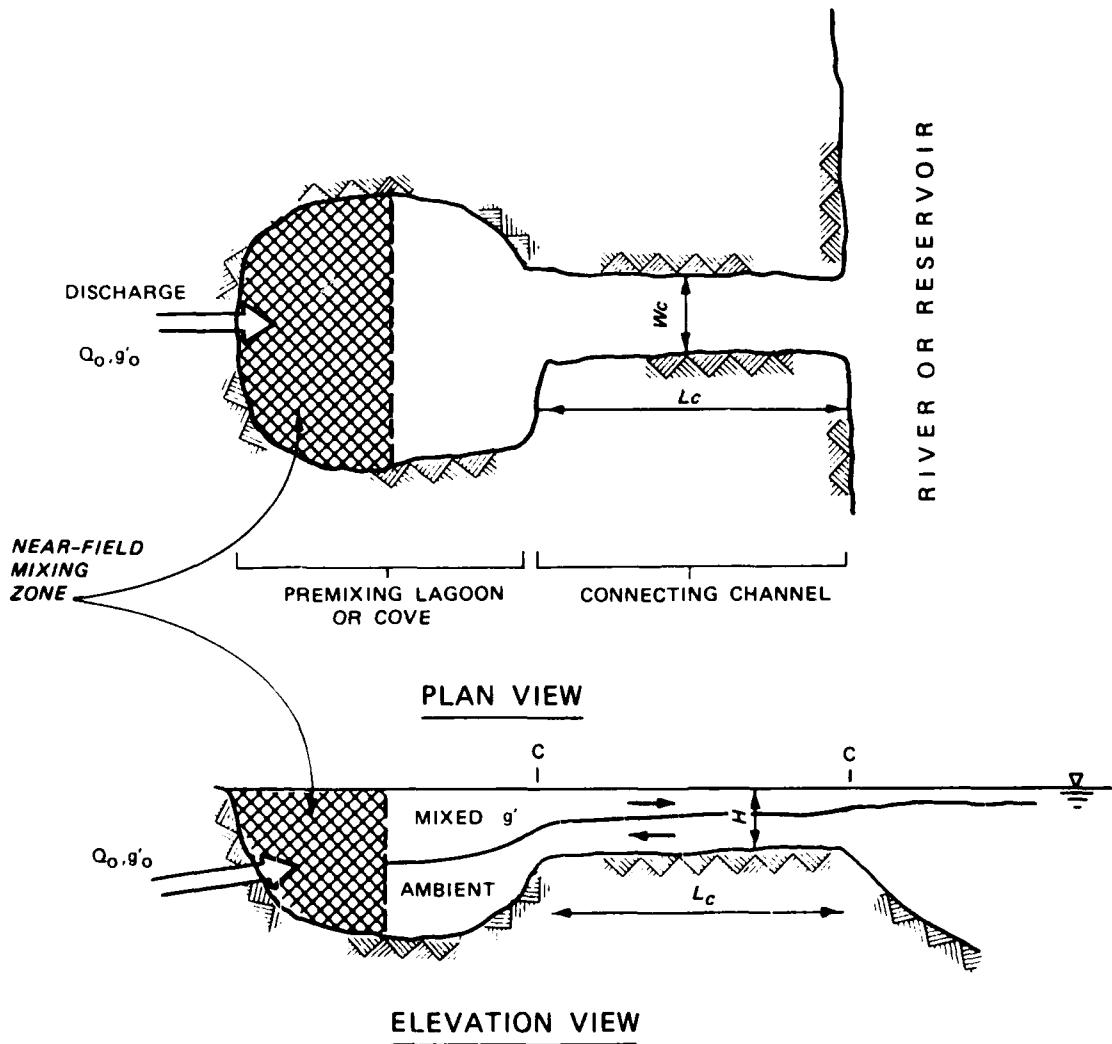
Figure 25. Stratified counterflow as a limit on near-field mixing

91

A solution diagram for the counterflow densimetric Froude number $q/(g'H^3)^{1/2}$ , where q is the flow rate per unit width in each layer, as a function of nondimensional channel length $f_o L_o/H$ is given in Figure 24c. Significantly, a maximum Froude number of 1/4 exists for zero channel length, i.e., a short opening between two reservoirs of different density water with equal discharges in the two layers. For any other channel length, there is a definite Froude number (say $F_c$ ), as given in the figure.

The maximum possible near-field dilution $S_{max}$ in this situation is computed by using the buoyancy ($g' = g_o'/S_{max}$) and the flow rate per unit width ($q = Q_o S_{max}/W_c$ where $Q_o$ and $g_o'$ are the initial discharge flow rate and buoyancy and $W_c$ is the channel width). Using the definition of $F_c$ , $S_{max}$ can be obtained as

$$S_{max} = F_c^{2/3}\left(\frac{g_o' H^3 W_c^2}{Q_o^2}\right)^{1/3} \tag{3.4.6}$$

Even if the near-field discharge within the lagoon or cove were designed to achieve higher dilutions, the stratified flow control represented by Eq. 3.4.6 would limit the mixing processes.

Similar types of analyses may be used to estimate the exchange flow that takes place between two reservoirs where the flow rates in the two layers are not constrained to be the same (Holley and Waddell 1976).

## 3.4.4 Lateral Buoyant Spread

The residual buoyancy of the mixed flow outside the near-field mixing zone can also induce lateral spreading perpendicular to the ambient flow. Such a situation is depicted in Figure 26. The lateral width $b_o$ of the initial mixing zone can usually be estimated from the details of the near-field dynamics, as discussed in the preceding sections. To analyze the spreading of $b(x)$ for the mixed water as it is advected in the downstream direction by the velocity $u_a$ , it can be

92
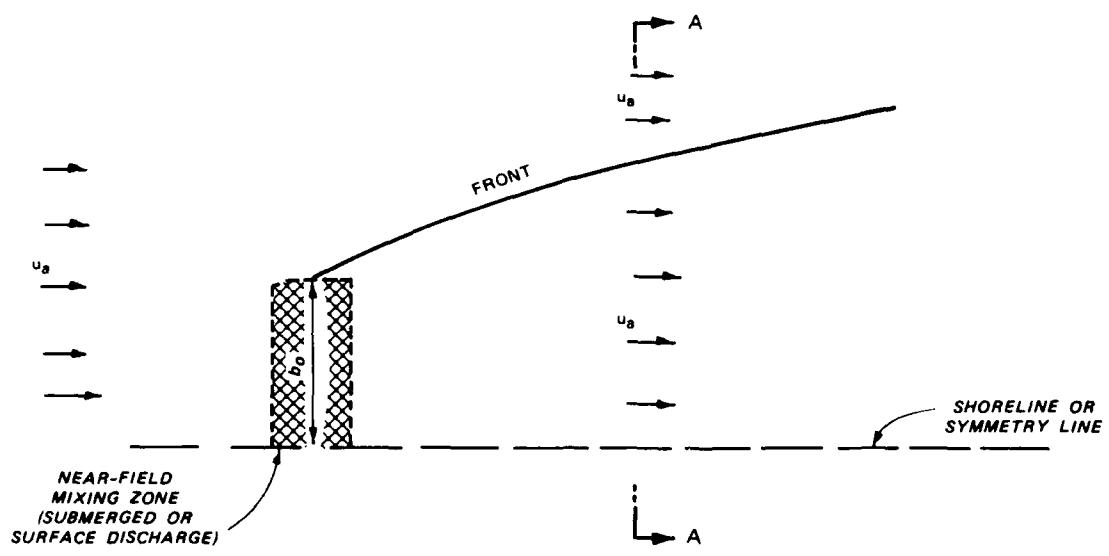
PLAN VIEW
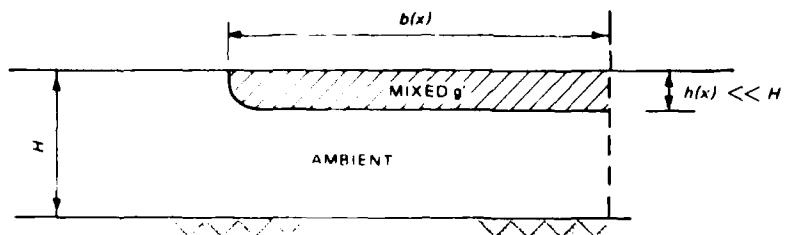


CROSS SECTION A-A

Figure 26. Lateral buoyant spread of mixed discharge in crossflow

assumed that no entrainment takes place so that the buoyancy and dis-
charge within the upper layer are conserved, i.e. $g' = g'_o/S$ = constant
and $Q = Q_o/S = u_a bh$ = constant (Figure 26). Assuming a simple bal-
ance of lateral buoyant forces and inertial accelerations, the spread-
ing relation is given by

$$\frac{b}{b_o} = \left( \frac{3}{2} \frac{x}{b_o} + 1 \right)^{2/3} \qquad (3.4.7)$$

93

while the thickness diminishes so that $h/h_o = b_o/b$ . This two-thirds power law (Eq. 3.4.7), first derived by Larsen and Sorensen (1968), usually gives a reliable estimation of the buoyant spreading even though some degree of turbulent entrainment may, in fact, be present in field situations.

## 3.5 INSTANTANEOUS RELEASES

If a mass of material is released suddenly into the water column at the water surface, either accidentally during a spill or purposely during a mixing experiment, some initial mixing takes place. This mixing is caused by the turbulence that is generated as the mass enters the water. Two force mechanisms can cause this turbulence: the initial impulse $P_o$ and/or the initial buoyant weight $W_o$ of the slug that has a density $\rho_o$ greater than that of the receiving water $\rho_a$ . These forces are quite analogous to the momentum flux and buoyancy flux in the continuous release situations.

The slug is characterized by its initial volume $V_o$ , buoyancy $g_o' = \dfrac{\rho_a - \rho_o}{\rho_a} g < 0$ , vertical velocity $w$ (i.e. the velocity with which it enters the water column), and concentration $c_o$ . An equivalent initial radius can be calculated as $r_o = \left(\dfrac{3}{4\pi} V_o\right)^{1/3}$ . The impulse is $P_o = w_o V_o$ and the buoyant weight is $W_o = -g_o' V_o$ (both in kinematic units). The following solutions given by Scorer (1978) apply.

### 3.5.1 Mixing Caused by Buoyant Weight

Bulk dilution

$$S = \frac{c_o}{c} = \frac{g_o'}{g'} \approx 0.016 \left(\frac{z}{r_o}\right)^3 \qquad \text{for} \quad z > 4r_o \qquad (3.5.1)$$

94
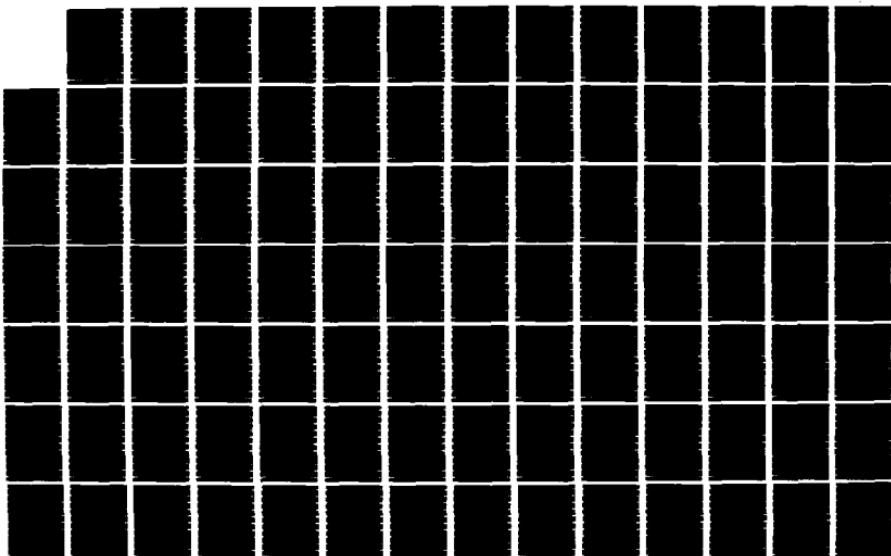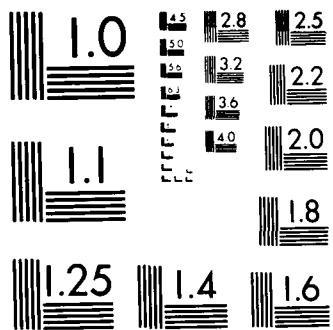
MICROCOPY RESOLUTION TEST CHART

NATIONAL BUREAU OF STANDARDS-1963-A

Geometry

$$z = 1.66 \, W_o^{1/4} t^{1/2} \, , \quad r = 0.25 \, z \qquad (3.5.2)$$

in which $z$ is the distance from the release level (e.g. water sur-
face), $t$ the time elapsed after release, and $r$ is the radius to
which the slug has grown by turbulent entrainment.

### 3.5.2 Mixing Caused by Initial Impulse

Bulk dilution

$$S \approx 0.016 \left( \frac{z}{r_o} \right)^3 \qquad \text{for} \quad z > 4r_o \qquad (3.5.3)$$

Geometry

$$z = 2.77 \, P_o^{1/4} t^{1/4} \, , \quad r = 0.25z \qquad (3.5.4)$$

Note that the dilution and the slug size as a function of depth
are the same in both cases; the rate of penetration, however, is quite
different. These equations may be used, for example, to arrive at an
estimate for the initial mixing caused over the total depth of a river,
$z = H$ . In case of a release with both $W_o$ and $P_o$ , it may be advis-
able for initial estimation purposes to compute the dilutions as a
function of time with both methods and to adopt the larger value. In
many cases, these will be the ones associated with the buoyancy-
enhanced dilution. Alternatively, the complete set of equations of
motion for an accelerating turbulent slug may be derived and solved
with the above information on growth rates, in a fashion analogous to
the procedure that was used for buoyant jets.

If the mass is released at the water surface with positive
buoyancy ($g_o' > 0$) and it has no impulse, the initial mixing may be

totally inhibited due to the damping of turbulence by the buoyancy. The slug will then simply spread along the water surface until it is affected by ambient diffusion.

Other release geometries (e.g. two-dimensional) are considered by Scorer (1978) as well. In many cases, however, it may be difficult to give precise estimates of the initial mixing of instantaneous releases, considering also the fact that the actual release is never quite instantaneous but may take place over a time period $\Delta t_o$. If primary interest is in the effluent dilution at large downstream distances where ambient diffusion has affected the released mass, then parametric calculations will show in most cases that the exact degree of initial mixing for instantaneous or short duration slug releases is of no great consequence.

CHAPTER 4.  DIFFERENTIAL EQUATIONS REPRESENTING
HYDRAULIC TRANSPORT PROCESSES

## 4.1  INTRODUCTION

### 4.1.1  Mass Balance Equations

The calculation of concentration distributions, whether done analytically or numerically, is useful both as a qualitative aid to visualizing the way in which pollutants are transported in rivers and as a means of making quantitative predictions of expected concentrations.  In performing these calculations, there are various levels of approximations ranging from three-dimensional numerical solutions, which can give concentration variations in all three spatial dimensions as well as in time for unsteady situations, to one-dimensional solutions.  Most present-day calculations proceed from some form of a differential equation which represents the mass conservation or mass balance of the pollutant.  The various terms in the differential equation represent the processes (hydraulic transport, reactions, etc.) which influence the concentration.  A general understanding of the terms in the differential mass balance equations is essential in order to have an appreciation for the way in which the hydraulics of a river are being represented in the calculations.  For example, the number of spatial dimensions included in a mathematical representation or model places a limit on the detail to which the velocity variations can be included and this limit, in turn, has strong implications on what must be represented in the diffusion or mixing terms and their associated coefficients.  These aspects of mathematical representations are discussed in more detail in the following sections in connection with the various forms of the differential mass balance equations, but some general comments are made in Section 4.2.2 about the relationship between advection and diffusion.

As an alternate to using differential mass-balance equations, a random-walk approach is sometimes taken.  This alternate approach, which is not widely used in engineering calculations, will be discussed

97

brie⸱⸱y in Chapter 6, where some results from the calculations are presented.

### 4.1.2 Boundary Conditions

Calculated concentrations ⸱⸱pend not only on the form of the differential mass balance equation, but also on the boundary conditions which are used to represent the effluent release or loading into the river. The boundary conditions are used to represent both the spatial and the temporal distributions of the effluent loading. In principle, it is possible to calculate concentrations (at least numerically) for almost any conceivable set of boundary (or release) conditions; frequently-used conditions correspond to the approximations of a continuous (and constant) effluent discharge rate or an instantaneous (or slug) release.

Most mathematical models for pollutant transport associated with natural river flow assume that steady flow exists in the river and that there are no density variations due either to natural causes or to effluent releases. (The effects of effluents with a different density from the river water are considered in Chapters 2 and 3.)

### 4.1.3 Major References

The mathematical development of the various forms of the differential mass balance equations in the remainder of this chapter follows very closely the development presented by Yotsukura (1977). Although that publication is not copyrighted and thus can be used and quoted extensively, the authors want to emphasize that much of this chapter is taken directly from Yotsukura's work. The parts taken verbatim from Yotsukura's paper are indicated by quotation marks. Equation and figure numbers have been changed to be consistent with this presentation, some of the notation has been changed, and "advection" was substituted for "convection." Yotsukura's derivations were done for conservative substances, but possible first-order reaction and transfer across the water surface and streambed have been included in this presentation. Some parts of the following derivations include rather detailed

98

mathematics because it is felt that the mathematics are needed for an understanding of the approximations and conditions applicable for each type of mass balance equation. The mathematical developments are preceded by physical interpretations and explanations of the processes being represented. Some of the physical interpretations follow a previous paper by Holley (1969).

## 4.2 GENERAL MASS BALANCE CONSIDERATIONS

### 4.2.1 General Approach

Differential mass balance equations, which are used as a basis for calculating concentration distributions, are normally developed for an infinitesimal or incremental control volume (CV). For this CV, mass balance states that the time rate of change (increase) of the mass of the pollutant in the CV must be equal to the net rate of influx of mass through all sides of the CV minus any decay of the mass inside the CV. In writing the general equation, rate of change and flux terms are written as positive quantities, but it is understood that any of them may be negative in a specific problem so that a negative rate of increase implies a decrease, a negative influx implies an efflux, and a negative decay implies a production. The hydraulics of the river flow are represented in the flux terms for the sides of the CV. The two types of flux which are considered are advective flux, i.e. movement of the pollutant associated with the water flow velocity, and diffusive or dispersive flux, i.e. mixing of the pollutant relative to the advective movement of the water. The actual mechanisms represented in the mixing terms depend strongly on the degree of resolution used in representing the actual, physical advective pattern in the advective terms in the differential equation.

For these developments related to ambient transport, it is assumed that the solute is neutrally buoyant so that it does not rise or sink due to gravity and so that the transport of the solute can be described using just the motion of the water.

"The three-, two-, and one-dimensional equations for turbulent-flow transport will be derived in sequence, starting from the

99

three-dimensional equations for instantaneous mass balance of water and
a solute. Time- and space-averagings are performed rigorously uti-
lizing Leibnitz's rule for reversing the order of integration and dif-
ferentiation, Reynolds' averaging rules, and necessary boundary condi-
tions (Leendertse 1970, Holley 1971). The procedure is devoid of such
assumptions as uniform distribution of solute concentration, stationary
flow boundaries, and steadiness or uniformity of flow, which are often
required in conventional derivations of transport equations. On the
other hand, each averaging process produces a covariance between the
deviations of concentration and velocity from their averaged values.
It is shown that an aggregate expression for the covariance, variously
called mixing, dispersion, and diffusion, is where major assumptions
and approximations are introduced into the advective-diffusion equa-
tion, which is otherwise exact. These covariances are expressed in
gradient-type flux forms following Boussinesq's and Taylor's phenomeno-
logical models (Hinze 1959, Taylor 1954).

"Various phases of the derivation have been reported in some of
the above references as well as in other recent papers (Sayre and Yeh
1973, Yotsukura and Sayre 1976). The only new aspect of the present
report is concerned with the one-dimensional equations. The entire
derivation, however, is documented in the present report as it should
prove useful and as it appears nowhere else in the literature."

4.2.2 Relationship Between Advection and Diffusion

Since a solute is dissolved in the water in a river, the solute
moves where the water moves, except for molecular diffusion which nor-
mally provides a negligible part of the total transport for rivers.
Thus, essentially all of the transport is advective flux or advection,
which is defined as the solute flux or transport associated with the
flow velocity. However, as will be seen in Sections 4.5-4.8, different
approximations for the advective transport are used in different equa-
tions. The difference between the actual advection and that in a
mathematical representation usually goes into a diffusive-type term.
Thus, the detail used in representing the advection dictates what type

100

of diffusive terms must be included in the mass balance equation. When less detail or resolution is used in the advective term(s), more of the transport is relegated to diffusive-type terms.

## 4.3  MATHEMATICAL TOOLS

### 4.3.1  Taylor Series

In deriving the differential mass balance equations, use is made of a Taylor series expansion of a function, say $\phi(p,q)$, which states that the value of $\phi$ at $p_2$ is related to $\phi$ at $p_1$ if $q$ is held constant, as follows:

$$\phi(p_2,q) = \phi(p_1,q) + \frac{\partial \phi}{\partial p} \Delta p + \frac{1}{2!} \frac{\partial^2 \phi}{\partial p^2} (\Delta p)^2$$

$$\tag{4.3.1}$$

$$+ \frac{1}{3!} \frac{\partial^3 \phi}{\partial p^3} (\Delta p)^3 + \dots$$

where all of the derivatives are evaluated at $p_1$ and $\Delta p = p_2 - p_1$. For very small $p$, all of the higher-order terms become negligible so that Eq. 4.3.1 reduces to

$$\phi(p_2,q) = \phi(p_1,q) + \frac{\partial \phi}{\partial p} \Delta p \tag{4.3.2}$$

which just states that, for small $\Delta p$, $\phi$ at $p_2$ is given by $\phi$ at $p_1$ plus the gradient or slope of a $\phi$ versus $p$ curve times the interval length $\Delta p$. Eq. 4.3.2 is used later with $\phi$ being various mass transport terms.

### 4.3.2  Leibnitz's Rule

"In carrying out the integration of equations with respect to time or space" as is required in the derivations to obtain the various forms of the mass balance equations, "Leibnitz's rule for reversing the order of integration and differentiation is frequently used. If $\phi$ is

101

a function of independent variables $p$ and $q$, and $\alpha$ and $\beta$ are parameters depending on $q$, this rule is written (Korn and Korn 1961) as follows:

$$\int_{\alpha(q)}^{\beta(q)} \frac{\partial}{\partial q} \phi(p,q)dp = \frac{\partial}{\partial q} \int_{\alpha(q)}^{\beta(q)} \phi(p,q)dp$$

$$- \phi(\beta,q) \frac{\partial \beta}{\partial q} + \phi(\alpha,q) \frac{\partial \alpha}{\partial q}$$

(4.3.3)

### 4.3.3 Reynolds' Rules

"In handling time or space averages of a quantity and its deviations from the averages, Reynolds' operational rules will be used frequently. For functions $\phi$ and $\psi$, the averages" with respect to time or vertical and/or transverse distance "are denoted by $\bar{\phi}$ and $\bar{\psi}$ and deviations from the averages by $\phi'$ and $\psi'$ so that, e.g., $\phi = \bar{\phi} + \phi'$. The following operational rules are generally valid for turbulent-flow analysis (Monin and Yaglom 1973):

$$\overline{\phi'} = 0 \tag{4.3.4}$$

$$\overline{\phi + \psi} = \bar{\phi} + \bar{\psi} \tag{4.3.5}$$

$$\overline{\bar{\phi}\,\bar{\psi}} = \bar{\phi}\,\bar{\psi} \tag{4.3.6}$$

$$\overline{\phi\psi} = \bar{\phi}\,\bar{\psi} + \overline{\phi'\psi'} \tag{4.3.7}$$

$$\overline{\frac{\partial \phi}{\partial x}} = \frac{\partial \bar{\phi}}{\partial x} \tag{4.3.8}$$

102

"In the following development, overbar and prime notations will be specified independently in each section to indicate whether they pertain to time-averaged, depth-averaged, or cross-section-averaged quantities. Since each section involves only one mode of averaging, notational conflicts are thereby averted."

### 4.3.4 Coordinate Transformations

Consider a variable $\phi$, which is a function of one set of coordinates, e.g. $\phi = \phi(a_1, a_2, a_3)$. It is desired to transform $\phi$ and its derivatives to another set of coordinates, e.g., $b_1$, $b_2$, $b_3$ so that $\phi = \phi(b_1, b_2, b_3)$. Since $b_1$, $b_2$, $b_3$ represent the same mathematical domain as $a_1$, $a_2$, $a_3$, there is some relation between the two sets of variables so that

$$b_i = b_i(a_1, a_2, a_3) , \quad i = 1, 2, 3 \tag{4.3.9}$$

Then, the first derivatives are related by

$$\frac{\partial \phi}{\partial a_i} = \frac{\partial \phi}{\partial b_1} \frac{\partial b_1}{\partial a_i} + \frac{\partial \phi}{\partial b_2} \frac{\partial b_2}{\partial a_i} + \frac{\partial \phi}{\partial b_3} \frac{\partial b_3}{\partial a_i} , \quad i = 1, 2, 3 \tag{4.3.10}$$

Eqs. 4.3.9 and 4.3.10 are both actually three equations with one equation being generated for each value of $i$.

### 4.4 NATURAL COORDINATE SYSTEM

"Use is made of an orthogonal curvilinear (natural) coordinate system, in which the longitudinal coordinate axis approximately follows the meandering longitudinal direction of a channel flow (Chang 1971, Fukuoka and Sayre 1973). This coordinate system is adopted in order to define quantities such as velocity and discharge in a manner consistent with the characteristics of a nonuniform flow, but, more importantly,

in order to utilize the scalar diffusivity concept properly in such a flow (Hinze 1959, Dagan, 1969, Fischer 1973)." The presentation also refers to simplified forms of the coordinate system as frequently used in engineering calculations.

"An orthogonal curvilinear coordinate system, hereinafter called the natural coordinate system, is illustrated in Figure 27 (Chang 1971, Fukuoka and Sayre 1973). The system is composed of three mutually
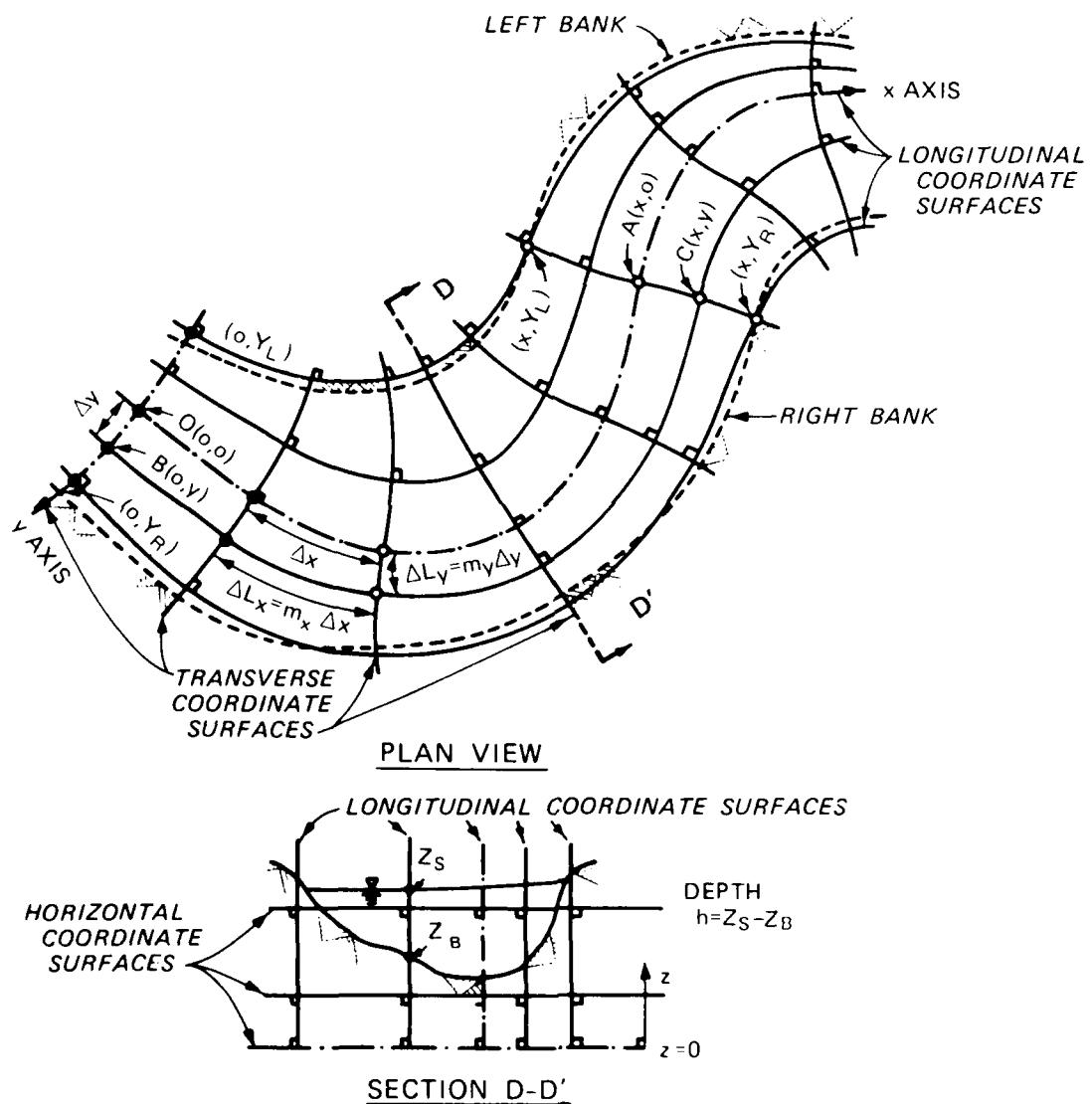


Figure 27. Orthogonal curvilinear (natural) coordinate
system for a river (after Yotsukura 1977)

104

orthogonal sets of coordinate surfaces, which may be called longitudinal, transverse, and horizontal coordinate surfaces. The longitudinal and transverse coordinate surfaces are vertical, typically curved, and nonparallel. The horizontal coordinate surfaces are all parallel, horizontal planes. For reasons that will become clear later, it is best to aline the longitudinal coordinate surfaces, at least approximately, in the direction of depth-averaged total velocity vectors.

"The origin, O , is located at the intersection point of three specially selected coordinate surfaces, as shown in Figure 27. The x axis is defined as the intersection of the longitudinal and horizontal coordinate surfaces (positive in the downstream direction), the y axis as the intersection of the transverse and horizontal surfaces (positive to the right), and the z axis as the intersection of the longitudinal and transverse surfaces (positive in the upward direction). Again for reasons to be explained later, it is best to locate the x axis in the midstream region of the channel," although in practice the origin is frequently located on one bank. "The x and y coordinates of a point, C , in Figure 27 are defined respectively as the horizontal distance, $L_{OA}$ , along the x axis from point O to point A and $L_{OB}$ along the y axis" from point O to point B. "Therefore, all points on a transverse coordinate surface have a common coordinate value, x , and, similarly, all points on a longitudinal coordinate surface have a common coordinate value, y . Coordinate values for z are measured vertically upward from the x-y plane.

"Due to curvature in channel alinement and (or) variations in width along the channel, horizontal distances measured along different longitudinal (or transverse) coordinate surfaces from one transverse (or longitudinal) coordinate surface to another are generally not equal," i.e., in general, the distances from B to C and from A to C are not equal to $L_{OA}$ and $L_{OB}$ even though $L_{OA}$, $L_{OB}$ are the coordinates of point C. "To take care of this, the metric coefficients, $m_x$ and $m_y$ are introduced to correct for differences between distances along curved coordinate surfaces and those measured along the respective axes. As illustrated in Figure 27, the horizontal distance along the

105

longitudinal coordinate surface from B to C is given by $L_{BC}$ " which is
the integral from 0 to A of $m_x dx$ and the horizontal distance along
the transverse coordinate surface from A to C is given by $L_{AC}$ which
is the integral from 0 to B of $m_y dy$ . In these expressions, x and
therefore dx are measured only along the x axis (from 0 to A) while
L is measured along the coordinate surface. The metric coefficient,
$m_x$ , gives the ratio of the incremental distance, $\Delta L_x$ along the coor-
dinate surface to the incremental distance along $\Delta x$ along the x axis.
Similarly, $m_y$ is the metric coefficient in the y direction. "The
values of $m_x$ and $m_y$ may vary from point to point and" $m_x$ and $m_y$
"are functions of both x and y , except that $m_x = 1$ on the x axis
and $m_y = 1$ on the y axis. Because all horizontal coordinate surfaces
are parallel, the metric coefficient $m_z$ is unity. The present nat-
ural coordinate system is thus based on the assumption that the total
velocity vector everywhere in the channel is predominantly oriented in
the horizontal direction. This is reasonable in most natural channels.
Note also that, if $m_x = m_y = 1$ everywhere, the coordinate system
reduces to a rectangular Cartesian system.

"Differential and integral operations in the natural coordinate
system follow those for a general orthogonal curvilinear coordinate
system (Kaplan 1953). For present purposes, it suffices to remember
that integration or differentiation of a function along a curved coor-
dinate surface is always related to an infinitesimal distance, such as
$dL_x = m_x dx$ or $dL_y = m_y dy$ . Notations $dL_x$ and $dL_y$ , however, will
not be used in the following development."

## 4.5 INSTANTANEOUS BALANCE EQUATIONS

The derivation of differential mass balance equations frequently
begins by applying the previously stated mass balance principle (Sec-
tion 4.2) in mathematical terms to an infinitesimal control volume (CV),
which in this case is at any arbitrary location in the natural coordi-
nate system described in Section 4.4 and is shown in Figure 28.
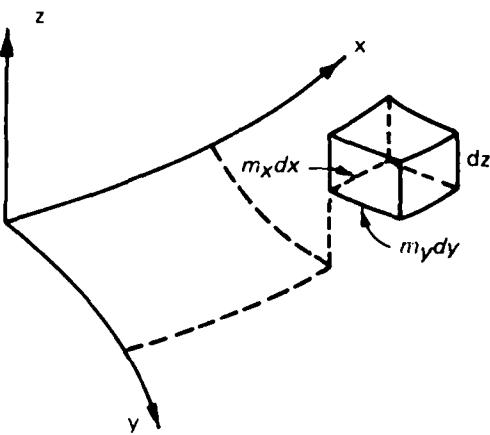
a. Control volume

$$\omega_z(m_xdx)(m_ydy) + \frac{\partial}{\partial z}\left(\omega_z(m_xdx)(m_ydy)\right)dz$$

$$\omega_x(m_ydy)dz \longrightarrow \boxed{dz} \longrightarrow \omega_x(m_ydy)dz + \frac{1}{m_x}\frac{\partial}{\partial x}(\omega_x(m_ydy)dz)m_xdx$$

$$m_xdx$$

$$\omega_z(m_xdx)(m_ydy)$$

b. Components of flux of water through upstream and downstream faces of the control volume

$$-D_m\frac{\partial\theta}{\partial z}(m_xdx)(m_ydy) + \frac{\partial}{\partial z}\left(-D_m\frac{\partial\theta}{\partial z}(m_xdx)(m_ydy)\right)dz$$

$$-\frac{D_m}{m_x}\frac{\partial\theta}{\partial x}(m_ydy)dz \longrightarrow \boxed{dz} \longrightarrow -\frac{D_m}{m_x}\frac{\partial\theta}{\partial x}(m_ydy)dz + \frac{1}{m_x}\frac{\partial}{\partial x}\left(-\frac{D_m}{m_x}\frac{\partial\theta}{\partial x}(m_ydy)dz\right)m_xdx$$

$$m_xdx$$

$$-D_m\frac{\partial\theta}{\partial z}(m_xdx)(m_ydy)$$

c. Components of diffusive flux of solute through upstream and downstream faces of the control volume

Figure 28. Infinitesimal control volume and flux terms in natural curvilinear coordinate system

107

## 4.5.1 Instantaneous Continuity of Water

If the water can be considered to be incompressible, the equation that is normally used is one which gives a balance of the volume of water rather than the mass. This equation is frequently called the continuity equation. For the upstream face of the CV, the area is $(m_y dy)(dz)$ . If $\omega_x, \omega_y, \omega_z$ are the instantaneous components of the velocity vector, then the volumetric flux through the upstream face is $\omega_x (m_y dy)(dz)$ . Letting $\phi$ be this volumetric flux, the volumetric flux through the downstream face is given from Eq. 4.3.2 as the expression shown in Figure 28b. The same procedure can be used to obtain the flux terms in the other two directions. If the water is incompressible, the volume of water in the CV cannot change with time so that at each instant, even for unsteady flow, the sum of the influxes must be zero, i.e., noting that an efflux is a negative influx,

$$
\begin{aligned}
&\omega_x m_y dy dz - \left[ \omega_x m_y dy dz + \frac{1}{m_x} \frac{\partial}{\partial x} \left( \omega_x m_y dy dz \right) m_x dx \right] \\
&+ \omega_y m_x dx dz - \left[ \omega_y m_x dx dz + \frac{1}{m_y} \frac{\partial}{\partial y} \left( \omega_y m_x dx dz \right) m_y dy \right] \quad (4.5.1) \\
&+ \omega_z m_x dx m_y dy - \left[ \omega_z m_x dx m_y dy + \frac{\partial}{\partial z} \left( \omega_z m_x dx m_y dy \right) dz \right] = 0
\end{aligned}
$$

Cancelling terms, recognizing that x , y , and z are independent variables so that dx , dy , and dz may be taken out of the derivatives, and dividing by the volume $(m_x dx)(m_y dy)(dz)$ as the volume approaches zero gives (Kaplan 1953, Chang 1971)

$$
\frac{1}{m_x m_y} \left[ \frac{\partial}{\partial x} \left( m_y \omega_x \right) + \frac{\partial}{\partial y} \left( m_x \omega_y \right) + \frac{\partial}{\partial z} \left( m_x m_y \omega_z \right) \right] = 0 \quad (4.5.2)
$$

## 4.5.2 Molecular Diffusion

The mass balance of the solute being transported can be obtained in a similar fashion except that for the solute both advective and diffusive fluxes must be considered, whereas for the water in Figure 28 and Eqs. 4.5.1 and 4.5.2, only advective flux needs to be considered. The instantaneous solute concentration ($\theta$, mass of solute per unit volume of solution) can, in general, be variable in both space and time.

Even though the part of the mass transport associated with molecular diffusion in rivers is usually small, molecular diffusion is discussed first since this process is included for completeness in the development of the equations and since the other diffusive-type processes and terms have some analogies to molecular diffusion.

For this discussion, and subsequent discussions in Section 4.6, visualize a specific case of transport as illustrated in Figure 29 which shows a side view of the CV in Figure 28. Flow is from left to right with a vertical distribution of the velocity $\omega_x$. A slug of some solute is released at time $t_1$. As the solute moves downstream, it also spreads out, and the maximum concentration in the cloud continually decreases. Along each vertical section through the tracer cloud, there is a distribution of concentration as shown at $t_2$.
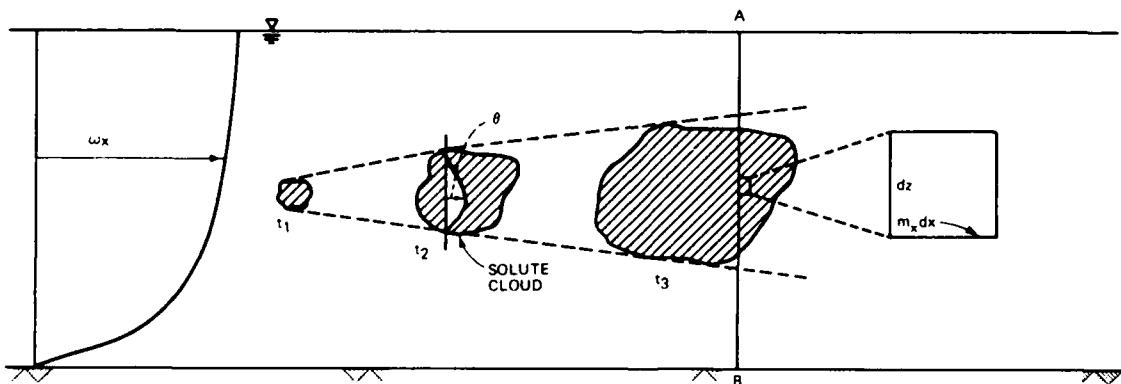


Figure 29. Transport in two-dimensional flow
(from Holley 1969)

109

Consider a case in which the spreading of the solute is due to molecular action. Figure 30 shows the conditions on line AB of Figure 29 at time $t_3$. Along line AB there is a concentration distribution such as that shown in Figure 30a. In effect, the concentration may be viewed as representative of the number of molecules of solute in a given small volume of fluid (for small concentrations). The dashed line in Figure 30b represents the distribution along AB of the fluid velocity $\omega_x$. This is the velocity when the fluid is considered as a continuum. Actually, at any instant, a large number of molecules is distributed along the region of the line AB. Some of the molecules (shown as open circles) are fluid molecules and some (filled circles) are the solute. As indicated by the arrows, the molecules move off in all directions with greatly varying velocities, most of which are much greater than $\omega_x$.

To write the mass balance equation, it is necessary to represent the amount of solute moving through the faces of the CV. One way to do this is to try to represent the motion of the molecules. One then needs to know how many solute molecules pass through the faces and the direction and displacement of each molecule. As time passes, molecules such as those shown along the time axis pass through the left side of the elemental area shown in Figure 30c. This series of molecules also has velocities varying in magnitude and direction. Approaching the representation of the molecular motion itself, even in a statistical manner as in random-walk representations, is often too cumbersome to be practical, although the approach has been used some, mostly in research studies as presented in Section 6.2.3. Engineers commonly use the continuum approach and are satisfied to say that the fluid carries the solute through the faces of the CV at a rate which depends on the concentration $\theta$ and the fluid velocity $\omega$, which is the average of the velocities of the molecules (Bird, Stewart, and Lightfoot 1960). However, the fluid velocity and the associated advective transport cannot completely represent the solute movement because the velocity $\omega$ does not account for the movement of the molecules which have directions and speeds different from $\omega$. This difference between the true molecular

110
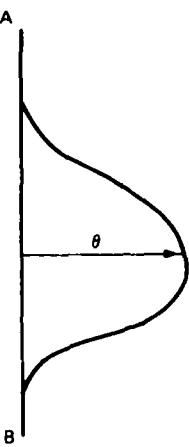
a. Concentration
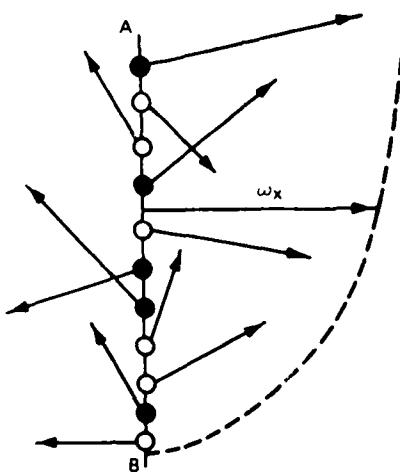
b. Velocity
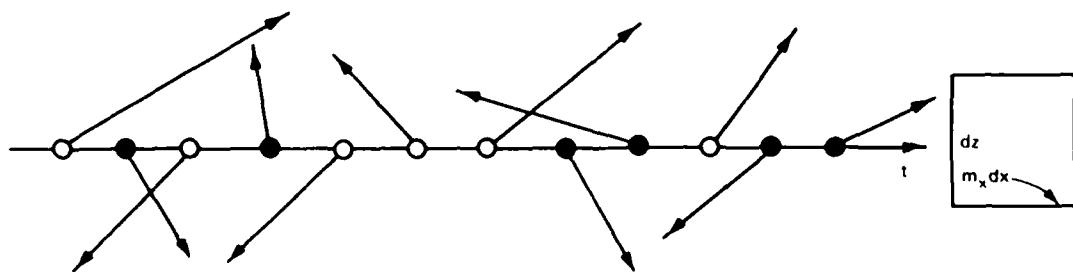
c. Sequence of molecules passing through upstream face

Figure 30. Transport due to molecular action
(from Holley 1969)

motion and the manner chosen to represent the motion (i.e. by $\omega$ ) is accounted for by terms referred to as molecular diffusion. Ficks first law (Bird, Stewart, and Lightfoot 1960) for molecular diffusion states that molecular diffusion is proportional to the concentration gradient. If $D_m$ is the molecular diffusion coefficient, then Ficks Law for the diffusive fluxes of the solute in the x and y directions through the upstream and bottom faces of the CV in Figure 28b are

$$j_x = - \frac{D_m}{m_x} \frac{\partial \theta}{\partial x} (m_y dy dz) \tag{4.5.3}$$

and

$$j_z = - D_m \frac{\partial \theta}{\partial z} (m_x dx m_y dy) \tag{4.5.4}$$

(See Figure 28c.) The diffusive flux terms have a negative sign since the flux, which is proportional to the concentration gradient, is in the direction opposite to the increasing concentration; i.e., regardless of the direction of advection, diffusion moves mass from regions of higher concentration to regions of lower concentration.

### 4.5.3 Instantaneous Mass Balance of Solute

The differential equation for the instantaneous mass balance of solute may be written from the general statement in Section 4.2. The advective flux of the solute can be obtained by multiplying by the velocity components in the various terms in Figure 28 and in Eq. 4.5.1 by $\theta$ since these terms give the rate at which the volume of water is being advected and $\theta$ gives the mass of solute in each unit volume of water. The diffusive flux is given by Eqs. 4.5.3 and 4.5.4 (plus a similar equation for $j_y$ ). See Figure 28c. Then, mass balance gives:

Time rate of increase of mass of solute in CV:

$$\frac{\partial}{\partial t}\left(\theta m_x dx m_y dy dz\right) =$$

Net advective flux of solute into CV:

$$\theta\omega_x m_y dy dz - \left[\theta\omega_x m_y dy dz + \frac{1}{m_x}\frac{\partial}{\partial x}\left(\theta\omega_x m_y dy dz\right)m_x dx\right]$$

$$+ \theta\omega_y m_x dx dz - \left[\theta\omega_y m_x dx dz + \frac{1}{m_y}\frac{\partial}{\partial y}\left(\theta\omega_y m_x dx dz\right)m_y dy\right]$$

$$+ \theta\omega_z m_x dx m_y dy - \left[\theta\omega_z m_x dx m_y dy + \frac{\partial}{\partial z}\left(\theta\omega_z m_x dx m_y dy\right)dz\right]$$

Net diffusive flux of solute into CV: (4.5.5)

$$-\frac{D_m}{m_x}\frac{\partial\theta}{\partial x}m_y dy dz - \left[-\frac{D_m}{m_x}\frac{\partial\theta}{\partial x}m_y dy dz + \frac{1}{m_x}\frac{\partial}{\partial x}\left(-\frac{D_m}{m_x}\frac{\partial\theta}{\partial x}m_y dy dz\right)m_x dx\right]$$

$$-\frac{D_m}{m_y}\frac{\partial\theta}{\partial y}m_x dx dz - \left[-\frac{D_m}{m_y}\frac{\partial\theta}{\partial y}m_x dx dz + \frac{1}{m_y}\frac{\partial}{\partial y}\left(-\frac{D_m}{m_y}\frac{\partial\theta}{\partial y}m_x dx dz\right)m_y dy\right]$$

$$- D_m\frac{\partial\theta}{\partial z}m_x dx m_y dy - \left[- D_m\frac{\partial\theta}{\partial z}m_x dx m_y dy + \frac{\partial}{\partial z}\left(- D_m\frac{\partial\theta}{\partial z}m_x dx m_y dy\right)dz\right]$$

Rate of decay of solute in CV:

$$- k\theta m_x dx m_y dy dz$$

where $k$ is a first-order decay rate coefficient. As was done with Eq. 4.5.1, cancel terms; take $dx$, $dy$, and $dz$ out of the derivatives and divide by the volume as it approaches zero. The result, since the metric coefficients are independent of $t$ and since $D_m$ is assumed to be constant, is

113

$$\frac{\partial \theta}{\partial t} + \frac{1}{m_x m_y} \left[ \frac{\partial}{\partial x} (m_y \theta \omega_x) + \frac{\partial}{\partial y} (m_x \theta \omega_y) + \frac{\partial}{\partial z} (m_x m_y \theta \omega_z) \right]$$

$$= \frac{D_m}{m_x m_y} \left[ \frac{\partial}{\partial x} \frac{m_y}{m_x} \frac{\partial \theta}{\partial x} + \frac{\partial}{\partial y} \left( \frac{m_x}{m_y} \frac{\partial \theta}{\partial y} \right) + \frac{\partial}{\partial z} \left( m_x m_y \frac{\partial \theta}{\partial z} \right) \right] - k\theta$$

$$(4.5.6)$$

"When $m_x = m_y = 1$, Eqs. 4.5.2 and 4.5.6 reduce to the familiar three-dimensional continuity and advective-diffusion equations in a rectangular Cartesian system. Eq. 4.5.6 is given in the so-called conservative form but may be simplified to the advection form by" expanding the derivatives of products and then subtracting $\theta$ times Eq. 4.5.2 from "the left-hand side (Crowley 1968). The following operations, however, will be performed throughout by use of the conservative form."

Eqs. 4.5.2 and 4.5.6 are the desired, general three-dimensional equations which are written in terms of the velocity components and concentration at a point in the flow and which include molecular diffusion terms since the molecular velocities are not represented by the continuum fluid velocities.

## 4.6 THREE-DIMENSIONAL TIME-AVERAGED EQUATIONS

Eqs. 4.5.2 and 4.5.6 apply for either laminar or turbulent flows provided that, for turbulent flows, the velocity components and concentrations are considered as instantaneous values including the relatively rapid variations (or fluctuations) associated with the turbulent nature of the flow. It may be noted that if these instantaneous values are used for turbulent flows, the balance equations do not need to have turbulent diffusion terms. However, the instantaneous values of the velocity usually are not known and, in many applications, the instantaneous concentrations are not needed. Thus, for turbulent flows, it is common to convert the equations to ones based on time-averaged quantities. In the process of performing the time averaging, turbulent diffusion terms are introduced.

114

### 4.6.1 Average Quantities and Temporal Fluctuations

Mathematically, the time average of any quantity $\phi$ is given by

$$\bar{\phi} = \frac{1}{T} \int_t^{t+T} \phi \, dt \tag{4.6.1}$$

An instantaneous value $\phi$ is

$$\phi = \bar{\phi} + \phi' \tag{4.6.2}$$

where $\phi'$ is the instantaneous deviation of $\phi$ from $\bar{\phi}$ and is frequently called a turbulent fluctuation. (Compare Section 4.3.3.) "The time interval $T$ (Eq. 4.6.1) should be long enough to damp out turbulent fluctuations and realistically should be defined for a specific problem based on the scales of flow and channel geometry under investigation."

Assume that the solute movement shown in Figure 29 is taking place in turbulent flow. In Figure 31a and b, the concentration and velocity distributions along the line AB at time $t$ are shown. The dashed lines indicate the time-averaged values of $\omega$ and $\theta$ (i.e., $\bar{\omega}$ and $\bar{\theta}$, the values with turbulent fluctuations $\omega'$ and $\theta'$ averaged out). These time-averaged values would be measured, for example, by collecting a sample over a sufficiently long time interval $T$ to determine the concentration and by counting the rotations of a current meter during T to determine the velocity. By looking in more detail, it is found that at any instant the turbulent fluctuations cause the concentration and velocity to be distributed as shown by the solid lines. From instant to instant, these irregular distributions fluctuate relative to the mean values indicated. The distributions to the left of the CV in Figure 31 indicate the concentration and the x-component of the velocity which pass through the upstream face as time elapses. This transport can be represented by using expressions like

115
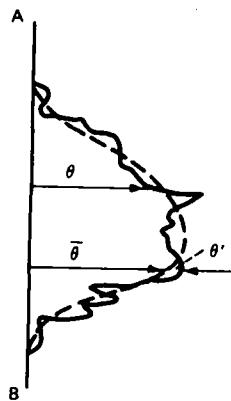
a. Concentration
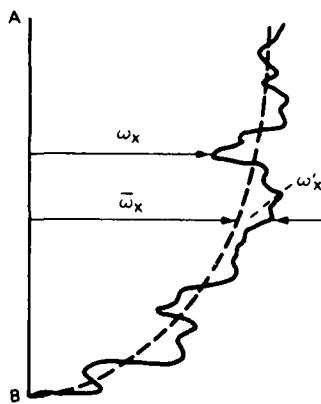
b. Velocity
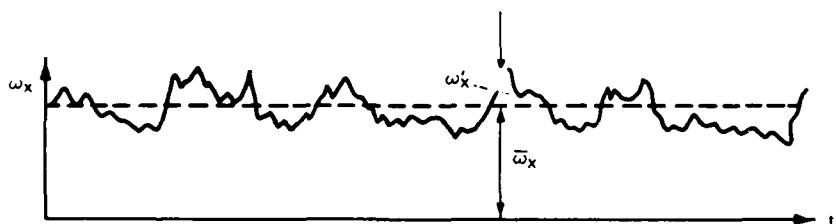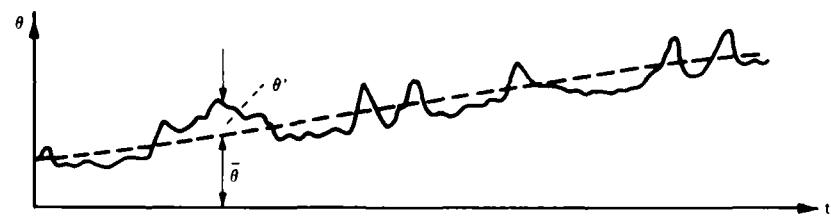
c. Sequence of $\omega$ and $\theta$ passing through upstream face

Figure 31.   Transport quantities in turbulent flow
(from Holley 1969)

116

Eq. 4.6.2 for each of the terms in the balance equations and then formally integrating the entire equation over the time interval $T$.

## 4.6.2 Time-Averaged Continuity of Water

"The integration of Eq. 4.5.2 over a time interval $T$ is carried out for each term by applying Leibnitz's rule (Eq. 4.3.3). Note that $m_x$ and $m_y$ are independent of time and thus are treated as constants in the integration. For an illustration, the first term of Eq. 4.5.2 is integrated as

$$\int_t^{t+T} \frac{\partial}{\partial x}(m_y \omega_x)dt = \frac{\partial}{\partial x}\left(m_y \int_t^{t+T} \omega_x dt\right)$$

$$= \frac{\partial}{\partial x}(m_y T \bar{\omega}_x) = T \frac{\partial}{\partial x}(m_y \bar{\omega}_x) \quad " \tag{4.6.3}$$

The order of integration and differentiation can be interchanged in Eq. 4.6.3 since $t$ and $T$ in the limits of integration are not functions of $x$, the variable with respect to which the differentiation is being done. "The other two terms of Eq. 4.5.2 may be integrated in the manner similar to that of Eq. 4.6.3."

"Introducing new symbols

$$u_x = \bar{\omega}_x$$

$$u_y = \bar{\omega}_y \tag{4.6.4}$$

$$u_z = \bar{\omega}_z$$

117

the three-dimensional continuity...equation averaged over the time
interval T becomes independent of T " after dividing the integrated
equation by T "and is written (Chang 1971) as follows:

$$\frac{1}{m_x m_y} \left[ \frac{\partial}{\partial x} (m_y u_x) + \frac{\partial}{\partial y} (m_x u_y) + \frac{\partial}{\partial z} (m_x m_y u_z) \right] = 0 \qquad (4.6.5)$$

Eq. 4.6.5 reduces to the familiar form in a Cartesian system when $m_x$
and $m_y$ are made unity."

### 4.6.3 Time-Averaged Mass Balance of Solute

"Integration of the first term of Eq. 4.5.6 requires the mean
theorem of integration for a continuous function (Kaplan 1953) so that

$$\int_t^{t+T} \frac{\partial \theta}{\partial t} dt = \theta(t+T) - \theta(t) = T \frac{\partial \bar{\theta}}{\partial t} \qquad (4.6.6)$$

"Integration of the advective terms on the left side of
Eq. 4.5.6 requires use of some of Reynolds' rules, in particular,
Eq. 4.3.7. For example, the first advection term may be integrated to
a form

$$\int_t^{t+T} \frac{\partial}{\partial x} (m_y \theta \omega_x) dt = \frac{\partial}{\partial x} \left( m_y \int_t^{t+T} \theta \omega_x dt \right)$$

$$\qquad (4.6.7)$$

$$= \frac{\partial}{\partial x} \left[ m_y T \left( \bar{\theta} \, \bar{\omega}_x + \overline{\theta' \omega_x'} \right) \right]$$

where $\bar{\theta}$ and $\bar{\omega}_x$ are the time-averaged values of concentration and
longitudinal velocity and $\theta'$ and $\omega_x'$ are instantaneous deviations
from the averaged values. Even though $\overline{\theta'}$ and $\overline{\omega_x'}$ are zero, the mean
of the product of the deviations or the covariance $\overline{\theta' \omega_x'}$ is not"

118

necessarily zero and represents the net transport in the x direction
associated with the turbulent fluctuations of velocity and concentra-
tion. This "effect is commonly expressed in analogy to molecular
diffusion as

$$\overline{\theta'\omega'_x} = - \frac{d_x}{m_x} \frac{\partial\overline{\theta}}{\partial x} \tag{4.6.8}$$

The symbol $d_x$ is the longitudinal turbulent diffusion coefficient
first introduced by Boussinesq (Hinze 1959). Integration of the other
two advection terms of Eq. 4.5.6 produces covariances, $\overline{\theta'\omega'_y}$ and $\overline{\theta'\omega'_z}$,
which are handled in the manner similar to that of Eq. 4.6.8" by intro-
ducing diffusion coefficients $d_y$ and $d_z$ for the y and z directions.

"The newly defined turbulent diffusion terms may be combined
with the molecular diffusion terms on the right-hand side of the inte-
grated form of Eq. 4.5.6. The remaining terms on the left-hand side of
the equation are the time-derivative term (Eq. 4.6.6) and the three
terms containing $\overline{\theta}\,\overline{\omega}_x$, $\overline{\theta}\,\overline{\omega}_y$, and $\overline{\theta}\,\overline{\omega}_z$, which may be called the
time-averaged advection terms."

Introducing the new symbol

$$s = \overline{\theta} \tag{4.6.9}$$

using Eq. 4.6.4 for $u = \overline{\omega}$, and dividing by $T$, the three-dimensional,
time-averaged, mass balance equation for the solute can be written
(Chang 1971) as

119

$$\frac{\partial s}{\partial t} + \frac{1}{m_x m_y}\left[\frac{\partial}{\partial x}(m_y s u_x) + \frac{\partial}{\partial y}(m_x s u_y) + \frac{\partial}{\partial z}(m_x m_y s u_z)\right]$$

$$= \frac{1}{m_x m_y}\left\{\frac{\partial}{\partial x}\left[\frac{m_y}{m_x}(d_x + D_m)\frac{\partial s}{\partial x}\right] + \frac{\partial}{\partial y}\left[\frac{m_x}{m_y}(d_y + D_m)\frac{\partial s}{\partial y}\right]\right. \qquad (4.6.10)$$

$$\left. + \frac{\partial}{\partial z}\left[m_x m_y(d_z + D_m)\frac{\partial s}{\partial z}\right]\right\} - ks$$

where it has been assumed that $k$ is constant, i.e., independent of the turbulent fluctuations. Eq. 4.6.10 reduces to the familiar form in a Cartesian system when $m_x$ and $m_y$ are made unity and symbols are defined for the overall mixing coefficients, $d_x + D_m$ and $d_y + D_m$, since "the molecular diffusion coefficient $D_m$...is normally an order of magnitude smaller than the turbulent diffusion coefficients" except near smooth boundaries where the turbulence must go to zero.

There is no approximation, only a time averaging, involved in obtaining the covariance terms from the advective terms of Eq. 4.5.6. Nevertheless, assumptions are introduced by expressions such as Eq. 4.6.8. One assumption is that the net turbulent transport as represented by the covariance terms can be represented by a gradient or Fickian-diffusion-type term as shown in Eq. 4.6.8. This assumption has "been shown to contain many theoretical deficiencies from the mechanics of turbulence (Hinze 1959)." On the other hand, it can be substantiated theoretically for some specific cases (Taylor 1921), and the use of diffusion terms has "been empirically established as a satisfactory working model in most natural-channel flows (Fischer 1973)." Also, "in utilizing the three principal (scalar) diffusion coefficients for approximation of $\overline{\theta' \omega'}$, however, a justification is that the principal axes of the diffusion tensor can be alined approximately with the three

coordinate directions when one adopts the natural coordinate system (Hinze 1959, Dagan 1969). If a stationary rectangular Cartesian coordinate system were used instead, it would be very difficult to satisfy the above alinement requirement in a generally meandering nonuniform channel, and it would thus be difficult to justify simple scalar expressions, as given in Eqs. 4.6.8 and 4.6.10. Overcoming these difficulties is a major advantage of utilizing the natural coordinate system over a Cartesian system."

## 4.7 TWO-DIMENSIONAL DEPTH-AVERAGED EQUATIONS

The three-dimensional time-averaged equations (Eqs. 4.6.5 and 4.6.10) apply for river flows as well as for many other types of flows. However, in order to use these two equations to obtain concentration distributions, it is necessary to know or to calculate the three velocity components ( $u_x$ , $u_y$ , and $u_z$ ) as functions of $x$ , $y$ , $z$ , and $t$ , i.e. throughout the length, depth, and width of the section of river being investigated. If these velocities, the boundary configuration (bed and water surface), the diffusion coefficients, and the release conditions are known, the three-dimensional variation of $s$ can be calculated as a function of $x$ , $y$ , $z$ , $t$ , i.e., the result is the temporal variation of $s$ over the length, depth, and width of the river. In some cases, this much detail about s may be required so that the effort of obtaining all of the required input information may be justified. However, in many situations in rivers, the concentration is rather uniform along each individual vertical line. As a result, there is no need to calculate the variation of $s$ with $z$ . The mathematical process by which this unnecessary variation is removed is integration or averaging of Eqs. 4.6.5 and 4.6.10 over the local flow depth producing two-dimensional equations. Also, even though the depth-averaging accomplishes the objectives of removing the unneeded variation of $s$ , it also removes the vertical variations of $u_x$ and $u_y$ from the advection terms. The effects of the variations of $u_x$

121

and $u_y$ , which can make a significant contribution to the transport process, are normally included in modified diffusion terms.

### 4.7.1 Depth Averages and Vertical Variations

The depth-average of any quantity $\phi$ is obtained by integrating (or averaging) the quantity over a vertical line in the flow. Mathematically, this process is expressed as

$$\bar{\phi} = \frac{1}{h} \int_{Z_B}^{Z_S} \phi dz \qquad (4.7.1)$$

where $h$ is the local depth, $z = Z_S$ is the water surface, $z = Z_B$ is the bed so that $h = Z_S - Z_B$ , and $\phi$ is a function of $x$ , $y$ , $z$ , and $t$ . The average $\bar{\phi}$ is a function of $x$ , $y$ , and $t$ since the variation with z has been integrated or averaged out. The value of $\phi$ at a point on the vertical line can be written as

$$\phi = \bar{\phi} + \phi' \qquad (4.7.2)$$

where now the primed quantity is a spatial (vertical) variation from the depth-averaged quantity which is the meaning of the overbar in this section.

Due to the boundary shear, there is normally a vertical variation of longitudinal velocity as shown in Figure 32a, which also illustrates the interrelationship among $u_x$ , $\bar{u}_x$ , and $u'_x$ .

Before looking at the depth-averaging of the transverse velocity $u_y$ , it may be helpful to consider the two primary types of transverse velocities. First consider net transverse velocities which, as illustrated in Figure 32b, are associated with changes in depth and velocity distributions along the river channel. Assume that the line AA' is the x axis along the center of the channel width and that the shape of the cross section changes as shown in the figure. Since velocities are

122
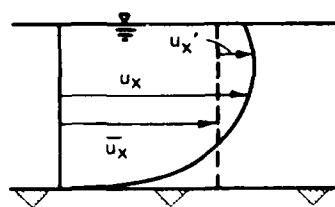
a. Vertical variation
of longitudinal
velocity
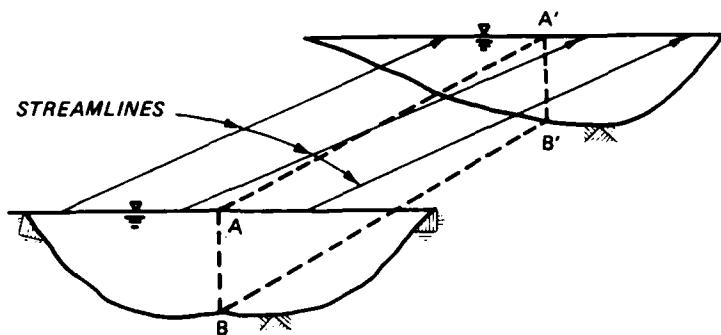
b. Net transverse velocity
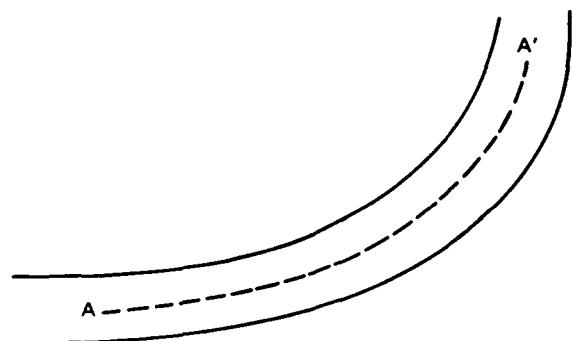
c. Helical secondary flow in a bend
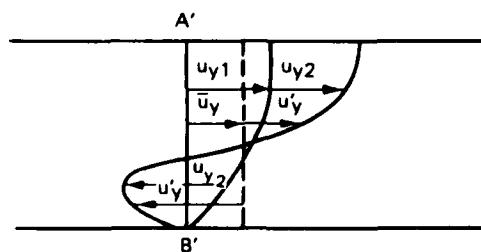
$u_{y1}$ - NET TRANSVERSE
VELOCITY

$u_{y2}$ - HELICAL SECONDARY
FLOW VELOCITY

d. Vertical variation of transverse velocity

Figure 32. Vertical variations of longitudinal and transverse velocity

123

generally higher in the parts of the cross section with the larger depths (Yotsukura and Sayre 1976), if AB divides the discharge in half (for example) at the first cross section, then more than half of the discharge will be to the right of A'B', indicating that there was a net flow to the right across the plane ABB'A', giving a net $u_y$ transverse velocity across the plane. As with $u_x$, this net transverse velocity would, in general, have a vertical distribution as indicated by $u_{y1}$ in Figure 32d. (As is seen in Section 4.7.4, it is possible to use a coordinate transformation so that the depth-averaged transverse velocity is eliminated from the equations.)

Next consider the secondary motion which develops in bends due to the combined effects of the vertical distribution of $u_x$ (Figure 32a), the centrifugal forces associated with the water particles needing to move along curved streamlines, and the centripedal pressure forces associated with the superelevation of the water surface on the outside of the bend. The net result is a helical secondary flow cell which becomes superimposed on the primary longitudinal flow with the water nearer the surface gradually migrating toward the outside of the bend and the water nearer the bottom gradually moving toward the inside. Looking along the channel, there is a rotating cell as illustrated in Figure 32c. The vertical distribution of the resulting transverse velocity is illustrated by $u_{y2}$ in Figure 32d. The depth average of $u_{y2}$ is zero since the same amount of water moves toward the outside and toward the inside along any vertical line.

The two components ($u_{y1}$ and $u_{y2}$) make up the total transverse velocity $u_y$ with a depth average of $\bar{u}_y$ as depicted in Figure 32d.

## 4.7.2  Depth-Averaged Continuity of Water

In principle, the depth-averaging process is just the integration of each term in Eq. 4.6.5 (or Eq. 4.6.10) over the depth as indicated in Eq. 4.7.1. However, the actual integration process is somewhat tedious since $Z_S$ and $Z_B$ are in general functions of $x$, $z$, and $t$ so that Leibnitz' rule (Section 4.3.2) must be used rather than

124

being able just to interchange orders of differentiation and integration as was done in the time averaging.

"In Eq. 4.6.5 (and Eq. 4.6.10), $m_x$ and $m_y$ are independent of $z$ and can be treated as constants in integration. Designate values of $z$ at flow boundaries as $Z$, so that $Z_B$ and $Z_S$ represent the channel bed and water surface, respectively. Note that $Z_S$ and $Z_B$ are functions of $x$, $y$, and $t$, whereas $z$ is an independent variable. Each term of Eq. 4.6.5 is now integrated with respect to $z$ from $Z_B$ to $Z_S$" and then Leibnitz's rule (Section 4.3.2) is applied to obtain

$$\int_{Z_B}^{Z_S} \frac{\partial}{\partial x} (m_y u_x)\, dz = \frac{\partial}{\partial x} \int_{Z_B}^{Z_S} m_y u_x dz - \overset{(1)}{m_y u_x\big|_{Z_S} \frac{\partial Z_S}{\partial x}} + \overset{(4)}{m_y u_x\big|_{Z_B} \frac{\partial Z_B}{\partial x}} \qquad (4.7.3)$$

$$\int_{Z_B}^{Z_S} \frac{\partial}{\partial y} (m_x u_y)\, dz = \frac{\partial}{\partial y} \int_{Z_B}^{Z_S} m_x u_y dz - \overset{(2)}{m_x u_y\big|_{Z_S} \frac{\partial Z_S}{\partial y}} + \overset{(5)}{m_x u_y\big|_{Z_B} \frac{\partial Z_B}{\partial y}} \qquad (4.7.4)$$

$$\int_{Z_B}^{Z_S} \frac{\partial}{\partial z} (m_x m_y u_z)\, dz = \overset{(3)}{m_x m_y u_z\big|_{Z_S}} - \overset{(6)}{m_x m_y u_z\big|_{Z_B}} \qquad (4.7.5)$$

The integrals on the right-hand sides of Eq. 4.7.3 and 4.7.4 are the desired terms. Fortunately, the other (numbered) terms in the three equations can be eliminated by using the kinematical boundary conditions at the surface and bed. This boundary condition is frequently stated as the requirement that water particles at the free surface remain there, with a similar condition applying at the bed. At first glance, this mathematical statement seems inconsistent with what can be readily observed at the water surface in a turbulent flow, namely that there are boils or turbulent eddies which continuously bring some water particles to the surface and carry others downward away from the surface. However, it must be recalled that the effects

125

of turbulence, including these boils or eddies just mentioned, have
been averaged out (Section 4.6) so that they need not be considered in
dealing with Eqs. 4.6.5, 4.7.3, and 4.7.4, and 4.7.5. (The effects are
in the turbulent diffusion terms in Eq. 4.6.10.) Thus, it is in a
time-averaging sense that a water particle must stay at the surface (or
the bed). Another way of stating this boundary condition is that, in
the absence of evaporation, precipitation, and influx or efflux seepage
across the bed, the time-averaged velocity at each boundary must be
tangent to the boundary. The incremental change in $Z_S$ for arbitrary
dt , dx , and dz is

$$dZ_S = \frac{\partial Z_S}{\partial t} dt + \frac{1}{m_x} \frac{\partial Z_S}{\partial x} m_x dx + \frac{1}{m_y} \frac{\partial Z_S}{\partial y} m_y dy \qquad (4.7.6)$$

since $Z_S = Z_S(x,y,t)$ . In order to apply Eq. 4.7.6 to the motion of a
fluid particle, select $m_x dx$ and $m_y dy$ as the displacements asso-
ciated with the time-averaged velocities during dt so that

$$m_x dx = u_x dt$$

$$\qquad (4.7.7)$$

$$m_y dy = u_y dt$$

Substitution into Eq. 4.7.6 and division by dt as dt approaches
zero gives the derivative $dZ_S/dt$ , which is the time rate of change of
the vertical position or simply $u_z$ , so that from Eq. 4.7.6,

$$u_z \big|_{Z_S} = \frac{\partial Z_S}{\partial t} + \frac{u_x}{m_x} \frac{\partial Z_S}{\partial x} + \frac{u_y}{m_y} \frac{\partial Z_S}{\partial y} \qquad (4.7.8)$$

"Multiplying Eq. 4.7.8 by $m_x m_y$ , the sum of the terms 1, 2, and 3 in
Eqs. 4.7.3, 4.7.4, and 4.7.5 is equal to $m_x m_y \partial Z_S / \partial t$ . A similar
boundary equation can be derived at the bed, and the sum of the terms

126

4, 5, and 6 can be shown to be equal to $-m_x m_y \partial Z_B / \partial t$ . The depth-integrated form of Eq. 4.6.5 thus reduces to

$$\frac{1}{m_x m_y}\left[\frac{\partial}{\partial x}\int_{Z_B}^{Z_S} m_y u_z dz + \frac{\partial}{\partial y}\int_{Z_B}^{Z_S} m_x u_y dz + m_x m_y \frac{\partial(Z_S - Z_B)}{\partial t}\right] = 0 \qquad (4.7.9)$$

Introducing the new notation

$$v_x = \bar{u}_x$$

$$\qquad (4.7.10)$$

$$v_y = \bar{u}_y$$

and using $h = Z_S - Z_B$ , the depth-averaged continuity equation for the water becomes

$$\frac{\partial h}{\partial t} + \frac{1}{m_x m_y}\left[\frac{\partial}{\partial x}(m_y h v_x) + \frac{\partial}{\partial y}(m_x h v_y)\right] = 0 \qquad (4.7.11)$$

### 4.7.3 Depth-Averaged Mass Balance of Solute

Integration of the left-hand side of Eq. 4.6.10 is similar to the integration of Eq. 4.6.5 as just presented in Section 4.7.2 except that each of the velocities in Eqs. 4.7.2-4.7.5 is multiplied by $s$ . Similarly, Eq. 4.7.8 (or the equivalent expression at $Z_B$ ) can be multiplied by $s$ at $Z_S$ (or $Z_B$ ) to allow elimination of several "terms arising from application of Leibnitz's rule, so that the depth-integrated left side of Eq. 4.6.10 is

$$\frac{\partial}{\partial t}\int_{Z_B}^{Z_S} s dz + \frac{1}{m_x m_y}\left[\frac{\partial}{\partial x}\left(m_y \int_{Z_B}^{Z_S} s u_x dz\right) + \frac{\partial}{\partial y}\left(m_x \int_{Z_B}^{Z_S} s u_y dz\right)\right] \qquad (4.7.12)$$

127

"Integration of the right side of Eq. 4.6.10 requires use of another boundary condition" related to any flux of the solute "across the water surface and the bed." Since evaporation, precipitation, and seepage were assumed to be zero in the previous section, there can be only sorptive-type transport of the solute across the boundary with no advective transport across the boundaries, in this derivation. In general, advective transport can also be included (Holley and Yotsukura 1979). Let $d\sigma_S$ be an increment of water surface area having a horizontal projection (on the x-y plane) of $dA_H$, where $dA_H = m_x m_y dx dy$. The unit normal outward vector at the water surface is

$$
\vec{n} = \left( -\frac{1}{m_x} \frac{\partial Z_S}{\partial x} \vec{i} - \frac{1}{m_y} \frac{\partial Z_S}{\partial y} \vec{j} + \vec{k} \right) \frac{dA_H}{d\sigma_S}
$$

$$
= \left( -\frac{1}{m_x} \frac{\partial Z_S}{\partial x} \vec{i} - \frac{1}{m_y} \frac{\partial Z_S}{\partial y} \vec{j} + \vec{k} \right) \left[ \left( \frac{1}{m_x} \frac{\partial Z_S}{\partial x} \right)^2 + 1 + \left( \frac{1}{m_y} \frac{\partial Z_S}{\partial y} \right)^2 \right]^{-1/2}
$$

(4.7.13)

where $\vec{i}$, $\vec{j}$, $\vec{k}$ are the unit vectors in the respective coordinate directions. A similar equation with opposite signs in the first term on the right-hand side of Eq. 4.7.13 would give the unit normal outward vector at the bed. Also, let $f$ be the unit diffusive flux vector:

$$
\vec{f} = -\frac{d_x + D_m}{m_x} \frac{\partial s}{\partial x} \vec{i} - \frac{d_y + D_m}{m_y} \frac{\partial s}{\partial y} \vec{j} - (d_z + D_m) \frac{\partial s}{\partial z} \vec{k} \qquad (4.7.14)
$$

Application of Leibnitz's rule in the depth integration of the right-hand side of Eq. 4.6.10 gives two terms with integrals over the depth plus three terms at the surface and a similar three terms at the bed. The sum of these six terms is equal to

$$- (\vec{f} \cdot \vec{n})_{Z_B} \frac{d\sigma_S}{dA_H} - (\vec{F} \cdot \vec{n})_{Z_B} \frac{d\sigma_B}{dA_H} = - f_S - f_B \qquad (4.7.15)$$

where $d\sigma_B$ is an increment of bed area having a horizontal projection of $dA_H$. In the first term in Eq. 4.7.15, $\vec{f} \cdot \vec{n}\, d\sigma_S$ is the normal diffusive flux for a water surface area of $d\sigma_S$. Having $dA_H$ in the denominator gives the flux per unit of horizontal area and makes the terms in Eq. 4.7.15 consistent with the terms in Eq. 4.7.12 and with other depth-averaged equations to follow. The final equations in Sections 4.5 and 4.6 were obtained after dividing by an incremental volume $(m_x dx m_y dy dz)$; in this section, the equations from Section 4.6 have been multiplied by $dz$ and integrated over the depth, meaning that the resulting terms have still effectively been divided by $m_x dx m_y dy$ and thus represent the various physical processes per unit of horizontal area. As indicated in Eq. 4.7.15, this flux at the surface is given the symbol $f_S$. The second term (without the negative sign) in Eq. 4.7.15 is a similar downward diffusive flux at the bed. If there are no sorptive transfers at the boundaries, then $f_S$ and $f_B$ must be zero. If there are sorptive transfers, then conservation of mass at the boundaries requires that $f_S$ (or $f_B$) be equal to the outward flux or efflux per unit area of the horizontal projection of the water surface (or bed). With these definitions, the depth-integration of the right-hand side of Eq. 4.6.10 gives

$$\frac{1}{m_x m_y} \left\{ \frac{\partial}{\partial x} \left[ \frac{m_y}{m_x} \int_{Z_B}^{Z_S} (d_x + D_m) \frac{\partial s}{\partial x}\, dz \right] + \frac{\partial}{\partial y} \left[ \frac{m_x}{m_y} \int_{Z_B}^{Z_S} (d_y + D_m) \frac{\partial s}{\partial y}\, dz \right] \right\}$$

$$\qquad (4.7.16)$$

$$- f_s - f_B - \int_{Z_B}^{Z_S} ks\, dz$$

129

"Before equating [Eqs.] 4.7.12 and 4.7.16 for the depth-integrated advection-diffusion equation, integrals in [Eq.] 4.7.12, such as $\int su_x dy$ , will be considered further.  In this section, over-lined and prime notations pertain only to depth averaging (Eq. 4.7.1).  The function $\phi(x,y,z,t)$  is the sum of  $\bar{\phi}(x,z,t)$  and  $\phi'(x,y,z,t)$ , where  $\phi'$  is a local deviation from the depth averaged  $\bar{\phi}$ .

"The integral in the second term of [Eq.] 4.7.12 may be written" using one of Reynolds' Rules (Eq. 4.3.7) as

$$\int_{Z_B}^{Z_S} su_x dz = h\,\overline{su_x} = h\,\left(\bar{s}\,\bar{u}_x + \overline{s'u'_x}\right) \tag{4.7.17}$$

"Note that the part of Eq. 4.7.17 in parentheses is analogous to the last parenthesized part of Eq. 4.6.7.  The difference is that Eq. 4.7.17 refers to depth averaging, whereas Eq. 4.6.7 refers to time averaging.  It is due to Taylor's (1954) longitudinal dispersion theory that this spatial covariance term  $\overline{s'u'_x}$ , may also be equated to a gradient-type flux form

$$\overline{s'u'_x} = -\frac{k_x}{m_x}\frac{\partial \bar{s}}{\partial x} \tag{4.7.18}$$

which is analogous to Eq. 4.6.8.  The symbol  $k_x$  [which has no relation to a first-order reaction rate coefficient] is the longitudinal advective-dispersion coefficient introduced by the depthwise variation of  $u_x$  [Figure 32a] and  s .  The other covariance  $\overline{s'u'_y}$  from [Eq.] 4.7.12" with  $u'_y$  shown in Figure 32d "may be handled in the manner similar to that of Eq. 4.7.18."

"The first integral of [Eq.] 4.7.16 may be written as

130

$$\int_{Z_B}^{Z_S} (d_x + D_m) \frac{\partial s}{\partial x} \, dz = h \, \overline{(d_x + D_m) \frac{\partial s}{\partial x}}$$

$$\text{(4.7.19)}$$

$$= h \left( \overline{(d_x + D_m) \frac{\partial \bar{s}}{\partial x}} + \overline{d'_x \frac{\partial s'}{\partial x}} \right)$$

The covariance term [the last term in the parentheses] is usually related to the product-of-averages term [the first term in the parentheses], but small relative to it, so that it is conveniently absorbed into the first term. Similar approximations will be applied to the second term of [Eq.] 4.7.16."

The depth-averaged advective-diffusion equation is obtained by equating Eqs. 4.7.12 and 4.7.16, substituting approximating expressions, such as Eqs. 4.7.18 and 4.7.19, and moving all diffusive flux terms to the right-hand side of the equation, so that

$$\frac{\partial}{\partial t}(h\bar{s}) + \frac{1}{m_x m_y}\left[\frac{\partial}{\partial x}(m_y h\bar{u}_x \bar{s}) + \frac{\partial}{\partial y}(m_x h\bar{u}_y \bar{s})\right]$$

$$= \frac{1}{m_x m_y}\left\{\frac{\partial}{\partial x}\left[\frac{m_y}{m_x} h(k_x + \bar{d}_x + D_m)\frac{\partial \bar{s}}{\partial x}\right]\right.$$

$$\text{(4.7.20)}$$

$$\left. + \frac{\partial}{\partial y}\left[\frac{m_x}{m_y} h(k_y + \bar{d}_y + D_m)\frac{\partial \bar{s}}{\partial y}\right]\right\} - f_S - f_B - kh\bar{s}$$

where it has been assumed that $k$ is independent of $z$ so that the last term in Eq. 4.7.16 equals $kh\bar{s}$. Introducing the new notation

131

$$c = \bar{s}$$

$$e_x = k_x + \bar{d}_x + D_m \qquad (4.7.21)$$

$$e_y = k_y + \bar{d}_y + D_m$$

where $e_x$ and $e_y$ are the overall mixing coefficients in the respective coordinate directions, the two-dimensional advective-diffusion equation is finally written (Yotsukura and Sayre 1976) as follows:

$$\frac{\partial}{\partial t} (hc) + \frac{1}{m_x m_y} \left[ \frac{\partial}{\partial x} (m_y h v_x c) + \frac{\partial}{\partial y} (m_x h v_y c) \right]$$

$$= \frac{1}{m_x m_y} \left[ \frac{\partial}{\partial x} \left( \frac{m_y}{m_x} h e_x \frac{\partial c}{\partial x} \right) + \frac{\partial}{\partial y} \left( \frac{m_x}{m_y} h e_y \frac{\partial c}{\partial y} \right) \right] \qquad (4.7.22)$$

$$- f_S - f_B - khc$$

"In going from the three-dimensional Eqs. 4.6.5 and 4.6.10 to the two-dimensional Eqs. 4.7.11 and 4.7.22, no assumptions were introduced except for those related to spatial covariance terms, such as Eqs. 4.7.18 and 4.7.19. One must remember that the advective-dispersion coefficient, as defined by Eq. 4.7.18, is an asymptotic approximation and thus applies only when the solute concentration is well distributed over the depth of flow (Fischer 1973). For a steady uniform flow, Taylor's longitudinal dispersion theory has been verified by Aris (1956), Elder (1959), Fischer (1966b), and Sayre (1967), among many others. Note that the mixing coefficient $e$ is the sum of the advective-dispersion coefficient $k$, the depth-averaged turbulent diffusion coefficient $\bar{d}$, and the molecular diffusion coefficient $D_m$, where $k \gg \bar{d} \gg D_m$, and also implicitly includes any net transport

132

associated with covariance terms such as the last term in the paren-
theses in Eq. 4.7.19.

### 4.7.4  Stream-Tube Model

By virtue of the depth averaging, Eqs. 4.7.11 and 4.7.22 do not
contain vertical variations but they do still contain a transverse
velocity term $(v_y)$. This term causes considerable difficulties when
seeking to obtain either approximate analytical solutions or numerical
solutions for concentration distributions. As discussed by Yotsukura
and Sayre (1976, 1977), there are at least two ways of eliminating the
$v_y$ term. The following derivations follow the general procedures of
Yotsukura and Sayre but combine points from the original paper (1976)
and the reply to comments on the paper (1977).

Rewrite the depth-averaged mass balance equation (Eq. 4.7.22) by
expanding the derivatives of products on the left-hand side, so that
the left-hand side becomes

$$h \frac{\partial c}{\partial t} + c \frac{\partial h}{\partial t} + \frac{1}{m_x m_y} \left[ c \frac{\partial}{\partial x} (m_y h v_x) + m_y h v_x \frac{\partial c}{\partial x} \right.$$
$$\left. + c \frac{\partial}{\partial y} (m_x h v_y) + m_x h v_y \frac{\partial c}{\partial y} \right] \qquad (4.7.25)$$

Then the continuity equation (Eq. 4.7.11) multiplied by $c$ can be used
to cancel three terms in Eq. 4.7.25. If the longitudinal diffusion
term can be neglected, Eq. 4.7.22 can be written as

$$h \frac{\partial c}{\partial t} + \frac{h v_x}{m_x} \frac{\partial c}{\partial x} + \frac{h v_y}{m_y} \frac{\partial c}{\partial y} = \frac{1}{m_x m_y} \frac{\partial}{\partial y} \left( \frac{m_x}{m_y} h e_y \frac{\partial c}{\partial y} \right) \qquad (4.7.26)$$

$$- f_S - f_B - khc$$

For steady river flow, $\partial h/\partial t = 0$ . Then the continuity equation
(Eq. 4.7.11) can be written as

133

$$\frac{\partial}{\partial x} (m_y h v_x) + \frac{\partial}{\partial y} (m_x h v_y) = 0 \qquad (4.7.27)$$

One way of eliminating the $v_y$ term is to choose a coordinate system aligned with the depth-averaged streamlines so that $v_y = 0$ (Fischer 1966b, Chang 1971, Sayre and Yeh 1973). However, Yotsukura and Sayre (1976, 1977) preferred using a coordinate transformation which allows $v_y$ to be eliminated by introducing the cumulative discharge

$$q = \int_{Y_L}^{y} m_y h v_x \, dy \qquad (4.7.28)$$

The cumulative discharge is the amount of discharge between the left bank $(Y_L)$ and any transverse position denoted by the value of $y$ in the upper limit of the integral. The coordinate transformation can be accomplished by integrating Eq. 4.7.27 with respect to $y$ from $Y_L$ to $y$ to obtain

$$m_x h v_y = -\frac{\partial}{\partial x} \int_{Y_L}^{y} m_y h v_x \, dy = -\frac{\partial q}{\partial x} \qquad (4.7.29)$$

The derivation of Eq. 4.7.29 makes use of Leibnitz's rule, the fact that $y$ and $x$ are independent so that $\partial y / \partial x = 0$, and the equivalent of Eq. 4.8.9 for $Y_L$ and for steady flow. (Yotsukura and Sayre assumed the special case of $v_x = v_y = 0$ at $Y_L$, but the use of Eq. 4.8.9 produces the same result with less restrictive assumptions.) Substitute Eq. 4.7.29 into Eq. 4.7.26 to obtain

134

$$h \frac{\partial c}{\partial t} + \frac{h v_x}{m_x} \frac{\partial c}{\partial x} - \frac{1}{m_x m_y} \frac{\partial q}{\partial x} \frac{\partial c}{\partial y} = \frac{1}{m_x m_y} \frac{\partial}{\partial y} \left( \frac{m_x}{m_y} h e_y \frac{\partial c}{\partial y} \right)$$

$$(4.7.30)$$

$$- f_S - f_B - khc$$

Using Eq. 4.3.10 with $a_1 = x$ , $a_2 = y$ , $a_3 = t$ , and $b_1 = x$ , $b_2 = q$ , $b_3 = t$ , the derivatives in Eq. 4.7.30 can be written as

$$\frac{\partial c}{\partial t} = \frac{\partial c}{\partial x} \frac{\partial x}{\partial t} + \frac{\partial c}{\partial q} \frac{\partial q}{\partial t} + \frac{\partial c}{\partial t} \frac{\partial t}{\partial t} = \frac{\partial c}{\partial t}$$

$$\frac{\partial c}{\partial x} = \frac{\partial c}{\partial x} \frac{\partial x}{\partial x} + \frac{\partial c}{\partial q} \frac{\partial q}{\partial x} + \frac{\partial c}{\partial t} \frac{\partial t}{\partial x} = \frac{\partial c}{\partial x} - m_x h v_y \frac{\partial c}{\partial q} \qquad (4.7.31)$$

$$\frac{\partial c}{\partial y} = \frac{\partial c}{\partial x} \frac{\partial x}{\partial y} + \frac{\partial c}{\partial q} \frac{\partial q}{\partial y} + \frac{\partial c}{\partial t} \frac{\partial t}{\partial y} = m_y h v_x \frac{\partial c}{\partial q}$$

This derviation assumes that longitudinal distances along the original coordinate system and the streamline coordinate system are identical; in general, this may not be exactly correct. By virtue of Eq. 4.7.31,

$$\frac{\partial}{\partial y} \left( \frac{m_x}{m_y} h e_y \frac{\partial c}{\partial y} \right) = m_y h v_x \frac{\partial}{\partial q} \left( \frac{m_x}{m_y} h e_y \frac{\partial c}{\partial y} \right)$$

$$= m_y h v_x \frac{\partial}{\partial q} \left[ \frac{m_x}{m_y} h e_y \left( m_y h v_x \frac{\partial c}{\partial q} \right) \right] \qquad (4.7.32)$$

$$= m_y h v_x \frac{\partial}{\partial q} \left( m_x h^2 v_x e_y \frac{\partial c}{\partial q} \right)$$

Substituting Eqs. 4.7.29, 4.7.31, and 4.7.32 into Eq. 4.7.30 and then dividing by $h$ gives

$$\frac{\partial c}{\partial t} + \frac{v_x}{m_x} \frac{\partial c}{\partial x} = \frac{v_x}{m_x} \frac{\partial}{\partial q} \left( m_x h^2 v_x e_y \frac{\partial c}{\partial q} \right) - \frac{f_S}{h} - \frac{f_B}{h} - kc \qquad (4.7.33)$$

135

This is the general (assuming that the effects of $e_x$ are negligible), depth-averaged stream-tube equation which derives its name from the fact that constant values of q represent depth-averaged streamlines or lines which, for all x values, have a certain, constant fraction of the total discharge to the left of them and the remainder to the right. Also, $q_2 - q_1$ or $\Delta q$ represents a stream tube containing a certain fraction of the total discharge. In a sense, $v_y$ disappears in the derivation of Eq. 4.7.33 because there is no flow across streamlines which are now used as part of the coordinate system.

Yotsukura and Sayre (1976) originally presented an expression for a steady-state concentration distribution for a conservative solute. For these conditions, Eq. 4.7.33 becomes

$$\frac{\partial c}{\partial x} = \frac{\partial}{\partial q}\left(m_x h^2 v_x e_y \frac{\partial c}{\partial q}\right)$$

(4.7.34)

## 4.8  ONE-DIMENSIONAL AREA-AVERAGED EQUATIONS

The depth-averaged two-dimensional (2D) equations which are presented in Section 4.7 apply to rivers regardless of the type of pollutant release and should be used for a large majority of prediction problems, if possible. However, the 2D approach requires information on the transverse variation of depth and of depth-averaged velocities. Historically, one-dimensional (1D) approaches have been used for many problems where they really were not appropriate. Nevertheless, because of this historical interest in 1D approaches and because occasionally 1D approaches are either justified physically or required for quick approximations, the derivation of the 1D equations is presented in this section.

### 4.8.1  Area Averages and Cross-Sectional Variations

The area average of any quantity is obtained by integrating (or averaging) the quantity over the cross-sectional area of the flow. This is a double integration which may be accomplished by first integrating over the depth and then integrating the result over the width.

136

Since the depth integration has already been done in Section 4.7, the results of that section can now be integrated over the channel width to obtain area-averaged equations. Mathematically, this integration over the width can be expressed as

$$\bar{\phi} = \frac{1}{A} \int_{Y_L}^{Y_R} \phi h m_y \, dy \qquad (4.8.1)$$

where $h$ is the local depth, $y = Y_L$ is the left edge of the water surface, $y = Y_R$ is the right edge, and $A$ is the cross-sectional area given by

$$A = \int_{Y_L}^{Y_R} h m_y \, dy \qquad (4.8.2)$$

The cross-sectional average $\bar{\phi}$ is a function of $x$ and $t$. The value of $\phi$ at any transverse point in the cross section can be written as

$$\phi = \bar{\phi} + \phi' \qquad (4.8.3)$$

where the overbar indicates an area-average value in this section and the primed quantity is a spatial (transverse) variation from the area-average.

Many aspects of the integration are very similar to the depth-averaging in Section 4.7 and thus are presented somewhat more briefly here. However, there is one distinct difference that arises from the way in which the integrations are done. Recall that it was mentioned that each of the terms in Eqs. 4.7.11 and 4.7.22 could be interpreted as representing various physical processes or quantities per unit of

137

horizontal area ($dA_H$) of the river. Since, at an arbitrary point in the river, the incremental longitudinal and transverse distances are respectively $m_x dx$ and $m_y dy$, then $dA_H = m_x m_y dx dy$. Because of the forms of Eq. 4.7.11 and 4.7.22, it is convenient to multiply by $m_x m_y dy$ and then perform the integration across the channel width rather than multiplying by just $m_y dy$ before integration. Most of the terms in the resulting 1D equation involve some type of width-average of $m_x$ to account for the fact that the actual amount of the physical process which is present at each point depends on the local length ($m_x dx$) along the channel while the terms being integrated represent the various processes per unit length ($dx$) along the x axis (Figure 27) by virtue of the multiplication by $m_x m_y dy$ before integration.

In Section 4.7.1, there is a brief discussion of the reasons for the existence of transverse velocities and the vertical variations of longitudinal and transverse velocities. In addition to those vertical variations, transverse variations of the various physical quantities are illustrated in Figure 32. For example, typical isovels of longitudinal velocity are shown in Figure 33a, along with a transverse distribution of longitudinal velocity (Figure 33b).
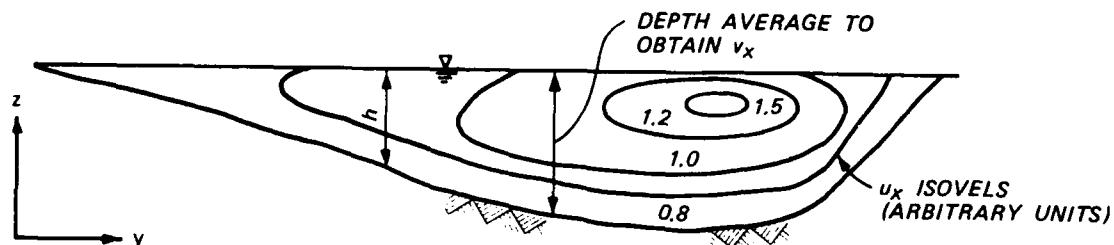
a. Cross-sectional variation
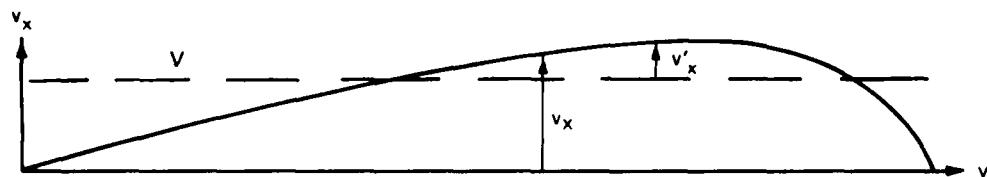
b. Transverse variation of depth-averaged velocity

Figure 33. Transverse variation of depth-averaged velocity

138

### 4.8.2 Area-Averaged Continuity of Water

Eq. 4.7.11 is first multiplied by $m_x m_y dy$ and then integrated with respect to $y$ from $Y_L$ to $Y_R$ . The integration of the three terms in Eq. 4.7.11 gives

$$\int_{Y_L}^{Y_R} m_x \frac{\partial h}{\partial t} m_y dy = \frac{\partial}{\partial t} \int_{Y_L}^{Y_R} m_x h m_y dy - (m_x m_y h)\big|_{Y_R} \frac{\partial Y_R}{\partial t} + (m_x m_y h)\big|_{Y_L} \frac{\partial Y_L}{\partial t} \qquad (4.8.4)$$

$$\int_{Y_L}^{Y_R} \frac{\partial}{\partial x} (m_z h v_x) \, dz = \frac{\partial}{\partial x} \int_{Y_L}^{Y_R} m_z h v_x dz - (m_z h v_x)_{Y_R} \frac{\partial Y_R}{\partial x} + (m_z h v_x)_{Y_L} \frac{\partial Y_L}{\partial x} \qquad (4.8.5)$$

$$\int_{Y_L}^{Y_R} \frac{\partial}{\partial y} (m_x h v_y) \, dy = \qquad\qquad + (m_x h v_y)_{Y_R} - (m_x h v_y)_{Y_L} \qquad (4.8.6)$$

In some cases, the depth and velocity are both zero at $Y_R$ and $Y_L$ so that the six terms to be evaluated at $Y_R$ and $Y_L$ in Eqs. 4.8.4–4.8.6 would be zero. However, in a more general case, with the depth and possibly the velocity being (mathematically) non-zero at the water's edge, there are conditions at the water's edge equivalent to those discussed in conjunction with Eqs. 4.7.6–4.7.8 for the surface and bed. In order for the depth-averaged flow to follow a (possibly) moving boundary at the water's edge, it is required that

$$dY_R = \frac{\partial Y_R}{\partial t} dt + \frac{1}{m_x} \frac{\partial Y_R}{\partial x} m_x dx \qquad (4.8.7)$$

since $Y_R = Y_R(x,t)$ . Select $m_x dx$ in Eq. 4.8.7 such that

$$m_x dx = v_x dt \qquad (4.8.8)$$

Then, as in Eq. 4.7.8 since $m_y dY_R/dt = v_y$ at $Y_R$

$$\frac{v_y}{m_y}\bigg|_{Y_R} = \frac{\partial Y_R}{\partial t} + \frac{v_x}{m_x}\frac{\partial Y_R}{\partial x} \qquad (4.8.9)$$

Multiplication by $m_x m_y h$ at $Y_R$ allows cancellation of three of the terms in Eqs. 4.8.4-4.8.6, while the same procedure at $Y_L$ allows cancellation of three more terms, leaving the area-averaged continuity equation as

$$\frac{\partial}{\partial t}\int_{Y_L}^{Y_R} m_x h m_y dy + \frac{\partial}{\partial x}\int_{Y_L}^{Y_R} h v_x m_y dy = 0 \qquad (4.8.10)$$

for situations with no seepage, precipitation, or other flow of water across the channel bed or water surface. Let the average value of $m_x$ be defined by

$$\int_{Y_L}^{Y_R} m_x h m_y dy = \bar{m}_x A \qquad (4.8.11)$$

and let

$$V = \bar{v}_x$$

$$\qquad (4.8.12)$$

$$M = \bar{m}_x$$

Then after assuming that $M$ is independent of $t$ and dividing by $M$, Eq. 4.8.10 becomes

140

$$\frac{\partial A}{\partial t} + \frac{1}{M} \frac{\partial (AV)}{\partial x} = 0 \qquad (4.8.13)$$

### 4.8.3  Area-Averaged Mass Balance of Solute

Integration of the left-hand side of Eq. 4.7.22 is similar to the integration of Eq. 4.7.11 just presented in Section 4.8.2 except that each $h$ in Eqs. 4.8.4–4.8.6 is multiplied by $c$. To perform the integration, multiply each term in the equation by $m_x m_y dy$ and then integrate from $Y_L$ to $Y_R$. Eq. 4.8.9 (or the equivalent at $Y_L$) can be multiplied by $m_x hc$ at $Y_R$ (or $Y_L$) to allow elimination of several terms arising from the application of Leibnitz's rule, so that the width-integrated left side of Eq. 4.7.22 becomes

$$\frac{\partial}{\partial t} \int_{Y_L}^{Y_R} c m_x h m_y \, dy + \frac{\partial}{\partial x} \int_{Y_L}^{Y_R} c v_x h m_y \, dy \qquad (4.8.14)$$

Integration of the right side of Eq. 4.7.22 requires another boundary condition similar to Eqs. 4.7.13–4.7.15. As before, if $h$ goes to zero at $Y_R$ and $Y_L$, then several of the terms arising from application of Leibnitz's rule are equal to zero since they contain $h$ at $Y_R$ and $Y_L$. For other, more general cases, let $d\lambda$ be an increment of length along the water's edge with $m_x dx$ being the length of the projection of $d\lambda$ on a longitudinal coordinates surface (Section 4.4) at the water's edge. Then, the normal unit outward vector at $Y_R$ is

$$\vec{n} = \left[\left(-\frac{m_y}{m_x}\frac{\partial Y_R}{\partial x}\vec{i} + \vec{j}\right)\left(\frac{1}{m_x}\frac{d\lambda}{dx}\right)\right]_{Y_R}$$

(4.8.15)

$$= \left\{\left(-\frac{m_y}{m_x}\frac{\partial Y_R}{\partial x}\vec{i} + \vec{j}\right)\left[\left(\frac{m_y}{m_x}\frac{\partial Y_R}{\partial x}\right)^2 + 1\right]^{-1/2}\right\}_{Y_R}$$

where $\vec{i}$ and $\vec{j}$ are the unit vectors along the respective coordinate surfaces. A similar expression with opposite signs in the first term on the RHS of Eq. 4.8.15 would give the unit normal outward vector at $Y_L$ . Also, let $f$ be the depth-averaged unit diffusive flux vector:

$$\vec{f} = -\frac{e_x}{m_x}\frac{\partial c}{\partial x}\vec{i} - \frac{e_y}{m_y}\frac{\partial c}{\partial y}\vec{j}$$

(4.8.16)

Application of Leibnitz's rule to the width integration of the right-hand side of Eq. 4.7.22 after it has been multiplied by $m_x m_y dy$ gives, among other terms, two terms evaluated at $Y_R$ and two similar terms at $Y_L$ . The sum of these four terms is equal to

$$-(m_x h\vec{f} \cdot \vec{n})_{Y_L}\left(\frac{1}{m_x}\frac{d\lambda}{dx}\right)_{Y_L} - (m_x h\vec{f}\cdot n)_{Y_R}\left(\frac{1}{m_x}\frac{d\lambda}{dx}\right)_{Y_R}$$

$$= -(m_x hf)_{Y_L} - (m_x hf)_{Y_R}$$

(4.8.17)

where, to be consistent with the other terms in the width-integrated mass balance equation, $f$ in Eq. 4.8.17 is defined as the boundary efflux per unit of vertical area so that $hf$ is the efflux per unit of length along the x axis, and $m_x$ is therefore needed on the right-hand side of Eq. 4.8.17 to give the correct flux per unit of length at the boundaries. The integrated right-hand side of Eq. 4.7.22 then becomes

$$\frac{\partial}{\partial x} \int_{Y_L}^{Y_R} \frac{m_y}{m_x} he_x \frac{\partial c}{\partial x} \, dy - (m_x hf)_{Y_L} - (m_x hf)_{Y_R}$$

$$(4.8.18)$$

$$- \int_{Y_L}^{Y_R} (f_S + f_B + khc) \, m_x m_y dy$$

Before equating Eqs. 4.8.14 and 4.8.18 for the width-integrated, 1D, advective-diffusion equation, some of the integrals need to be considered further.

"The integral in the first term of [Eq.] 4.8.14 may be written as

$$\int_{Y_L}^{Y_R} cm_x hm_y dy = \overline{Acm_x} = A \, \overline{c} \, \overline{m_x} + \overline{c'm_x'}$$

$$(4.8.19)$$

The covariance term i.e. $\overline{c'm_x'}$ is a peculiar term resulting from the use of the natural coordinate system (as noted in Section 4.8.1). The term will be kept in the present form for later comments.

"The integral in the second term of [Eq.] 4.8.14 is written as

$$\int_{Y_L}^{Y_R} cv_x hm_y dy = \overline{Acv_x} = A \, \overline{c} \, \overline{v_x} + \overline{c'v_x'}$$

$$(4.8.20)$$

The covariance term of Eq. 4.8.20 is analogous to [similar terms in] Eqs. 4.6.7 and 4.7.17. In extending Taylor's longitudinal dispersion

143

theory to natural streams, Fischer (1966) showed that "under rather restrictive conditions as presented in Section 6.3" this covariance can also be expressed in a gradient-type flux form. In the natural coordinate system, the flux form may be written as

$$\overline{c'v_x'} = -\frac{K_x}{\overline{m}_x}\frac{\partial \overline{c}}{\partial x} \tag{4.8.21}$$

which is analogous to Eqs. 4.6.8 and 4.7.18. The symbol $K_x$ is the longitudinal advective-dispersion coefficient induced by the widthwise variation of $v_x$ and $c$.

"The integral in [Eq.] 4.8.18 is written as

$$\int_{Y_L}^{Y_R}\frac{e_x}{m_x}\frac{\partial c}{\partial x}hm_y\,dy = A\,\overline{\frac{e_x}{m_x}\frac{\partial c}{\partial x}} = A\left[\overline{\left(\frac{e_x}{m_x}\right)}\overline{\left(\frac{\partial c}{\partial x}\right)} + \overline{\left(\frac{e_x}{m_x}\right)'\left(\frac{\partial c}{\partial x}\right)'}\right]\text{''} \tag{4.8.22}$$

In order to express $\overline{(\partial c/\partial x)}$ in terms of $\partial \overline{c}/\partial x$, apply Leibnitz's rule again to obtain

$$\overline{\frac{\partial c}{\partial x}} = \frac{1}{A}\int_{Y_L}^{Y_R}\frac{\partial c}{\partial x}hm_y\,dy = \frac{1}{A}\int_{Y_L}^{Y_R}\left[\frac{\partial}{\partial x}(chm_y) - c\frac{\partial(hm_y)}{\partial x}\right]dy$$

$$\tag{4.8.23}$$

$$= \frac{\partial \overline{c}}{\partial x} - \frac{1}{A}(chm_y)_{Y_R}\frac{\partial Y_R}{\partial x} + \frac{1}{A}(chm_y)_{Y_L}\frac{\partial Y_L}{\partial x} - \frac{1}{A}\int_{Y_L}^{Y_R}c\frac{\partial(hm_y)}{\partial x}\,dy$$

With presently used analyses, it is not necessary to try to evaluate the covariance term (the last term in the brackets) in Eq. 4.8.22 and

144

the last three terms in the final form of Eq. 4.8.23 because the net contribution of all of these terms is probably small compared to the first term in the brackets in Eq. 4.8.22, which in turn normally provides a small contribution to the total longitudinal mixing when compared to the mixing mechanisms represented in Eq. 4.8.21. (Also, if all of the terms in Eqs. 4.8.22 and 4.8.23 had to be evaluated, there would be little benefit in using a 1D representation.)

The last terms in Eq. 4.8.18 may be integrated as follows, where it is assumed that $k$ is not a function of $y$ :

$$\int_{Y_L}^{Y_R} (f_S + f_B + khc) \, m_x m_y \, dy = \int_{Y_L}^{Y_R} m_x \left( \frac{f_S}{h} + \frac{f_B}{h} + kc \right) h m_y \, dy$$

$$= \left[ \overline{\left( \frac{m_x f_S}{h} \right)} + \overline{\left( \frac{m_x f_B}{h} \right)} + k \, \overline{m_x c} \right] A \qquad (4.8.24)$$

$$= A \left[ \overline{\left( \frac{m_x f_S}{h} \right)} + \overline{\left( \frac{m_x f_B}{h} \right)} \right] + A \overline{m}_x k \overline{c} + A k \, \overline{m'_x c'}$$

Recall that $f_S$ and $f_B$ are fluxes at the free surface and bed per unit of horizontal area. Thus, $f/h$ is a flux per unit of volume in the vertical water column where the flux $f$ is taking place. In the averages of $f_S$ and $f_B$ , $m_x$ is retained to give the correct horizontal area per unit of transverse length ($m_y dy$).

From Eqs. 4.8.14 and 4.8.17, the width-integrated form of Eq. 4.7.24 may be written as

$$\frac{\partial}{\partial t}\left(A\,\bar{c}\,\bar{m}_x\right) + \frac{\partial}{\partial t}\left(A\,\overline{c'm_x'}\right) + \frac{\partial}{\partial x}\left(A\,\bar{c}\,\bar{v}_x\right) = \frac{\partial}{\partial x}\left(A\,\frac{K}{\bar{m}_x}\,\frac{\partial\bar{c}}{\partial x}\right)$$

$$+ \frac{\partial}{\partial x}\left[A\,\overline{\left(\frac{e_x}{m_x}\right)}\frac{\partial\bar{c}}{\partial x} - \frac{1}{A}\,(chm_y)^{\circledast}_{Y_R}\,\frac{\partial Y_R}{\partial x} + \frac{1}{A}\,(chm_y)^{\circledast}_{Y_L}\,\frac{\partial Y_L}{\partial x}\right.$$

$$- \frac{1}{A}\int_{Y_L}^{Y_R} \overset{\circledast}{c}\,\frac{\partial(hm_y)}{\partial x}\,dy + \overset{\circledast}{\overline{\left(\frac{e_x}{m_x}\right)'\left(\frac{\partial c}{\partial x}\right)'}} \tag{4.8.25}$$

$$\left. - (m_x f)_{Y_L} - (m_x f)_{Y_R} - A\,\overline{\left(\frac{m_x f_S}{h}\right)} + \overline{\left(\frac{m_x f_B}{h}\right)}\right] - A\bar{m}_x k\bar{c}$$

$$- Ak\,\overline{m_x' c'}$$

Use the definition of $V$ and $M$ in Eq. 4.8.12 and let

$$C = \bar{c}$$

$$\tag{4.8.26}$$

$$E = K_x + M\,\overline{\left(\frac{e_x}{m_x}\right)}$$

It is normally implicitly assumed, since the terms marked with an asterisk (*) in Eq. 4.8.25 apparently contribute very little to the transport process, that any influence of the terms can just be included in $E$ as a mixing coefficient. Then, since $M$ is independent of $t$, Eq. 4.8.25 can be written as

146

$$\frac{\partial}{\partial t}(AC) + \frac{\partial}{\partial t}\left(\frac{A\overline{c'm'_x}}{M}\right) + \frac{1}{M}\frac{\partial}{\partial x}(AVC) = \frac{1}{M}\frac{\partial}{\partial x}\left(\frac{AE}{M}\frac{\partial C}{\partial x}\right)$$

$$- A\left[\overline{\left(\frac{m_x f_S}{h}\right)} + \overline{\left(\frac{m_x f_B}{h}\right)} + kC\right] - \frac{A}{M}\,k\overline{c'm'_x} \tag{4.8.27}$$

$$- \frac{1}{M}\left[(m_x hf)_{Y_L} + (m_x hf)_{Y_R}\right]$$

Writing $f_S$ and $f_B$ in Eq. 4.8.27 in terms of cross-sectional averages to be consistent with the other terms may tend to obscure the physical meaning of the terms, for example,

$$A\,\overline{\left(\frac{m_x f_B}{h}\right)} = A\left(\frac{1}{A}\int_{Y_L}^{Y_R}\frac{m_x f_B}{h}\,hm_y\,dy\right) = \int_{Y_L}^{Y_R} m_x f_B m_y\,dy \tag{4.8.28}$$

so that this term represents the bottom efflux per unit of channel length (dx), while the $f_S$ , $(m_x hf)_{Y_L}$ , and $(m_x hf)_{Y_R}$ terms are similar terms at the surface, left edge, and right edge, so that the sum of these four terms, which is called $F$ , is the total efflux per unit of channel length (dx):

$$F = A\left[\overline{\left(\frac{m_x\,f_S}{h}\right)} + \overline{\left(\frac{m_x f_B}{h}\right)}\right] + \frac{1}{M}\left[(m_x hf)_{Y_L} + (m\,hf)_{Y_R}\right] \tag{4.8.29}$$

With this definition, Eq. 4.8.27 may be written as

$$\frac{\partial (AC)}{\partial t} + \frac{\partial (A\overline{c'm_x'})}{\partial t} + \frac{1}{M} \frac{\partial}{\partial x} (AVC) = \frac{1}{M} \frac{\partial}{\partial x} \left( \frac{AE}{M} \frac{\partial C}{\partial x} \right)$$

(4.8.30)

$$- F - AkC - \frac{A}{M} \overline{kc'm_x'}$$

"In going from the depth-averaged Eqs. 4.7.11 and 4.7.22 to the cross-section-averaged Eqs. 4.8.13 and 4.8.30 no assumptions were introduced except for those related to the spatial covariance terms, such as in Eqs. 4.8.21" and the terms marked by an asterisk in Eq. 4.8.25. "As was the case with $k_x$ , the advective dispersion coefficient, $K_x$ , induced by the widthwise variation of $v_x$ and $c$ , is an asymptotic approximation." Thus, its application assumes that the solute concentration is well distributed over the channel width (Fischer 1973). The overall mixing coefficient, $E$ , as defined by Eq. 4.8.26 is more complicated than that for a rectangular Cartesian coordinate system, which may be obtained by letting $M = m_x = 1$ in Eq. 4.8.26. Nevertheless, Eq. 4.8.26 clearly shows that contributions to the mixing coefficient are additive if one recalls that $e_x$ (the two-dimensional mixing coefficient) is the sum of the advective dispersion coefficient $(k_x)$ induced by depth integration, a depth-averaged value of the turbulent diffusion coefficient $(d_x)$, and the constant molecular diffusion coefficient $(D_m)$. According to Fischer's (1966) study and other studies, the contribution of $K_x$ to $E$ is by far the most significant of all the contributions. Fischer's theory, as an extension of Taylor's, has been satisfactorily verified in a steady uniform open-channel flow.

The covariance terms involving $m_x'$ "in Eq. 4.8.30 are terms unique to the natural coordinate system, since they will be zero in a rectangular Cartesian system, wherein $m_x' = 0$ . Note that $m_x'$ is determined predominantly by the geometry of the coordinate system, whereas $c$ is dependent on the widthwise distribution of solute concentration," and $f'$ , as a surface flux, in many cases might be proportional to $c'$ . In a sharp bend, $m_x'$ might be large enough to cause

148

a small contribution from the $\overline{m'_x c'}$ terms, but even that is doubtful since one of the conditions for using a one-dimensional advective-dispersion coefficient (E), as mentioned above, is that the concentration distribution be well mixed transversely. This means that in order to use a 1D equation, c' must be small. Thus, for most cases, the covariance terms involving m' and c' or f' are probably insignificant. If these terms are neglected and M is assumed to be approximately unity, Eq. 4.8.30 may be written as

$$\frac{\partial C}{\partial t} + V \frac{\partial C}{\partial x} = \frac{1}{A} \frac{\partial}{\partial x} \left( AE \frac{\partial C}{\partial x} \right) - \frac{F}{A} - kC \qquad (4.8.31)$$

after using C times Eq. 4.8.13 to eliminate some of the terms which result from expanding the derivatives on the left-hand side of Eq. 4.8.30.

## 4.9 FURTHER COMMENTS

"As outlined in the introduction, merits of the transport equations derived herein are drawn mostly from analytical considerations. By use of the natural coordinate system, one can define a stationary coordinate system for an entire flow field, in which the channel axis meanders and the width and depth vary from point to point. As no assumptions are introduced in the derivation process except those related to covariance terms between solute concentration and advective velocities, the transport equations thus derived apply to unsteady or nonuniform natural channel flows with moving boundaries.

"On the other hand, in order to apply gradient-type diffusive flux models to various covariance terms, solute concentration must be well distributed over the depth and [or] the channel width. Another restriction is that, because of the present configuration of the natural coordinate system, the predominant flow direction must be horizontal." This restriction is not a severe one for many rivers.

"Gradient-type diffusive flux models were introduced into the advection-diffusion equations with only cursory references to the

149

mechanics of turbulent flows. Understanding the mechanics, however, is an essential prerequisite to applying the equations properly to a real turbulent flow. The reader is referred to Fischer's (1973) comprehensive review of the mechanics of mixing. [See also Fischer et al. 1979.] Briefly, the gradient-type flux models for dispersion and diffusion have been verified as asymptotic approximations only in a steady uniform flow. Their applicability in an unsteady flow is less certain theoretically and experimentally. The advective-diffusion equations are workable models in most natural rivers and estuaries," where the magnitude of the turbulent velocity fluctuations is small relative to the longitudinal velocity.

"Transport equations in the natural coordinate system have two additional parameters, $m_x$ and $m_y$, compared with those in a rectangular Cartesian coordinate system. Significance of these parameters beyond their analytical utility is not well known currently." At the very least, the inclusion of these metric coefficients shows the level of approximation involved when a meandering $x,y,z$ system is superimposed on a river and $m_x$ and $m_y$ are assumed to be unity. "Sayre and Yeh (1973) found that the range of $m_x$ is from 0.84 to 1.14 for the Aspinwall Bend in the Missouri River near Cooper Nuclear Station, which probably represents one of the sharpest bends in a large river. It is thus apparent that, for one-dimensional equations, the metric coefficient, $M$, will tend to unity if one locates the x axis in the central part of a channel as Sayre and Yeh did in their Missouri study.

"Despite some uncertainties and limitations arising from the current knowledge on the mechanics of turbulent mixing, Eqs. 4.6.5 and 4.6.10 for three (space) dimensions, Eqs. 4.7.11 and 4.7.22 (or Eq. 4.7.33 or 4.7.34) for two dimensions, and Eqs. 4.8.13 and 4.8.30 for one dimension represent one of the most workable sets of equations for solute transport by turbulent flow in a natural channel."

(The passages in quotations in Chapter 4 were taken from Yotsukura (1977); see Section 4.1.3.)

150

# CHAPTER 5. CALCULATED CHARACTERISTICS OF STEADY-STATE CONCENTRATION DISTRIBUTIONS

## 5.1 STEADY-STATE DISTRIBUTIONS

Concentration distributions in a river may be approximated as being steady-state distributions if the river flow, the upstream concentration distribution (e.g. from an effluent discharge or tributary inflow), and the rate coefficients for any distributed sources and sinks (e.g. reaction, production, surface transfer, etc.) are approximately constant. For such steady-state situations, the longitudinal concentration gradients in rivers are frequently small enough that the effects of longitudinal mixing (which is proportional to the concentration gradient times a mixing coefficient, Eqs. 4.5.3, 4.7.18, and other similar expressions in Chapter 4) are negligible compared to the other processes influencing the concentration distributions.

In this chapter, concentration distributions are given for typical 3D, 2D, and 1D steady-state situations. There are many situations for which concentration distributions could be calculated; only a few examples are illustrated. Also, in this chapter only calculated results are presented; comparisons of data and calculations are presented in Chapter 7. In discussing the solutions, the terms "point source" and "line source" are used to refer to the mathematical representation of effluent discharge conditions at the upstream end of the reach, while the term "distributed sources or sinks" refers to the reactions, decay, surface transfer, etc., that take place within the reach.

Most of the calculated distributions are given in terms of dimensionless variables since these variables allow the general characteristics of the distributions to be demonstrated and discussed without needing to use specific hydraulic characteristics (depth, velocity, etc.). These dimensionless variables also form the basis for comparing measured concentration distributions from different rivers with each other and for interpreting the calculated distributions for specific situations. It is highly desirable to become accustomed to thinking in terms of the dimensionless variables when considering questions such as

151

the relative shapes of the concentration distributions, degree of mixing, etc., for transport problems in rivers.

Various dimensionless variables are introduced as needed for the calculations. However, there is one variable (called the dimensionless longitudinal distance) that occurs with so much regularity that it deserves special mention. This variable relates the time for which transport has been taking place (the flow time, $x/V$, from the point of release to the cross section of interest) to a characteristic time ($t_c$) for mixing. The characteristic time ($t_c$) is defined as the time required for a given amount of mixing to take place. The time for the mixing process to transport mass over a distance $L$ is proportional to the distance squared (if the mixing coefficient is constant); in a simple diffusion problem, four times as much time is needed for the mixing process to increase the width of a concentration distribution to $2L$ as to increase it to $L$. For example, consider a steady-state release into steady, uniform flow in a rectangular channel. Four times as much time is needed for mass to mix across the full channel width as for it to mix across half of the width. Thus, if mass released at the center of the channel reaches the banks in a time $t_1$, then mass released at one edge of the channel requires $4t_1$ to mix across to the far side. The same type of comparison can be made for the concentration distributions for the two release conditions to reach any specified degree of uniformity, not only for the time for mixing to carry mass to the edge of the channel. Similarly, for a 1D longitudinal mixing process which can be described with a dispersion coefficient, if $t_2$ is required for the length of the distribution to increase from zero at the release point to some specified length, then $4t_2$ is required for the length to increase to twice that amount. Furthermore, the time for a given degree of mixing to take place is inversely proportional to the mixing coefficient, as would be expected from the fact that the rate of mass transport in a diffusive-type process is proportional to the mixing coefficient (Eqs. 4.5.3, 4.5.4, and other similar equations in Chapter 4). Thus, if $L$ is defined as a significant distance for the mixing process in a given problem and $D$ is the mixing coefficient,

152

then a characteristic mixing time to be used for nondimensionalization of the problem can be defined as

$$t_c = \frac{L^2}{D} \qquad (5.1.1)$$

The nondimensional distances are given various symbols as appropriate for the various mixing problems considered in subsequent sections, but if a general nondimensional distance is defined as $x_*$ , then

$$x_* = \frac{x/V}{L^2/D} \qquad (5.1.2)$$

For unsteady transport problems, dimensionless time is similarly defined as

$$t_* = \frac{t}{L^2/D} \qquad (5.1.3)$$

Converting between dimensionless and actual distances is considered in Chapters 7 and 8.

## 5.2  THREE-DIMENSIONAL SOLUTIONS

### 5.2.1  Assumptions

Eq. 4.6.10 forms the basis for obtaining 3D analytical solutions. However, several assumptions and simplifications are normally reasonable:

<u>a</u>.  $\partial s/\partial t = 0$ . This is inherent in the specification of steady state.

<u>b</u>.  Negligible effects of longitudinal mixing. The term involving $d_x$ is deleted. (See Section 5.1.)

<u>c</u>.  $u_y = u_z = 0$ . As is shown later (Sections 5.2.6 and 5.2.7), the flow distance over which 3D effects are significant is normally relatively short in the absence of density differences. In this short

153

distance it is common to assume that changes in depth may be neglected (so the vertical velocity, $u_z$ , is zero), that the x axis of a Cartesian coordinate system may be aligned with the mean flow direction (so that the depth average of the transverse velocity, $u_y$ , is zero), and that any variations of $u_x$ and $u_y$ over the depth have negligible influence. (See assumption f below, also.)

$\underline{d}$. $u_x = v_x$ = constant . If $u_y = u_z = 0$ , then by virtue of Eq. 4.6.5 and assumption f below, $u_x$ cannot vary with x and can then be taken out of the derivative on the left-hand side of Eq. 4.6.10. Furthermore, the vertical variations of $u_x$ contribute only to longitudinal spreading, which is usually unimportant in 3D steady-state transport. Thus, $u_x$ may be replaced with its depth average ($v_x$, Eq. 4.7.10), which is taken as constant.

$\underline{e}$. h = constant . The flow is steady, so h does not change with time. Also, for the short distances in the 3D region, h is assumed not to change with either longitudinal or transverse distance.

$\underline{f}$. $m_x = m_y = 1$ . For short distances, channel curvature is neglected. (See assumption c above, also.)

$\underline{g}$. $d_y$ = constant , $d_z$ = constant . $D_m$ is normally absorbed into the definitions of the turbulent diffusion coefficients ($d_y$, $d_z$), and these coefficients are assumed to be constant for the short 3D region. They may then be taken out of the derivatives on the right-hand side of Eq. 4.6.10.

$\underline{h}$. k = constant in the nondimensionalization of the equations (Section 5.2.2). The solutions in Section 5.2.4 are presented for k = 0 , but for steady-state distributions, the effect of a first-order reaction can be taken into account by multiplying the given solutions by $\exp(-kx/v_x)$ , or by $\exp(-k_3 x_3)$ using the dimensionless variables and parameters in Section 5.2.2.

$\underline{i}$. $\partial s/\partial z = 0$ at the water surface and streambed. Any absorption, adsorption, or other transfer of the solute across the surface and bed can be neglected within the short 3D region.

$\underline{j}$. Constant density.

154

With these assumptions, Eq. 4.6.10 may be written as

$$v_x \frac{\partial s}{\partial x} = d_y \frac{\partial^2 s}{\partial y^2} + d_z \frac{\partial^2 s}{\partial z^2} - ks \qquad (5.2.1)$$

In sequence from left to right, the terms represent longitudinal advection, transverse mixing, vertical mixing, and distributed sources and sinks.

5.2.2 Dimensionless Variables and Differential Equation

In order to define dimensionless variables and then to write Eq. 5.2.1 in dimensionless form, the depth h is used as the characteristic distance for mixing. The dimensionless variables, which are given the subscript 3 to indicate that they are for 3D distributions, are then defined as

$$x_3 = \frac{x/v_x}{h^2/d_z} = \frac{d_z x}{h^2 v_x}$$

$$y_3 = \left(\frac{d_z}{d_y}\right)^{1/2} \frac{y}{h}$$

$$z_3 = \frac{z}{h} \qquad (5.2.2)$$

$$k_3 = \frac{h^2/d_z}{1/k} = \frac{h^2 k}{d_z}$$

$$s_3 = \frac{s}{\dot{m} / \left[h^2 v_x \left(\frac{d_y}{d_z}\right)^{1/2}\right]} = \frac{h^2 v_x \left(\frac{d_y}{d_z}\right)^{1/2} s}{\dot{m}}$$

where $\dot{m}$ is the mass of solute released per unit time in the effluent

155

discharge and $h$ is the flow depth. The dimensionless variables may be interpreted as follows:

$x_3$ — ratio of flow time $(x/v_x)$ to characteristic time $(h^2/d_z)$ for vertical mixing over the depth.

$y_3$ — relative transverse coordinate which is scaled so that the diffusion rates are the same with respect to $y_3$ and $z_3$ even though $d_y$ and $d_z$ may not be equal.

$z_3$ — vertical coordinate relative to the depth.

$k_3$ — ratio of characteristic vertical mixing time $(h^2/d_z)$ to characteristic decay or reaction time $(1/k)$.

$s_3$ — concentration relative to a reference concentration which is the concentration that would exist after complete mixing of the given $\dot{m}$ in a hypothetical section $h$ deep and $h(d_y/d_z)^{1/2}$ wide.

Introduction of the dimensionless variables into Eq. 5.2.1 gives

$$\frac{\partial s_3}{\partial x_3} = \frac{\partial^2 s_3}{\partial y_3^2} + \frac{\partial^2 s_3}{\partial z_3^2} - k_3 s_3 \tag{5.2.3}$$

Solution of this equation, with the appropriate boundary conditions, gives the concentration distributions as a function of $x_3$, $y_3$, and $z_3$.

### 5.2.3  Coordinate Origin and Boundary Conditions

The upstream condition to be represented is a passive point source with a mass discharge rate $(\dot{m})$ located at a distance "a" above the stream bed. The origin of the coordinate system is located on the stream bed directly below the source so that the coordinates of the source are $x_3 = 0$, $y_3 = 0$, $z_3 = a_3 = a/h$. The mathematical boundary conditions may then be expressed as

156

$$s_3 = \delta(y_3)\delta(z_3 - a_3) \quad \text{on} \quad x_3 = 0$$

$$\frac{\partial s_3}{\partial z_3} = 0 \quad \text{on} \quad z = 0 \quad \text{and} \quad 1 \qquad (5.2.4)$$

$$s_3 = 0 \quad \text{for} \quad x_3 \to \infty$$

where $\delta(\ )$ is the Dirac delta function.

## 5.2.4 Analytical Solutions

The analytical solution for the concentration distributions $(s_3)$ as a function of $x_3$, $y_3$, and $z_3$ is given from Eqs. 4.3.2 and 5.2.4 using the method of images as

$$s_3 = \frac{1}{4\pi x_3} \sum_{i=-\infty}^{\infty} \sum_{j=1}^{2} \exp\left\{-\frac{\left[z_3 - (-1)^j a_3 - 2i\right]^2 + y_3^2}{4x_3}\right\} \qquad (5.2.5)$$

or, if $a_3 = 0$, as

$$s_3 = \frac{1}{2\pi x_3} \sum_{i=-\infty}^{\infty} \exp\left[-\frac{\left(z_3 - 2i\right)^2 + y_3^2}{4x_3}\right] \qquad (5.2.6)$$

Using the method of separation of variables, the solution may also be written as

$$s_3 = \frac{1}{2\left(\pi x_3\right)^{1/2}} \exp\left(-\frac{y_3^2}{4x_3}\right)\left[1 + 2\sum_{i=1}^{\infty} \cos(i\pi a_3)\cos(i\pi z_3)\exp\left(-i^2\pi^2 x_3\right)\right] \qquad (5.2.7)$$

## 5.2.5 Concentration Distributions

Various characteristics of the concentration distributions are shown in Figures 34 and 35 for $a_3 = 0$ and $a_3 = 0.2$ for a conservative solute $(k_3 = 0)$. For $k_3 \neq 0$, the effects of a first-order decay or reaction can be included by multiplying the calculated concentrations

157
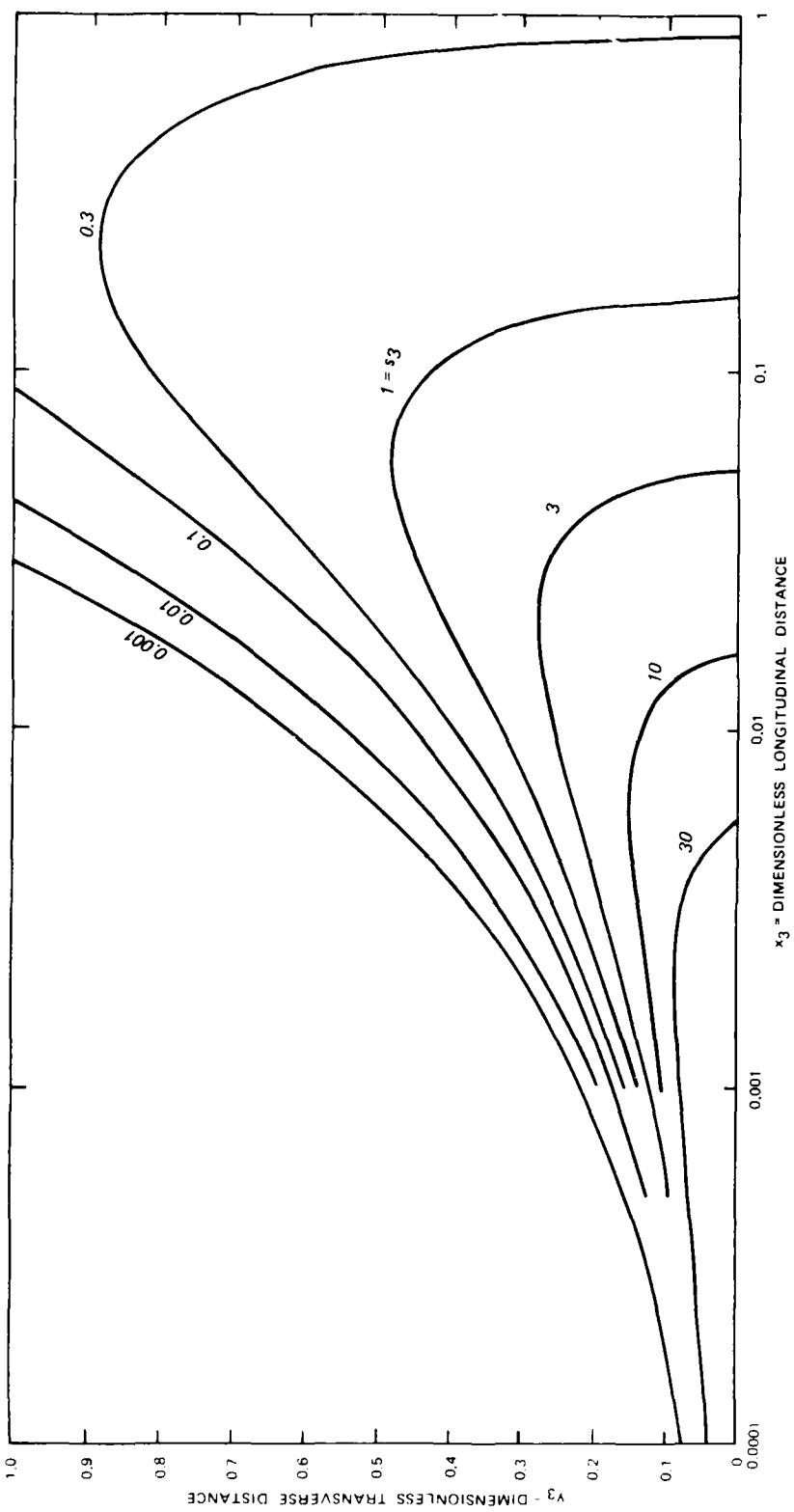
a. Contours of concentration at bed

Figure 34. Calculated concentration distributions for point source at bed (3D, $a_3 = 0$) (Sheet 1 of 6)

158
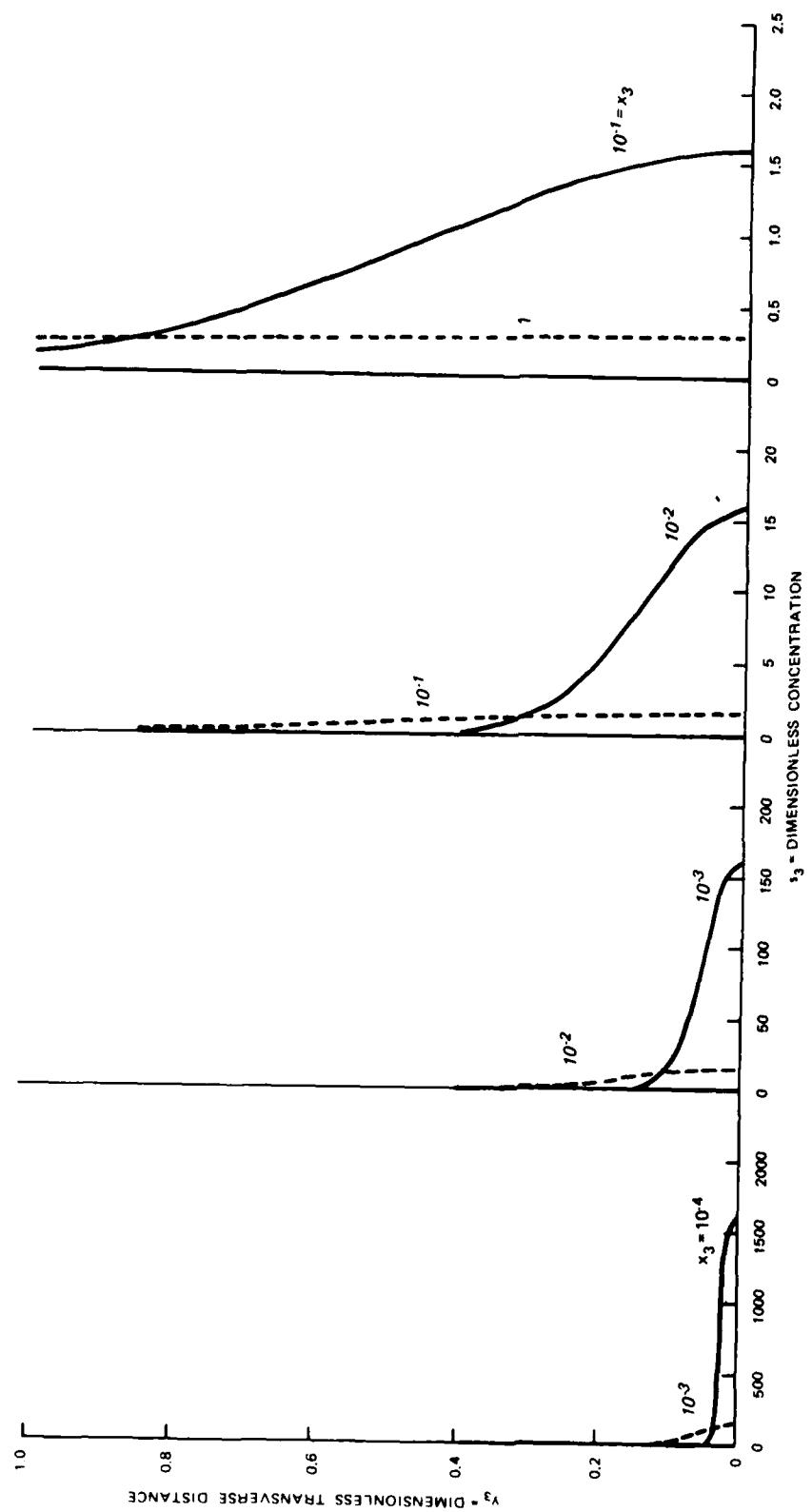
b. Concentration distributions at bed

Figure 34. (Sheet 2 of 6)
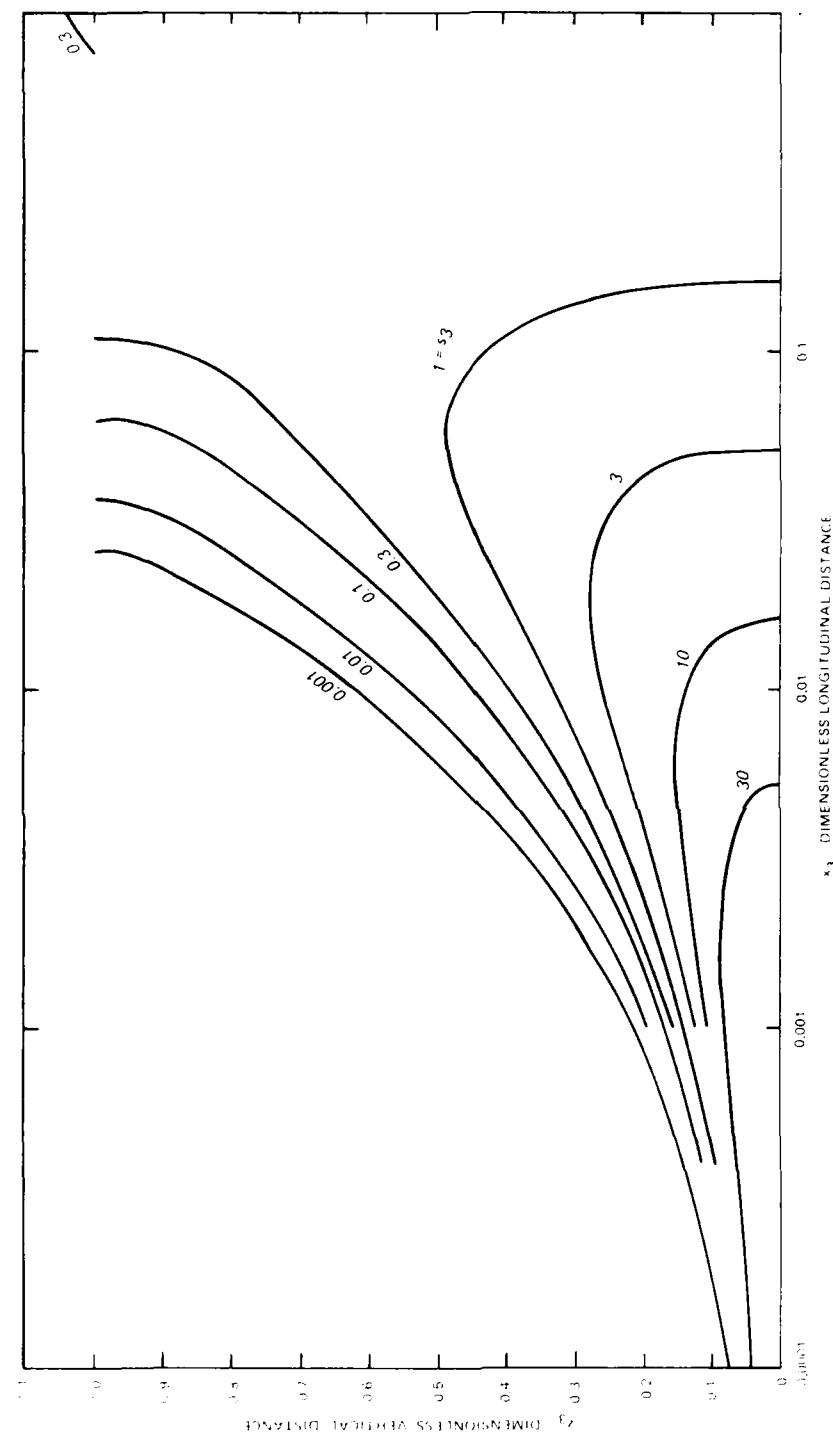
c. Contours of concentration on vertical plane ($y_3 = 0$) through source

Figure 34. (Sheet 3 of 6)

160
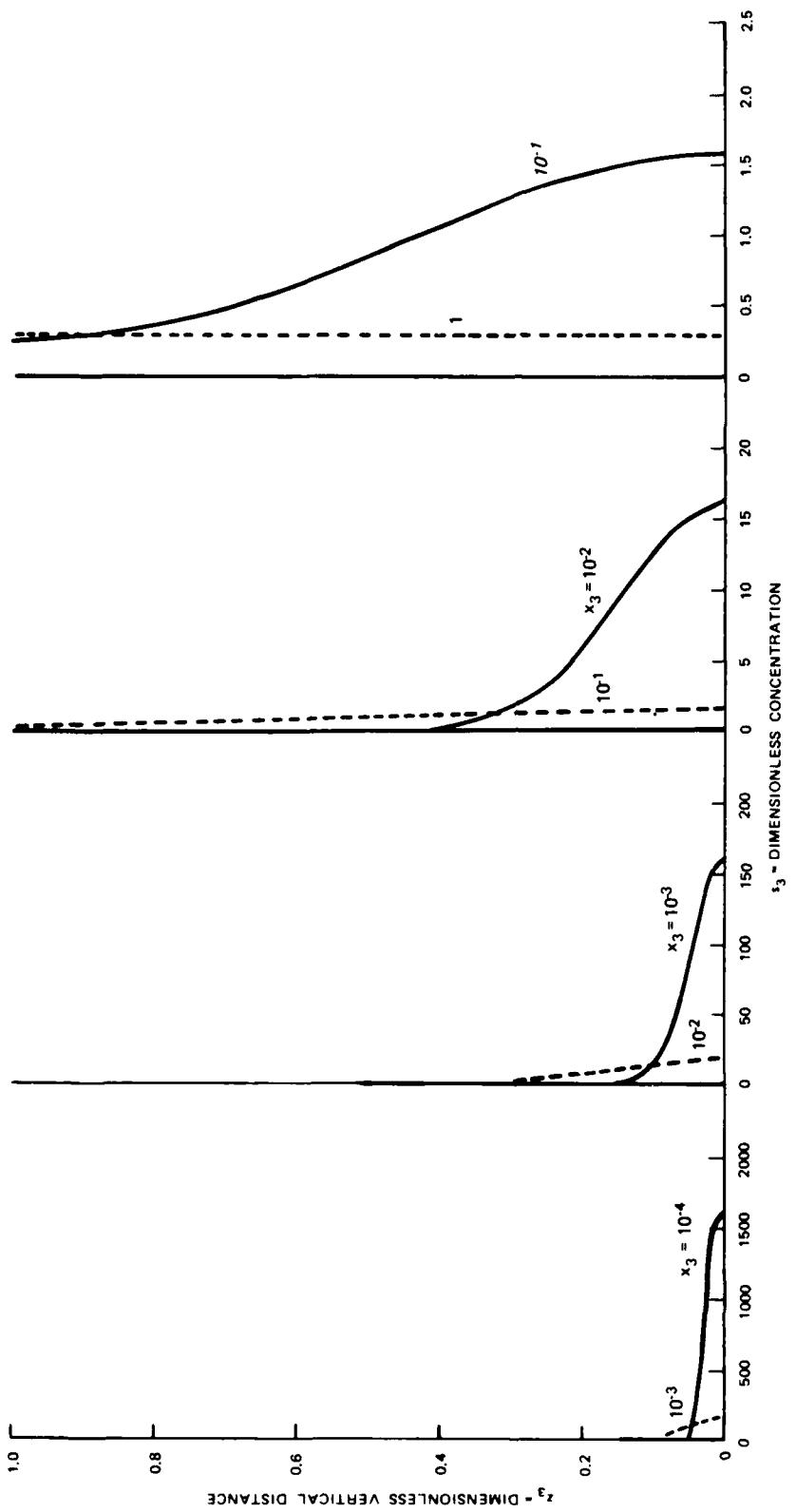
d. Concentration distributions on vertical plane ($y_3 = 0$) through source

Figure 34. (Sheet 4 of 6)

161
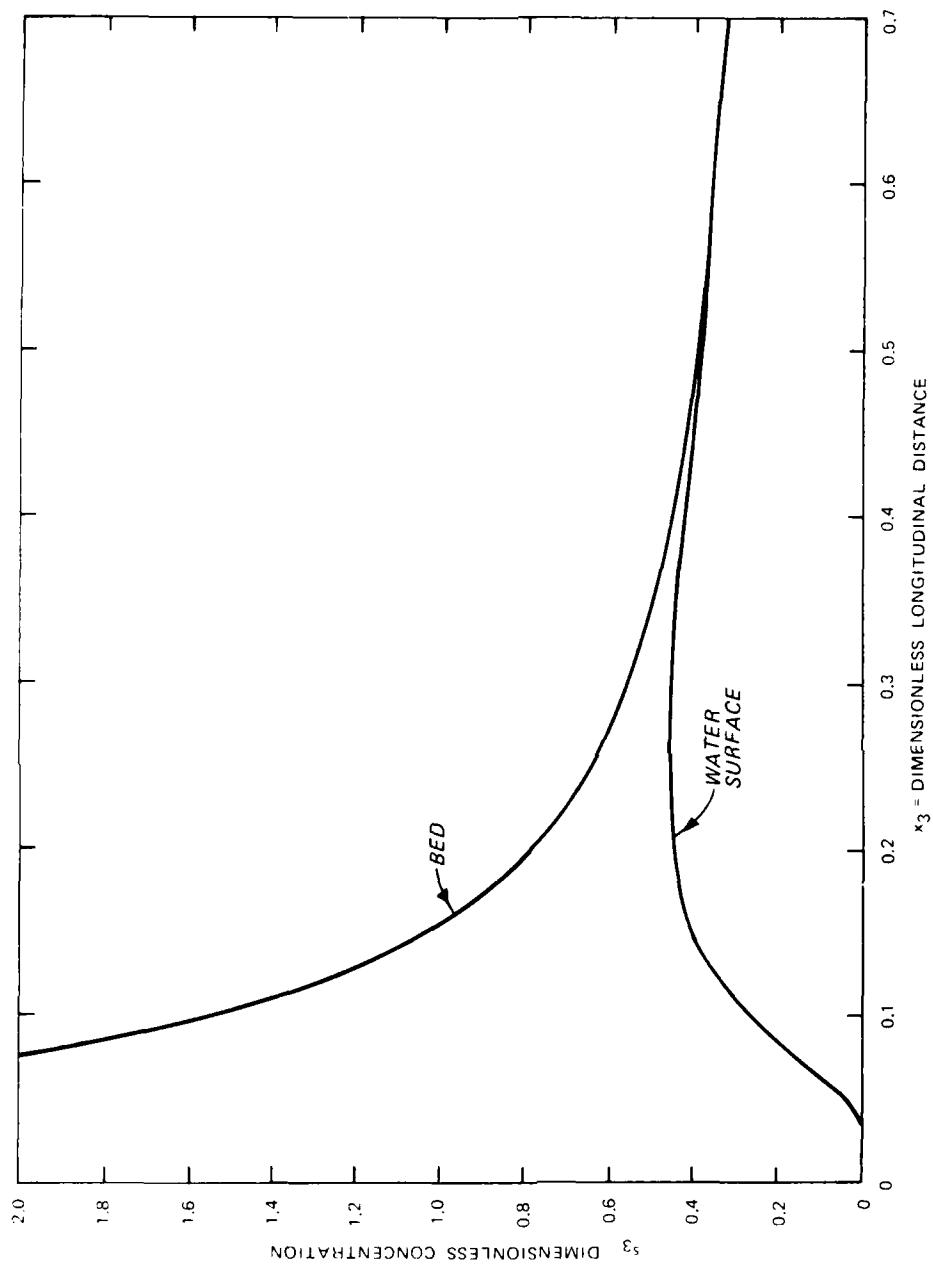
e. Concentration variation at bed and water surface (linear plot)

Figure 34. (Sheet 5 of 6)
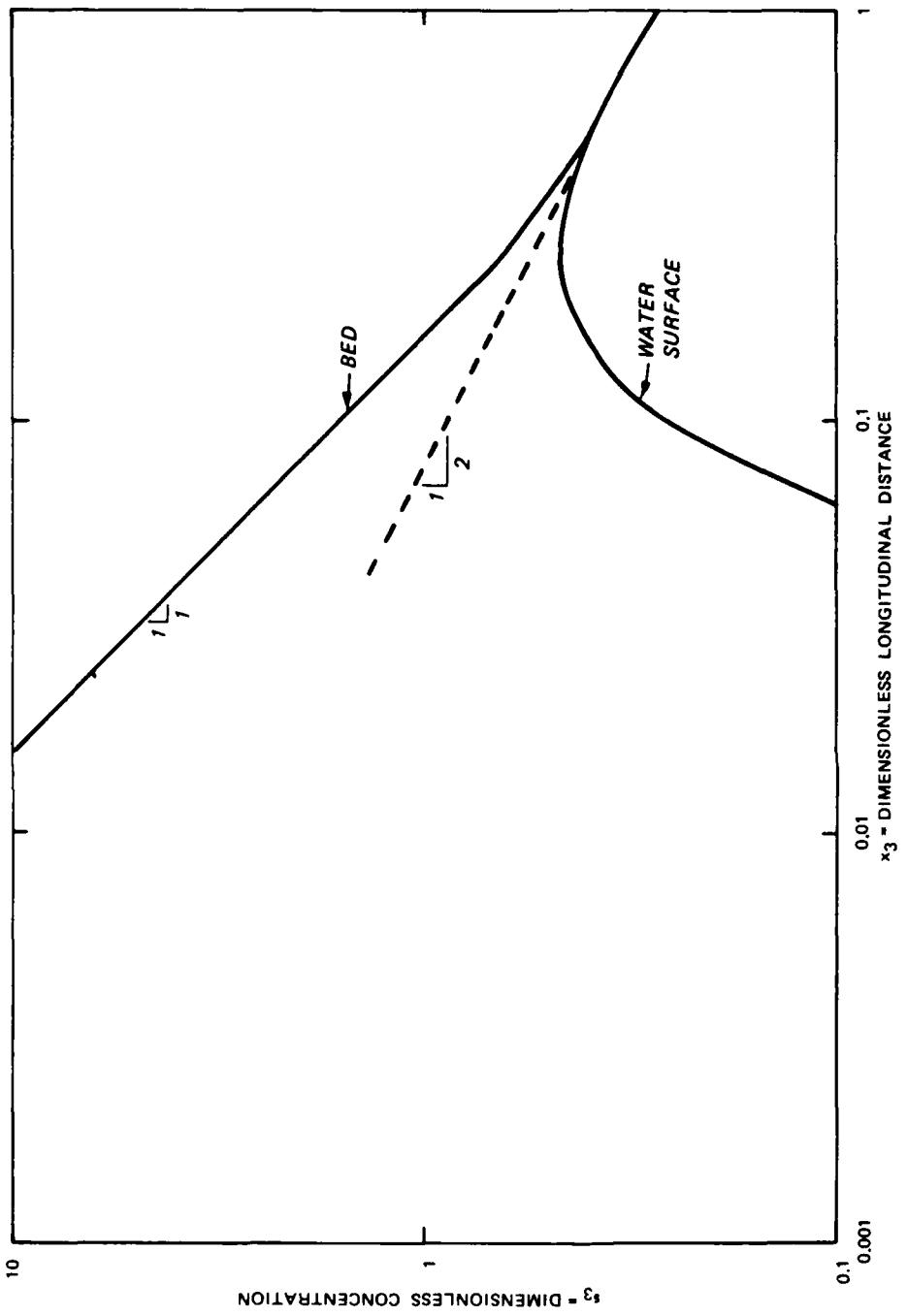
f. Concentration variation at bed and water surface (log-log plot)

Figure 34. (Sheet 6 of 6)
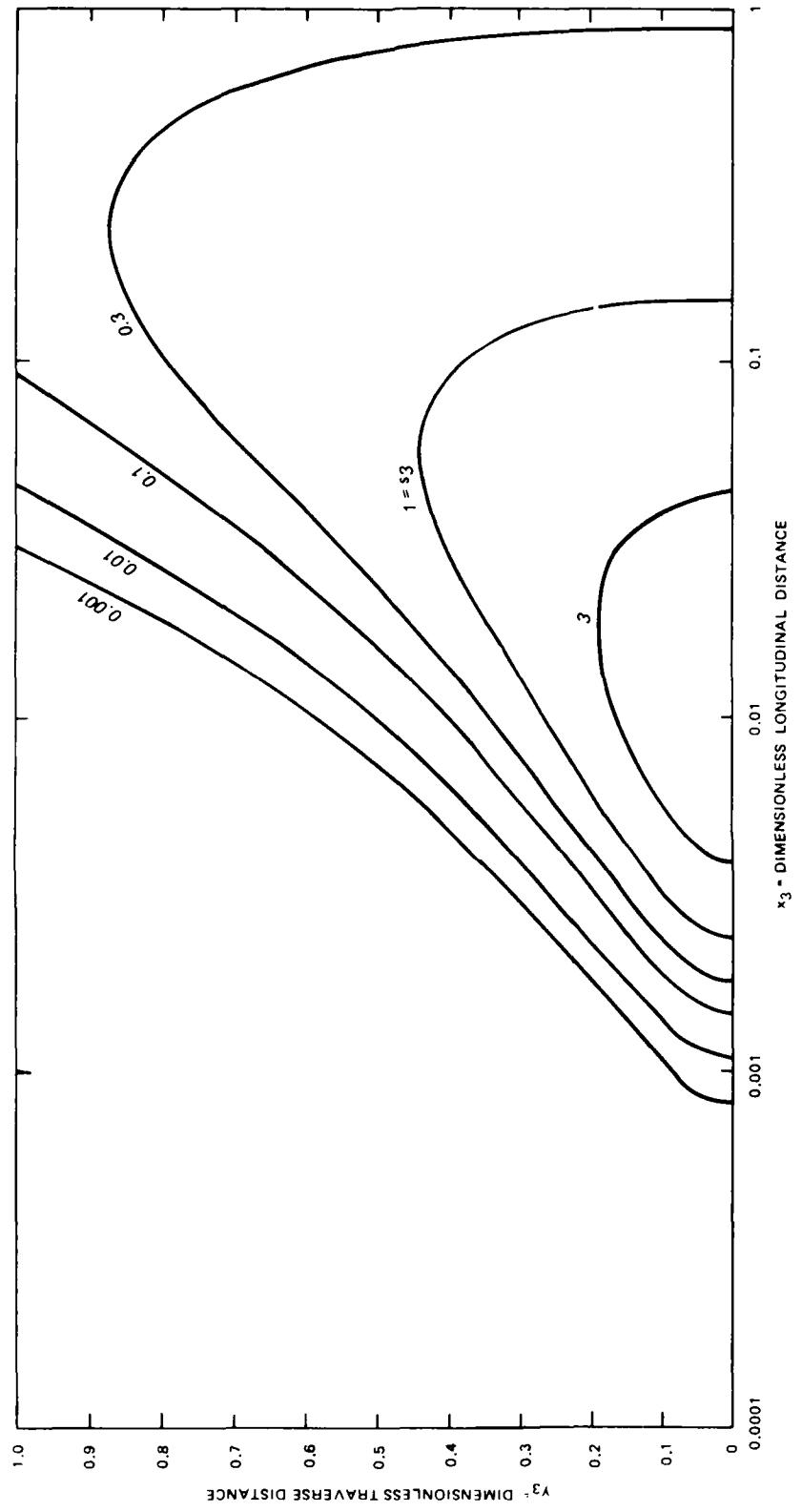
a. Contours of concentration at bed

Figure 35. Calculated concentration distributions for point source at $a_3 = 0.2$ (3D)
(Sheet 1 of 6)

164
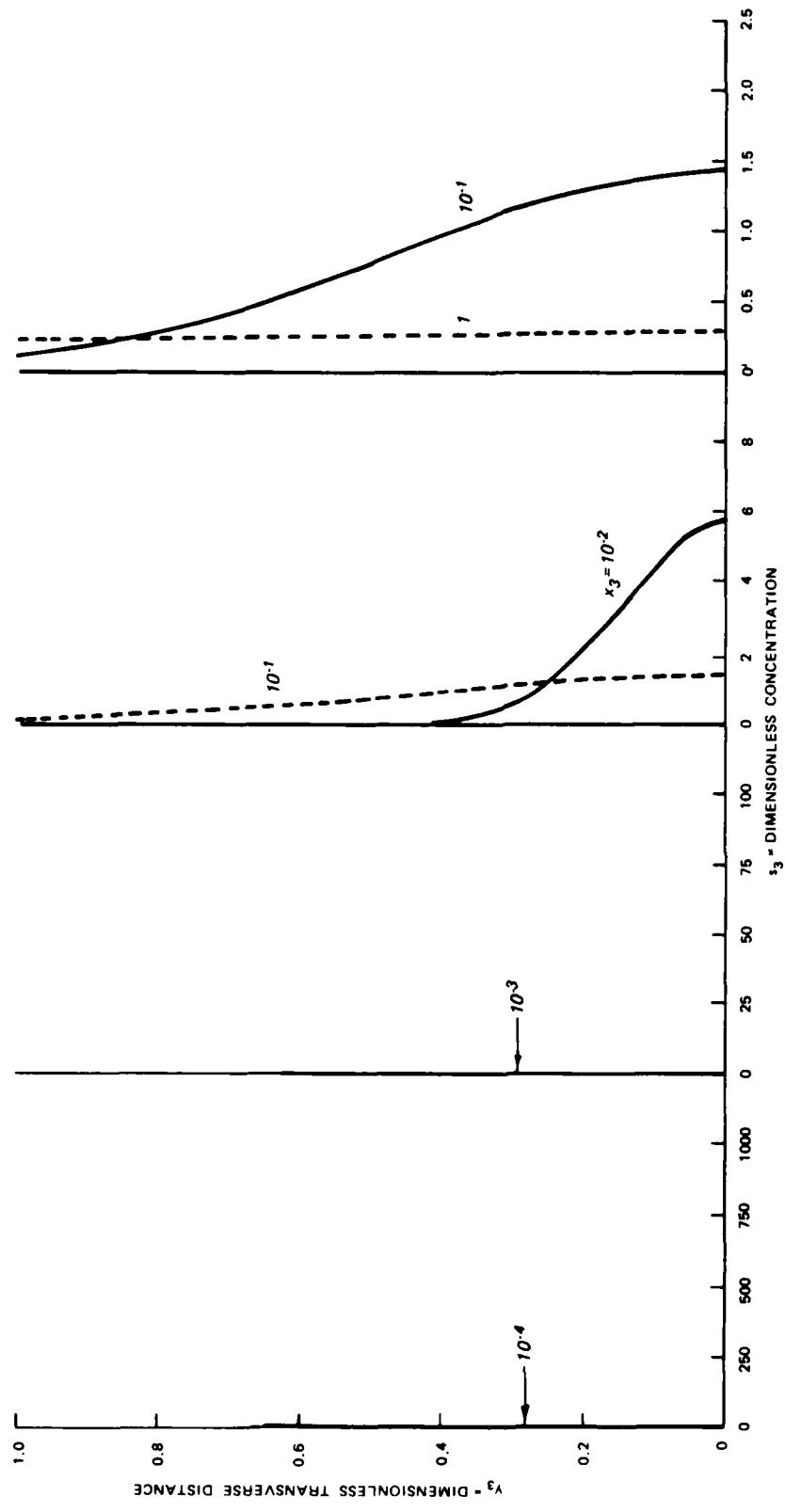
b. Concentration distribution at bed

Figure 35. (Sheet 2 of 6)
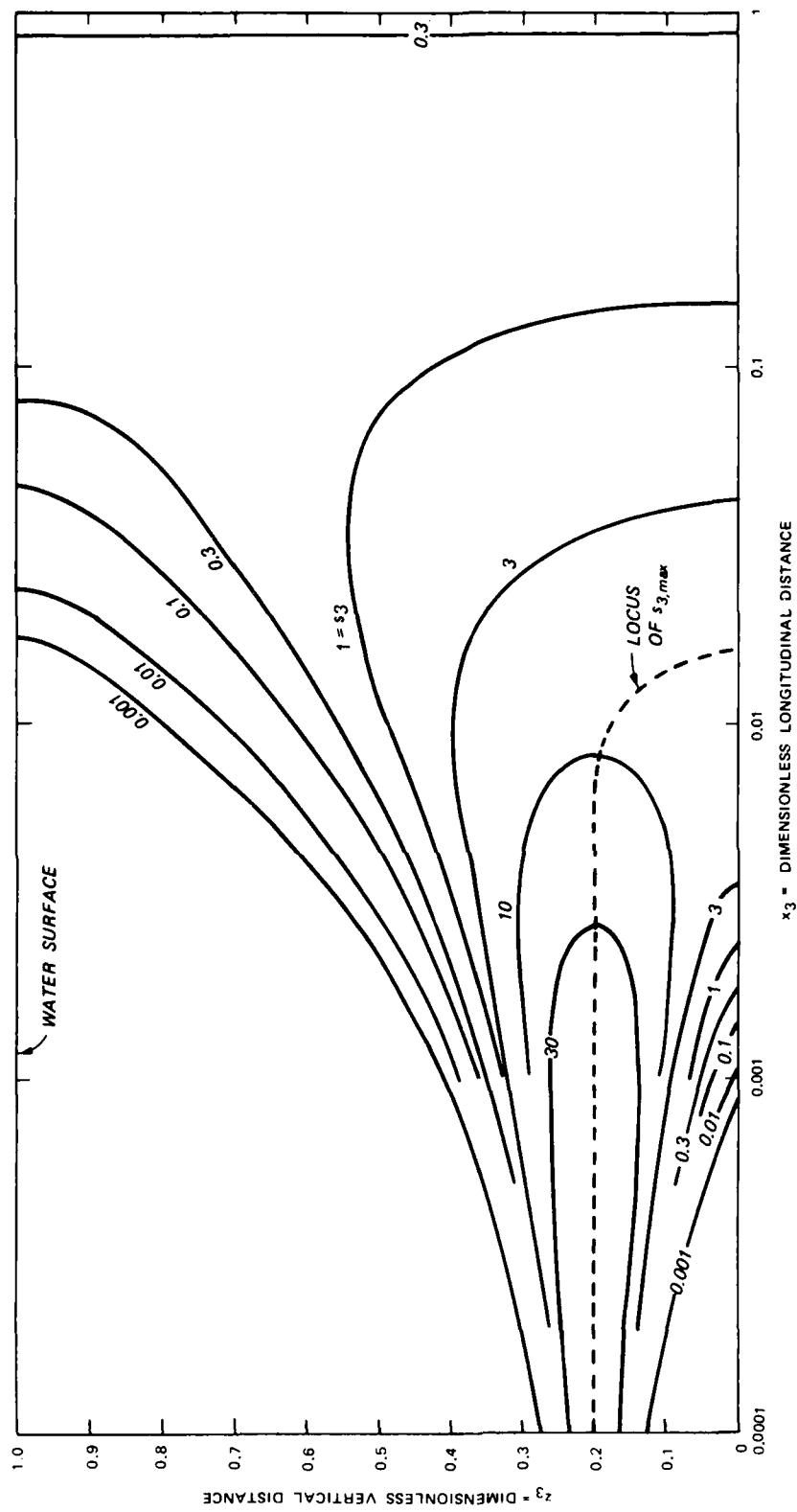
c. Contours of concentration on vertical plane ($y_3 = 0$) through source

Figure 35. (Sheet 3 of 6)

166
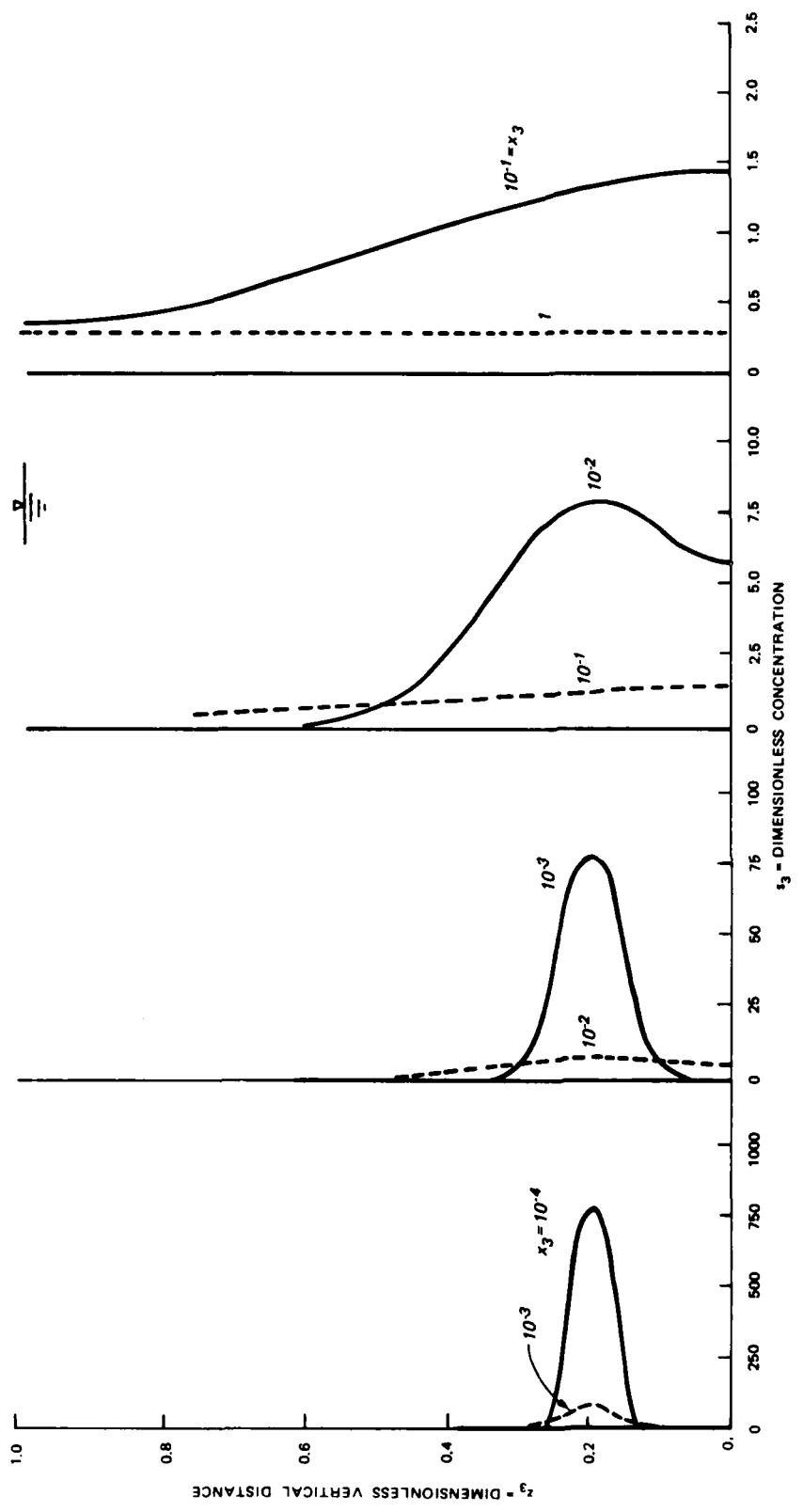
d. Concentration distributions on vertical plane ($y_3 = 0$) through source

Figure 35. (Sheet 4 of 6)
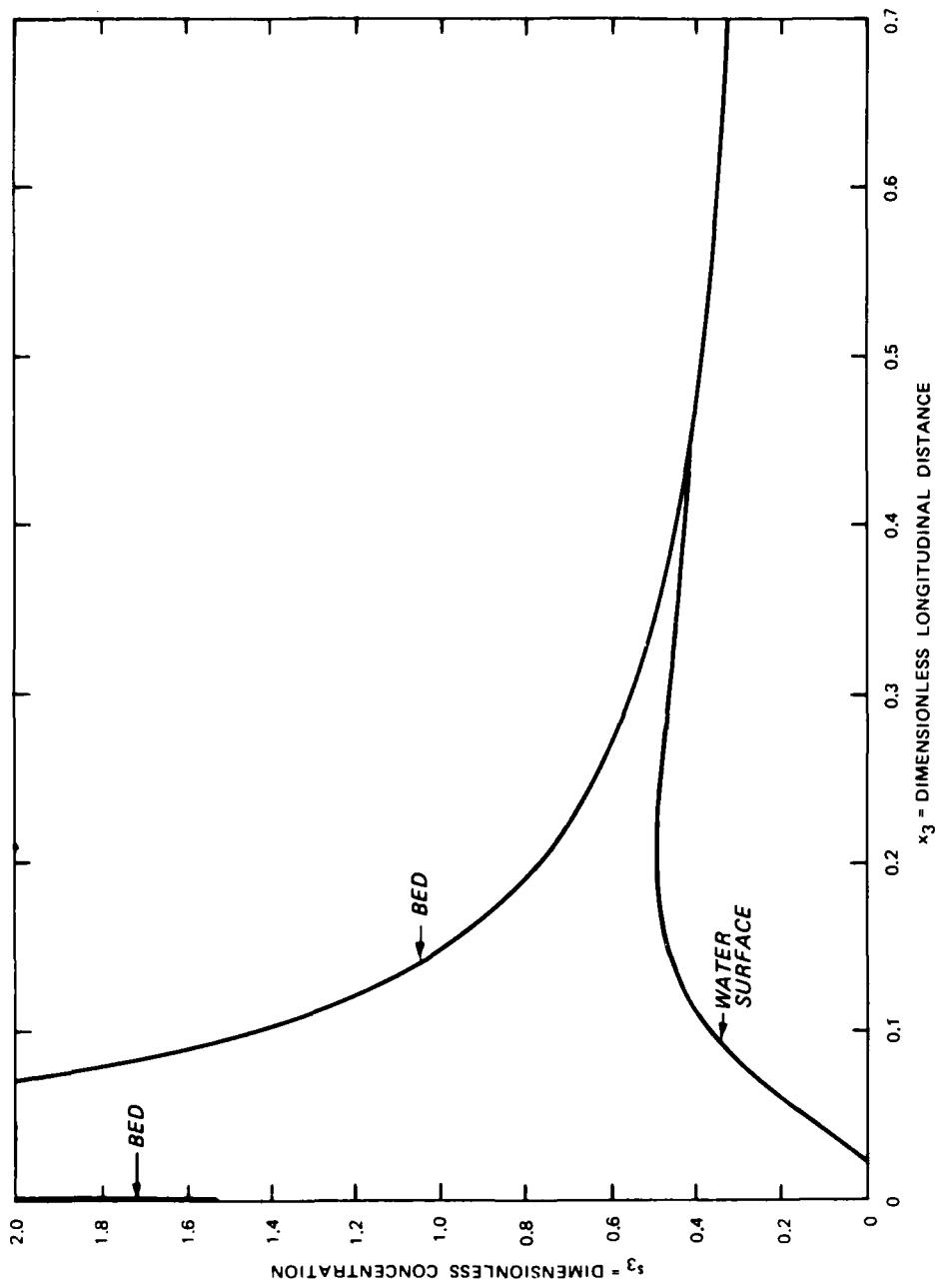
e. Concentration variation at bed and water surface (linear plot)

Figure 35. (Sheet 5 of 6)
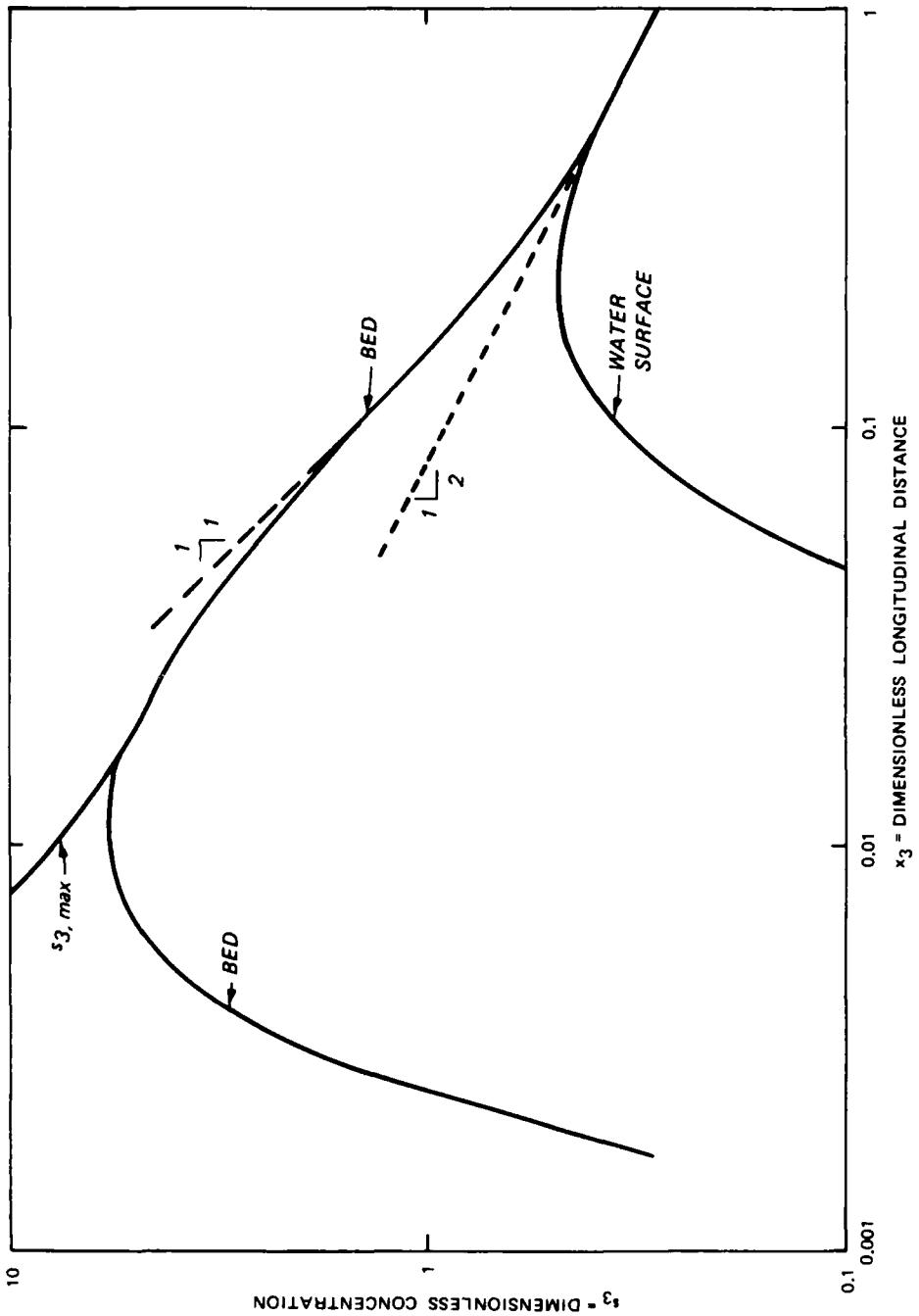
f.  Concentration variation at bed and water surface (log-log plot)

Figure 35.  (Sheet 6 of 6)

169

by $\exp(-k_3 x_3)$ if the longitudinal concentration gradients are much smaller than the vertical and transverse gradients, as is usually the case for steady-state distributions in rivers. Figure 34a shows concentration contours at the bed for the left half of the distributions. The transverse distributions of concentration (Figure 34b) are Gaussian or normal curves for all $x_3$ (if no lateral boundaries are considered). Concentration contours for the vertical plane through the source are shown in Figure 34c. The distributions (Figure 34d) are Gaussian for the shorter distances (smaller $x_3$ values), but when the solute reaches the free surface, the "reflection" of the solute from the surface due to the required zero vertical gradient or "no flux" condition at the surface (Eq. 5.2.4) begins to change the shapes of the distributions until, because of the finite depth, the solute ultimately becomes well mixed over the vertical (as illustrated by the nearly vertical contour for $s_3 = 0.3$ in Figure 34c and the distribution for $x_3 = 1$ in Figure 34d. Figures 34e and 34f give the surface and bed concentrations for a vertical plane straight downstream from the source. The -1 slope for the maximum bed concentration (Figure 34f) is characteristic of 2D mixing (vertical and transverse in this case) with constant mixing coefficients while the -1/2 slope corresponds to 1D mixing (transverse in this case) with a constant coefficient after the solute becomes well mixed over the depth. (Recall that longitudinal mixing is negligible for most steady-state problems such as this one. Thus, even though the concentration distribution is three dimensional, there is only advection in one of the dimensions so that the maximum number of dimensions for mixing is two.) As can be seen in Figure 34f, the characteristic slope of -1 applies only in the region where the reduction of the maximum concentration is not affected by "reflections" from the boundaries. If lateral boundaries were present, the -1/2 slope would change when the reflections from those boundaries began to influence the maximum concentration.

With the source located above the bed at $a_3 = 0.2$ (Figure 35), many characteristics of the concentration contours and distributions are similar to those in Figure 34 for $a_3 = 0$ . The primary

170

differences are that the initial vertical Gaussian distribution begins to be destroyed as soon as the lower part of the distribution reaches the bed and that the maximum concentration moves to the bed (Figures 35c, d). Depending on the value of $a_3$, a vertical Gaussian distribution with the maximum concentration at the bed may be reestablished before reflection from the free surface begins. The reason that the maximum moves to the bed (or, in a more general case, to a boundary) can be explained as follows. Initially, vertical mixing moves mass both upward and downward from the source location since diffusive mass flux is always in the direction of decreasing concentration. When the diffusing mass reaches the bed (or any boundary with a no-flux boundary condition), the mass must accumulate there. Thus, the concentration increases at the boundary (e.g., $x_3 = 10^{-2}$, Figure 35d) while the maximum concentration away from the boundary continues to decrease due to mixing. The boundary concentration increases until it is ultimately equal to the maximum concentration away from the boundary (Figures 35c, f). Then the decreasing gradient is only away from the boundary. Thus, from that point on downstream, the maximum concentration remains at the boundary with diffusion taking place away from it.

## 5.2.6  Vertical-Crossing Distance

For each source condition, there is a downstream distance (called the vertical-crossing distance, $x_{3,c}$) at which the solute concentration distribution reaches the free surface (Figures 34c, d and 35c, d). Nevertheless, the crossing distance cannot be mathematically defined as the distance at which the concentration at the surface ($z_3 = 1$) changes from zero; since the calculated concentration even for very small $x_3$ approaches zero asymptotically, there is a calculated non-zero value of $s_3$ at $z_3 = 1$ for all $x_3 > 0$. Thus, some specified non-zero value of $s_3$ at $z_3 = 1$ must be used to define $x_{3,c}$. This non-zero $s_3$ might correspond to a certain value of $s$; on the other hand, for illustrative purposes, it is convenient to take a relative value of $s_3$ since $x_{3,c}$ can then be calculated without needing to specify $\dot{m}$, $h$, $v_x$, etc. Thus, $x_{3,c}$ can be defined as the value of

171

$x_3$ for which the concentration at the surface ($y_3 = 0$, $z_3 = 1$) first reaches some specified small fraction (e.g. 0.01) of the maximum concentration on the plane $y_3 = 0$ for the same $x_3$ . One advantage of using dimensionless variables is that the crossing distance (and the mixing distance, Section 5.2.7, or the distance for any other relative degree of mixing) is just a constant value of $x_3$ for a given effluent discharge position. This condition is directly related to the physical interpretation of the dimensionless longitudinal distance variable as the ratio of the flow time to the characteristic mixing time. Thus, regardless of the values of the individual variables (depth, velocity, mixing coefficient, etc.), the same relative amount of mixing takes place between the release point and any specified dimensionless longitudinal distance (for a given relative location of the source, i.e., $a_3$ in this case).

The values of $x_{3,c}$ for various source locations ($a_3$) are shown in Figure 36 for $s_{3,surface}/s_{3,max} = 0.01$ and $0.05$ . These results were calculated using Eq. 5.2.5. For $a_3$ approaching 0.5 (i.e. mid-depth), the calculated $x_{3,c}$ values are of questionable worth since
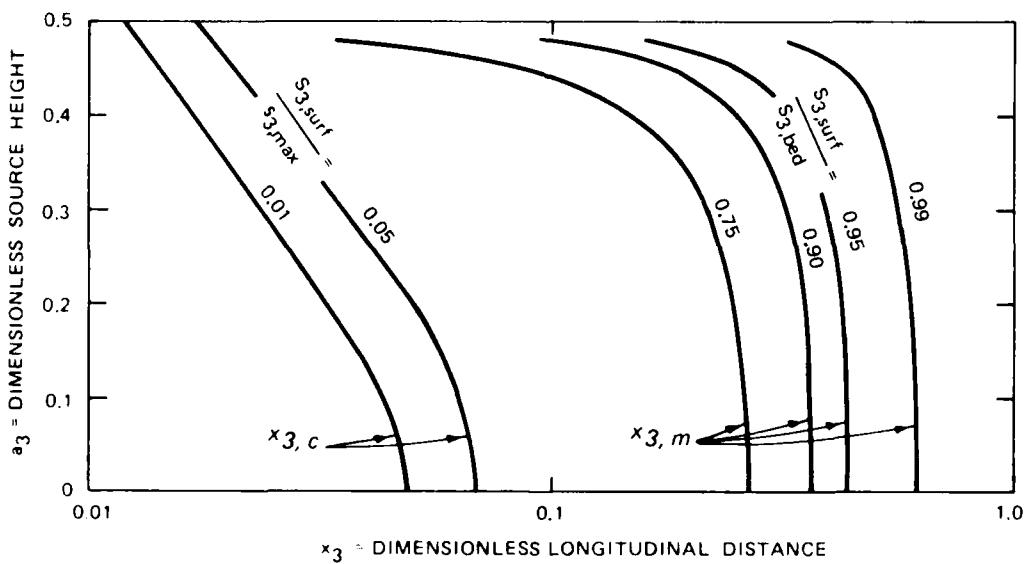


Figure 36. Vertical crossing and mixing distances for various point sources (3D)

the calculated concentration distributions approach an exact mathematical symmetry (for $a_3 = 0.5$) that would never be realized physically.

5.2.7 Vertical-Mixing Distance

In a manner similar to the crossing distance, the vertical-mixing distance ($x_{3,m}$) can be defined as the distance required to achieve a specified degree of relative vertical uniformity. Again, relative uniformity must be specified because absolute mathematical uniformity is approached asymptotically as $x_3$ approaches infinity. Based on Eq. 5.2.6, Figure 36 gives four curves for $x_{3,m}$ for different uniformity criteria expressed as the ratio of $s_{3, surface}$ to $s_{3,bed}$. For nearly uniform concentration distributions in the vertical, the distributions have a mathematical "odd symmetry" about the mid-depth so that for large $x_3$

$$\frac{s_{3,surf} - c_d}{c_d} = \frac{1}{2} \frac{s_{3,surf} - s_{3, bed}}{c_d} \tag{5.2.8}$$

where $c_d$ is the depth-averaged concentration along a vertical line. Thus, the maximum deviation from the average concentration is about half of 1 minus the values shown on the $x_{3,m}$ curves.

The value of $x_{3,m}$ has a fairly strong dependence on the specified degree of uniformity. For example, for $a_3 = 0$ in Figure 36, the flow distance to reach the 0.95 tolerance is about 65 percent greater than for the 0.75 tolerance. Nevertheless, regardless of the tolerance selected to define $x_{3,m}$, the actual flow distance required to obtain vertical uniformity is frequently relatively short. For example, taking $d_z = hU_*/15$ (Section 7.4.1) where $U_*$ is the shear velocity, $x_3$ can be written as

$$x_3 = \frac{1}{15} \left(\frac{f}{8}\right)^{1/2} \frac{x}{h} \tag{5.2.9}$$

173

where  f  is the Darcy-Weisbach friction factor.  For example, if
$x_{3,m}$ = 0.3  and  f = 0.02 , then  $x_m/h$  would be 90.  For this set of
values, the concentration distributions would be essentially uniform
over the flow depth for downstream distances greater than 90 times the
local depth.  However, as illustrated by the figures showing calculated
concentration distributions, nonuniform transverse distributions of
concentration remain downstream of the vertical mixing distance.

## 5.3  TWO-DIMENSIONAL SOLUTIONS

In Section 5.2, it was shown that the region with significant 3D
aspects downstream of a passive point source is relatively short.  With
any initial mixing, the 3D region would be even shorter.  Thus, rela-
tively close to the effluent structure, the concentration distributions
become essentially uniform over the depth.  Downstream from that point,
the important variations in the concentrations are in the longitudinal
and transverse directions, so these distributions may be treated as
being two dimensional.  In 2D steady problems, the mass can be consid-
ered as being advected along the depth-averaged streamlines and as
being mixed normal to the streamlines.  Thus, these 2D problems are
analyzed in this section using the streamtube model (Eq. 4.7.34).
Since the solutions apply for any depth and velocity distributions,
they can be used to represent the simplified case of a rectangular
channel with a constant velocity by using a constant depth and
velocity.

### 5.3.1  Assumptions

The assumptions that are used for the 2D solutions are as
follows:

a.  $\partial c/\partial t = 0$  for steady state.

b.  Negligible effects of longitudinal mixing.  As was pointed
out for the 3D assumptions in Section 5.2.1, the longitudinal concen-
tration gradients for steady-state situations are frequently small
enough that the rate of longitudinal mass transport by the mixing mech-
anism is negligibly small.  For the depth-averaged case, the longitudi-
nal mixing is due primarily to the differential advection associated

174

with the velocity variations along a vertical line (Section 4.7.3).

<u>c</u>. $m_x h^2 v_x e_y = D_f$ = constant. This series of terms which appears in Eq. 4.7.34 is called the diffusion factor ($D_f$) and is assumed to be constant in the sections dealing with analytical solutions. This assumption is discussed in Section 7.3 on the estimation of mixing coefficients. In general, this assumption is more reasonable for releases and concentration distributions in the deeper, higher velocity regions where the percentage changes in h and $v_x$ are smaller than in the regions near the banks where the percentage changes are larger. The assumption of constant $D_f$ is also useful for studying transport characteristics over long distances since the local variations of $D_f$ then do not have a large influence on the overall behavior of the transport.

<u>d</u>. k = constant, $f_S$ = constant times concentration, $f_B$ = constant times concentration. For general analytical considerations, it could be assumed that all of the distributed sources and sinks along a vertical line could be combined into one first-order reaction term with a constant rate coefficient K . This one term would then represent both decay or reactions within the flow and transfer across the flow boundaries at the water surface and the streambed (Section 4.7.3). See also assumption h in Section 5.2.1.

<u>e</u>. $m_x h^2 v_x e_y (\partial c/\partial q) = 0$ at the left and right banks. This condition states that there is no mass transport transversely at the banks and is satisfied if any of the individual variables (depth, velocity, concentration gradient, etc.) is zero at the banks. This condition is independent of the assumption of constant $D_f$.

## 5.3.2 Dimensionless Variables and Differential Equation

In order to define dimensionless variables, the characteristic length for mixing is taken as the channel width since, for 2D transport problems, interest is frequently in the concentration distributions across the width and in the flow time required for various degrees of uniformity of the concentration across the width. However, when using the streamtube model, traversing the stream from one bank to the other

175

is represented by crossing the total flow (Q) rather than by crossing the physical width of the stream. (Nevertheless, for lack of another more desirable term, the term "distance" is still used for the transverse coordinate even though it is actually discharge; each amount of the discharge corresponds to some distance across the stream. See Section 7.5.) Also, the mixing is represented by the diffusion factor (dimensions $L^5T^{-2}$) rather than a mixing coefficient such as $e_y$ (dimensions $L^2T^{-1}$). As a result, the form of the dimensionless longitudinal distance $(x_d)$ may at first appear to be different from the general form previously discussed. As explained below, $x_d$ is basically the same type of variable as $x_*$ (Eq. 5.1.2) and $x_3$ (Eq. 5.2.2). For these 2D problems, the dimensionless variables are denoted by a subscript d to indicate the 2D depth-averaged situation.

The dimensionless variables are defined as

$$x_d = \frac{D_f x}{Q^2}$$

$$q_d = \frac{q}{Q}$$

$$c_d = \frac{c}{\dot{m}/Q}$$

$$v_d = \frac{v_x}{V} \tag{5.3.1}$$

$$h_d = \frac{h}{H}$$

$$k_d = \frac{kQ^2}{D_f V}$$

$$f_d = \frac{fQ^3}{\dot{m} H D_f V}$$

where  Q  is the river flow rate.  The variables may be interpreted as follows:

$x_d$ – dimensionless longitudinal distance.  The functional equivalence of $x_d$ and the previous dimensionless distances can be seen by considering an ideal case where all of the variables in $D_f$ (depth, velocity, and mixing coefficient) and in Q (depth, velocity, and width) are constant.  Substitution of these constants into Eq. 5.3.1 with $m_x = 1$ gives $x_d = (x/V)/(B^2/e_y)$, in accordance with the previous variables.  Thus, the form of $x_d$ shows that $Q^2/D_f$ is a characteristic distance for transverse mixing; the characteristic time analogous to $t_c$ of Eq. 5.1.1 is then $Q^2/(D_f V)$ .

$q_d$ – transverse position as a fraction of the total discharge so that constant  $q_d$  corresponds to a depth-averaged streamline.

$c_d$ – concentration relative to the concentration if the initial effluent discharge were diluted in the entire river flow.

$v_d$ – velocity relative to the cross-sectional average velocity (V).

$h_d$ – depth relative to the cross-sectional average depth (H).

$k_d$ – ratio of characteristic transverse mixing time $(Q^2/D_f V)$ to characteristic decay or reaction time (1/k).

$f_d$ – ratio of characteristic transverse mixing time $(Q^2/D_f V)$ to characteristic time for transfer across the flow boundaries $(f/\dot{m}H)$.  Note that, in applications,  f  would normally be written as a transfer coefficient times a concentration or a concentration difference which, when made nondimensional, would absorb the  $\dot{m}$  in the definition of  $f_d$ .

Introduction of these variables into Eq. 4.7.33 gives the dimensionless streamtube form of the mass balance equation as

$$v_d \frac{\partial c_d}{\partial x_d} = v_d \frac{\partial^2 c_d}{\partial q_d^2} - f_{d,S} - f_{d,B} - k_d c_d \qquad (5.3.2)$$

177

Solution of this equation, with the appropriate boundary conditions, gives the concentration distribution as a function of $x_d$ and $q_d$. Except for Section 5.3.8, only solutions for conservative substances ($f = 0$, $k = 0$) are considered. As is the case for the 3D solutions considered previously, the effects of first-order reactions may be approximated by multiplying the concentrations for conservative substances by $\exp(-k_d x_d)$ or by a similar expression with $k$ replaced by the rate coefficient for transfer across the flow boundaries as represented by $f$. This type of approximation neglects the type of behavior considered in Section 5.3.8.

### 5.3.3  Coordinate Origin and Boundary Conditions

For these calculated distributions with passive sources (no initial mixing), the origin is placed so that $x_d = 0$ corresponds to the cross section containing the source, and the origin for $q_d$ is at one bank (the right bank for the solutions presented in this section). The values of $q_d$ then range from 0 to 1. There are many upstream source configurations which could be considered, but only two types are illustrated in this section. One is a point source located at $q_{d,I}$. The other, which is called a partial line source, is a line source extending across the stream from $q_{d,1}$ to $q_{d,2}$ with $q_{d,1} < q_{d,2}$. This type of partial line source could correspond to conditions at the junction of two tributaries having different concentrations, or it might be used to approximate the conditions at the end of an initial mixing region. For these solutions, it is assumed that the initial mass flux ($\dot{m}$) is uniformly distributed along the region from $q_{d,1}$ to $q_{d,2}$. This assumption corresponds to a uniform concentration along the partial line source. For the upstream boundary, the mathematical boundary conditions then may be written for the point source as

$$c_d = \delta(q_{d,I}) \quad \text{on} \quad x_d = 0 \tag{5.3.}$$

and for the partial line source as

178

$$c_d = 0 \quad \text{on} \quad x_d = 0 , \quad q_d < q_{d,1} \quad \text{and} \quad q_d > q_{d,2}$$

$$c_d = \frac{1}{q_{d,2} - q_{d,1}} \quad \text{on} \quad x_d = 0 , \quad q_{d,1} \leq q_d \leq q_{d,2}$$

(5.3.4)

For any upstream condition, assumption e in Section 5.3.1 gives boundary condition at the banks as

$$\frac{\partial c_d}{\partial q_d} = 0 \quad \text{on} \quad q_d = 0 \text{ and } 1$$

(5.3.5)

### 5.3.4 Analytical Solutions

The analytical solutions for the concentration distributions $(c_d)$ as a function of $x_d$ and $q_d$ can be obtained from Eqs. 5.3.2, 5.3.3, and 5.3.4. For a point source, the solution for a conservative substance using the method of images can be written as

$$c_d = \frac{1}{(4\pi x_d)^{1/2}} \sum_{i=-\infty}^{\infty} \sum_{j=1}^{2} \exp \left\{ - \frac{\left[ q_d - (-1)^j q_{d,I} - 2i \right]^2}{4x_d} \right\}$$

(5.3.6)

Using separation of variables, the equivalent solution for a point source is

$$c_d = 1 + 2 \sum_{n=1}^{\infty} \cos (n\pi q_{d,I}) \cos (n\pi q_d) \exp (-n^2\pi^2 x_d)$$

(5.3.7)

For a partial line source using the method of images, the solution is

$$c_d = \frac{1}{2(q_{d,2} - q_{d,1})} \sum_{i=-\infty}^{\infty} \sum_{j=1}^{2} \left\{ \text{erf} \left[ \frac{q_{d,2} - (-1)^j q_d - 2i}{2(x_d)^{1/2}} \right] \right.$$

$$\left. - \text{erf} \left[ \frac{q_{d,1} - (-1)^j q_d - 2i}{2(x_d)^{1/2}} \right] \right\} \tag{5.3.8}$$

Using separation of variables, the equivalent solution for a partial line source is

$$c_d = 1 + \frac{2}{\pi(q_{d,2} - q_{d,1})} \sum_{n=1}^{\infty} \frac{1}{n} \left[ \sin(n\pi q_{d,2}) \right.$$

$$\left. - \sin(n\pi q_{d,1}) \right] \cdot \cos(n\pi q_d) \exp\left(-n^2 \pi^2 x_d\right) \tag{5.3.9}$$

### 5.3.5 Concentration Distributions

Various concentration distributions can be calculated from the analytical solutions given in the previous section in order to obtain some general insight into the transport processes. For illustrative purposes, three specific situations (namely, a point source located at $q_{d,I} = 0$, a point source at $q_{d,I} = 0.2$, and a partial line source from $q_{d,1} = 0$ to $q_{d,2} = 0.2$) have been selected for presentation of various aspects of the concentration distributions. For these three situations, Figures 37-39 give various aspects of the concentration distributions to parallel the information in Figures 34 and 35 for the 3D transport situation. For the 2D situations depicted in Figures 37-39, the concentrations are uniform over the depth so that the 2D figures give the entire description of the evolving concentration distributions in terms of $x_d$ and $q_d$. The relationship between $q_d$ and actual transverse distance (y) is illustrated in Section 7.5.
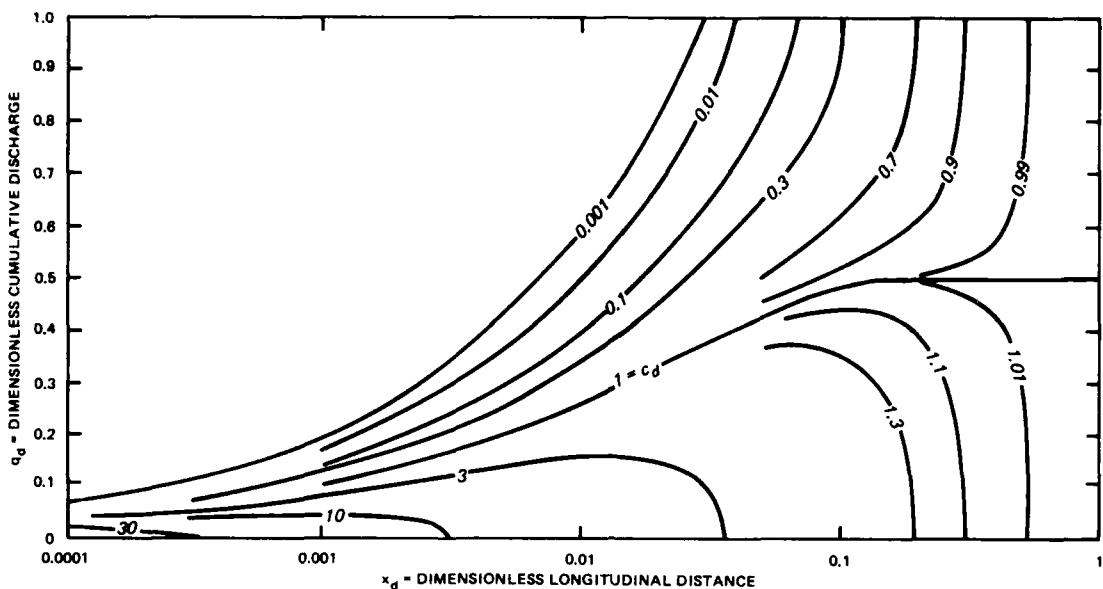
a. Contours of concentration
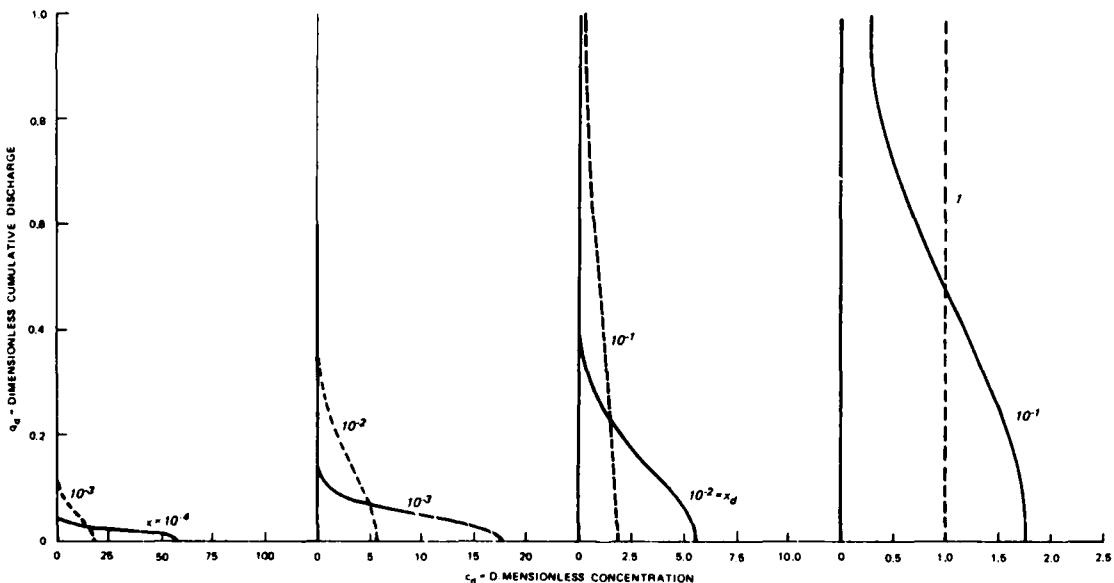


b. Concentration distributions

Figure 37. Calculated concentration distributions for point source at bank (2D, $q_{d,I} = 0$) (Continued)
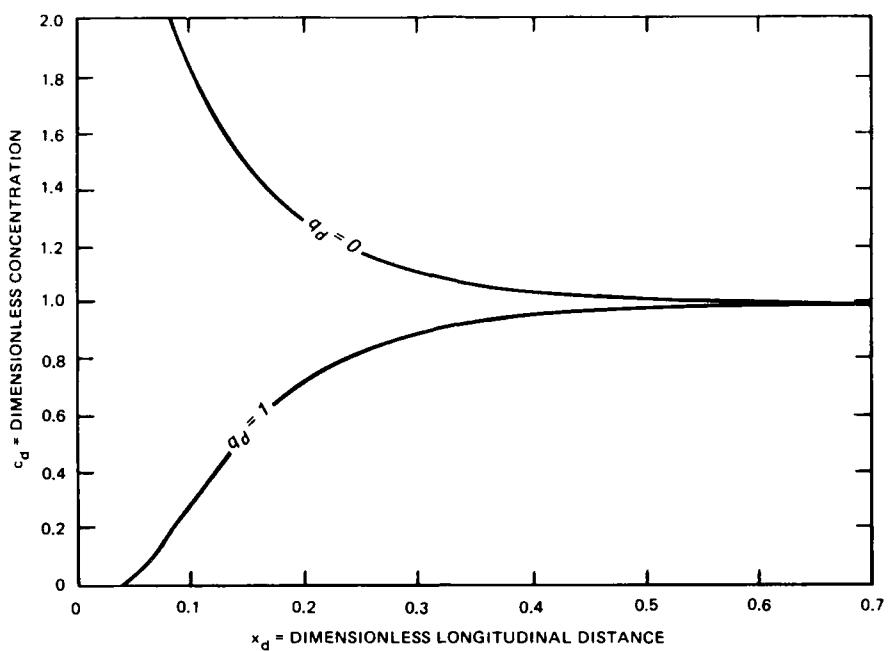
181

c. Concentration variation at banks (linear plot)



d. Concentration variation at banks (log-log plot)

Figure 37. (Concluded)

182
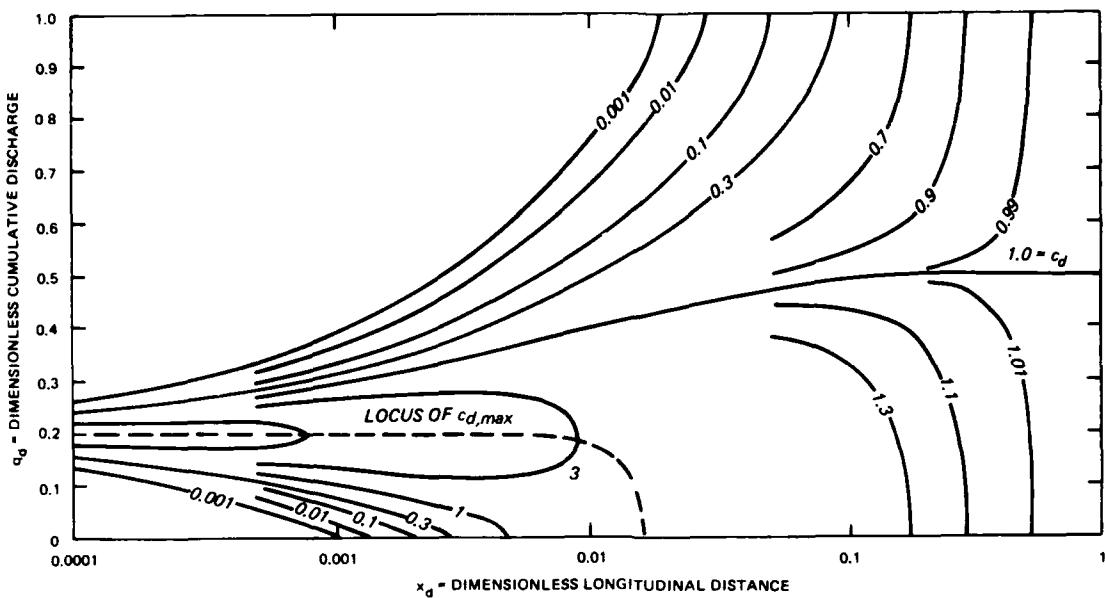
a. Contours of concentration
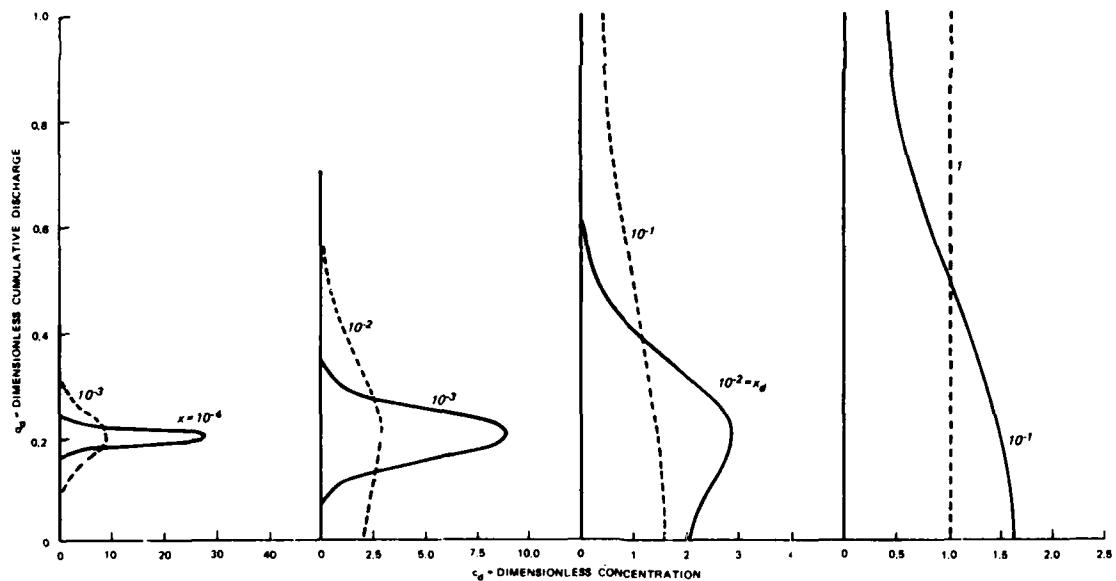


b. Concentration distributions

Figure 38. Calculated concentration distributions for point source at $q_{d,I}$ = 0.2 (2D) (Continued)
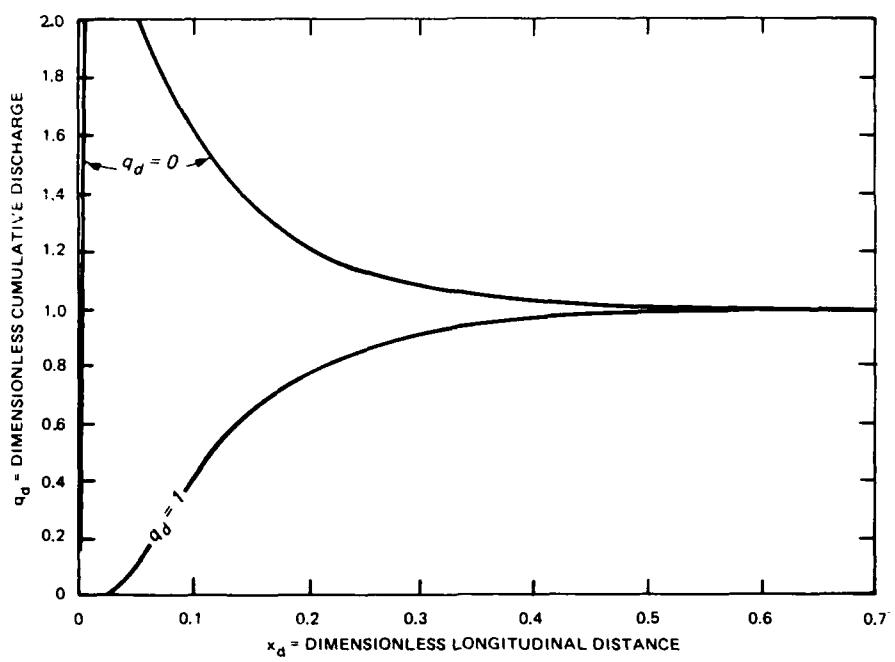
c.  Concentration variation at banks (linear plot)
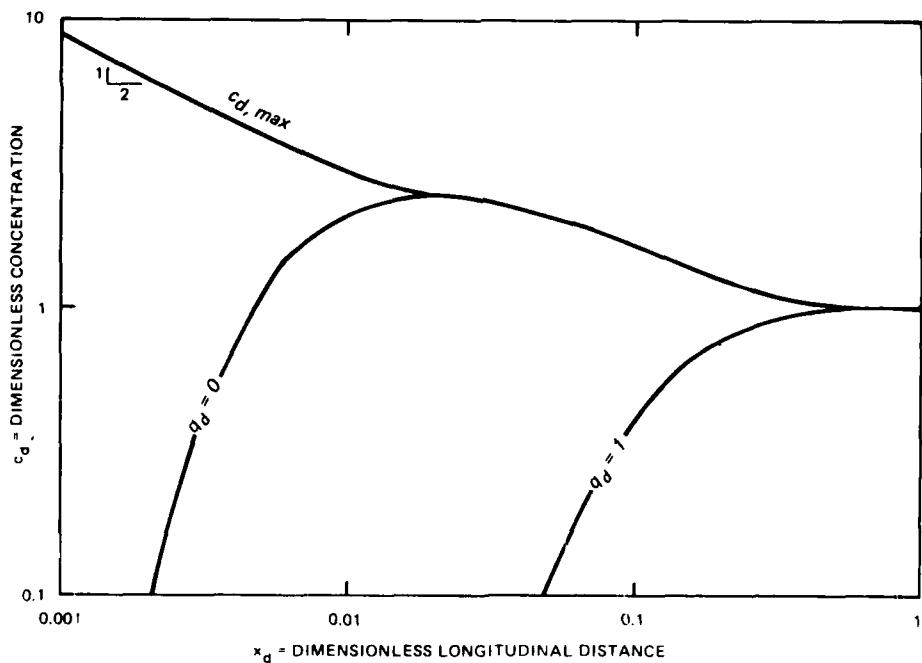


d.  Concentration variation at banks (log-log plot)

Figure 38.  (Concluded)

184
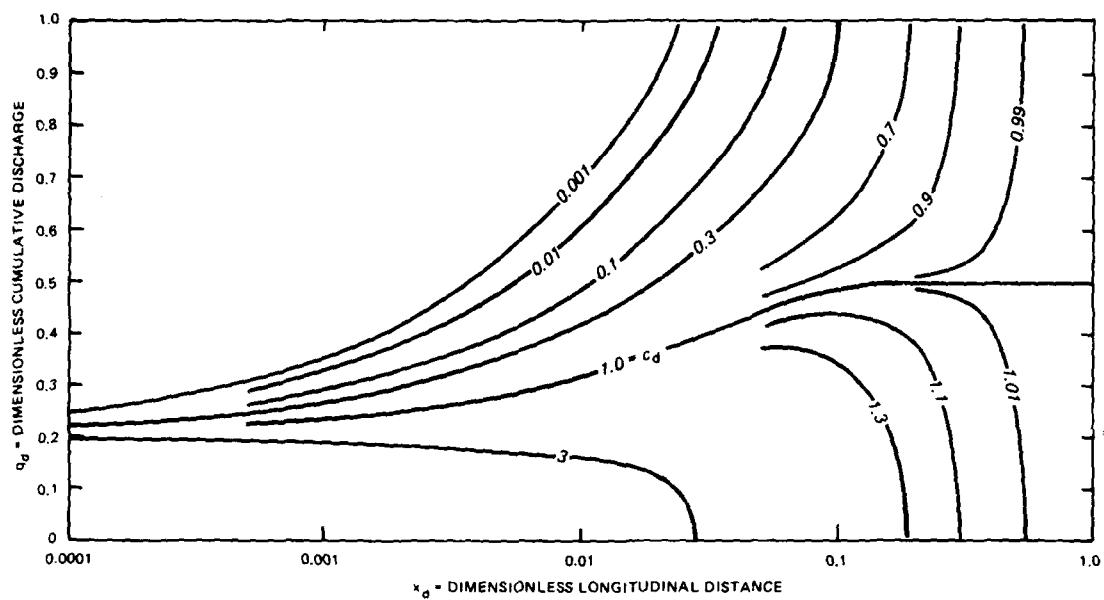
a.  Contours of concentration
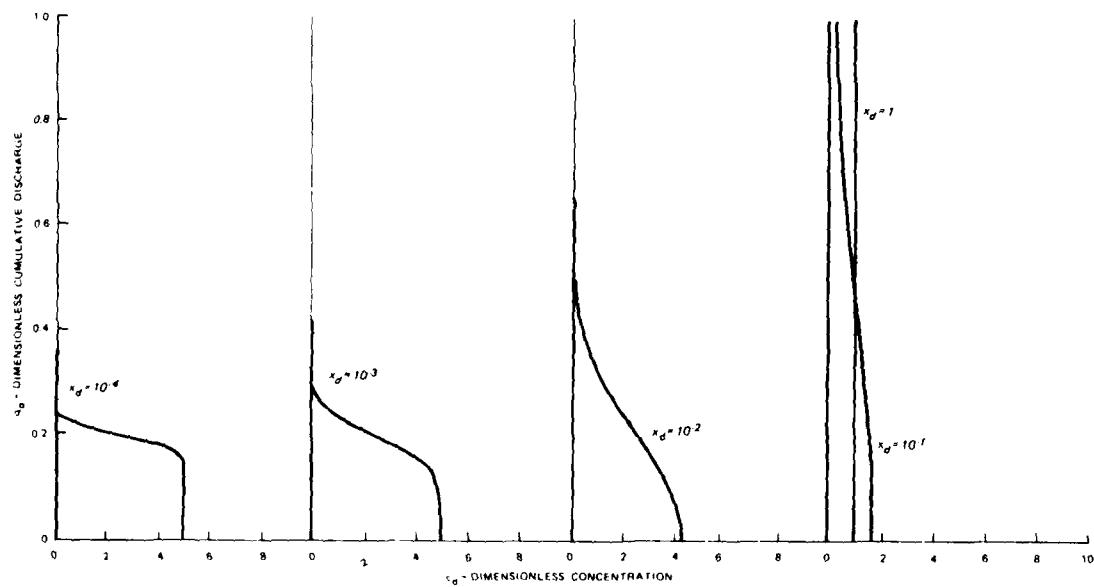


b.  Concentration distributions

Figure 39.  Calculated concentration distributions for line source
from $q_{d,1} = 0$  to $q_{d,2} = 0.2$ (2D) (Continued)
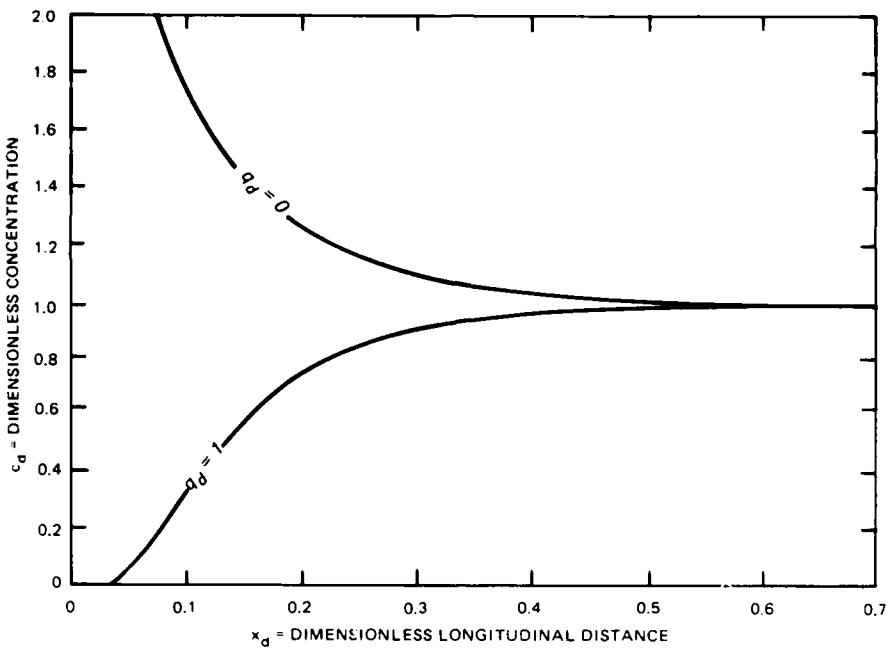
185

c.   Concentration variation at banks (linear plot)
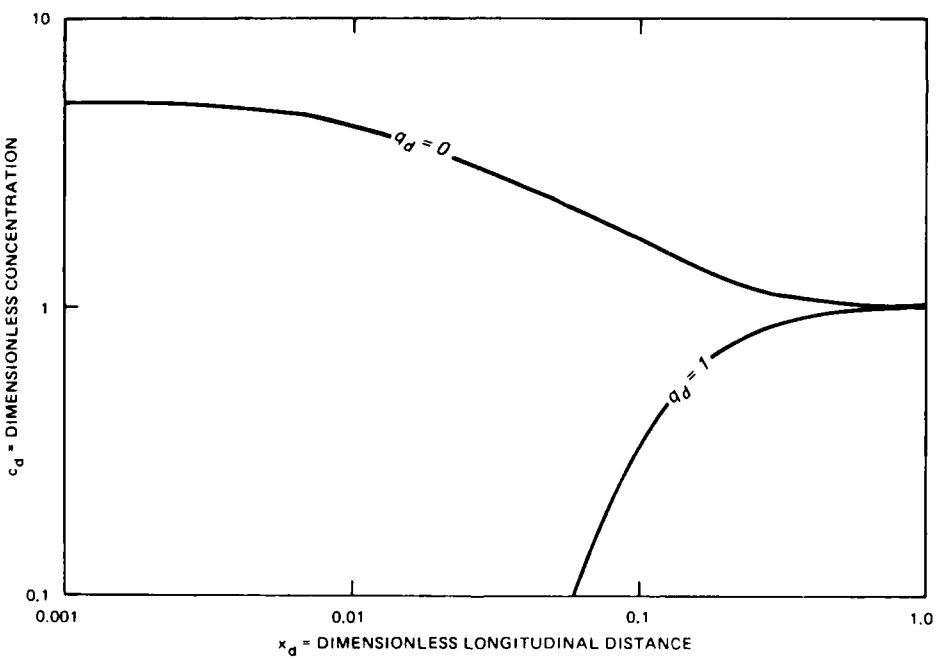


d.   Concentration variation at banks (log-log plot)

Figure 39.   (Concluded)

186

The maximum and minimum concentrations are shown for the three source configurations in parts c and d of Figures 37-39. More information on maximum and minimum concentrations is given in Figures 40 and 41. For Figures 40a and 41a, each curve is for a single point source located at the indicated value of $q_{d,I}$ , while each curve in part b of the figures is for a line source extending from $q_{d,1} = 0$ to the indicated value of $q_{d,2}$ . Figure 40 gives the maximum concentrations as functions of longitudinal distance. For the point sources, the actual location of the maximum concentration starts at the transverse location of the source but eventually moves to the nearer bank, as shown in Figure 38a. For the partial line source, the maximum concentration is always at the bank. Figure 41 is a companion graph to Figure 40 and gives the ratio of maximum and minimum concentrations. The curves are given as semilogarithmic graphs of $(1 - c_{d,min}/c_{d,max})$ since the analytical solutions indicate that these curves become straight lines for large values of $x_d$ .

For the point sources, the log-log plots in Figures 37d and 38d show that the maximum concentrations decrease in proportion to $x_d^{-1/2}$ in the early part of the transport process. After "reflection" from the boundaries begins to affect the maximum concentrations, the slope of the $c_{d,max}$ versus $x_d$ curves becomes progressively flatter until the slope becomes zero when transverse uniformity is obtained and the concentration distribution no longer changes with $x_d$ . The different values of $x_d$ at which the slope changes from -1/2 for the two point sources can be used to illustrate the use of a dimensionless longitudinal distance defined on the basis of the significant distance over which mixing must take place to achieve a specified result. In this case, the specified result is the modification of the rate of decrease of the maximum concentration due to reflection from the boundaries. The significant distance is the distance from the source to the boundary (for the mixing to carry the concentration distribution to the boundary) and back (for the mixing to carry the effect of the reflection back to the point of the maximum concentration). Since $x_d$ is defined using the total distance across the stream as the significant

187

a. Point sources
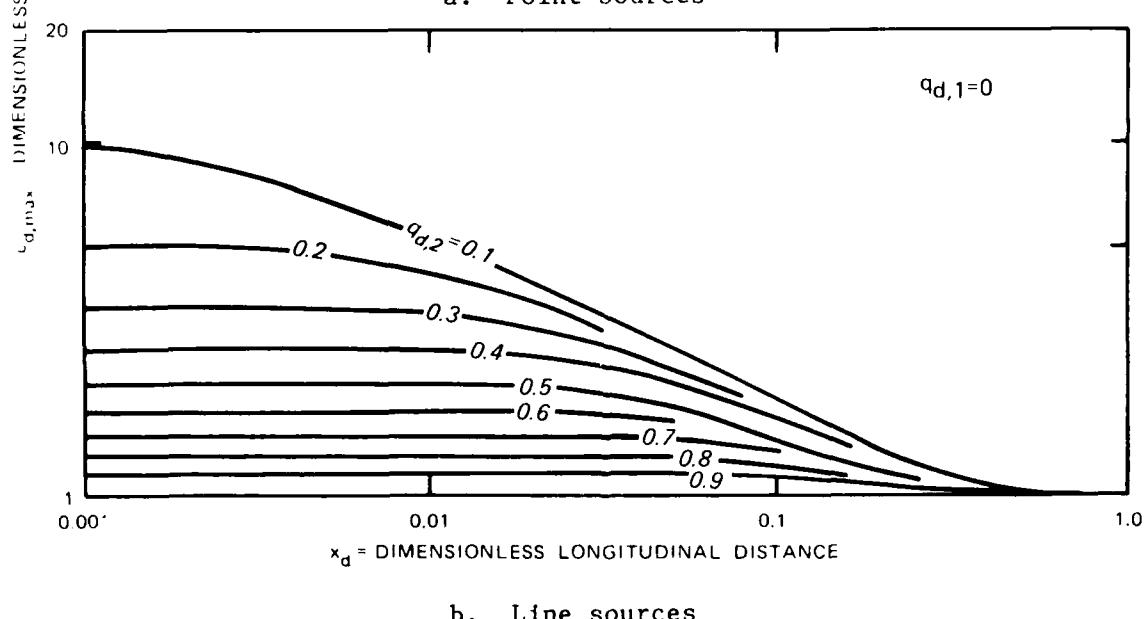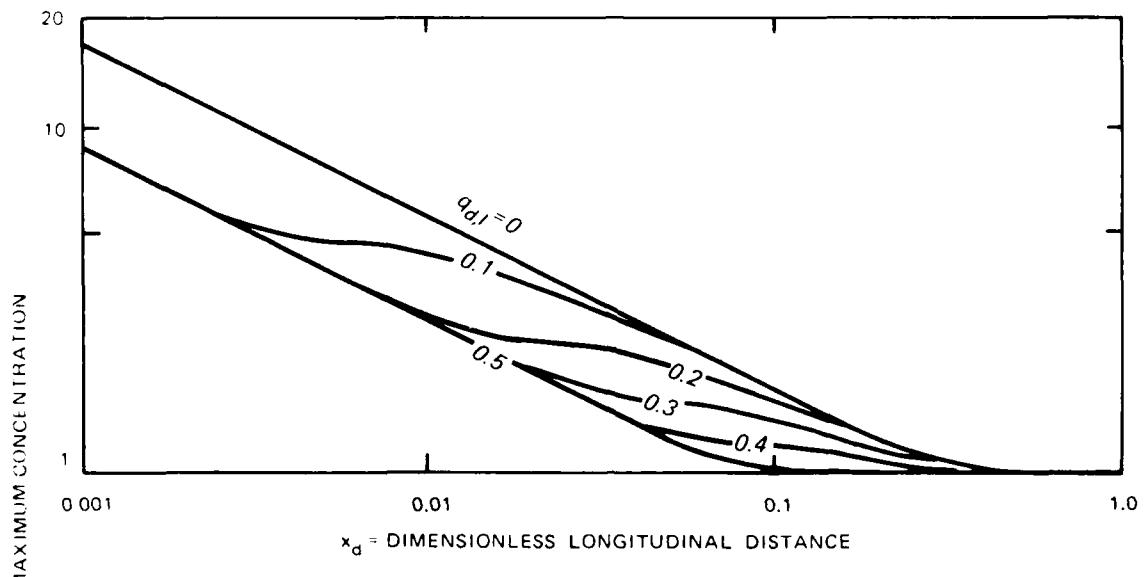


b. Line sources

Figure 40. Calculated maximum concentrations for various
sources (2D)

188
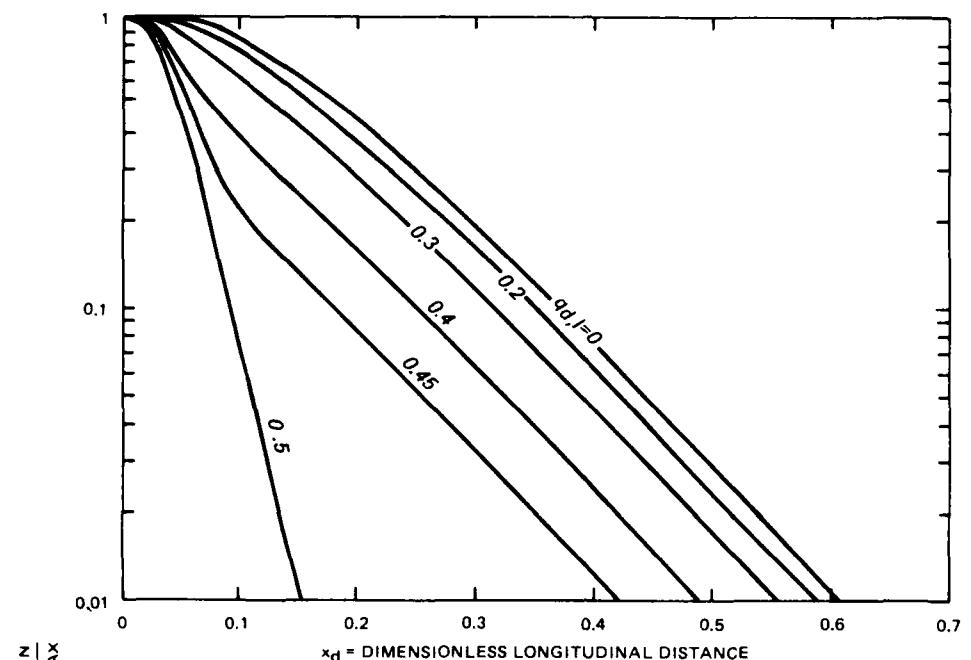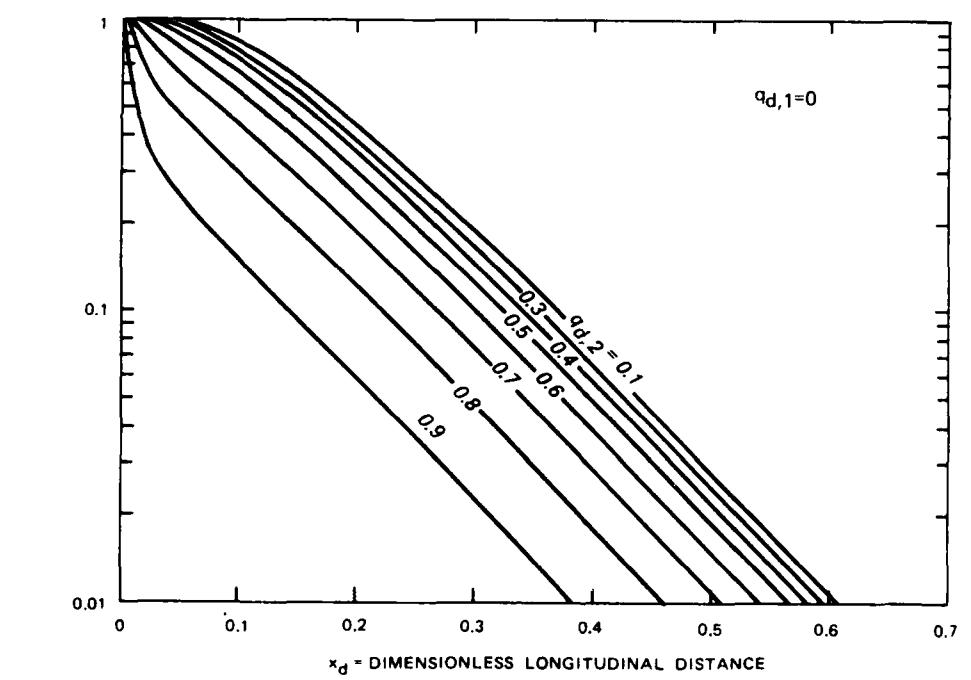
a. Point sources



b. Line sources

Figure 41. Calculated relative concentrations variation across channel width for various sources (2D)

189

distance, the effect of reflection is seen at different values of $x_d$ for the different locations for the point sources. For $q_{d,1} = 0$, the slope changes at about $x_d = 0.2$, while for $q_{d,1} = 0.2$, the change occurs at about $x_d = 0.008$. The ratio of these two values of $x_d$ is 25 since the significant distance for the first case is five times larger than for the second (0 to 1 and back, as contrasted to 0.2 to 0 and back) and the definition of $x_d$ involves the significant distance squared (Eqs. 5.2.2 and 5.3.1). If, for the specific purpose of considering the rate of decrease of the maximum concentration, the significant distance applicable to each situation (Q in one case and 0.2Q in the other case) were used in defining another dimensionless longitudinal variable (say, $x_d'$), then the rate of decrease of $c_{d,max}$ would change at the same value of $x_d'$ for both sources.

Returning to the dimensionless distance $(x_d)$ as previously defined (Eq. 5.3.1) and as used in the figures, Figure 40b illustrates that the longitudinal distance required for the concentration at the bank for each of the line sources to begin dropping from its initial value is inversely proportional to the square of the length of the original line source. For example, for $q_{d,2} = 0.2$, the decrease in the maximum concentration begins at about $x_d = 0.0025$, while for $q_{d,2} = 0.4$, $x_d$ is four times larger at about 0.01, and for $q_{d,2} = 0.8$, $x_d$ is again four times larger at about 0.04. This behavior results from the fact that the concentration starts dropping at a distance which is large enough for the mixing to have carried water from outside the end of the source to the bank, and the longitudinal distance (or flow time) required for a certain amount of mixing to take place is proportional to the square of the (transverse) distance over which the mixing takes place.

### 5.3.6 Transverse-Crossing and Transverse-Mixing Distances

Vertical-crossing and vertical-mixing distances were discussed in Sections 5.2.6 and 5.2.7. This section and Figure 42 present the analogous distances for transverse mixing with depth-averaged 2D concentration distributions. Figure 42a for point sources and Figure 42b

190
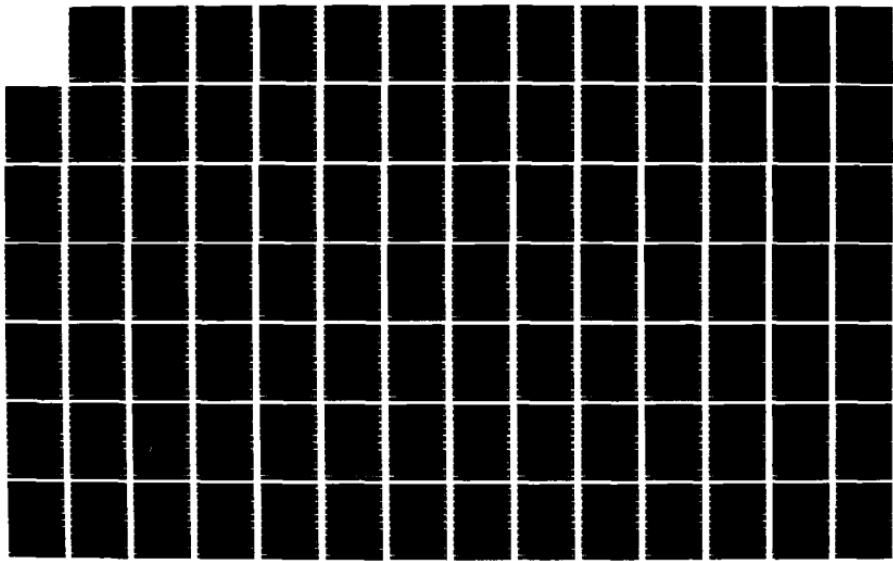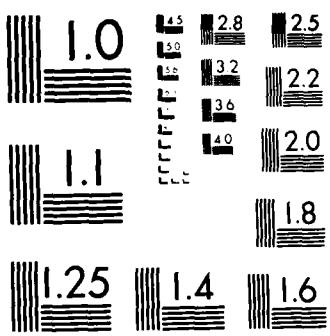
MICROCOPY RESOLUTION TEST CHART

NATIONAL BUREAU OF STANDARDS 1963 A
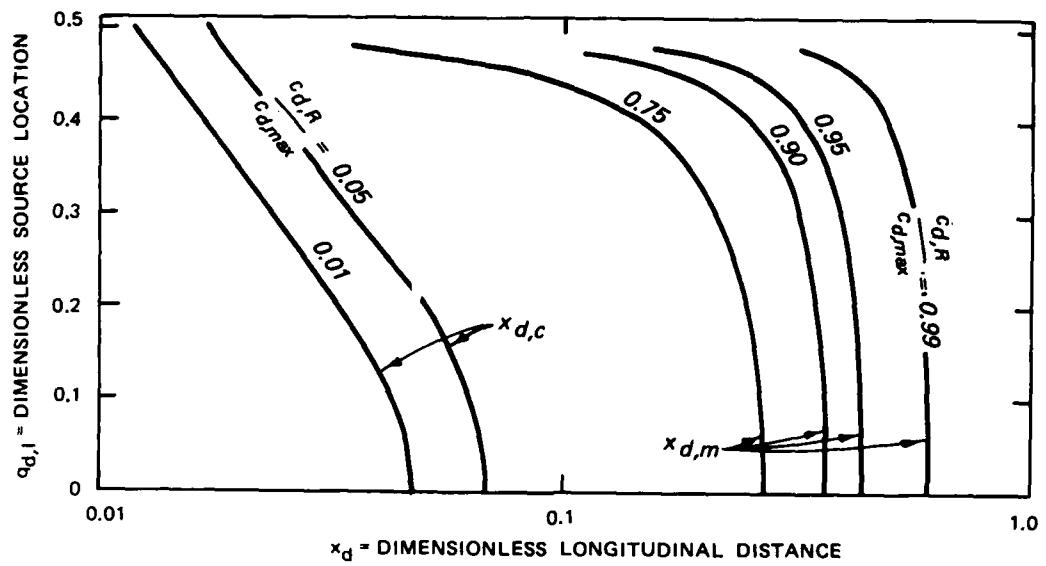
a. Point sources
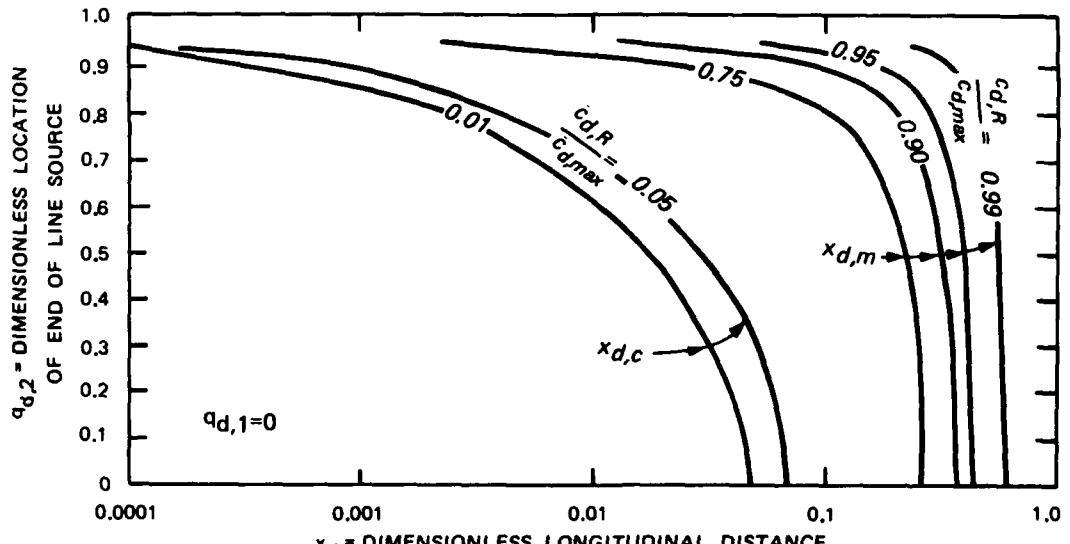


b. Line sources

Figure 42. Calculated crossing and mixing distances
for various sources (2D)

191

for partial line sources give the transverse-crossing distance $(x_{d,c})$
and the transverse-mixing distance $(x_{d,m})$ for several tolerances. For
medium to large rivers, the transverse mixing distance may be many
miles, or many tens of miles, so that within a reach of interest,
transverse uniformity may never be achieved, especially when it is con-
sidered that any tributary inflows will make the approach to transverse
uniformity of concentration slower than is depicted in the figures.
Some specific situations are considered in Section 7.5. Nevertheless,
as a general indication of the distances involved, consider three
rivers:

| River | Width ft | Depth ft | Velocity fps | $V/U_*$ | $x_m$ miles |
|-------|----------|----------|--------------|---------|-------------|
| A | 50 | 1 | 0.6 | 8 | 2 |
| B | 150 | 6 | 3 | 14 | 6 |
| C | 800 | 13 | 5 | 19 | 110 |

The calculation of $x$ is based on $x_{d,m} = 0.3$ and a typical trans-
verse mixing coefficient of $e_y = 0.5HU_*$ (Section 7.4). The value of
$V/U_*$ is indicative of the flow resistance since this value is equal to
$(8/f)^{1/2}$, where $f$ is the Darcy-Weisbach friction factor. For the
smaller river, transverse mixing takes place rapidly enough that most
of a reach of interest might be in the region where the concentration
distribution is essentially one dimensional, although the maximum con-
centrations in the river would still be in the region near the origin
where 2D aspects are important. For the larger rivers, the mixing dis-
tances can be so great that the majority of a reach of interest may be
in the region where 2D aspects of the transport and mixing processes
are important.

### 5.3.7 Overall Mixing Parameters

The previous sections deal with various aspects of the concen-
tration distributions across and along a channel. Sometimes, it is
useful to have a single parameter to represent the degree of uniformity
of the concentration distribution across the width of the channel. The

192

two primary parameters that have been used for this purpose are the coefficient of variation $(C_v)$ and the degree of mixing (P). Using the dimensionless concentration, $C_v$ is defined as

$$C_v = \left[ \int_0^1 (c_d - 1)^2 \, dq_d \right]^{1/2} \qquad (5.3.10)$$

Values of $C_v$ decrease in the downstream direction as the uniformity increases. The limiting values are infinity at a point source and zero at complete mixing. (A zero value can never be obtained experimentally because of random measurement errors.) The degree of mixing, P, is a closely related parameter which is defined by

$$P = 1 - \frac{1}{2} \int_0^1 |c_d - 1| \, dq_d \qquad (5.3.11)$$

and increases in the downstream direction. The limiting values are 0 at a point source and 1 at complete uniformity. For a partial line source, the initial value of P is equal to the fraction of the discharge covered by the source. For example, for a partial line source from $q_{d,1} = 0.2$ to $q_{d,2} = 0.5$, the initial value of P is 0.3. Values of $C_v$ and P for point sources and for partial line sources beginning at one bank are shown in Figures 43 and 44. The graphs are plotted on semilogarithmic axes and the P values are plotted $(1 - P)$ since both graphs then give straight lines as $x_d$ increases. (In analyzing data, it is sometimes helpful to be able to plot the data so that the anticipated behavior gives a straight line. However, field data seldom give a straight line because the slope of the line is related to $D_f$, and $D_f$ is not exactly constant for rivers as assumed in the analysis. Rather, it tends to vary about an average value.) For large $x_d$, the ratio of $C_v$ to $(1 - P)$ is constant and equal to $\pi/2^{1/2} = 2.22$.

a. Point sources

b. Line sources (2D)
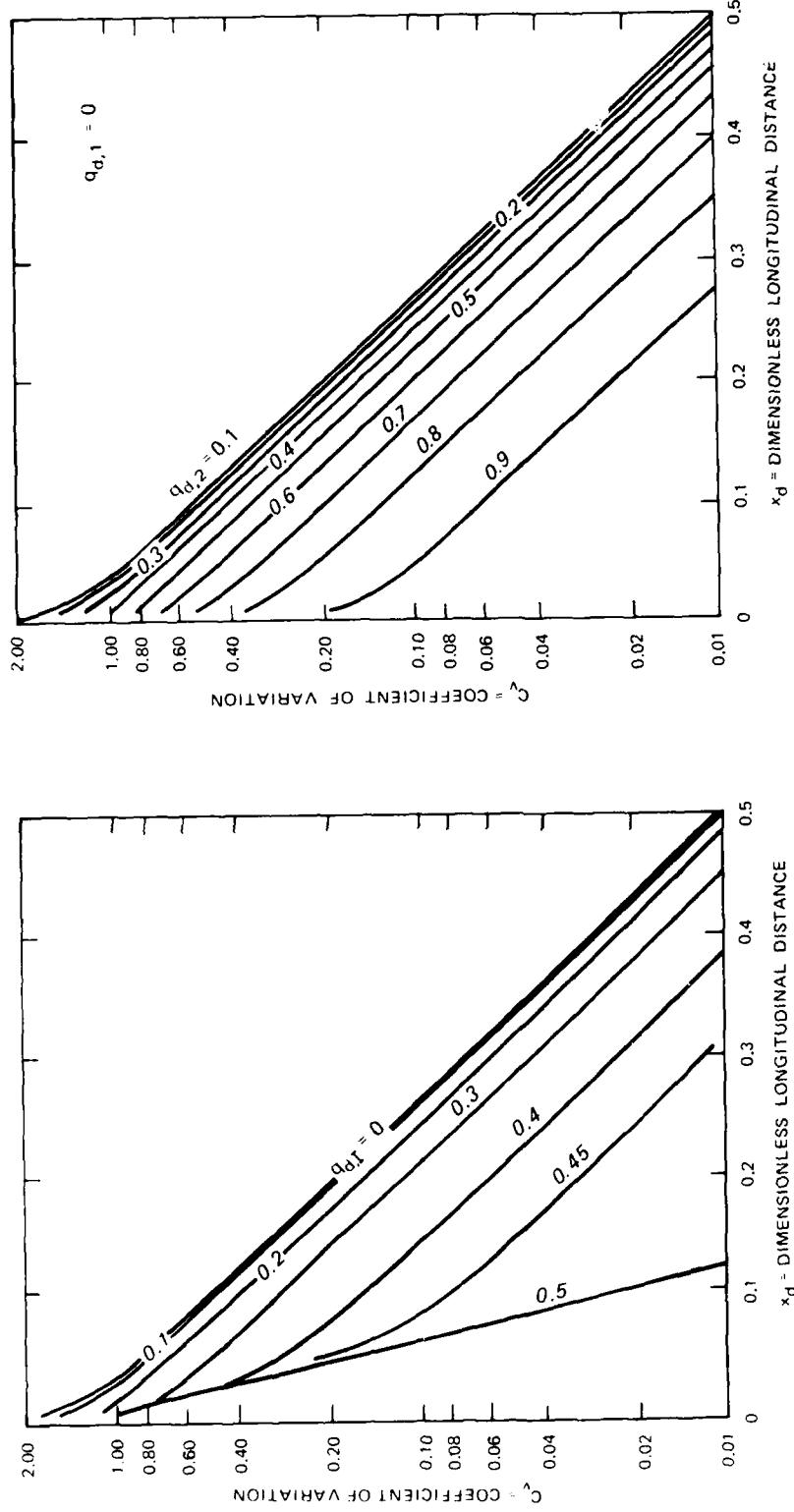
Figure 43. Calculated coefficients of variation for various sources

a. Point sources

b. Line sources
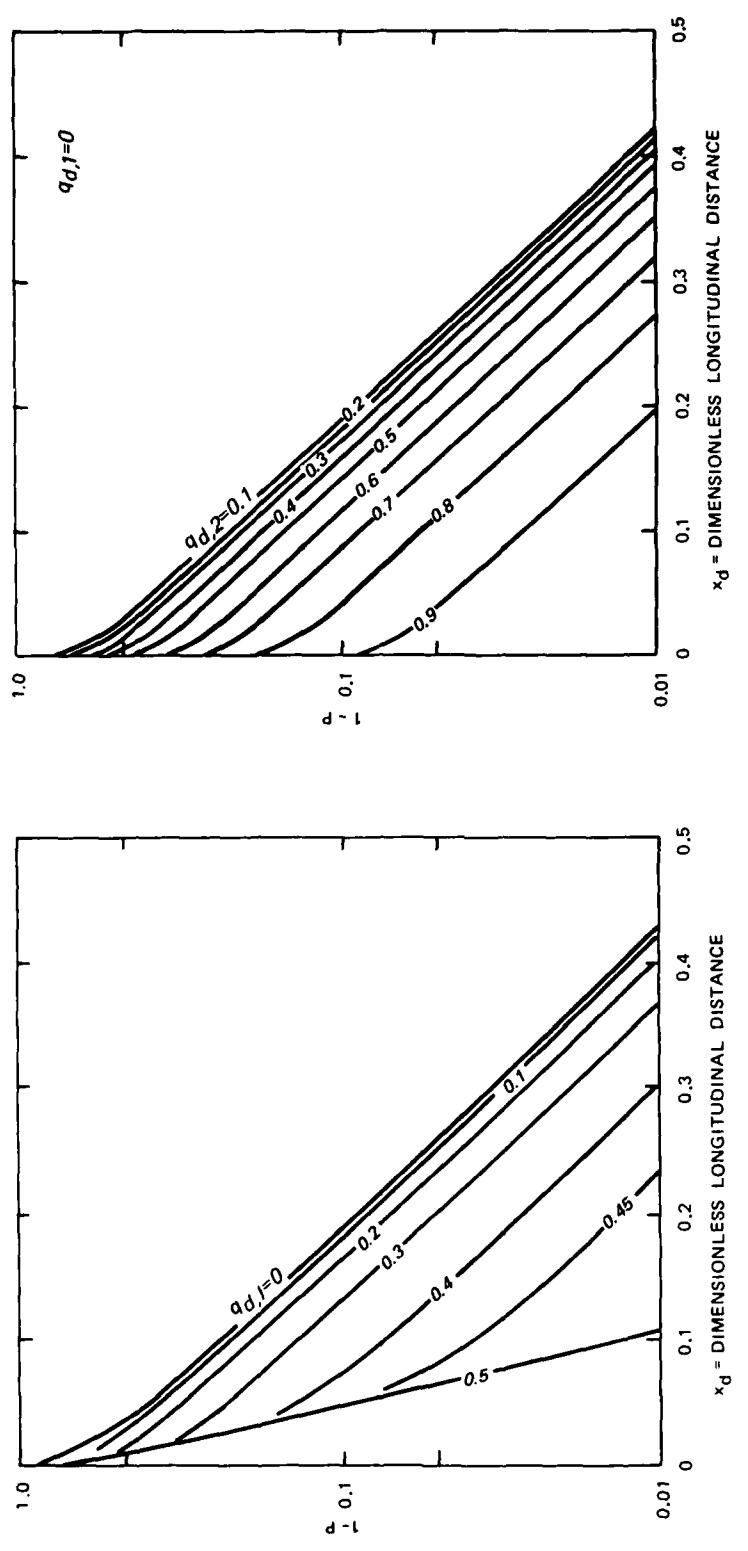
Figure 44. Calculated mixing parameter for various sources (2D)

195

### 5.3.8 Equilibrium Concentration Distributions with Distributed Sources or Sinks

The previous discussion of concentration distributions and mixing relates primarily to conservative substances, but it also gives a general indication of the amount of transverse mixing to be expected for nonconservative substances. One definite difference is that conservative substances theoretically approach a uniform concentration distribution as $x_d$ increases. However, for nonconservative substances, the equilibrium distribution at large $x_d$ for the dimensionless concentration may be nonuniform, with the amount of nonuniformity depending on the type of distributed source or sink and on the river hydraulics. The physical explanation for the existence of an ultimate equilibrium nonuniform concentration distribution varies somewhat depending on the type of distributed sources and sinks for the problem being considered.

In order to have a specific situation to discuss, consider the case of simple reaeration in a straight, prismatic channel with the flow having an initial oxygen saturation deficit and no distributed sources or sinks other than reaeration. Typically, the water nearer to the edges of the channel moves more slowly than the water in the central part of the river so that between any two cross sections, the water nearer the banks has a larger travel time and therefore more time for reaeration to take place. In addition, the depths are smaller near the banks so that the absorbed oxygen is distributed into a smaller amount of water. Thus, both the velocity distribution and depth profile contribute to having higher oxygen concentrations or lower deficits nearer to the banks. (There is probably also some transverse variation of the reaeration rate coefficient $(K_a)$. Since this type of variation has not been well documented, it is not included in this discussion.) Transverse mixing tends to bring the transverse concentration distribution toward uniformity, but the rate of transverse mixing is proportional to the concentration gradients. Ultimately, regardless of the initial concentration distribution at $x_d = 0$, a balance or equilibrium is reached between the tendency of the velocity and depth

variations to cause lower deficits near the banks and the tendency of the transverse mixing to cause an approach to uniformity. Once this equilibrium is reached, a properly defined dimensionless concentration distribution does not change with increasing $x_d$ .

For this reaeration situation, consider a steady-state concentration distribution in a straight, prismatic channel. Let the dimensionless variables be

$$v_d = \frac{v_x}{V}$$

$$c_d' = \frac{C_s - c}{C_s - C_o}$$

$$y_d = \frac{y}{B} \qquad (5.3.12)$$

$$f_d = \frac{K_L B^2}{He_y}$$

$$h_d = \frac{h}{H}$$

where $C_s$ is the saturation concentration, $C_o$ is the initial concentration, and $K_L$ is the mass transfer coefficient so that $f_S = -K_L (C_S - c)$ . The parameter $f_d$ is similar to the previously defined $k_3$ (Eq. 5.2.2) and $k_d$ (Eq. 5.3.1) in that it represents the ratio of a characteristic time for transverse mixing to a characteristic time for surface transfer of oxygen, i.e. a characteristic time proportional to the time required for the deficit to change by any given amount due to surface gas transfer. For example, for simple first-order reaeration in a mixing tank, $H/K_L$ , is the time required for the deficit to decrease to 37% of its original value since for $t = H/K_L$ ,

$$\exp\left(-\frac{K_L t}{H}\right) = \exp\left(-1\right) = 0.37. \qquad (5.3.13)$$

Either one of the two characteristic times in $f_d$ could be used to nondimensionalize the longitudinal distance; $x_d$ based on the transverse mixing time is used in this analysis to be consistent with the analyses in the previous sections. From Eq. 4.7.33, using the definitions in Eq. 5.3.12, the nondimensional mass balance equation for $c_d'$ may be written as

$$v_d \frac{\partial c_d'}{\partial x_d} = \frac{1}{h_d} \frac{\partial}{\partial y_d} \left( h_d \frac{\partial c_d'}{\partial y_d} \right) - f_d c_d' \qquad (5.3.14)$$

The distribution of $c_d'$ can be obtained for specified depth and velocity distributions by solving Eq. 5.3.14 numerically. From these numerical solutions (and from a theoretical analysis based on the separation of variables technique), it can be observed that for large $x_d$ values, an equilibrium is reached such that the transverse distribution of $c_d'$ relative to its cross-sectional average value does not change with $x_d$. Thus, a new dimensionless concentration can be defined to give the distribution relative to the average:

$$c_d'' = \frac{(C_s - c)}{(C_s - C)} \qquad (5.3.15)$$

where C is the cross-sectional average of c . For specified dimensionless distributions of velocity and depth, the equilibrium distribution of concentration as represented by $c_d''$ depends only on the parameter $f_d$ . As $f_d$ increases, the time required for a given amount of cross-channel mixing increases relative to the time for a given amount of gas transfer, so that it is more difficult for the mixing to eliminate the deficit differences being created, as described previously, by the interaction of the gas transfer and the stream hydraulics. The result is that the amount of cross-channel variation of deficit is larger for a stream with large $f_d$ than for a stream with a small

198

$f_d$ , if the hydraulics (relative depth and velocity distributions) for the two streams are the same.

To illustrate the variation of the equilibrium distribution of $c''_d$ with $f_d$ and stream hydraulics, calculations were made for two cases. For Case A, there was a rectangular cross section and $v_d$ varied over each half of the channel width as the 1/10th power of the distance from the edge of the channel. Thus, there was no depth variation and the velocity distribution was relatively flat. For Case B, the bottom profile was half of a sine wave, and the velocity varied in proportion to the 2/3rds power of the depth (Yotsukura and Sayre 1976). This case had a relatively strong variation of both depth and velocity. Both channels were prismatic. For each case, $f_d$ was varied as an input parameter for the calculations. Figure 45 shows $\Delta c''_{d,max}$ , which is defined as the maximum difference in $c''_d$ across the channel width, i.e. the difference between the center-line and bank values. As expected, $\Delta c''_{d,max}$ increased as $f_d$ increased for each case, and for a given $f_d$, $\Delta c''_{d,max}$ increased from Case A to Case B as the transverse variations of depth and velocity became more pronounced.

Even though the dimensionless deficit reaches an equilibrium distribution for a prismatic channel, that does not mean that the distribution of the actual deficit $(C_s - c)$ remains constant. Rather, an equilibrium $c''_d$ means that $(C_s - c)$ continually decreases with $x_d$ since the average deficit $(C_s - C)$ in the denominator of $c''_d$ continually decreases in the downstream direction.

## 5.4  ONE-DIMENSIONAL SOLUTIONS

As discussed in Section 5.3.6 for the 2D solutions, there are some rivers for which the flow distance required to obtain transverse uniformity of the concentration distribution can be extremely large in terms of absolute distances. On the other hand, there are other types of rivers (e.g. very narrow streams or pool and riffle streams) for which transverse uniformity may be achieved rapidly, so that transport problems may reasonably be analyzed using 1D approaches. For these

199
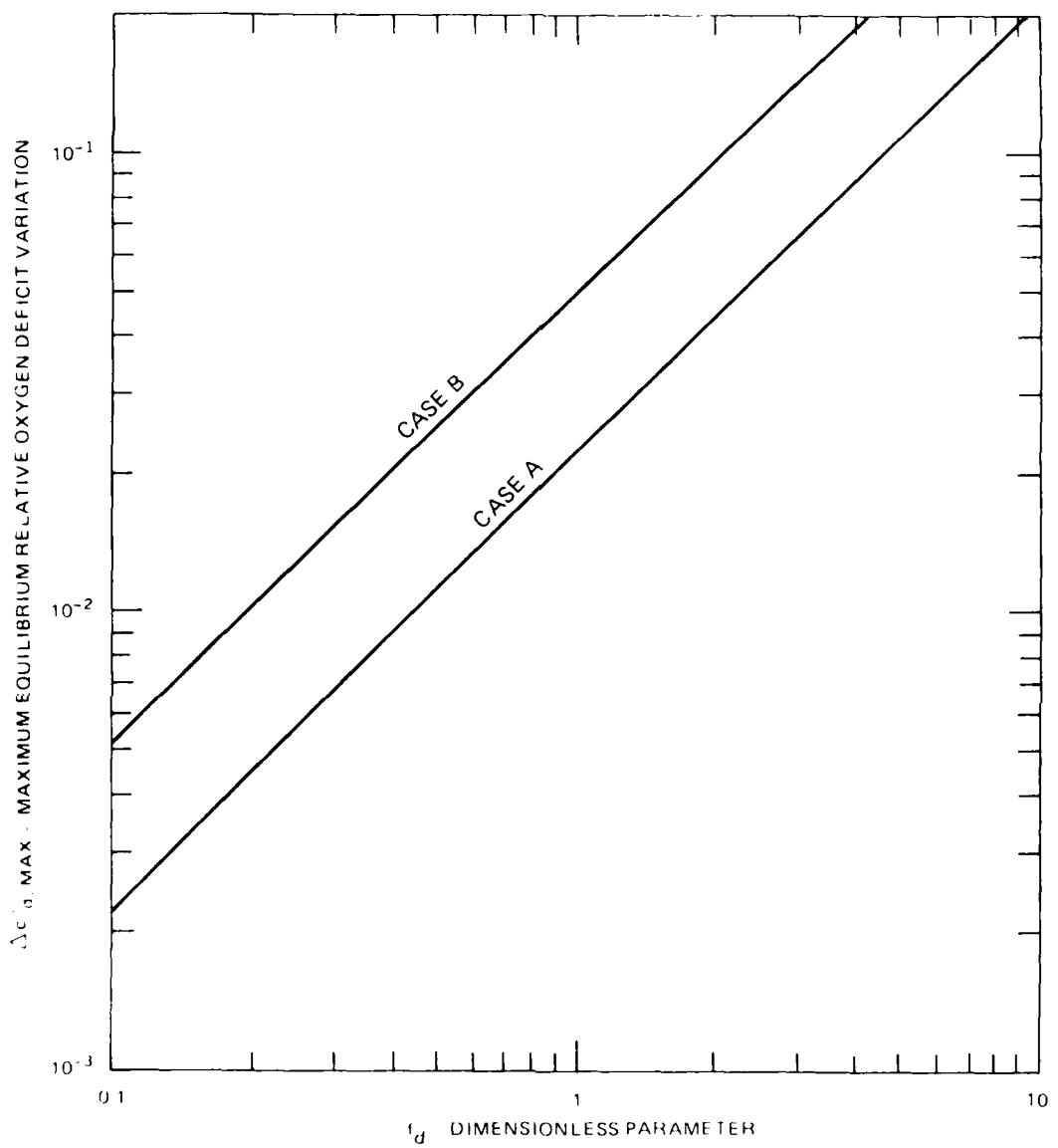
Figure 45. Calculated magnitude of equilibrium variation
of oxygen concentration

cases, some elementary 1D solutions for concentration distributions are presented in this section.

## 5.4.1 Assumptions

The assumptions that are used for the 1D solutions are as follows:

a. $\partial C/\partial t = 0$ for steady state.

b. A = constant, V = constant, E = constant. As with the previous cases, the hydraulic and transport parameters are assumed to be constant for the basic analytical solutions.

c. K = constant where all of the distributed source and sink terms in Eq. 4.8.30 are assumed to be represented by a single first-order "reaction" term with rate coefficient of K .

d. M = 1 for a straight, prismatic channel.

With these assumptions, the 1D mass balance equation may be written as

$$V \frac{\partial C}{\partial x} = E \frac{\partial^2 C}{\partial x^2} - KC \qquad (5.4.1)$$

From left to right, the terms in this equation represent the advective mass flux, the dispersive mass flux, and the removal of mass from the river by the combined "reaction" processes.

## 5.4.2 Dimensionless Variables and Differential Equation

For the 1D problems, the dimensionless variables are denoted by a subscript a to indicate the area-averaged situation. However, for a 1D transport problem in a river which is assumed to be infinitely long, there is no significant finite length over which the mixing process causes the concentration distribution to approach uniformity and thus there is no length which can be used to form the same type of dimensionless longitudinal distance as was used for the 3D and 2D problems. Rather, the dimensionless distance is based on the other two primary

201

processes in the problem, namely longitudinal advection and the first-order reaction.

The dimensionless variables are defined as

$$x_a = \frac{Kx}{V}$$

$$C_a = \frac{C}{\dot{m}/Q}$$

(5.4.2)

The variables may be interpreted as follows:

$x_a$ – dimensionless longitudinal distance which is equal to the ratio of a characteristic advection time $(x/V)$ to a characteristic reaction time $(1/K)$.

$C_a$ – concentration relative to the concentration $(\dot{m}/Q)$ which would exist if the effluent discharge were simply diluted in the total riverflow.

Introduction of these variables into Eq. 5.4.1 gives the dimensionless equation as

$$\frac{\partial C_a}{\partial x_a} = \beta \frac{\partial^2 C_a}{\partial x_a^2} - C_a$$

(5.4.3)

where $\beta = KE/V^2$. (Some analyses include a factor of 4 in the definition of a parameter analogous to $\beta$.) If $\beta \ll 1$, as is frequently the case, Eq. 5.4.3 reduces to

$$\frac{\partial C_a}{\partial x_a} = C_a$$

(5.4.4)

which represents a simple plug flow model with a first-order reaction.

### 5.4.3  Analytical Solutions

The origin is placed with $x_a = 0$ corresponding to the location of the source which has an initial mass flux of $\dot{m}$. The steady-state 1D concentration distribution from Eq. 5.4.3 may be written as

$$C_a = \frac{1}{(1 + 4\beta)^{1/2}} \quad \exp\left[-\frac{(1 + 4\beta)^{1/2} - 1}{2\beta} x_a\right] \tag{5.4.5}$$

For $\beta \ll 1$, Eq. 5.4.5 can be reduced to

$$C_a \approx \exp(-x_a) \tag{5.4.6}$$

This solution may also be obtained directly from Eq. 5.4.4.

### 5.4.4  Concentration Distributions

If $K = 0$, then the concentration for $x_a > 0$ is constant and equal to $\dot{m}/Q$, which is the dilution ratio between the mass influx and the streamflow. For $K \neq 0$, the concentration decreases exponentially with downstream distance as shown in Figure 46. The values of $\beta$ used in the figure are relatively large and are used primarily to illustrate the behavior of the concentration distributions in the event that $\beta$ is large. (For many free-flowing streams, $\beta$ based on natural biological and physical processes for $K$ and natural dispersion for $E$ is on the order of 0.1 or smaller. For pool and riffle streams or very sluggish streams, larger values of $\beta$ may be found.) One means of indicating the effect of $\beta$ on the concentration distributions is in terms of $C_{a,max}$ (at $x_a = 0$), which is given by

$$C_{a,max} = \frac{1}{(1 + 4\beta)^{1/2}} \tag{5.4.7}$$

The parameter $\beta$ must be greater than 0.03 before $C_{a,max}$ is reduced below 0.95.

203

b. Semilogarithm plot

a. Linear plot
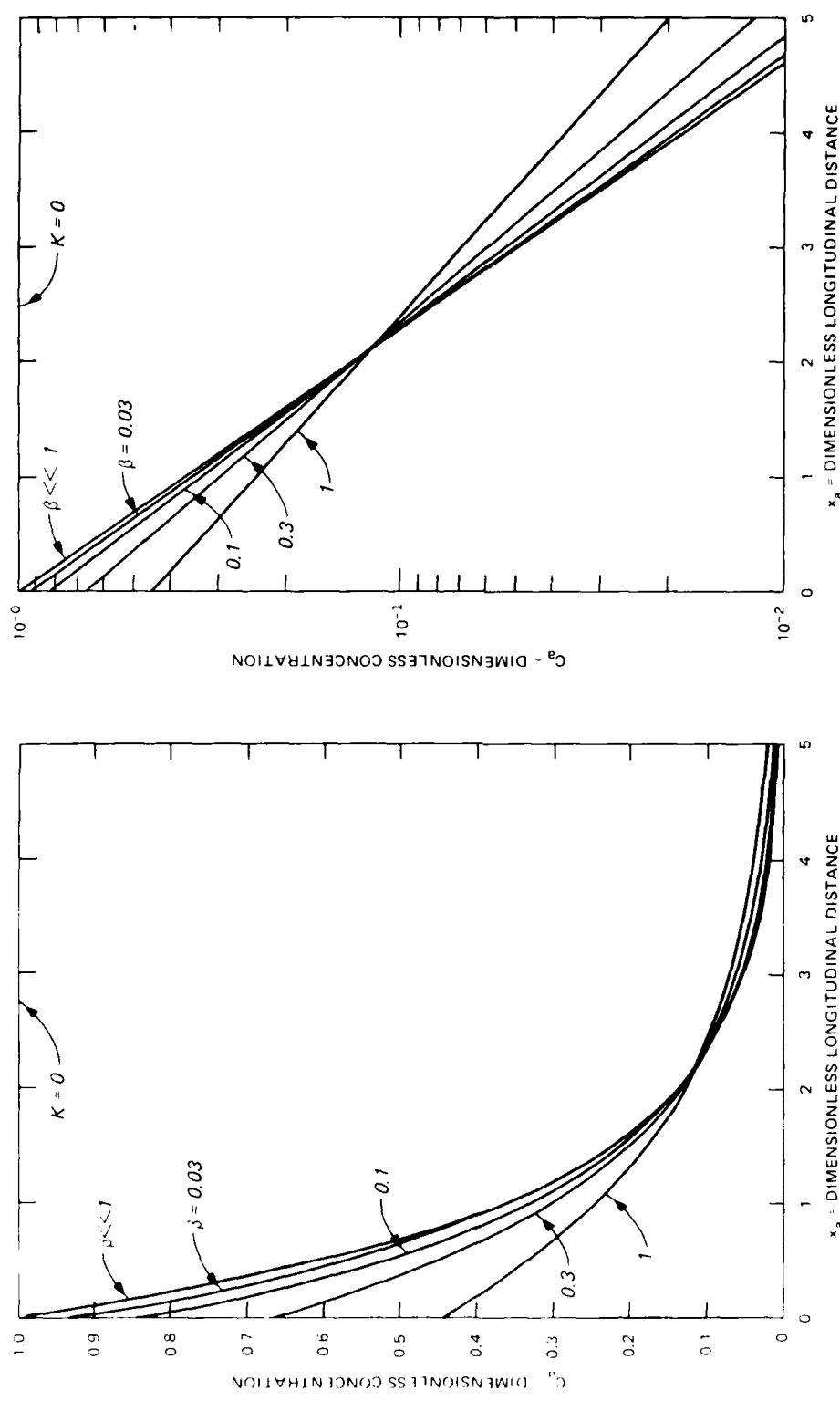
Figure 46. Calculated concentration distributions (1D)

204

One way of interpreting the effect of $\beta$ is in terms of its representing $E$ for a constant $K$ and $V$. In Figure 46, as $\beta$ increases so does the relative influence of longitudinal dispersion so that the maximum concentrations decrease and the smaller concentrations increase as dispersion transports mass down the concentration gradient from the upstream high concentrations to the downstream regions of lower concentrations.

# CHAPTER 6. CALCULATED CHARACTERISTICS OF UNSTEADY CONCENTRATION DISTRIBUTIONS

## 6.1  UNSTEADY DISTRIBUTIONS

### 6.1.1  Introduction

Chapter 5 deals with some characteristics of steady-state concentration distributions. This chapter presents similar considerations for unsteady distributions. Some of the general considerations from Chapter 5 on topics such as crossing and mixing distances and on the distance required to achieve vertical uniformity can be used as general guidelines for the unsteady case as well as the steady case and thus are not repeated in this chapter. Since the 3D region is relatively short, as shown in Section 5.2.7, no unsteady 3D distributions are presented. Nevertheless, as illustrated in Section 6.2.3, it can be important to account for the effects of the vertical distribution of velocity in the early part of the transport process.

Unsteady concentration distributions exist in rivers for a variety of reasons such as having a "slug" release, having a continuous but time-variable release rate, or having time-variable distributed sources and sinks. The term "slug" release refers to a discharge or spill that takes place essentially instantaneously; this condition is also sometimes called an "instantaneous" or "puff" release. Unsteadiness exists as the slug of released material travels downstream. The slug mixes transversely until essentially uniform conditions are achieved in the transverse direction and continually mixes longitudinally. The advecting and spreading slug of material is sometimes called a "cloud." If there is a continuous but time-variable effluent discharge, then a time-variable or unsteady concentration distribution results in the river. This type of situation is not considered explicitly in this manual; Thomann (1973) presented an analysis of unsteady 1D distributions resulting from variable effluent discharge rates. Perhaps one of the best known examples of the third type of unsteadiness is the varying dissolved oxygen (DO) distribution that results

from the diurnal variation of photosynthetic production of oxygen. For all three cases, the unsteadiness is associated with some aspect of the substance being transported but the flow is steady. Most of the presentation in this chapter is related to slug releases, both because many of the essential features of transport problems can be demonstrated for slug release and because many other types of releases can be represented as a superposition of slug releases (Carslaw and Jeager 1959, Yotsukura et al. 1983, Kilpatrick and Cummings 1972, Yotsukura and Kilpatrick 1973). Situations with unsteady river flow are not considered in this manual. There have not been extensive analyses for such situations, although some cases are considered by Jobson (1981).

In free-flowing rivers, the important mechanisms influencing the longitudinal transport process are the average longitudinal velocity, the distribution of velocity, mixing across the velocity distribution, and temporary storage zones, if any are present (Section 6.2.4b). The average velocity influences the general rate of downstream movement of the cloud. The velocity distribution produces the differential advection that provides much of the longitudinal spreading. The mixing moves particles randomly from point to point and therefore from velocity to velocity within the cross section. By influencing how long a particle remains in a region with a given velocity, the mixing across the velocity distribution also influences the rate of longitudinal spreading. The temporary delay or retention of parts of the cloud in storage zones can influence both the general rate of downstream movement of the cloud and the rate of longitudinal spreading.

Since differential advection is a significant mechanism in longitudinal spreading processes, it is important to have a reasonable means of representing the velocity distribution for unsteady transport problems. It is preferable to have the velocity distribution represented explicitly in the analysis. This is done for the transverse distribution of velocity in the first three methods discussed in Section 6.2. The fourth method does not properly account for the velocity distribution and is therefore normally not as desirable as the other methods. Nevertheless, it is sometimes used because of the ease of

207

calculation. For 1D problems, the effects of the distribution of velocity and the mixing across the velocity distribution are included in the longitudinal mixing coefficient or in other spreading coefficients for representations which do not use mixing coefficients.

## 6.1.2 Moments of Concentration Distributions

There are sometimes benefits in studying the moments of concentration distributions resulting from slug releases. For example, the rate of movement of the centroid gives the average stream velocity (if there are no temporary storage mechanisms present, Section 6.2.4b), and the rate of change of the variance can be used to obtain a longitudinal mixing coefficient. Since the calculation of moments involves integration over (and therefore elimination of) one of the independent variables on which the concentration depends (Eq. 6.1.2), the presentation and interpretation of some of the important features of concentration data can be done more efficiently by using moments. Also, in making predictions, it is frequently much easier to calculate the moments of the distributions than to calculate the concentrations themselves. Even though direct calculation of moments does not give the actual concentrations, the calculated moments do give much useful information about the transport process. Furthermore, means are being developed to be able to estimate concentrations from calculated moments (Tso 1982; Section 6.2.4h).

In a general case, the depth-averaged concentration may be a function of longitudinal distance, transverse distance, and time so that

$$c = c(x,y,t) \tag{6.1.1}$$

With measurements made at some specific longitudinal and transverse locations, i.e. at specific $x$ and $y$ values, the measured distributions would be functions of $t$. For such distributions, the temporal moments ($n_p$) are defined as

208

$$n_p = \int_0^\infty ct^p \, dt \qquad (6.1.2)$$

The zeroth ($p = 0$) moment gives the area under the  c  versus  t
curve.  The centroid ($\bar{t}$) can be obtained from the zeroth and first
moments since

$$\bar{t} = \frac{n_1}{n_0} \qquad (6.1.3)$$

The variance comes from the second and zeroth moments (and the first
moment in $\bar{t}$):

$$\sigma^2 = \frac{n_2}{n_0} - \bar{t}^2 \qquad (6.1.4)$$

The square root of the variance, i.e. the standard deviation ($\sigma$) is a
measure of the "width" of the  c  versus  t  distribution.  The skew-
ness (S) of the distribution comes from the third and lower moments and
is defined as

$$S = \frac{\dfrac{n_3}{n_0} - 3\bar{t}\sigma^2 - \bar{t}^3}{\sigma^3} \qquad (6.1.5)$$

In general, as the order (p) of the moments increases, it becomes pro-
gressively more difficult to obtain accurate calculations of the
moments from data because small variations in  c  values on the tails
of the distribution can cause relatively large variations in the
moments.

## 6.2 TWO-DIMENSIONAL SOLUTIONS

### 6.2.1 General Comments

The dimensionless flow distances required to achieve various degrees of transverse uniformity of concentration for steady-state conditions are considered in Section 5.3.6. Approximately the same flow distances are required to achieve transverse uniformity for unsteady concentration distributions. Thus, there are many unsteady situations which are two dimensional and need to be analyzed as such. In spite of this fact, there have been relatively few analyses of the general characteristics of 2D unsteady transport problems in rivers. Thus, most of the examples that are presented in this section are for the simple case of a rectangular channel with a parabolic transverse distribution of longitudinal velocity.

For 2D unsteady transport problems, the longitudinal spreading is associated primarily with the differential advection due to the distribution of velocity and the mixing across the velocity distribution, as discussed in Sections 4.8.3 and 6.1.1. The accuracy of calculated concentration distributions depends to a large degree on the accuracy with which the important mechanisms are represented in the calculations. In the following four subsections, results are presented from four different methods for analyzing 2D unsteady transport problems. The first three methods have the capability of directly representing the primary mechanisms. The effects of temporary storage are included in only the third method; in principle, they could be included in any of the methods. The last method does not properly account for the important aspect of the transverse distribution of velocity and the related differential advection.

The differential mass balance equation representing 2D unsteady transport using general curvilinear coordinates may be written from Eq. 4.7.26 (retaining the $e_x$ term from Eq. 4.7.22) as

210

$$h \frac{\partial c}{\partial t} + \frac{h v_x}{m_x} \frac{\partial c}{\partial x} + \frac{h v_y}{m_y} \frac{\partial c}{\partial y} = \frac{1}{m_x m_y} \frac{\partial}{\partial x} \left( \frac{m_y}{m_x} h e_x \frac{\partial c}{\partial x} \right)$$

$$+ \frac{\partial}{\partial y} \left( \frac{m_x}{m_y} h e_y \frac{\partial c}{\partial y} \right) - Khc \qquad (6.2.1)$$

In Eq. 6.2.1, the transfers across the surface $(f_S)$ and the bed $(f_B)$ and the reaction within the water column as represented by $k$ have been combined into a single first-order reaction term represented by $K$. As demonstrated by the depth-averaging process leading to Eq. 4.7.22, $e_x$ in Eq. 6.2.1 represents the effects of differential advection associated with the vertical distribution of velocity and vertical mixing (Eqs. 4.7.18 and 4.7.21). If the y axis is along the streamlines, then $v_y = 0$ in Eq. 6.2.1. On the other hand, if the streamtube model is used, the mass balance equation can be written from Eq. 4.7.33 as

$$\frac{\partial c}{\partial t} + \frac{v_x}{m_x} \frac{\partial c}{\partial x} = \frac{1}{m_x m_y h} \frac{\partial}{\partial x} \left( \frac{m_y}{m_x} h e_x \frac{\partial c}{\partial x} \right)$$

$$+ \frac{v_x}{m_x} \frac{\partial}{\partial q} \left( m_x h^2 v_x e_y \frac{\partial c}{\partial q} \right) - \frac{f_S}{h} - \frac{f_B}{h} - Kc \qquad (6.2.2)$$

where the longitudinal mixing term has been retained in the development from Eq. 4.7.22 to 4.7.33.

The calculated results given in the following sections are for a straight, rectangular channel so that Eq. 6.2.1 can be used with $m_x = 1$, $m_y = 1$, $v_y = 0$, and $h = $ constant. As with the steady-state solutions in Chapter 5, the calculated results for the unsteady distributions are presented in dimensionless form with the dimensional variables being

$$x_r = \frac{x/V}{B^2/e_y} = \frac{xe_y}{B^2 V}$$

$$t_r = \frac{t}{B^2/e_y} = \frac{te_y}{B^2}$$

$$y_r = \frac{y}{B}$$

$$V_r = \frac{V_x}{V}$$

$$e_r = \frac{e_x e_y}{(BV)^2}$$

$$(6.2.3)$$

where the subscript $r$ indicates a depth-averaged dimensionless repre-
sentation in a rectangular channel. See Sections 5.1.2, 5.2.2, and
5.3.2 for a discussion of the interpretation of similar dimensionless
variables. The parameter $e_r$ is generated as a coefficient in the
differential equation in the process of nondimensionalizing other terms
in the equation. Eq. 6.2.1 may now be written as

$$\frac{\partial c}{\partial t_r} + \frac{v_x}{V} \frac{\partial c}{\partial x_r} = e_r \frac{\partial^2 c}{\partial x_r^2} + \frac{\partial^2 c}{\partial y_r^2} \qquad (6.2.4)$$

In Eq. 6.2.4, it is assumed that the substance being transported is
conservative ($K = 0$); the concentration has not been nondimensionalized.

6.2.2 Numerical Solutions

The amount of published work for 2D unsteady transport is much
less than that for steady 2D problems. One reason is that even for a
straight rectangular channel and for a conservative substance, it gen-
erally is not possible to obtain analytical solutions to Eq. 6.2.4 when
$v_x$ is a function of $y$, but this dependence on $y$ must be included
to properly represent the longitudinal spreading. Thus, most of the

212

solutions which have been published for unsteady problems have been obtained numerically, but even then the 2D results have frequently been averaged transversely with only the width-averaged results being presented.

A thorough discussion of various numerical solution techniques is beyond the scope of this manual. Only two points will be mentioned. One is that it is not a trivial matter to obtain a numerical scheme which does not have significant numerical dispersion (i.e. one for which the numerical scheme itself does not cause attenuation of the peak concentration and spreading of the cloud) and which does not cause oscillations of the tail of the concentration distribution. The other point is that, in recent years, there has been considerable attention in the literature to obtaining improved numerical schemes; so, early publications should be used with care. Even so, most of the more recent publications deal with the numerical schemes themselves (frequently for 1D problems) rather than with the characteristics of the concentration distributions which exist for various situations. As a result, it is not possible to draw generalized information from the literature. Thus, concentrations were calculated for one idealized flow situation to provide some insight into the transport processes and into the types of information which can be obtained from calculations.

The situation considered in these calculations is a rectangular channel with a parabolic transverse distribution of velocity. The effects of longitudinal dispersion associated with the vertical distribution of velocity are demonstrated in the results of the calculations. A scheme was used which had zero numerical dispersion. In order to accomplish this condition of zero numerical dispersion, the velocity distribution had to be modified slightly, but was still approximately a parabolic distribution. (Thus, in a general problem, it may not be possible to use this type of scheme since the velocity distribution had to be adjusted slightly to achieve the zero numerical dispersion. Also, the scheme depends on having a prismatic channel where the velocity distribution does not change with downstream distance.) Because of symmetry, calculations were made for only half of the channel;

213

10 filaments were used. Figure 47 shows contours of the calculated
concentrations for a vertical line source in the filament next to the
channel centerline. Note the changes in the scaling for the $x_r$ axis.
The solid curves are for $e_r = 0.00001$ in Eq 6.2.4. One condition
that would give rise to this value would be $e_x/HU_* = 6$ (Elder 1959),
$e_y/HU_* = 0.5$, $B/H = 40$, $V/U_* = 14$. (See Chapter 7.) For a
centerline source, the mass is originally in a small region and is not
exposed to significant differential advection due to the transverse
distribution of velocity so that the initial increase in the cloud
length is due primarily to the effects of the vertical distribution of
velocity as represented by $e_x$ and $e_r$ in the calculations. However,
as transverse mixing increases the width of the cloud, differential
advection associated with the transverse distribution of velocity
begins to increase the cloud length also; eventually, the effects of
$e_x$ become negligible. Ultimately, mixing causes the concentration
distributions to approach, but never totally achieve (Fischer et al.
1979; Fig. 47; Section 6.2.5e), transverse uniformity.

The dotted curves in Figure 47 show the contours for $e_r$ or
$e_x = 0$. Since this numerical scheme has no numerical dispersion, this
latter condition is equivalent to the frequently used assumption of
negligible effects of the vertical distribution of velocity on the
longitudinal transport process. The figure demonstrates the types of
errors which are introduced by assuming that $e_x = 0$. Especially for
the small dimensionless times, using $e_x = 0$ gives distributions which
are much too steep on the leading edge and gives maximum concentrations
which are much too large (Figure 48). The same general types of errors
should be expected in calculations for actual flows. (The abrupt
fronts in Figure 47 are sometimes not evident because of numerical dis-
persion in solutions. It is the authors' opinion that, whenever prac-
tical, numerical dispersion should not be used to represent actual
physical dispersion. It is generally desirable to be able to control
the calculated dispersion independently from the factors which influ-
ence the numerical dispersion, namely the finite difference grid size
and the difference scheme used in the calculations.)
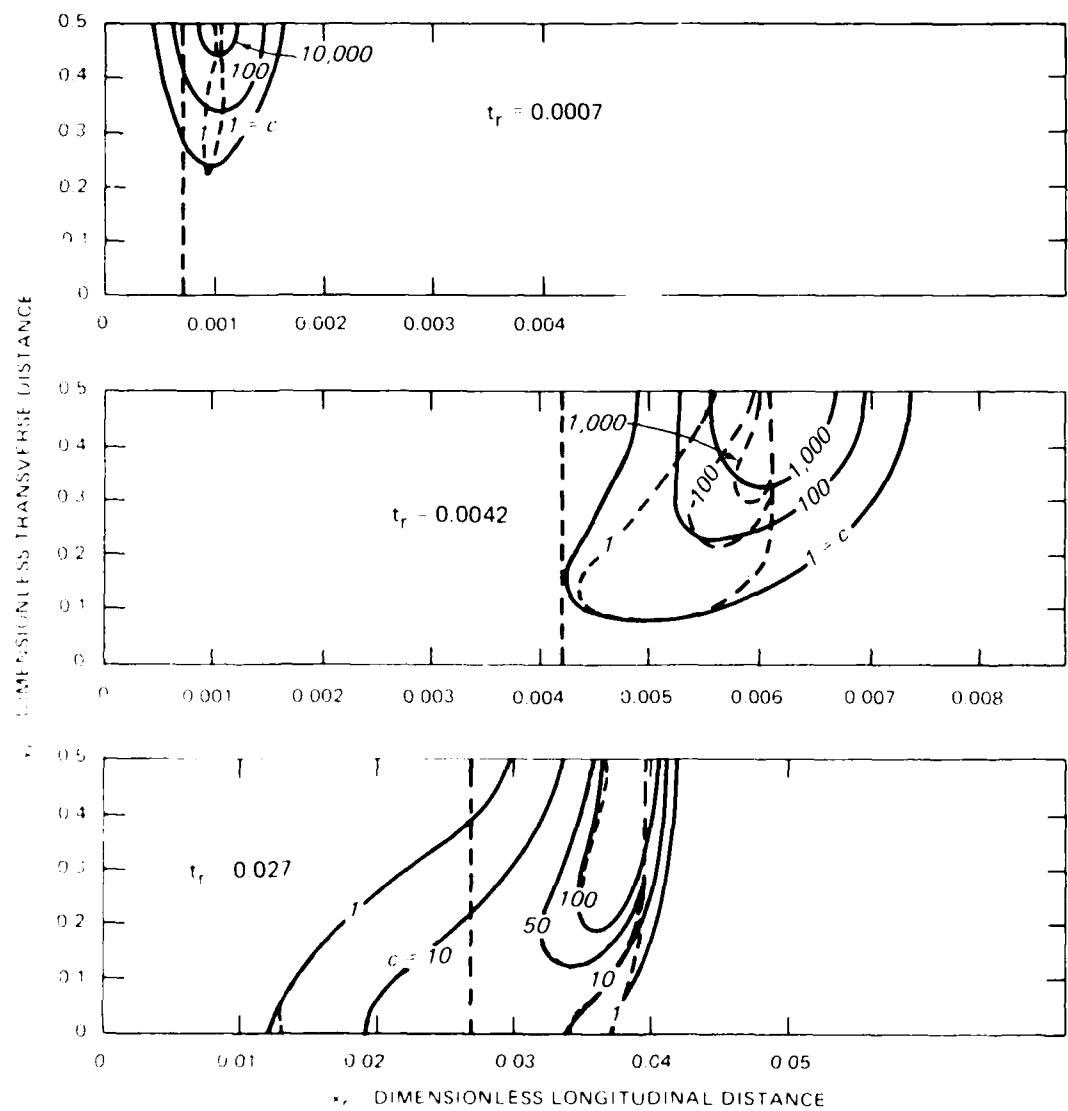
Figure 47. Calculated two-dimensional concentration contours with and without longitudinal dispersion (Continued)
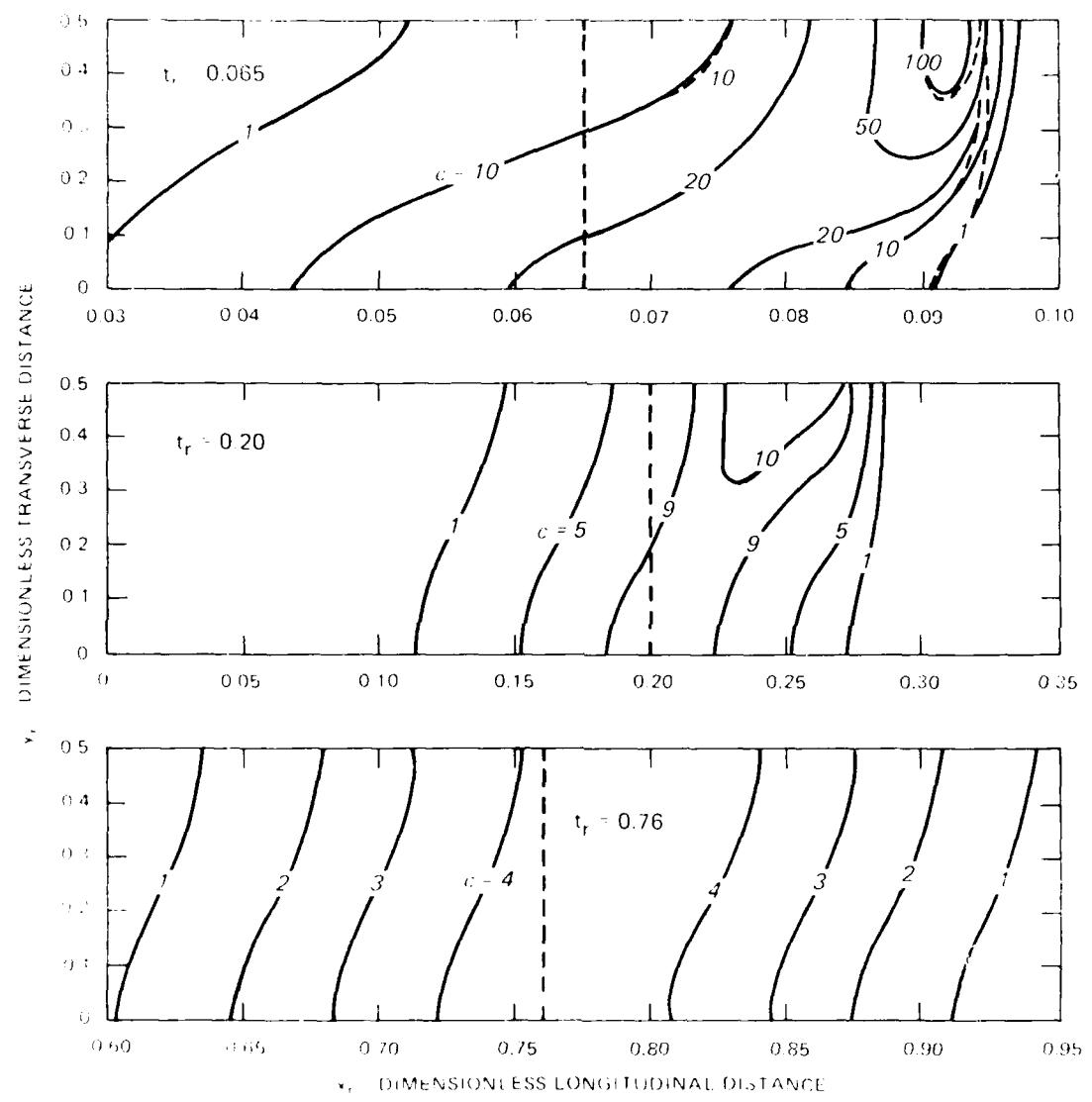
Figure 47. (Concluded)
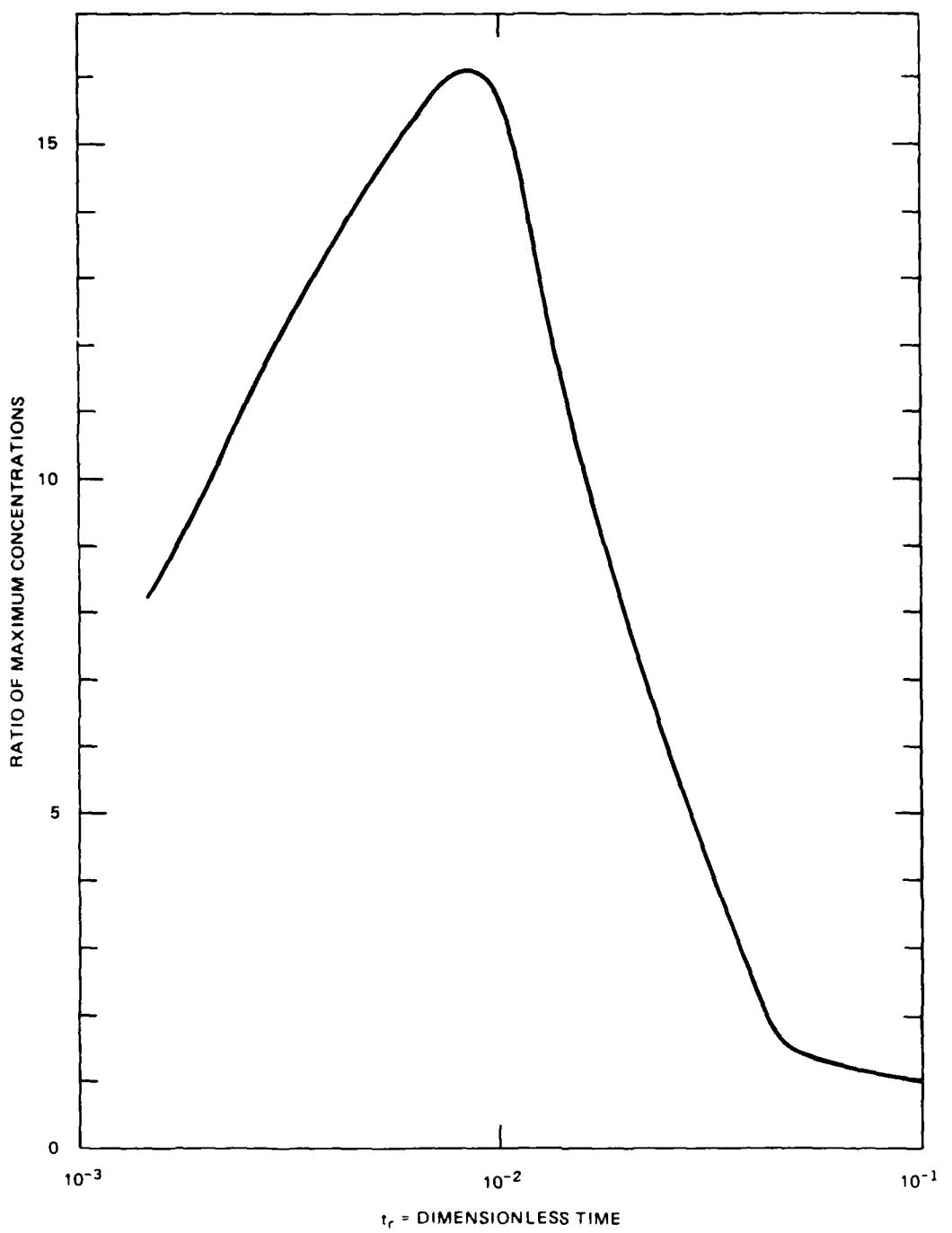
Figure 48. Ratio of maximum calculated concentrations for two-dimensional situations with $e_x = 0$ and with $e_x \neq 0$

217

The general characteristics of the concentration distributions are discussed further in the next section as the results of the random walk simulations are presented.

### 6.2.3  Random Walk Simulations

Most of the calculated concentration distributions that are presented in this manual and in the technical literature in general are based on solutions to the differential mass balance equations for various situations.  The random walk approach is an alternative approach which has been presented in the literature (Bugliarello and Jackson 1964, Sullivan 1971), but has not been widely used for idealized channel flows or for rivers even though it is a Lagrangian scheme that has zero numerical dispersion.  The usefulness of the method for natural streams with varying cross-sectional shapes and varying velocity distributions has recently been demonstrated (Jeng and Holley 1986).

Fundamentally, one of the main differences between solving differential mass balance equations and using the random walk approach is that the mass balance equations represent the time-averaged mixing mechanisms by using mixing coefficients in diffusion-type terms while the random walk approach has discrete particles that undergo random displacements to represent the mixing, and ensemble averages for large numbers of particles can be used to represent the concentration distributions.  In the present case, the advection is in the longitudinal direction and the random displacements are in the transverse direction to represent transverse mixing.  No longitudinal mixing comparable to $e_x$ is included in these sample calculations.  Thus, these results are valid only for $t_r$ greater than about 0.05 (Figure 48).  The effects of $e_x$ can be included in the calculations (Jeng and Holley 1986).

Since mixing processes are normally characterized in terms of mixing coefficients rather than in terms of random walk parameters, it is necessary to have a relationship between the two types of representations, but the relationship depends on the way in which the random mixing is represented in the simulation and on the probability distributions used for the random steps of the discrete particles.  One means

218

of bridging between the two methods is to apply the relationship $e_y = 0.5 \partial \sigma^2 / \partial t$ for each time step in the random walk simulation, with $\sigma^2$ being the transverse variance of the concentration distribution. In that case, $\partial \sigma^2 / \partial t$ is equal to the variance of the probability distribution divided by $\Delta t$ for the simulation since the variance of the probability distribution is equal to the increase of $\sigma^2$ for one time step for a large number of particles. In these calculated results, a rather elementary representation was used for the random transverse steps of the particles. The step length (L) was taken as constant and equal to 1/20th of the channel width. For each time step ($\Delta t$), each particle had equal probabilities of moving one step to the right, remaining at the original transverse position, or moving one step to the left. For this situation, the relationship between $e_y$ and $\partial \sigma^2 / \partial t$ then gives

$$e_y = \frac{1}{2} \frac{\partial \sigma^2}{\partial t} = \frac{L^2}{3 \Delta t} \tag{6.2.5}$$

Substitution into the nondimensional expression for $\Delta t_r$ (Eq. 6.2.3) leads to

$$\Delta t_r = \frac{L_r^2}{3} \tag{6.2.6}$$

where $L_r = L/B$ . Thus $\Delta t_r$ corresponding to each step of the particles was fixed by the selected $L_r$ of 0.05.

The simulation was done by releasing a large number of particles (5000, in this case) with an initial distribution corresponding to the assumed initial condition. For each time step, each particle was advected a distance downstream based on $\Delta t_r$ and on the flow velocity at the particle's initial transverse location and was displaced transversely in a random manner. (The velocity could be taken from the initial position of the particle before the random transverse step or from the average velocity over the path length. In this example, the

219

former method was used.)  The velocity distribution was the same as
that used in the numerical solution discussed in the previous section.
The no-flux or reflective boundary condition was satisfied by simple
reflection of the transverse path if a particle's path would have moved
across one of the side boundaries.  At various times and locations, the
particles in $\Delta x_r \Delta y_r$ cells were counted, with $\Delta y_r$ always being 0.05
and with $\Delta x_r$ being increased from 0.002 to 0.05 as the length of the
cloud increased.  The number of particles in each grid should be
divided by the grid area $(\Delta x_r \Delta y_r)$ and by the total number of particles
released to obtain concentrations corresponding to an initial release
of a unit mass.

Tables 7 and 8 give samples of the calculated results for a
plane source and a centerline source.  The moment-related quantities
were calculated from the actual particle distributions, not from the
summed particle counts shown in the tables.  First, consider the spa-
tial distributions for the plane source (Table 7).  Since longitudinal
advection is faster than transverse mixing (and since the effects of $e_x$
are not included in these calculations), the distributions for the small
times result primarily from the advection with the original line source
being distorted into the shape of the velocity distribution.  Thus, a
source which is originally uniform across the flow area becomes non-
uniform due to the differential advection.  The resulting transverse
concentration gradients give rise to transverse mixing so that the con-
centration distributions gradually approach transverse uniformity, but
absolute transverse uniformity is never achieved in unsteady transport
problems (Taylor 1953, 1954; Fischer et al. 1979; Section 6.2.5e).  The
length of the cloud continually increases.  For all times except at the
very beginning of the transport process, the total length of the cloud
is less than would be indicated by the differential advection based on
the total differences between the maximum and minimum velocities; since
transverse mixing moves particles from point to point with different
velocities at the different points, there is no particle that stays on
the streamline with the maximum velocity to continually be advected with

# Table 7

## Random Walk Simulation for a Plane Source

DIMENSIONLESS TIME = .00333

SPATIAL PARTICLE COUNT MAP:

FIL*

| 1 | 480 | 0 | 0 |
| 2 | 504 | 0 | 0 |
| 3 | 337 | 175 | 0 |
| 4 | 179 | 324 | 0 |
| 5 | 0 | 508 | 0 |
| 6 | 0 | 348 | 170 |
| 7 | 0 | 145 | 348 |
| 8 | 0 | 0 | 491 |
| 9 | 0 | 0 | 505 |
| 10 | 0 | 0 | 486 |

DIMENSIONLESS DISTANCE * 1000
　　　-2　0　2

LATERALLY INTEGRATED PARTICLE COUNT:
　　150015002000

MOMENTS:

| FILAMENT | RELATIVE COUNT | CENTROID * 1000 | STD DEV * 1000 | VARIANCE | SKEW COEF |
|---|---|---|---|---|---|
| 1 | .0960 | -2.544 | .425 | .00000018 | .69719 |
| 2 | .1008 | -2.015 | .699 | .00000049 | .00791 |
| 3 | .1024 | -1.182 | .621 | .00000039 | -.07211 |
| 4 | .1006 | -.495 | .541 | .00000029 | -.04494 |
| 5 | .1016 | .129 | .454 | .00000021 | -.13431 |
| 6 | .1036 | .621 | .365 | .00000013 | -.14031 |
| 7 | .0986 | 1.048 | .284 | .00000008 | -.31934 |
| 8 | .0982 | 1.316 | .204 | .00000004 | -.21433 |
| 9 | .1010 | 1.530 | .120 | .00000001 | -.53560 |
| 10 | .0972 | 1.622 | .047 | .00000000 | -.77702 |
| TOTAL | 1.0000 | .004 | 1.481 | .00000219 | -.61718 |

(Continued)

* Filament 1 is next to the channel boundary. Filament 10 is next to the centerline.

(Sheet 1 of 6)

221

Table 7 (Continued)

DIMENSIONLESS TIME = .01000

SPATIAL PARTICLE COUNT MAP:

FIL

| | | | | | | | |
|---|---|---|---|---|---|---|---|
| 1 | 299 | 169 | 39 | 0 | 0 | 0 | 0 |
| 2 | 147 | 192 | 98 | 77 | 0 | 0 | 0 |
| 3 | 37 | 111 | 109 | 135 | 82 | 0 | 0 |
| 4 | 0 | 40 | 65 | 178 | 190 | 29 | 0 |
| 5 | 0 | 0 | 30 | 87 | 215 | 159 | 17 |
| 6 | 0 | 0 | 0 | 21 | 139 | 189 | 116 |
| 7 | 0 | 0 | 0 | 0 | 42 | 225 | 268 |
| 8 | 0 | 0 | 0 | 0 | 0 | 75 | 408 |
| 9 | 0 | 0 | 0 | 0 | 0 | 0 | 521 |
| 10 | 0 | 0 | 0 | 0 | 0 | 0 | 491 |

DIMENSIONLESS DISTANCE * 1000
    -8  -6  -4  -2   0   2   4

LATERALLY INTEGRATED PARTICLE COUNT:
   483 512 341 498 668 6771821

MOMENTS:

| FILAMENT | RELATIVE COUNT | CENTROID * 1000 | STD DEV * 1000 | VARIANCE | SKEW COEF |
|---|---|---|---|---|---|
| 1 | .1014 | -7.094 | 1.421 | .00000202 | .95193 |
| 2 | .1028 | -5.565 | 2.052 | .00000421 | .22168 |
| 3 | .0948 | -3.507 | 2.289 | .00000524 | -.17886 |
| 4 | .1004 | -1.581 | 1.961 | .00000385 | -.36606 |
| 5 | .1016 | .234 | 1.790 | .00000320 | -.43692 |
| 6 | .0930 | 1.765 | 1.441 | .00000208 | -.39420 |
| 7 | .1070 | 2.843 | 1.090 | .00000119 | -.44564 |
| 8 | .0966 | 3.843 | .804 | .00000065 | -.77454 |
| 9 | .1042 | 4.451 | .501 | .00000025 | -1.14042 |
| 10 | .0982 | 4.759 | .257 | .00000007 | -1.80637 |
| TOTAL | 1.0000 | .012 | 4.341 | .00001884 | -.56842 |

(Continued)

Table 7 (Continued)

DIMENSIONLESS TIME = .03000

SPATIAL PARTICLE COUNT MAP:

FIL

| 1 | 10 | 67 | 119 | 72 | 55 | 51 | 30 | 29 | 21 | 21 | 14 | 7 | 4 | 1 | 1 | 0 | 0 | 0 | 0 | 0 | 0 |
| 2 | 12 | 48 | 69 | 56 | 44 | 48 | 39 | 37 | 39 | 23 | 26 | 23 | 11 | 16 | 7 | 2 | 0 | 0 | 0 | 0 | 0 |
| 3 | 0 | 16 | 34 | 37 | 42 | 45 | 36 | 44 | 39 | 37 | 37 | 38 | 28 | 23 | 23 | 17 | 6 | 4 | 0 | 0 | 0 |
| 4 | 0 | 4 | 6 | 17 | 28 | 26 | 20 | 33 | 38 | 42 | 29 | 42 | 49 | 42 | 34 | 32 | 30 | 12 | 9 | 0 | 0 |
| 5 | 0 | 0 | 0 | 3 | 9 | 4 | 14 | 13 | 14 | 19 | 30 | 33 | 61 | 54 | 50 | 43 | 51 | 52 | 31 | 11 | 0 |
| 6 | 0 | 0 | 0 | 0 | 0 | 2 | 2 | 4 | 5 | 9 | 20 | 26 | 26 | 38 | 31 | 49 | 52 | 63 | 67 | 56 | 20 |
| 7 | 0 | 0 | 0 | 0 | 0 | 0 | 1 | 1 | 0 | 4 | 8 | 8 | 15 | 22 | 29 | 43 | 61 | 76 | 87 | 97 | 69 |
| 8 | 0 | 0 | 0 | 0 | 0 | 0 | 0 | 0 | 0 | 0 | 4 | 0 | 2 | 8 | 7 | 17 | 28 | 60 | 72 | 125 | 171 |
| 9 | 0 | 0 | 0 | 0 | 0 | 0 | 0 | 0 | 0 | 0 | 0 | 0 | 0 | 0 | 0 | 5 | 8 | 15 | 37 | 50 | 115 | 284 |
| 10 | 0 | 0 | 0 | 0 | 0 | 0 | 0 | 0 | 0 | 0 | 0 | 0 | 0 | 0 | 1 | 0 | 0 | 4 | 11 | 37 | 81 | 374 |

DIMENSIONLESS DISTANCE * 1000
       -26 -24 -22 -20 -18 -16 -14 -12 -10  -8  -6  -4  -2   0   2   4   6   8  10  12  14

LATERALLY INTEGRATED PARTICLE COUNT:
       22 135 228 185 178 176 142 161 156 155 168 177 196 205 187 211 247 315 353 485 918

MOMENTS:

| FILAMENT | RELATIVE COUNT | CENTROID * 1000 | STD DEV * 1000 | VARIANCE | SKEW COEF |
|---|---|---|---|---|---|
| 1 | .1004 | -17.955 | 5.577 | .00003110 | .90541 |
| 2 | .1000 | -14.985 | 7.246 | .00005250 | .55261 |
| 3 | .1012 | -10.517 | 7.966 | .00006345 | .22153 |
| 4 | .0986 | -5.598 | 8.157 | .00006653 | -.15797 |
| 5 | .0984 | .208 | 7.133 | .00005087 | -.60978 |
| 6 | .0940 | 4.646 | 6.304 | .00003975 | -.68151 |
| 7 | .1042 | 7.823 | 5.116 | .00002617 | -1.07304 |
| 8 | .0988 | 10.805 | 3.749 | .00001406 | -1.65859 |
| 9 | .1028 | 12.366 | 2.627 | .00000690 | -1.58241 |
| 10 | .1016 | 13.380 | 1.791 | .00000321 | -2.48701 |
| TOTAL | 1.0000 | .053 | 12.578 | .00015820 | -.50036 |

(Continued)

# Table 7 (Continued)

```
DIMENSIONLESS TIME -  .10000

SPATIAL PARTICLE COUNT MAP:

FIL

 1    1   3  31  43  49  37  37  41  33  21  26  24  16  30  26  17  13  11   8   9   9   1   2   1   0   0   0   0

 2    0   1  15  21  35  40  37  34  31  30  19  25  28  23  17  18  19   9  14   6   6   8   8   6   2   1   0   0

 3    0   1   9  14  18  30  36  31  31  35  33  19  33  23  25  22  21  23  18  15  16  16  13  19   6   4   0   0

 4    0   0   2  14  11  24  29  20  17  25  26  24  17  26  27  20  24  17  24  23  22  27  18  20  20  11   2   0

 5    0   0   2   4   5   5  13  15  27  22  25  14  26  21  14  26  20  22  18  22  24  35  29  21  40  25  14   0

 6    0   0   0   0   4   5   8  10  13   9  17  13  18  18  22  11  14  29  24  27  33  29  30  55  52  55  46   1

 7    0   0   0   0   0   0   2   3   4  10   9  10  11  10  18  20  12  23  24  23  32  35  29  38  45  52  77   3

 8    0   0   0   0   0   1   1   3   1   4   7   6   6   6  10   9  10  13  12  24  23  21  28  46  68  96 113  13

 9    0   0   0   0   0   0   0   2   1   1   1   1   4   3   9   6   6  12  10  11  24  28  29  28  44  77 123  27

10    0   0   0   0   0   0   0   1   0   0   1   2   2   1   4   3   7  10   6  10  15  19  26  31  60  94 173  60

DIMENSIONLESS DISTANCE * 1000
    -85 -80 -75 -70 -65 -60 -55 -50 -45 -40 -35 -30 -25 -20 -15 -10  -5  -0   5  10  15  20  25  30  35  40  45  50

LATERALLY INTEGRATED PARTICLE COUNT:
     1   5  59  96 126 142 163 160 158 157 164 138 161 161 172 152 146 169 158 170 204 218 212 265 337 448 554 104
```

MOMENTS:

| FILAMENT | RELATIVE COUNT | CENTROID * 1000 | STD DEV * 1000 | VARIANCE | SKEW COEF |
|---|---|---|---|---|---|
| 1 | .0978 | -41.785 | 25.078 | .00062891 | .58306 |
| 2 | .0914 | -35.380 | 27.121 | .00073554 | .62046 |
| 3 | .1022 | -24.817 | 29.513 | .00087104 | .32532 |
| 4 | .0980 | -15.210 | 31.674 | .00100325 | .01291 |
| 5 | .0980 | -3.525 | 31.247 | .00097637 | -.23367 |
| 6 | .1104 | 10.208 | 29.308 | .00085895 | -.72912 |
| 7 | .1000 | 17.271 | 25.317 | .00064096 | -.80955 |
| 8 | .1022 | 25.954 | 22.616 | .00051147 | -1.46992 |
| 9 | .0950 | 30.910 | 18.673 | .00034867 | -1.63997 |
| 10 | .1050 | 35.404 | 15.558 | .00024205 | -2.06279 |
| TOTAL | 1.0000 | .468 | 37.227 | .00139583 | -.40204 |

(Continued)

(Sheet 4 of 6)

224

Table 7 (Continued)

DIMENSIONLESS TIME = .30000

SPATIAL PARTICLE COUNT MAP:

FIL

| 1 | 2 | 11 | 13 | 31 | 37 | 39 | 44 | 41 | 44 | 25 | 23 | 44 | 35 | 36 | 23 | 18 | 6 | 1 | 0 |
| 2 | 1 | 5 | 17 | 21 | 26 | 41 | 36 | 43 | 41 | 42 | 43 | 32 | 31 | 37 | 23 | 20 | 20 | 0 | 0 |
| 3 | 2 | 4 | 17 | 24 | 19 | 18 | 37 | 34 | 27 | 27 | 37 | 38 | 31 | 44 | 36 | 29 | 22 | 6 | 0 |
| 4 | 0 | 4 | 9 | 22 | 22 | 26 | 37 | 33 | 37 | 42 | 39 | 36 | 38 | 39 | 27 | 38 | 28 | 16 | 3 |
| 5 | 0 | 1 | 4 | 6 | 23 | 20 | 32 | 35 | 37 | 38 | 41 | 37 | 39 | 42 | 43 | 49 | 49 | 34 | 5 |
| 6 | 0 | 1 | 2 | 11 | 20 | 20 | 14 | 27 | 37 | 24 | 28 | 44 | 50 | 47 | 44 | 52 | 59 | 45 | 7 |
| 7 | 0 | 0 | 1 | 2 | 8 | 9 | 22 | 29 | 27 | 49 | 33 | 34 | 35 | 47 | 54 | 52 | 66 | 58 | 17 |
| 8 | 0 | 0 | 0 | 2 | 7 | 12 | 15 | 18 | 25 | 27 | 24 | 33 | 41 | 41 | 55 | 58 | 76 | 71 | 25 |
| 9 | 0 | 0 | 0 | 2 | 2 | 7 | 14 | 11 | 20 | 26 | 32 | 33 | 26 | 41 | 40 | 40 | 59 | 68 | 35 |
| 10 | 0 | 0 | 0 | 2 | 3 | 4 | 9 | 15 | 22 | 28 | 27 | 50 | 29 | 34 | 44 | 53 | 61 | 85 | 38 |

DIMENSIONLESS DISTANCE * 1000
-220-200-180-160-140-120-100 -80 -60 -40 -20 -0 20 40 60 80 100 120 140

LATERALLY INTEGRATED PARTICLE COUNT:
5 26 63 123 167 196 260 286 317 328 327 381 355 408 389 409 446 384 130

MOMENTS:

| FILAMENT | RELATIVE COUNT | CENTROID * 1000 | STD DEV * 1000 | VARIANCE | SKEW COEF |
|---|---|---|---|---|---|
| 1 | .0946 | -54.927 | 77.779 | .00604950 | .06742 |
| 2 | .0958 | -43.941 | 77.086 | .00594222 | .04785 |
| 3 | .0904 | -29.023 | 83.130 | .00691058 | -.19643 |
| 4 | .0992 | -22.571 | 81.581 | .00665551 | -.09534 |
| 5 | .1070 | .839 | 80.376 | .00646034 | -.25018 |
| 6 | .1064 | 13.204 | 79.845 | .00637525 | -.49274 |
| 7 | .1086 | 26.751 | 74.524 | .00555389 | -.41966 |
| 8 | .1060 | 40.078 | 72.334 | .00523226 | -.68157 |
| 9 | .0912 | 44.238 | 71.508 | .00511334 | -.60784 |
| 10 | .1008 | 47.438 | 69.897 | .00488562 | -.63041 |
| TOTAL | 1.0000 | 3.196 | 84.684 | .00717143 | -.32918 |

(Continued)

(Sheet 5 of 6)

225

Table 7 (Concluded)

DIMENSIONLESS TIME = 1.00000

SPATIAL PARTICLE COUNT MAP:

FIL

| 1 | 1 | 2 | 8 | 16 | 37 | 35 | 42 | 54 | 33 | 38 | 54 | 48 | 32 | 17 | 7 | 7 | 4 | 0 |
| 2 | 0 | 6 | 3 | 22 | 32 | 36 | 44 | 48 | 60 | 56 | 52 | 38 | 43 | 37 | 21 | 8 | 1 | 0 |
| 3 | 0 | 2 | 9 | 15 | 25 | 35 | 32 | 44 | 48 | 43 | 57 | 46 | 30 | 30 | 18 | 11 | 3 | 1 |
| 4 | 1 | 4 | 7 | 10 | 36 | 55 | 34 | 44 | 43 | 50 | 54 | 49 | 52 | 45 | 26 | 16 | 2 | 1 |
| 5 | 1 | 1 | 7 | 18 | 35 | 30 | 27 | 45 | 42 | 64 | 65 | 52 | 39 | 37 | 36 | 15 | 3 | 4 |
| 6 | 1 | 0 | 9 | 9 | 24 | 35 | 33 | 47 | 43 | 47 | 72 | 58 | 53 | 43 | 44 | 21 | 5 | 3 |
| 7 | 0 | 1 | 6 | 12 | 19 | 22 | 30 | 44 | 48 | 66 | 67 | 53 | 47 | 37 | 32 | 20 | 5 | 4 |
| 8 | 0 | 0 | 6 | 10 | 26 | 26 | 23 | 43 | 45 | 64 | 63 | 48 | 56 | 53 | 43 | 18 | 7 | 1 |
| 9 | 0 | 2 | 0 | 6 | 14 | 18 | 23 | 33 | 45 | 40 | 76 | 44 | 52 | 56 | 42 | 17 | 9 | 3 |
| 10 | 0 | 0 | 3 | 7 | 10 | 20 | 26 | 36 | 36 | 46 | 62 | 61 | 63 | 51 | 41 | 18 | 5 | 2 |

DIMENSIONLESS DISTANCE * 1000
  -450-400-350-300-250-200-150-100 -50  -0  50 100 150 200 250 300 350 400

LATERALLY INTEGRATED PARTICLE COUNT:
   4  18  58 125 258 312 314 438 443 514 622 497 467 406 310 151  44  19

MOMENTS:

| FILAMENT | RELATIVE COUNT | CENTROID * 1000 | STD DEV * 1000 | VARIANCE | SKEW COEF |
|---|---|---|---|---|---|
| 1 | .0870 | -40.014 | 158.550 | .02513801 | .04991 |
| 2 | .1014 | -22.574 | 159.916 | .02557327 | -.07596 |
| 3 | .0898 | -14.716 | 163.256 | .02665248 | -.04416 |
| 4 | .1058 | -4.545 | 169.373 | .02868709 | -.12096 |
| 5 | .1042 | 7.321 | 169.602 | .02876467 | -.15297 |
| 6 | .1094 | 27.032 | 167.462 | .02804337 | -.22953 |
| 7 | .1026 | 26.415 | 159.209 | .02534758 | -.18489 |
| 8 | .1064 | 35.039 | 161.899 | .02621134 | -.26150 |
| 9 | .0960 | 59.015 | 154.106 | .02374880 | -.30690 |
| 10 | .0974 | 57.547 | 150.137 | .02254111 | -.37163 |
| TOTAL | 1.0000 | 13.856 | 164.633 | .02710404 | -.17756 |

## Table 8

### Random Walk Simulation for a Centerline Source

DIMENSIONLESS TIME = .00167

SPATIAL PARTICLE COUNT MAP: DELTA X FOR COUNTING = .0002

FIL*

| | |
|---|---|
| 1 | 0 |
| 2 | 0 |
| 3 | 0 |
| 4 | 0 |
| 5 | 0 |
| 6 | 0 |
| 7 | 0 |
| 8 | 569 |
| 9 | 1664 |
| 10 | 2767 |

DIMENSIONLESS DISTANCE * 10000
    8

LATERALLY INTEGRATED PARTICLE COUNT:
    5000

MOMENTS:

| FILAMENT | RELATIVE COUNT | CENTROID * 1000 | STD DEV * 1000 | VARIANCE | SKEW COEF |
|---|---|---|---|---|---|
| 1 | 0 | 0 | 0 | 0 | 0 |
| 2 | 0 | 0 | 0 | 0 | 0 |
| 3 | 0 | 0 | 0 | 0 | 0 |
| 4 | 0 | 0 | 0 | 0 | 0 |
| 5 | 0 | 0 | 0 | 0 | 0 |
| 6 | 0 | 0 | 0 | 0 | 0 |
| 7 | 0 | 0 | 0 | 0 | 0 |
| 8 | .1138 | .750 | 0 | 0 | 0 |
| 9 | .3328 | .750 | .000 | .00000000 | .00000 |
| 10 | .5534 | .750 | .000 | .00000000 | .00000 |
| TOTAL | 1.0000 | .750 | .000 | .00000000 | .00000 |

(Continued)

---

* Filament 1 is next to the channel boundary. Filament 10 is next to the centerline.

(Sheet 1 of 7)

227

Table 8 (Continued)

DIMENSIONLESS TIME = .00500

SPATIAL PARTICLE COUNT MAP:  DELTA X FOR COUNTING = .0002

FIL

| | | | | |
|---|---|---|---|---|
| 1 | 0 | 0 | 0 | 0 |
| 2 | 0 | 0 | 0 | 0 |
| 3 | 0 | 0 | 0 | 0 |
| 4 | 2 | 0 | 0 | 0 |
| 5 | 15 | 36 | 0 | 0 |
| 6 | 8 | 58 | 139 | 0 |
| 7 | 6 | 54 | 58 | 252 |
| 8 | 0 | 7 | 172 | 733 |
| 9 | 0 | 0 | 511 | 463 |
| 10 | 0 | 0 | 131 | 833 |

DIMENSIONLESS DISTANCE * 10000
         16  18  20  22

LATERALLY INTEGRATED PARTICLE COUNT:
         31 155 533 4281

MOMENTS:

| FILAMENT | RELATIVE COUNT | CENTROID * 1000 | STD DEV * 1000 | VARIANCE | SKEW COEF |
|---|---|---|---|---|---|
| 1 | 0 | 0 | 0 | 0 | 0 |
| 2 | 0 | 0 | 0 | 0 | 0 |
| 3 | 0 | 0 | 0 | 0 | 0 |
| 4 | .0004 | 1.583 | 0 | 0 | 0 |
| 5 | .0102 | 1.783 | .107 | .00000001 | -.71485 |
| 6 | .0410 | 1.956 | .131 | .00000002 | -.90780 |
| 7 | .0940 | 2.085 | .134 | .00000002 | -1.16213 |
| 8 | .1824 | 2.178 | .093 | .00000001 | -1.60452 |
| 9 | .3028 | 2.224 | .051 | .00000000 | -2.91412 |
| 10 | .3692 | 2.242 | .025 | .00000000 | -4.66705 |
| TOTAL | 1.0000 | 2.194 | .107 | .00000001 | -2.65604 |

(Continued)

(Sheet 2 of 7)

Table 8 (Continued)

DIMENSIONLESS TIME = .01000

SPATIAL PARTICLE COUNT MAP: DELTA X FOR COUNTING = .0002

FIL

| 1 | 1 | 0 | 1 | 1 | 0 | 0 | 1 | 0 | 1 | 0 | 0 | 0 | 0 | 0 | 0 | 0 | 0 | 0 | 0 | 0 | 0 | 0 | 0 |
| 2 | 0 | 0 | 1 | 0 | 0 | 2 | 2 | 4 | 0 | 2 | 1 | 1 | 3 | 0 | 0 | 0 | 0 | 0 | 0 | 0 | 0 | 0 | 0 |
| 3 | 0 | 0 | 1 | 0 | 3 | 1 | 3 | 2 | 0 | 4 | 4 | 2 | 8 | 7 | 8 | 2 | 1 | 0 | 0 | 0 | 0 | 0 | 0 |
| 4 | 0 | 0 | 0 | 1 | 1 | 1 | 1 | 4 | 4 | 4 | 10 | 4 | 17 | 12 | 8 | 13 | 11 | 9 | 4 | 0 | 0 | 0 | 0 |
| 5 | 0 | 1 | 0 | 0 | 0 | 0 | 0 | 0 | 0 | 1 | 0 | 7 | 6 | 14 | 9 | 25 | 28 | 31 | 36 | 28 | 41 | 6 | 0 |
| 6 | 0 | 0 | 0 | 0 | 0 | 0 | 0 | 1 | 0 | 1 | 1 | 3 | 0 | 9 | 11 | 26 | 37 | 33 | 53 | 72 | 79 | 90 | 22 | 0 |
| 7 | 0 | 0 | 0 | 0 | 0 | 0 | 0 | 1 | 0 | 0 | 0 | 2 | 1 | 3 | 3 | 13 | 14 | 22 | 51 | 70 | 118 | 168 | 181 | 0 |
| 8 | 0 | 0 | 0 | 0 | 0 | 0 | 0 | 0 | 0 | 0 | 0 | 0 | 0 | 0 | 0 | 2 | 8 | 12 | 11 | 27 | 65 | 88 | 202 | 349 | 158 |
| 9 | 0 | 0 | 0 | 0 | 0 | 0 | 0 | 0 | 0 | 0 | 0 | 0 | 0 | 0 | 0 | 0 | 3 | 4 | 6 | 17 | 23 | 57 | 154 | 508 | 457 |
| 10 | 0 | 0 | 0 | 0 | 0 | 0 | 0 | 0 | 0 | 0 | 0 | 0 | 0 | 0 | 0 | 0 | 2 | 3 | 8 | 10 | 33 | 115 | 471 | 718 |

DIMENSIONLESS DISTANCE * 10000

2  4  6  8  10  12  14  16  18  20  22  24  26  28  30  32  34  36  38  40  42  44  46

LATERALLY INTEGRATED PARTICLE COUNT:

1  1  3  2  4  4  9  10  7  11  27  14  54  44  91  112  118  201  272  416  735 1531 1333

MOMENTS:

| FILAMENT | RELATIVE COUNT | CENTROID * 1000 | STD DEV * 1000 | VARIANCE | SKEW COEF |
|---|---|---|---|---|---|
| 1 | .0010 | .958 | .577 | .00000033 | .29995 |
| 2 | .0032 | 1.810 | .570 | .00000032 | -.04849 |
| 3 | .0092 | 2.344 | .684 | .00000047 | -.82813 |
| 4 | .0208 | 2.742 | .647 | .00000042 | -.63232 |
| 5 | .0466 | 3.380 | .550 | .00000030 | -1.16171 |
| 6 | .0876 | 3.719 | .488 | .00000024 | -1.06397 |
| 7 | .1294 | 4.035 | .410 | .00000017 | -1.70012 |
| 8 | .1844 | 4.236 | .309 | .00000010 | -1.83458 |
| 9 | .2458 | 4.371 | .213 | .00000005 | -2.86795 |
| 10 | .2720 | 4.425 | .150 | .00000002 | -3.65021 |
| TOTAL | 1.0000 | 4.150 | .533 | .00000028 | -2.55350 |

(Continued)

Table 8 (Continued)

```
DIMENSIONLESS TIME = .02500

SPATIAL PARTICLE COUNT MAP:  DELTA X FOR COUNTING = .0010

FIL
```

| FIL | | | | | | | | | | | | | | | | | | | | | | | |
|---|---|---|---|---|---|---|---|---|---|---|---|---|---|---|---|---|---|---|---|---|---|---|
| 1 | 1 | 2 | 0 | 7 | 1 | 3 | 7 | 7 | 11 | 14 | 8 | 16 | 18 | 9 | 12 | 12 | 8 | 9 | 2 | 1 | 0 | 0 | 0 |
| 2 | 0 | 0 | 3 | 2 | 2 | 2 | 4 | 5 | 10 | 13 | 6 | 12 | 13 | 17 | 14 | 17 | 15 | 17 | 14 | 11 | 5 | 0 | 0 |
| 3 | 0 | 0 | 1 | 0 | 3 | 2 | 4 | 0 | 3 | 3 | 13 | 14 | 9 | 17 | 12 | 22 | 18 | 26 | 28 | 26 | 16 | 6 | 0 |
| 4 | 0 | 0 | 1 | 0 | 0 | 2 | 1 | 4 | 3 | 5 | 6 | 8 | 11 | 15 | 10 | 24 | 24 | 33 | 49 | 52 | 44 | 33 | 1 |
| 5 | 0 | 0 | 1 | 0 | 0 | 0 | 2 | 1 | 2 | 3 | 3 | 4 | 4 | 10 | 14 | 21 | 22 | 40 | 54 | 63 | 97 | 62 | 17 |
| 6 | 0 | 0 | 0 | 0 | 0 | 0 | 0 | 0 | 2 | 0 | 1 | 1 | 5 | 3 | 7 | 17 | 25 | 35 | 47 | 90 | 119 | 145 | 84 |
| 7 | 0 | 0 | 0 | 0 | 0 | 0 | 0 | 2 | 0 | 1 | 1 | 2 | 2 | 5 | 3 | 7 | 11 | 25 | 33 | 68 | 107 | 177 | 198 |
| 8 | 0 | 0 | 0 | 0 | 0 | 0 | 0 | 0 | 0 | 0 | 0 | 0 | 0 | 2 | 2 | 6 | 5 | 12 | 36 | 54 | 113 | 184 | 333 |
| 9 | 0 | 0 | 0 | 0 | 0 | 0 | 0 | 0 | 0 | 1 | 1 | 0 | 1 | 0 | 0 | 2 | 1 | 10 | 13 | 35 | 75 | 201 | 474 |
| 10 | 0 | 0 | 0 | 0 | 0 | 0 | 0 | 0 | 0 | 0 | 0 | 0 | 0 | 0 | 0 | 1 | 4 | 3 | 7 | 23 | 63 | 217 | 599 |

```
DIMENSIONLESS DISTANCE * 1000
   -11 -10 -9  -8  -7  -6  -5  -4  -3  -2  -1   0   1   2   3   4   5   6   7   8   9  10  11

LATERALLY INTEGRATED PARTICLE COUNT:
     1   2   6   5   6   9  18  19  31  40  39  57  63  79  74 129 133 210 293 423 639 1025 1706
```

MOMENTS:

| FILAMENT | RELATIVE COUNT | CENTROID * 1000 | STD DEV * 1000 | VARIANCE | SKEW COEF |
|---|---|---|---|---|---|
| 1 | .0296 | -.053 | 3.971 | .00001577 | -.37334 |
| 2 | .0364 | 2.188 | 4.212 | .00001774 | -.50222 |
| 3 | .0446 | 4.175 | 3.890 | .00001513 | -.87441 |
| 4 | .0652 | 5.890 | 3.535 | .00001250 | -1.25756 |
| 5 | .0840 | 7.194 | 2.962 | .00000878 | -1.72342 |
| 6 | .1162 | 8.471 | 2.183 | .00000477 | -1.59194 |
| 7 | .1284 | 9.204 | 2.085 | .00000435 | -2.40003 |
| 8 | .1494 | 9.816 | 1.511 | .00000228 | -1.91870 |
| 9 | .1628 | 10.278 | 1.275 | .00000163 | -3.61440 |
| 10 | .1834 | 10.493 | .919 | .00000085 | -2.49309 |
| TOTAL | 1.0000 | 8.483 | 3.437 | .00001181 | -2.11044 |

(Continued)

# Table 8 (Continued)

DIMENSIONLESS TIME = .05000

SPATIAL PARTICLE COUNT MAP:  DELTA X FOR COUNTING = .0020

FIL

```
 1    2  4  1  4  3  12  8  11  12  12  23  18  23  23  26  23  32  25  18  14  25  16   6    3    0    0
 2    0  1  3  4  4   7  7  11   8  17  13  19  15  16  25  18  25  31  26  19  36  16  24   11    6    0
 3    1  0  1  2  5   6  5   6   9   9   9  15  11  19  15  25  21  22  35  33  36  32  34   26   13    0
 4    0  0  1  0  0   3  3   6   4   8   7  17  12  14  18  20  21  31  19  29  29  41  50   54   29    2
 5    0  0  0  0  2   5  4   2   3   5   9   9   6  11  12  15  27  25  24  32  37  45  61   76   65    9
 6    0  0  0  0  0   0  0   0   0   3   4   9   7   7  10  10  17   5  25  20  22  43  49   80  111  116  39
 7    0  0  0  0  0   0  1   1   2   2   2   6   5   6   5  17  17  16  14  29  15  49  72   88  134   69
 8    0  0  0  0  0   0  0   0   0   2   0   1   4   5  10   6   8   8  22  15  30  55  59   98  171  130
 9    0  0  0  0  0   1  0   2   0   0   0   1   2   6   3   9   4   5   8  16  25  32  54  109  144  193
10    0  0  0  0  0   0  0   0   0   0   1   2   3   1   1   4   8   5   8  13  24  34  32  102  204  195
```

DIMENSIONLESS DISTANCE * 1000
```
-28 -26 -24 -22 -20 -18 -16 -14 -12 -10 -8 -6 -4 -2  0  2  4  6  8  10  12  14  16  18  20  22
```

LATERALLY INTEGRATED PARTICLE COUNT:
```
 3  5  6  10  14  34  28  39  41  59  73  95  88  111  125  154  168  193  194  222  300  369  472  678  882  637
```

MOMENTS:

| FILAMENT | RELATIVE COUNT | CENTROID * 1000 | STD DEV * 1000 | VARIANCE | SKEW COEF |
|---|---|---|---|---|---|
| 1 | .0688 | -.638 | 10.001 | .00010002 | -.41050 |
| 2 | .0724 | 2.268 | 10.476 | .00010976 | -.48925 |
| 3 | .0780 | 5.494 | 10.251 | .00010509 | -.78822 |
| 4 | .0836 | 8.375 | 9.459 | .00008947 | -.81956 |
| 5 | .0968 | 10.821 | 9.033 | .00008160 | -1.23275 |
| 6 | .1154 | 13.874 | 7.495 | .00005617 | -1.46834 |
| 7 | .1100 | 14.950 | 7.129 | .00005082 | -1.62623 |
| 8 | .1248 | 16.768 | 5.746 | .00003302 | -1.81284 |
| 9 | .1228 | 17.710 | 5.552 | .00003082 | -2.53915 |
| 10 | .1274 | 18.347 | 4.700 | .00002209 | -2.45258 |
| TOTAL | 1.0000 | 12.147 | 9.843 | .00009639 | -1.30678 |

(Continued)

(Sheet 5 of 7)

Table 8 (Continued)

DIMENSIONLESS TIME = .10000

SPATIAL PARTICLE COUNT MAP:  DELTA X FOR COUNTING = .0050

FIL

| 1 | 0 | 0 | 4 | 9 | 8 | 7 | 14 | 21 | 28 | 28 | 29 | 31 | 39 | 40 | 34 | 46 | 39 | 37 | 17 | 8 | 0 | 0 |
|---|---|---|---|---|---|---|---|---|---|---|---|---|---|---|---|---|---|---|---|---|---|---|
| 2 | 0 | 0 | 5 | 3 | 11 | 13 | 14 | 11 | 18 | 29 | 33 | 37 | 43 | 48 | 39 | 42 | 35 | 30 | 33 | 14 | 1 | 0 |
| 3 | 1 | 0 | 2 | 2 | 5 | 7 | 8 | 15 | 11 | 23 | 37 | 32 | 30 | 34 | 43 | 33 | 48 | 48 | 42 | 24 | 8 | 0 |
| 4 | 0 | 0 | 3 | 5 | 2 | 7 | 6 | 8 | 16 | 22 | 33 | 33 | 34 | 41 | 46 | 49 | 47 | 31 | 47 | 40 | 21 | 0 |
| 5 | 0 | 0 | 3 | 1 | 3 | 0 | 7 | 6 | 14 | 22 | 25 | 32 | 37 | 36 | 39 | 47 | 58 | 58 | 62 | 66 | 34 | 3 |
| 6 | 0 | 0 | 0 | 0 | 5 | 7 | 8 | 8 | 11 | 11 | 17 | 23 | 31 | 25 | 43 | 33 | 44 | 51 | 43 | 81 | 57 | 8 |
| 7 | 0 | 0 | 0 | 0 | 1 | 3 | 2 | 6 | 11 | 10 | 14 | 23 | 33 | 38 | 36 | 46 | 45 | 45 | 63 | 110 | 73 | 7 |
| 8 | 0 | 0 | 0 | 0 | 0 | 0 | 2 | 6 | 4 | 17 | 12 | 20 | 10 | 30 | 27 | 50 | 52 | 57 | 72 | 88 | 98 | 11 |
| 9 | 0 | 0 | 0 | 0 | 0 | 0 | 0 | 2 | 7 | 9 | 8 | 26 | 12 | 26 | 26 | 29 | 49 | 41 | 52 | 105 | 82 | 18 |
| 10 | 0 | 0 | 0 | 0 | 0 | 0 | 0 | 1 | 5 | 2 | 5 | 13 | 16 | 25 | 12 | 45 | 52 | 40 | 61 | 80 | 111 | 17 |

DIMENSIONLESS DISTANCE * 1000
-60 -55 -50 -45 -40 -35 -30 -25 -20 -15 -10 -5 -0 5 10 15 20 25 30 35 40 45

LATERALLY INTEGRATED PARTICLE COUNT:
1 0 17 20 35 44 61 84 125 173 213 270 285 343 345 420 469 438 492 616 485 64

MOMENTS:

| FILAMENT | RELATIVE COUNT | CENTROID * 1000 | STD DEV * 1000 | VARIANCE | SKEW COEF |
|---|---|---|---|---|---|
| 1 | .0878 | .404 | 19.933 | .00039733 | -.44675 |
| 2 | .0918 | 2.039 | 19.964 | .00039856 | -.43876 |
| 3 | .0906 | 7.070 | 19.863 | .00039456 | -.54944 |
| 4 | .0982 | 9.298 | 19.774 | .00039101 | -.57410 |
| 5 | .1106 | 14.174 | 18.880 | .00035644 | -.70713 |
| 6 | .1012 | 16.690 | 19.992 | .00039970 | -.80422 |
| 7 | .1132 | 19.881 | 17.726 | .00031421 | -.82411 |
| 8 | .1112 | 22.535 | 16.586 | .00027510 | -.93367 |
| 9 | .0984 | 23.559 | 16.340 | .00026699 | -.93149 |
| 10 | .0970 | 25.916 | 14.581 | .00021260 | -.97480 |
| TOTAL | 1.0000 | 14.621 | 20.238 | .00040956 | -.71851 |

(Continued)

Table 8 (Concluded)

DIMENSIONLESS TIME = .20000

SPATIAL PARTICLE COUNT MAP:  DELTA X FOR COUNTING = .0100

FIL

| 1 | 0 | 3 | 9 | 11 | 25 | 39 | 33 | 53 | 50 | 55 | 57 | 34 | 27 | 23 | 15 | 6 | 1 |
| 2 | 0 | 2 | 8 | 20 | 27 | 31 | 41 | 47 | 56 | 40 | 49 | 48 | 53 | 34 | 19 | 8 | 3 |
| 3 | 2 | 4 | 6 | 15 | 27 | 24 | 34 | 43 | 59 | 51 | 44 | 43 | 45 | 35 | 20 | 9 | 4 |
| 4 | 2 | 4 | 6 | 12 | 19 | 33 | 29 | 42 | 68 | 53 | 61 | 59 | 46 | 48 | 27 | 21 | 3 |
| 5 | 0 | 6 | 11 | 13 | 27 | 25 | 25 | 49 | 53 | 45 | 48 | 68 | 59 | 55 | 26 | 17 | 4 |
| 6 | 0 | 10 | 7 | 6 | 15 | 23 | 17 | 50 | 68 | 42 | 47 | 83 | 54 | 58 | 35 | 26 | 10 |
| 7 | 1 | 4 | 3 | 10 | 16 | 17 | 19 | 51 | 56 | 33 | 40 | 72 | 64 | 59 | 42 | 26 | 13 |
| 8 | 0 | 3 | 3 | 5 | 5 | 13 | 23 | 42 | 57 | 35 | 34 | 74 | 48 | 62 | 45 | 33 | 18 |
| 9 | 0 | 3 | 7 | 9 | 10 | 7 | 14 | 46 | 40 | 43 | 45 | 61 | 55 | 58 | 46 | 30 | 10 |
| 10 | 0 | 1 | 5 | 2 | 13 | 13 | 11 | 44 | 46 | 34 | 31 | 47 | 64 | 91 | 38 | 30 | 13 |

DIMENSIONLESS DISTANCE * 1000
    -80 -70 -60 -50 -40 -30 -20 -10 -0 10 20 30 40 50 60 70 80

LATERALLY INTEGRATED PARTICLE COUNT:
    5  40  65 103 184 225 246 467 553 431 456 589 515 523 313 206  79

MOMENTS:

| FILAMENT | RELATIVE COUNT | CENTROID * 1000 | STD DEV * 1000 | VARIANCE | SKEW COEF |
|---|---|---|---|---|---|
| 1 | .0882 | 3.854 | 30.438 | .00092649 | -.00851 |
| 2 | .0972 | 7.756 | 32.216 | .00103787 | -.11164 |
| 3 | .0930 | 8.566 | 32.678 | .00106783 | -.17858 |
| 4 | .1066 | 12.867 | 32.697 | .00106908 | -.27423 |
| 5 | .1062 | 13.375 | 33.654 | .00113260 | -.40416 |
| 6 | .1102 | 18.292 | 32.949 | .00108566 | -.45497 |
| 7 | .1052 | 21.119 | 32.847 | .00107892 | -.47052 |
| 8 | .1000 | 25.297 | 31.478 | .00099086 | -.41585 |
| 9 | .0968 | 23.915 | 32.161 | .00103436 | -.58611 |
| 10 | .0966 | 26.764 | 31.480 | .00099099 | -.59135 |
| TOTAL | 1.0000 | 16.350 | 33.164 | .00109988 | -.33418 |

that velocity nor any particle that stays on the streamline with the minimum velocity.

The temporal distributions would be somewhat like the reverse of the spatial distributions. For a given cross section (given $x_r$), the cloud would arrive first in the center of the channel where the velocities are the highest and would arrive later at the sides. Farther downstream as the concentration distributions become more nearly uniform, the percentage difference between the time of first arrival at the center and at the edges would decrease. Also, since the longitudinal spreading process continues as the cloud passes a cross section, the temporal distributions are generally longer and more highly skewed than the corresponding spatial distributions when compared in terms of the dimensionless variables.

The behavior of the transport for a centerline source (Table 8) using the random walk simulation is naturally similar to the results seen from the numerical solution in the previous section. The mass is originally in a small region and is not exposed to significant differential advection due to the transverse distribution of velocity so that the cloud length does not increase very rapidly at first (if the effects of the vertical distribution of velocity as represented by $e_x$ are not included as in the calculations). However, as transverse mixing increases the width of the cloud, differential advection begins to increase its length also. Ultimately, transverse mixing causes the concentration distributions to approach (but never totally accomplish) transverse uniformity. For each time, the length of the distributions (as represented for example by the standard deviation) is smaller for the centerline source than for the plane source because of the smaller amount of differential advection in the early part of the process when the cloud width is small. Again, the general behavior of the temporal distributions could be deduced from thinking of the spatial distributions being measured as they are advected past the specified cross sections and accounting for the continued longitudinal spreading as the distributions pass.

234

## 6.2.4  Temporary Storage

The rate of longitudinal displacement of a solute being trans-
ported by flowing water can be viewed as being the flow rate divided by
the storage capacity per unit length of the channel.  For a simple
channel, the storage capacity is just the volume of the channel so that
the storage capacity per unit length is the channel area and the rate
of displacement is the discharge divided by the area, i.e. the flow
velocity.  However, if a channel has storage capacity in addition to
the cross-sectional area where the flow is taking place, the displace-
ment rate for the transported substance is slower than would be indi-
cated by measurement of the flow velocities in the channel (and there
are also other possible changes in the transport process, as discussed
in Section 6.2.5f).  The additional storage can be in any region of
water which does not have continuous downstream flow, e.g., the wake
regions behind sand dunes or behind cobbles in mountain streams, "dead
water" regions caused by debris or vegetation along the banks, separa-
tion zones on the inside of sharp bends, or the regions between groins
(jetties) or other bank protection structures.  These types of storage
regions are variously called separation zones, dead zones, or pockets.
There can also be temporary storage in the pools of pool and riffle
streams when the pools are not totally flushed within one mean resi-
dence time (volume of pool divided by flow rate).  Another storage
mechanism is the deposition and resuspension of sediment with absorbed
substances.

Naturally, if any of these mechanisms is present in a stream,
they are there for both steady and unsteady transport situations.  How-
ever, for steady state, the storage comes to equilibrium with the con-
centration in the main flow; the storage is permanent as long as steady
conditions persist and thus has no net effect on the transport process.
On the other hand, for unsteady problems, the storage is temporary with
the solute moving into the storage region as the front part of the
cloud passes and then moving back out from storage into the main flow
as the tail of the cloud passes.  It is this temporary storage which

235

can influence not only the rate of displacement of the solute but also the variance and skewness of the solute cloud (Section 6.2.5f).

The means of including the storage mechanism in the mathematical representation of the transport process depends on the type of mechanism which is present. For example, for storage zones, some of the factors to be considered are the shape, size, and location of the storage zones, the exchange rate between the main flow and the storage zones, and the degree of mixing within the storage zones. The only situation which is considered here is the case of well-mixed storage zones which are distributed uniformly along the stream bed. It is assumed that the storage zones are not interconnected longitudinally or laterally.

In order to include the effects of the storage zones in the analysis, additional variables are needed:

$c^*$ – concentration in the storage zones. In general, $c^*$ is a function of longitudinal position $(x)$, transverse position $(y)$, and time $(t)$.

$h^*$ – depth of storage zones. In this discussion, $h^*$ is taken to be constant, but this is not a necessary assumption in general.

$A^*$ – fraction of the bed area occupied by the storage zones.

$K^*$ – mass exchange rate coefficient between the main flow and the storage zones. The mass flux per unit plan area of the storage zones is then $K^*(c - c^*)$ , with a positive flux being from the main flow into the storage zones.

The effects of the temporary storage are not included in the calculations presented in Sections 6.2.2 and 6.2.3, but they are included in some of the results in the next section.

6.2.5 Temporal Moments Analysis

a. General comments. As is mentioned in Section 6.1.2, much information about unsteady transport problems can be obtained from just the moments of the concentration distributions without knowing the concentrations themselves. Aris (1956) introduced the concept of analyzing certain aspects of the transport by converting the

236

differential mass-balance equation into an equation for the spatial moments of the concentration distribution ( c  versus  x  at a given time). One advantage of the moments approach is that the 2D moment equations for unsteady situations have one less independent variable and thus can be solved more easily than the 2D mass balance equation for the concentration while all of the transport mechanisms are retained in the analysis. Sayre (1969; 1975), among others, used Aris' type of analysis extensively. A disadvantage of Aris' analysis is that it is for the moments of the spatial distributions (i.e.,  c  versus  x  for given transverse coordinates and given times), while most measurements are temporal distributions (i.e.,  c  versus  t  at given longitudinal  x and transverse  y  positions). Thus, Holley and Tsai (1978) and Tsai and Holley (1978) extended the analysis so that temporal moments could be calculated and compared directly with moments from measured concentration distributions. Another disadvantage of any moment analysis is that it gives only the moments of the concentration distributions, not the concentrations themselves. Thus, for making approximate predictions of concentrations, Tso (1982) investigated the use of similarity functions for estimating concentrations from the moments. (See Section 6.2.5g.)

　　　b. Dimensionless variables and differential equations. The same dimensionless variables given in Eq. 6.2.3 are used here since the same situation (namely a prismatic rectangular channel with a parabolic transverse distribution of velocity) is being considered. In these examples of the temporal moments analysis, the velocity distribution is exactly parabolic rather than the slightly modified distribution used in the examples in Sections 6.2.2 and 6.2.3. Also, $e_x$ is zero; these results were calculated before the importance of longitudinal mixing associated with the vertical velocity distribution was recognized. If $e_x$ were to be included, the character of the differential equations for the moments and the method for solving the equations would change.

237

Following the work of Holley and Tsai (1978) and Tsai and Holley (1978, 1979), the additional dimensionless variables for the moment calculations are defined as

$$c_r = \frac{B^3 HVc}{Me_y}$$

$$c_r^* = \frac{B^3 HVc^*}{Me_y}$$

(6.2.7)

$$\lambda = \frac{h^*}{H} A^*$$

$$\theta = \frac{B^2/e_y}{h^*/K^*} = \frac{B^2 K^*}{e_y h^*}$$

The mass of substance released at $x = 0$ and $t = 0$ is $M$. The parameter $\lambda$ is the ratio of the volume of storage zones to volume of main flow per unit length of channel. The parameter $\theta$ is the ratio of a characteristic time for cross-sectional mixing $(B^2/e_y)$ to a characteristic time for mass exchange with the storage zones $(h^*/K^*)$. The individual parameters $\lambda$ and $\theta$ have physical interpretations as given, but in the analysis of the various moments, $\lambda$ and $\theta$ occur in specific combinations that are given the symbol $\Omega$ where

$$\Omega_1 = (1 + \lambda) \theta$$

$$\Omega_2 = (1 + \lambda)^2 \theta_1 = \Omega_1 \frac{(1 + \lambda)}{\lambda}$$

(6.2.8)

$$\Omega_3 = \frac{(1 + \lambda)^3 \theta^2}{\lambda} = \Omega_1 \Omega_2$$

While $\Omega_1$ and $\Omega_2$ are independent parameters that can replace $\lambda$ and $\theta$ in the analysis, $\Omega_3$ is just a convenient combination of the other

238

two parameters. For most natural channels, $\theta > 1$ and $\lambda < 1$ so that $\Omega_1 < \Omega_2 < \Omega_3$ (Holley and Tsai 1978).

The differential mass balance equations for the main flow and the storage zones may now be written in dimensionless form as

$$\frac{\partial c_r}{\partial t_r} + v_r \frac{\partial c_r}{\partial x_r} = \frac{\partial^2 c_r}{\partial y_r^2} + \theta\lambda(c_r^* - c_r)$$

$$(6.2.9)$$

$$\frac{\partial c_r^*}{\partial t_r} = -\theta(c_r^* - c_r)$$

The last term in each expression accounts for the mass transfer between the main flow and the storage zones. In writing Eq. 6.2.9, it is assumed that $K^*$ , $e_y$ , $h$ , and $h^*$ are constant and that $e_x = 0$ .

c. Differential moment equations. The situation considered here is transport in rectangular channels with constant depth storage zones, as described above. Similar results for other cross-sectional shapes are given by Tsai and Holley (1979). Although the major aspects of analysis by the use of moments can be seen by considering rectangular channels, there were some unexpected differences which appeared in the results for other shapes. A similar type of analysis has also been done for meandering channels by applying the moment analysis to the streamtube equations with $e_x \neq 0$ (Bird and Holley 1985). For rectangular channels, the equations for both the spatial and the temporal moments are presented, but most of the calculated results are for temporal moments since temporal distributions are normally the ones that are measured.

The p-th spatial moment of a $c_r$ versus $x_r$ distribution along any $y_r$ and at any $t_r$ in the main flow is defined as

$$\mu_p = \int_{-\infty}^{\infty} c_r x_r^p dx_r$$

$$(6.2.10)$$

239

A similar expression defines $\mu_p^*$ as the p-th spatial moment of $c_r^*$ for the concentration in the storage zones. The differential equations for the dimensionless spatial moments are obtained by multiplying Eq. 6.2.9 by $x_r^p$ and integrating with respect to $x_r$ from $-\infty$ to $\infty$ (Tsai and Holley 1978, 1979) to obtain

$$\frac{\partial \mu_p}{\partial t_r} = \frac{\partial^2 \mu_p}{\partial y_r^2} + p v_r \mu_{p-1}$$

$$\frac{\partial \mu_p^*}{\partial t_r} = - \theta(\mu_p^* - \mu_p)$$

(6.2.11)

When Eq. 6.2.11 is applied for $p = 0$, $\mu_{-1}$ is defined as being zero.

The p-th temporal moment of a $c_r$ versus $t_r$ distribution for any $x_r$ and $y_r$ is defined as

$$\nu_p = \int_0^\infty c_r t_r^p dt_r$$

(6.2.12)

A similar expression defines $\nu_p^*$ as the p-th temporal moment of $c_r^*$ for the concentration in the storage zones. The differential equations for the dimensionless temporal moments are obtained by multiplying Eqs. 6.2.9 by $t_r^p$ and integrating with respect to $t_r$ from 0 to $\infty$ so that the p-th temporal moments for the main flow and storage zones are given by

$$v_r \frac{\partial v_0}{\partial x_r} = \frac{\partial^2 v_0}{\partial y_r^2}$$

$$v_r \frac{\partial v_p}{\partial x_r} = \frac{\partial^2 v_p}{\partial y_r^2} + p v_{p-1} + \lambda\theta(v_p^* - v_p) \quad \text{for} \quad p > 0 \qquad (6.2.13)$$

$$v_p^* = v_p + p \frac{v_{p-1}}{\theta}$$

As with the spatial moments, the -1 moments are defined as being zero.

In order to obtain these forms of the equations, some integration by parts has to be done. In general, the equations must be integrated numerically to obtain the moments, with the solutions for the moments being obtained recursively beginning with the zeroth moments. Also, some additional considerations, which are not presented here, are needed in the derivation of Eqs. 6.2.13. These considerations, as well as the initial conditions to be used for the numerical integration, were discussed by Tsai and Holley (1978, 1979).

d. Calculated spatial moments. Since measured concentrations are normally in terms of temporal rather than spatial distributions and since some characteristics of spatial distributions are presented in Sections 6.2.2 and 6.2.3, no further results for spatial distributions are given here. Moments for spatial distributions have been presented by Aris (1956) and Tsai and Holley (1978, 1979) for flows with no storage zones, by Valentine and Wood (1977) for flows with storage zones, and by Sayre (1969, 1975) for different types of storage mechanisms. Tsai and Holley (1978, 1979, 1980) discussed the relationships between spatial and temporal moments.

e. Calculated temporal moments with no temporary storage. Eq. 6.2.13 was solved for a rectangular channel with a parabolic velocity distribution and with no storage zones for a plane source across the full width of the channel (Figure 49) and for a point source on the channel centerline (Figure 50). In these calculations, $y_r = 0$ was

Figure 49. Calculated temporal moments for a plane source

c. Variances

b. Centroids

a. Zeroth Moments

242
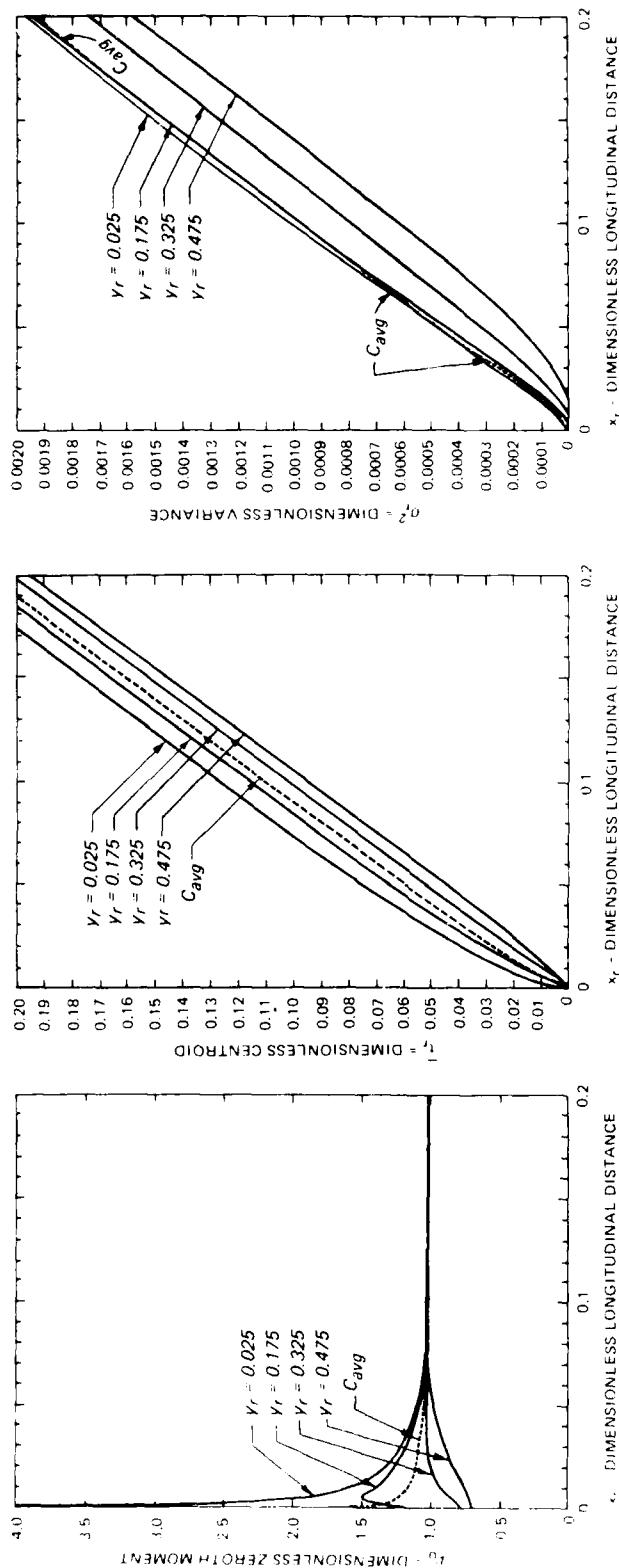
a. Zeroth Moments

b. Centroids
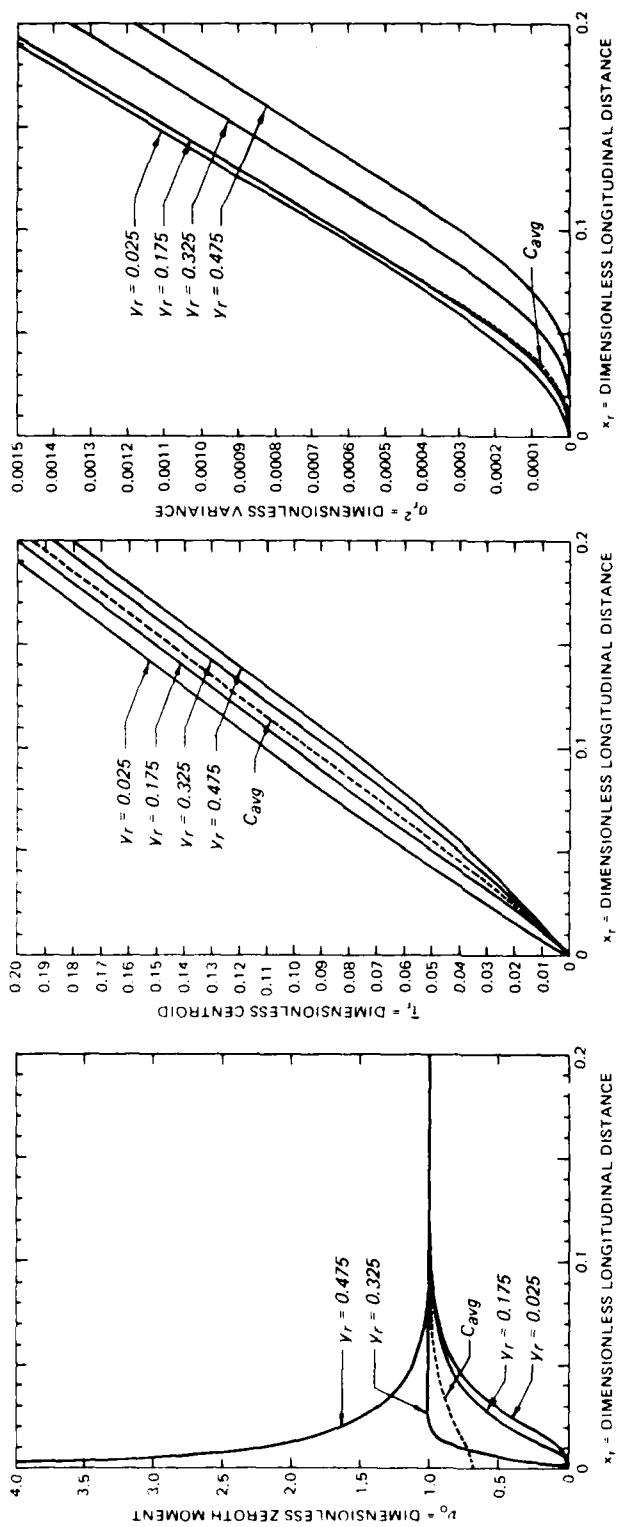
c. Variances

Figure 50. Calculated temporal moments for average concentrations in a rectangular channel

243

at the edge of the channel and $y_r = 0.5$ was at the center. The figures give the results for four transverse locations with equal intervals of 0.150 of the channel width between the locations. The results are also shown for the cross-sectionally averaged concentration ($C_{avg}$).

First consider Figure 49 for the plane source. In this case, the mass is initially distributed uniformly across the channel width. The zeroth moments are initially smaller in the central part of the channel and larger near the banks because of the velocity distribution; in the center the mass moves rapidly because of the higher velocity and thus gives smaller temporal moments, while nearer the banks, the mass moves more slowly and gives longer $c_r$ versus $t_r$ curves and thus larger temporal moments. As the mass is transported downstream, transverse mixing causes the concentrations distribution to become progressively more nearly uniform so the differences between the various transverse positions gradually disappear and for $x_r > 0.05$, the areas under the concentration curves are all within 5% of the average value. However, as can be seen from the higher moments (the centroids and the variances), the concentrations themselves are not totally uniform across the width.

The influence of the velocity distribution on the transport can also be seen in the time of occurrence of the centroids. For all $x_r$, $\bar{t}_r$ is smaller in the central part of the channel than near the banks. As $x_r$ increases, the rate of increase of $\bar{t}_r$ eventually becomes the same across all of the channel. However, the concentration distributions near the banks always lag behind those in the center of the channel. This effect is seen in the fact that $\bar{t}_r$ is always larger near the banks, even for large $x_r$. As $x_r$ continues to increase, the difference in the times of occurrence of the centroids at the center and at the banks remains constant, but this difference becomes proportionally smaller since all of the $\bar{t}_r$ values are continually increasing. The behavior of the variances is generally similar to that of the centroids with smaller variances for the concentration distributions in the central part of the channel than for the sides of the channel. Proportionately, the differences in the variances across the width of

244

the channel are larger than the differences in the centroids. Significant differences exist in the variances even in the central 20% to 30% of the channel width. Thus, in conducting longitudinal mixing tests, it can be important, as pointed out by Holley and Tsai (1978), to properly account for the streamline on which measurements are made.

Figure 50 gives the temporal moments for a centerline source. Since all of the mass is initially in the center of the channel, the zeroth moments are initially large there and zero near the banks. The zeroth moments begin to increase from zero for each $y_r$ as transverse mixing brings mass to that $y_r$ . Note that the dimensionless moment is greater than unity for many positions (e.g. for $x_r < 0.1$ in the central part of the channel). Thus, if concentrations were measured for any of these positions and taken as being the average for the cross section and then integrated with respect to time to check the mass balance, it would appear that more mass had been recovered than was released into the flow. When comparing the plane source case and the centerline case, there are marked differences in the zeroth moments and there are some differences in the development, during Fischer's initial period (Section 6.3.2), of the transverse distributions of centroids and variances. Nevertheless, the ultimate behavior and relative distribution of the centroids and variances is the same for both cases (and for any other type of initial condition which might be considered) because, as Fischer et al. (1979) showed, the ultimate, equilibrium transverse concentration distribution depends on the channel shape, the velocity distribution, and the transverse mixing, but not on the initial condition. Also, even though the changes in the concentrations can be represented by 1D analyses for $x_r$ greater than about 0.1, 1D analyses cannot properly account for the transport processes and the development of the concentration distributions within the initial period. The calculations also show that there can be significant differences between the moments for the average concentration, as would be represented in a 1D analysis, and the concentration on the center line of the channel. Recall that $x_r$ of 0.1 can correspond to very large actual distances for medium and large streams (Section 5.3.6).

245

<u>f</u>.   <u>Calculated temporal moments with temporary storage</u>.   The re-
sults of Holley and Tsai (1978) can be used to demonstrate the influ-
ence of temporary storage on the transport process.   The calculations
were for a rectangular channel with a parabolic velocity distribution,
with a plane source across the full width of the main flow, and with
uniformly distributed storage zones of constant depth on the channel
bottom.   Calculated results for other cases were given by Tsai and
Holley (1979).   For the rectangular channel, the results were given
(Figure 51) for the moments of only the cross-sectionally averaged con-
centrations with $N_0$ , $\bar{T}$ , $\bar{\sigma}^2$ , and $\bar{S}$ being the zeroth moment, cen-
troid, variance, and skewness for the averaged concentrations in the
main flow and $\bar{T}^*$ being the centroid for the average concentration in
the storage zones.   Some of the observations that are made below are
based on analytical results (Holley and Tsai 1978, Tsai and Holley
1979) as well as on the results shown in the figure.   The analytical
work was done for any shape prismatic channel with constant depth
storage zones and with the initial instantaneous upstream source being
in only the main flow.

Figure 51 shows no dependence of $N_0$ on the storage zones since
all of the mass must eventually move downstream even if some of it is
delayed temporarily by storage.   Comparison of $N_0$ in Figure 51 with
the curve in Figure 49 for the cross-sectionally averaged concentration
shows that the two curves are the same.   Consideration of the centroids
begins to reveal how the storage mechanism can influence the transport
process.   Rather than plotting the centroids themselves, Figure 51b
gives the quantity $\bar{T}/(1 + \lambda) - x_r$ .   Thus, this figure shows the dif-
ference between the time of occurrence of the centroid (after account-
ing for the slower cloud travel associated with $\lambda$) and the centroidal
time ($\bar{T} = x_r$) which would exist for a simple 1D transport problem.

If $\Omega_1$ is large (say, greater than 1000), then there is rapid
exchange between the main flow and storage zones so that the concentra-
tion distributions in the two regions move downstream in phase with
each other and with $\bar{T} = \bar{T}^*$ .   This condition is called "concentration
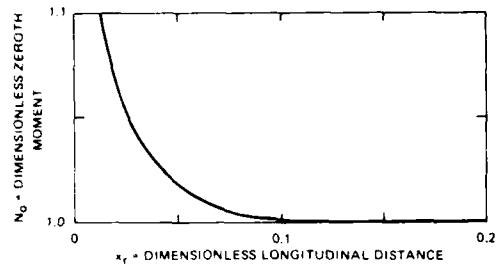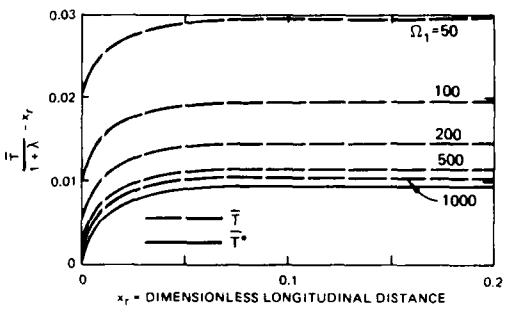
a. Zeroth moments        b. Centroidal differentials
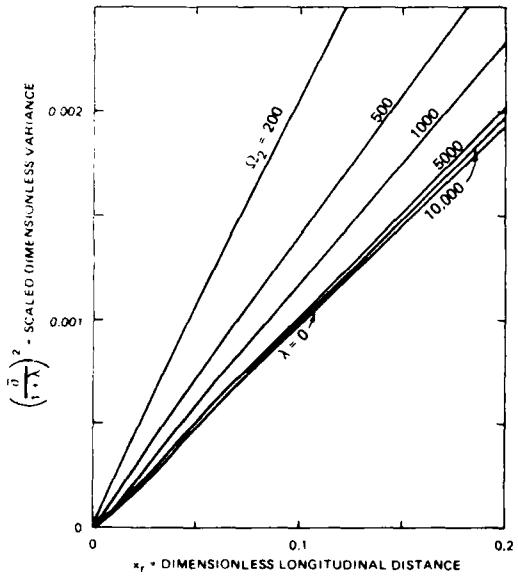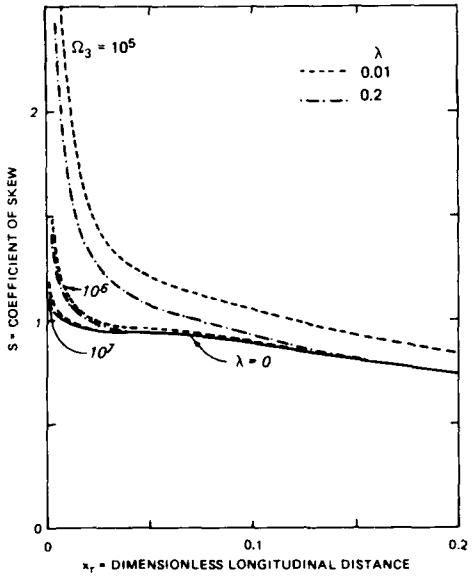
c. Variances        d. Skewness

Figure 51. Calculated effects of storage zones on temporal moments for area average concentrations in rectangular channel

equilibrium" between the main flow and storage zones. When concentration equilibrium exists, the primary effect of the storage is to slow the cloud movement relative to the flow velocity in proportion to the ratio of the total storage capacity to the storage in the main flow, i.e. in proportion to $(1 + \lambda)$. See Eq. 6.3.20. Thus, this factor has been included in the plots of the centroids (and variances) so that all of the remaining variation depends only on $\Omega_1$ (and $\Omega_2$), as shown in the figure. For $\Omega_1 < 1000$, the exchange with the storage zones is slow enough that the concentration distributions in the storage zones lag behind the downstream movement in the main flow. This lag is shown by the fact that $\bar{T}^*/(1 + \lambda) > \bar{T}/(1 + \lambda)$ for the smaller values of $\Omega_1$ in Figure 51. As the lagging mass in the storage zones mixes back into the main flow, it adds to the upstream tail of the cloud, increasing the variances and skewnesses (Figures 51c and 51d). Even for $\lambda = 0.2$, S for large $x_r$ is only slightly greater than for $\lambda = 0$ and decreases as $x_r$ increases.

The values of the $\Omega$'s and $\lambda$ for natural streams are frequently small enough that concentration equilibrium exists (Holley and Tsai 1978). While these calculations for a rectangular channel with a parabolic velocity distribution are indicative of many of the essential types of influences of storage zones, some of the details of the behavior are different for different shapes of channels and for different distributions of storage zones. Other cases were considered by Tsai and Holley (1979).

g. Estimated concentration distributions. In principle, the shape of a concentration distribution is uniquely determined if the infinite series of moments of the distribution is known. Since it is not practical to calculate all of the moments to determine concentration distributions, Tso (1982) investigated the possibility of using the first four (zeroth through third) calculated moments to estimate the concentrations. Since only four moments were used, it was necessary to make some additional assumptions; he assumed that the concentration distributions are similar, i.e., that they may be estimated from a similarity function whose area, centroid, variance, and skewness are

248

determined by the calculated moments. He investigated five similarity functions to determine which one most nearly represented the shapes of 114 concentration distributions measured in 10 tests in laboratory flumes and in 27 fields studies. The Pearson Type III (PT-III) distribution was the best of the ones that he investigated. The same similarity function had been used by previous investigators (Sayre 1975, Liu and Cheng 1978) without presenting considerations as to why it was selected. A further discussion of the general shapes of measured concentration distributions is given in Section 7.7.3c and the PT-III distribution is illustrated in Figures 72 and 82. The mathematical expression for the PT-III distribution as a concentration distribution may be stated as

$$c = \frac{n_o}{a_P \Gamma(b_P)} \left( \frac{t - g_P}{a_P} \right)^{b_P - 1} \exp \left( - \frac{t - g_P}{a_P} \right) \tag{6.2.14}$$

where

$$b_P = \left( \frac{2}{S} \right)^2$$

$$a_P = \left( \frac{\sigma^2}{b_P} \right)^{1/2} \tag{6.2.15}$$

$$g_P = \bar{t} - \left( \sigma^2 b_P \right)^{1/2}$$

with $n_o$ = the zeroth moment , $\bar{t}$ = the centroid , $\sigma^2$ = the variance , and $S$ = the skew coefficient .

## 6.2.6  Pseudo Two-Dimensional Analysis

In 2D unsteady problems, the transverse distribution of longitudinal velocity is a major part of the longitudinal spreading process, but the inclusion of this velocity distribution makes it impractical to try to obtain analytical solutions for concentration distributions and even means that it is not a trivial matter to obtain accurate numerical

249

solutions. Thus, strictly as an expedient, it has sometimes been assumed that the transport can be represented by using the cross-sectionally averaged velocity (V) for the advection and using longitudinal and transverse mixing coefficients to represent the spreading. This approach normally cannot correctly represent the transport mechanisms since transport is not one dimensional during the early part ($x_d$ < 0.2) of the process (Fischer et al., 1979). Even though a longitudinal mixing coefficient really should not be used from the standpoint of the mechanics of the transport, if one is used, it probably should be one that increases with downstream distance or flow time. (See Section 7.7.3b for 1D situations.) This type of approach should be recognized as generally being more of an approximation than the methods discussed previously. If a decision is made to assume a constant coefficient, there is no rational basis for specifying the "correct" longitudinal mixing coefficient in general terms (except perhaps for the very early part of the process when the longitudinal spreading is due to the vertical distribution of velocity, Section 6.2.2).

For a constant velocity $V$, constant area $A$, and constant mixing coefficients $E$ and $e_y$ in a rectangular channel of width $B$, the differential mass balance equation may be written as

$$\frac{\partial c}{\partial t} + V \frac{\partial c}{\partial x} = E \frac{\partial^2 c}{\partial x^2} + e_y \frac{\partial^2 c}{\partial y^2} - Kc \qquad (6.2.16)$$

where all of the reactions are combined into one first-order term. For a slug of mass $M$ released at $x = 0$, $y = a$, and $t = 0$, the concentration is given by the method of images to be

$$c = \frac{M}{4\pi\sqrt{Ee_y}} \exp(-Kt) \sum_{i=-\infty}^{\infty} \sum_{j=1}^{2} \left[ \exp - \frac{(x - Vt)^2}{4Et} \right.$$

$$\left. - \frac{(y - (-1)^j a - 2iB)^2}{4e_y t} \right] \qquad (6.2.17)$$

A modification of this expression can be used if $E$ is assumed to be a function of $x$ (Section 7.7.3b). If Eq. 6.2.17 were to be used, it probably is best to use it for estimating conditions for limiting cases where the largest and smallest reasonable mixing coefficients are assumed to determine if there are potential problems that require a more detailed analysis.

## 6.3 ONE-DIMENSIONAL SOLUTIONS

This section gives some of the solutions that have been presented in the literature for 1D conditions. However, it should be noted that some of these solutions apply only under rather restrictive conditions (Section 6.3.1) and that the 2D approaches discussed in the Section 6.2 can be used for calculations from the release point, through the 2D region, and on into the region where 1D conditions exist. Thus, if one has the capability of making the 2D calculations discussed earlier, there is really no need (other than some savings in computational time) to also have a separate capability for 1D calculations and, in general, better representation of the transport processes in free-flowing streams is obtained with 2D models.

### 6.3.1 Criteria for Existence of One-Dimensional Conditions

Basically, the criterion for using a 1D mathematical analysis is that 1D physical conditions exist, i.e. that the variation of the concentration across the width of the channel for the majority of the cloud is small compared with the average concentration at that cross section. Sayre (1968) and Fischer et al. (1979) discussed specific criteria for the existence of 1D conditions. Sayre (1968) and Tsai and Holley (1979) showed that the dimensionless flow distance required to obtain 1D conditions depends on the stream hydraulics (cross-sectional shape and velocity distribution) and the location of the initial source within the cross section. Fischer et al. (1979) recommended assuming 1D conditions only for $x_d > 0.2$ . The calculations of Tsai and Holley (1979) indicate that the critical value of $x_d$ is $0.1 \pm 0.05$ for the various conditions that they investigated. The examples in

Sections 7.5 and 7.8 include illustrations of the relationship between actual flow distances and dimensionless distances. For very small streams, the actual distance may be only a few hundreds of feet. For medium to large rivers, the distance may be so great that the transport is two dimensional throughout the region of interest. If the required distance is large, then a possible 50% variation in the critical value for 1D conditions can correspond to a very long distance. Nevertheless, there are some aspects of transport calculations for rivers (e.g. the mixing coefficients) where it may not be possible to know the parameters with an accuracy of 50%.

The above considerations are for free-flowing streams with continuous cross sections where the differential advection associated with the velocity distributions is responsible for the longitudinal spreading. For pool and riffle streams where the mixing within the pools and the gradual depletion of solute stored in the pools accounts for the longitudinal spreading, 1D conditions may be obtained after the flow has passed through one or two pools.

## 6.3.2 Fischer's Initial Period

Fisher (1966a, 1966b) was the first to demonstrate explicitly for rivers that $x_d$ must be greater than some critical value $(x_{d,1D})$ for 1D conditions to exist. This fact was implicit in Taylor's (1953, 1954) pioneering work on longitudinal dispersion but, before Fisher's work, most persons working with transport problems in rivers had not recognized the great importance of accounting for the processes within the region where 2D conditions exist. Fischer's original presentation was in terms of flow times instead of distances, so the time (or region, $x_d < x_{d,1D}$ ) for which 2D conditions exist has come to be known as Fischer's initial period. Among other things, Fischer pointed out that the velocity distribution is all that is needed to account for the highly skewed concentration distributions that are frequently observed to occur in streams. His observation is supported by much subsequent work, including the skewnesses in observed distributions (Section 7.8). Since 2D conditions exist in the initial period, 2D calculations should

252

be used to represent the transport in the initial period. As mentioned above, 2D calculations correctly represent the transport in the 1D region also, so they can be continued as far downstream as desired, or some provision can be made for switching from 2D to 1D computations at the end of the initial period. If the latter approach is taken, the transverse differences in the concentration distributions (as represented for example by the differences in the centroids and variances in Figures 49 and 50) will not be obtained from the subsequent 1D calculations. Also, even for calculations for cross sections beyond the initial period, provision must be made to account for the skewness and other characteristics of the concentration distributions which develop during the initial period.

## 6.3.3 Distributions with No Temporary Storage

When 1D conditions exist, the transport may be represented by Eq. 4.8.31. If it is assumed that all of the sources and sinks can be represented by one first-order reaction term with a rate coefficient of K , that the cross-sectional area, velocity, longitudinal mixing coefficient, and first-order rate coefficient are constant, and that the effects of temporary storage are negligible, then the differential mass balance equation may be written as

$$\frac{\partial C}{\partial t} + V \frac{\partial C}{\partial x} = E \frac{\partial^2 C}{\partial x^2} - KC \tag{6.3.1}$$

For unsteady situations, advection and dispersion are frequently the primary mechanisms, with decay or reaction taking place relatively slowly. For these situations, the dimensionless terms can be defined based on V and E with the effects of K being represented in a parameter for the problem rather than in the variables:

253

$$x_E = \frac{Vx}{E}$$

$$t_E = \frac{V^2 t}{E}$$

$$C_E = \frac{AEC}{VM}$$

(6.3.2)

$$\beta = \frac{KE}{V^2}$$

where $M$ is the mass initially released into the flow and the other variables are defined in Section 4.8.3.

In dimensionless terms, the solution to Eq. 6.3.1 for a slug of mass $(M)$ released instantaneously at $x_E = 0$ and $t_E = 0$ (with 1D conditions existing immediately after the release) is

$$C_E = \frac{1}{\left(4\pi t_E\right)^{1/2}} \exp\left[-\frac{\left(x_E - t_E\right)^2}{4 t_E} - \beta t_E\right]$$

(6.3.3)

This type of solution implies that 1D conditions exist for all $x_E > 0$ and thus does not account for the skewness of the concentration distribution that develops during Fischer's initial period. If the initial period is a significant fraction of the total study reach, Eq. 6.3.1 should be solved beginning at the end of the initial period (i.e. at $x_{E,1D}$) rather than beginning at $x_E = 0$, and the initial condition should be the skewed distribution that exists at the end of the initial period. Since Eq. 6.3.3 does not account for the skewness that develops during the initial period, it does not apply until after the cloud has traveled long enough in the 1D period for the initial skewness to be eliminated by the longitudinal mixing. Fischer et al.

254

(1979) suggested that Eq. 6.3.3 should be used only for $x_d$ $(= xe_y/VB^2)$ > 1 . This distance is so great for medium and large rivers that Eq. 6.3.3 has very little region of strict applicability for such rivers.

  <u>a</u>.  <u>Spatial distributions.</u> If Eq. 6.3.3 does apply, it gives a Gaussian or normal spatial distribution which has the following characteristics:

    (1) It is being advected with the velocity V and the centroid is always at $\bar{x}_E = t_E$.

    (2) The area under the $C_E$ versus $x_E$ curve is continually decreasing because of the reaction (if $\beta \neq 0$ ) and is given by

$$\int_{-\infty}^{\infty} C_E dx_E = \exp\ (-\beta t_E) \qquad\qquad (6.3.4)$$

and is thus decreasing exponentially due to the first-order reaction.

    (3) The maximum concentration is given by

$$C_{E,max} = \frac{1}{\left(4\pi t_E\right)^{1/2}}\ \exp\ (-\beta t_E) \qquad\qquad (6.3.5)$$

The maximum concentration decreases in proportion to $t_E^{-1/2}$ due to the mixing and simultaneously has an exponential decrease if there is a first-order reaction.

    (4) The nondimensional spatial variance grows linearly with time according to

$$\sigma_{E,x}^2 = 2t_E \qquad\qquad (6.3.6)$$

so that the length of the distribution, which is proportional to $\sigma_{E,x}$ , grows in proportion to the square root of time.

255

b. __Temporal distributions.__ The characteristics of the temporal distributions ($C_E$ versus $t_E$) represented by Eq. 6.3.3 for a fixed location ($x_E$) are somewhat different from what would be observed if the spatial distribution described above were "frozen" and simply advected past the observation location. The differences are due to the fact that, as the cloud passes the observation location, it is both dispersing due to the longitudinal mixing and decaying due to the first-order reaction. Both of these processes cause some difference in the variations of the moments for the temporal distributions compared to the spatial distributions, including the fact that the temporal distributions are slightly skewed while the spatial ones are symmetrical (but the skewness of the calculated 1D temporal distributions is much less than the skewness that develops during the initial period). Some of the characteristics of the temporal distributions are given below. In the following equations

$$A = \frac{(1 + 4\beta)^{1/2} - 1}{2}$$

$$B = \frac{1}{(1 + 4\beta)^{1/2}}$$

$$(6.3.7)$$

For $\beta \ll 1$, $A \approx \beta$ and $B \approx 1$.

(1) The area under the concentration curve is

$$\int_0^\infty C_E dt_E = B \exp(-Ax_E) \tag{6.3.8}$$

It is only for $\beta \ll 1$ that

$$\int_0^\infty C_E dt_E = \exp(-\beta x_E) \tag{6.3.9}$$

256

For this case, the area under the temporal concentration curve decreases exponentially due to the first-order reaction in a fashion similar to that for the spatial distributions (Eq. 6.3.4). For the larger values of $\beta$, the combined effects of the mixing and the reaction give a different rate of decrease of the area.

(2) The centroid is given by

$$\bar{t}_E = Bx_E + 2B^2 \tag{6.3.10}$$

If the cloud velocity $(V_{E,c})$ is derived from the rate of change of the centroids, then

$$V_{E,c} = \left(\frac{dt_E}{dx_E}\right)^{-1} = B \tag{6.3.11}$$

Thus, the reaction gives an apparent cloud velocity which is too large unless $\beta \ll 1$ so that $B \approx 1$.

(3) The variance is

$$\sigma_{E,t}^2 = 2B^3 x_E + 8B^4 \tag{6.3.12}$$

so that

$$\frac{d\sigma_{E,t}^2}{dx_E} = 2B^3 \tag{6.3.13}$$

or, in terms of the original dimensional variables,

$$\frac{d\sigma_t^2}{dx} = \frac{2E}{V^3(1 + 4\beta)^{3/2}} \tag{6.3.14}$$

257

For a conservative solute ($\beta = 0$), the rate of increase of the variance can be used directly to obtain the longitudinal mixing coefficient ($E$). However, for $\beta > 0$, the derivative in Eq. 6.3.14 is smaller than it would be for a conservative solute in the same flow; thus the mixing coefficient indicated by the rate of change of the variance would be too small if this derivative were used without accounting for the reaction. Even for relatively small values of $\beta$, the error in calculating the longitudinal mixing coefficient can be significant because of the three-halves power on the term containing $\beta$ in Eq. 6.3.14. Eq. 6.3.14 also shows that the calculated value of $E$ depends strongly on the value of $V$ for given concentration data, but the values of $V$ can frequently be obtained rather accurately from the concentration data. (See also Section 7.8.)

Even though Eqs. 6.3.11 and 6.3.14 were derived from a mathematical solution based on the assumption of 1D conditions for all $x > 0$, it can be shown using superposition that these expressions involving the gradients of $\bar{t}_E$ and $\sigma^2_{E,t}$ are also valid for the 1D transport which follows a 2D initial period if Eq. 6.3.1 is valid.

## 6.3.4  Distributions with Temporary Storage

Thackston and Schnelle (1970) analyzed the 1D equivalent of the problem considered in Section 6.2.5, i.e., a channel with storage zones distributed uniformly along the stream bed. They considered the case of uniform flow with constant velocity, mixing coefficient, and exchange rate coefficient with the storage zones. For this situation, the mass balance equations for the main channel and the storage zones may be written for conservative substances as

$$\frac{\partial C_a}{\partial t_a} + V \frac{\partial C}{\partial x} = E \frac{\partial^2 C}{\partial x^2} - \frac{K^* A^*}{H} (C - C^*) \tag{6.3.15}$$

and

258

$$\frac{\partial C_a^*}{\partial t_a} = \frac{K^*}{h^*} (C - C^*) \qquad (6.3.16)$$

(The sign is wrong on the last term of Eq. 6.3.15 in the original paper.) The variables are defined in Sections 4.8.3 and 6.2.5. Thackston and Schnelle considered only the case with $A^* = 1$, but the results can be scaled to other values of $A^*$. They assumed an instantaneous initial source at $x_a = 0$ and $t_a = 0$ and used LaPlace transforms to solve the differential equation. The transforms had to be inverted numerically, so their results were presented graphically for a limited number of situations, as shown in Figures 52 and 53. The figures are given as originally presented by Thackston and Schnelle. In addition to previously defined quantities, the parameters for the calculations were $Pe = Vx/E$ and

$$R = \frac{h^*/K^*}{x/\ V/(1 + \lambda)} = \frac{h^* V}{K^* (1 + \lambda)x} \qquad (6.3.17)$$

where $R$ is the ratio of characteristic times for exchange with the storage zones and for movement of the cloud through the reach of length $x$ (when concentration equilibrium exists). All of the calculated results were for $Pe = 1000$ and $\bar{t} = 6.95$ hr. In retrospect, there are two unfortunate things about the way that the results were given. First, the results were not given in totally dimensionless form; specifically, the time axes on the graphs are not dimensionless. Thus, the results cannot be interpreted as broadly as might have otherwise been the case. Second, the dimensionless variables and parameters have the original dimensional variables and parameters intertwined in such a way that extreme care must be used in interpreting some of the graphical results. For example, there may be a tendency to view Figure 52 as showing the change in concentration versus time at a given distance if the amount of storage capacity is changed. Thackston and Schnelle apparently did this and came to the incorrect conclusion that the

259
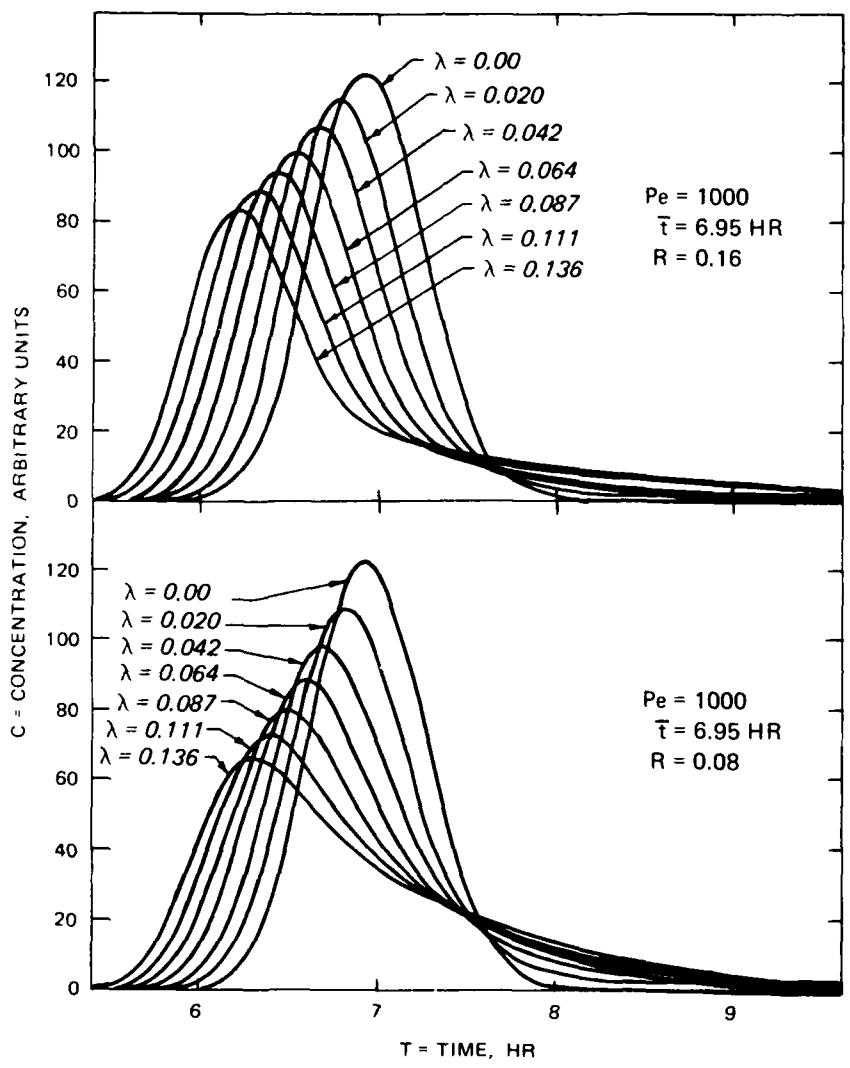
Figure 52. Calculated (1D) concentration distributions with temporary storage (Thackston and Schnelle (1970), Fig. 3)
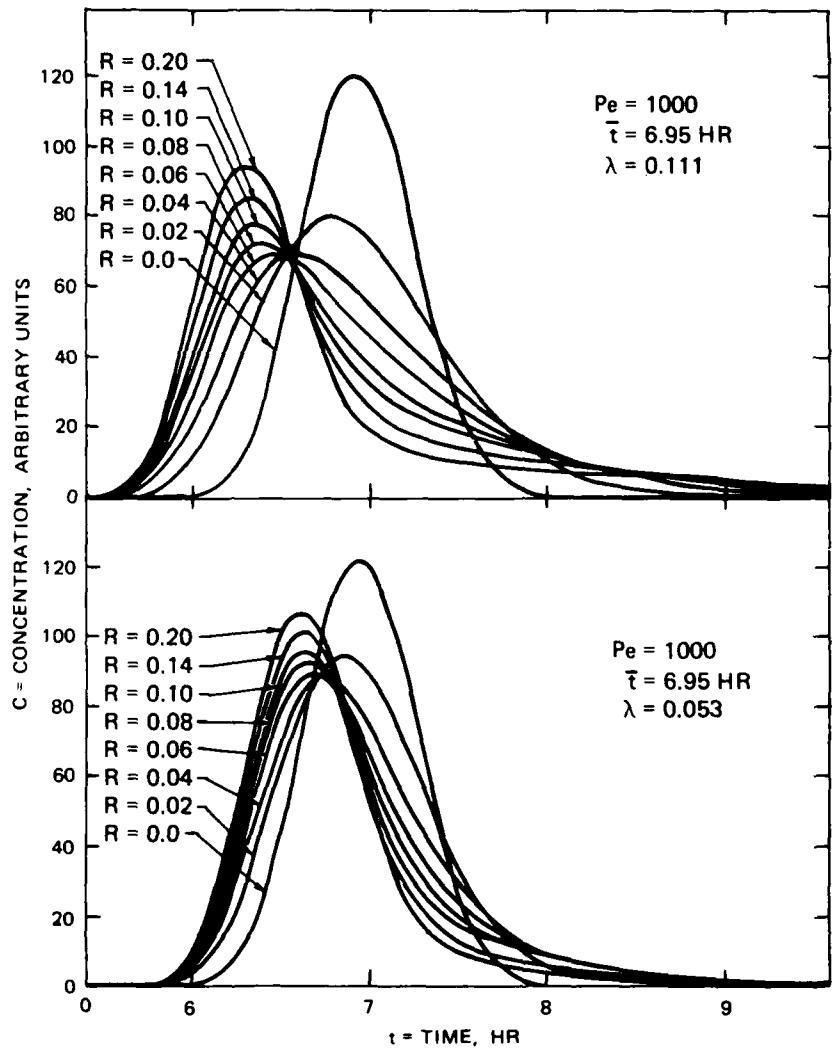
Figure 53.  Calculated (1D) concentration distributions with
temporary storage (Thackston and Schnelle (1970), Fig. 4)

261

presence of storage zones decreases the residence time, or increases the effective advective transport rate, for a given reach of a river. The problem is that, while $x$ is in Pe , $x$ and $\lambda$ are both in R so that changing $\lambda$ while holding R constant means that $x$ cannot be constant for the curves in Figure 53. If the type of analysis used by Thackston and Schnelle were done in such a way as to look at the effect that increasing $\lambda$ would have on concentration distribution at a given $x$ , it would be seen that the residence time would be increased for the stream reach and that the changes in the shapes of the concentration distributions would be in accord with the discussion presented in Section 6.2.4 for the 2D analysis.

(Thackston and Schnelle's results are presented to demonstrate the calculated effects of temporary storage on the concentration distributions. However, they did not account for Fischer's initial period (Section 6.3.2) in their analysis so that much of the effect which they attributed in their data analysis to the storage mechanism probably was probably due to the effect of the transverse velocity distribution.)

While there are no simple analytical solutions for Eq. 6.3.15, an analytical solution can be obtained for the case of concentration equilibrium between the main flow and the storage zones (the limiting case of very rapid exchange between the main flow and the storage zones or very large $K^*$ ). For this case the mass balance equation can be written as

$$(1 + \lambda) \frac{\partial C}{\partial t} + V \frac{\partial C}{\partial x} = E \frac{\partial^2 C}{\partial x^2} \tag{6.3.18}$$

Since $\lambda$ appears only in the time-derivative term, a new variable can be introduced with

$$t' = \frac{t}{1 + \lambda} \tag{6.3.19}$$

262

thereby reducing Eq. 6.3.18 to the mathematical form of Eq. 6.3.1 (with $K = 0$). In dimensionless terms, the solution for a slug of mass $M$ released at $x = 0$ and $t = 0$ is

$$C_E = \frac{1}{\left(4\pi t_E'\right)^{1/2}} \exp\left[-\frac{\left(x_E - t_E'\right)^2}{4 t_E'}\right] \tag{6.3.20}$$

where $t_E' = V^2 t/[E(1 + \lambda)] = t_E/(1 + \lambda)$. Thus, the only effect of storage for the case with concentration equilibrium is to slow the whole transport process down in proportion to $1/(1 + \lambda)$.

### 6.3.5 Cells-in-Series Model

Stefan and Demetracopoulos (1981) analyzed the transport of a slug of mass through a series of well-mixed cells in the context of transport in rivers. They used this type of representation as an approximation for the transport through a reach of the Upper Mississippi River with irregular cross sections. They also mentioned that this type of representation might be used as an approximation of the conditions in a pool and riffle stream. The mass balance equation for any cell may be written as

$$\frac{dC}{dt} = \frac{W}{\Psi} - \frac{Q}{\Psi} - KC \tag{6.3.21}$$

where $C$ is the concentration in the cell, $t$ is time, $W$ is the rate of mass input into the cell either from the upstream cell or from an external source, $\Psi$ is the volume of the cell, $Q$ is the flow rate out of the cell, and $K$ is a first-order rate coefficient. They solved Eq. 6.3.21 for constant $\Psi$, $Q$, and $K$, and with the only external input being an instantaneous release of mass $M$ into the first cell at $t = 0$. The concentration may be written in dimensionless terms for the j-th cell ($j \geq 1$) as

$$C_s = \frac{t_s^{j-1}}{(j-1)!} \quad \exp\left[-(1 + K_s)t_s\right] \tag{6.3.22}$$

where the dimensionless variables are

$$C_s = \frac{C\Psi}{M}$$

$$t_s = \frac{Qt}{\Psi} \tag{6.3.23}$$

$$K_s = \frac{K\Psi}{Q}$$

The concentration distribution may be integrated to determine the temporal moments and these may be used to evaluate the following parameters for the $C_s$ versus $t_s$ curves:

$$N_{s,o} = \int_0^\infty C_s dt_s = \frac{1}{\left(1 + K_s\right)^j}$$

$$\bar{t}_s = \frac{j}{(1 + K_s)}$$

$$\sigma_s^2 = \frac{j}{\left(1 + K_s\right)^2} \tag{6.3.24}$$

$$S_s = \frac{2}{j^{1/2}}$$

In sequence, these quantities (all in terms of the dimensionless concentration, $C_s$, for the j-th cell) are the area under the concentration versus time curve, the centroid of the distribution, the variance, and the skew coefficient. The effects of the first-order reaction can be seen by comparing these results with the equivalent terms with $K_s = 0$ . This type of comparison shows that any reaction not only

causes less mass to pass through a given cell so that $N_{s,o}$ decreases as $K_s$ increases, but also causes the centroid of the concentration curve to occur earlier since the reaction has more time to reduce the concentrations on the tail than on the rising limb of the distribution. The reaction also causes the total width of the distribution to decrease because of the additional reduction of the concentrations on the tail, so that $\sigma_s$ also decreases for a given cell (or a given $x$) as $K_s$ increases. However, all effects of $K_s$ compensate in such a way that $S_s$ is independent of $K_s$. The dependence of the concentration distributions on $K_s$ is similar to the dependence on $\beta$ in Eqs. 6.3.7-6.3.12.

Stefan and Demetracopoulos used Eqs. 6.3.22 and 6.3.24 to rewrite the concentration distribution in terms of time relative to the centroidal time for the j-th cell. An alternate version of their equation may be written as

$$C_s = \frac{1}{(j-1)!} \left( \frac{j}{1 + K_s} \frac{t_s}{\bar{t}_s} \right)^{j-1} \exp\left( -j \frac{t_s}{\bar{t}_s} \right) \tag{6.3.25}$$

Sample concentration distributions from Eq. 6.3.25 are plotted in Figure 54a as given by Stefan and Demetracopoulos for a conservative solute ($K_s = 0$). Note that this method of plotting continuously distorts the scales as $j$ increases since $C_s$ is multiplied by $j$ and since $\bar{t}_s$ increases linearly with $j$. This type of scaling results in a vertical exaggeration and a horizontal compression as $j$ (or $\bar{t}_s$) increases. A similar plot is given in Figure 54b for $K_s = 0.05$. This value implies that 5% of the mass is lost due to reaction in a time equal to the residence time in one cell (since $[1 - \exp(-0.05)] = 0.05$). One effect of the reaction, namely the reduction of mass, can be seen by comparing the area under the curve for a given $j$ in Figure 54a with the area for the same $j$ in Figure 54b. The graphs also demonstrate that the reaction reduces the concentrations on the

265
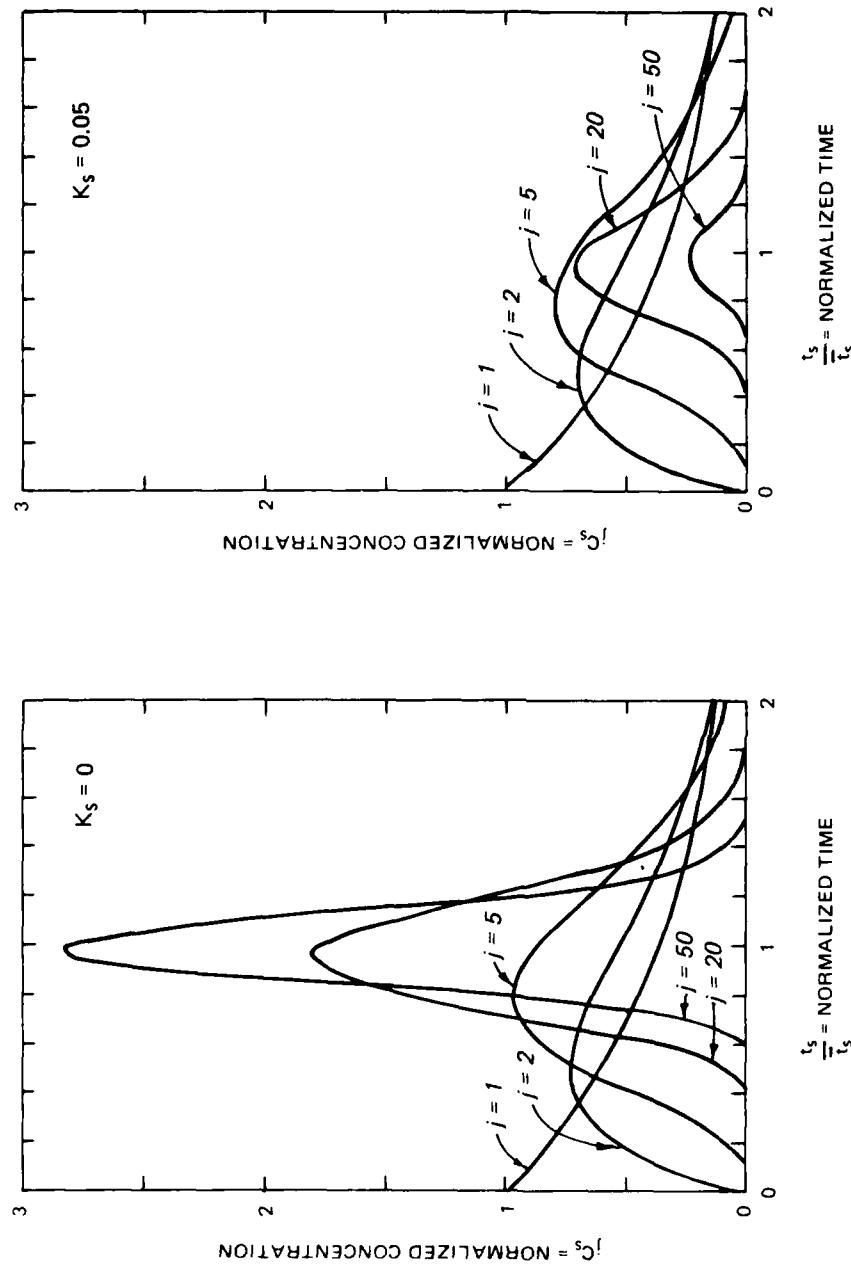
a. Conservative substance

b. Nonconservative substance

Figure 54. Calculated 1D concentrations with cells-in-series model (after Stefan and Demetracopoulos 1981)

tails of the distributions more than on the rising and central parts of the distributions.

This cells-in-series model is a specific case of general lumped parameter analyses discussed by Martin (1976) and Beer and Young (1980, 1983).

# CHAPTER 7. EXPERIMENTAL CONSIDERATIONS

## 7.1 INTRODUCTION

This chapter presents some considerations related to experimental programs, gives some information on numerical values and related considerations for mixing coefficients, and summarizes some experimental results from field studies. Both steady and unsteady problems are considered, but 1D steady-state experiments are not included because they are influenced primarily by distributed sources and sinks such as biological and chemical processes which are not within the scope of this manual.

In this chapter, a brief summary is given of the types of data which are desirable for field studies. Then some data analysis techniques are presented (particularly for determining mixing coefficients), available results for mixing coefficients are summarized and discussed, and finally a few sets of data from the literature are presented. These types of information are given first for steady-state transverse mixing experiments and then for unsteady, longitudinal transport experiments.

### 7.1.1 Steady-State Transverse Mixing Experiments

The literature contains data and data analyses for both laboratory and field studies. Much of the available data has been summarized by Fischer et al. (1979). Most of the laboratory studies have been conducted in rectangular flumes. There has also been a very limited number of laboratory studies in rectangular meandering channels and an even more limited number in meandering laboratory channels with cross-sectional shapes approximating those of natural channels. Some of the field studies have been for relatively short reaches, for example, reaches which were contained within one bend or which were short enough that the tracer being used to study the transport did not disperse across the channel width since the reach was shorter than the crossing distance. In other studies, the reaches were longer, and some studies have been conducted with the reach length being on the order of

the mixing distance. Most studies of transverse mixing have been conducted with steady-state injection and concentration distributions; Beltaos (1975) presented a method for using a slug injection for transverse mixing tests. This method is illustrated in Section 7.5.4.

The primary objectives of experiments on steady-state 2D transport problems have been (a) the determination of transverse mixing coefficients, (b) the evaluation of characteristics of concentration distributions, and (c) the demonstration of the utility of the streamtube model.

### 7.1.2 Unsteady Longitudinal Mixing

With very few exceptions, the data collection and analysis programs for experiments on unsteady longitudinal transport and mixing have assumed that 1D conditions existed, even though this assumption frequently has not been checked either experimentally or by estimating the mixing distances necessary to achieve approximately 1D conditions. Nordin and Sabol (1974) summarized the results from 51 experiments in 24 rivers for slug-type injections. For small streams, the tracer injection has frequently been made by simply dumping the tracer near midstream; for larger streams, there has sometimes been an attempt to spread the tracer across the stream width to approximate a line source condition. However, if the criteria for 1D conditions are actually met, the details of the release method should be of little importance. There have also been numerous laboratory studies, again mostly in rectangular channels. Most of the available results for longitudinal mixing coefficients for both laboratory and field studies were summarized by Fischer et al. (1979).

Some of the primary objectives of the unsteady experiments have been (a) determination of the longitudinal mixing coefficient, (b) demonstration of the importance of the transverse distribution of velocity in the longitudinal mixing process, and (c) investigation of the causes and characteristics of the "long tails" often observed on temporal concentration distributions.

269

## 7.2  DESIRABLE FIELD DATA

This section presents a summary of the types of data which would be de·irable for a thorough experimental field study. It is generally desirable to have the types of data described here regardless of the objectives of the experiments. However, it is recognized that it may not be feasible to collect all of these data for each experiment. The discussion assumes that an artificial tracer is used to determine the transport patterns. The necessary changes should be apparent if a naturally present tracer is used.

### 7.2.1  Hydraulic Characteristics

a.  Stream discharge. The discharge can generally be obtained from US Geological Survey stream gaging records to define the flow conditions for the study and to provide a check of the velocity and depth measurements discussed in paragraph 7.2.1d below.

b.  Stream stage. The stage can also be obtained from stream gaging records. In addition, a temporary staff gage should be installed and read periodically during the test to monitor for possible unsteadiness. Measuring the water height on bridges or other permanent structures can prove useful for resolving discrepancies which sometimes appear during data analysis.

c.  Plan-form geometry. The information which is needed to define the plan-form geometry includes the stream width at the injection cross section, at each of the measurement cross sections, and at any significant changes in width and alignment of the stream. Meandering streams are frequently characterized as a series of approximately circular arcs connected by approximately straight sections. The arcs are described by the location of the center of curvature, the radius of curvature for the stream centerline, the length of arc, and the stream width. The straight sections are described by their length, direction, and width. Any channel islands or other significant physical features should be included in the description. All of these features of the plan-form geometry should be shown on a scale drawing of the study reach, including enough of the stream upstream and downstream of the

270

study reach to indicate how the flow enters and leaves the reach. As is seen in Section 7.4, this type of information and the general characteristics of the cross-sectional shapes (paragraph 7.2.1d below) are useful for estimating mixing coefficients and for comparing the results of a particular study with other experimental results.

d. Cross sections and velocity profiles. Standard stream gaging procedures (Buchanan and Somers 1968) should be used to determine the cross-sectional shapes and the velocity profiles for the injection and measurement cross sections and for any other particularly significant cross sections. Notes should be made and photographs taken to document the general types of cross sections (well-defined and unobstructed, patches of sediment and weeds, highly irregular, etc.). The distributions of depth and velocity are needed in the data analysis to determine mixing coefficients and in subsequent predictions of concentration distributions. Also, immediately after each cross section is gaged, it frequently is convenient to mark (by means of a tag line, anchors and floats, etc.) the locations where concentrations are to be measured, if river traffic will allow this.

Although it is most desirable to have complete stream gaging at each significant cross section, velocities can be obtained somewhat easier by the moving boat method (Smoot and Novak 1969) if appropriate equipment is available. In the absence of time or resources for direct measurement of velocities, they can be estimated from the depth distributions for free-flowing streams with regular cross sections (Yotsukura and Sayre 1976).

e. Flow time. For each measurement cross section, it is helpful to know the time-of-travel from the injection site and to know the time ($t_A$) at which the concentration from a slug injection starts rising from zero and the time ($t_B$) at which it falls back to zero (Section 7.2.2a). This information can be obtained with standard time-of-travel procedures (Hubbard et al. 1982). Preliminary time-of-travel estimates can be made with the average velocities obtained from the stream gaging. There are at least two potential problems with this approach. One is that the average of the velocities measured at a few

271

cross sections may not be the average for the entire study reach, particularly if the cross sections where velocities are measured include constricted sections (such as bridge openings) that are frequently used for stream gaging purposes. The other is that the average flow velocity in the main channel may not give the average velocity of a tracer cloud because of temporary storage effects (Section 6.2.4b).

$\underline{f}$. $\underline{Slope}$. The slope of the energy grade line is needed to calculate a resistance coefficient (Manning's n, Darcy-Weisbach f, Chezy C, etc.). Low Froude number flows have small velocity heads relative to the flow depth, so the slope of the energy grade line can be assumed to be equal to the slope of the water surface. Standard surveying techniques can be used if benchmarks are present in the vicinity of the study reach. Care should be taken to ensure that the water surface elevations are obtained at representative points, i.e. not in sharp bends where superelevation may cause a significant transverse slope of the water surface nor in high-velocity regions where obstructions (rocks, debris, etc.) cause a disturbance of the water surface. When surveying is not feasible, the slope can sometimes be estimated from the general land slope obtained from topographic maps. For short study reaches, an accurate determination of the slope may require considerable effort because of the difficulty of measuring small changes in water surface elevation. If the flow is undisturbed so that the slope in the short study reach is the same as for a longer reach, then the slope for the longer reach may be used, of course.

$\underline{g}$. $\underline{Bed\ material\ and\ bed\ forms}$. It is helpful to have notes and/or photographs about the bed materials and bed forms (flat bed, dunes, etc.) at representative points through the study reach. This information, along with the cross-sectional size and shape and the velocity, can be used to check the resistance coefficient and to provide a general characterization of the test reach.

$\underline{h}$. $\underline{Storage\ zones}$. For unsteady transport problems, it is important to have information on storage zones along the stream bed and/or banks. This type of information has not been obtained very frequently in the past so there are no generally accepted procedures.

272

The types of information which are needed are the size (area exposed to the main flow and volume in the storage zone), location, and distribution for storage zones such as wakes behind sand dunes of other bed forms, cobbles or larger stones in the stream, irregularities or debris along the banks, etc. Visual inspection will frequently reveal whether possible storage zones along the banks are being continually flushed by the flow or whether there is a time lag in the exchange with the main flow. Although the quantitative information will probably need to be estimated, even estimates are an aid in trying to assess the possible influence of the temporary storage mechanism.

## 7.2.2 Tracer Injection

This section presents some considerations related to tracer injection; the following section discusses concentration measurements. More extensive considerations are given by Hubbard et al. (1982).

a. Steady-state tests. A frequently used procedure for steady-state experiments is to inject a tracer at a constant rate at a known location in the stream for a duration great enough to provide for the desired length of steady-state conditions at the cross section which is farthest downstream. The information which is generally needed concerning the injection includes the longitudinal, transverse, and vertical location of the injection tube, the concentration of the injected tracer, the injection rate, and the times at which the injection is started and stopped. It is desirable for stream gaging to be done at the injection cross section (as well as the measurement cross sections) so that the cumulative discharge can be determined for the transverse location of the injection.

If Rhodamine is being used as the tracer, the injection location should normally be selected (for example, near the water surface) to keep the highly concentrated injection solution away from bed sediments because of possible adsorption losses. Some investigators (for exam ple, Yotsukura, Fischer, and Sayre 1970) have added light-weight liquids such as methanol to the injection solution to bring the

273

specific gravity to approximately unity. Although adjustment of the specific gravity is the recommended procedure, it may be possible in some cases to make the injection of diluted Rhodamine near the water surface in such a way that the mixing associated with the falling dye plume and with the turbulence in the stream prevent the tracer from sinking immediately to the stream bed. The analyses of Section 3.6 may be used to estimate the dilution of the negatively buoyant jet or plume of injected tracer as it travels over the water depth. This type of analysis does not include the effects of ambient turbulence and thus gives a conservative estimate.

The tracer normally is prepared to give a predetermined injection concentration. Estimated mixing characteristics of the stream and tracer decay rates are used to determine the injection concentration which is required to provide accurately measurable concentrations at the last cross section. Even with a predetermined injection concentration, samples should be taken periodically from the injected tracer for later analysis for concentration. At least three samples should be taken from each container of tracer which is prepared for injection, with one sample when injection from the container begins, one when about half of the tracer has been injected, and one when the container is almost empty. In case there is any nonuniformity in the tracer, the location from which the sample was taken in the container should be noted.

The two most common devices for obtaining a constant injection rate are battery- or generator-operated diaphragm pumps and mariotte vessels. When operating properly, either type of device is capable of providing a constant flow rate over many hours. Pumps have the advantage of providing a definite pumping mechanism, and a properly selected pump generally can operate for several hours from a fully _____ 12-volt automobile battery. Pumps have the disadvantage of possible mechanical or electrical failure. Mariotte vessels have no mechanical parts which can fail, and they require no power source. However, the flow rate usually depends to some degree on the fluid viscosity and the tube diameter so that adjustments may need to be made

274

during a long injection to compensate for changes in temperature. Also, the injection tube generally must be open to the atmosphere near the bottom of the vessel with the injection flow passing out of a tube coming from the vessel, through the atmosphere, then into a collection device, and finally into a tube to the stream. Care must be taken to keep the tube going to the stream from becoming air-locked due to bubbles brought from the collection device. Before going to the field, the selected injection system should be set up and tested for the expected duration of the actual injection and under conditions as nearly like those in the field as possible.

Whichever injection device is used, the volumetric injection rate should be determined periodically (say at about 15- to 30-minute intervals, since the adverse consequences of a change in injection rate can be very severe). It generally is acceptable to interrupt the tracer flow to the stream for about 30 seconds to measure the flow rate with a graduated cylinder and a stop water. The volume should be read as rapidly as possible and the collected tracer immediately reintroduced into the injection system in such a way that it flows directly to the stream to help compensate for the interruption. (The collected tracer should not be poured back into the tracer reservoir.)

The required duration of tracer injection to obtain a given duration of steady-state conditions can be determined as shown in Figure 55. Figure 55a illustrates the concentration response curve at a given measurement point for an instantaneous injection at $t = 0$. The time when the concentration first starts increasing above zero is $t_A$, and the time when the falling limb of the curve reaches zero (or, say, 2% of the maximum concentration) is $t_B$. As illustrated in Figure 55b, an injection started at $t = 0$ with a duration of $\tau_I$ gives a steady-state concentration at the measurement point from $t_B$ to $\tau_I + t_A$ (Yotsukura et al. 1983). Note that this means that steady-state may exist at some downstream stations even after the injection is stopped. When it is crucial to know the limits of the steady-state period accurately, the actual response curve should be determined with a slug dye test. In other cases, the response curve can be

275

INSTANT INJECTION OF MASS M

$\tau = 0$

f(t) FOR CONSERVATIVE TRACER

$t = 0$    $t_A$    $t_B$
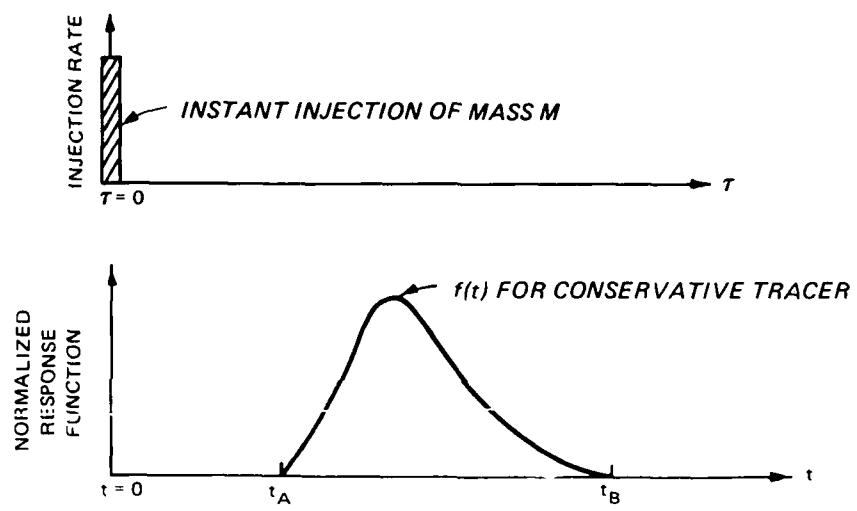
a.   Input-output relation for an instantaneous injection

$\dot{m}d\tau$

$\tau = 0$    $\tau_I$

STEADY STATE

$t = 0$   $t_A$    $t_B$   $t_A + \tau_I$    $t_B + \tau_I$
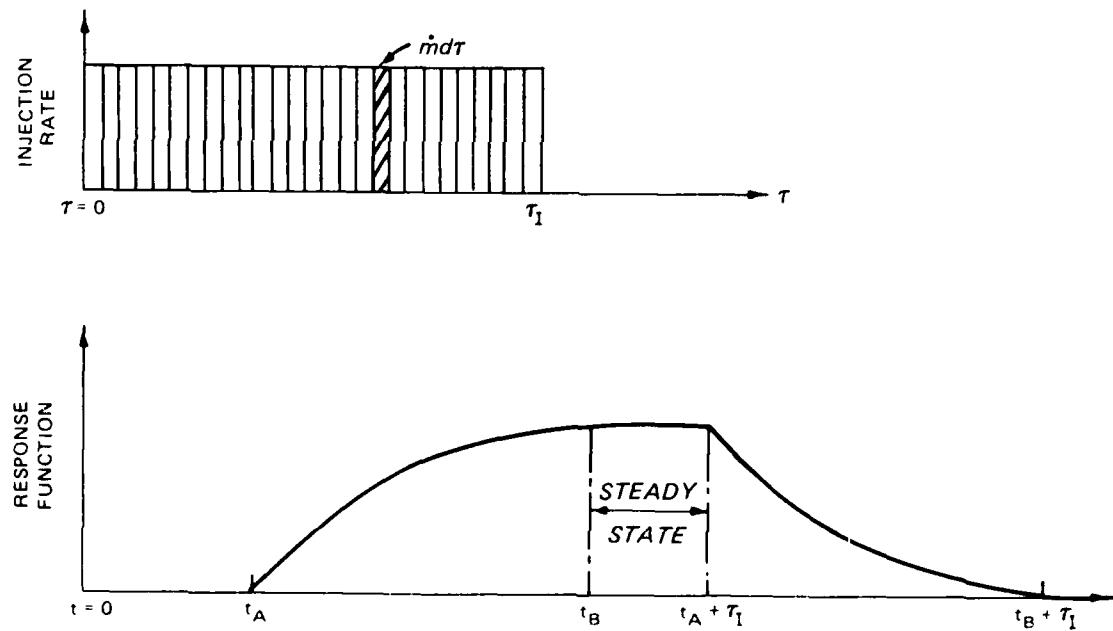
b.   Input-output relation for a finite-duration injection

Figure 55.   Relationship between duration of injection and concentration (after Yotsukura et al. 1984)

276

approximated from the time-of-travel and from estimated longitudinal mixing characteristics for the stream. In such cases, if measurements of concentration are made near $t = t_B$, it should be directly determined from the concentration measurements that steady conditions exist.

b. Transient tests. For transient (unsteady) tests, the injection of dye is much simpler than for steady-state tests. The injection frequently consists of simply dumping a known quantity of tracer at the desired location, after adjusting the specific gravity with a fluid such as methanol, as for the steady-state case. The injection location should be known in terms of longitudinal and transverse position and cumulative discharge. The injection generally should not be made in shallow or stagnant regions of the stream. By estimating the amount of longitudinal mixing through the study reach and the expected tracer decay and by specifying the minimum desirable concentration at the downstream end of the reach, the required amount of tracer can be specified for the injection.

In mathematical terms, dumping tracer at one location corresponds to a point source. Occasionally, an attempt has been made to dump tracer rapidly across the width of a stream in order to approximate a line source. In some situations, this type of injection may be justified, but frequently it is not needed. Sometimes, this type of injection has been used on the mistaken assumption that the mixing distance (Section 5.3.6) is significantly shorter for a line source than for a point source. Also, it should be noted that the practical aspects of trying to achieve a line source usually prevent the physical condition from corresponding exactly to the normally assumed mathematical condition, namely a constant initial concentration across the stream cross-sectional area. Under field conditions, the best that can normally be expected (except in very small streams) is to be able to release tracer at a constant rate from a boat which travels at a constant speed straight across the river. Even if this ideal is achieved, the concentration will not be uniform; it will be higher in the shallower parts of the river.

277

As with the steady injection, consideration should be given to keeping the highly concentrated injection solution away from bed sediments as much as is practical.

### 7.2.3 Concentration Measurements

a. Steady-state tests. For steady-state tests the objective is generally to determine the time-averaged transverse distribution of tracer concentration at specified cross sections. The same method used to define the transverse locations for the depth and velocity distributions can be used for the concentration distributions. As mentioned previously, the locations for the concentration measurements frequently are marked in conjunction with the stream gaging at the measurement cross sections. For cross sections where the tracer plume occupies only a fraction of the width of the stream, it may be desirable to locate the concentration measurements closer together in the transverse direction than the velocity or depth measurements. Although the test reach for studies to determine transverse mixing coefficients normally should extend beyond the crossing distance, it is not necessary for the test reach to extend to the mixing distance (Section 5.3.6). The latter part of the approach to transverse uniformity may contribute very little additional information about the transverse mixing process since the transverse concentration gradients are very small.

It frequently is assumed (Section 5.2.7) that complete mixing exists over the depth in rivers so that concentrations need to be measured at only one point in the vertical for each transverse location. However, in bends the helical motion may distort the concentration distribution faster than vertical mixing can restore vertical uniformity. This potential situation has not been analyzed thoroughly enough to be able to give definitive conditions under which vertically nonuniform conditions might be expected. As a general guide and until more detailed information is available, it is advisable to take three or more samples along the vertical at each sampling point for bends for which $UH/U_* R_c > 0.04$ (Section 7.4.2). Any tendency toward vertical nonuniformity should decrease as the transverse concentration gradients

278

decrease, but again this behavior has not been quantified.

In seeking to define time-averaged concentrations, it is helpful to recognize that the turbulent fluctuations of concentration are greater in the regions where the transverse gradients of concentration are greater. (See the example for the IJssel River data in Section 7.5.2.) Thus, for some cross sections it is necessary to take definite steps to provide for time-averaging over a sampling period $(t_s)$, which should be on the order of 100H/V where H is the stream depth and V is the flow velocity. In some situations, a sampling time of 100H/V is prohibitively long so that some compromise is necessary in selecting $t_s$. One method for obtaining time averages is to make (say) 10 concentration determinations at equally spaced intervals during the selected $t_s$. This approach also gives some information on the concentration fluctuations, which may be of interest in water quality considerations. The amplitude of turbulent fluctuations of concentration in the stream is damped if the sample flows through a tube (as contrasted to being measured directly in, or collected directly from, the stream). The amount of possible damping can be estimated from longitudinal dispersion theory for tubes (Taylor 1953, 1954). Another method for determining the time-averaged concentration is to use sample bottles which are designed to fill at a uniform rate during $t_s$.

b. Transient tests. For transient tests with slug-type injection of tracer, the objective is generally to measure the concentration versus time distributions at selected locations. For distances larger than the mixing distance, the measurements usually are made at only one transverse location for each cross section. The sampling location is then normally near the center of the stream, but the exact location is not very important if there is no significant transverse variation of concentration. For distances shorter than the mixing distance, the transverse extent of the cloud for each measurement cross section should be estimated from transverse mixing considerations, and sampling should be done at enough transverse locations to describe the variation of the concentration with both time and transverse position in the stream. (See Section 7.5.4.) If a slug-type injection is being used

279

for a transverse mixing test, then the concentration versus time curves should be integrated to provide the zeroth moment ($n_o$) for use in the subsequent analyses (Section 7.5.4 and Eq. 6.1.2).

For the steady-state tests discussed previously, the timing of sampling is not crucial once it has been established that a steady state actually exists. For transient tests, the timing is extremely crucial in terms of knowing the time at which sampling should be started, knowing the approximate time of passage of the tracer cloud so that an appropriate sampling interval can be selected, and knowing the time at which each reading is made during the sampling. In some cases where a sampling tube is being used with a pump to a concentration measurement instrument, it is necessary to correct the time of sampling to account for the flow time in the tube. Temporal concentration distributions are essentially always positively skewed, i.e., the rising part of the curves is steeper than the falling part. For some distributions (especially for distances much less than the mixing distance), the rising part of the curves may be extremely steep so that rather small time intervals between the first samples are needed to define the curves.

## 7.3 DATA ANALYSIS FOR STEADY-STATE EXPERIMENTS

This section summarizes possible methods of data analysis assuming that the streamtube model is being used to determine a transverse mixing coefficient and that the mixing coefficient is to be correlated with the hydraulic characteristics of the stream. (The same type of results can be obtained by using a coordinate system which follows the streamlines but without making the variable transformation from y to q .) It is assumed that the data are from an experiment using a conservative tracer to determine the hydraulic and mixing characteristics of a stream; since these characteristics are independent of any biological and chemical processes in a stream (assuming that these processes do not change the water density or the ambient flow pattern), information from conservative tracers can be used in models which also incorporate distributed sources and sinks for other types of substances.

An analysis based on the simplifying assumption of a rectangular cross-sectional shape would be generally the same as what is discussed here but with fewer variables in some parts of the analysis. The appropriate changes for the assumption of a rectangular channel are briefly noted in the discussion.

It is important that the same degree of detail be used in describing the hydraulics in the data analysis and in the subsequent use of mixing coefficients obtained from that analysis because the mixing coefficients effectively represent all of the transport processes which are not explicitly included in the model. For example, it is not appropriate to calculate a mixing coefficient using a streamtube model and then use that coefficient to calculate concentration distributions from a model assuming a rectangular cross section.

### 7.3.1 Coordinate System

Longitudinal and transverse coordinates need to be established. In order to minimize the deviations of $m_x$ from unity, the longitudinal coordinate should be along the center of the river with transverse distances measured from this longitudinal axis. However, except in sharp bends or in very wide, meandering rivers, the difference in longitudinal distances between two cross sections, whether taken along the inside or along the outside of bends, is small so that $m_x$ can frequently be approximated as being equal to unity. Then, as a practical matter, the origin of the transverse coordinate can be taken at either bank, but the longitudinal distances should be measured along the center of the stream. Vertical distances are normally measured relative to the water surface.

### 7.3.2 Cumulative Discharge

In the streamtube model, the transverse mixing is considered as taking place relative to the depth-averaged streamlines (Section 4.7.4). Thus, the concentration distributions are viewed as being a function of the cumulative discharge in the transverse direction so that this variable accounts for the stretching and compressing of the concentration

281

distribution associated with the transverse velocities; the remaining changes in the transverse direction are attributed to transverse mixing.

To obtain the cumulative discharge (q) as a function of  y (Eq. 4.7.28), the measured velocities along each vertical line are integrated to give  $hv_x$ .  If the metric coefficients are needed, then $m_y$  is evaluated from the plan-form geometry, and Eq. 4.7.28 is integrated to various  y  values. The velocity, depth, and cumulative discharge distributions are frequently presented as shown in the examples in Section 7.5.

### 7.3.3  Concentration Simulation

This section and the next one on change of moments summarize alternate methods for obtaining transverse mixing coefficients.  The simulation method has the advantages that it avoids the large effect that small concentrations at the edges of concentration distributions can have on calculated moments and that it is somewhat easier to include spatial variations of the hydraulics and of  $e_y$  in the simulation method.

In the simulation method, the 2D mass balance equation is solved numerically using the measured hydraulic characteristics as inputs and trying various values of the transverse mixing coefficient to obtain the best fit of the calculations with the concentration measurements. The magnitude of the mixing coefficient can be varied for different sections of the stream depending on the hydraulic characteristics. (See Sections 7.4 and 7.5, where correlations with  H  and  $U_*$  and with positions along a channel bend are presented.)  The longitudinal computational steps usually are significantly shorter than the distance between measurement cross sections so that some interpolation from the measured depths and velocities is needed to obtain the inputs for the numerical solutions.  Yotsukura and Sayre (1976) and Holly (1975) presented examples using the simulation method.  Rather elementary numerical techniques can frequently be used to solve the mass balance equation since numerical errors giving rise to numerical dispersion in

282

the longitudinal direction are not very important for steady-state problems. However, it is important to use the best possible estimate of the distributions of depth and velocity across and along the stream since these distributions can have a significant influence on the calculated concentration distributions. To illustrate this point, a calculated example is given in Figure 56 for a rectangular channel with two source conditions and with power-law velocity distributions in the transverse direction. An exponent (n) of 1 in the power law gives a triangular velocity distribution; $n = 1/2$ gives a parabolic distribution while $n = 1/10$ gives a rather flat distribution across the stream. Changes in the depth distributions would give effects similar to those shown in the figure. However, in the determination of $e_y$ from concentration data (by either the simulation method or the change-of-moments method in the next section), there has not been a definitive evaluation of the possible effects of errors in the depth and velocity distributions used in the data analysis.

### 7.3.4 Change of Moments

Mixing coefficients (for processes where the rate of mass transport is proportional to the gradient of concentration) are linearly related to the rate of increase of the variance of the concentration distribution, if the variance is not affected by tracer decay or by channel boundary. In general, this type of relationship exists because the rate of increase of the variance is a measure of how rapidly mass is being transported outward (from the regions of high concentration) due to the mixing process. The analysis to calculate mixing coefficients from the rate of increase of the variance has come to be known as the change-of-moments analysis. Some references have derived the basis for the change-of-moments analysis from analytical solutions for concentration distributions, but such derivations are, in principle, limited to the conditions for which the analytical solutions are valid. A more general analysis can be based on the differential mass balance equation. Fischer (1966a) was one of the first to derive this type of relationship for rivers; his application was for the problem of

283

b.  Center-line source
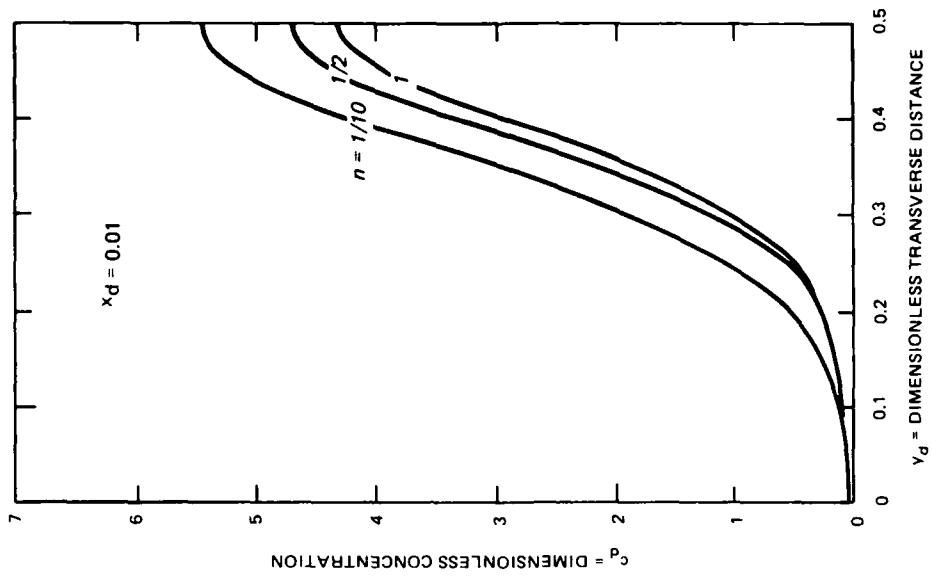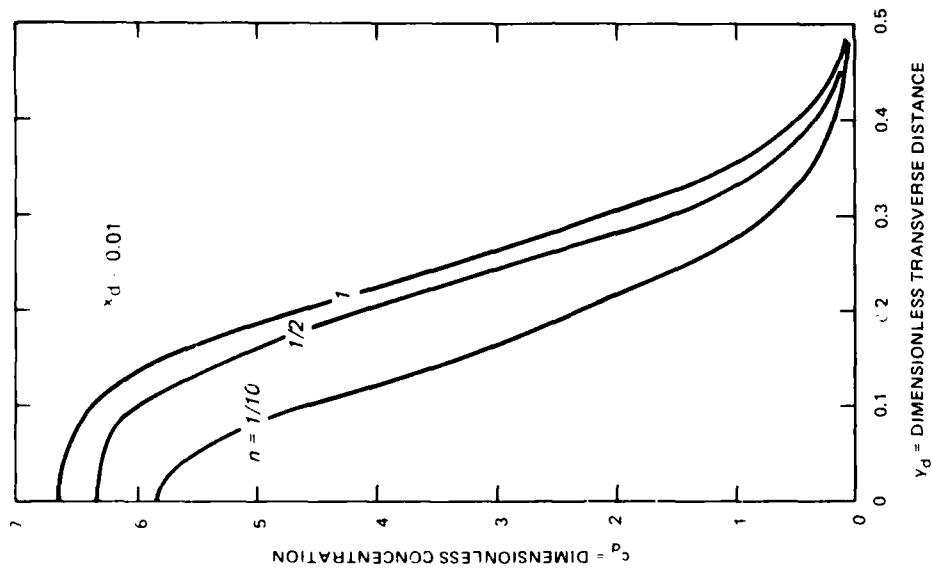
a.  Edge source

Figure 56.  Effect of velocity distribution on calculated steady-state concentration distributions

longitudinal mixing, but the subsequent extension to transverse mixing was based on Fischer's analysis. However, for the longitudinal problem, rivers are effectively infinitely long so that the concentration distributions can continue to spread indefinitely. For transverse mixing, the concentration distributions may eventually reach the river banks. Thus, Holley (1971) and Holley, Siemons, and Abraham (1972) developed a generalized change-of-moments (GCM) analysis for transverse mixing problems to allow inclusion of concentration distributions downstream of the crossing distance (Section 5.3.6) into the analysis. The GCM analysis also allows inclusion of variable depths, velocities, and mixing coefficients. Beltaos (1978) combined some aspects of the GCM analysis with the streamtube model. The development which is summarized below is also a combination of the GCM analysis and the streamtube model and is thus called the GCM-ST analysis. The analysis presented here takes a somewhat different approach from, and is believed to be more nearly complete than, previously published work. However, this analysis is based on the assumption of a constant total flow (Q) in the study reach. A similar, but somewhat more involved, analysis can be done to account for the frequently encountered situation with Q being a function of longitudinal distance. The first part of the discussion relates to obtaining the mixing coefficient $e_y$ , and then the diffusion factor $D_f$ is considered.

a. **Mixing coefficient.** From Eq. 4.7.34, the mass balance equation for steady conditions, for $m_x = 1$ , and for a conservative tracer can be written as

$$\frac{\partial c}{\partial x} = \frac{\partial}{\partial q} \left( h^2 v_x e_y \frac{\partial c}{\partial q} \right) \tag{7.3.1}$$

The steps in the derivation of the basic equation for the GCM-ST analysis are as follows:

(1) Select an appropriate streamline about which to take moments of the concentration distributions and call this streamline $q_o$ . In the analysis, $q_o$ is arbitrary, but might typically be taken as the bank for a side injection or the injection streamline for a

285

central injection. Note that $q_o$ is constant for all $x$, even if the maximum concentration moves to another streamline (e.g. following a central injection).

(2) Multiply Eq. 7.3.1 by $q_1^2 dq$, where $q_1 = q - q_o$, and integrate from $q_L$ to $q_R$, where $q_L$ and $q_R$ are the cumulative discharge values at the left and right banks, respectively.

(3) On the left-hand side (LHS) of the equation, take $q_1^2$ into the derivative. The additional term generated by this process is zero since $q$ and $x$ are independent variables and since $q_o$ is constant.

(4) Integrate the right-hand side (RHS) by parts. The resulting term which is evaluated at $q_L$ and $q_R$ is zero because of the no-flux boundary condition at the banks.

(5) Interchange the order of integration and differentiation on the LHS (Section 4.3.2). The two additional terms generated by this process are zero since $q_L$ and $q_R$ are constant if $Q$ is constant.

(6) Divide both sides by the longitudinal mass flux,

$$QC = \int_0^Q c\,dq \qquad (7.3.2)$$

which is constant for a conservative tracer and thus can be taken inside the derivative on the LHS. The definition of C (the average concentration) is obtained by dividing Eq. 7.3.2 by Q.

(7) Define

$$\sigma_1^2 = \frac{1}{QC} \int_0^Q cq_1^2\,dq \qquad (7.3.3)$$

Depending on the location of $q_o$ relative to the concentration distribution, $\sigma_1^2$ may not be the variance since $q_o$, from which $q_1$ is measured, may not be the centroid of the distribution. On the other hand, when the maximum concentration and $q_o$ are both at the same bank, then $\sigma_1^2$ is the variance of the concentration distribution.

286
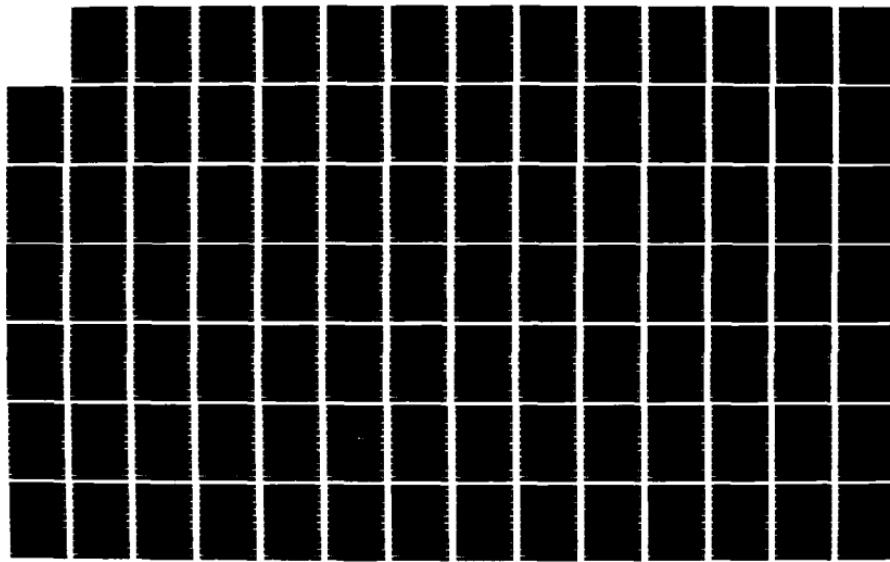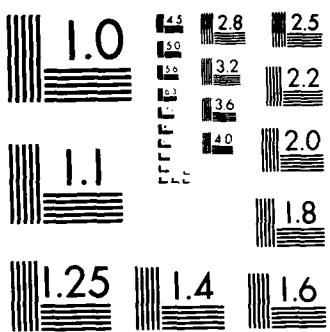
MICROCOPY RESOLUTION TEST CHART
NATIONAL BUREAU OF STANDARDS-1963-A

(8) The resulting equation may be written as

$$\frac{d\sigma_1^2}{dx} = -\frac{2}{QC} \int_0^Q h^2 v_x e_y \frac{\partial c}{\partial q} q_1 dq \qquad (7.3.4)$$

Since $c$ is in the numerator and $C$, which is constant for the problem being considered, is in the denominator, the analysis is sometimes done in terms of a dimensionless concentration which may be defined as

$$c_d = \frac{c}{C} \qquad (7.3.5)$$

If it is assumed that $e_y$ does not vary across the channel width as postulated by Holly (1975) and by Lau and Krishnappan (1981), then $e_y$ can be taken out of the integral so that

$$\frac{d\sigma_1^2}{dx} = -\frac{2e_y}{QC} \int_0^Q h^2 v_x \frac{\partial c}{\partial q} q_1 dq \qquad (7.3.6)$$

An alternate form of this equation can be obtained by integrating the RHS by parts. The terms which are evaluated at $q_L$ and $q_R$ are zero if the depth and/or the velocity is zero at the banks. The result may be written as

$$\frac{d\sigma_1^2}{dx} = \frac{2e_y}{QC} \int_0^Q c \frac{\partial}{\partial q} (h^2 v_x q_1) dq \qquad (7.3.7)$$

287

Eqs. 7.3.6 and 7.3.7 are mathematically equivalent forms; in either form, care must be exercised to use compatible values of $q$ and $Q$ and of $c$ and $C$ for each cross section to be sure that Eq. 7.3.2 is satisfied. Part of the RHS of Eqs. 7.3.6 and 7.3.7 is called $f(x)$ :

$$f(x) = -\frac{1}{QC} \int_0^Q h^2 v_x \frac{\partial c}{\partial q} q_1 dq = \frac{1}{QC} \int_0^Q c \frac{\partial}{\partial q} (h^2 v_x q_1) dq \qquad (7.3.8)$$

so that

$$\frac{d\sigma_1^2}{dx} = 2e_y f(x) \qquad (7.3.9)$$

or

$$\frac{d\sigma_1^2}{dF} = 2e_y \qquad (7.3.10)$$

where

$$F = \int_0^x f(x) dx \qquad (7.3.11)$$

In an application, the evaluation of $f(x)$ from either of the integrals in Eq. 7.3.8 can present difficulties because of the need to obtain derivatives of either the $c$ or the $h^2 v_x q_1$ distributions; in general, the distributions of the data are scattered, making the evaluation of derivatives difficult. Thus, two different approaches are considered. First, if either the $c$ or the $h^2 v_x q_1$ distributions are smooth enough that the required derivatives can be evaluated with reasonable accuracy, then $f$ may be evaluated directly from Eq. 7.3.8. On the other hand, if the data are too scattered for the derivatives to be evaluated, the integrands may be rewritten to eliminate the need to obtain the derivatives. A similar procedure may be used with either of

288

the forms in Eq. 7.3.8; the procedure is illustrated for the first form
and is based on

$$\int\limits_{o}^{Q} \eta \, \frac{\partial c}{\partial q} \, dq = \int\limits_{o}^{q=Q} \eta dc \qquad (7.3.12)$$

where $\eta = h^2 v_x q_1$ so that the second form in Eq. 7.3.12 is just the
area under a curve of $\eta$ plotted versus $c$ . This curve is obtained
by selecting various $q$ (or y) values, finding the corresponding $\eta$
and $c$ values for each $q$ (or y), and plotting these values versus
each other. A smooth curve can then be drawn through the scattered
data and the area obtained. Care must be used to assign the proper
signs to the area since the integral still must correspond to inte-
grating from lower to higher $q$ . The appropriate procedure is illus-
trated schematically in Figure 57 for two types of concentration dis-
tributions. After f is obtained, it is integrated in accordance with
Eq. 7.3.11 to obtain a value of $F$ for each cross section.

To evaluate $e_y$ from the data, $\sigma_1^2$ is calculated from the mea-
sured distributions of concentration, depth, and velocity for each
measurement cross section. Then graphically or by some other means,
the rate of change of $\sigma_1^2$ with $F$ is obtained. If the measurement
cross sections are relatively close together and if the $\sigma_1^2$ data do
not have much scatter, it may be possible to fit a smooth curve through
the data and to obtain local values of the derivative and then of $e_y$
(Sayre and Yeh 1973). In other cases, it may be possible to obtain
only an average $e_y$ for the entire study reach.

The method just described for calculating $e_y$ accounts for the
transverse and longitudinal variations of depth and velocity. Thus,
the resulting values of $e_y$ should be used in a model which includes
these same types of variations. Some considerations are presented
below for the case where it is desired to use the mixing coefficient in
a model with reach-averaged values of depth and velocity.

289
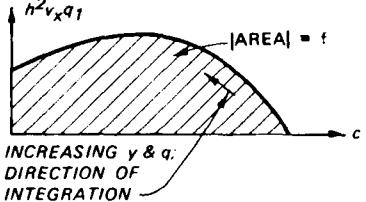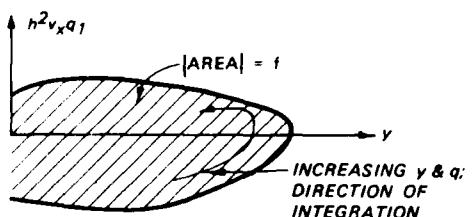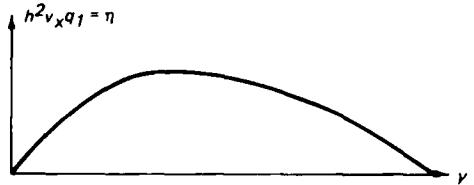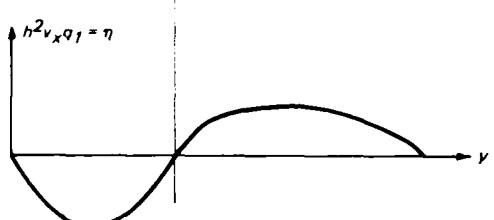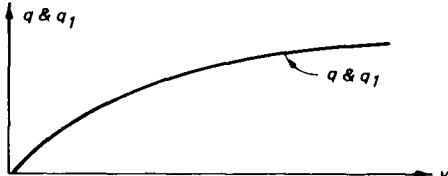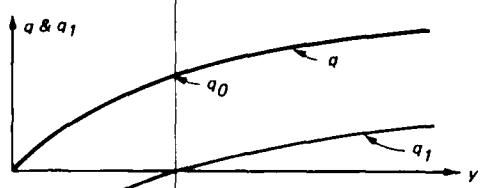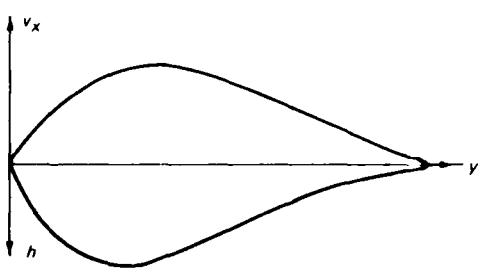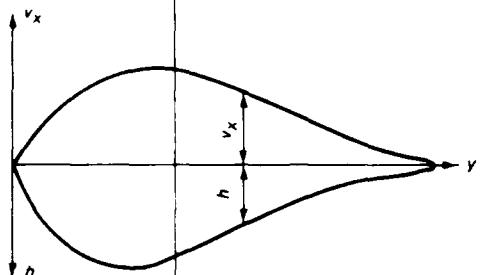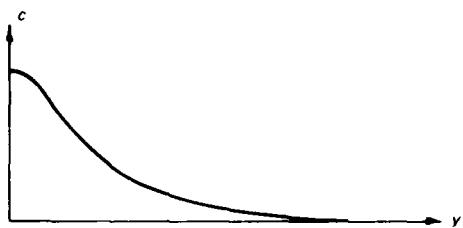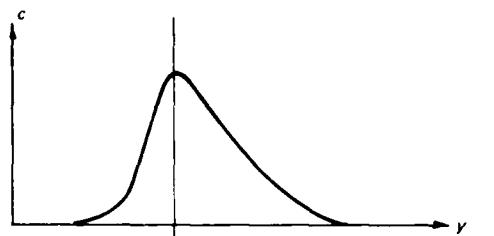
a. Central injection          b. Side injection

Figure 57. Integration procedure for generalized change of
moments in curvilinear coordinates

290

If a rectangular channel is assumed with the depth, velocity, and width constant and equal to their average values (H, V and B), then dq = HVdy so that the integrals with respect to q may be converted to integrals with respect to y . The key expressions corresponding to the ones above are

$$\sigma_{r,1}^2 = \frac{1}{C} \int_0^B cy_1^2 dy \qquad (7.3.13)$$

where $y_o$ , $y_1$ , $y_L$ , and $y_R$ are analogous to the corresponding values of q , and sub r indicates quantities for a rectangular channel approximation,

$$\frac{d\sigma_{r,1}^2}{dx} = 2e_y f_r(x) \qquad (7.3.14)$$

and

$$f_r(x) = -\frac{1}{V} \int_0^B \frac{\partial c}{\partial y} y_1 dy = \frac{1}{V} \left[ B - \frac{(y_1 c)_R - (y_1 c)_L}{C} \right] \qquad (7.3.15)$$

The first form for $f_r$ is the more difficult to evaluate because of the integral, but it is also probably the more accurate for actual application because the second form depends on the individual values of $c_R$ and $c_L$ . Scatter and uncertainty of the data (e.g. Figure 68d) cause possible inaccuracies in seeking to determine values of $c_L$ and $c_R$ . (The terms involving $c_L$ and $c_R$ in Eq. 7.3.15 result from the integration by parts in going from the first form of $f_r$ to the second form; the corresponding terms are zero for the stream-tube representation in Eq. 7.3.8.)

The assumption of a rectangular channel in the calculations effectively lumps into $e_y$ the influences of both the actual

transverse mixing and the transverse spreading due to transverse velocities. As a result, the variation of $\sigma_{r,1}^2$ with distance can be very irregular. The assumption of a rectangular channel should be used only to provide a rough indication of the value of $e_y$ and should be used only for reaches that include several bends in a meandering river or that are otherwise long enough to provide a reasonable average value for other types of rivers.

   <u>b</u>. <u>Diffusion factor.</u> Since the first introduction of a pre-liminary form of the streamtube model (Yotsukura and Cobb 1972), there has been interest in the possibility of replacing $h^2 v_x e_y$ in Eq. 7.3.1 by a constant diffusion factor $(D_f)$ which is defined as

$$D_f = \frac{1}{Q} \int_o^Q h^2 v_x e_y \, dq \qquad (7.3.16)$$

At least part of this interest has stemmed from the convenience of being able to obtain analytical solutions with a constant diffusion factor (Yotsukura and Cobb 1972, Yotsukura and Sayre 1976, and others). The present evidence, although not complete, indicates that it is more reasonable to assume a constant $e_y$ than a constant $D_f$ , at least for situations where the concentration distributions are not mixed across the channel width. Also, using the analyses given above to evaluate $e_y$ by either the simulation or the change-of-moments method, it is no more difficult (and perhaps more reasonable) to evaluate $e_y$ rather than $D_f$ . Nevertheless, the following analysis is presented because of the long-standing interest in $D_f$ and because the assumption of a constant $D_f$ does allow analytical solutions to be obtained easily to approximate the concentration distributions (Chapter 5). For some situations, the calculated concentrations near the bank when $D_f$ is constant are much lower than the actual concentrations (Figure 58). For other situations, a constant $D_f$ gives a reasonable representation of the concentrations even near the banks (Figure 59). The conditions under which a constant $D_f$ is an acceptable assumption have not been

292
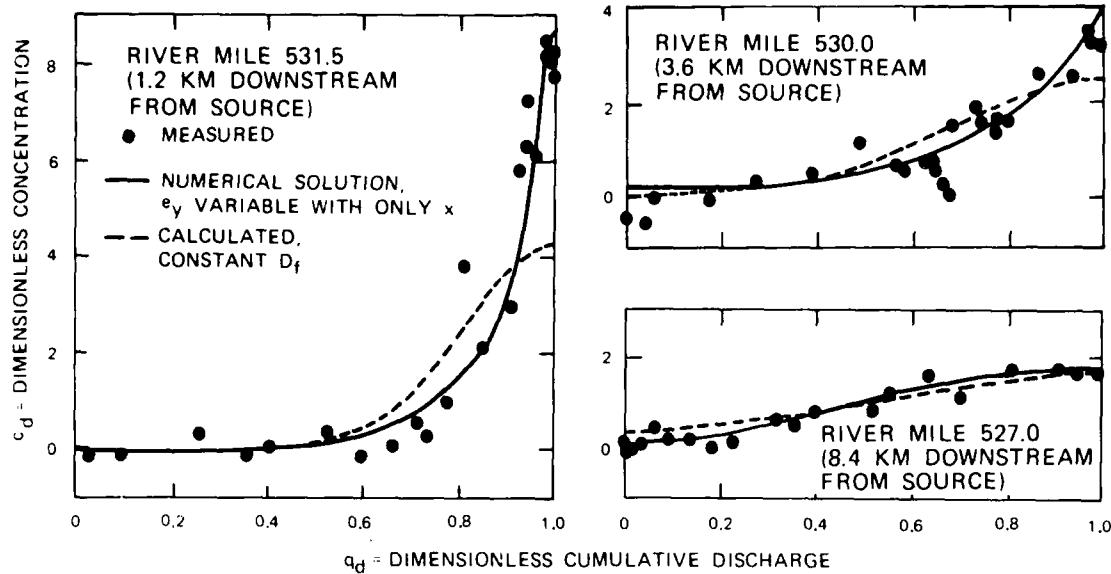
Figure 58. Comparison of measured and calculated transverse distributions of concentration for Missouri River (after Yotsukura and Sayre 1976)

well defined. Nevertheless, in general, a constant $D_f$ can be expected to be a better assumption for injections and concentration distributions in the central parts of streams where the depths and velocities are more nearly constant than for the bank releases when the majority of the concentration distribution is in a region with strong variations of depth and velocity. (Note that the use of a curvilinear coordinate system that follows the streamlines is independent of any assumption concerning the possible variation of $e_y$ or $D_f$ .)

The assumption of a constant $D_f$ can be included in the simulation method mentioned above in order to evaluate $D_f$ . A constant $D_f$ can also be evaluated by a change-of-moments (Beltaos 1980). In deriving expressions for $D_f$ , previous analyses have effectively first assumed that $e_y$ is constant and taken it out of the integral
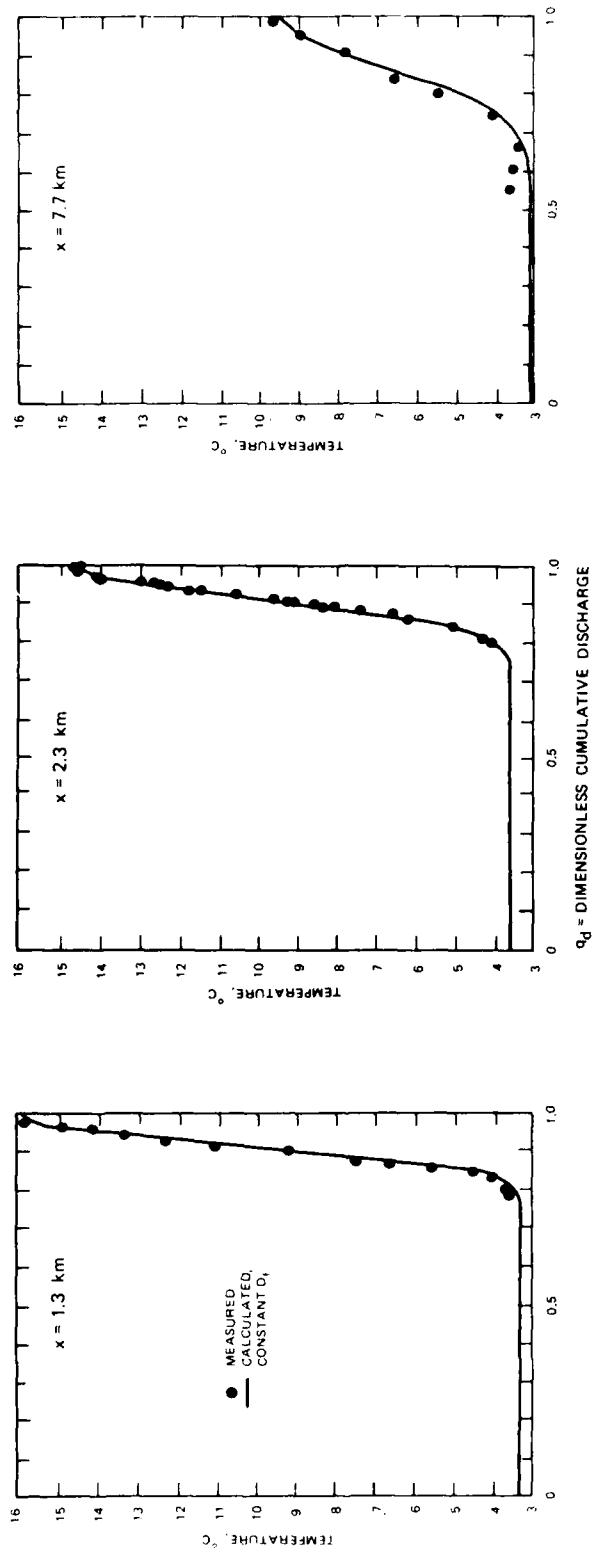
Figure 59. Comparison of measured and calculated transverse distributions of concentration for Missouri River (after Yotsukura and Sayre 1976)

(Eq. 7.3.16) and, since $D_f$ then involves an integral of $h^2$ and $v_x$, have defined a "shape factor" ($\psi$) such that

$$D_f = e_y(\psi H^2 V) \tag{7.3.17}$$

where

$$\psi = \frac{1}{H^2 VQ} \int_0^Q h^2 v_x dq \tag{7.3.18}$$

However, the previous change-of-moments analyses have apparently not derived the appropriate analytical relationship between $\sigma_1^2$ and $D_f$. This relationship can be obtained by essentially the same steps as given above for evaluating $e_y$ by first multiplying and dividing the RHS of Eq. 7.3.1 by $D_f$ and then by taking $D_f$ in the numerator out of the integral in step 2. The result can be written as

$$\frac{d\sigma_1^2}{dx} = 2D_f f_D(x) \tag{7.3.19}$$

where

$$f_D(x) = \frac{1}{\psi H^2 V} f(x) \tag{7.3.20}$$

Thus,

$$\frac{d\sigma_1^2}{dF_D} = 2D_f \tag{7.3.21}$$

295

where

$$F_D = \int\limits_0^x f_D(x)\,dx \qquad\qquad (7.3.22)$$

The data analysis to determine $D_f$ now exactly parallels that presented earlier to determine $e_y$ .

Yotsukura (personal communication) estimated $\psi$ to have an average or typical value of 1.5. He also considered the need to obtain a longitudinal average of $\psi$ if $D_f$ is taken as constant with respect to $x$ as well as $y$ . In the present analysis, the integration of $f_D(x)$ to obtain $F_D(x)$ accomplishes the same objective if the longitudinal variations of $h$ and $v_x$ are included in Eq. 7.3.18 so that $\psi$ becomes a function of $x$ . (It is also possible to include other types of variations of $e_y$ or $D_f$ in the analysis (Holley 1971; Holley, Siemons, and Abraham 1972).) Beltaos (1980) used measured distributions of depth and velocity to evaluate $\psi$ and found values in the range 1.7–3.6.

## 7.4  TRANSVERSE MIXING COEFFICIENTS

(Much of this discussion on transverse mixing coefficients is taken from Almquist and Holley 1985.)

### 7.4.1  Straight Channels

The experiments described in this section are divided into two general categories: laboratory experiments and field experiments. In a few instances (particularly for the field experiments), the designation of a channel as "straight" does not imply an absolute geometric condition but rather refers to the lack of any influence of channel curvature on the transport process. "Straight" channels may show mild curvature (or the flow itself may meander within a geometrically straight channel); however, this curvature is often so slight as to prevent even a rough estimation of the radius of curvature.

296

Section 7.5.1 provides an approximate quantitative criterion for classifying channels as straight or meandering in terms of the effects on transverse mixing.

a. Results from laboratory experiments. Only some general conclusions from laboratory experiments in straight channels are reviewed here since reviews of most of the available experiments have been given by others, including Okoye (1970), Fischer (1973), and Lau and Krishnappan (1977).

Assuming similarity between mass and momentum transport and assuming that the primary shear involved in the production of turbulence is associated with the vertical profile of longitudinal velocity over the depth, Elder (1959) concluded that the vertical mixing coefficient for wide, open-channel flow could be given by

$$e_z = 0.067U_*H \qquad (7.4.1)$$

He further reasoned that, since essentially all of the turbulence in such a flow is generated by the shear due to the vertical profile of longitudinal velocity, the lateral mixing coefficient should also be proportional to $U_*H$ . His own experiments, after a correction described by Sullivan (1968), gave a constant of proportionality $\alpha$ of 0.16, yielding

$$e_y = \alpha U_*H = 0.16U_*H \qquad (7.4.2)$$

It seems reasonable that $e_y$ is larger than the vertical coefficient since there are effectively no lateral boundaries to restrict the formation of larger-scale turbulence in the lateral direction in a wide, open-channel flow. Okoye (1970), based on his own experiments in rectangular channels and on experiments of others, concluded that $\alpha$ increased with increasing $B/H$ ; he found $\alpha$ values varying from slightly less than 0.1 for $B/H \approx 5$ to about 0.25 for $B/H \approx 65$ . Lau and Krishnappan (1977), using their own experiments and those of Miller and Richardson (1974), found more scatter in a plot of $\alpha$ versus $U_*H$

than did Okoye. They suggested that a more definitive correlation could be obtained by considering $e_y/U_* B$ rather than $\alpha \; (= e_y/U_* H)$ to be a function of $B/H$; however assuming that $\alpha = 0.15$, which is the average value for all the data considered, gives a correlation which is essentially as good as theirs.

Lau and Krishnappan also suggested that the rate of lateral mixing should depend on the friction factor, $f$, reasoning that increased relative bottom roughness results in higher turbulent intensities, increasing the mixing rate. However, turbulent intensity is proportional to $U_*$, so that much of this type of variation should already be included in the nondimensional coefficient based on $U_* H$. Nevertheless, some of the data presented by Lau and Krishnappan support their hypothesis, but no clear trends were evident.

Holley and Abraham (1973) conducted experiments with a straight rectangular flume with and without groins, and in an undistorted fixed-bed river model with groins; the model river had very slight curvature. The objectives of their experiments included a study of the effects on transverse mixing of variations in depth and width (river model) and of the effects of extra side roughness, such as groins (rectangular flume). In the rectangular channel ($B/H = 8.0$) without groins, they found $\alpha = 0.16$, consistent with previous studies. When groins were placed at the sides of the channel, with $B/H$ still equal to 8.0, $\alpha$ increased appreciably, ranging from 0.36 to 0.49 for different groin lengths and injection positions. The increase was ascribed to additional, larger-scale lateral eddies associated with the separation zones on the lee side of the groins. They also found that for otherwise identical experiments, $\alpha$ was 0.36 for a centerline injection and 0.48 for side injections, indicating that transverse variations of $e_y$ (due to the separation zones at the sides) could have an effect on the rate of spreading of a tracer plume.

The aspect ratio of the river model with groins was $B/H = 13.6$; the cross-sectional shape was modeled from a river (and thus was not rectangular nor prismatic), but there were no large bottom irregularities such as islands or sand dunes. The value of $\alpha$ obtained in

this channel ranged from 0.45 to 0.77, depending on injection location. Because those values were higher than for the rectangular flume and because the channel had only slight curvature, it seems likely that the increased mixing was associated with the transverse bed slope. Although experimental data are not available for precisely identifying the mechanism involved, it may be hypothesized that a transverse bed slope can give rise to lateral gradients of longitudinal velocity which, in turn, generate turbulence with a relatively large horizontal scale. It may be concluded from Holley and Abraham's (1973) results that groins and transverse bed slopes can significantly increase lateral mixing coefficients over those found in straight, smooth-walled rectangular channels.

F. M. Holly (1975) performed experiments in a straight flume with a triangular cross section, using two bottom roughnesses giving friction factors of 0.041 and 0.021. One objective of his study was to determine if $e_y$ could be related to local parameters by an expression such as $e_y = \alpha u_* h$ , where $u_*$ and $h$ are local values of shear velocity and flow depth. Using both streamtube simulation and generalized change-of-moments methods, Holly concluded that the best results were obtained by using cross-sectionally averaged values, i.e., $e_y = \alpha U_* H$ , and obtained $\alpha = 0.32$ for the smooth flume experiments and $\alpha = 0.62$ for the rough flume experiments. Both values are larger than would be expected for rectangular flumes, again indicating that a transverse bed slope can give rise to increased lateral mixing. The apparent dependence on bottom roughness is in qualitative agreement with Lau and Krishnappan's (1977) hypothesis. Although there are not enough data to be certain if, or why, the change in f in Holly's experiments should cause such a change in $\alpha$ , it is possible that the increase in roughness caused a more pronounced transverse gradient of velocity and thereby generated more turbulence and increased $\alpha$ . On the other hand, it may be that the apparent change in $\alpha$ was due to the fact that some of Holly's data exhibited considerable scatter.

The fact that better correlation was obtained by Holly using depth-averaged rather than local values of shear velocity and flow

depth was qualitatively explained by Yotsukura (1981), who stated that "transverse mixing requires a certain time or distance to pass through an initial advection-dominated period before it behaves like a diffusion process. Therefore, $[e_y]$ cannot possibly be a local quantity, and, moreover, is probably correlated with averaged values of  H  and $U_*$  within a certain time or space."

b.  Results from field experiments.  Fischer (1967) performed transverse mixing experiments in a straight reach of the Atrisco Feeder Canal near Albuquerque, N. Mex., and determined that  $\alpha \approx 0.24$  for both centerline and side injections.  This value is somewhat higher than that obtained in straight laboratory channels with comparable width-to-depth ratios, possibly due to the slight variations of depth. Another possibility is that the reported tendency of the flow to meander  thin the essentially straight channel may hav  introduced a weak secondary circulation, possibly causing additional lateral transport.

Yotsukura and Cobb (1972) performed experiments in a similar canal (the Bernardo Conveyance Channel) and obtained an average  $\alpha$  of 0.3.  The fact that there was more variation of depth in this canal than in the Atrisco Canal may have accounted for the larger value of $\alpha$ .

Holley and Abraham (1973) calculated the transverse mixing coefficient downstream of a cooling water discharge into the Waal River in the Netherlands.  There was almost no curvature of the channel and the depth was fairly uniform over the test reach, with groins at the banks. They obtained  $\alpha = 0.36$ ; as is typical for river experiments, the data showed considerable scatter.  Again, the value of  $\alpha$  is higher than observed in laboratory channels, which is probably due to the slight depth variation and the presence of the groins on the river banks.

Beltaos (1980) measured transverse mixing on a fairly straight reach of the Athabasca River in Canada, for both ice-covered and open-water conditions.  According to Beltaos' description, this reach of the river has a very nonuniform cross-sectional geometry, with many alternating bars of mud, sand, and weeds and several islands.  For the open-water condition (the case considered here), he found  $\alpha = 0.75$ .  This

value is higher than that obtained in the other field studies for straight channels. A feature of the reach of river studied by Beltaos is that many large-scale irregularities, such as islands and bars of mud and sand with heights on the order of the flow depth, existed in the channel. Such large-scale irregularities can be expected to cause large-scale splitting and intertwining of the flow streamlines (in much the same fashion as flow around grains in a porous medium, but on a much larger scale) and may also cause additional turbulence due to separation zones. Such bottom irregularity (as opposed to transverse variations of depth mentioned earlier) would thus be expected to increase the rate of lateral mixing, as was observed by Beltaos.

Yotsukura et al. (1984) obtained an $\alpha$ of approximately 0.75 for the Chenango River near Binghamton, N.Y., in a reach with a highly irregular geometry.

### 7.4.2 Meandering Channels

As in Section 7.4.1, the experiments described in this section are divided into laboratory and field experiments, but first a classification scheme is given to provide a framework for understanding some of the experimental results.

a. Classification of meandering channels. One conclusion to be drawn from the experiments in straight channels is that the lateral mixing coefficient, $e_y$, depends on several factors, including bottom shear velocity, water depth, channel width, bottom roughness, depth variations, bed irregularities and, to some extent, the lateral source position. The studies in straight channels indicate that the strongest influences on the nondimensional mixing coefficient $\alpha = e_y/U_*H$ are the width-to-depth ratio (B/H), transverse bed slope, and bed irregularity.

In a meandering channel, secondary circulation in the bends may generate additional lateral transport (Figure 60), which may or may not be of the gradient transport type. For bends that are long enough to develop gradient-type transport, Fischer (1969; also Fischer et al.

301

a. Prior to bend

b. Entering bend

c. Within bend
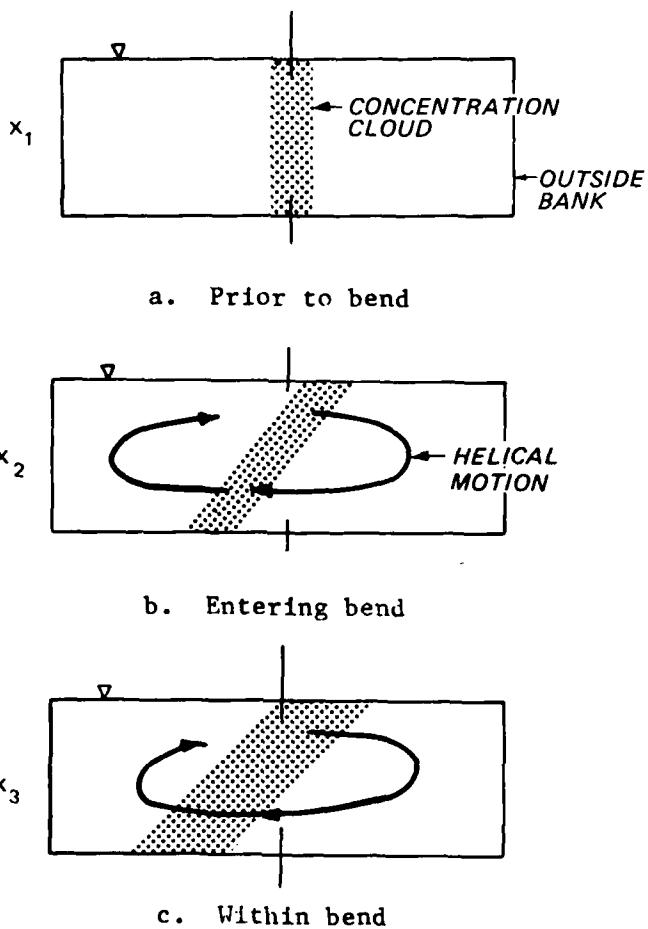
Figure 60. Effects of helical motion on tracer

1979) developed a theoretical expression for the additional transverse mixing coefficient ($\Delta\alpha$) due to secondary circulation:

$$\Delta\alpha = 25 \left( \frac{VH}{U_* R_c} \right)^2 \qquad (7.4.3)$$

where $R_c$ is the radius of curvature. This expression should be expected to apply only after a "long enough" initial period after the flow enters the bend. (See Figure 61, which is discussed later.) Eq. 7.4.3 was derived for flow in a hypothetical infinitely wide channel. Therefore, there was no channel width in the analysis. Yotsukura and Sayre (1976) and Sayre and Caro-Cordero (1979) found that a better correlation was obtained by including the width-to-depth ratio on the RHS of Eq. 7.4.3. For field data, their analysis gave

$$\alpha = 0.4 \, \frac{B}{H} \left( \frac{VH}{U_* R_c} \right)^2 = 0.4 \left( \frac{VB}{U_* R_c} \right)^2 \qquad (7.4.4)$$

based on the data in Figure 62. The coefficient in Eq. 7.4.4 was about seven times smaller (0.06) for the laboratory data. A possible explanation for this fact is presented in Section 7.6, after the data upon which the relationship is based are discussed. The inclusion of B/H in Eq. 7.4.4 has no theoretical basis. Nevertheless, the trend is the general one shown by the field and laboratory data in Figure 62. No correlations which are better than that given by Eq. 7.4.4 have been proposed.

Starting with these analyses, Almquist and Holley (1985) presented an approach to classifying transverse mixing in various types of meandering channels based on the assumption that the parameter $(VH/U_* R_c)^2$ can be used to indicate whether the secondary currents in a given bend are strong enough to induce additional transverse transport. If $\Delta\alpha$ computed by Eq. 7.4.3 is much less than a typical value for straight channels, then the secondary currents are probably too weak to

303
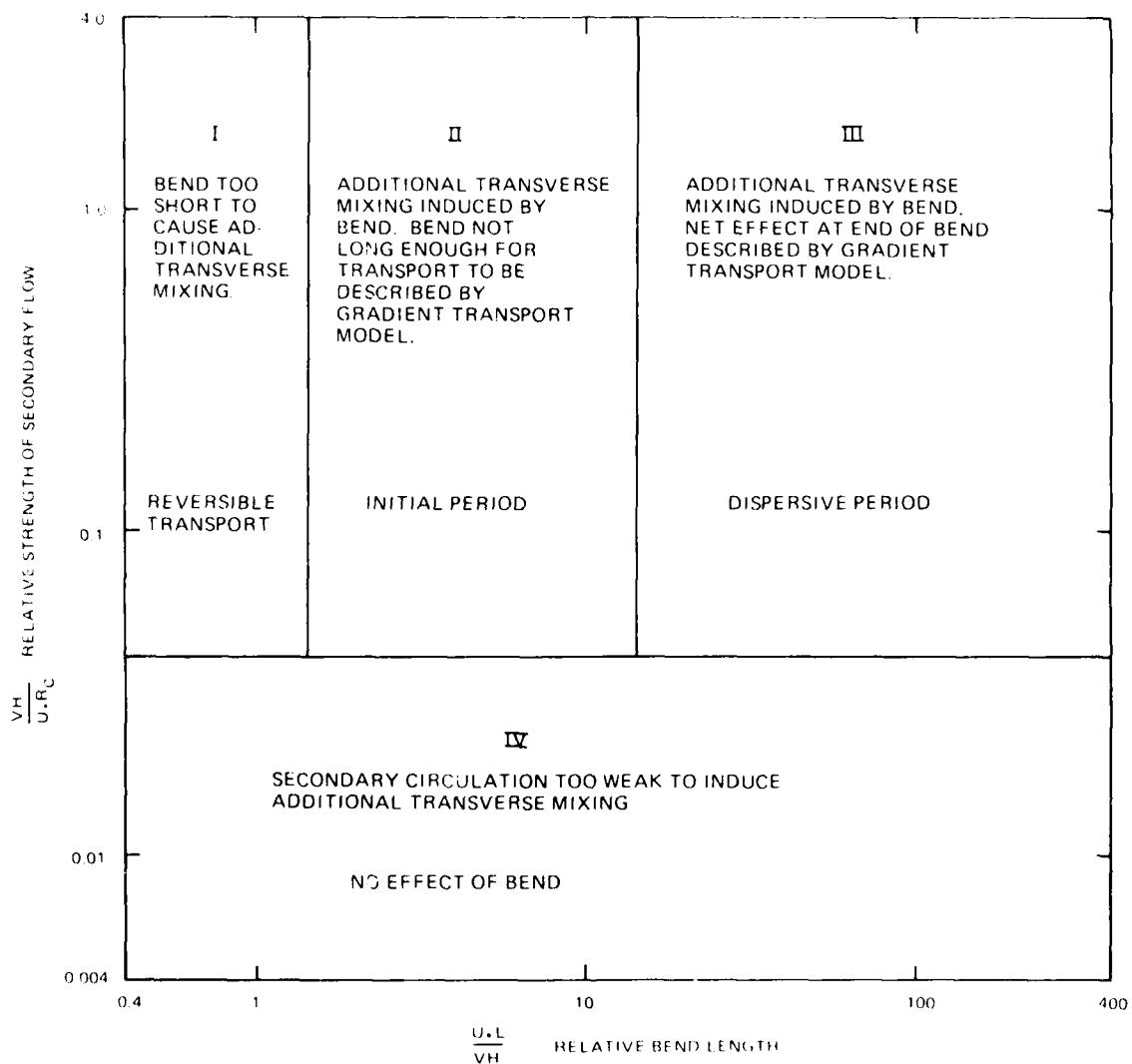
Figure 61. Classification scheme for meandering channels
(after Almquist and Holley 1985)
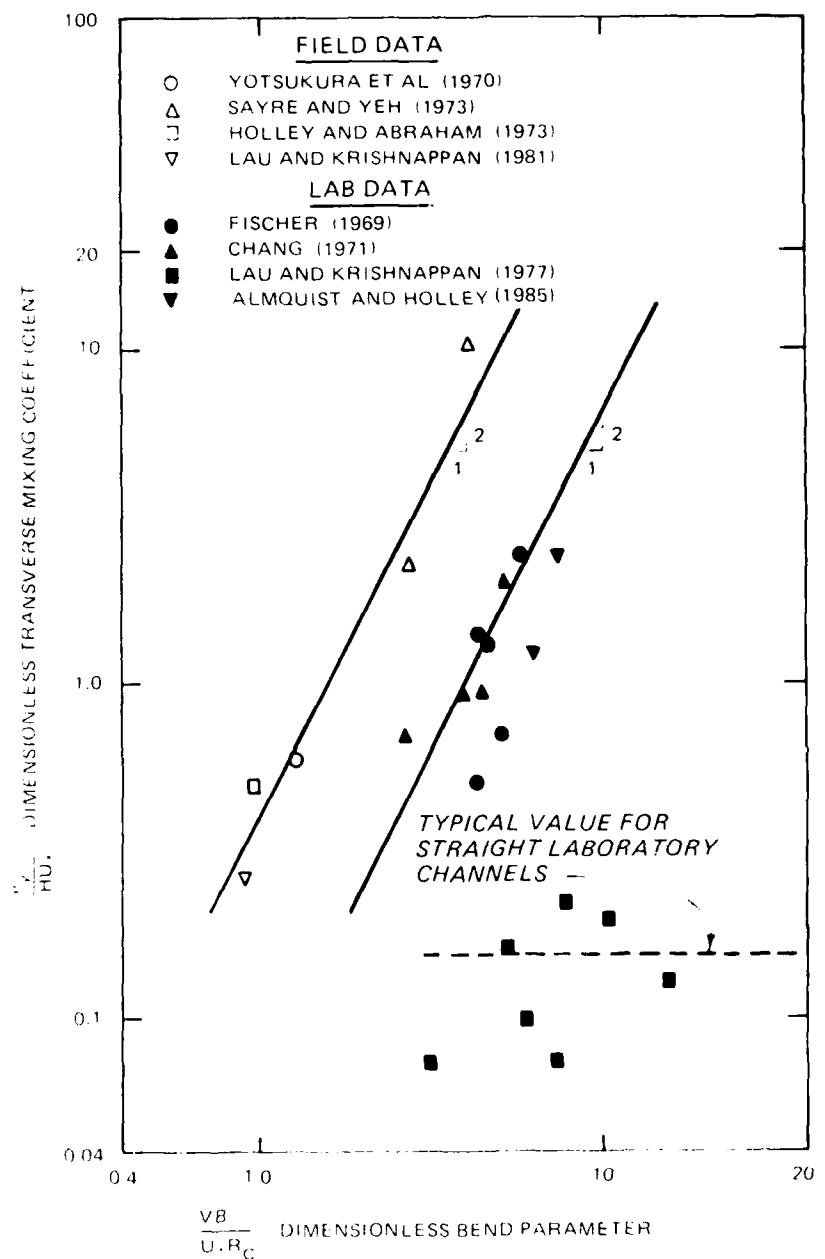
Figure 62. Transverse mixing coefficient in meanders
(adapted from Yotsukura and Sayre 1976)

induce additional mixing. If $\alpha$ for a straight channel is taken as 0.4 (Section 7.4.1b) and if a 10% increase in the mixing coefficient is deemed to be significant, the secondary flow in a given bend may be estimated to have the potential of a significant effect on the mixing coefficient if

$$25 \left(\frac{VH}{U_* R_c}\right)^2 > (0.1)(0.4) \quad \text{or} \quad \frac{VH}{U_* R_c} > 0.04 \tag{7.4.5}$$

Inasmuch as the parameter $(VH/U_* R_c)$ is an indicator of the potential for additional mixing due to circulatory transport, it would be expected that--all other things being equal--larger values of this parameter should be associated with larger mixing coefficients. Other parameters may also be important, however, as discussed below.

If the flow in a given bend is such that the criterion of Eq. 7.4.5 indicates potentially enhanced mixing due to secondary circulation, the question may then be asked whether the bend is long enough for this transport to be described by a gradient transport model, i.e. whether there is enough flow time within the bend for the vertical concentration differences which are generated from the transverse displacement due to the helical motion (Figure 60) to become essentially uniformly mixed over the depth. This time for vertical mixing over the depth in order for gradient-type dispersion to result from the velocity distribution associated with the helical motion is analogous to the time for mixing over the width in the longitudinal dispersion process (Sections 4.8.3 and 6.3.2). For flow through bends, Almquist and Holley (1985) suggested

$$\frac{U_* L}{VH} > 14 \tag{7.4.6}$$

as a minimum criterion for the gradient assumption to apply for the transverse transport. Thus, if the criterion of Eq. 7.4.5 is met,

306

Eq. 7.4.6 provides a criterion for judging whether or not the enhanced transport will be of the gradient transport type.

On the other hand, even if Eq. 7.4.5 is satisfied, a bend may be so short that no significant vertical mixing can take place while a tracer plume passes through the bend. Then, if the secondary flow reverses itself in the next bend, no appreciable net mixing due to secondary circulation takes place since the transverse advection associated with the first bend is just reversed in the second bend (for identical bends). If it is assumed that a bend is too short for additional mixing to take place when the travel time through the bend is less than one-tenth the time required for vertical diffusion over the depth of flow, then Eq. 7.4.6 gives

$$\frac{U_* L}{VH} < 1.4 \tag{7.4.7}$$

as the criterion which indicates that the bend is too short for any net additional mixing to take place through a series of bends, regardless of the value of the secondary flow parameter $(UH/U_* R_c)$, assuming that the downstream bend essentially reverses the helical motion of the previous upstream bend.

The classification scheme described by Eqs. 7.4.5, 7.4.6, and 7.4.7 is summarized in Figure 61. Four regions describing different transverse transport regimes are shown. These are: (I) bend too short to cause additional mixing, regardless of the strength of the secondary circulation; (II) additional mixing caused by secondary circulation but not of gradient transport type; (III) additional mixing caused by the secondary circulations and of a gradient transport type; and (IV) secondary circulation too weak to cause additional mixing.

The classification scheme illustrated in Figure 61 does not, however, include all the parameters which might affect transverse mixing (and circulation-induced mixing in particular) in a river bend. For example, the width-to-depth ratio may have an effect, as the discussion leading up to and following Eq. 7.4.4 demonstrates. (See next

307

paragraph.) Similarly, transverse gradients of depth and bed irregularities may also have an effect on α in bends. The intent of Figure 61 is to determine if a given river bend may reasonably be expected to have the potential for increased lateral mixing due to circulatory transport, and whether or not that transport may be expected to be of a gradient transport type. Because of the other factors which must be involved, the simple fact that two sets of experiments lie near each other in Figure 63 does not imply that they will exhibit the same rates of transverse mixing, a fact which is illustrated in the following discussion.

To consider a possible means of including the effect of channel width on the classification scheme, the analysis leading to Eq. 7.4.5 could be started with Eq. 7.4.4 (which is an empirical scheme for the total α ) instead of Eq. 7.4.3 (which is an analytical expression for Δα for a hypothetical infinitely wide channel). Then, the equivalent of Eq. 7.4.5 for field experiments would be

$$0.4 \left( \frac{VB}{U_* R_c} \right)^2 > 1.1(0.4) \quad \text{or} \quad \frac{VB}{U_* R_c} > 1 \tag{7.4.8}$$

which could be used as an alternate basis for a classification scheme. Nevertheless, the criterion of Eq. 7.4.5 is used in the remainder of the discussion.

This discussion of possible classification schemes for transverse mixing has been given to demonstrate that, even for meanders, the processes are not fully understood nor fully quantified and to provide an aid for classifying and interpreting mixing rates observed in experiments. However, at present, the state-of-the-art is to use a gradient mixing representation (i.e. a diffusion coefficient) for all bends, even the ones in Regimes I and II of Figure 61. Furthermore, the classification scheme itself, although apparently the only rational one yet presented, should be viewed as a preliminary scheme until more data can be obtained.
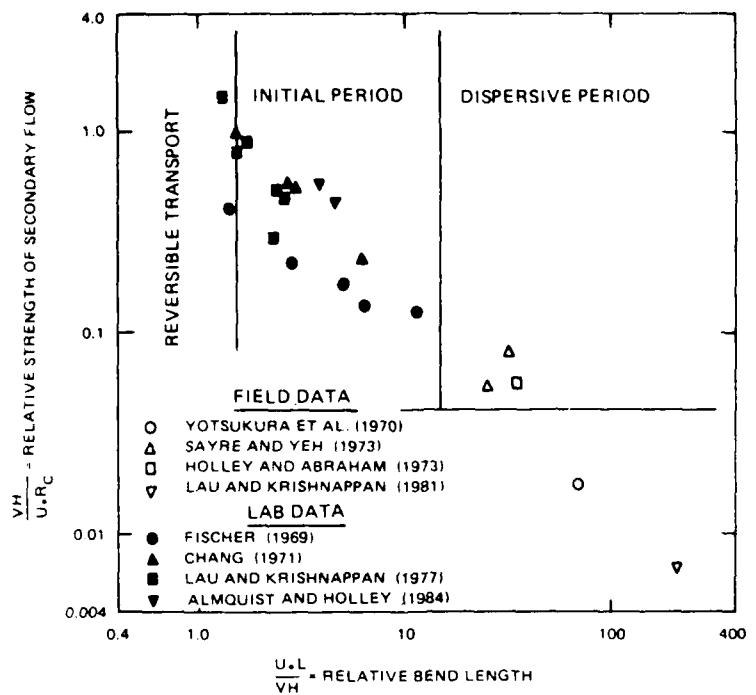
Figure 63. Classification of laboratory and field
experiments in meandering channels (after Almquist
and Holley 1985)

b. Results from laboratory experiments. Pertinent parameters
for laboratory studies on transverse mixing in open-channel flows with
significant curvature are summarized by Almquist and Holley (1985), and
the data are plotted according to the classification scheme in Fig-
ure 63 and according to Yotsukura and Sayre's (1976) correlation shown
in Figure 62.

Fischer (1969) made measurements of transverse mixing in the
circular flume, not a meandering channel; nevertheless, the results are
closely related to the problem at hand. Assuming the bend length, L ,
to be equal to the distance from the point of injection to the last
measurement cross section, Figure 63 shows that Fischer's experiments
should exhibit additional mixing due to secondary circulation, but not
necessarily of the gradient transport type. The α values did in-
crease with increasing values of $VH/U_*R_c$ , showing conclusively that

rate of transverse mixing can indeed be significantly increased by the secondary flow in a bend.

Chang (1971) performed experiments in two meandering flumes with rectangular cross sections and with circular arcs connected by straight tangent sections. The width-to-depth ratios ranged from 4.5 to 7.4; these ratios are small compared to natural streams. Because of the unusually small width-to depth ratio, experimental results from the smaller of the two channels are not included here. Chang's analysis allowed $e_y$ and $\alpha$ to be functions of longitudinal position. He thus was able to quantify the variation in transverse mixing as a function of position along a bend. A plot of the average value of $\alpha$ from six runs as a function of position in the bend is given in Figure 64. The results showed no clearly discernible trend as a function of lateral
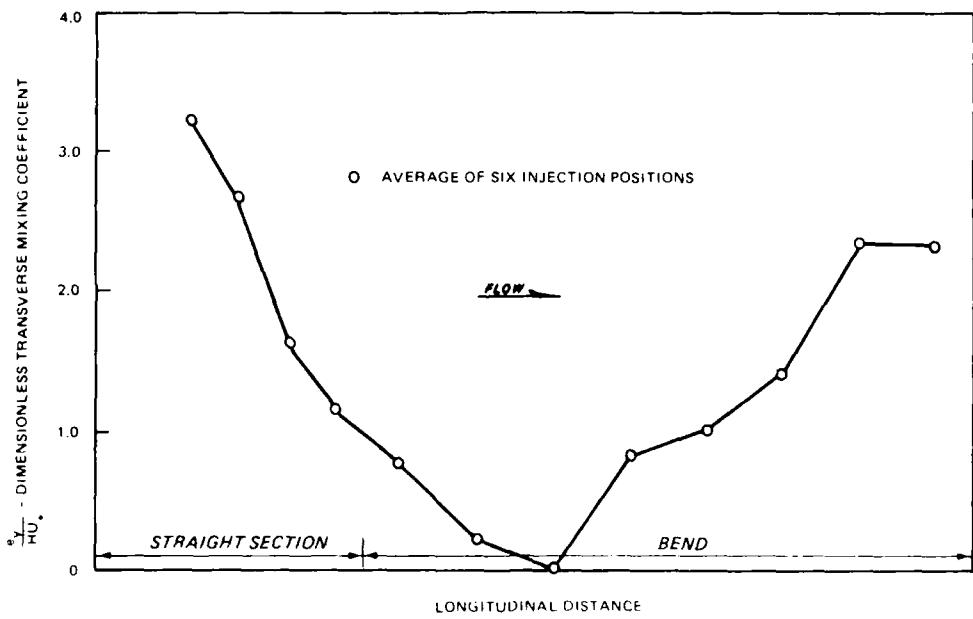


Figure 64. Variation of transverse mixing coefficient
through a bend in Chang's (1970) experiments

source position. In all of Chang's experiments, the maximum values for $\alpha$ were observed near the exit of a bend, while minimum values were observed about one-fourth to one-third of the way into a bend. Chang's data clearly show the effect of meandering, as opposed to a single curve, on the transverse mixing process. Since the secondary flow must

310

change its sense of rotation in going from one bend to the next, it must diminish in strength and then reverse at some point during the transition. At that point, circulatory transport should also diminish, then increase as the secondary flow develops in the downstream bend. The observed values of $\alpha$ are relatively large when compared to those found in natural rivers (Section 7.5.3). Qualitatively, this behavior can be explained by referring to Fig. 7.4.4; Chang's experiments are seen to lie at a relatively large value of $VH/U_*R_c$ compared to the field studies, indicating that secondary flow had a strong influence on transverse mixing in his experiment.

Krishnappan and Lau (1977a, 1977b) performed experiments in relatively small channels, with three plan-form geometries, all of which were sine curves (not the sine-generated curves of Langbein and Leopold 1966) with relatively long, approximately straight sections connected by rather sharp bends. The channel bottom was formed by allowing the flow to shape a sand bottom, and then fixing the equilibrium bed form with a hardening agent. Although the channel bottom was thus "shaped" by the flow, the resulting bottom profiles did not seem to be typical of natural streams. The thalweg always moved completely to the outside bank, with the vertical flume walls meeting the bed below the water surface at nearly right angles; at the crossovers, the flow was also bounded by vertical walls. Only bend-averaged transverse mixing coefficients ($\iota = 0.075$ to $0.225$) were presented. These values are in the same range as those for straight rectangular channels. The bends in Lau and Krishnappan's experiments were relatively short (Figure 63), indicating that most of the effects of secondary circulation in one bend may have been reversed in the next bend. Also, the channels typically had long, approximately straight sections connecting the bends, so that the overall mixing may have been dominated by the turbulent transport characteristics of straight channels. With the definitions of $L$ and $R_c$ being used here, the experiments of Lau and Krishnappan are in the same range of parameters for the other laboratory experiments in Figure 63.

Almquist and Holley (1985) performed transverse mixing experiments in a meandering laboratory channel with circular arcs connected by straight sections. The plan form of their channel was similar to Chang's (1970); Almquist and Holley used both a rectangular cross section and "natural" cross sections which were shaped to give the general features of the natural depth variations found in meandering rivers. They used four injection conditions, namely right and left bank injections at Station 2 (which was in a straight section before a bend to the left), and at Station 6 (which contained the deepest point of the thalweg in a bend to the left). Their experiments were aimed primarily at quantifying and analyzing the various mechanisms contributing to transverse mixing, but they also calculated $\alpha$ values which are shown in Figure 65 for the four tests that are identified by the injection locations as 2R, 2L, 6R, 6L. (Recall that only the average trend is shown in Figure 64 for Chang's data.)

The $\alpha$ values observed by Almquist and Holley were of the same magnitude as those obtained by Chang's experiments. The $\alpha$ values typically peaked between 3.0 and 4.0, and reached a minimum of from -0.2 to 0.4. The peaks typically occurred in the last one-third of a bend, and the minimums occurred in the first one-third of a bend. These general features parallel the trends shown in Figure 64. However, at essentially every point along the channels, $\alpha$ is smaller for the natural channel than for the rectangular channel. The arithmetic average $\alpha$ values for each run are

| Test | $\alpha$ Value Rectangular | Natural |
|------|------------|---------|
| 2L | 3.0 | 1.6 |
| 2R | 1.9 | 1.1 |
| 6L | 2.0 | 1.0 |
| 6R | 1.8 | 1.1 |
| Overall Average | 2.2 | 1.2 |
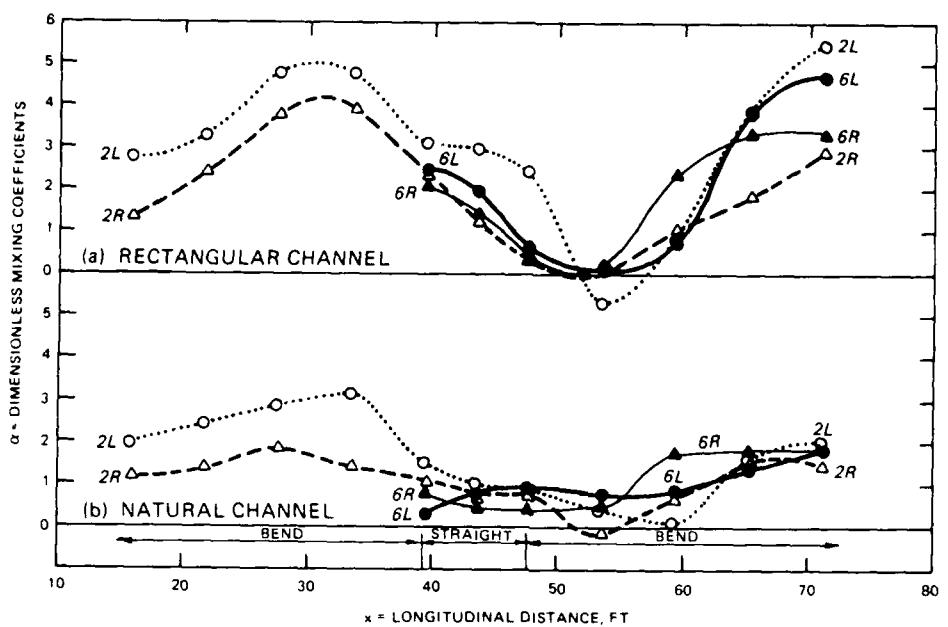
Figure 65. Variations of transverse mixing coefficient through
bends in Almquist and Holley's (1985) experiments

In summary, the laboratory experiments of Fischer (1969), Chang (1970), and Almquist and Holley (1985) show conclusively that secondary circulation in a bend can contribute to transverse mixing. Chang's and Almquist and Holley's experiments show a direct connection between transverse mixing and secondary circulation; those portions of a bend with high secondary circulation were associated with large values of $\alpha$, and vice versa. Almquist and Holley's results show a smaller $\alpha$ for a channel with "natural" cross sections than for a rectangular channel with the same average hydraulic conditions. The experiments of Lau and Krishnappan indicate that if the bends in a meandering channel are too short or if the straight sections of a meandering channel are relatively long, then very little additional transverse mixing due to secondary circulation takes place.

c. Results from field experiments. Although several field experiments for measuring rates of transverse mixing in rivers have been performed, none has been designed specifically to investigate the influence of bends on the transverse mixing process. In fact, only one

313

study (Sayre and Yeh 1973) even attempted to investigate the variation in transverse mixing through a bend.

Almquist and Holley (1985) listed most of the meandering river field experiments which have been reported in the general literature and for which sufficient information on channel geometry and hydraulics were reported to allow the data to be discussed in the framework of the classification scheme in Figure 61. Some other experiments, with less complete data, are also discussed below. The primary purpose in this section is to discuss the $\alpha$ values; the rivers and experiments for some of these tests are discussed in more detail in Section 7.5.

The first study of transverse mixing in a meandering river was reported by Glover (1964) who analyzed temperature distributions downstream of a heated water discharge from a power plant on the Columbia River; Glover reported only that "the river makes a very gradual S-curve" in the reach analyzed. He found $\alpha = 0.72$. This value is comparable to those found for straight rivers with transverse bed slopes or irregular cross sections, as summarized in Section 7.4.1. One possible interpretation is that the bends on the river were not sharp enough to induce additional lateral transport (i.e. that the flow was in Region IV of Figure 61), an interpretation which is in qualitative agreement with the description of the bends as "gradual." Without additional data, a more conclusive interpretation is difficult.

Yotsukura, Fischer, and Sayre (1970) performed a dye experiment in a stretch of the Missouri River containing an S-bend and obtained $\alpha = 0.6$. For the same data, Yotsukura and Cobb (1972) computed $\alpha$ as a function of position in the bends and found that $\alpha$ ranged from 0.34 to 0.65. The only discernible trend was for $\alpha$ to increase somewhat with increasing distance along the bends. Since the cross sections apparently were not irregular, the values of $\alpha$ indicate that transverse bed slopes may have made a significant contribution to the transverse mixing. This conclusion is qualitatively supported by locating the parameters for this study in Figure 63; it can then be seen that the relative strength of the secondary flow for this reach was probably not great enough to cause significant additional mixing.

314

Sayre and Yeh (1973) performed a dye experiment on a reach of the Missouri River with significant curvature. Their results yielded an average $\alpha$ of 3.4. By the classification scheme of Figure 63, the experiments were performed in a bend with sufficient circulation to cause additional mixing and with sufficient length that the additional mixing could be described by a gradient transport model, at least by the end of the bend. The observed dimensionless dispersion coefficients are the largest of the field data reviewed in this chapter. The data of Sayre and Yeh do, however, follow the general trend of the field data presented in Figure 62.

Holley and Abraham (1973) conducted separate experiments with left-bank and right-bank injections in the IJssel River (The Netherlands). The average trend of the data yielded $\alpha = 0.5$. According to the classification scheme of Figure 63, the IJssel River reach should be similar in mixing properties to the reach of the Missouri River used in the experiments of Sayre and Yeh. However, the nondimensional mixing coefficient of $\alpha = 0.5$ is smaller than that found by Sayre and Yeh and is, in fact, more typical of a relatively straight river with irregular geometry or with significant transverse bed slopes. One significant difference between the two rivers is the width-to-depth ratio; for the Missouri River $B/H \approx 50$, whereas for the IJssel River, $B/H \approx 19$. When plotted in Figure 62, which takes the width-to-depth ratio into account, the data of Holley and Abraham follow the general trend of the field data.

Lau and Krishnappan (1981) conducted a dye experiment on the Grand River (Ontario). The $\alpha$ values ranged from 0.18 to 0.39, with an average of 0.27. These values indicate that the effects of secondary circulation on transverse mixing was small; this conclusion is qualitatively supported by Figure 63, where it can be seen that the relative strength of the secondary currents in this bend was probably small. It also appears that there was a relatively small contribution from transverse bed slopes or irregular cross sections since the average $\alpha$ is about the same as that found in artificial canals (Section 7.4.1b).

315

### 7.4.3 Synthesis and Summary

In straight uniform channels, the primary transverse mixing mechanism is turbulent diffusion; dimensional and theoretical considerations show that $e_y$ can be related to hydraulic properties by $e_y = \alpha\, U_* H$ . In laboratory experiments, $\alpha$ shows some increase with increasing width-to-depth (B/H) ratio, with $\alpha$ ranging from about 0.1 to 0.25. Field experiments on very straight canals with relatively constant depths yield $\alpha$ values from about 0.2 to 0.3.

Field experiments in "straight" rivers (not canals) and laboratory experiments in nonrectangular channels yield higher values of $\alpha$ ranging from 0.27 to 0.75. In such relatively straight channels, at least three possible mechanisms for the increased lateral mixing can be identified:

<u>a</u>. Groins or other large side-channel irregularities may generate large-scale turbulence (Holley and Abraham 1973).

<u>b</u>. The variation of depth with transverse position may generate transverse gradients of longitudinal velocity, and these gradients may increase the horizontal scale of turbulence. Such a mechanism may have caused the increased lateral mixing in, for instance, the IJssel River model of Holley and Abraham (1973).

<u>c</u>. Large-scale bottom irregularities, such as sandbars or islands, which may cause local splitting and intertwining of the flow, causing additional net transverse spreading of a tracer in a manner similar to that observed in dispersion in a porous medium. This mechanism probably contributed to the relatively high mixing coefficient observed by Beltaos (1980) in the Athabasca River.

In meandering channels, a fourth mechanism, namely the helical secondary flow induced in a river bend can contribute to transverse mixing. To accomplish this increase, the bend must be "curved enough" to induce significant secondary currents and it must be "long enough" for vertical mixing to interact with the secondary currents to produce irreversible lateral mixing. "Curved enough" and "long enough" are defined in Section 7.4.2a in conjunction with a classification scheme

for meandering rivers. Even if the secondary currents can induce additional lateral mixing, a gradient transport model strictly applies only after an initial period for shear dispersion in the bend (although, at present, it is common practice to use a gradient or diffusive model for all bends for engineering calculations).

Yotsukura and Sayre (1976) and Sayre and Caro-Cordero (1979) reasoned that the width-to-depth ratio should be an important parameter for lateral dispersion, and included this parameter in an empirical correlation which was based on Fischer's (1969) analysis. The correlation that they found, extended by the inclusion of more recent data, supports this hypothesis, although field and most laboratory data follow different trends. A possible explanation for this fact lies in Figure 63. All of the laboratory experiments were conducted in channels for which the relative bend lengths $(VH/U_*L)$ were less than about 12; on the other hand, the relative bend lengths for the river experiments were all greater than 30. According to the classification scheme (Figure 61), this indicates that the transverse mixing observed in the field experiments may have been of the gradient transport type, whereas that observed in the laboratory experiments probably was not. Thus, the fundamental difference between the two sets of data in Figure 60 may not be a difference between laboratory and field, but rather a difference between small and large values of $VH/U_*L$ .

In the laboratory, Chang's (1971) and Almquist and Holley's (1985) experiments provided details on transverse mixing in a meandering channel capable of inducing lateral mixing due to secondary currents. They found that secondary currents increased overall mixing considerably, with minimum rates of mixing being observed near the entrance of a bend and maximum rates being observed near the exit. In laboratory channels, typical measured local values of $\alpha$ have ranged from 0 to 5 for rectangular channels and 0 to 3 for a channel with "natural" cross sections.

Field data on transverse mixing is also sparse. Only Sayre and Yeh (1973) investigated the variation of $\alpha$ along a bend. Their field results were in qualitative agreement with the laboratory results. The

317

average value they found for $\alpha$ was 3.4. Other experiments on river reaches which included bends showed lower values of $\alpha$, ranging from 0.26 to 0.6; the lower values can generally be explained by the fact that the secondary currents in the bends were probably not strong enough to induce significant additional mixing.

All investigators have analyzed their data using gradient transport models with $\alpha$ values being obtained using either a change-of-moments analysis or a simulation method.

## 7.5 EXAMPLES OF FIELD EXPERIMENTS ON TRANSVERSE MIXING

In this section, some examples of field experiments are summarized (in chronological order according to the dates of publication). This summary is not intended to be an exhaustive coverage of previous related field work. There is a more comprehensive summary of experimental values of $\alpha$ in Section 7.4 for both laboratory and field experiments. The purpose of this section is to give some examples of the types of data that have been collected and the types of analyses that have been performed. Although several field studies have been conducted, many of them did not have data on both the hydraulics (including slope or resistance coefficient) and the concentration at each measurement cross section. Thus, it has not been possible to apply some of the more recent techniques for data analysis to some of the earlier data sets.

### 7.5.1 Missouri River (Yotsukura, Fischer, and Sayre 1970)

In 1967, Yotsukura, Fischer, and Sayre (1970) conducted a field experiment in a 33,000-ft-long reach of the Missouri River about 85 miles downstream of Sioux City, Iowa. As shown in Figure 66a, this is a gently meandering reach. Hydraulic data were collected at only two cross sections (Figure 66b), with one being in a bend and the other one being near a crossover. The channel width was maintained at 500-800 ft by a system of dikes and jetties. The depth at the thalweg was generally less than 25 ft. The flow rate was about 33,000 cfs, with a Manning's n of about 0.020. According to the criteria of

318
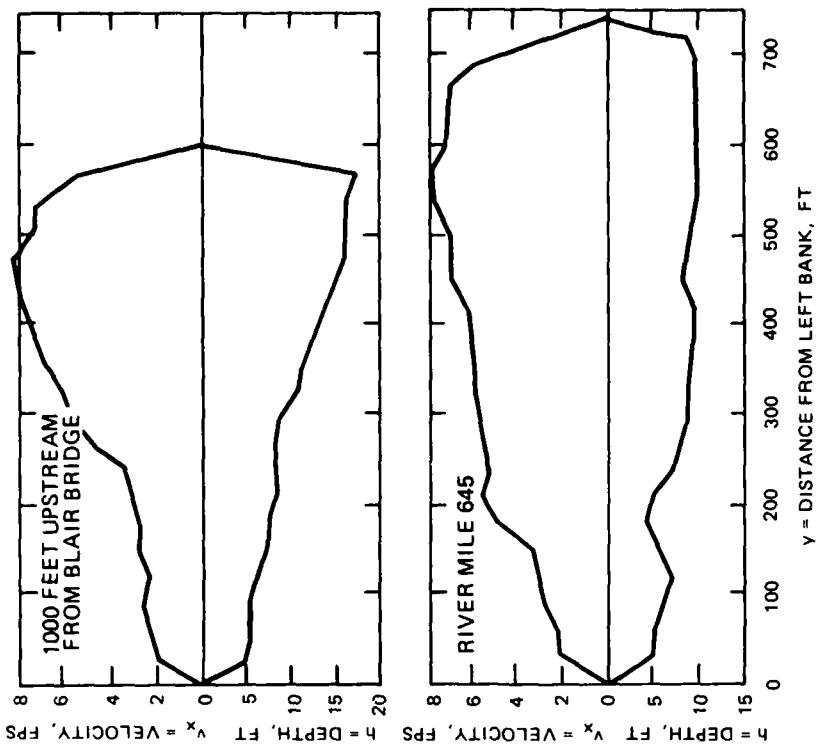
b. Depth and velocity profiles

a. Test reach

Figure 66. Data for Missouri River study on transverse mixing
(after Yotsukura, Fischer, and Sayre 1970) (Continued)

319
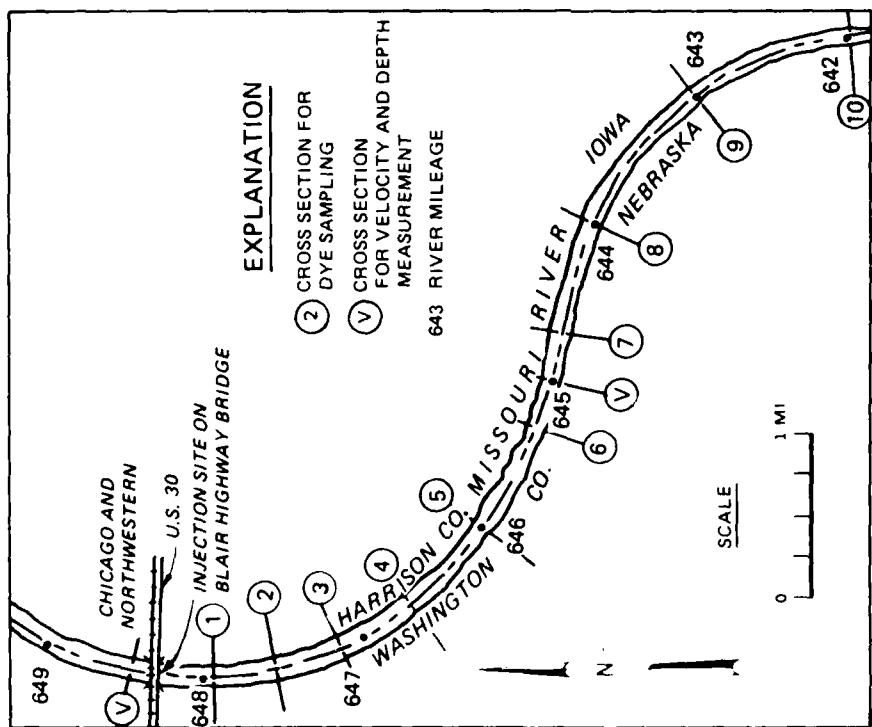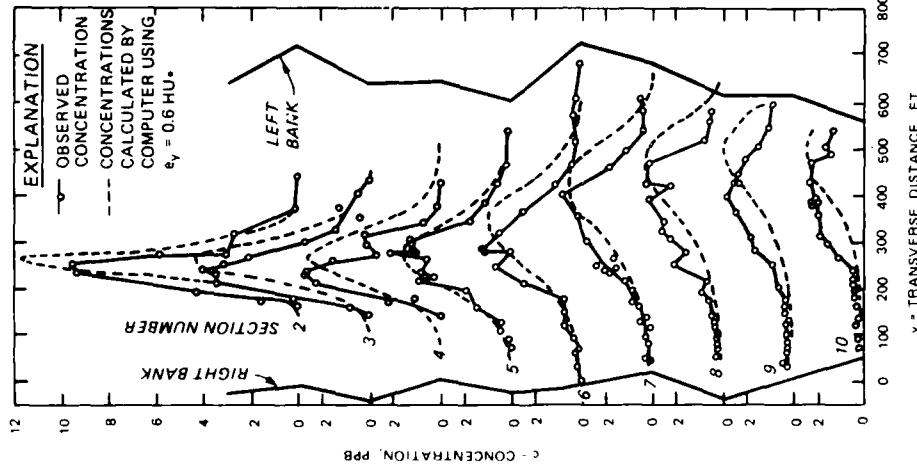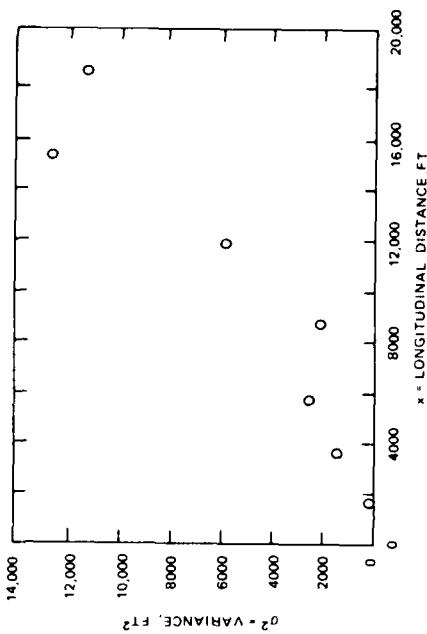
d. Variance of transverse tracer distribution



c. Measured and calculated transverse distributions of concentration

Figure 66. (Concluded)

320

Almquist and Holley (1985), the bends in this reach are gentle enough that the helical secondary motion probably did not contribute significantly to the transverse mixing. Based on approximate values of $B = 625$ ft , $H = 10$ ft , and $n = 0.02$ , the last measurement cross section corresponds to $x_d$ (Section 5.3.2) of 0.03.

The tracer (Rhodamine BA) was injected in the central region of the river for about 4 hours using a 50-gal mariotte vessel. Concentration samples were collected at 10 cross sections, with the transverse sampling locations being determined by triangulation from the shore during sample collection. The recovery ratios (integrated tracer flux divided by the mass injection rate) at the 10 cross sections were 1.34, 0.58, 0.58, 0.49, 0.65, 0.56, 0.66, 0.64, 0.60, 0.58, respectively, for sections 1-10. The concentration distributions, after correction for dye loss, are shown in Figure 66c. The data show that the maximum concentration migrated toward the left bank (which is on the right side of the figure).

Even though it is not really desirable (as the authors pointed out) to make the assumption of a rectangular cross section for a natural channel, this assumption was used by Yotsukura, Fischer, and Sayre (1970) for a preliminary analysis of the data using the method of moments (Section 7.3.4). The variances obtained from the transverse distributions of concentration are shown in Figure 66d. The primary analysis was done using the simulation method (Section 7.3.3) with 20 streamtubes and with the assumption of a constant $e_y$ . The velocities, depths, and widths were estimated from the available measurements. The initial conditions were taken from the measurements at cross section 1. It was concluded that $\alpha = 0.6$ gave the best agreement between the measurements and the calculations, which are also shown in Figure 66c. The degree of agreement between measurements and calculations was undoubtedly affected by the need to estimate the hydraulic characteristics, by the fact that the measurements gave instantaneous rather than time-averaged concentrations, and by the assumption of a constant $\alpha$ for the entire reach.

## 7.5.2  IJssel River (Holley and Abraham 1973)

In 1970, Holley and Abraham (1973) conducted two transverse mix-
ing tests on a 3900-meter-long reach of the IJssel River in the eastern
part of The Netherlands (Figure 67a).  (More detailed information on
these tests and similar tests in other rivers is given by Holley 1971.)
The discharges were 282 $m^3$/sec during the first test (right-side injec-
tion) and 268 $m^3$/sec during the second test (left-side injection).  The
Chezy coefficient was 40 $m^{1/2}$/sec.  The average area and depth were
278 $m^2$ and 4.0 m.  The depth profiles for the measurement cross sec-
tions are shown in Figure 67b.  The banks were protected by groins
(dikes) in the upstream part of the reach.  In the new channel down-
stream of cross section 5, the banks were lined with stones.  According
to the criteria of Almquist and Holley (1985), the bends in this reach
are gentle enough that the helical secondary motion probably did not
contribute significantly to the transverse mixing.  The value of $x_d$
for the last measurement cross section was about 0.13.  (Holley 1971
reported more limited measurements to $x_d = 0.26$ for the left-side
injection.  See Figure 67e.)

The tracer (Rhodamine WT solution prepared from crystals) was
injected from a mariotte vessel, with the injection tubes being posi-
tioned at the end of a groin for both injections.  The recovery ratios
could not be determined accurately because of recrystallization of the
dye due to cold weather and because of an apparent error in calculation
of the injection rates.  The integrated tracer flux for the left-side
injection did show a rather consistent decrease, with the value at the
end of the reach being approximately 70% of that at the beginning of
the reach.  Transverse distances were measured with an optical range
finder approximately 1 m long.  The concentration measurements for the
right-side injection are shown in Figure 67c.  As mentioned previously,
the concentration fluctuations decreased as the transverse gradients
decreased.  The concentration distributions shown in Figure 67d repre-
sent the data trend determined from 2-minute averages of the concentra-
tion readings.  Also, the concentrations have been scaled to give the
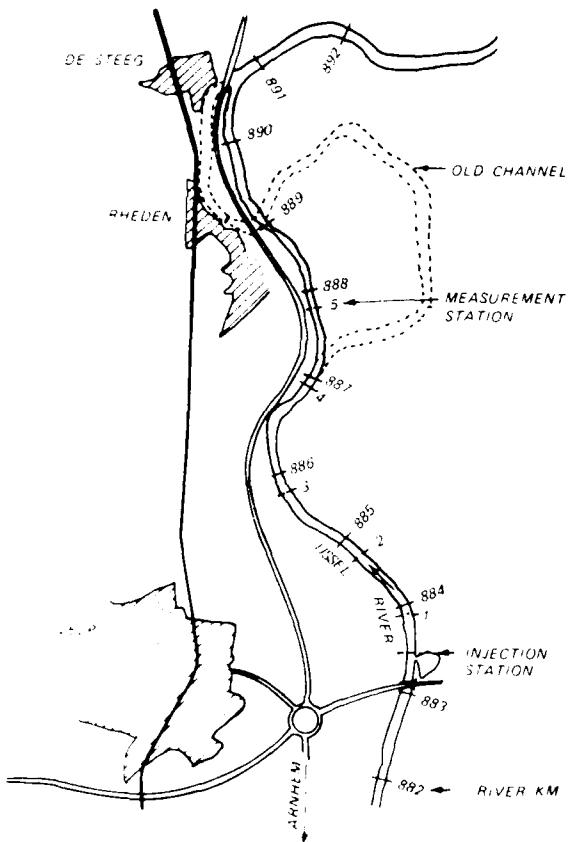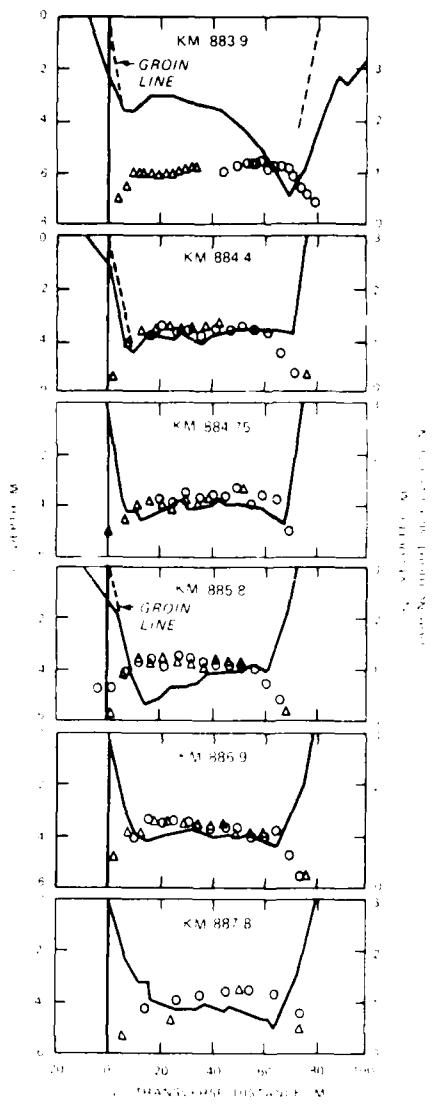
a. Test reach          b. Depth and velocity profiles

Figure 67.  Data form IJssel River study on transverse mixing
(after Holley and Abraham 1973) (Sheet 1 of 4)

323
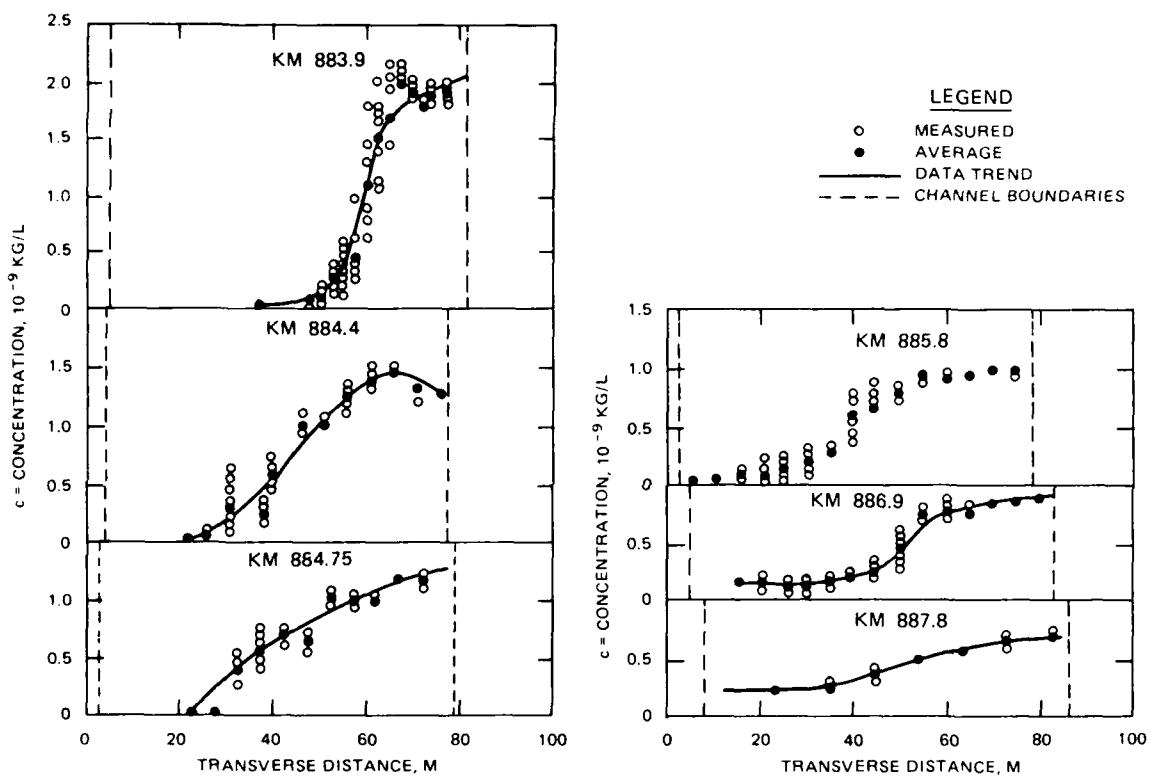
c. Concentration measurements for right-side injection

Figure 67. (Sheet 2 of 4)
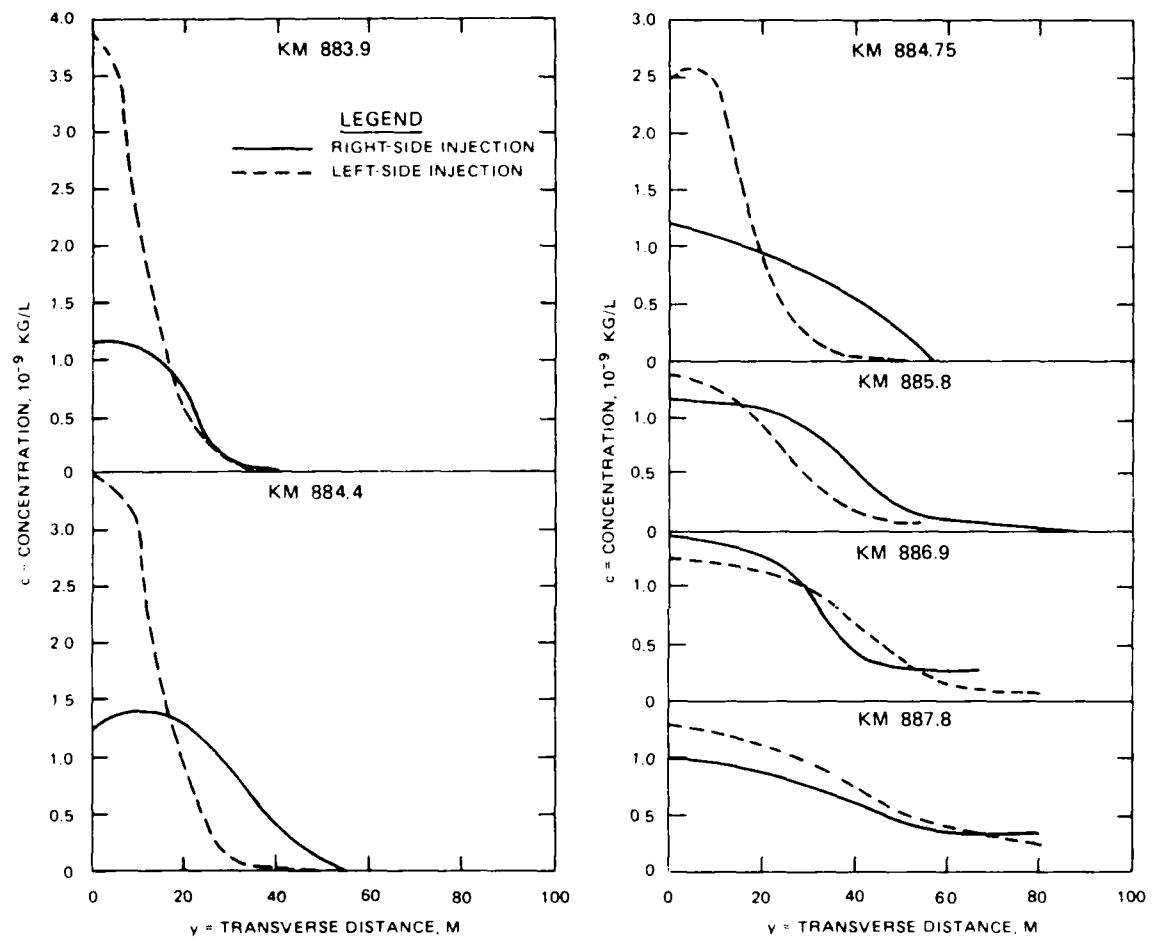
d. Comparison of concentration distributions from right
and left injections

Figure 67. (Sheet 3 of 4)
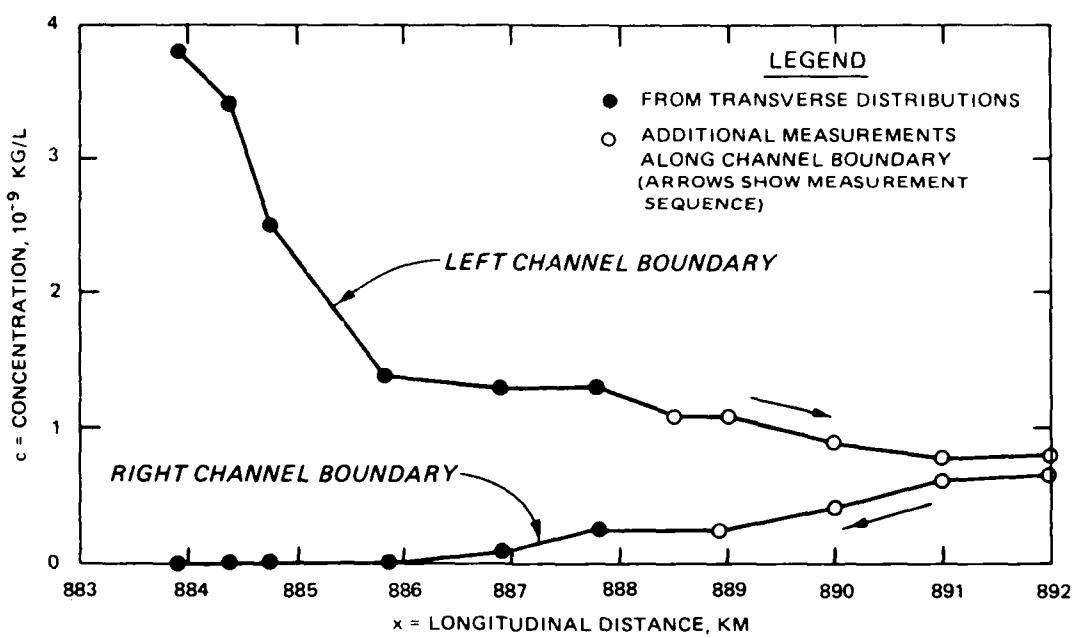
e. Concentrations at channel boundaries for
left-side injection
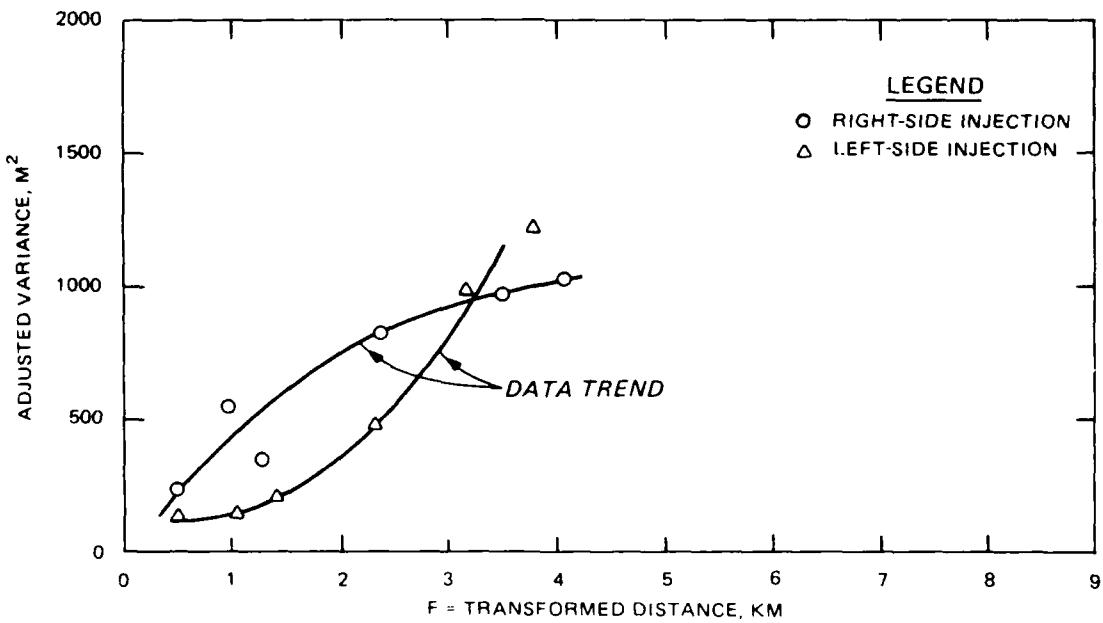


f. Generalized change of moments analysis

Figure 67. (Sheet 4 of 4)

same tracer flux for all cross sections for both injections. The distributions show the higher concentrations for the left injection due to the smaller depths and velocities on the left side downstream of the injection location. Also, the different rates of transverse spreading can also be seen, particularly at cross sections 2, 3, and 4.

The data were analyzed by the generalized change-of-moments method (GCM, Section 7.3.4). Even using the GCM method, the trends of the variance versus distance curves (Figure 67f) showed a definite correlation with the channel curvature, with the trends being concave downward for the right-side injection and concave upwards for the left. The two curves formed a loop; taking the average slope gave an average $\alpha$ of 0.5.

### 7.5.3 Missouri River (Sayre and Yeh 1973)

In 1972, Sayre and Yeh (1973) conducted a transverse mixing test that provided an extensive set of field data for a strongly meandering river in which the helical motion contributed significantly to the transverse mixing. The test reach, as shown in Figure 68a, was about 32,500 ft long. The channel width was maintained at 700 to 900 ft by dikes and jetties. The average depths of the channel and thalweg were about 13 ft and 22 ft, respectively. The discharge was 56,100 cfs. The measured depth and velocity profiles are given in Figure 68b, with the velocities having been measured 3 ft below the water surface. The figure also shows relative values of the discharge per unit width; these values can be integrated from one bank to any transverse position (y) to obtain the value of the cumulative discharge (q) at that $y$ . The average slope for the test reach was 0.00019, giving n = 0.018 , using an average width of 700 ft determined from the depth profiles in Figure 68b. Using an average $\alpha$ of 3.3, the last measurement cross section corresponds to $x_d$ of 0.11.

The tracer (Rhodamine WT solution) was introduced into the cooling water from the power plant using two mariotte vessels made from 55-gallon drums. The injection continued for about 5.5 hours. The cooling water flow, which was about 2.6% of the total river flow,

327
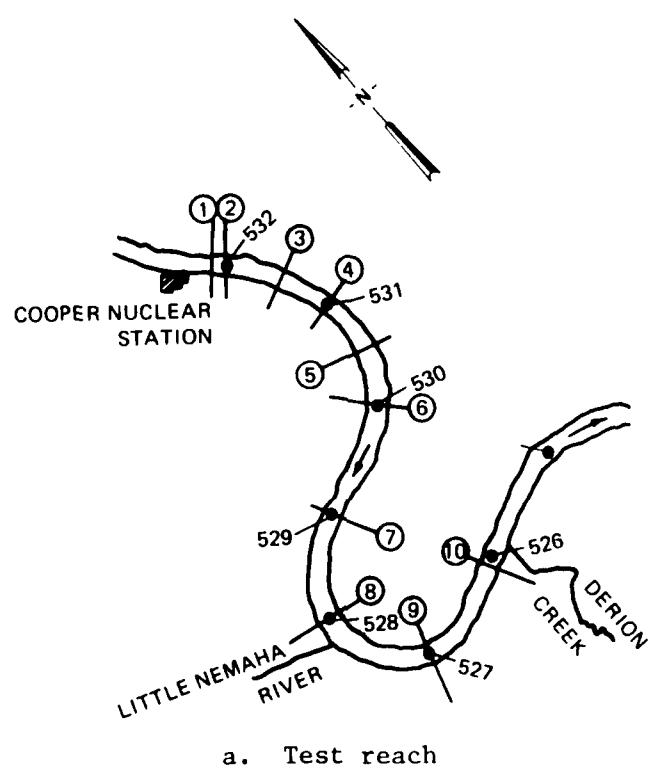
a. Test reach

Figure 68. Data from Missouri River study on transverse
mixing (after Sayre and Yeh 1973) (Sheet 1 of 5)
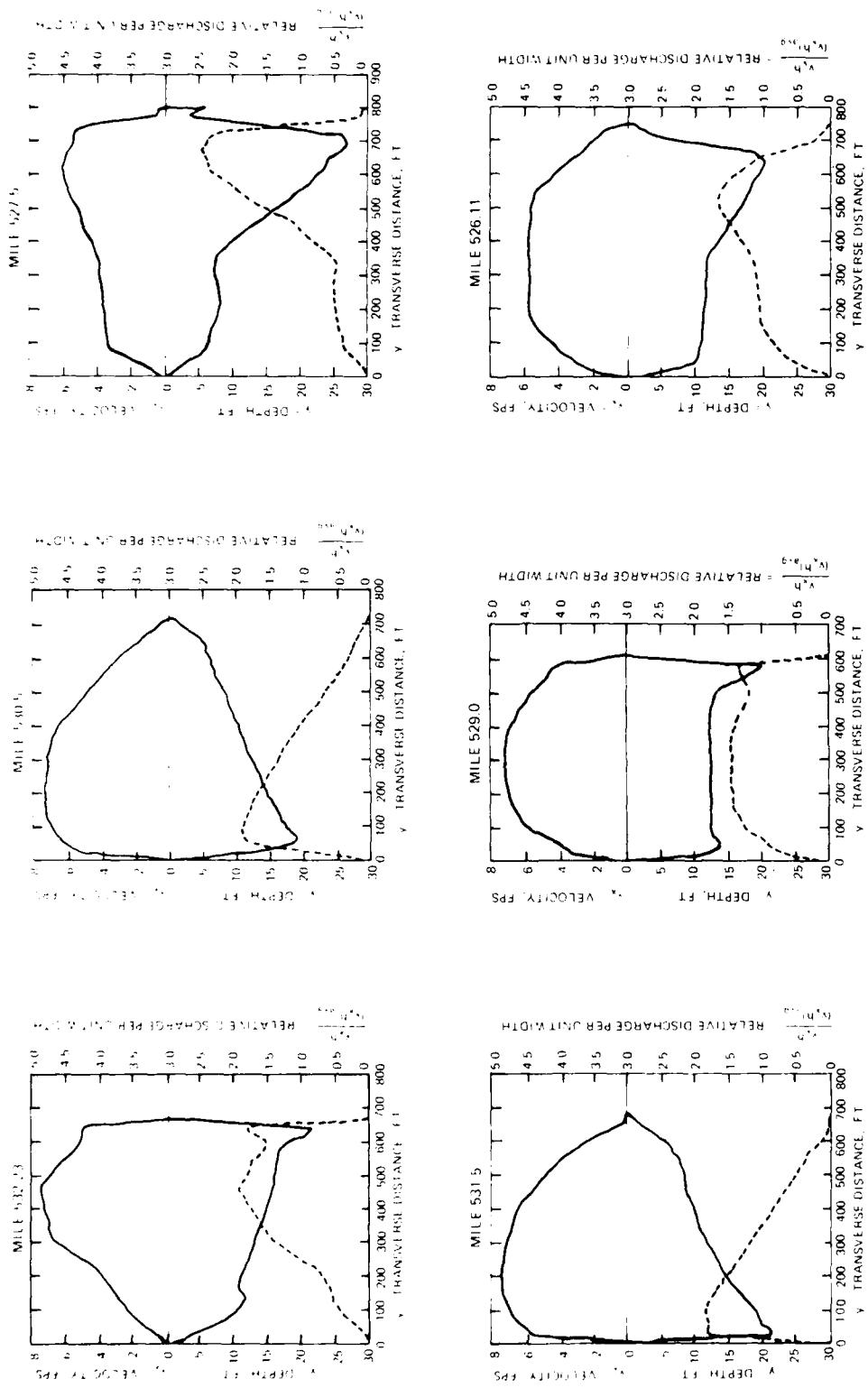
b. Depth, velocity, and discharge distributions

Figure 68. (Sheet 1 of 5)

329
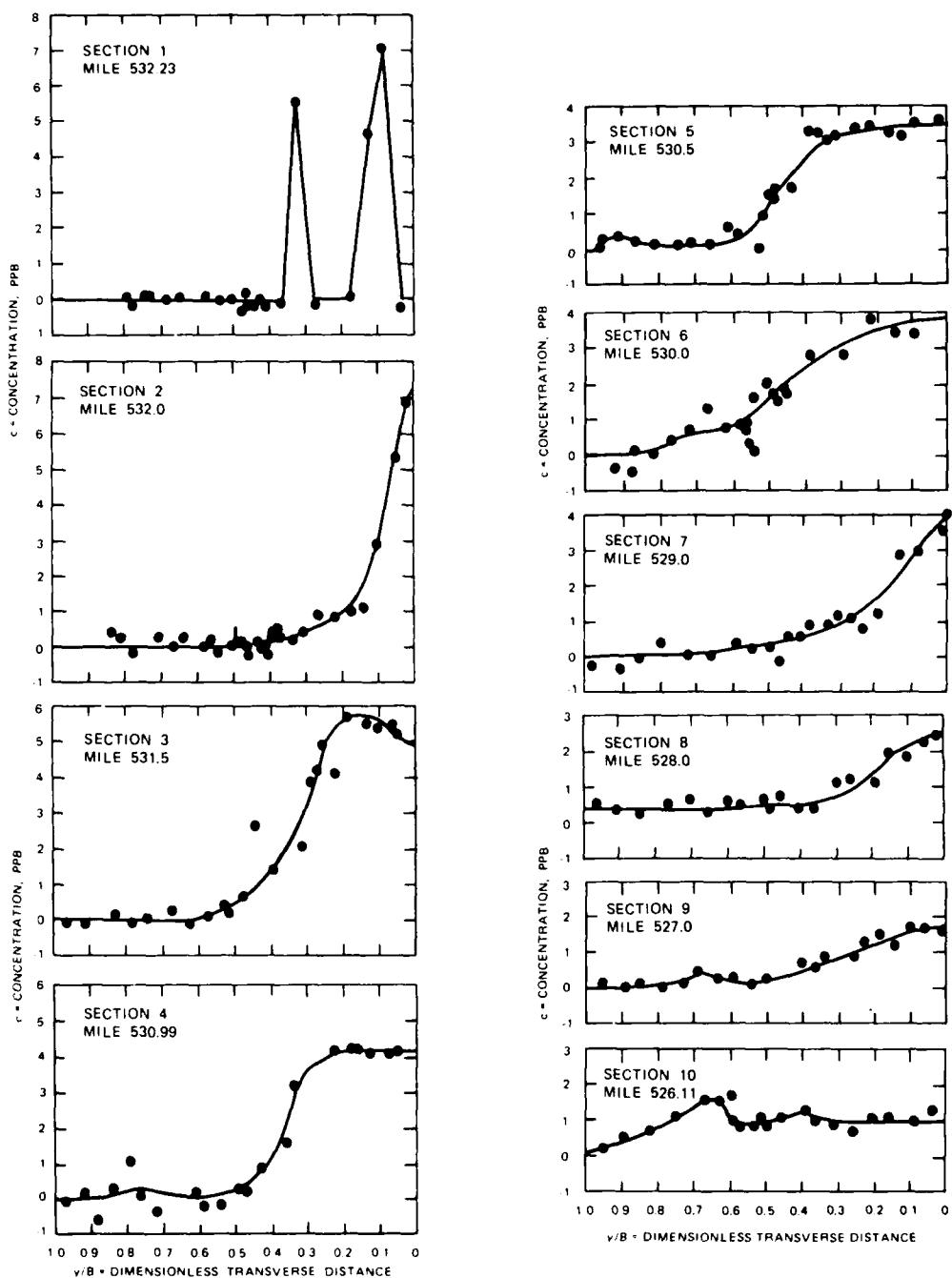
c. Concentration measurements (as a function of transverse distance)

Figure 68. (Sheet 3 of 5)
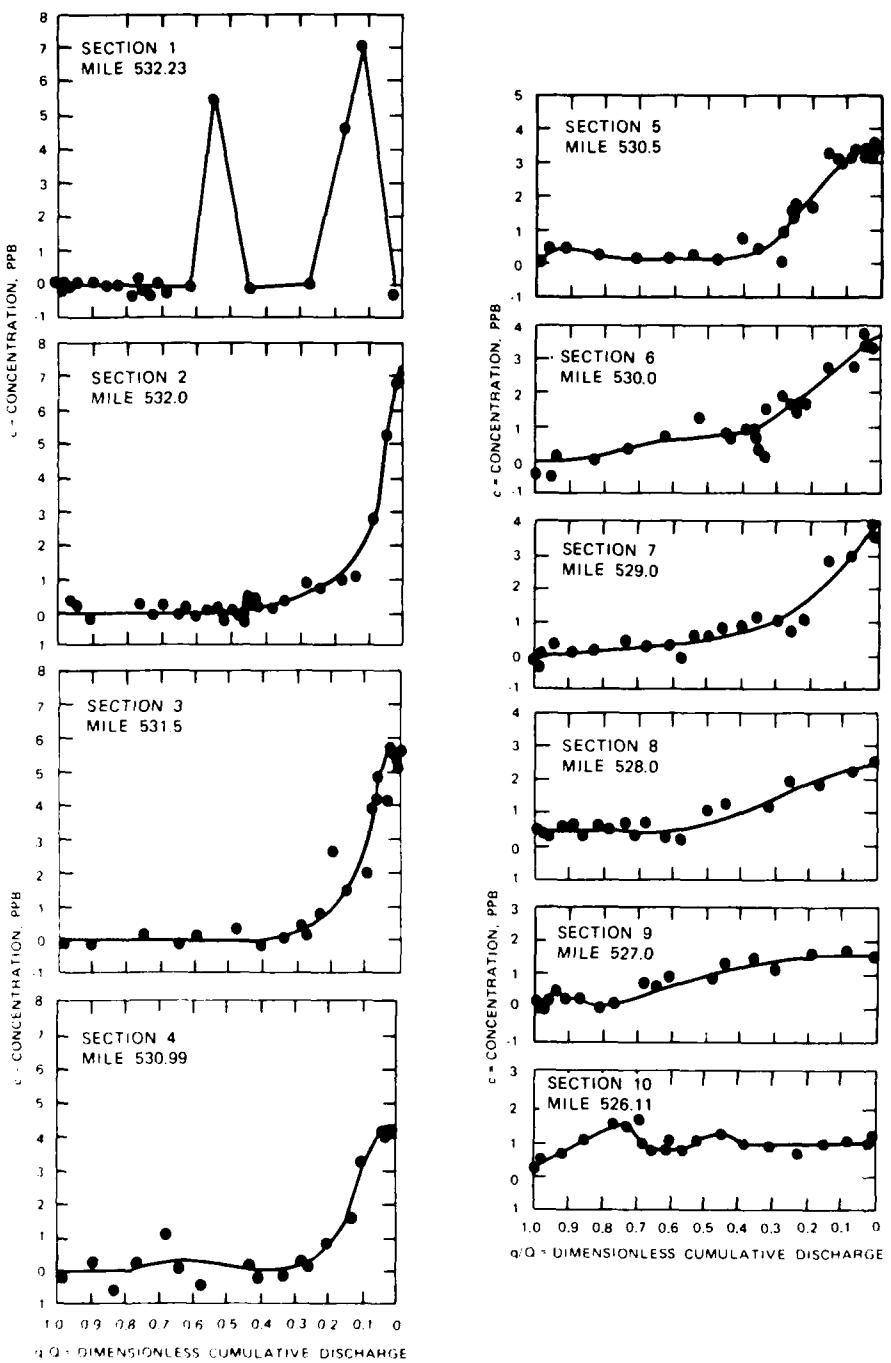
d.   Concentration measurements (as a function of
cumulative discharge)

Figure 68.   (Sheet 4 of 5)

331
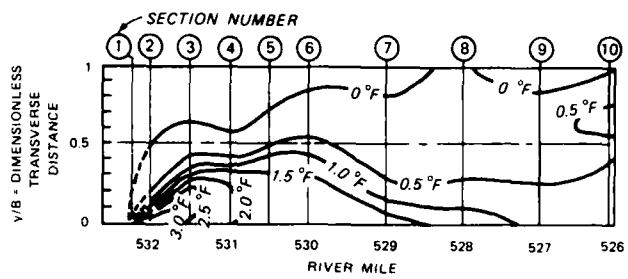
e.  Excess temperature isotherms based on dye experiment
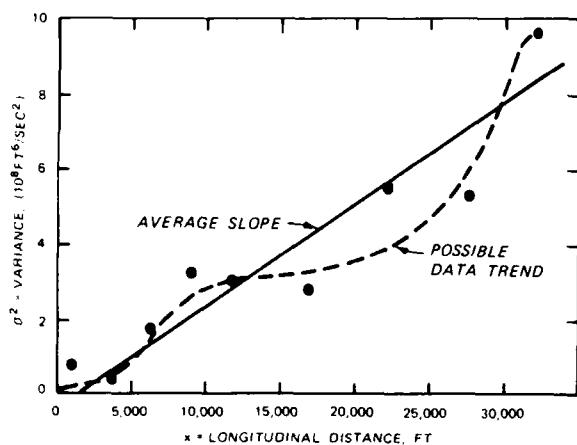


f.  Variances
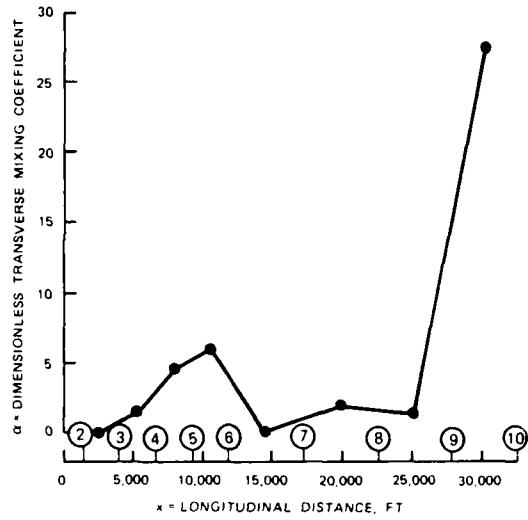


g.  Dimensionless transverse
mixing coefficients
determined by simulation
method

Figure 68.  (Sheet 5 of 5)

332

entered at the right bank of the river with essentially no initial mixing due to either momentum or buoyancy. Grab samples for concentration distributions were collected at 10 cross sections. Transverse locations during the sampling were determined by triangulation using the same methods reported by Yotsukura, Fischer, and Sayre (1970). For the four cross sections (nos. 3, 5, 7, and 10) for which both hydraulic data and concentration data were collected, the recovery ratios were 0.71, 0.91, 0.99, and 1.05, proceeding in the downstream direction. The concentration distributions are shown in Figures 68c and 68d with the concentrations plotted against both relative transverse distance and cumulative discharge. The curves through the data points are the ones drawn by Sayre and Yeh. Apparently, the concentrations in these figures were not corrected for dye loss. The concentrations were also used to construct isotherms, as shown in Figure 68e. These isotherms demonstrate the influence of net transverse velocities on transverse distributions. For example, between cross sections 6 and 8, a significant part of the flow moves from the left side of the channel to the right side due to the changes in depth and velocity distributions associated with the bends. The effects can be seen, for example, in the 0.5° F contour which moves toward the right bank between cross sections 6 and 8. Then, as the flow comes out of the second bend, the 0.5° F contour starts moving back toward the left bank.

In addition to using the data to study the isotherms, transverse mixing coefficients were determined using essentially the same simulation approach as Yotsukura, Fischer, and Sayre (1970). The resulting values of $\alpha$ are shown in Figure 68g. This is the only known field study (for a river with a significant influence from channel curvature) where enough data were collected to allow investigation of the variation of $\alpha$ through individual bends. Concerning the variation of $\alpha$ shown in Figure 68g, Sayre and Yeh stated that "the two maxima occur toward the downstream ends of the two bends, and that the minima occur at about the beginning of the first bend and in the relatively straight reach between the first and second bends. This is consistent with the results obtained in Chang's (1971) laboratory flume experiments..."

333

The results are also generally consistent with the laboratory experiments of Almquist and Holley (1985), as discussed in Section 7.4.2b. The value of $\alpha$ of 27 between sections 9 and 10 is the largest reported in the literature, and perhaps should be viewed with caution until additional data can be obtained for similar bends.

Sayre and Yeh also calculated the variances of the concentration distributions with respect to q (Figure 68f). Even using q , they found that the variances sometimes decreased in the downstream direction. The average slope of the variance versus distance curve was used as a preliminary guide for the selection of the values of $e_y$ to be tried in the simulation.

### 7.5.4 Athabasca River (Beltaos 1980)

In 1974, Beltaos (1980) conducted a transverse mixing test in the Athabasca River using a slug injection and the integrals of the concentration versus time curves, as mentioned in Section 7.1.1. (The data and figures used here were taken from Beltaos 1978, which served as the basis for the 1980 reference.) The study reach, which is shown in Figure 69a, was 37 km downstream of Fort Murray, Alberta, and was 17.6 km long. As the figure shows, this is a rather straight reach with interspersed patches of mud, sand, and weeds giving an irregular variation of the cross-sectional size and shape (Figure 69a). It appears from Figure 69b that most of the measurement cross sections may have been placed at relatively unobstructed locations. Velocity profiles were measured at sections O, B, C, D, and F, and were simulated at the other cross sections using Yotsukura and Sayre's (1976) power-law relation between discharge per unit width and local depth. The discharge was 776 $m^3$/sec with an average area of 820 $m^2$, a width of 373 m, a depth of 2.20 m, a velocity of 0.95 m/sec, a shear velocity of 0.056 m/sec, and a friction factor of 0.028.

The tracer (Rhodamine WT) was dumped 85 m from the left bank, corresponding to a relative cumulative discharge of 0.5. Concentration versus time distributions were measured at various longitudinal and transverse positions. (A sample of such distributions is given in
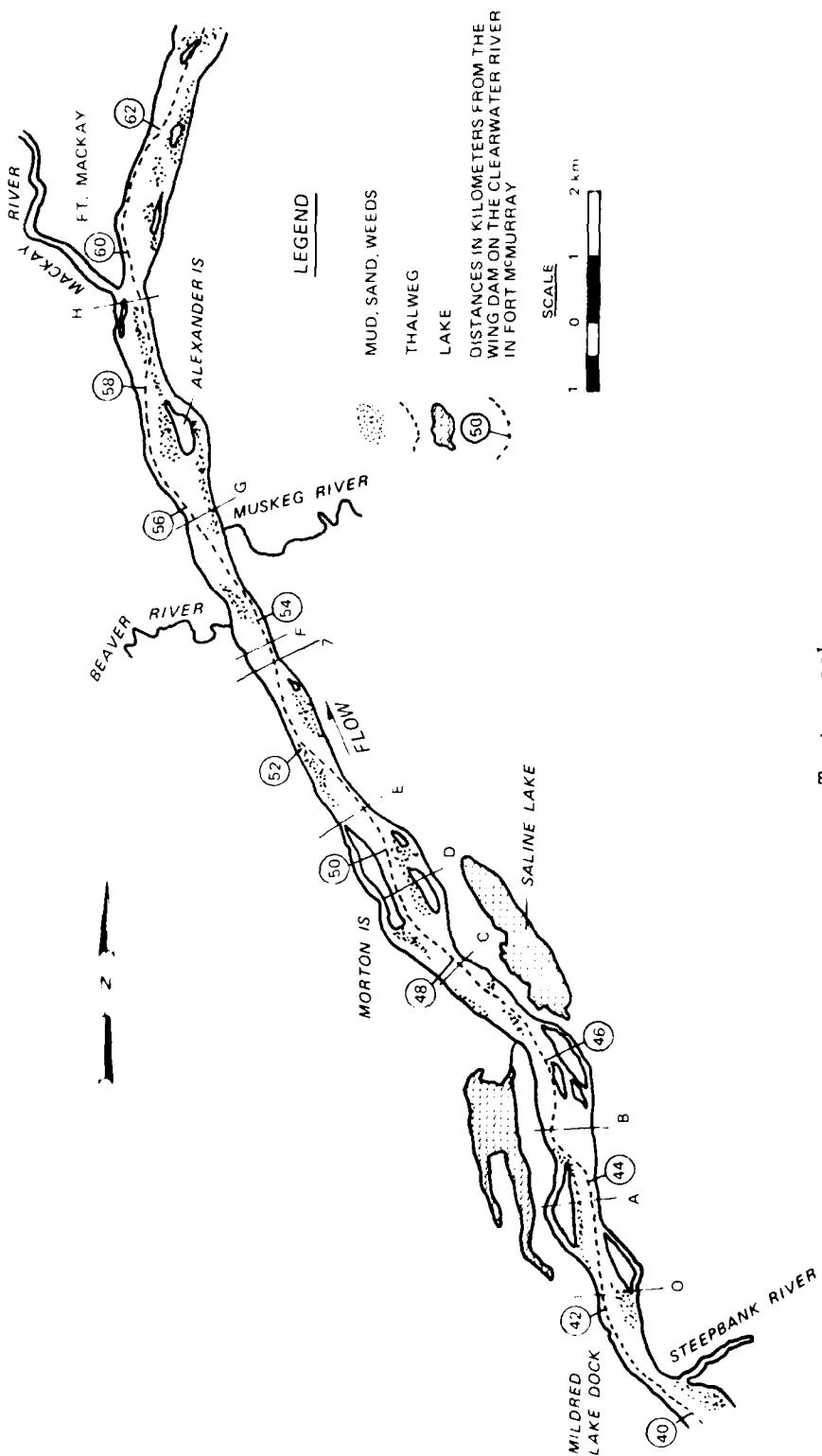
a. Test reach

Figure 69. Data from Athabasca River study on transverse mixing
(after Beltaos 1980) (Sheet 1 of 4)

335
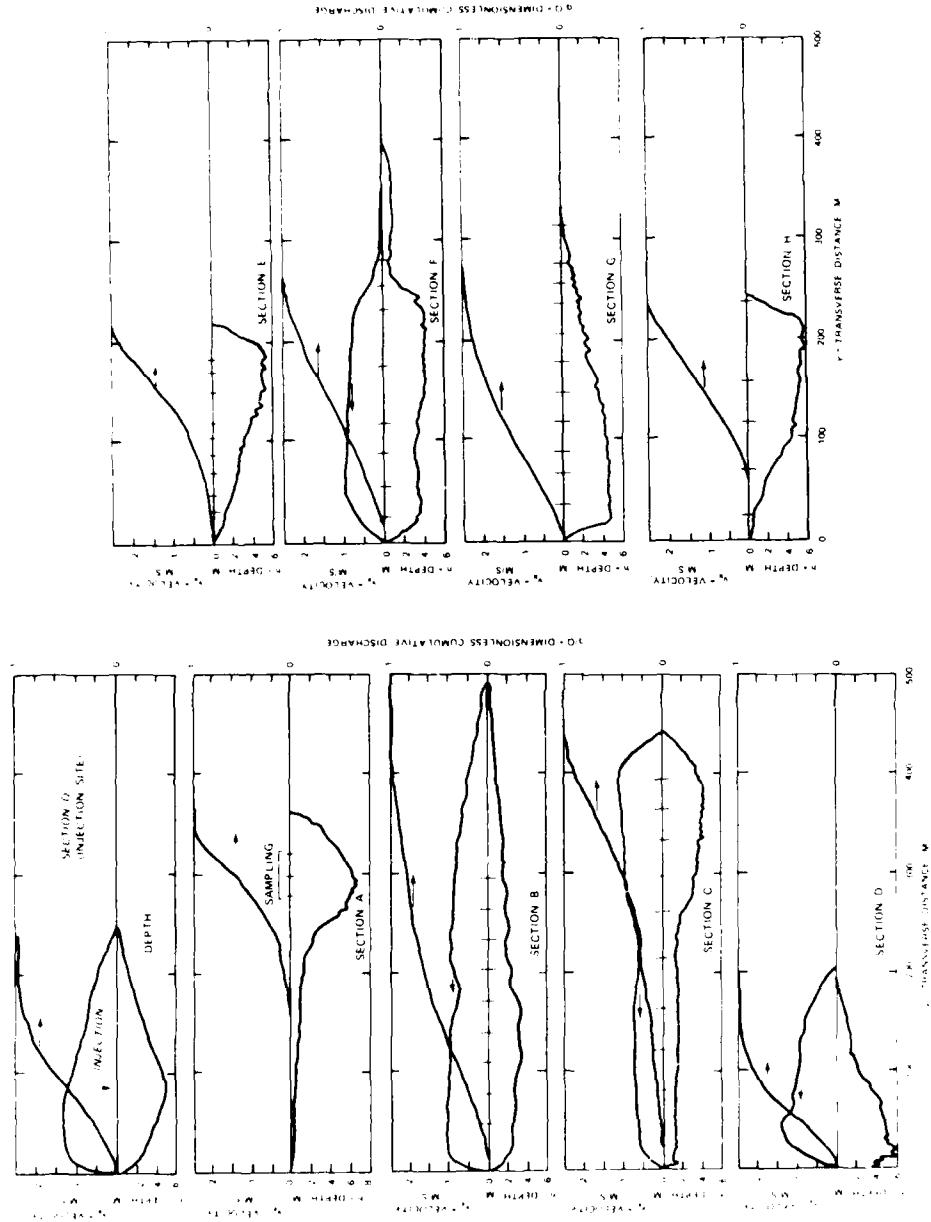
b. Depth, velocity and cumulative discharge distributions

Figure 69. (Sheet 2 of 4)
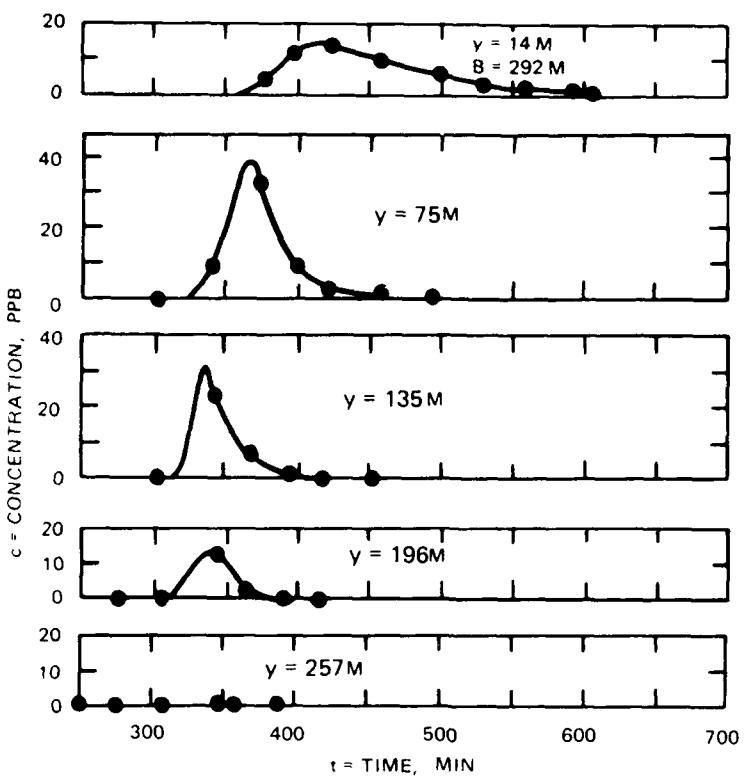
c. Measured concentration distributions at section 7
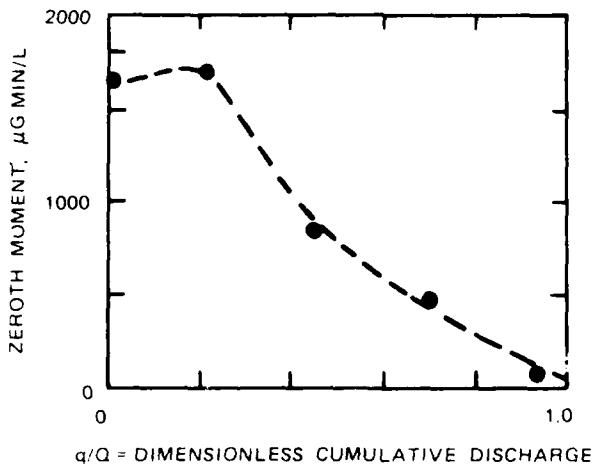


d. Transverse distribution of zeroth moments
at section 7

Figure 69. (Sheet 3 of 4)

337
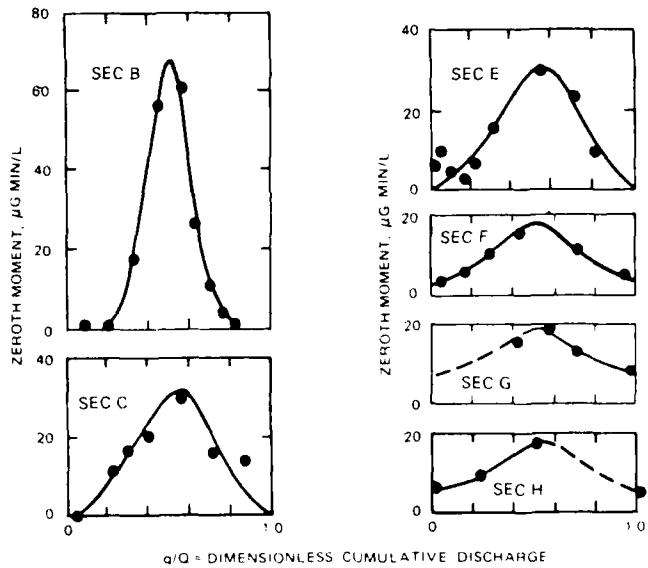
e. Transverse distributions of dosage
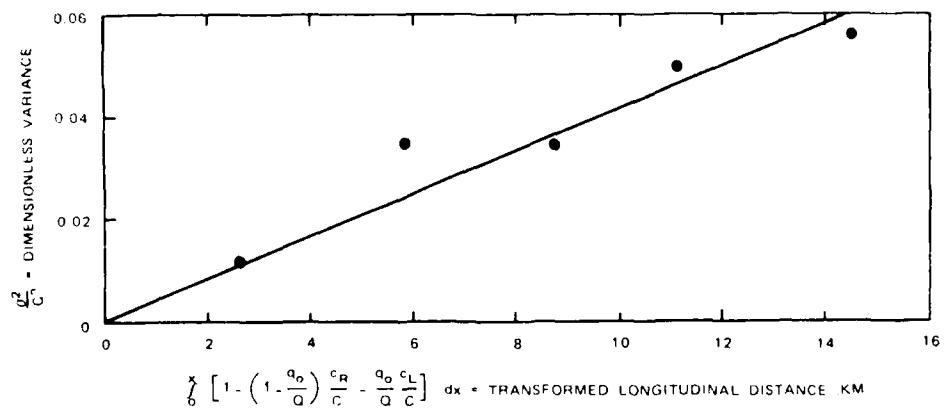


f. Variances

Figure 69. (Sheet 4 of 4)

Figure 69c, which is from an earlier preliminary test in the same reach but for ice-covered conditions. The resulting distribution of the zeroth moments is shown in Figure 69d. The concentration versus time curves were not given for the open-water test being discussed.) In a similar manner, the areas under all of the curves for the open-water tests were obtained to give the zeroth moments, which were distributed as shown in Figure 69e. Somewhat surprisingly, the maximum zeroth moment (concentration) apparently remained on the injection stream line (relative cumulative discharge of 0.5) throughout the study reach. Frequently, for a degree of mixing as great as that at the last cross section for this study, the maximum concentration moves toward, or perhaps even to, one of the banks (see Figure 66c). No values were given for the recovery ratios for the data in Figure 69e.

The data were analyzed using a generalized change-of-moments method based on the streamtube model (Figure 69f and Section 7.3.4), but in the derivation of the equations, it was effectively assumed at the beginning of the analysis that the depth and velocity were constant so that the $f(x)$ in this analysis was more nearly like the second part of Eq. 7.3.15 than like Eq. 7.3.8. Also, an average value of $\psi$ was used to obtain $e_y$ from $D_f$ rather than including $\psi$ in the integral to obtain $F_D$. Although the data have not been reanalyzed using the more general form of $f(x)$, the results that were obtained for $\alpha$, namely $\alpha = 0.75$, are probably of the correct order of magnitude. The length of the study reach corresponded to $x_d = 0.012$.

## 7.6  DATA ANALYSIS FOR UNSTEADY TRANSPORT

This section summarizes some of the primary considerations for analysis of data from unsteady tracer tests conducted to determine the longitudinal mixing characteristics of a stream. The comments in Sections 7.3.1 and 7.3.2 apply for data analysis for unsteady mixing problems as well as for the steady-state transverse mixing problems considered previously. For the transverse mixing problem, a significant part of the mixing process can be represented by a single coefficient ($e_y$), so much of the data analysis is directed at obtaining

339

numerical values for this coefficient or for the dimensionless equivalent ($\alpha$). For unsteady transport, if one-dimensional conditions exist, there is the analogous longitudinal dispersion coefficient (E) which has been the object of many of the experimental studies. As is seen in Section 7.7, there is even less reliability in generalized relationships for E than for $e_y$ (and $\alpha$). For two-dimensional unsteady transport problems, there is no single coefficient which can be used to characterize the mixing process. For these cases, it is preferable to include the velocity distribution and the transverse mixing in the representation of the transport.

Since the transverse distributions of velocity are a major part of the longitudinal spreading process, the approaches to data analysis need to be categorized according to the hydraulics of the stream, and of all of the possible cases, only a few have been studied explicitly in enough detail that any general comments can be made. These few include 2D situations in free-flowing streams with regular cross sections and 1D situations in various types of streams (with the hydraulics of the stream sometimes not being well described in the publications presenting the data). Two-dimensional problems in rivers with highly irregular geometries have not been studied in enough detail that general comments can be made about them even though there is a large number of problems which fall into this category. Another problem which has not been generalized is 2D transport in run-of-the-river reservoirs where the transport may have significant influences from both the river hydraulics and wind shear on the water surface.

The discussion in this section is presented in terms of analyses based on various forms of the conservation equations containing mixing coefficients. For 1D situations, similar analyses can be performed for lumped-parameter representations (Section 6.3.5).

### 7.6.1 Two-Dimensional Situations

For 2D situations within the initial period or with the initial period corresponding to a significant part of the total reach, there is no single coefficient which characterizes the transport process in the

340

same sense that $e_y$ does for transverse mixing and that $E$ does for 1D problems. Thus, for 2D unsteady situations, data analysis frequently must be done by testing a simulation scheme against the data. Since the longitudinal transport and mixing are controlled primarily by the transverse distribution of longitudinal velocity, by transverse mixing, and by temporary storage if any is present (Sections 6.2.5b, f; 6.3.4), the quality of the simulation generally increases in direct proportion to the degree with which these mechanisms are accurately represented in the simulation process; even a rather crude representation of these processes is generally better for 2D situations than trying to use some sort of 1D mixing coefficient, even one which may vary with longitudinal distance (Liu and Cheng 1980), in the opinion of the authors (but such a comparison has not been documented).

Any of the methods discussed in Section 6.2 for calculating concentration distributions can be used for simulation. Since the random walk is only currently being adapted for field situations and since the pseudo two-dimensional representation is considered to be inferior to the other methods (i.e. it seems inappropriate to use this degree of simplification for any situation where the time and expense have been expended to obtain field data), attention is focused on numerical solutions of the mass balance equation and of the temporal moment equations. The two methods are highly interrelated since the same physical mechanisms must be represented by the mathematics in both methods. In fact, even when the mass balance equation is being used to calculate concentrations, it is sometimes helpful to compare the moments of the calculated and measured concentration distributions.

a. Mass balance equation. Some numerical simulations of two-dimensional transport problems seek first to calculate the hydraulics (velocity distributions, water surface elevations, etc.) for the specified discharge, cross-sectional shapes, resistance coefficient, etc., and then to use this hydraulic information along with transverse mixing coefficients to calculate the concentration distributions. A discussion of this type of simulation is beyond the scope of this report. It is assumed here that the hydraulic characteristics are known from

341

measurements so that the objective is to develop numerical solutions of a 2D mass balance equation to represent the transport and to be able to reproduce measured concentration distributions.

Without going into the details of numerical solution techniques, some general observations are as follows. Even with hydraulic measurements, it is normally impractical to measure the depths and velocities at enough cross sections to correspond to every computational step in the model. Thus, interpolation is needed to ob ain the inputs required for the numerical solution (Yotsukura, Fischer, and Sayre 1970; Bird and Holley 1985). Also, care must be used in numerical solutions to prevent excessive numerical dispersion from the advection terms (Fischer 1981). Numerical solutions are somewhat easier if the stream-tube model is used or if the longitudinal coordinates are along the streamlines (as contrasted with using Cartesian coordinates) since only one advection term is then needed in the solution.

Considerable attention has been given to the question of what constitutes an acceptable numerical simulation of transport problems (Fischer 1981), but not much of the attention has been focused on transport in rivers. For this problem, there are at least four major aspects of the simulation that should be considered. Unfortunately, the last three aspects are interrelated so that trial-and-error adjustments may be needed (within the range of physically reasonable values, of course).

(1) Mass conservation. It should be verified that the simulation, without any distributed sources and sinks in the numerical solutions, conserves mass within an acceptable tolerance for the entire computational reach. Also, in comparing calculated and measured concentrations, any actual loss of mass during the tracer test should be taken into account either by scaling up the measured concentrations or by scaling down the calculated concentrations. Erroneous conclusions can be drawn by comparing a calculated concentration distribution representing one amount of mass with a measured distribution representing another amount.

342

(2) Time-of-travel. The time of travel, i.e. the time of occurrence of the centroid ($\bar{t}$) of the calculated and measured concentration versus time curve, should match for the various longitudinal and transverse measurement points. In 2D computations in the early part to the initial period, the primary aspects affecting $\bar{t}$ are the mean velocity along each stream line and temporary storage (dead zones). Thus, if the centroids are wrong, the problem probably stems from interpolated velocities not matching the actual ones, in terms of mean velocities and/or velocity distributions, or from the effects of temporary storage not being estimated properly. However, the time-of-travel can also be affected by the transverse mixing coefficient ($e_y$) used in the simulations. For example, consider a tracer injection made in the central, high-velocity part of a stream with no temporary storage. If $e_y$ is too small, then the tracer in the computations stays in the high-velocity region too long, so that once it does mix out to another streamline, $\bar{t}$ is too small.

(3) Transverse mixing. Even though $e_y$ has some influence on the time-of-travel, it has a primary influence on the transverse mass distribution at each cross section. The value of $e_y$ should be checked to ensure that it gives the correct distribution of the zeroth moments of the measured concentration curves. However, at least in the early part of the transport process, the velocity distribution also influences the zeroth moment; the value of $e_y$ influences the amount of mass on a given streamline, but the velocity influences the time required for the mass to pass a given point and thereby influences the zeroth moment.

(4) Longitudinal spreading. For a given stream geometry, the longitudinal spreading relative to the centroid is controlled by the vertical and transverse distributions of velocity and by the vertical and transverse mixing. In using a 2D model, the effects of the vertical distribution of velocity and the vertical mixing can be represented by using a longitudinal dispersion coefficient ($e_x \approx 6HU_*$). (In many numerical schemes, the numerical dispersion may be larger than the value of $e_x$. If this is the case, it will be difficult to accurately

343

represent the transport in the early part of the process.) The effects of spreading should be checked only after the zeroth moments and the centroids of the calculated and measured concentration distributions agree, even if either the calculated or measured distributions have to be shifted slightly in time (for the centroids) and the concentrations have to be scaled (for the zeroth moments). It can be a frustrating and fruitless task to try to adjust velocity distributions to improve agreement between data and calculations when the problem actually lies in the mean velocities or in a decay of mass during the experiment.

There have been relatively few published detailed examples of the use of 2D numerical simulations for rivers. Many times, 1D conditions have been assumed without checking (either empirically or by estimating the dimensionless longitudinal distances in comparison to the initial period) to ascertain whether 1D conditions actually existed.

b. _Temporal moment equations._ The objective of simulation of the temporal moments is to develop a numerical solution that correctly represents the moments of the measured concentration distributions. The comparison is in terms of the moments (areas, centroids, and variances, which represent the amount of longitudinal spreading), rather than in terms of the concentrations themselves. Nevertheless, the approach to simulation by temporal moments essentially parallels the preceding discussion for the mass balance equation since the directly calculated moments are influenced by essentially the same inputs as the analogous aspects in the solutions of the mass balance equation. The skewnesses of measured distributions are frequently very sensitive to relatively small errors or variations in the concentration versus time curves, so that it may be difficult to obtain a good comparison between calculated and empirical skewnesses. In general, as the order (zeroth, first, etc.) of the moments increases, it becomes progressively more difficult to obtain good agreement between calculations and data.

344

One advantage of simulating the temporal moments rather than the concentrations is that it is normally easier to obtain numerically accurate solutions of the moment equations, yet they still represent the significant aspects of the transport process and they avoid the primary numerical problem with the mass balance equations, namely the numerical dispersion arising from the advection term. The disadvantage with using the moment equations is that the concentrations then have to be obtained by the use of similarity functions (Section 6.2.5g) rather than by direct calculation. The use of temporal moments is a relatively new approach and has not been extensively used. Nevertheless, it appears to provide a relatively easy method for simulating the primary transport processes.

Holley and Tsai (1978) gave examples of comparisons of calculated and empirical temporal moments, including the effects of temporary storage. Tso (1982) and Bird and Holley (1985) used temporal moments and similarity functions to compare calculations and measurements for not only the moments but also for the concentration distributions.

## 7.6.2 One-Dimensional Situations

a. Numerical simulations. When the initial period represents only a small percentage of the total reach of interest, the entire transport process can be simulated as being one dimensional. One of the primary objectives of the data analysis is then the evaluation of the longitudinal mixing coefficient (E). Trial values of E are used in a numerical solution of Eq. 4.8.31 to determine the value which gives the best agreement between calculated and measured concentrations. The hydraulic inputs which are needed are the area (A) and the velocity (V). If temporary storage is a significant mechanism, then values are also needed for $\lambda$ and for $K^*$. If V is obtained from time-of-travel studies or other similar techniques using the speed of movement of a tracer cloud, then the effects of temporary storage are inherently included in V and should not be represented separately in the advection term. As with 2D simulations, the area under the

345

concentration versus time curves, the centroids, and the spread of the
distributions should be independently compared to each other with
adjustments being made in  V  and in the parameters for the storage
zones to get the centroids to agree, and in  E  to get the amount of
longitudinal spreading relative to the centroids to agree.  Generally,
agreement must be considered in some reach-averaged sense (especially
if constant values are used for the entire reach for  A ,  V , and
E ), but it still is essential that the amounts of longitudinal
spreading relative to the centroids be compared even if the centroids
do not match exactly.  It is normally very difficult to achieve a high
level of agreement for each distribution unless the simulation is
adjusted by having  V  and  E  vary with longitudinal distance.  Also,
it frequently is found that the 1D equation cannot adequately represent
changes in the concentration distribution between the release point and
the first measurement cross section, so that the first measurements are
taken as the initial condition for the calculations for the remaining
part of the reach to determine E (Fischer 1966a).  While this is a
reasonable approach for evaluating  E , it leaves still unanswered a
question concerning how the transport upstream of the first measurement
cross section should be represented in subsequent calculations to
predict concentration distributions.  At present the answer apparently
lies either in using a 2D analysis including  $e_x$  to account for the
effects of the vertical velocity distribution, at least for the early
part of the transport, or in using site-specific analyses.

   b.  Change of moments.  The objective of this type of analysis
is to determine  E  from the rate of growth of the variance of measured
versus  t  distributions.  Since it frequently is difficult to
obtain a good definition of the time at which the measured concentra-
tion reaches the background level on the falling limb of the distri-
butions and since small variations in the concentrations at the tail of
the distributions have a relatively large influence on the moments
because of the long moment arms relative to the centroid, it is common
practice to use the variances of the  C  versus  t  curves above some
small percentage (typically 1% or 2%) of the maximum concentration for

346

each curve. The variances can be plotted versus longitudinal distance, and the slope of a straight line through the points is used to evaluate $\Delta\sigma_t^2/\Delta x$ and then $E$ since

$$E = \frac{V^3}{2} \frac{\Delta\sigma_t^2}{\Delta x} \qquad (7.6.1)$$

The calculated value of $E$ is very sensitive to the value of $V$ since $V^3$ is in the calculation. The dependence of the calculated $E$ on $V$ can be reduced to $V^2$ if $\sigma^2$ is plotted versus $\bar{t}$ instead of $x$ since

$$E = \frac{V^2}{2} \frac{\Delta\sigma_t^2}{\Delta\bar{t}} \qquad (7.6.2)$$

There generally is considerable scatter of the plotted points, so that again $E$ must be considered as a reach-averaged value corresponding to a best straight-line approximation to the plotted points (Section 7.8). Although it would probably be possible to develop a 1D generalized change of moments to account for variations of hydraulic character- istics through the study reach, this has not been done; it is common to assume constant values of $A$, $V$, and $E$ in the change-of-moments analysis.

## 7.7 ONE-DIMENSIONAL LONGITUDINAL DISPERSION COEFFICIENTS

### 7.7.1 Significance of Dispersion Coefficients

As discussed in Section 6.3, longitudinal dispersion coeffic- ients (E) should be expected to represent the transport process only after an initial period, i.e. only when the concentration distributions are one dimensional. When it is appropriate to use dispersion coeffic- ients, they embody the combined effects of differential advection asso- ciated with the transverse distribution of velocity and transverse mix- ing. Attempts to find generalized expressions for $E$ have been made primarily for free-flowing streams since they have some degree of

347

consistency in the velocity distributions (as contrasted to streams with highly irregular cross-sectional geometries or pool-and-riffle streams). In principle, the effects of temporary storage can be represented by using separate mass balance equations for the main flow channel and for the storage zones. Sometimes, this has not been done, so the longitudinal spreading due to the coupling between the main channel and the storage zones may be a third mechanism contributing to the magnitude of a gross dispersion coefficient. For pool-and-riffle streams and streams with highly irregular cross-sectional shapes, E is a bulk coefficient which must represent all of the longitudinal spreading processes. Even a brief consideration of the extremely wide possible variations of the details and degrees of the contributing mechanisms, even in free-flowing rivers with fairly regular geometries, gives an insight into the reason that it has not yet been possible to find widely applicable, accurate means of predicting dispersion coefficients from bulk hydraulic parameters of streams. With the present knowledge of the transport processes in rivers, it seems apparent that any future efforts at obtaining general prediction equations should consider a categorization of rivers according to the characteristics of the primary mechanisms contributing to the dispersion process (including whether any effects of temporary storage are to be included directly in E or are to be modeled by using separate equations for the main channel and the storage zones) and should use only data that do in fact come from the 1D dispersive period following the initial period. This philosophy has not been followed in some of the published attempts at generalizing expressions for dispersion coefficients, with the result that the available values have a large scatter relative to the prediction equations for E .

## 7.7.2  Analytical Predictions of Dispersion Coefficients

The expressions which are given in this section for E are intended to apply only for free-flowing streams with regular and systematic variations in cross-sectional shapes along the length of the stream. Equivalent expressions are not available for other cases.

a. <u>Uniform flow.</u> For steady, uniform flow, Fischer et al. (1979) showed that $E$ can be calculated from

$$E \approx I \; \frac{B^2 \overline{v_x'^2}}{e_y}$$

(7.7.1)

where $B$ = channel width, $e_y$ = transverse diffusion coefficient, $v_x' = v_x - V$, i.e. the deviation of $v$ from the cross-section average $V$, $\overline{v_x'^2}$ = mean squared variation of $v_x$. The coefficient $I$ represents the combined effects of the differential advection and transverse mixing in dimensionless terms and is given by

$$I = - \frac{1}{AB^2 \overline{v_x'^2}} \int_0^B v_x' h \left[ \int_0^y \frac{1}{h} \left( \int_0^y v_x' h \, dy \right) dy \right] dy$$

(7.7.2)

Even though these expressions may look unwieldy, they are definitely manageable; Fischer et al. (1979) showed the results of calculations for $E$ using these equations.

Jain (1976) rewrote Eq. 7.7.1 as

$$E = \beta_J \; \frac{V^2 B^2}{e_y}$$

(7.7.3)

and evaluated $\beta_J$ from an expression similar to Eq. 7.7.2 for uniform flow in generalized quadralateral cross sections using synthesized velocity distributions based on Yotsukura and Sayre's (1976) power-law relationship between depth and velocity. Jain's calculated results are shown in Figure 70.

At least as important as the numerical values which can be calculated for $E$ from Eqs. 7.7.1 and 7.7.2 is the fact that these

349
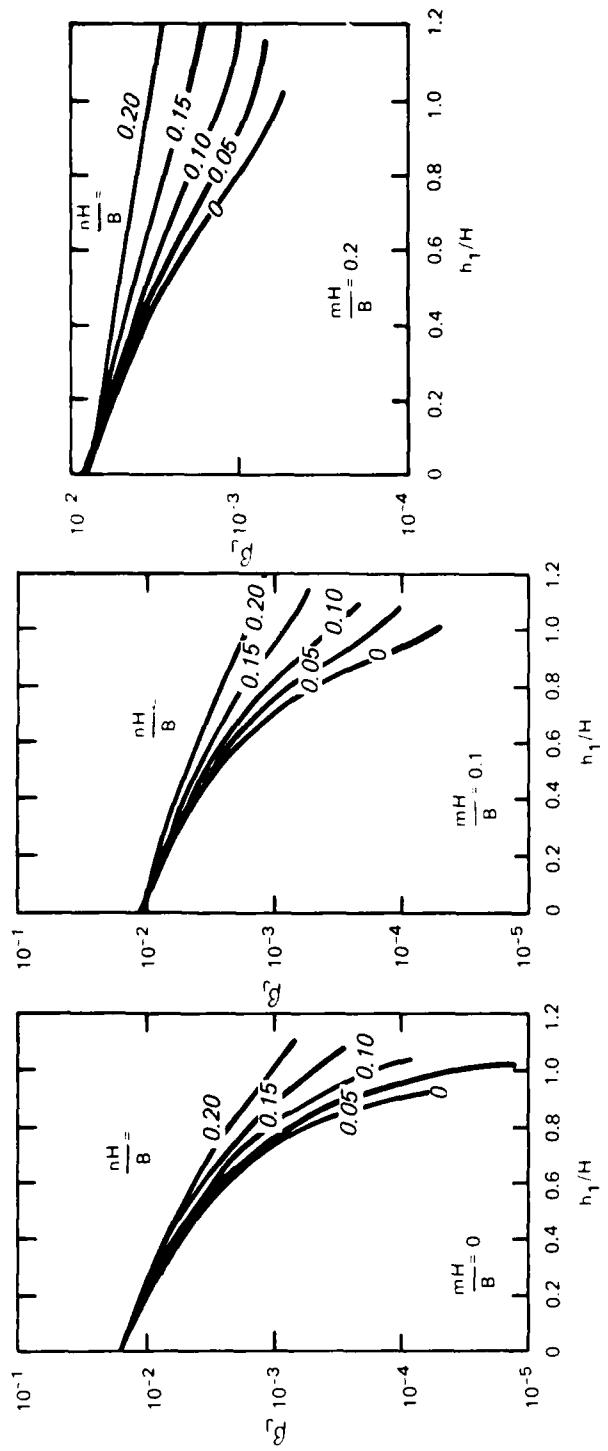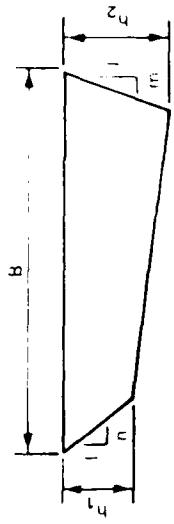
Figure 70. Dimensionless longitudinal dispersion coefficients for prismatic channels (after Jain 1976)

equations demonstrate how E depends on hydraulic characteristics of the flow. Eqs. 7.7.1 and 7.7.2 are written in the forms shown because I is dimensionless and therefore is independent of the absolute size of the river; I depends only on the relative distributions of $v_x$ and h, if $e_y$ is taken as a constant. (The original form of the equations includes the possibility of having $e_y$ be variable across the width of the stream.) Thus, Eq. 7.7.1 shows the general way in which E varies with the width of the river, with the amount of variation of velocity within the cross section, and with the magnitude of the transverse mixing coefficient. Nevertheless, since natural streams are not prismatic channels with uniform flow, Eqs. 7.7.1 and 7.7.2 are more useful for understanding the makeup of E than for direct practical application. The applications which Fischer et al. (1979) developed from these equations for natural streams are presented in the following paragraphs and in Section 7.7.3.

b. _Meandering streams._ For uniform flow, the velocity along any streamline is the same at all cross sections. Even though mass is being continually redistributed transversely by mixing, whatever mass is on a specific streamline at any instant always moves downstream with the same velocity, which is either faster than, or slower than, the average velocity. With this type of differential advection, the dispersion coefficient associated with a particular velocity distribution is as given above. In a meandering channel, the velocity on a given streamline may be larger than the average when that streamline is on the outside of a bend and then lower than the average farther downstream when the streamline is on the inside of a bend. This variation of velocity along a streamline, as contrasted to a constant velocity for each streamline for uniform flow, has the potential for reducing the amount of differential advection and thus reducing the longitudinal spreading. As Fischer (1969) and Fischer et al. (1979) showed, the dimensionless length (L') of the bend determines whether E is smaller than it would be for a uniform flow with the same velocity distribution as exists in a bend. The dimensionless length is defined as

351

$$L' = \frac{L/V}{B^2/e_y} = \frac{Le_y}{B^2V} \qquad\qquad (7.7.4)$$

where $L'$ is the ratio of the flow time through a bend of length $L$ to the characteristic time for transverse mixing over the width $B$, and is thus a measure of the amount of transverse mixing that can take place while the flow is moving through the bend. The dimensionless length can be interpreted as an indication of whether the flow time though the bend is longer than the period needed for the velocity distribution within the bend to fully develop its dispersive potential (Fischer et al. 1979). From very limited results (two cases), Fischer et al. concluded that if $L' > 0.04$, a bend is long enough that $E$ can be calculated from Eqs. 7.7.1 and 7.7.2 using velocity distributions measured within the bend. (The distributions used in their examples were specified (Fischer 1969), but no general guidelines were given concerning where in a bend the velocities should be measured.) For another example with $L' = 0.008$, $E$ was found from experimental results and by numerical simulation to be about eight times smaller than that given by Eqs. 7.7.1 and 7.7.2.

## 7.7.3  Empirical Approaches

There have been many methods presented in the literature for estimating dispersion coefficients or other dispersion-related parameters from stream hydraulics. Only three of the methods are summarized here. Other than the statement by Fischer et al. (paragraph 7.7.3a) that the effects of storage zones were not included in their equation, no mention was made by the various authors of any attempt to categorize the rivers according to the major mechanisms contributing to the longitudinal dispersion process. All of the methods in the literature are based on subsets of the available data, and there has been almost no independent verification or evaluation of the methods by disinterested persons.

a. Fischer et al. (1979) used results from measured velocity
distributions and from transverse mixing tests to obtain representative
values of $\overline{v_x'^2}/V^2$ and $e_y$ (0.2 and $0.6HU_*$, respectively) which could
be substituted into Eqs. 7.7.1 and 7.7.2 to give

$$E = 0.011 \frac{V^2 B^2}{HU_*} \tag{7.7.5}$$

They stated that this expression is intended only as a rough estimate
and that it does not include the effects of storage zones on longi-
tudinal spreading. Also, it could be concluded that the equation per-
haps should not be used in highly meandering streams because of the
value of $e_y$ incorporated into the equation and because no considera-
tion was given to the possible reduction of E due to small L'
(Eq. 7.7.4). Fischer et al. compared Eq. 7.7.5 with 16 measured values
of E and found the agreement to be within a factor of about 4. In
one sense, this is a very large amount of variation; nevertheless, it
is relatively good when compared with other prediction equations.
Fischer et al. also pointed out that the amount of longitudinal spread
of concentration distributions is proportional to the square root of
E , so that overall errors in the concentration distributions are gen-
erally less than errors in E .

b. Liu (1977) used 15 measured values of E, with some of the
experiments being different from the ones used by Fischer et al.
(1979), to obtain

$$E = \beta_L \frac{V^2 B^2}{HU_*} \tag{7.7.6}$$

where

$$\beta_L = 0.18 \left( \frac{U_*}{V} \right)^{3/2} \qquad (7.7.7)$$

This prediction method agreed with the empirical values of E to within a factor of about 6. On the basis of physical reasoning, Christiansen (1977) concluded that the exponent in Eq. 7.7.7 should be 2. From fitting his equation to Liu's data, he suggested that $\beta_L$ should be given by

$$\beta_L = 0.41 \left( \frac{U_*}{V} \right)^2 \qquad (7.7.8)$$

This equation differed from the experimental values of E by as much as a factor of 10.

Liu and Cheng (1980) extended Liu's approach in an effort to account for the variation of the effective dispersion coefficient (i.e. the slope of the $\sigma^2$ versus distance curve, e.g. Figure 76e) during the initial period. Their analysis gave

$$E' = E \left\{ 1 - \frac{t_o}{t} \left[ 1 - \exp \left( -\frac{t}{t_o} \right) \right] \right\} \qquad (7.7.9)$$

where E' is a dispersion coefficient which varies with time during the transport process and E is the dispersion coefficient for large times. The expression which Liu and Cheng gave for E and $t_o$ can be written as

$$E = 0.5 \frac{U_* A^2}{H^3} \qquad (7.7.10)$$

and

$$t_o = 2.5 \frac{B^2}{HU_*} \qquad\qquad (7.7.11)$$

Eq. 7.7.10 can be written in the form of Eq. 7.7.6 with

$$\beta'_L = 0.5 \left(\frac{U_*}{V}\right)^2 \qquad\qquad (7.7.12)$$

Liu and Cheng concluded that this approach predicted the observed dispersion coefficients from 32 of 33 cases within a factor of 2.5, the lone exception being the Missouri data summarized in Section 7.8.3. (This conclusion apparently applies only to the values of E for large times since some of the individual points for E' in their Fig. 6 differ from their equation by a factor of 4.) They also reported that this approach materially improved the representation of the variation of $C_{max}$ and of the concentration distributions compared to previous approaches. They recommended using a Pearson Type III concentration distribution rather than a Gaussian distribution. (See Section c below.)

While Liu and Cheng's approach takes into account some of the aspects of transport during the initial period, their approach is inherently one dimensional while the transport process within the initial period is two dimensional. Thus, the dependence of the concentrations on transverse position within the channel cannot be represented by this approach.

c. Weaver and Holley (1985) analyzed the measured concentration distributions at 225 cross sections from 54 experiments in 24 streams. Rather than seeking to represent the results in terms of dispersion coefficients, they presented nondimensionalized graphs of the data so that the results can be used directly for predictive purposes.

The dimensionless variance is shown in Figure 71 as a function of dimensionless downstream distance for all of the tests, with each experiment being indicated by a different symbol. The dimensionless variables were defined as

$$\sigma_d'^2 = \int_0^x \left(\frac{e_y}{B^2}\right)^2 \frac{d\sigma^2}{dx} \; dx \quad \text{or} \quad \left(\frac{e_y \sigma}{B^2}\right)^2 \qquad (7.7.13)$$

and

$$x_d' = \int_0^x \frac{e_y}{VB^2} \; dx \quad \text{or} \quad \frac{e_y x}{VB^2} \qquad (7.7.14)$$

The first (integral) form of each equation was used together with the available information on the variation of hydraulic parameters with flow distance; the second form can be used when only average depths, velocities, etc., are available. These dimensionless variables are similar to those used by Holley and Tsai (1978) and by others, with the exception of using the integrals to account for the variations of the various parameters with distance.

The general trend of the data is clear although there are certainly some individual experiments which do not agree with the general trend either in terms of the numerical values or in terms of the trend. Although the data trend should not be expected to be a straight line in this type of graph (Holley and Tsai 1978), the best-fit straight line is shown on the graph for simplicity. The coefficient of variation of the data about the line is 5.2, so that a variance estimated from this graph should be expected to be within a factor of 5.2, on the average, compared to the actual variance. Since the height (i.e. $C_{max}$) and

356
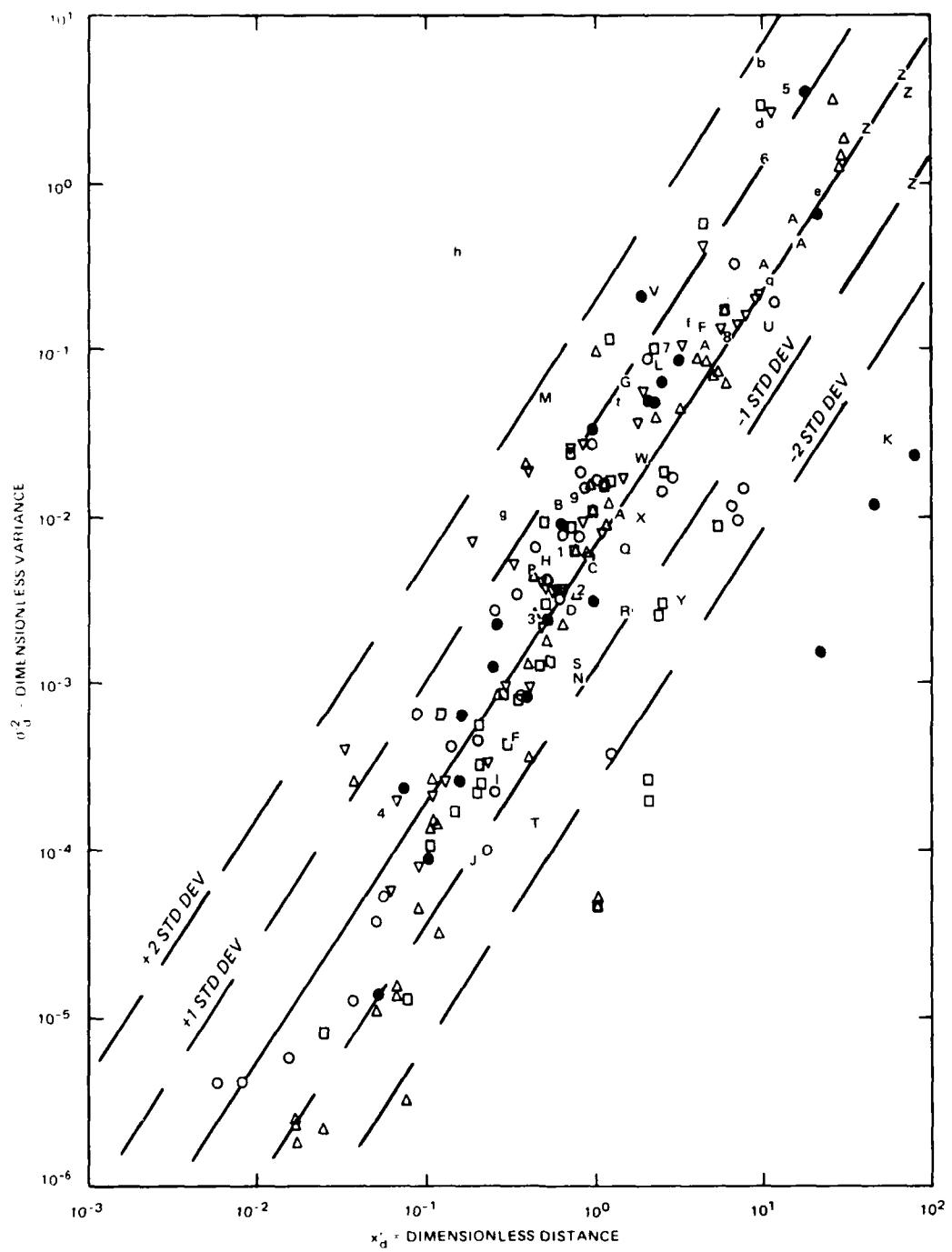
Figure 71. Dimensionless longitudinal variance of
concentration distributions

357

width of the concentration distribution are proportional to the standard deviation (square root of the variance of the concentration distribution), these features of the distributions can be estimated within a factor of 2.3 on the average. (Note that these values are given in terms of a measure of the average error while the possible errors for the prediction equations for E were given in the preceding sections in terms of the total range, as originally reported by the authors who presented the equations for E .)

It was found that the shapes of most of the concentration distributions were very similar to each other when properly nondimensionalized. If the highly spiked distributions for small dimensionless distances (e.g., as shown in Figures 75c and 76b) are excluded, the average shape for all of the remaining distributions is as shown in Figure 72, which also gives some of the statistics of the spread of the measured concentrations about the average. The dimensionless variables in Figure 72 are

$$t' = \frac{t - \bar{t}}{\sigma} \qquad (7.7.15)$$

and

$$C' = \frac{C\sigma}{\int_0^\infty C dt} \qquad (7.7.16)$$

The average distribution in Figure 72 has a mean of zero, a standard deviation of unity, and a coefficient of skew of 0.90. These parameters were used to superimpose a Pearson Type III distribution (Eq. 6.2.14) on the figure; the averages of the measured distributions and the Pearson Type III distribution are essentially the same.

For this analysis, a highly spiked distribution was defined as one having a dimensionless maximum concentration greater than 0.6; this
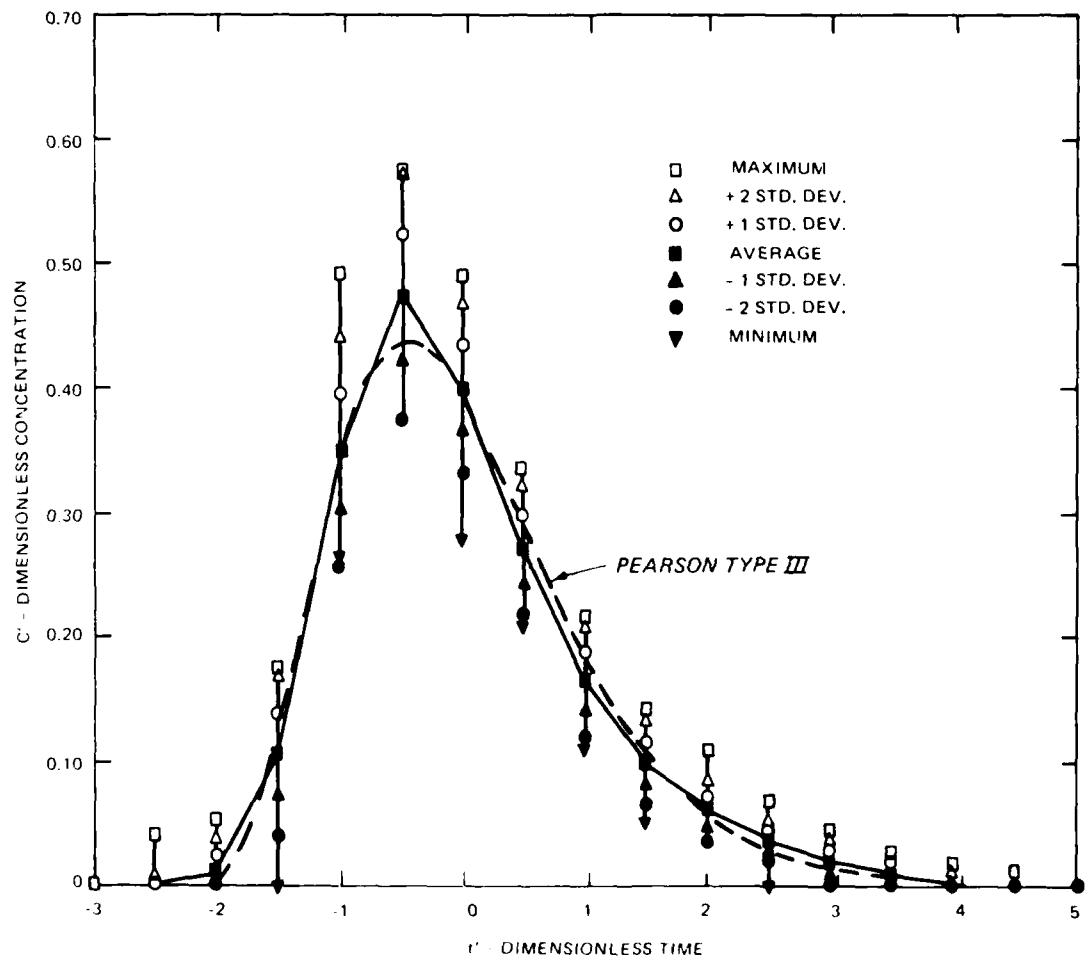
Figure 72.   Dimensionless concentration distribution
for longitudinal mixing problem (with highly spiked
distributions omitted)

359

criterion was obtained simply by inspection of the shapes of the concentration distribution curves. Figure 73 shows the actual dimensionless maximum concentrations ($C'_{max}$) as a function of dimensionless distance ($x'$). From this figure, it can be concluded that the distribution in Figure 72 should be a reasonable representation for dimensionless longitudinal distances greater than about 0.1 or 0.2. Since this is a
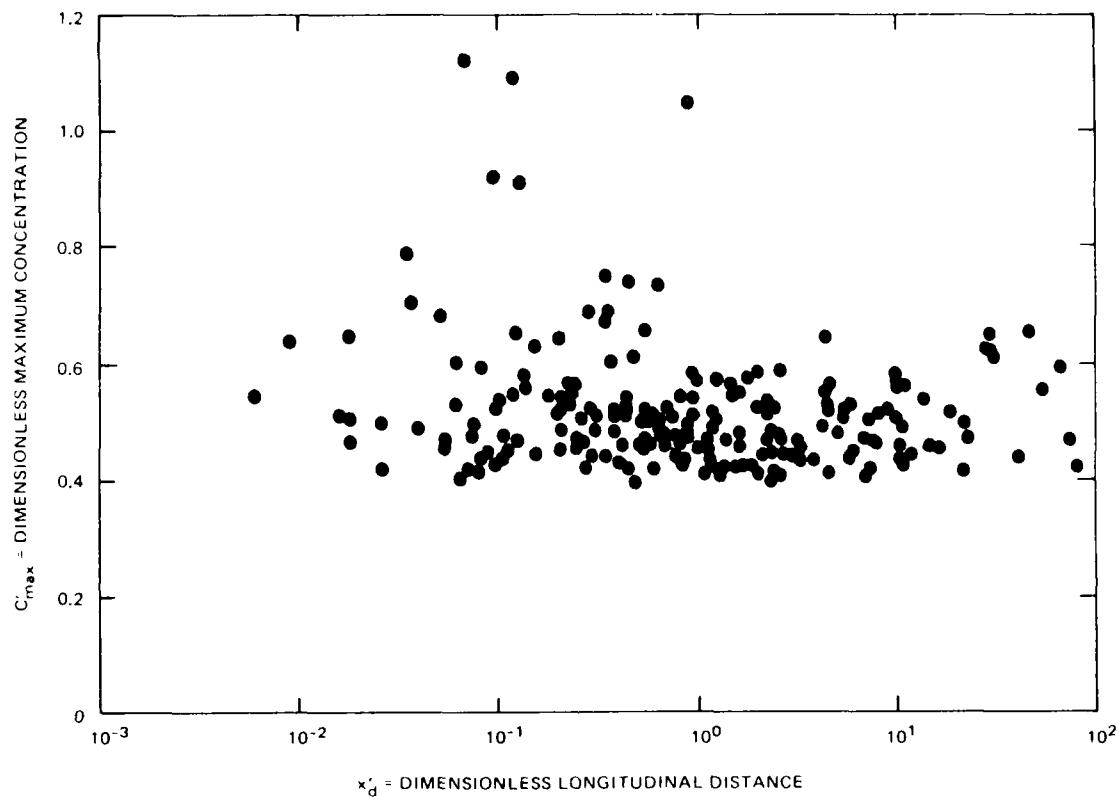


Figure 73. Dimensionless maximum concentrations for longitudinal mixing problem (including all distributions)

one-dimensional analysis, it is reasonable to expect that it may not accurately represent the behavior for all cases at small distances. For comparison, Figure 74 shows the average concentration distribution when all measurements were included in the analysis.

In order to use this information in a predictive mode, it is necessary to know average or representative values of $B$, $V$, $Q$, and $e_y$ for the stream and $M$ for the released mass of pollutant. For the selected values of $x$ for which the concentration

360
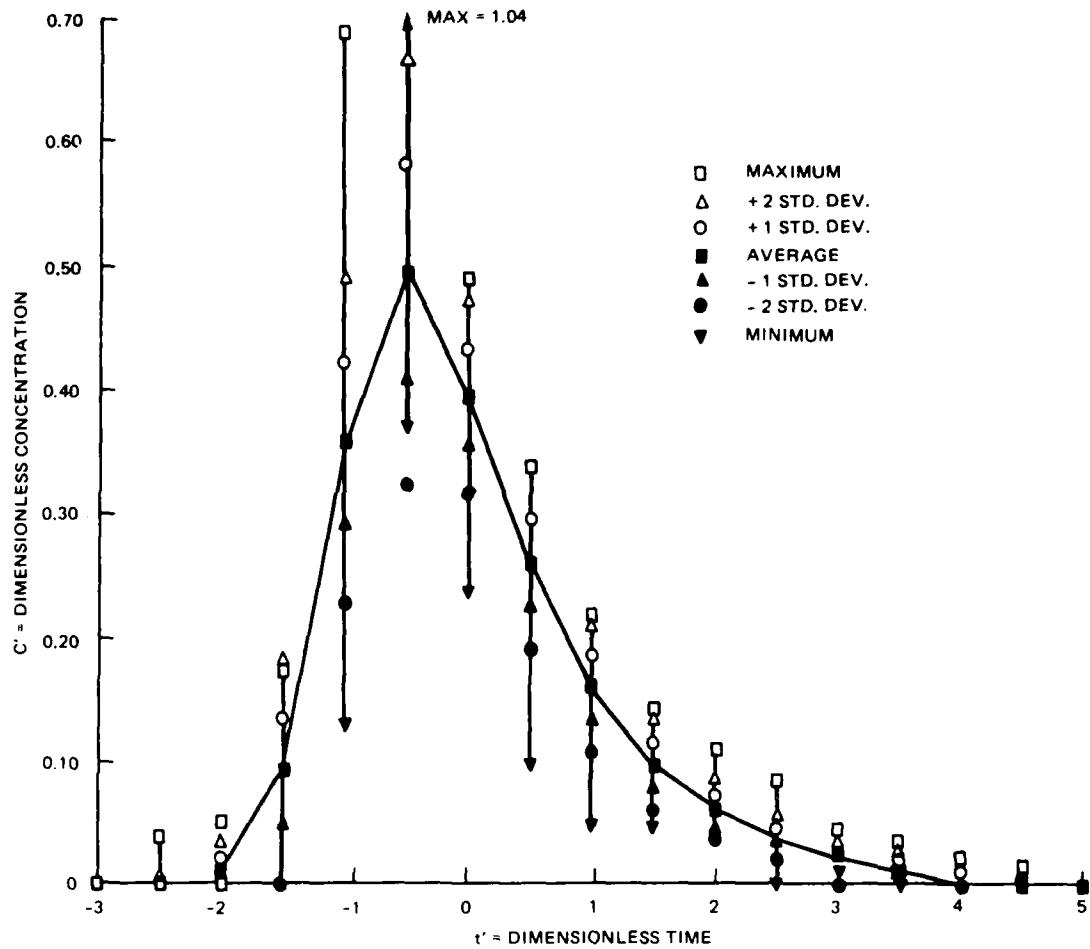
Figure 74. Dimensionless concentration distribution for longitudinal mixing problem (including all distributions)

distributions are desired, calculate $x'$, estimate $\sigma'^2$ from Figure 71, and use the values of $e_y$ and B to calculate $\sigma$. Use $x/V$ as an estimate for $\bar{t}$. Read $C'$ versus $t'$ values from Figure 72 and obtain the estimated concentration distribution from

$$C = \frac{C'M}{\sigma Q} \qquad (7.7.17)$$

and

$$t = \bar{t} + \sigma t' \qquad (7.7.18)$$

## 7.8  EXAMPLES OF FIELD EXPERIMENTS ON LONGITUDINAL MIXING

In this section, some experiments on longitudinal mixing are summarized in chronological order. (Nordin and Sabol (1974) presented the results from 51 longitudinal mixing tests in 24 rivers.) This section parallels Section 7.5 on transverse mixing, and many of the general comments in the introductory paragraph of that section apply to the experiments on longitudinal mixing also.

### 7.8.1  Copper Creek (Godfrey and Frederick 1963)

From 1959 to 1961, Godfrey and Frederick (1963, 1970) conducted 11 longitudinal mixing tests in six different reaches of three rivers and one canal. That series of studies still is the most complete, well documented, published set of experiments on longitudinal mixing. In all of the studies, the hydraulics (distributions of both depth and velocity) were measured first, with the injections being made and the concentrations measured on subsequent days. Unfortunately, for most of the studies, the river flow changed between collecting the hydraulic data and conducting the dye tests. For four of the tests, the flow changes were from 19% to 40%. For the others, the changes were 11% or less. The types of data collected and the analyses of the data were essentially the same for all of the tests. From the studies with the smaller flow changes, the Copper Creek study (Test 3-59 in Godfrey and Frederick (1963) and Test 3 in Godfrey and Frederick (1970)) was selected arbitrarily as a study in a small, meandering creek.

The general alignment of the study reach, which was 27,550 ft long, is shown in Figure 75a. The depth profiles and the depth-averaged velocities for the six measurement cross sections are given in Figure 75b. From the hydraulic measurements, average values were obtained as  $Q = 35$ cfs ,  $B = 56$ ft ,  $H = 1.3$ ft , and  $n = 0.21$ . The average of the measured velocities was 0.53 fps; using the centroids of the concentrations distributions for a time-of-travel study gave a velocity of 0.64 fps. The dimensionless distances  $(x_d)$  for the measurement cross sections were 1.4, 3.0, 4.4, 5.6, 7.4, and

362

INJECTION SECTION

SECTION 1

SECTION 2

SECTION 3

SECTION 4

SECTION 5

SECTION 6

SCALE

0    1000    2000    3000    4000    5000 FT
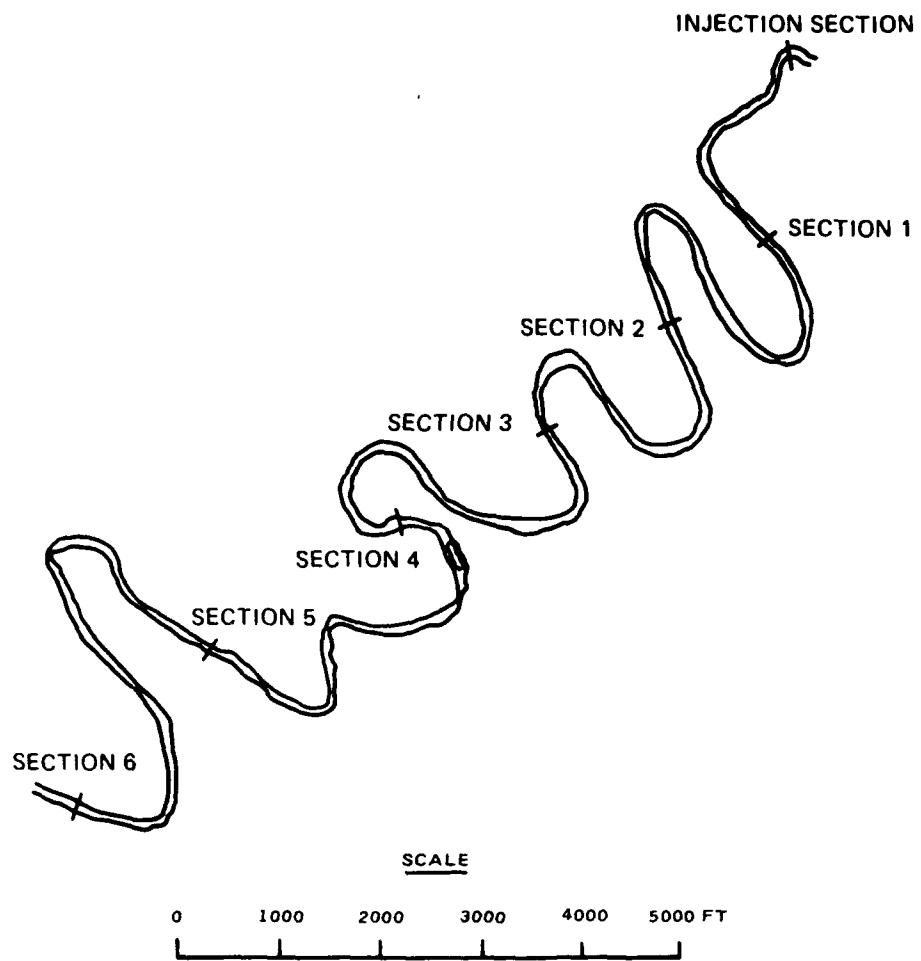
a.  Test reach

Figure 75.  Data from Copper Creek study
on longitudinal mixing (after Godfrey and
Frederick 1963) (Sheet 1 of 4)

363
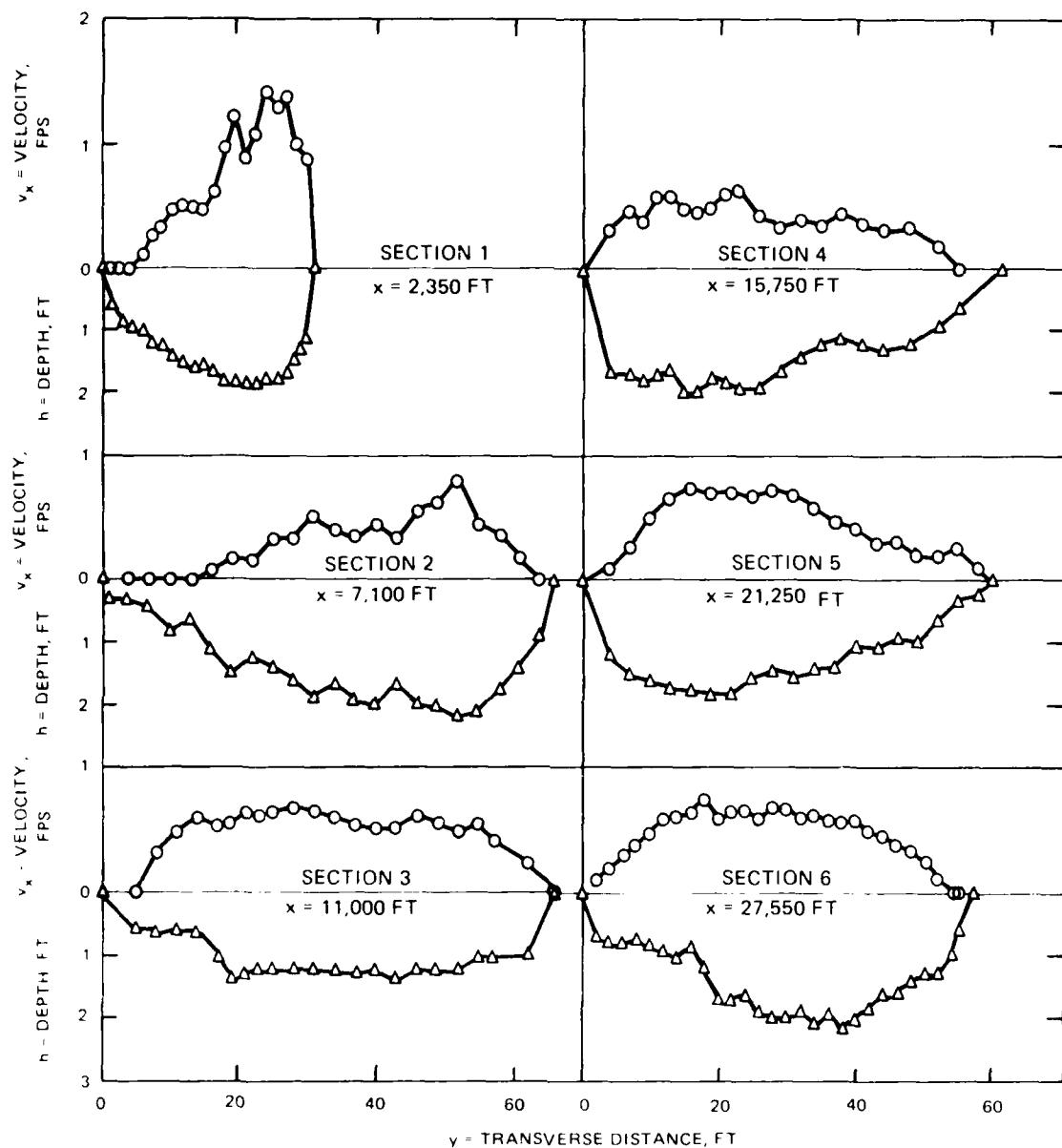
b. Depth and velocity profiles

Figure 75. (Sheet 2 of 4)
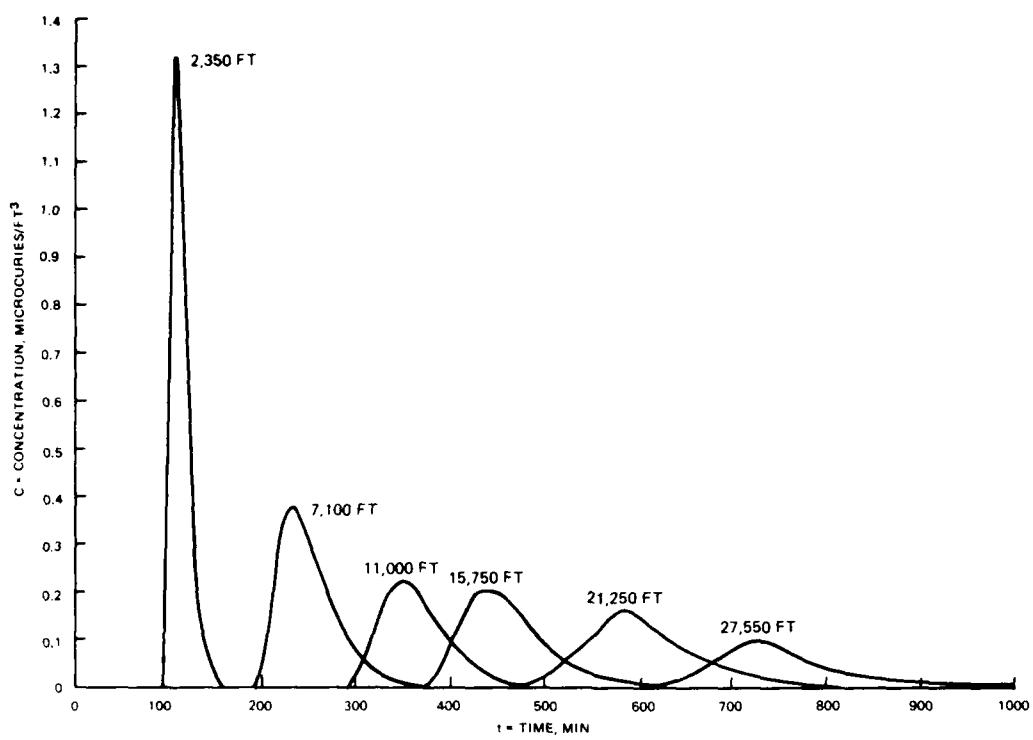
c.  Concentration measurements
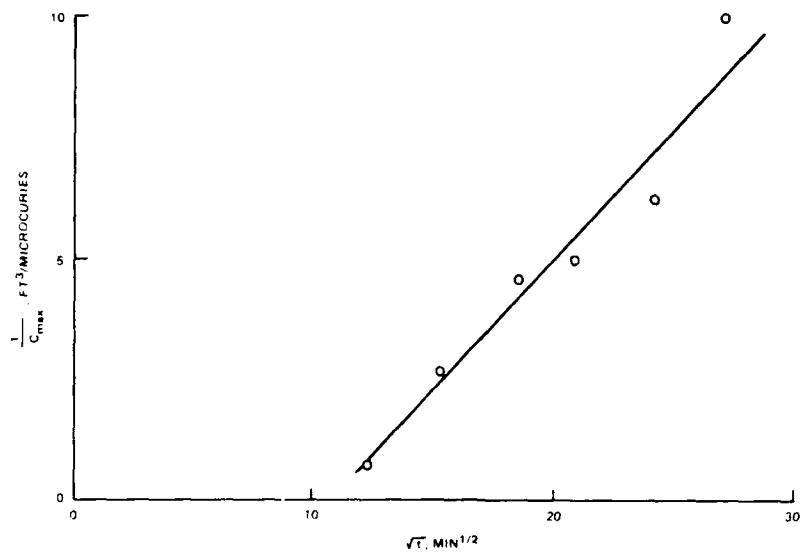


d.  Variation of maximum concentration

Figure 75.  (Sheet 3 of 4)

365
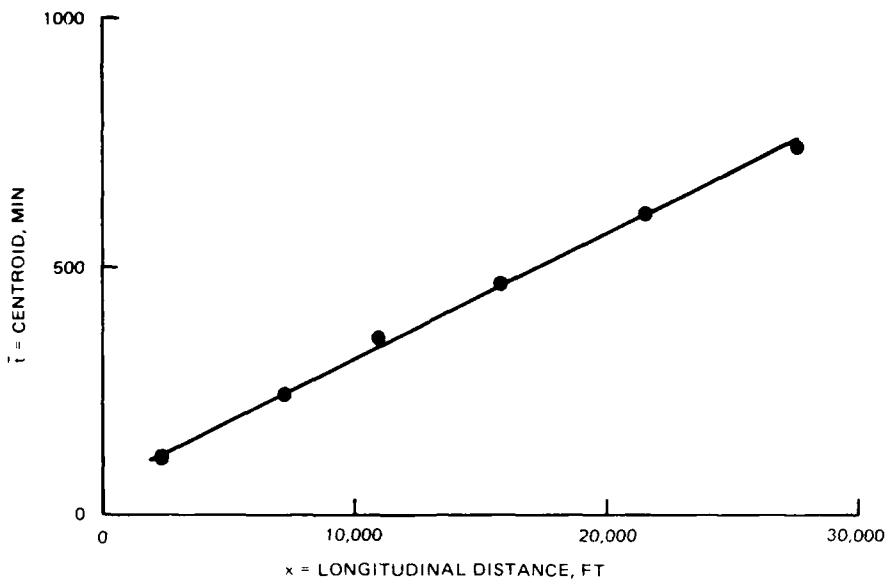
e. Variation of centroid
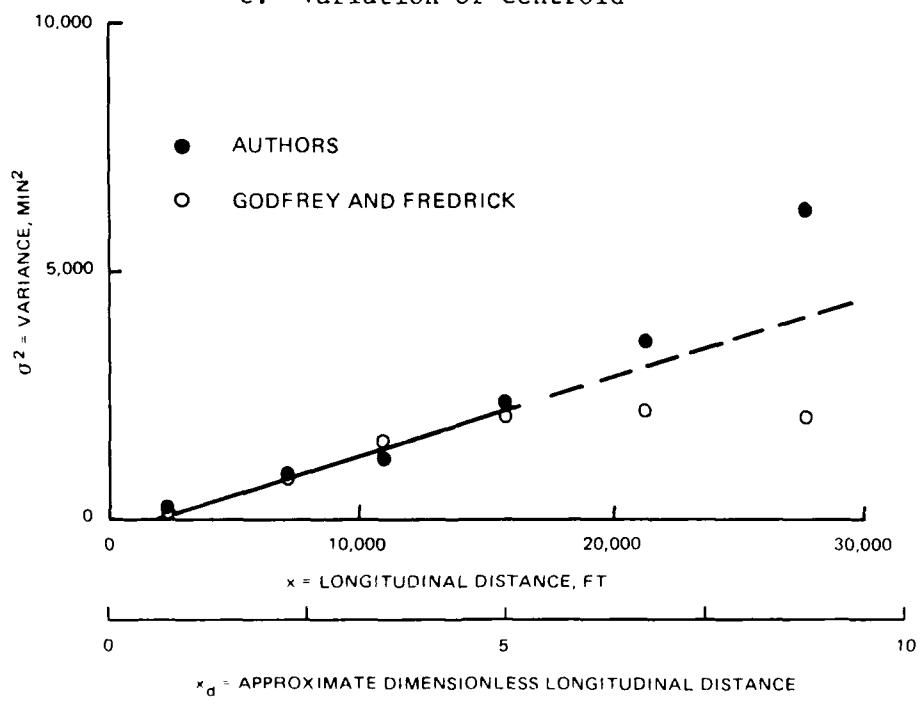


f. Variation of variance

Figure 75. (Sheet 4 of 4)

9.1 using $x/V = \bar{t}$ , $U_* = 0.49$ fps , and $\alpha = 1.0$ which is strictly an estimated value of $\alpha$ .

The tracer injection consisted of 0.064 curies of Au 198 released between 9:49.5 and 9:50.5 on June 18, 1959 as a line source across most of the width of the stream (except immediately adjacent to the banks). The measured concentration distributions are shown in Figure 75c. The next part of the figure shows the longitudinal distributions of the inverse of the maximum concentration ($C_{max}$) as presented by Godfrey and Frederick; $C_{max}$ would be expected to decrease in proportion to the inverse square root of flow time (as represented by the centroid) or distance since the transport process should be one dimensional for the dimensionless distances at which these measurements were made. This type of variation would give a linear increase of $1/C_{max}$ with $t^{1/2}$ . The centroids ($\bar{t}$) are shown as given by the authors (Figure 75e). The inverse of the slope of the line through the centroids gives the average cloud velocity. Figure 75f shows the variances ($\sigma^2$) both as calculated directly from the concentration distributions by the writers and as given by the authors from a method which was based on the assumption that the concentration distributions fit a Pearson Type III distribution so that $\sigma$ could be obtained from the widths of the distributions at heights corresponding to various percentages of the maximum concentrations. Also, Godfrey and Frederick converted the temporal variances to spatial variances before presenting them; the values shown in Figure 75f have been converted back to temporal variances. The growth of the variances is approximately linear, as would be expected for these values of dimensionless distances. The large values of $\sigma^2$ obtained from the concentration distributions for the last two cross sections may be due to the fact that the entire tail of the distributions was used in the calculations. (See the discussion of the calculation of variances in Section 7.8.3.) The slope of the line shown in Fig. 75f corresponds to $E$ 80 $ft^2$/sec and $E/HU_*$ 120 . The calculated value of $E$ is very sensitive to the value of $V$ since $V^3$ is in the calculation:

367

$$E = \frac{V^3}{2} \frac{\Delta\sigma^2}{\Delta x} \qquad (7.8.1)$$

The dependence of the calculated $E$ on $V$ can be reduced to $V^2$ if $\sigma^2$ is plotted versus $\bar{t}$ instead of $x$ since

$$E = \frac{V^2}{2} \frac{\Delta\sigma^2}{\Delta\bar{t}} \qquad (7.8.2)$$

### 7.8.2 Coachella Canal (Godfrey and Frederick 1963)

This study was done in a man-made canal with a relatively straight alignment and relatively uniform cross section. The total reach was 63,750 ft (12.1 mi) long. The depth profiles and the depth-averaged velocities for the measurement cross sections are given in Figure 76a. From the hydraulic measurements, average values were obtained as $Q = 900$ cfs , $B = 81$ ft , $H = 5.1$ ft , and $n = 0.02$ . The average of the measured velocities was 2.2 fps; using the centroids of the concentrations distributions for a time-of-travel study gave a velocity of 2.3 fps. Tracer tests were conducted on 2 consecutive days with measurements being made at a total of seven cross sections. The hydraulic data just given are for the first day; on the second day, the discharge increased by only 6% so there should be only small changes in the hydraulic variables. The dimensionless distances $(x_d)$ for the measurement cross sections were 0.02, 0.05, 0.11, 0.17, 0.25, 0.35, and 1.18 using $x/V = \bar{t}$ , $U_* = 0.14$ fps , and $\alpha = 0.4$ which is based on the straight alignment of the channel. These values of $x_d$ indicate that part of the reach was within the initial period where 2D concentration distributions should be expected to exist.

On the first day, the tracer injection consisted of 1.58 curies of Au 198 released between 11:01 and 11:02 on May 11, 1960 as a line source across most of the width of the stream (except immediately adjacent to the banks). On the second day, a similar injection of 1.21 curies was made from 9:06 to 9:07. The measured concentration
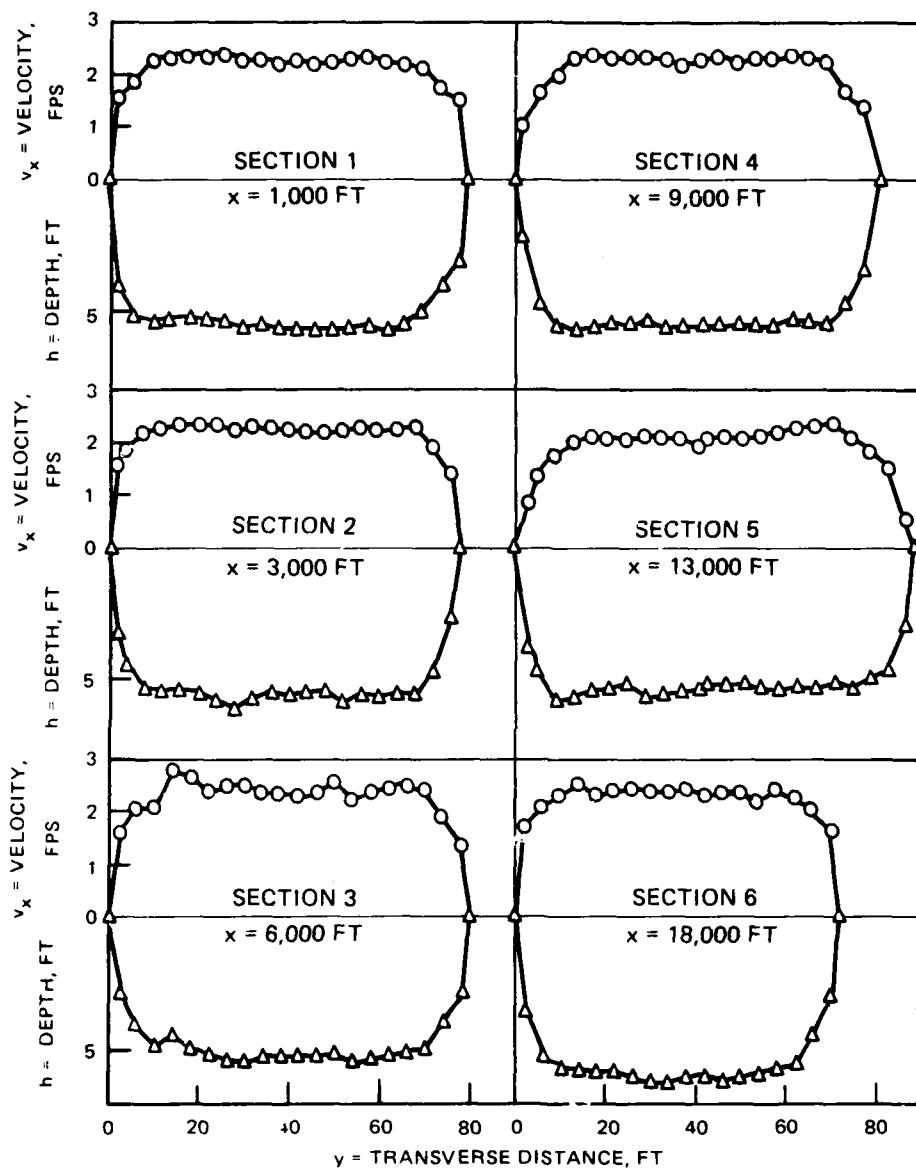
a. Depth and velocity profiles

Figure 76. Data from Coachella Canal study on longitudinal
mixing (after Godfrey and Frederick 1963) (Sheet 1 of 3)

369

b. Concentration measurements



c. Variation of maximum concentration

Figure 76. (Sheet 2 of 3)

370

a. Depth and velocity profiles

Figure 76. Data from Coachella Canal study on longitudinal
mixing (after Godfrey and Frederick 1963) (Sheet 1 of 3)

369

b. Concentration measurements



c. Variation of maximum concentration

Figure 76. (Sheet 2 of 3)

370
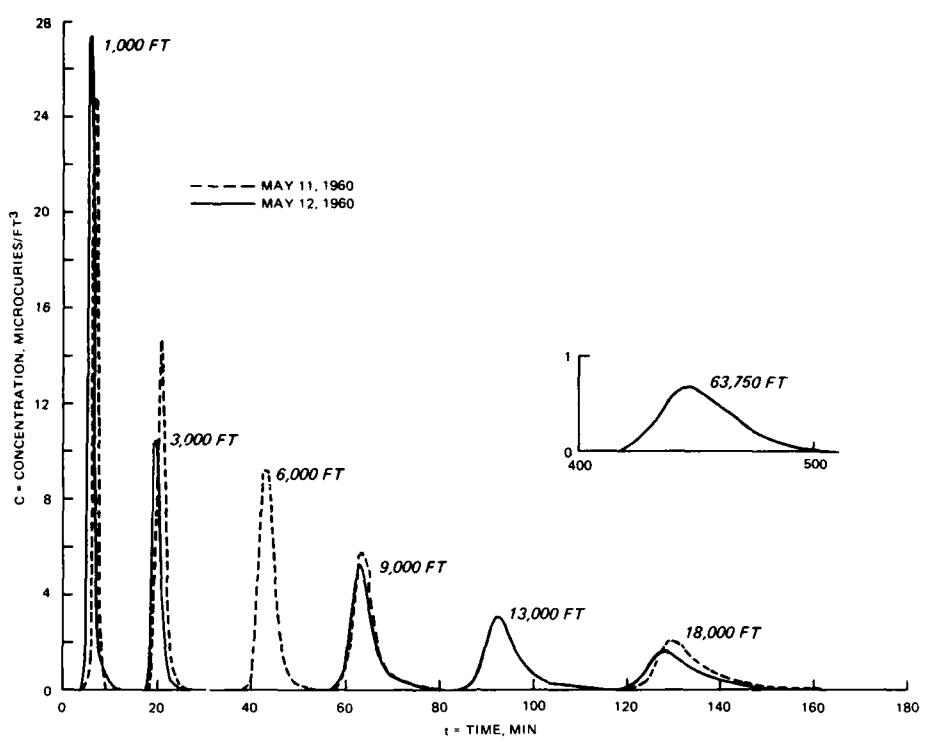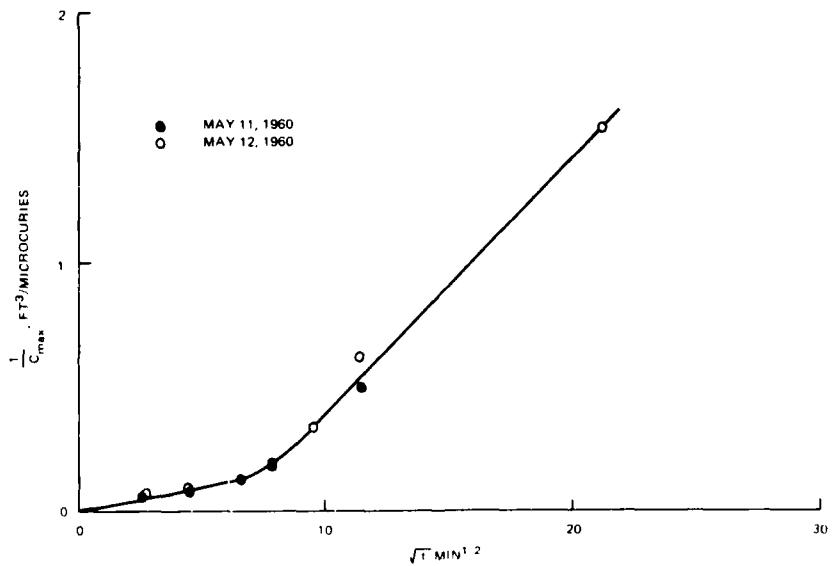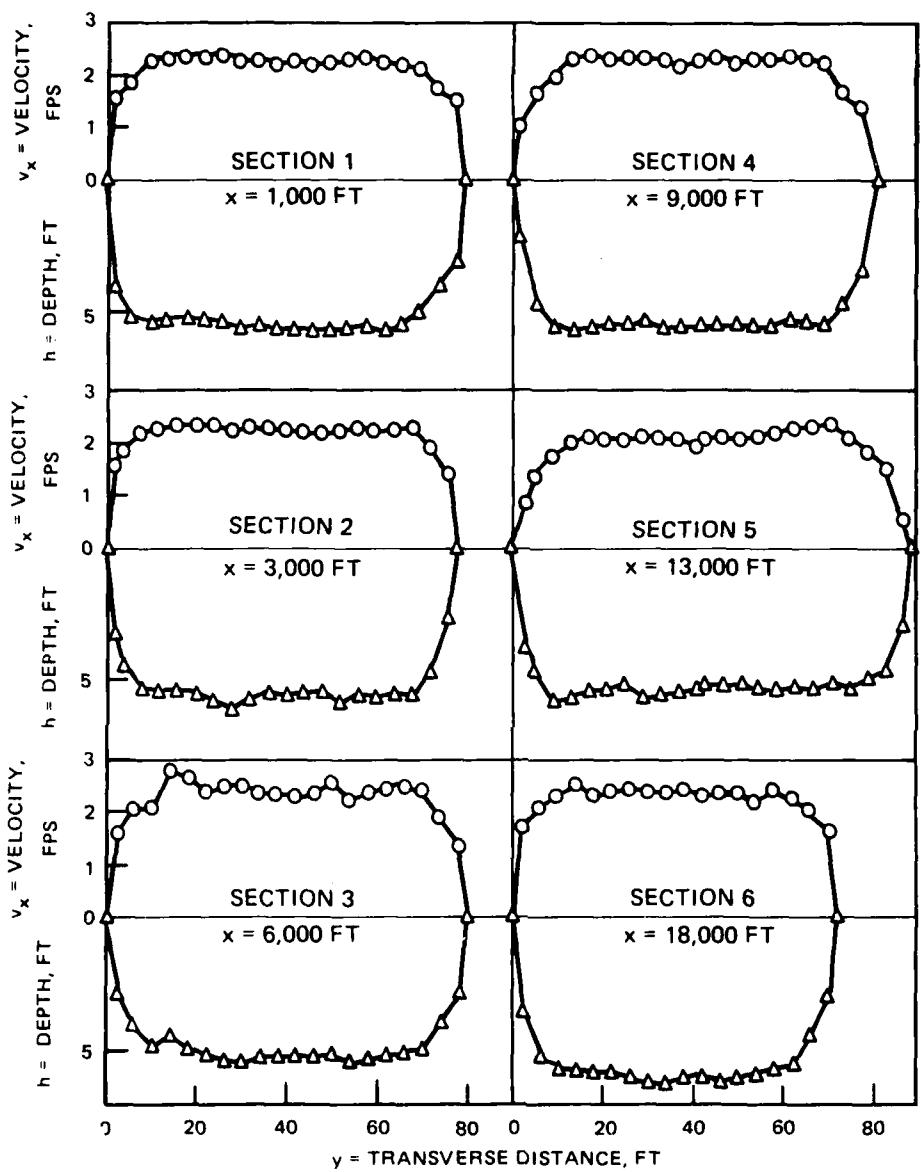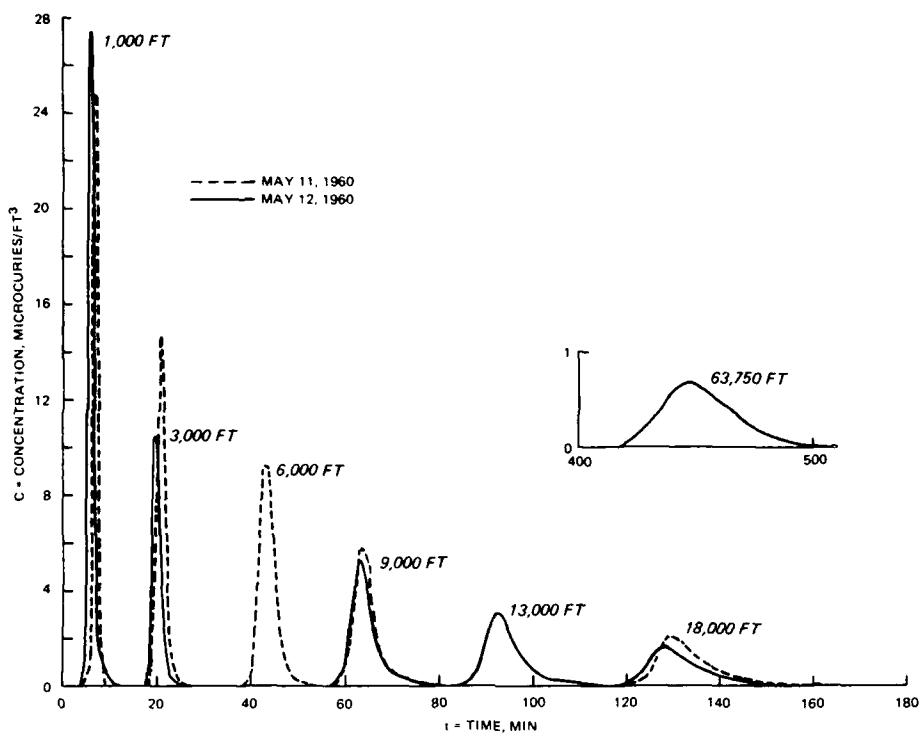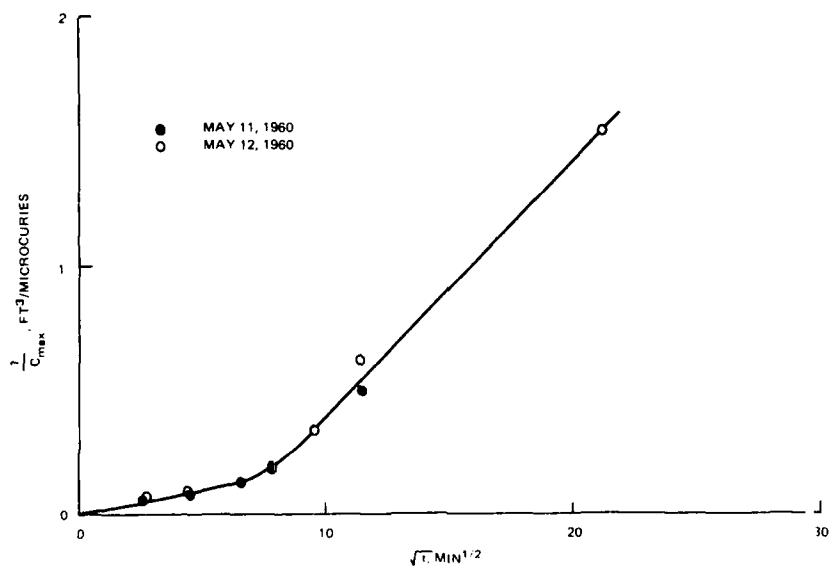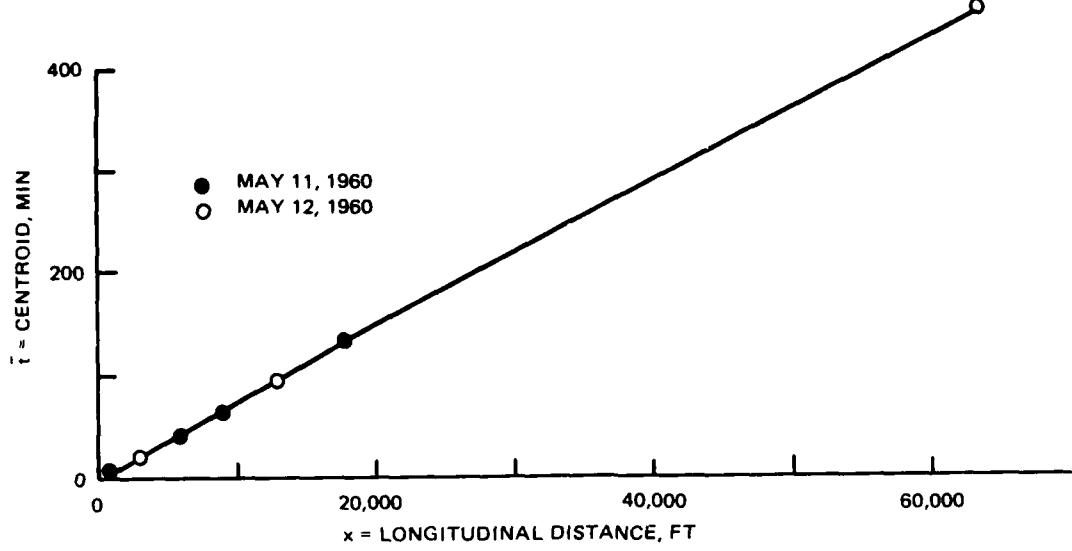
d. Variation of centroid
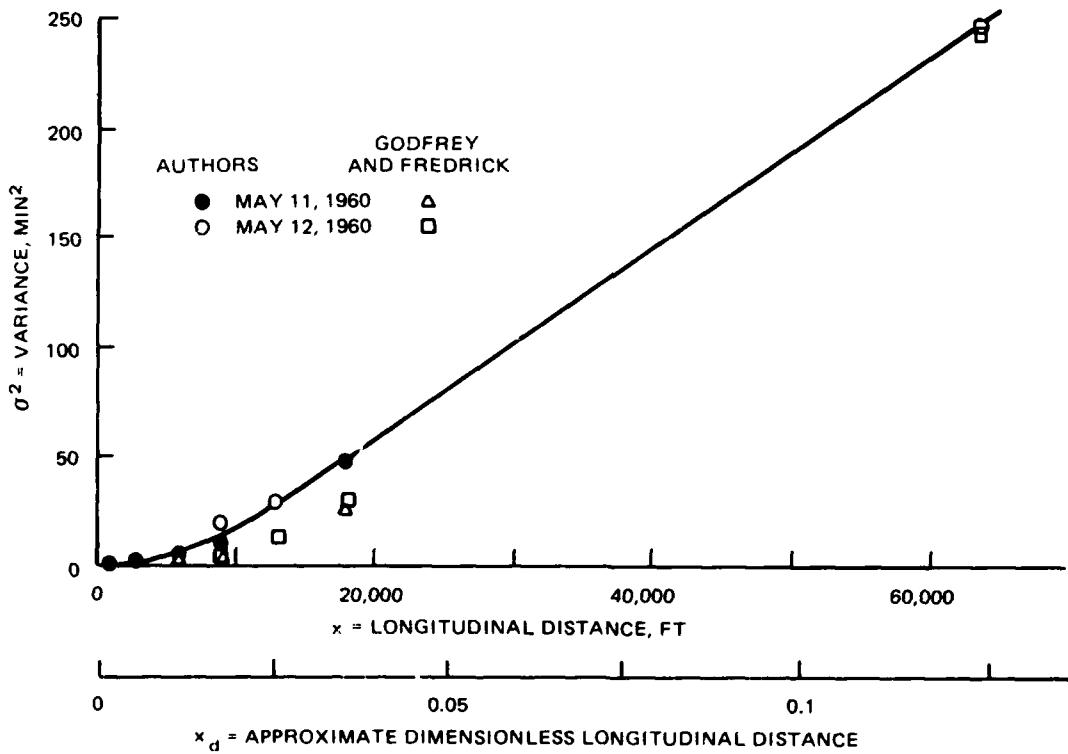


e. Variation of variance

Figure 76. (Sheet 3 of 3)

371

distributions are shown in Figure 76b in terms of time since release
and with the concentrations for the second test multiplied by the ratio
1.58/1.21 to account for the different injection strengths. Fig-
ures 76c, d, and e show the longitudinal distributions of the maximum
concentrations ($C_{max}$), centroids ($\bar{t}$), and variances ($\sigma^2$) in a manner
similar to those in Figure 75. The two sets of values for the vari-
ances are as calculated by the writers and by the authors, as was the
case for the Copper Creek data in the previous section. The increase
in the centroids is approximately linear as would be expected in a
relatively uniform channel. The influence of the 2D transport in the
initial period can be seen in the variation of both $C_{max}$ and $\sigma^2$.
Initially, $C_{max}$ decreases more rapidly (or $1/C_{max}$ increases more
rapidly) than for 1D transport and the variance increases less rapidly.
Since some of the data were collected in the 2D initial region, the
transverse location of the sampling point would be an important part of
the data, but the exact sampling position was not given. It was stated
that the concentrations were measured at or near the centerline of each
stream.

The value of E was calculated from the slope of the curve
through the last data points; however, as the values of $x_d$ on the
figure indicate, these cross sections may not have been far enough
downstream of the injection location to be certain that they were
within the dispersive period. Also, this calculation may be subject to
large errors since only two data points were used to define the
straight line. The value of E was found to be approximately
90 $ft^2$/sec giving $E/HU_* $ 120 . As stated above, these values should
be viewed with caution.

### 7.8.3 Missouri River (Yotsukura, Fischer, and Sayre 1970)

In 1967, Yotsukura, Fischer, and Sayre (1970) conducted a longi-
tudinal transport and mixing experiment in 141-mile long reach of the
Missouri River between Sioux City, Iowa, and Plattsmouth, Neb. (Fig-
ure 77a). The tabulated discharges for the study reach varied from
31,200 cfs to 34,100 cfs. It was stated that the Platte River was the
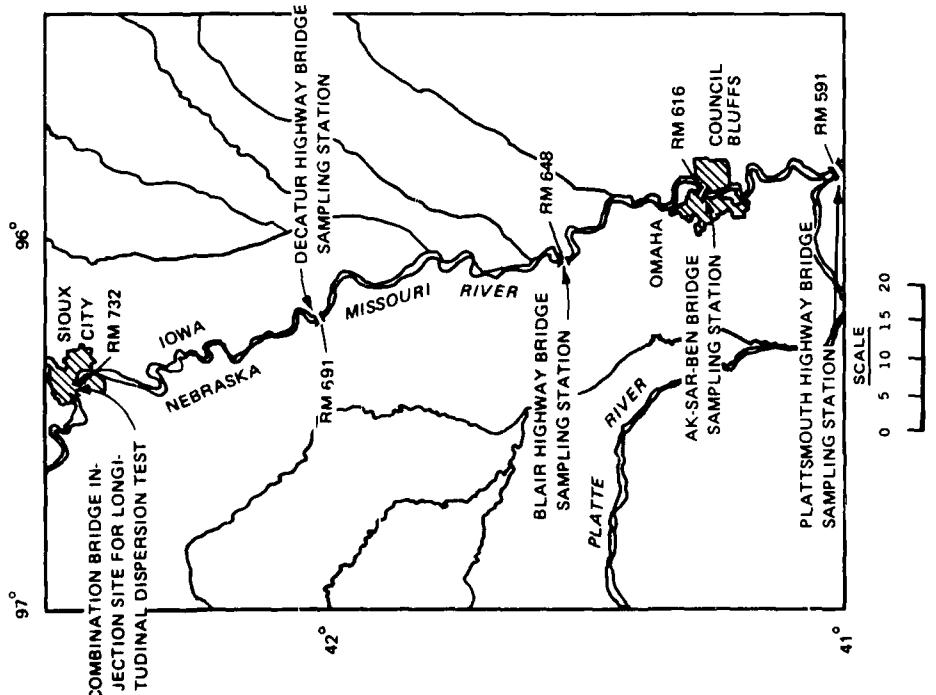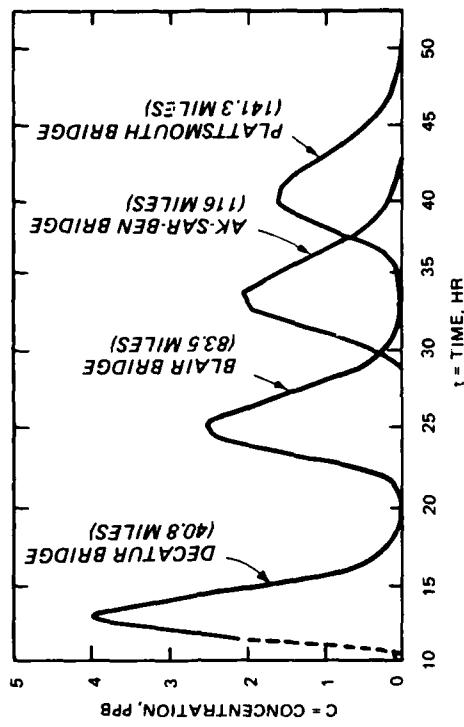
b. Concentration measurements

Figure 77. Data from Missouri River study on longitudinal mixing
(after Yotsukura, Fischer, and Sayre 1970) (Continued)
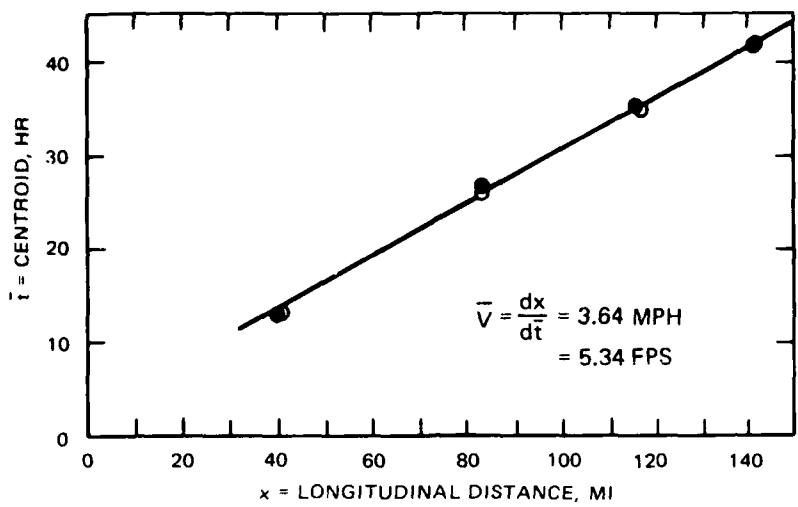
a. Study reach

c. Variation of centroid
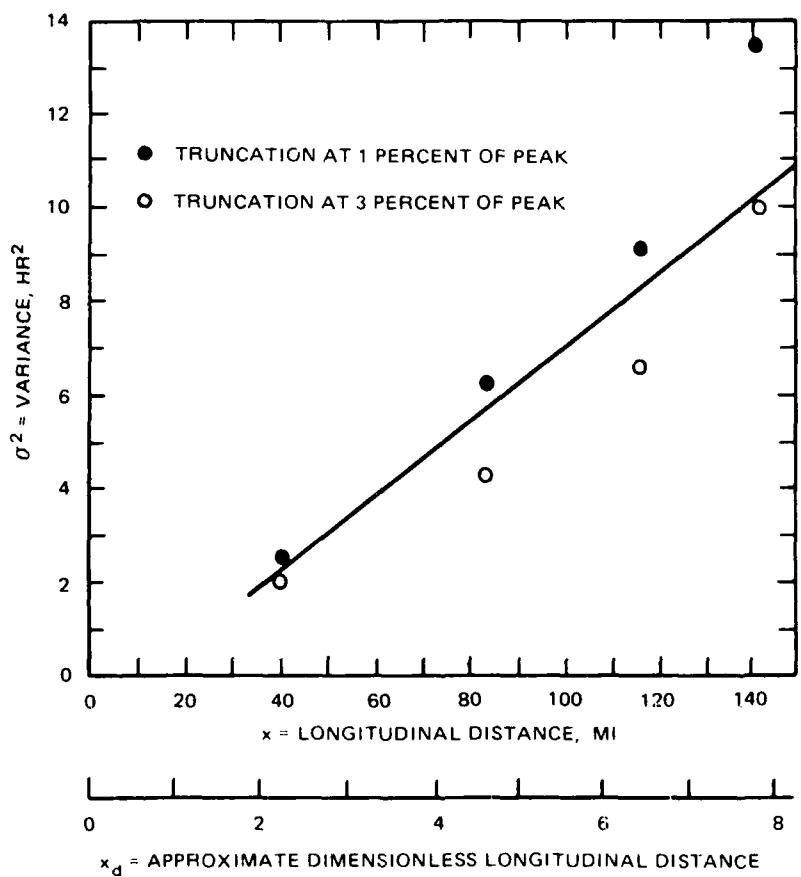


d. Variation of variance

Figure 77. (Concluded)

374

only significant tributary entering the study reach, but the discharge data do not show a significant increase at the Plattsmouth Highway Bridge. The channel width was maintained at 500 ft to 800 ft by dikes and jetties. The depth of the thalweg was generally less than 25 ft. At the time of the test, the bed form was primarily flat or plane bed with a Manning's n of 0.015. The corresponding slope of the energy grade line was 0.0002. One of the tables shows that the average depth and shear velocity were 9.7 ft and 0.25 fps; the average of the depths for seven cross sections in another table is 10.6 ft. The measured velocities varied from 3.9 fps at the upstream end of the reach to 6.0 at the downstream end; the time-of-travel analysis of the data indicated an average velocity of 5.34 fps (Figure 77c). No depth profiles or velocity distributions were given.

The dye release consisted of 600 lb of 20% solution of Rhodamine WT, which was released as a line source across the middle of the channel just downstream of the Combination Bridge at Sioux City. Concentrations were measured at the Decatur Highway Bridge, the Blair Highway Bridge, the Ar-sar-ben Bridge, and the Plattsmouth Bridge corresponding to flow distances of 40.8, 83.5, 116.0, and 141.3 miles or dimensionless distances $(x_d)$ of 2.4, 4.7, 6.2, and 7.4 based on $\alpha = 0.6$ , $B = 640$ ft , and $x/V = \bar{t}$ from the tracer measurements. At the Decatur Bridge, measurements were made at five transverse positions in the channel; at the other stations, three transverse locations were used. Only the cross-sectional average concentrations were reported, but the values of $x_d$ indicate that the concentrations should have been relatively uniform across the channel width for all of the measurement stations.

The concentration distributions are shown in Figure 77b with the corresponding centroids $(\bar{t})$ in Figure 77c and the variances $(\sigma^2)$ in Figure 77d based on truncating the distributions at both 1% and 3% of the maximum concentrations, as given by the authors. As the figure shows, the amount of truncation can have a significant effect on the calculated values of $\sigma^2$ and therefore on the calculated value of E . The line shown on the figure is the one originally drawn by the authors

375

and gives an E of 15,000 $ft^2$/sec. Because of the sensitivity of $\sigma^2$ and E to the tails of the distributions, the authors recommended using a routing procedure (or simulation, Section 7.6.2) starting with the first measured distribution. They demonstrated that the values of E obtained with this procedure were not very sensitive to truncation of the tails of the distributions; for various subreaches, the E values changed by -17% to +14% when the distributions were truncated. The difference in the slopes of lines through the two sets of data points in Figure 77d is on the order of 30%, but that is a comparison of 1% and 3% truncation, not a comparison of truncation and no truncation as was done for the routing procedure. Based on the routing procedure, the authors concluded that E was approximately 16,000 $ft^2$/sec, corresponding to $E/HU_* = 6,600$ . This is the largest non-dimensional longitudinal dispersion coefficient that is known to the writers; there has been no subsequent explanation of this value in comparison to the more frequently encountered range of dimensionless values of 100 to 1000 (Fischer et al. 1979).

### 7.8.4  Lower Mississippi River (McQuivey and Keefer 1976b)

In 1974, McQuivey and Keefer (1976b) performed a longitudinal dispersion experiment in 179-mile-long reach of the Mississippi River below Baton Rouge, La. (Figure 78a). The flow rate was 792,000 cfs at Baton Rouge at the time of the release and 798,000 cfs at Belle Chase, 152 miles downstream of the injection site, when the tracer arrived there. The hydraulic parameters for this reach of the river were given (McQuivey and Keefer 1976a) as hydraulic radius = 55.0 ft, $U_* = 0.19$ fps , B = 2845 ft , and V = 4.85 fps . The movement of the peak concentration indicates a velocity of 4.6 fps. No cross-sectional profiles or velocity distributions were given. For the width-to-depth ratio which existed, the average depth would be approximately equal to the hydraulic radius.

At 9 a.m. on April 24, 1974, a dye release consisting of 4,000 lb of 20% solution of Rhodamine WT was made near the center of the channel at river mile 228 near Baton Rouge, La. Concentrations

376
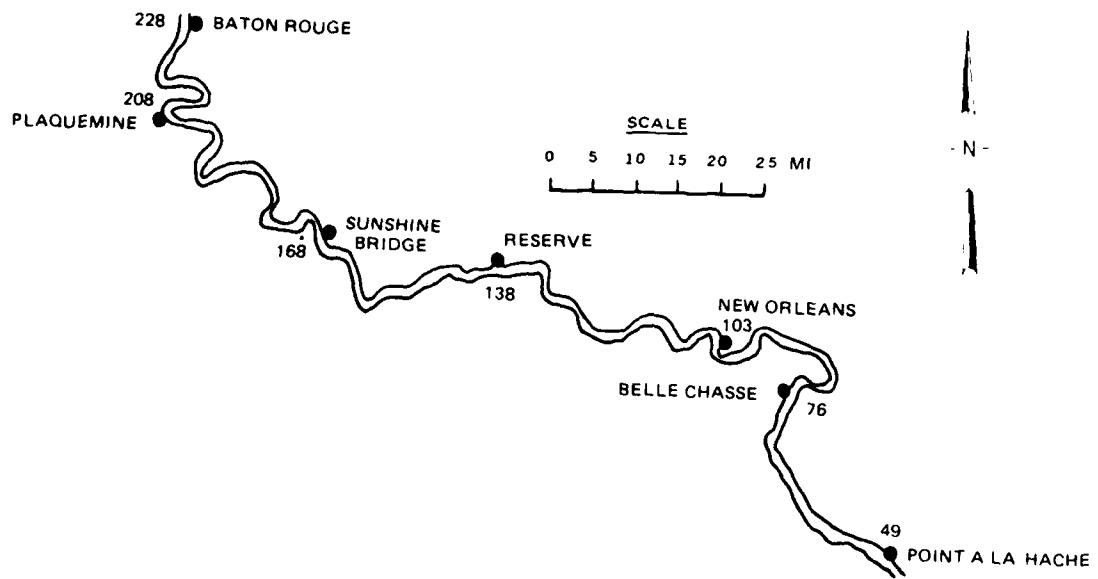
a. Study reach
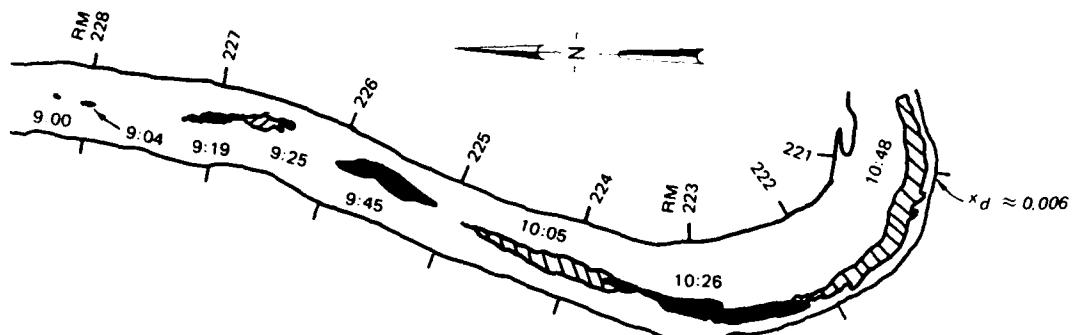


b. Outlines of tracer cloud

Figure 78. Data from Mississippi River study on longitudinal mixing (after McQuivey and Keefer 1976b) (Sheet 1 of 3)
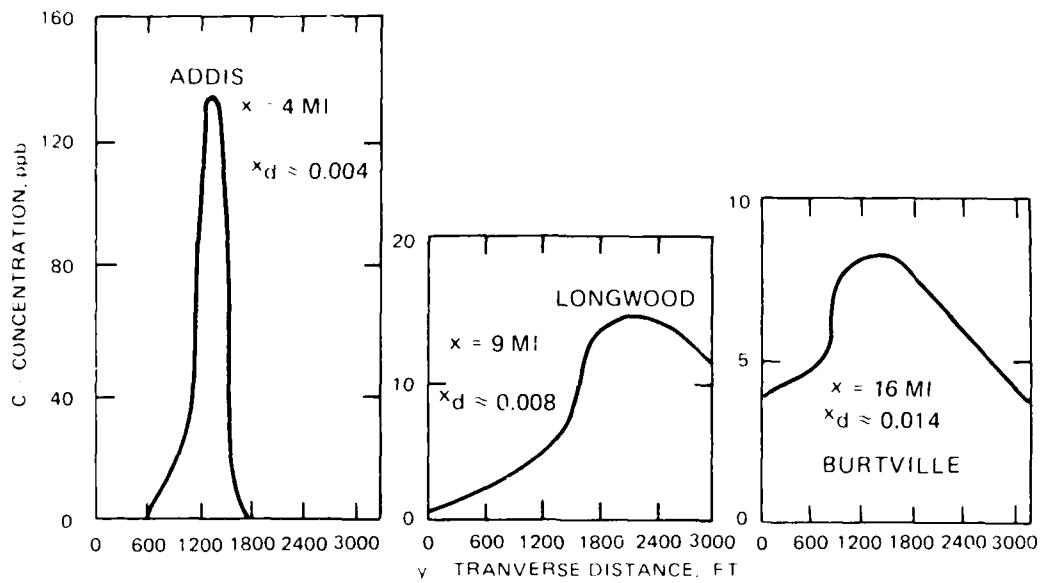
c. Transverse concentration distributions
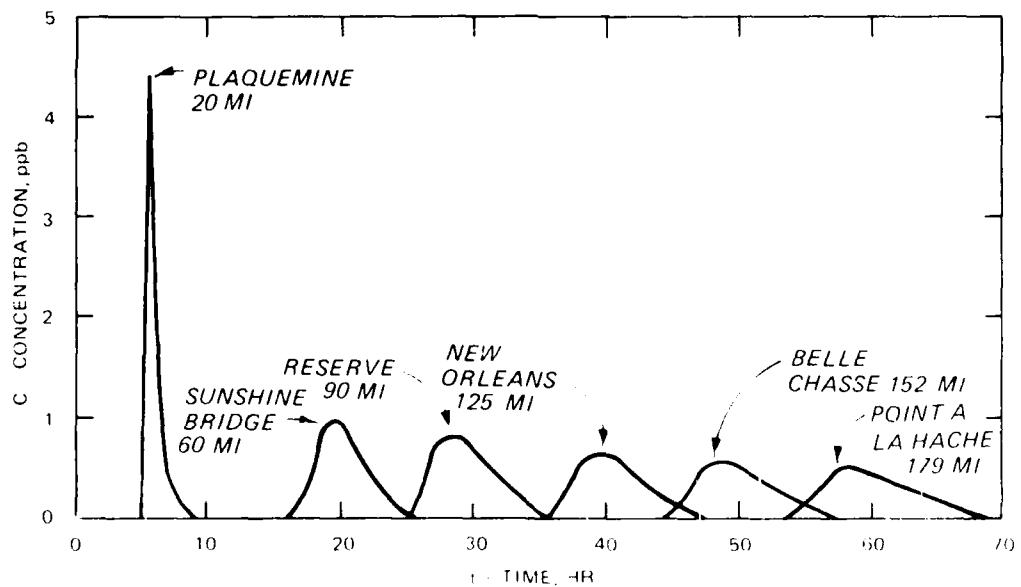


d. Concentration measurements

Figure 78. (Sheet 2 of 3)

378
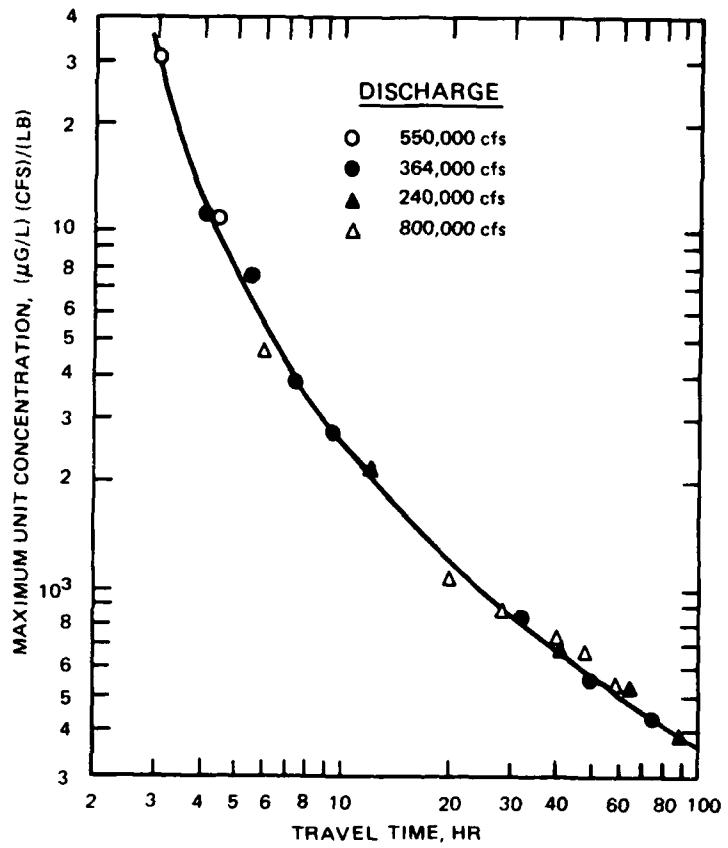
e. Variation of maximum unit concentration (after
Martens et al. 1974)

Figure 78. (Sheet 3 of 3)

379

were measured at nine downstream locations corresponding to dimension-
less distances ($x_d$) of 0.004, 0.008, 0.014, 0.018, 0.053, 0.080, 0.11,
0.13, and 0.16, using the hydraulic parameters given above and an
assumed $\alpha$ of 0.6. These values of $x_d$ indicate that much, it not
all, of the study reach was in the initial period and that the dye
cloud would not be expected to fill the channel width at the upstream
stations. At the first three stations, samples were collected near the
surface and at a depth of 50 ft to determine the degree of vertical
mixing and across the surface to determine the degree of lateral
mixing.

Figure 78b shows the outline of the dye cloud as obtained from
aerial photographs during the early period while the cloud was visible.
The cloud is seen to move toward the right bank as it enters the bend,
as would be expected because of the larger depths and velocities on the
outside of the bend. Also, it seems apparent that much of the early
longitudinal stretching of the cloud must have been associated with the
vertical distribution of velocity since the amount of transverse varia-
tion of velocity within the cloud probably was not great enough to
cause the observed amount of elongation.

At Addis ( $x_3$ = 1.1 , where $x_3$ is the nondimensional distance
based on the depth for 3D transport), the concentrations near the sur-
face were observed to be about twice those at 50-ft depth. The ana-
lysis of Section 5.2.7 indicates that vertical uniformity should have
been achieved at this value of $x_3$ . Since details of the measurements
were not given, it is difficult to provide a definite explanation con-
cerning why vertical uniformity did not exist, but one possibility is
that the helical motion of the flow entering the bend was distorting
the cloud and the measurements were made in a part of the cloud with
higher surface concentrations. (See Figure 61.) Vertical uniformity
was found at Longwood and the downstream stations. Some of the mea-
sured transverse distributions are shown in Figure 78c. These distri-
butions were apparently obtained as the peak concentration passed the
measurement stations.

380
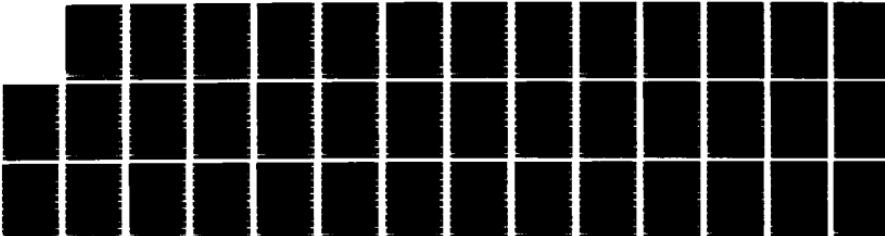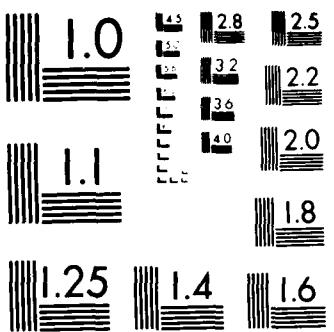
MICROCOPY RESOLUTION TEST CHART
NATIONAL BUREAU OF STANDARDS-1963 A

Figure 78d gives the distributions of cross-sectionally averaged
concentrations as measured at the six downstream stations. No informa-
tion was given on the sampling points within the cross sections or on
the method of obtaining the cross-sectional average. The centroids and
variances of the distributions were not given. The longitudinal dis-
persion coefficient was obtained by McQuivey and Keefer as approxi-
mately 7,500 $ft^2$/sec or 900 $HU_*$ by a method similar to the 1D simula-
tion procedure (Section 7.6.2a). Figure 78e (Martens et al. 1974)
shows a correlation of the variation of the maximum concentration from
four tracer tests in the same reach of the river but with different
discharges. The correlation of all of the tests was obtained by mul-
tiplying the observed maximum concentrations times the river flow rate,
dividing by the weight of the tracer, and plotting the results versus
travel time (not distance). This particular curve is applicable to
only this reach of the Mississippi River; the same type of correlation
was discussed by Hubbard et al. (1982) in a more general context.

## 7.8.5  Susquehanna River (Environmental Laboratory, WES)

In 1981, personnel of the Environmental Laboratory of the Water-
ways Experiment Station conducted longitudinal dispersion experiments
in the West Branch of the Susquehanna River immediately upstream of
Williamsport, Pa. The flow rate was 4,200 cfs. The average hydraulic
parameters were approximately $V = 0.6$ fps , $B = 700$ ft , $H = 10$ ft ,
and $n = 0.035$ . This section of the river was essentially straight
with the depths increasing gradually in the downstream direction due to
a low dam.

At 11:45 a.m. on October 12, 1981, a release of Rhodamine WT dye
was made by navigating a boat directly across the river and releasing
the dye continuously across the width. Even if the release rate were
constant, this method of injection gives higher initial concentrations
in the regions of lower depths and velocities. Concentrations were
measured at downstream cross sections with a submersible pump and a
flow-through fluorometer on a boat which continuously traversed back
and forth across the river. The resulting measurements were used to

381

produce 3D graphs giving the variation of concentration with distance across the river and time. An example is shown in Figure 79 for a longitudinal distance of 13,100 ft or $x_d$ of about 0.01.

As far as the writers know, these are the only available data that simultaneously illustrate the effects of the vertical and transverse variations of velocity for the early part of the longitudinal spreading process in a river. The effects of the transverse distribution of velocity can be seen in the fact that the cloud, for this relatively small value of $x_d$, becomes distorted in the general shape of the velocity distribution with the dye arriving first in the central part of the river and later along the sides. Thus, it can be seen that the primary effect of the transverse distribution of velocity was to provide differential advection of the different parts of the cloud but that transverse mixing had not yet had sufficient time to mix the dye cloud across the width of the river. Thus, the transverse distribution of velocity was contributing to an elongation of the cloud, but not to the mixing or dispersion. Nevertheless, at each transverse position across the width, the cloud has been dispersed longitudinally as indicated by the time required for the cloud to pass that transverse position (e.g., about 0.5 hr at a transverse position of 400 ft). This dispersion must have been due primarily to the dispersion caused by the combined effects of the vertical distribution of velocity and the vertical mixing.

Analysis and publication of these data have not been completed; therefore, the information on the hydraulic parameters must be taken as being approximate. Nevertheless, this brief description of one of the tests and Figure 79 are included because of the uniqueness of the data.

7.8.6  Comment

While there are many general comments that could be made from these and other examples of field studies, the only one which will be made concerns the dimensionless distance variable $x_d$. Regardless of the absolute size of a river, from the small Copper Creek to the lower Mississippi River, this variable gives a general indication of the
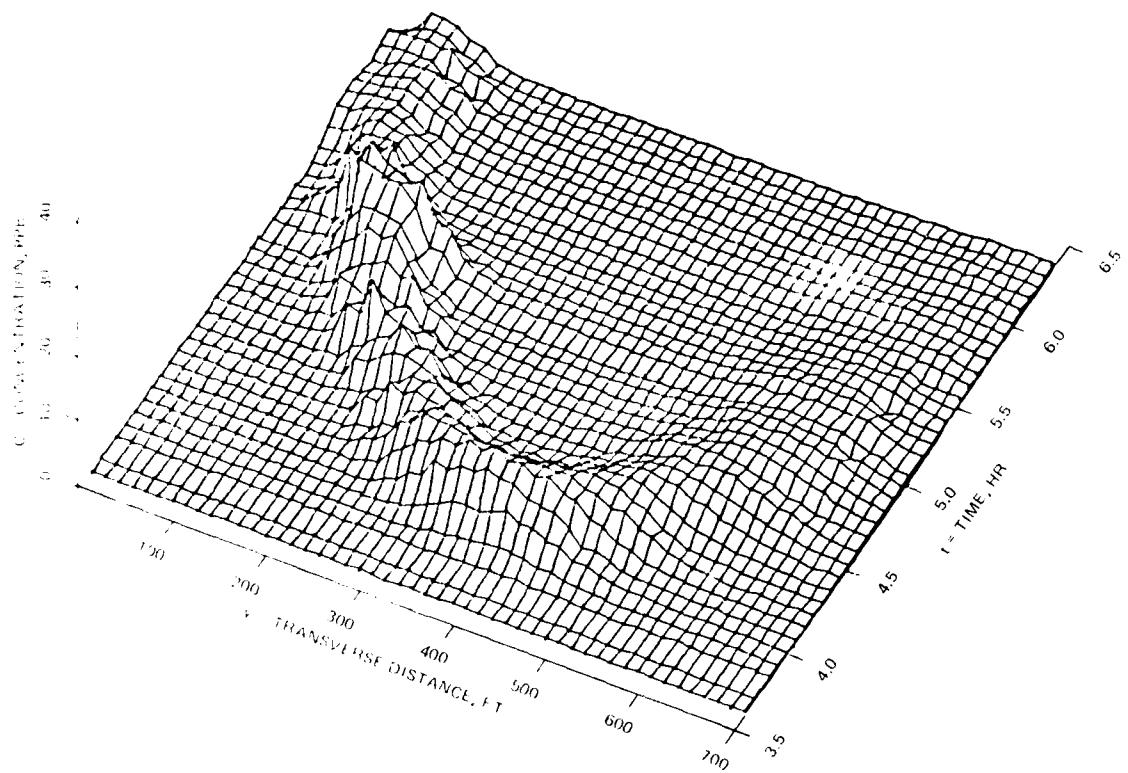
Figure 79.  Data from Susquehanna River study
on longitudinal mixing

degree of transverse uniformity of concentration distributions to be
expected and therefore also an indication of the regions in which to
expect 1D behavior of the transport process.

# CHAPTER 8. APPLICATIONS

## 8.1 INTRODUCTION

In this chapter some calculated examples are given for both
initial mixing and ambient transport to illustrate the application of
the principles discussed in the previous chapters. It must be empha-
sized that it would definitely be a mistake to try to use these illu-
strative examples as the primary source of information for making cal-
culations for transport problems. The extensive discussion in the
preceding chapters is intended to show the bases, assumptions, limi-
tations, etc., for the various types of analyses; as in any type of
problem, it is inappropriate to try to apply the calculation methods
without thoroughly understanding them.

## 8.2 SUMMARY OF PROCEDURES

There are so many types of discharges, types of rivers, and ob-
jectives of analysis that it is essentially impossible to summarize in
a concise form all of the information that is needed and all of the
steps that should be taken for any general type of analysis. Recogniz-
ing this limitation, Table 9 presents some of the major types of infor-
mation and decisions that are needed in many situations to calculate
the location and magnitude of concentrations which result from a
discharge.

There are at least two types of situations missing in Table 9
and in the earlier parts of this manual (because the literature does
not contain well-defined means of addressing these situations). First,
there is not a clear definition of how to define the transition point
between initial mixing and ambient transport. The types of analyses
normally done for these two parts of a problem are fundamentally dif-
ferent. In the initial mixing analysis, there is no consideration of
the turbulence in the ambient flow or the receiving water, and the
analysis is based on the integral of the fluxes while the ambient
transport analysis deals directly with the continuous distributions of
concentration, velocity, depth, etc. Thus, it is not possible to have

384

Table 9

Summary of Procedure

| Activity | Information Required |
|---|---|
| 1) Define environmental impact problem, objectives of analysis, and region of interest. | What is the problem associated with the pollutant?<br><br>Where is the area of concern, i.e., where do concentrations need to be known?<br><br>Define $x_{min}$ = minimum downstream distance for discharge or spill location at which concentrations need to be determined.<br><br>Define $x_{max}$ = maximum downstream distance from discharge or spill location at which concentrations need to be determined. |
| 2) Characterize receiving water. | River geometry - depth (h = local depth, H = average depth), width (B), alignment, meandering, type of cross-sectional shapes, potential storage zones (Section 7.2.1).<br><br>Hydraulic characteristics - mean velocity ($u_a$ or V), resistance coefficient (f = friction factor, n = Manning's coefficient, etc.) or slope (S) (Section 7.2.1).<br><br>Diffusive/dispersive characteristics - shear velocity ($U_*$); vertical diffusivity ($e_z$), if needed for 3D problems; transverse mixing coefficient ($e_y$); longitudinal mixing coefficient (E), if needed for unsteady problems (Sections 7.4, 7.7). |

(Continued)

(Sheet 1 of 5)

385

Table 9 (Continued)

| Activity | Information Required |
|---|---|
| 3) Determine initial characteristics of discharge. | a) <u>Continuous</u>.<br>Geometry - cross-sectional area for single port or channel discharges ($a_o$ and $L_o$) (Sections 3.1.1, 3.3.1); length ($L_D$), port diameter (D), and port spacing (L) for diffusers (Section 3.2.1); direction of discharge relative to vertical and relative to ambient flow.<br><br>Fluxes - total momentum flux ($M_o$), total buoyancy flux ($J_o$), discharge ($Q_o$), mass flux of solute ($Q_{co}$) (Section 2.2.2).<br><br>b) <u>Instantaneous</u> (Section 3.5).<br>Geometry - typical length dimension.<br><br>Quantities - impulse, buoyancy, volume, mass of solute. |
| 4) Determine if initial mixing analysis and/or ambient transport analysis is necessary. | Estimate initial-mixing length scale ($L_{IM}$).<br><br>a) <u>Continuous</u>: $L_{IM} = \max (\ell_{Mu} = M_o^{1/2}/u_a$ , $\ell_{Ju} = J_o/u_a^3$, H, $L_D$). |

(Continued)

386

Table 9 (Continued)

| Activity | Information Required |
|---|---|
| 4) Determine if initial mixing analysis and/or ambient transport analysis is necessary. (Continued) | b) Instantaneous: $L_{IM} = \max(\ell_o, H)$. <br><br> Estimate ambient transport transverse mixing length scale as standard deviation developed solely by transverse mixing: <br><br> $L_{AT} = (2e_y x_{min}/V)^{1/2}$. <br><br> Test 1: Test for low velocity or region of interest - Is $x_{min} < 10\ L_{IM}$ ? <br><br> Yes - Initial mixing analysis required due to low ambient velocity or small region of interest. <br> No - Initial mixing analysis may not be required. Go to Test 2 below. <br><br> If Yes above, is $x_{max} < 10L_{IM}$ ? <br><br> Yes - Only initial mixing analysis required. <br> No - Both initial mixing and ambient transport analyses required. <br><br> Test 2: Test for memory of initial mixing - Is $L_{AT} > 10L_{IM}$ or $> B/2$ ? <br><br> Yes - Only ambient transport analysis required. Use outfall geometry for initial condition for ambient transport analysis. <br> No - Initial mixing analysis required, followed by ambient transport analysis. <br><br> (Continued) |

387

(Sheet 3 of 5)

Table 9 (Continued)

| Activity | Information Required |
|---|---|
| 5) Initial-mixing analysis. | a) Continuous. Submerged single-port outlet – Check discharge stability for deep or shallow conditions (Section 3.1.4). Use appropriate model depending on discharge and ambient conditions (Sections 3.1, 8.3.1). Submerged multiport diffuser – Check discharge stability for deep or shallow conditions (Section 3.2.2). Use appropriate model depending on discharge and ambient conditions (Sections 3.2, 8.3.2). Surface discharge – Check discharge stability for deep or shallow conditions (Section 3.3.2). Use appropriate model depending on discharge and ambient conditions (Sections 3.3, 8.3.3). Results: Position, width, and dilution (concentration) of mixed discharge at desired points along trajectory. b) Instantaneous. See Section 3.5. |
| 6) Ambient-transport analysis. | a) Continuous. Initial conditions from location and geometry of outfall, if initial mixing analysis not required, or from conditions at end of initial mixing analysis. 3D analysis required if $x_{min} < x_{3,m} h^2 v_x / d_z$ (Figure 36). See text. |

(Continued)

388

Table 9 (Concluded)

| Activity | Information Required |
|---|---|
| 6) Ambient-transport analysis. (Continued) | 2D analysis required if $x_{min} < x_{d,m} B^2 V/e_y$ (Figure 42). Analytical solutions (Section 5.3) or numerical solution of Eq. 4.7.33 or 4.7.34. (May switch to 1D analysis at $x$ corresponding to $x_{d,m}$ using results at end of 2D region as initial conditions for 1D calculations.) |
| | 1D analysis acceptable if $x_{min} > x_{d,m} B^2 V/e_y$ (Figure 42). Analytical solution (Section 5.4) or numerical solution of Eq. 4.8.31. |
| | b) Instantaneous.<br>Initial conditions from spill or release information. |
| | 2D analysis required if $x_{min} < x_{d,m} B^2 V/e_y$ (Figure 42). Numerical solution of Eqs. 6.2.1 or 6.2.2. See also Figures 47 and 48 for very general indication of concentration distributions, and Section 6.2.4. (May switch to 1D analysis at $x$ corresponding to $x_{d,m}$ using results at end of 2D region as initial conditions for 1D calculation.) |
| | 1D analysis acceptable if $x_{min} > x_{d,m} B V/e_y$ (Figure 42). Empirical approach (Section 7.7.3c) for $x > x_{d,m} B^2 V/e_y$ or analytical solutions (Section 6.3) for $x > B^2 V/e_y$. |

(Sheet 5 of 5)

389

a smooth transition from the initial mixing analysis to the ambient
transport analysis; rather, the first must just be stopped at some
point and the second begun. It is still largely a matter of case-by-
case evaluation and judgment in picking a reasonable point at which to
change from one to the other. For example, if there is a discharge
normal to the axis of a river so that the discharge behaves as a jet in
a crossflow, the slope of the bent-over trajectory might be used to
select the point at which to end the initial mixing analysis. When the
slope becomes 1 (across the river) to 5 (longitudinal) or 1 to 10, the
cross-channel momentum is probably so low that the initial mixing
analysis could be stopped. In any case, it is usually advisable to do
a sensitivity analysis to determine whether the results that are needed
are very sensitive to the assumed end of the initial mixing region. If
there is a high and unacceptable sensitivity, then a different type of
analysis may be needed. Two possibilities would be a physical model
study or a calculation based on a higher-level turbulence closure
scheme (e.g., Rodi 1980).

A second item that is missing is an analysis for vertically
stratified flow conditions which might exist downstream of a buoyant
discharge if the effects of the initial momentum of the discharge
become unimportant (due to a vertical or cross-channel discharge, for
example) before the initial density difference is totally mixed with
the ambient water. While there have been many analyses of vertically
stratified flows, there has not been a general application and inter-
pretation of these analyses for riverine situations.

## 8.3 EXAMPLES OF INITIAL MIXING ANALYSIS

The following three examples illustrate the use of the predic-
tive equations and diagrams that were presented in Chapters 2 and 3.
Some variability in the ambient conditions is assumed in order to
demonstrate the solution sensitivity. Note, in particular, that the
examination of discharge stability is a common step in all cases in
order to ascertain whether "deep-water" or "shallow-water" conditions
prevail at the discharge site and to select the appropriate model.

390

### 8.3.1  Vertical Single-Port Discharge

An industrial effluent is discharged by means of a vertical single-port pipe of diameter $D = 0.5$ m at the bottom of a run-of-the-river reservoir. The discharge has a flow rate $Q_o = 0.6$ m$^3$/sec , giving $U_o = 3.06$ m/sec , and is lighter than the ambient water with a relative density difference $(\rho_a - \rho_o)/\rho_a = 0.01$ giving a buoyant acceleration $g'_o = 0.098$ m/sec$^2$ . The initial concentration of a pollutant is 200 ppm. The reservoir is unstratified with a water depth $H = 8$ m at the discharge site and the ambient velocities vary between $u_a = 0$ to 0.5 m/sec due to variable river flow and reservoir operation.

<u>a</u>.  <u>Stagnant conditions</u>.  A vertical buoyant jet will result, characterized by the Froude number (Table 5)

$$F_o = \frac{U_o}{\sqrt{g'_o D}} = 13.8$$

and the momentum length scale (Table 6)

$$\ell_M = \frac{M_o^{3/4}}{J_o^{1/2}} = \frac{(U_o Q_o)^{3/4}}{g'_o Q_o^{1/2}} = 6.5 \text{ m}$$

First, the discharge stability is checked by computing the ratio

$$\frac{\ell_m}{H} = 0.81 < 4.3$$

This comparison to Eq. 3.1.8 indicates that the discharge is operating well in the deep-water regime, and a well-defined jet will result with a surface impingement zone of thickness $h_i = 0.08 H = 0.6$ m (Section 3.1.4c). Hence, the effective level up to which entrainment takes place is $z_i = 8.0 - 0.6 = 7.4$ m .

The centerline dilution $S_c$ at the level $z_i$ is found from Eq. 3.1.3 or Figure 5. These indicate that at the level $z_i/(DF_o)$ = 1.30 corresponding to $z_i = 7.4$ m , the centerline dilution is

$$S_c = 3.5$$

Thus, the maximum pollutant concentration that can be found in the "boil" region at the free surface is

$$c_c = \frac{c_o}{S_c} = \frac{200}{3.5} = 57 \text{ ppm}$$

Observe also from Figure 5 that the buoyant jet operates, for the largest part, in the pure jet regime and only commences its transition to the plume at the level of impingement.

b. Crossflow conditions. The applicable parameters are the crossflow ratio (Table 5)

$$R = \frac{u_a}{U_o} = \frac{0.5}{3.06} = 0.16$$

the jet-crossflow length scale (Eq. 2.10.1)

$$\ell_{Mu} = \frac{M_o^{1/2}}{u_a} = \frac{(U_o Q_o)^{1/2}}{u_a} = 2.7 \text{ m}$$

and the plume-crossflow length scale (Eq. 2.10.2)

$$\ell_{Ju} = \frac{J_o}{u_a^3} = \frac{g_o' Q_o}{u_a^3} = 0.47 \text{ m}$$

Since $\ell_M/\ell_{Mu} > 1$ the buoyant jet deflection and dilution will

392

initially be governed by the pure jet laws (two phases, $z \sim x^{1/2}$ and $z \sim x^{1/3}$) as depicted in Figure 8. However, as the buoyant jet has some buoyancy, there is a possibility that the final phase ($z \sim x^{2/3}$) of the pure plume (Figure 9) will be entered. This possibility is examined below.

The jet trajectory as determined from Figure 8 is plotted in dimensional form in Figure 80a. It shows the initial and the final phases of pure jet deflection. Also shown in the figure is the final phase of the pure plume deflection (as obtained from Figure 9) and its intersection with the pure jet trajectory. This intersection occurs at a vertical distance of $z = 15$ m , which is higher than the actual water depth $H = 8$ m . Thus, for the present example, the conclusion is that the deflection of the buoyant jet within the available water column and for the ambient velocity of $u_a = 0.5$ m/sec is governed solely by pure jet conditions.

The jet trajectory in a linear coordinate system is shown in Figure 80b, indicating that surface impingement occurs at a downstream distance of about 9 m. Center-line dilutions are shown in Figure 80a. At the surface impingement point,

$$S_c = 10$$

giving a maximum pollutant concentration

$$c_c = \frac{c_o}{S_c} = \frac{200}{10} = 20 \text{ ppm}$$

Comparison to the stagnant result ($c_c = 57$ ppm) demonstrates the significant mixing action induced by an ambient crossflow.

### 8.3.2  Co-flowing Submerged Multiport Diffuser

A multiport diffuser discharges waste heat from a thermoelectric power plant into an adjacent river. The discharge flow is $Q_d = 15$ m$^3$/sec at a temperature rise $\Delta T_o = 20°$ C . The river is well
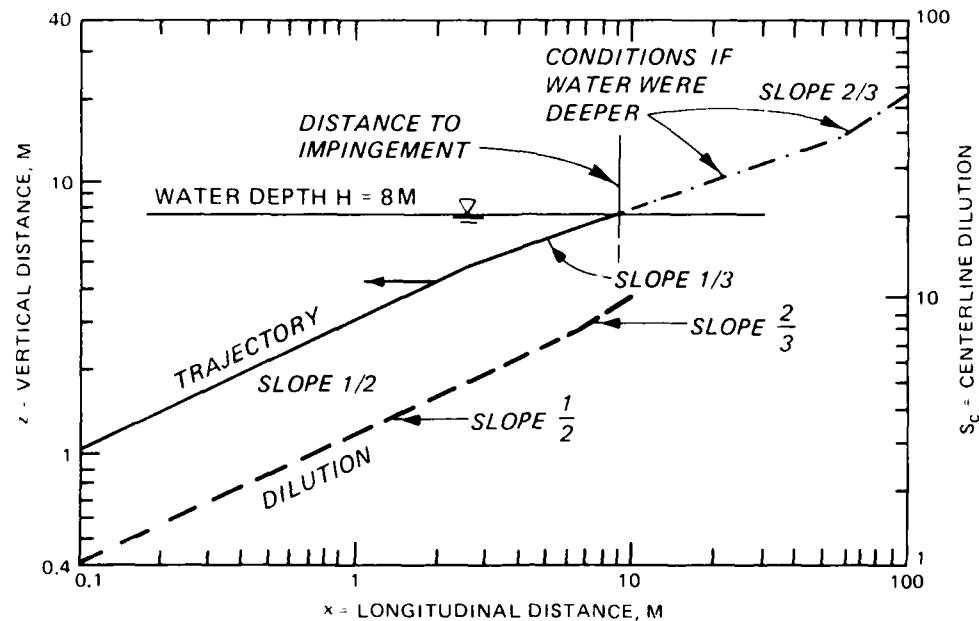
a.  Log-log coordinates
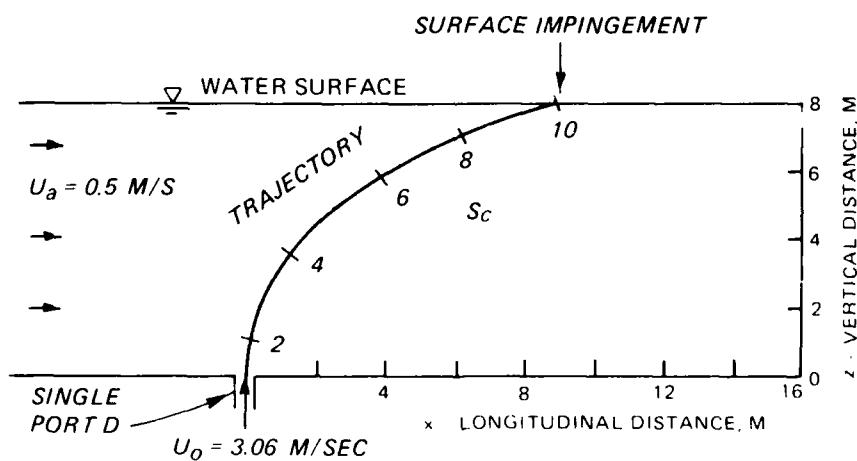


b.  Linear coordinates

Figure 80.  Example of vertical single-port
discharge in crossflow

channelized with a width of 300 m. The river depth and velocity vary from $H = 3$ m and $u_a = 0.6$ m/sec for average flow conditions (river flow rate $Q_R = 540$ m$^3$/sec ) down to $H = 2$ m and $u_a = 0.3$ m/sec for low-flow conditions ($Q_R = 180$ m$^3$/sec). The ambient water temperature is $T_a = 15°$ C . The diffuser pipe length is $L_d = 100$ m commencing at one bank of the river and extending across one third of the width. There are 20 attached ports (spacing $L = 5$ m, diameter $D = 0.4$ m) pointing in the downstream direction, thereby forming a co-flowing unidirectional multiport diffuser (Figure 18).

a. Low-flow conditions. The discharge velocity through each port is $U_o = Q_d/(20D^2\pi/4) = 6.0$ m/sec . The relative density difference corresponding to the temperature rise is $(\rho_a - \rho_o)/\rho_a = 0.0047$ and the buoyant gravitational acceleration is $g_o' = 0.046$ m/sec$^2$ . The momentum flux and discharge per unit length from the diffuser are $m_o = M_o/L = U_o Q_d/L_d = 0.90$ m$^2$/sec (Eq. 3.2.3) and $q_o = Q_d/L_d = 0.15$ m$^2$/sec , respectively. The diffuser parameters are the equivalent slot with (Eq. 3.2.4)

$$B = \frac{D^2\pi}{4L} = 0.025 \text{ m}$$

and the slot densimetric Froude number

$$F_s = F_o \left(\frac{4L}{D\pi}\right)^{1/2} = \frac{U_o}{\sqrt{g_o'D}} \left(\frac{4L}{D\pi}\right)^{1/2} = 176$$

The momentum length is $\ell_m = BF_s^{4/3} = 24.6$ m (Table 6). The discharge stability can be evaluated from the criterion (Eq. 3.2.5, even neglecting the effect of ambient velocity)

$$\frac{H}{\ell_m} = 0.12 < 1.84 \ (1 + \cos^2 \theta_o)^2 = 7.36$$

since for the horizontal discharge $\theta_o = 0$ deg . Thus, the diffuser operates in the unstable shallow-water domain. This fact would be emphasized even more if the additional destabilization due to ambient momentum (criterion of Eq. 3.2.7) were consulted. Unstable conditions are quite typical for cooling water diffusers.

The characteristics of the fully mixed diffuser plume are predicted by the bulk dilutions $S$ (Eq. 3.2.14). The ambient volume flux parameter is $V = u_a H/(Q_d/L_d) = 4.0$ , giving

$$S = 8.6$$

and a contraction coefficient $C_c = 0.65$ (Eq. 3.2.16), so that the downstream width of the fully mixed plume is $C_c L_d = 65$ m . The average excess temperature downstream will be

$$\Delta T = \frac{\Delta T_o}{S} = 2.3^\circ \text{ C}$$

Note that excess temperature acts exactly like a tracer or pollutant concentration $c$ . The total ambient flow drawn over the diffuser line is

$$(S-1)Q_d = 114 \text{ m}^3/\text{sec}$$

or 63% of the river flow ($Q_R = 180$ m$^3$/sec). Thus, there is no recirculation tendency, which might arise, however, if the riverflow were even lower than this low-flow condition.

b. <u>Normal-flow conditions.</u> With an increased volume flux parameter $V = u_a H/(Q_d/L_d) = 12.0$ , the bulk dilution is now (Eq. 3.2.14)

$$S = 15.8$$

396

and the contraction is less severe, $C_c = 0.85$ (Eq. 3.2.16). The mixed temperature rise is lower

$$\Delta T = \frac{\Delta T_o}{S} = 1.3° \text{ C}$$

Only $(S-1)Q_d = 41\%$ or $222 \text{ m}^3/\text{sec}$ of the river flow ($Q_R = 540 \text{ m}^3/\text{sec}$) participates in the mixing that is now much more influenced by the river flow.

### 8.3.3 Surface Buoyant Jet

Blowdown water from an industrial cooling process enters a run-of-the-river reservoir in the form of a surface channel of width $2b_o = 2 \text{ m}$ and depth $h_o = 0.5 \text{ m}$. The total discharge flow rate is $1.5 \text{ m}^3/\text{sec}$ giving a velocity $U_o = 1.5 \text{ m/sec}$. The relative density difference is 0.0025 ($g_o' = 0.025 \text{ m/sec}^2$), and the concentration of a discharged radioactive substance is $c_o = 5 \text{ µCi/cm}^3$. The topography of the river channel drops rapidly to a relatively constant water depth of $H = 4 \text{ m}$. The ambient velocities are weak varying from essentially stagnant, $u_a = 0$, to mild crossflow conditions, $u_a = 0.10 \text{ m/sec}$.

a. **Stagnant conditions.** The relevant parameters are the length scale (Eq. 3.3.1)

$$L_o = \sqrt{h_o b_o} = 0.71 \text{ m}$$

the aspect ratio (Eq. 3.3.2), and the Froude number (Eq. 3.3.3)

$$A = \frac{h_o}{b_o} = 0.5 , \quad F_o' = \frac{U_o}{\sqrt{g_o' L_o}} = 11.3$$

giving the momentum length scale (Eq. 3.3.4)

$$\ell_M = 2^{1/4} L_o F_o' = 9.5 \text{ m}$$

The maximum jet penetration depth (Eq. 3.3.5) is

$$h_{max} = 0.35 \; \ell_M = 3.3 \text{ m}$$

occurring at a distance $x_{max} = 4.6 \; \ell_M = 44$ m (Eq. 3.3.6) from the shoreline. Thus, considering the criterion, Eq. 3.3.9,

$$\frac{h_{max}}{H} \approx 0.83 > 0.75$$

the discharge is affected by shallow-water conditions. Therefore, the centerline dilution predictions (Figure 20 or Eq. 3.3.8) must be adjusted by the dilution reduction factor $r_S = 0.93$ (Eq. 3.3.11). This gives the stable dilution (from Eq. 3.3.8)

$$r_S S_{cs} = (0.93)(1.0 \; F_o') = 10.5$$

This means that the radioactivity level after mixing is

$$c = c_o/10.3 = 0.5 \; \mu Ci/cm^3$$

which is attained after a distance (Eq. 3.3.7)

$$x_t = 13 \; \ell_M = 124 \text{ m}$$

Unless the reservoir is significantly wider than this, the jet would be affected by the opposite bank.

b. <u>Crossflow conditions.</u> Even under these weak crossflow conditions (Table 5),

$$R = u_a/U_o = 0.067$$

398

The criterion of Eq. 3.3.12 indicates

$$R \left(\frac{h_{max}}{H}\right)^{3/2} = 0.8 > 0.05$$

so that the buoyant jet becomes shoreline-attached. This is quite a common occurrence for buoyant surface discharges into rivers.

As mentioned in Section 3.3.2, the prediction for surface jets in crossflow is difficult, in particular under shoreline-attached conditions. For a first, conservative approximation, one may take the dilution as 50% of the non-attached or stagnant case, giving $S = 5$ in this case and $c = c_o/S = 1\mu Ci/cm^3$. The initial width of the recirculating zone is of order (Eq. 3.3.13)

$$\ell_{Mu} = M_o^{1/2}/u_a = 15 \text{ m}$$

These initial dilution and width estimates may be starting points for far-field calculations.

## 8.4 EXAMPLES OF STEADY AMBIENT TRANSPORT ANALYSIS

### 8.4.1 Point Source

A 3-ft-diam pipe discharges 10.6 cfs of water with a loading rate $(\dot{m})$ of a conservative pollutant of 150 g/sec at river mile (RM) 531.5 of the Missouri River (in the reach shown in Figure 68). For this stage of the river, the end of the outfall pipe is 150 ft from the left bank of the river. It is desired to determine the concentration distribution at RM 526.11. The river flow is 56,100 cfs, and the average depth and width are approximately 13 ft and 700 ft, giving an average river flow velocity of 6.2 fps.

For this situation, enough data are available on the alignment of the river and on the depth and velocity profiles that the most desirable approach would be to obtain the concentration distribution by using a numerical solution of Eq. 4.7.33 with interpolated values of h

and $v_x$ for each computational grid point and with $e_y$ obtained from Figure 62 for each computational cross section. Nevertheless, in this example, the concentration distribution is estimated from the analytical solutions given in Eq. 5.3.6 or 5.3.7. These solutions are based on the assumption of a constant diffusion factor $(D_f)$. For reaches containing many bends, a value of $D_f$ might be selected based on an average or typical bend. For the present example, it would be expected that the diffusion coefficients and therefore the diffusion factors might be significantly different in the two bends between the outfall and RM 526.11. The analysis below includes an illustration of the appropriate means of obtaining an average $D_f$ for reaches such as this one.

The effects of initial mixing should be negligible for this problem (if there is no significant temperature difference between the effluent and the river). The discharge velocity is about 1.5 fps while the river flow velocity is about 6.2 fps. Thus, the discharge momentum would not be sufficient to cause any significant penetration of the effluent across the river. Also, there is only a negligible increase in the effluent density associated with the pollutant load. As a rule-of-thumb, the density increase can be estimated as being 60% of the concentration. The initial concentration is $c_o = \dot{m}/Q_o = 150$ g/sec divided by 10.6 cfs (with the appropriate conversion factors) = 500 mg/$\ell$. The density increase is thus approximately 300 mg/$\ell$ (or 300 mg per 1000 g of water) or 0.03%.

From Section 7.5.3 the slope (S) is 0.00019, and for this width-to-depth ratio, it is reasonable to estimate the hydraulic radius $(R_H)$ as being equal to the depth. The shear velocity is then

$$U_* = (gR_HS)^{1/2} = 0.28 \text{ fps}$$

Based on the planform geometry (Figure 68a), the reach is schematized as four subreaches consisting of a bend to the right, a straight section, a bend to the left, and another straight section, as follows:

400

| Reach | RM | $\Delta x$, ft | $R_c$ ft | $\dfrac{VB}{U_* R_c}$ | $\alpha$ | $e_y$ ft$^2$/sec | $D_f$ ft$^5$/sec$^2$ |
|---|---|---|---|---|---|---|---|
| 1 | 531.5–529.9 | 8450 | 5200 | 3.0 | 3.6 | 13.1 | 20,600 |
| 2 | 529.9–528.8 | 5800 | -- | -- | 0.6 | 2.2 | 3,500 |
| 3 | 528.8–526.5 | 12150 | 3500 | 4.4 | 7.7 | 28.0 | 44,000 |
| 4 | 526.5–526.1 | 2100 | -- | -- | 0.6 | 2.2 | 3,500 |

For the straight reaches, $\alpha$ is assumed to be 0.6. For the bends, $\alpha$ is obtained from Figure 62. Since the values of $\alpha$ for field conditions in Figure 62 were obtained by a method which accounted for the effects of the variation of h and $v_x$, these effects must also be included in the use of these values of $\alpha$ for predictive purposes. This can be accomplished in an approximate way by the inclusion of $\psi$ in the definition of $D_f$ (Eq. 7.3.17). For the present calculation, $\psi$ is assumed to be equal to 1.5 for all subreaches.

The appropriate means for obtaining an average $D_f$ can be obtained from the concept that each value of $D_f$ is representative of the rate of transverse spreading in each subreach and that the total amount of spreading at any cross section is the accumulated effect of all upstream subreaches. This leads to the conclusion that the average diffusion factor should be taken as

$$\bar{D}_f = \frac{\Sigma (D_f \Delta x)_i}{\Sigma \Delta x_i}$$

The mathematical basis for this expression can be seen starting with Eq. 4.7.34 and replacing $m_x h^2 v_x e_y$ with a diffusion factor that is function of x but not of q or y so that

$$\frac{\partial c}{\partial x} = D_f(x) \frac{\partial^2 c}{\partial q^2}$$

Nondimensionalization would give

$$x_d = \int_o^x \frac{D_f}{Q^2} \, dx$$

rather than the expression in Eq. 5.3.1, but with this new definition of $x_d$, the analytical solutions of Eqs. 5.3.6–5.3.9 would still be applicable. If an average $D_f$ is defined for a given reach, then the value should be such that

$$x_d = \frac{\bar{D}_f x}{Q^2}$$

A comparison of these last two expressions leads to the conclusion that

$$D_f = \frac{1}{x} \int_o^x D_f \, dx$$

and discretization of this integral leads to the expression given above for $\bar{D}_f$. Application to the tabulated values of $D_f$ gives $\bar{D}_f = 25,800 \text{ ft}^5/\text{sec}^2$. The value of $x_d$ for the total reach length of 28,500 ft is then 0.23. Thus, it can be anticipated that the concentration distribution will be relatively uniform across the channel width (Fig. 42a) with the values being on the order of completely-mixed concentration which is $\dot{m}/Q = 94 \text{ µg}/\ell$.

In determining the concentration distributions, the value is required for

$$q_I = \int_o^{y_I} h v_x \, dy$$

402

This integral can be evaluated from the distribution of $hv_x$ in Figure 68b using $(v_x h)_{avg} = Q/B = 80.1 \text{ ft}^2/\text{sec}$ ; the result is $q_I = 20,900 \text{ cfs}$ for $q = 0$ at the left bank. The definitions of the dimensionless variables in Eq. 5.3.1 can be substituted into Eq. 5.3.6 or 5.3.7 (using $\bar{D}_f$) to obtain an expression for the concentration in terms of the original dimensional variables. Evaluation of this expression gives:

| q (cfs) | 0 | 10,000 | 20,000 | 30,000 | 40,000 | 50,000 | 56,100 |
|---|---|---|---|---|---|---|---|
| y (ft) | 0 | 185 | 310 | 425 | 515 | 610 | 750 |
| c (µg/ℓ) | 102 | 101 | 98 | 94 | 90 | 88 | 87 |

The conversion between q and y is accomplished in a manner similar to the evaluation of $q_I$ since

$$q = \int_0^y hv_x dy$$

## 8.4.2  Line Source

For the low-flow situation for the multiport diffuser discussed in Section 8.3.2, it is desired to determine if a temperature rise of 1° C will exist at any point along the left bank (assuming that the diffuser extends outward from the right bank of the river), and if so, to identify the region where the specified temperature rise exists. For this purpose, the temperature distribution which exists at the end of the initial mixing region downstream of the diffuser can be approximated as a line source across part of the width of the stream.

The temperatures along the left bank are estimated using the analytical solution (Eq. 5.3.8 or 5.3.9) based on the streamtube model with a constant diffusion factor. From Section 8.3.2, some of the hydraulic parameters are $H = 2 \text{ m}$ and $Q = 195 \text{ m}^3/\text{sec}$ ($180 \text{ m}^3/\text{sec}$ upstream of the diffuser and $15 \text{ m}^3/\text{sec}$ from the diffuser). The river is relatively straight, so $\alpha$ (Eq. 7.4.2) is taken as 0.5 and $\psi$

403

(Eq. 7.3.17) is taken as 1.5. The river slope is $10^{-5}$. For the large width-to-depth ratio the hydraulic radius is approximately equal to the mean depth so that the shear velocity can be calculated from

$$U_* = (gHS) \quad = 0.014 \text{ m/sec}$$

The diffusion factor (Eq. 7.3.17) is then

$$D_f = \psi H^2 V e_y = \psi H^2 V(\alpha H U_*) = 0.025 \text{ m}^5/\text{sec}$$

The conversions from dimensionless distances and temperatures (concentrations) to dimensional values using Eq. 5.3.1 are

$$x(\text{km}) = \frac{x_d Q^2}{D_f} = 1,520 x_d$$

$$\Delta T \ (^\circ C) = c_d \dot{m} \exp\left(-\frac{Kx}{V}/Q\right) = 1.54 c_d \exp\left(-\frac{Kx}{V}\right)$$

where $\dot{m}$ represents the temperature (heat) flux given by the product of the initial $\Delta T$ ($20^\circ$ C) and the diffuser discharge (15 m$^3$/sec) and the exponential decay term accounts for the surface heat transfer (Section 5.3.2). The first-order reaction rate coefficient (K) for surface heat transfer for this river is $5 \times 10^{-6}$ sec$^{-1}$ or 0.43 day$^{-1}$. Using Eq. 5.3.8 or 5.3.9 with $q_{d,1} = 0$ and $q_{d,2} = 0.66$ (since the calculation in Section 8.3.2 shows that 66% of the riverflow [(114 + 15)/195] was in the mixed diffuser flow), the calculated temperatures for the left bank ($q_d = 1$) and the right bank ($q_d = 0$) are

| Bank | $\Delta T$ ($^\circ$C) at Locations x (in kilometers downstream of diffuser) |
|------|----|----|----|----|-----|-----|-----|-----|-----|-----|-----|-----|
|      | 20 | 40 | 60 | 80 | 100 | 120 | 140 | 160 | 180 | 200 | 220 | 240 |
| Left | 0.08 | 0.27 | 0.41 | 0.49 | 0.53 | 0.55 | 0.55 | 0.54 | 0.52 | 0.50 | 0.48 | 0.45 |
| Right | 2.14 | 1.96 | 1.77 | 1.59 | 1.42 | 1.26 | 1.13 | 1.00 | 0.90 | 0.80 | 0.72 | 0.65 |

(The temperatures are given with two decimal places to show the variation in the calculations, since there is very little change in the temperature over a large distance along the left bank.) Even though 66% of the river flow has an excess temperature of 2.3° C due to the diffuser action, the slow transverse mixing, coupled with the surface heat transfer, produces a maximum temperature of 0.55° C along the left bank, with the calculated maximum being 130 km downstream of the diffuser. Along the right bank, the temperature rise drops to 1° C at 160 km. (These distances are so large that the length of the initial mixing region can be neglected. Also, over these distances, changes in the hydraulics, such as tributary inflow and changes in $D_f$ caused by changes in depth and velocity, may be significant.)

Since the temperature along the left bank is also the minimum temperature at each cross section, the temperature distributions along the left bank for various values of $x_d$ could be estimated by obtaining $c_{d,max}$ from Figure 40b and then $c_{d,min}$ from Figure 41b. As was done in the calculations above, these values of $c_d$ would have to be converted to dimensional values and then reduced to account for surface heat loss.

## 8.5 EXAMPLES OF UNSTEADY AMBIENT TRANSPORT ANALYSIS

### 8.5.1 One-Dimensional Conditions

There is an accidental spill of 200 lb of a substance in a river. It is desired to estimate the concentration distribution at a point 20 miles downstream with a river flow rate (Q) of 1,440 cfs. For the purpose of this calculation, the substance is assumed to be conservative (no decay or reaction). For this reach of the river and for this $Q$, the average hydraulic characteristics are $H = 6$ ft, $B = 200$ ft, and $S = 10^{-4}$. Manning's n is estimated to be 0.04 giving an average $V$ of 1.2 fps. The shear velocity, $U_* = (gR_H S)^{1/2}$, is then 0.14 fps. The alignment of the channel and the bed form and materials are such that the effects of temporary storage are probably negligible ( $\lambda < 0.05$ , Section 6.2.4) so that the average flow

405

velocity should also be the average cloud velocity (i.e. the average speed with which the pollutant cloud moves downstream).

First calculate the value of $x_d'$ (Eq. 7.7.14) for $x = 20$ miles to determine whether the concentration distribution will be one dimensional or two dimensional with significant transverse variations. The river is gently meandering; an investigation of several typical bends in the river shows that they fall in Region IV of Figure 62, so that the meandering does not contribute significantly to the transverse mixing process. Since this is a free-flowing river with well-defined cross sections, the value of $\alpha$ is estimated to be 0.6 giving $e_y = \alpha H U_* = 0.50$ ft$^2$/sec and $x_d' = e_y x/VB^2 = 1.1$ so that the concentration distribution will be one dimensional. (Since a one-dimensional analysis is to be used, the transverse location of the spill is not needed.)

The empirical correlation of Weaver and Holley (Section 7.7.3c) is used to estimate the concentration distribution. In order to convert the $C'$ versus $t'$ distribution of Figure 72 into a $C$ versus $t$ distribution, values are needed for $\sigma$ and $\bar{t}$. For $x_d' = 1.1$, Figure 71 gives $\sigma_d'^2 = 8.1 \times 10^{-3}$ (with a $\pm$ one standard deviation range from $1.6 \times 10^{-3}$ to $4.3 \times 10^{-2}$). The value of $\sigma$ is

$$\sigma = \left(\sigma_d'^2\right)^{1/2} \frac{B^2}{e_y} = 7{,}150 \text{ sec} \quad (\text{range:} \quad 3{,}180\text{--}16{,}460 \text{ sec})$$

and $\bar{t}$ can be estimated as

$$\bar{t} = \frac{x}{V} = 88{,}000 \text{ sec}$$

Starting with $C'$ and $t'$ from Figure 72, the concentration distribution is obtained using

$$C = \frac{C'M}{\sigma Q}$$

and

$$t = \bar{t} + \sigma t'$$

The resulting distributions are shown in Figure 80 with the solid curve corresponding to the average $\sigma$ and the two dashed curves showing the possible variation associated with the range of $\sigma$ values (i.e. due to the uncertainty in the value of $\sigma$ from Figure 72). Uncertainty in the hydraulic parameters, in $e_y$ , etc., would give additional possible variation in the calculated concentrations. The possible range of concentrations shown in Figure 80 is typical of uncertainty to be expected in problems of this type.

The concentration distribution can also be estimated by using Eq. 6.3.3 with $E$ from one of the expressions in Section 7.7.3a or b. For illustrative purposes, Eq. 7.7.5 is used, giving $E = 750$ $ft^2$/sec . (Note that this expression should be used only when $e_y$ is approximately $0.6HU_*$ .) The concentration distribution obtained from Eq. 6.3.3 is shown as the dotted curve in Figure 81. The possible variation in $E$ (Section 7.7.3a) could be used to obtain other curves to demonstrate the uncertainty in $C$ by this method also, but this is not done in order to keep the figure from becoming too cluttered. The range in $C$ values based on the range of $E$ values would be smaller than that of Weaver and Holley's analysis; this result is probably due to the fact that Eq. 7.7.5 for $E$ was based on a selected set of data (14 tests) whereas Figure 71 includes many more tests with no criteria having been applied to select or eliminate any of the data that were available for the correlation. Also, the relative shape of the $C$ versus $t$ curve from Figure 72 normally is more realistic than the one from Eq. 6.3.3.

8.5.2 Two-Dimensional Calculation

Due to an accident on a bridge, 5 curies of a radioactive liquid are spilled near the center of a river whose alignment is shown in Figure 82a. The concentrations need to be known for the central part of

407
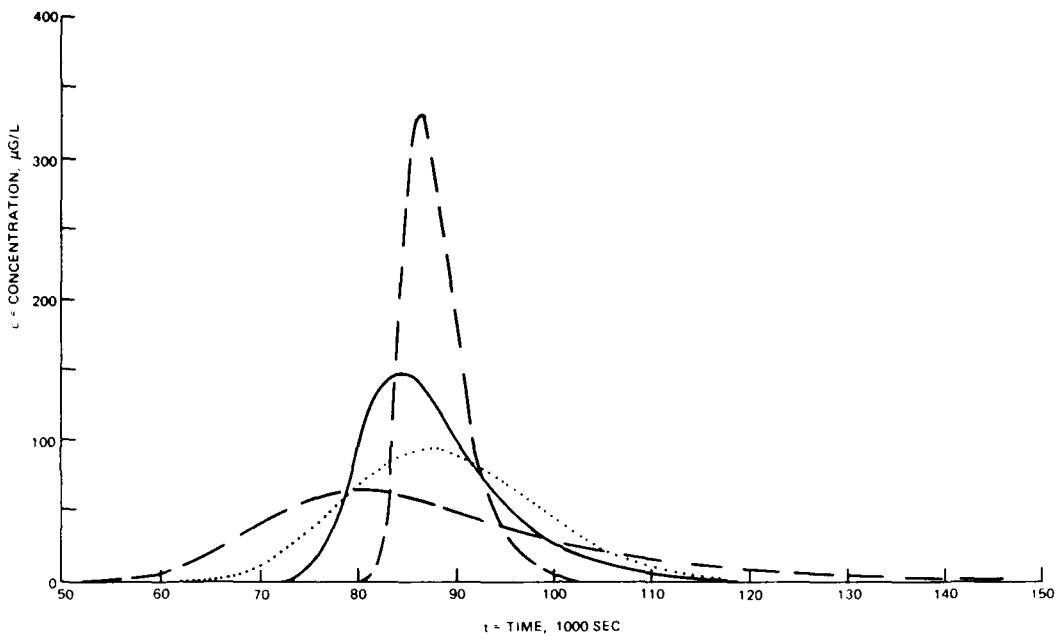
Figure 81. Estimated one-dimensional concentration distributions for unsteady conditions

the river at a point 5,500 ft downstream (cross section 2 on the figure). The river flow rate is 150 cfs. The average width is 110 ft and the average depth is 2.8 ft, giving a velocity of 0.5 fps. The slope is $3.2 \times 10^{-4}$ so that the shear velocity $U_* = (gR_H S)^{1/2}$ is 0.17 fps. For an approximate calculation, $\alpha$ is estimated to be 1.0 because of meandering of the stream. (An average value of $\alpha$ could be obtained by first getting $\alpha$ for each bend using Figure 60 and then averaging the values, with each value being weighted by the flow length for which it applies, as was done to obtain an average $D_f$ in Section 8.4.1). The value of $x_d$ at 5,500 ft is 0.4. Even though the concentration distribution is probably essentially one dimensional at this cross section (Figure 42), a significant part of the reach is in the initial period where the concentration distributions are two dimensional. Thus, a 2D calculation is needed.

Temporal moments will be used, with the concentration being estimated using a Pearson Type III distribution (Section 6.2.4). From prior measurements in the stream, the depth profile and velocity

408
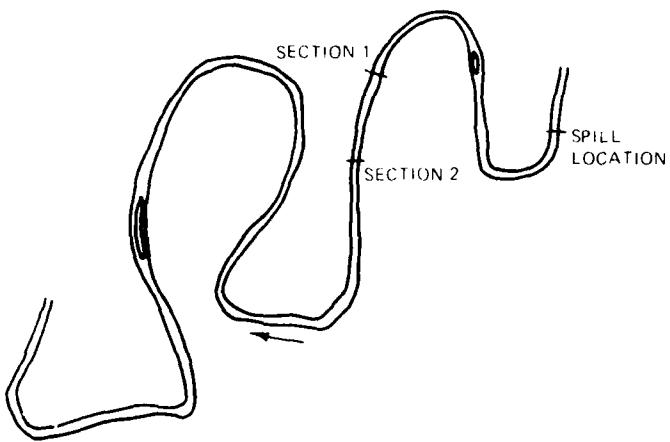
a. River reach
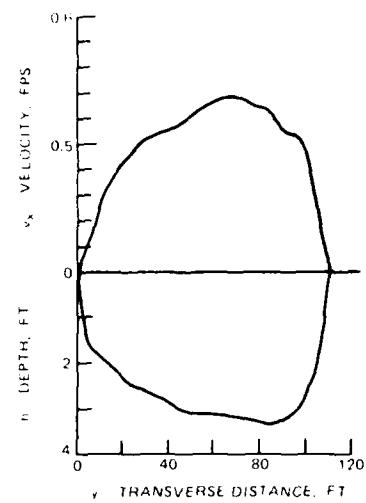
b. Velocity and depth distributions
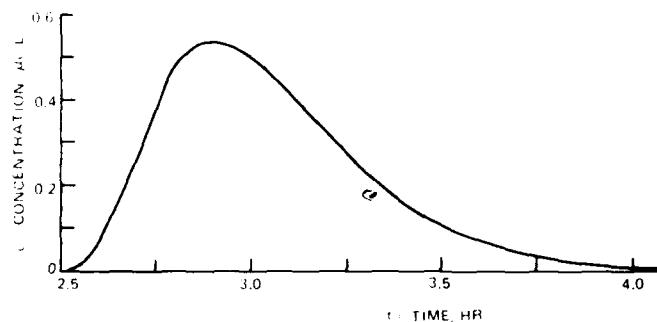
c. Concentration distributions

Figure 82. Example using 2D temporal moment calculation

distribution at Section 1 in Figure 82a are known to be as shown in Figure 82b. Since this is the only information available on depth and velocity distributions, the calculations will be made assuming a prismatic channel. However, the measured distributions are from a cross-over region between bends and the differences in depths and velocities within the cross section are not as large as they would be in the bends. Thus, the calculated longitudinal spreading may be somewhat smaller than would be the actual case. The 2D calculations give the following results for the center line of the stream: zeroth moment = 1,180 $\mu$c-sec/$\ell$ , $\bar{t}$ = 10,981 sec = 3.05 hr, $\sigma^2$ = 976,000 sec$^2$ or $\sigma$ = 988 sec = 0.27 hr , and S (skew coefficient) = 1.03 . Substitution of these values into Eq. 6.2.14 allows the concentration distribution for the centerline of the stream to be calculated as shown in Figure 82c. As with the previous example, these calculations must be viewed as being a general approximation. In particular, even if the average velocity is correct, the elapsed time to the first arrival of the cloud may be as much as 20% smaller than indicated, since the velocity distributions in the bends (where there are larger differences of velocity within the cross section) are not represented in the calculations.

# REFERENCES

Abdelwahed, M. S. T., and Chu, V. H. 1978. "Bifurcation of Buoyant Jets in Crossflow," Technical Report 78-1, Department of Civil Engineering and Applied Mechanics, McGill University, Montreal, Canada.

Abraham, G. 1963. "Jet Diffusion in Stagnant Ambient Fluid," Publ. No. 29, Delft Hydraulics Laboratory, The Netherlands.

_____. 1967. "Jets with Negative Buoyancy in Homogeneous Fluid," J. Hydr. Research, Vol 5, No. 4.

_____. 1970. "The Flow of Round Buoyant Jets Issuing Vertically into Ambient Fluid Flowing in a Horizontal Direction," Proc., 5th Intern. Water Pollution Res. Conf., San Francisco, Calif.

Adams, E. E. 1982. "Dilution Analysis for Unidirectional Diffusers," J. Hydr. Div. Vol 108, No. HY3.

Adams, E. E., Stolzenbach, K. D., and Harleman, D. R. F. 1975. "Near and Far Field Analysis of Buoyant Surface Discharges into Large Bodies of Water," Tech. Rep. 205, R. M. Parsons Laboratory for Water Resources and Hydrodynamics, Dept. of Civil Engineering, Massachusetts Institute of Technology, Cambridge, Mass.

Almquist, C. W., and Holley, E. R. 1985. "Transverse Mixing in Meandering Laboratory Channels with Rectangular and Naturally Varying Cross Sections," Report 205, Center for Research in Water Resources, Univ. of Texas at Austin, 223 pp.

Anwar, H. O. 1972. "Measurements on Horizontal Buoyant Jets in Calm Ambient Fluid," La Houille Blanche, Vol 27, No. 4.

Aris, R. 1956. "On the Dispersion of a Solute in a Fluid Flowing Through a Tube," Proc. Royal Soc. London, Vol 235A, pp 67-77.

Beer, T., and Young, P. C. 1980. "On the Characterization of Longitudinal Dispersion in Natural Streams," Rept. AS/R42 1980, Centre for Resource and Envir. Studies, Australian National Univ., Canberra.

_____. 1983. "Longitudinal Dispersion in Natural Streams," J. Envir. Engrg. Div., ASCE, Vol 109, No. 5, pp 1049-1067.

Beltaos, S. 1975. "Evaluation of Transverse Mixing Coefficients from Slug Tests," J. Hydr. Research, Vol 13, No. 4, pp 351-360.

_____. 1978. "Transverse Mixing in Natural Streams," Rep. SWE-78/01, Alberta Research Council.

_____. 1980. "Transverse Mixing Tests in Natural Streams," J. Hydr. Div., ASCE, Vol 106, No. HY10, pp 1607-1625.

Bird, S., and Holley, E. R. 1985. "An Evaluation of a Two-Dimensional Model for Transport of a Slug Release in a Meandering Channel," Report 207, Center for Research in Water Resources, Univ. of Texas, Austin, Tex., 87 pp.

411

Bird, R. B., Stewart, W. E., and Lightfoot, E. N. 1960. Transport Phenomena, John Wiley and Sons, New York.

Buchanan, T. J., and Somers, W. P. 1968. "Discharge Measurement at Gaging Stations," Techniques of Water Resources Investigations, US Geological Survey, Book 3, Chap. A8.

Bugliarello, G., and Jackson, E. D. 1964. "Random Walk Study of Convective Diffusion," J. Engrg. Mech. Div., ASCE, Vol 90, No. EM4, pp 49-77.

Carslaw, H. S., and Jaeger, J. C. 1959. Conduction of Heat in Solids, Oxford Press, 2d ed.

Cederwall, K. 1963. The Initial Mixing of Jet Disposal into a Recipient," Tech. Rep. 14 and 15, Div. of Hydraulics, Chalmers Institute of Technology, Goteborg, Sweden.

_____. 1971. "Buoyant Slot Jets into Stagnant or Flowing Environments," Rep KH-R-25, W. M. Keck Laboratory for Water Resources and Hydraulics, California Institute of Technology.

Chang, Y. C. 1971. "Lateral Mixing in Meandering Channels," Ph. D. Dissert., Iowa Univ., Iowa City.

Chen, C. J., and Rodi, W. 1980. Vertical Buoyant Jets: A Review of Experimental Data, Pergamon Press, Oxford.

Christensen, B. A. 1977. "Discussion of 'Predicting Dispersion Coefficients of Streams,' by H. Liu," J. Envir. Engrg. Div., ASCE, Vol 103, No. EE6, pp 1144-1146.

Crowley, W. P. 1968. "Numerical Advection Experiments," Monthly Weather Rev., Vol 96, No. 1, pp 1-11.

Dagan, G. 1969. "Dispersivity Tensor for Turbulent Uniform Channel Flow," J. Hydr. Div., ASCE, Vol 95, No. HY5, pp 1699-1712.

Daily, J. W., and Harleman, D. R. F. 1968. Fluid Dynamics, Addison-Wesley Publishing Co., Inc. Cambridge, Mass.

Elder, J. W. 1959. "The Dispersion of Marked Fluid in Turbulent Shear Flow," Fluid Mechanics, Vol 5, Part 4, pp 544-560.

Fan, L. N. 1967. "Turbulent Buoyant Jets into Stratified or Flowing Ambient Fluids," Rep. KH-R-15, W. M. Keck Laboratory for Hydraulics and Water Resources, California Institute of Technology, Pasadena, Calif.

Fan, L. N., and Brooks, N. H. 1967. "Numerical Solution of Turbulent Buoyant Jet Problems," Rep. KH-R-18, W. M. Keck Laboratory for Hydraulics and Water Resources, California Institute of Technology, Pasadena, Calif.

Fischer, H. B. 1964. "Determination of Dispersion Coefficients by the Change of Moments Method," Tech. Memo. 64-6, Keck Lab., Caltech, Pasadena, Calif.

Fischer, H. B. 1966a. "A note on the One-Dimensional Dispersion Model," Air and Water Pollution, Intern. Journal, London, Vol 10, pp 443-452.

_____. 1966b. "Longitudinal Dispersion in Laboratory and Natural Streams," Rep KH-4-12, Calif. Inst. Technology, W. M. Keck Laboratory for Hydraulics and Water Resources, Pasadena, Calif.

_____. 1967. "Transverse Mixing in a Sand-Bed Channel," Prof. Paper No. 575-D, US Geological Survey, pp D267-D272.

_____. 1969. "Effects of Bends on Dispersion in Streams," Water Resources Research, Vol 5, No. 2, pp 496-506.

_____. 1973. "Longitudinal Dispersion and Turbulent Mixing in Open-Channel Flow," Annual Review of Fluid Mechanics, Vol 5, pp 59-78, Annual Reviews, Inc., Palo Alto, Calif.

_____, ed. 1981. Transport Models for Inland and Coastal Waters, Academic Press, New York.

Fischer, H. B., et al. 1979. Mixing in Inland and Coastal Waters, Academic Press, New York.

Fox, D. C. 1970. "Forced Plume in a Stratified Fluid," J. Geophys. Res., Vol 75, No. 33.

Fukuoka, S., and Sayre, W. W. 1973. "Longitudinal Dispersion in Sinuous Channels," J. Hydr. Div, ASCE, Vol 99, No. HY1, pp 195-217.

Glover, R. E. 1964. "Dispersion of Dissolved or Suspended Materials in Flowing Streams," Prof. Paper No. 433-B, US Geological Survey.

Godfrey, R. G., and Frederick, B. J. 1963. "Dispersion in Natural Streams," US Geological Survey Open File Rep., Washington, DC.

_____. 1970. "Stream Dispersion at Selected Sites," Prof. Paper No. 433-K, US Geological Survey, Washington, DC.

Harleman, D. R. F. 1961. "Stratified Flow," Handbook of Fluid Dynamics, V. L. Streeter, ed., McGraw-Hill, New York.

Hinze, J. O. 1959. Turbulence, McGraw-Hill, New York, pp 275-375.

Hirst, E. A. 1972. "Buoyant Jets with Three-Dimensional Trajectories," J. Hydr. Div., ASCE, Vol 98, No. HY11.

Holley, E. R. 1969. "Unified View of Diffusion and Dispersion," J. Hydr. Div., ASCE, Vol 95, No. HY2, pp 621-631.

_____. 1971. "Transverse Mixing in Rivers," Rep. S132, Delft Hydr. Lab., Delft, Netherlands.

Holley, E. R., and Abraham, G. 1973. "Field Tests on Transverse Mixing in Rivers," J. Hydr. Div., ASCE, Vol 99, No. HY12, pp 2313-2331.

Holley, E. R., Siemons, J., and Abraham, G. 1972. "Some Aspects of Analyzing Transverse Mixing in Rivers," J. Hydr. Research, Vol 10, No. 1, pp 27-57.

Holley, E. R., and Tsai, Y. H. 1978. "Effects of Separation Zones on Temporal Moments for Longitudinal Mixing in Rivers," Proc., Intern. Symp. on Envir. Effects of Hydr. Engrg. Works, E. E. Driver and W. O. Wunderlich, eds., Tennessee Valley Authority, Knoxville, Tenn.

Holley, E. R., and Waddell, K. M. 1976. "Stratified Flow in Great Salt Lake Culvert," J. Hydr. Div., Proc. ASCE, Vol 102, No HY7.

Holley, E. R., and Yotsukura, N. 1979. "Thermal Boundary Conditions for Water Flow with Moving Boundaries," Open-File Rep 79-743, US Geological Survey, Reston, Va.

Holly, F. M. 1975. "Two-Dimensional Mass Dispersion in Rivers," Hydrology Paper 78, Colorado State Univ., Fort Collins, Colo.

Hubbard, E. F., et al. 1982. "Measurement of Time of Travel and Dispersion in Streams by Dye Tracing," Techniques of Water-Resources Investigations, US Geological Survey, Book 3, Chap A9.

Jackman, A. P. and Yotsukura, N. 1977. "Thermal Loading of Natural Streams," Prof. Paper No. 991, US Geological Survey, Washington, DC.

Jain, S. C. 1976. "Longitudinal Dispersion Coefficients for Streams," J. Envir. Engrg. Div., ASCE, Vol 102, No. EE2, pp 465-474.

Jeng, S. W., and Holley, E. R. 1986. "Two-Dimensional Random Walk Model for Pollutant Transport in Natural Rivers" in press, Center for Research in Water Resources, Austin, Tex.

Jirka, G. H. 1982a. "Turbulent Buoyant Jets in Shallow Fluid Layers," Turbulent Buoyant Jets and Plumes, W. Rodi, ed., Pergamon Press, Oxford.

_____. 1982b. "Multiport Diffusers for Heat Disposal - A Summary," J. Hydr. Div., ASCE, Vol 108, No. HY12.

Jirka, G. H., Abraham, C., and Harleman, D. R. F. 1975. "An Assessment of Techniques for Hydrothermal Prediction," Tech. Rep. 203, MIT, R. M. Parsons Laboratory for Water Resources and Hydrodynamics, Cambridge, Mass. (also published by US Nuclear Regulatory Commission, Rep. No. NUREG-0044, 1976).

Jirka, G. H., Adams, E. E., and Stolzenbach, K. D. 1981. "Buoyant Surface Jets," J. Hydr. Div., ASCE, Vol 107, No. HY11.

Jirka, G. H., and Fong, H. L. M. 1981. "Vortex Dynamics and Bifurcation of Buoyant Jets in Crossflow," J. Engrg. Mech. Div., ASCE, Vol 107, No. EM3.

Jirka, G. H., and Harleman, D. R. F. 1973. "The Mechanics of Submerged Multiport Diffusers for Buoyant Discharges in Shallow Water," Tech. Rep. No. 169, R. M. Parsons Laboratory for Water Resources and Hydrodynamics, Massachusetts Institute of Technology.

_____. 1979. "Stability and Mixing of Vertical Plane Buoyant Jet in Confined Depth," J. Fluid Mech., Vol 94, pp 275-304.

Jobson, H. E. 1981. "Temperature and Solute-Transport Simulation in Streamflow Using a Lagrangian Reference Frame," Water-Resources Investigation 81-2, US Geological Survey, NSTL Station, Bay St. Louis, Miss.

Kaplan, W. 1953. Advanced Calculus, Addison-Wesley Publishing Co., Inc., Cambridge, Mass., pp 151-158.

Kilpatrick, F. A., and Cummings, T. R. 1972. "Tracer Simulation Study of Potential Solute Movement in Port Royal Sound, South Carolina," Water-Supply Paper 1586-J, US Geological Survey, Washington, DC.

Korn, G. A., and Korn, T. M. 1961. Mathematical Handbook for Scientists and Engineers, McGraw-Hill, New York, p 100.

Krishnappan, B. G., and Lau, Y. L. 1977a. "Transverse Dispersion in Meandering Channels," Scientific Series No. 75, Canada Centre for Inland Waters, Burlington, Ontario.

_____. 1977b. "Transverse Mixing in Meandering Channels with Varying Bottom Topography," J. Hydr. Research, Vol 5, No. 4 pp 351-372.

Langbein, W. B., and Leopold, L. B. 1966. "River Meanders--Theory of Minimum Variance," Prof. Paper US Geological Survey.

Larsen, J., and Sorensen, T. 1968. "Buoyancy Spread of Wastewater in Coastal Regions," Vol 2, Eleventh Conference on Coastal Engineering, London.

Lau, Y. L., and Krishnappan, B. G. 1977. "Transverse Dispersion in Rectangular Channels," J. Hydr. Div., ASCE, Vol 103, No. HY10, pp 1173-1189.

_____. 1981. "Modeling Transverse Mixing in Natural Streams," J. Hydr. Div., ASCE, Vol 107, No. HY2, pp 209-226.

Lee, J. H., and Jirka, G. H. 1980. "Multiport Diffuser as Line Source of Momentum," Water Resources Research, Vol 16, No. 4.

Leendertse, J. J. 1970. "A Water-Quality Simulation Model for Well-Mixed Estuaries and Coastal Seas; Vol 1, Principles of Computation," Memo. Rm-6230-RC, Rand Corp., Santa Monica, Calif.

List, E. J. 1982. "Mechanics of Turbulent Buoyant Jets and Plumes," Turbulent Buoyant Jets and Plumes, W. Rodi, ed., Pergamon Press, Oxford.

Liu, H. 1977. "Predicting Dispersion Coefficient of Streams," J. Envir. Engrg. Div., ASCE, Vol 103, No. EE1, pp 59-69.

Liu, H., and Cheng, H. D. 1980. "Modified Fickian Model for Predicting Dispersion," J. Hydr. Div., ASCE, Vol 106, No. HY6, pp 1021-1040.

Martens, L. A., et al. 1974. "Time of Travel of Solutes in Mississippi River from Baton Rouge to Pointe a la Hache, Louisiana," Tech. Rept. 9, Louisiana Dept. of Public Works, Baton Rouge, La.

Martin, B. 1976. "Comparing Methods for Modeling Dispersion in Flowing Media," Rept. AS/RB 1976, Centre for Resource and Envir. Studies, Australian National Univ., Canberra. (See also, Utilitas Mathematica, Vol 15, 1979, pp 307-322.)

McQuivey, R. S., and Keefer, T. N. 1976a. "Convective Model of Longitudinal Dispersion," J. Hydr. Div., ASCE, Vol 102, No. HY10, pp 1409-1424.

_____. 1976b. "Dispersion--Mississippi River Below Baton Rouge, La.," J. Hydr. Div., ASCE, Vol 102, No. HY10, pp 1425-1437.

McQuivey, R. S., Keefer, T. N., and Shirazi, M. A. 1971. "Basic Data Report on the Turbulent Spread of Heat and Matter," US Geological Survey, Open File Report, Bay St. Louis, Miss.

Miller, A. C., and Richardson, E. V. 1974. "Diffusion and Dispersion in Open Channel Flow," J. Hydr. Div., ASCE, Vol 100, No. HY1, pp 159-171.

Monin, A. S., and Yaglom, A. M. 1973. Statistical Fluid Mechanics; Mechanics of Turbulence, Massachusetts Inst. Technology Press, Cambridge, Mass., pp 205-218.

Morton, B., Taylor, G. I., and Turner, J. S. 1956. "Turbulent Gravitational Convection from Maintained and Instantaneous Sources," Proc. Roy. Soc., London, Series A, Vol 234, pp 1-23.

Nordin, C. F., and Sabol, C. V. 1974. "Empirical Data on Longitudinal Dispersion in Rivers," Water-Resources Investigations, US Geological Survey, Lakewood, Colo.

Okoye, J. K. 1970. "Characteristics of Transverse Mixing in Open-Channel Flows," Rep. KH-R-23, W. M. Keck Laboratory for Water Resources and Hydraulics, California Institute of Technology, Pasadena, Calif.

Roberts, P. J. W. 1977. Dispersion of Buoyant Waste Water Discharged from Outfall Diffusers of Finite Length," Rep. KH-R-35, W. M. Keck Laboratory for Hydraulics and Water Resources, California Institute of Technology, Pasadena, Calif.

Rodi, W. 1980. "Turbulence Models and Their Application in Hydraulics: A State-of-the-Art Review," Intern. Assn. for Hydr. Research, Delft, The Netherlands.

Sayre, W. W. 1967. "Dispersion of Mass in Open-Channel Flow," Ph. D. Dissert., Colorado State Univ., Fort Collins, Colo. (see also Sayre 1975).

_____. 1968. "Discussion of The Mechanics of Dispersion in Natural Streams," by H. B. Fischer, J. Hydr. Div., ASCE, Vol 94, No. HY6, pp 1549-1556.

_____. 1969. "Dispersion of Silt Particles in Open Channel Flow," J. Hydr. Div., ASCE, Vol 95, No. HY3, pp 1009-1038.

Sayre, W. W. 1975. "Dispersion of Mass in Open-Channel Flow," Hydrology Paper 75, Colorado State Univ., Fort Collins, Colo. (see also Sayre 1967).

Sayre, W. W. and Caro-Cordero, R. 1979. "Shore-Attached Thermal Plumes in Rivers," Chap. 15, Modeling of Rivers, H. W. Shen, ed., Wiley Interscience Publ., New York.

Sayre, W. W., and Yeh, T. P. 1973. "Transverse Mixing Characteristics of the Missouri River Downstream from the Cooper Nuclear Station," Rep. 145, Iowa Inst. of Hydr. Research, Univ. of Iowa, Iowa City, Iowa.

Schatzmann, M. 1978. "The Integral Equations for Round Buoyant Jets in Stratified Flows," J. Applied Math. and Physics (ZAMP), Vol 29, pp 608-630.

Schlichting, H. 1968. Boundary Layer Theory, McGraw-Hill, New York.

Scorer, R. S. 1978. Environmental Aerodynamics, Ellis Norwood, Chichester, England.

Shirazi, M. A., and Davis, L. R. 1974. "Workbook of Thermal Plume Prediction; Vol 1 - Submerged Discharge," Report No. EPAR2-72-005a, US Environmental Protection Agency.

Smoot, G. F., and Novak, C. E. 1969. "Measurement of Discharge by the Moving Boat Method," Techniques of Water-Resources Investigations, US Geological Survey, Book 3, Chap. All.

Stefan, H., and Demetracopoulos, A. 1981. "Cell-in-Series Simulation of Riverine Transport," J. Hydr. Div., ASCE, Vol 102.

Stolzenbach, K. D., and Harleman, D. R. F. 1971. "An Analytical and Experimental Investigation of Surface Discharges of Heated Water," Report 135, MIT, Parsons Lab. for Water Resources and Hydrodynamics, Cambridge, Mass.

Sullivan, P. J. 1968. "Dispersion in Turbulent Shear Flow," Ph. D. Dissertation, Univ. of Cambridge, Cambridge, U. K.

_____. 1971. "Longitudinal Dispersion Within a Two-Dimensional Turbulent Shear Flow," J. Fluid Mech., Vol 49, Part 3, pp 551-576.

Taylor, G. I. 1921. "Diffusion by Continuous Movements," Proc., London Math. Soc., Ser. A, Vol 20, pp 196-211.

_____. 1953. "Dispersion of Soluble Matter in Solvent Flowing Slowly Through a Tube," Proc. Royal Soc. of London, Ser. A, No. 219, pp 186-203.

_____. 1954. "The Dispersion of Matter in Turbulent Flow Through A Pipe," Proc., Royal Soc., London, Ser. A, Vol 223, pp 446-468.

Thackston, E. L., and Schnelle, K. B. 1970. "Predicting Effects of Dead Zones on Stream Mixing," J. San. Engrg. Div., ASCE, Vol 96, No. SA2, pp 319-331.

Thomann, R. V. 1973. "Effect of Longitudinal Dispersion on Dynamic Water Quality Response of Streams and Rivers," Water Resources Research, Vol 9, No. 2, pp 353-366.

Tsai, Y. H., and Holley, E. R. 1978. "Temporal Moments for Longitudinal Dispersion," J. Hydr. Div., ASCE, Vol 104, No. HY12, pp 1617-1634.

_____. 1979. "Temporal and Spatial Moments for Longitudinal Mixing in Rivers with Separation Zones," Hydr. Engrg. Series, Dept. of Civil Engrg., Univ. of Illinois, Urbana, Ill.

_____. 1980. Closure to Discussions of "Temporal Moments for Longitudinal Dispersion," J. Hydr. Div., ASCE, Vol 106, No. HY12, pp 2063-2066.

Tso, D. J. 1982. "Accuracy of Concentration Predictions for Rivers Using Temporal Moments with Similarity Functions," M.S. Thesis, Univ. of Texas at Austin.

Valentine, E. M., and Wood, I. R. 1977. "Longitudinal Dispersion with Dead Zones," J. Hydr. Div., ASCE, Vol 103, No. HY9, pp 975-990.

Weaver, J., and Holley, E. R. 1985. "Empirical Analysis of Longitudinal Dispersion in Streams (in press)," Center for Research in Water Resources, Univ. of Texas, Austin, Tex.

Wright, S. J. 1977. "Mean Behavior of Buoyant Jets in a Crossflow," J. Hydr. Div., ASCE, Vol 103, No. HY5.

Yotsukura, N. 1977. "Derivation of Solute-Transport Equations for a Natural-Channel Flow," J. Research, US Geological Survey, Vol 5, No. 3, pp 277-284.

_____. 1981. "Discussion of 'Modeling Transverse Mixing in Natural Streams' by Y. L. Lau and B. G. Krishnappan," J. Hydr. Div., ASCE, Vol 107, No. HY11, pp 1577-1579.

Yotsukura, N., and Cobb, E. D. 1972. "Transverse Diffusion of Solutes in Natural Streams," Prof. Paper No. 582-C, US Geological Survey, Washington, DC.

Yotsukura, N., Fischer, H. B., and Sayre, W. W. 1970. "Measurement of Mixing Characteristics of the Missouri River Between Sioux City, Iowa and Plattsmouth, Nebraska," US Geological Survey Water Supply Paper 1899-G.

Yotsukura, N. and Kilpatrick, F. A. 1973. "Tracer Simulation of Soluble Water Concentration," J. Envir. Engrg. Div., ASCE, Vol 99, No. EE4, pp 499-515.

Yotsukura, N., and Sayre, W. W. 1976. "Transverse Mixing in Natural Channels," Water Resources Research, Vol 12, No. 4, pp 695-704 (copyright by the American Geophysical Union).

_____. 1977. "Reply to Comments on 'Transverse Mixing' in Natural Channels," Water Resources Research, Vol 13, No. 2, p 497.

Yotsukura, N., et al. 1983. "An Assessment of Steady-State Propane-Gas Tracer Method for Reaeration Coefficients--Cowaselon Creek, New York," Water-Resources Investigations, Rep. 83-4183, US Geological Survey, Reston, Va.

_____. 1984. "An Assessment of Steady-State Propane-Gas Tracer Method for Reaeration Coefficients -- Chenango River, New York, (in press)" Water-Resources Investigations, US Geological Survey, Reston, Va.

END

1-81

DTIC